
Environmental
Studies
Research
Fund

218

Integrated Beaufort Observatory

Observatoire intégré dans la mer de Beaufort

Environmental Studies Research Funds
Report No. 218

July 2019

Integrated Beaufort Observatory

By

ArcticNet Inc.
Université Laval, Québec, QC

The correct citation for this report is:

ArcticNet Inc. (2019). Integrated Beaufort Observatory. Environmental Studies Research Funds Report No. 218. Quebec, QC. 474 pages.

TABLE OF CONTENTS

Executive Summary	5
Résumé	8
Part 1 – iBO Technical Report 2015	11
Part 2 – iBO Technical Report 2016	138
Part 3 – iBO Technical Report 2017	273
Part 4 – iBO Technical Report 2018	406

EXECUTIVE SUMMARY

The integrated Beaufort Observatory (iBO) is a four-year mooring program (2015-2018) managed by ArcticNet in partnership with Fisheries and Oceans Canada and Golder Associates Ltd. The project aims to contribute key oceanographic information required for decisions on development and regulations in the offshore Canadian Beaufort Sea by extending existing time-series measurements and integrating regional understanding of the shelf and slope environment through year-round measurements acquired by autonomous measuring systems on subsurface moorings. iBO builds upon extensive time-series acquired by DFO since the 1970's and through ArcticNet and related projects (e.g. Canadian Arctic Shelf Exchange Study, ArcticNet-Industry partnership, Beaufort Regional Environmental Assessment) from 2002 to 2015. Data from the iBO program are available publicly through the Polar Data Catalogue. This report is composed of a series of four comprehensive Technical Reports which provide information on the data collection approach, quality assurance/quality control method, and overview of results.

The main iBO sampling platform is composed of 7 tautline moorings located in waters ranging from 20 to 750 m depth at key locations from the Mackenzie Canyon, to the mid- and outer central shelf and slope, up to the remote northwestern area off Banks Island. The moorings are equipped with state-of-the-art instrumentation, including acoustic Doppler current profilers from 75 to 2000 MHz to measure current velocity, current direction, ice drift and plankton/particulates backscattering; ice-profiling sonars for the measurement of sea ice thickness, under-ice topography and for assessing waves and storm surges; water quality sensors for salinity, temperature, turbidity, chlorophyll and dissolved oxygen; and automated sediment traps that collect sinking particles for the measurement of biogeochemical fluxes. Fieldwork to recover and redeploy the moorings was conducted from the research icebreaker CCGS Amundsen in 2015 and 2016, and subsequently from the CCGS Sir Wilfrid Laurier in 2017 and 2018. Note that in 2018, heavy ice conditions prevented the recovery of 5 out of the 7 iBO moorings from the Laurier. These moorings will be recovered in September 2019.

The following are key observations derived from the full dataset:

- The high data recovery rates (>90% on average) reflect the success of the iBO field program. Attention to quality control detail, continuous application of lessons learned have resulted in a near-continuous dataset at 7 sites from 2014-2018 with few gaps.
- Sea ice conditions in the southern Beaufort Sea from 2015 to 2018 are characterized by earlier than normal break up in the spring and near record minimum seasonal ice coverage each September except for 2018. Available results from the iBO IPS dataset reflect a similar trend towards longer ice-free seasons and slightly thinner ice.
- Current profilers and current meters at the 7 mooring sites provided measurements of ocean current through the water column from 2014 to 2018 and were used to

characterize currents across the shelf, shelf-break, and slope and provide evidence and insight into large- and small-scale circulation patterns. Current speeds are consistent from year-to-year; similar large- and small-scale circulation patterns were observed from year-to-year with some temporal and spatial variation.

- The temperature and salinity time-series from 2014 to 2018 consistently show that most of the variability in terms of water mass physical properties occurs in the upper 200 m. Each year several water mass shifts resulting in the upper 200 m from upwelling or downwelling were identified primarily on the slope moorings. Below 200 m, temperature-salinity diagrams show little variability from year-to-year in water mass physical properties.
- The near-continuous four-year dataset provides important insight into the marine physical environment of the Beaufort Sea. An initial review of the datasets is presented in yearly Technical Reports and identifies key features of the physical environment. The dataset provides the opportunity to further investigate and understand ice-ocean processes in the southern Beaufort Sea.

In 2018, the iBO team initiated a synthesis work entitled “Variability of the Beaufort Ice-Ocean Environment Synthesis: A Synthesis Report” to be developed over 2018-2021. The Synthesis Report will be a building block of the Indigenous and Northern Affairs Canada (INAC) Beaufort Regional Strategic Environmental Assessment (BRSEA). The goal of this synthesis work is to develop an informative document summarizing the physical marine environment by incorporating analysis and review of existing data and new data obtained from the mooring observatories and state-of-the-art modelling products. The project seeks to continue liaison and coordination with relevant Inuvialuit and Industry stakeholder in the Beaufort Sea for communication and delivery of research and data products. The report will provide integrated perspective on the iBO dataset into a synthesis of 8 years of (2009-2017) of enhanced observations of the marine physical environment in the southern Beaufort Sea.

In summary, the iBO program consisted in a four-year extension of sea ice and ocean time series at long-standing sites in the Beaufort Sea: ice drift, thickness and ridging, ocean current, temperature and salinity, storm waves and surge, plankton presence from acoustic scattering, and other studied variables. The project contributed to improve ocean and sea-ice climatology (means, extremes, seasonal cycle, co-variability, etc.) derived by statistical analysis from mooring observations. The project has enhanced the description of ocean circulation over the slope of the Beaufort, including upwelling and downwelling, the water-parcel trajectories, the characteristics and propagation of eddies, and the coherence scale of oceanic motion. New types of data (e.g. on biogeochemical cycling, downward particle flux) suited to guiding engineering to mitigate anticipated impacts of Beaufort offshore development were acquired.

The iBO program demonstrates that long-term monitoring is essential to assess and eventually predict inter-annual variations in oceanographic processes of importance for the development

of offshore resources, including the role of climate change and natural variability. Once established, the value of long-term observatories, such as those provided by the iBO project, exponentially increases every year. However, due to a model of relatively short-term funding in Canada and to rapidly evolving priorities in the Beaufort Sea, a multi-stakeholder approach should be developed to ensure long-term viability of observations.

RÉSUMÉ

L'Observatoire intégré dans la mer de Beaufort (OIB) est un programme de corps d'amarrage s'échelonnant sur quatre ans (2015-2018) géré par ArcticNet en partenariat avec Pêches et Océans Canada (MPO) et Golder Associates Ltée. Le projet vise à fournir les données océanographiques clés requises pour la prise de décisions sur la mise en valeur et la réglementation dans la zone extracôtière de la mer de Beaufort au Canada, en prolongeant les mesures de séries chronologiques et en intégrant les connaissances régionales de l'environnement de plateaux et de talus obtenues par la prise de mesures toute l'année effectuées par des systèmes de mesure indépendants sur les corps d'amarrage sous-marin. L'OIB mise sur les séries chronologiques obtenues par le MPO depuis les années 1970, par ArcticNet et dans le cadre de projets connexes réalisés de 2002 à 2015 (l'étude internationale du plateau continental arctique canadien, le partenariat établi entre ArcticNet et l'industrie, l'évaluation environnementale régionale de Beaufort, par exemple). Les données provenant du programme de l'OIB sont accessibles au public dans le Polar Data Catalogue (catalogue sur les données polaires). Le présent rapport comporte une série de quatre rapports techniques exhaustifs fournissant de l'information sur la méthode de collecte de données, la méthode d'assurance et de contrôle de la qualité et un aperçu des résultats.

La principale plate-forme d'échantillonnage de l'OIB se compose de sept corps d'amarrage par cordeau tendu localisés stratégiquement dans des eaux de 20 à 750 m de profondeur, à partir du canyon Mackenzie en passant par le milieu et par la partie centrale externe des plateaux et des talus, jusqu'à la région nord-ouest éloignée au large de l'île Banks. Les corps d'amarrage sont équipés d'instruments de pointe, y compris des profileurs de courant à effet Doppler de 75 à 2 000 MHz pour mesurer la vitesse et la direction des courants, la dérive de la glace, la rétrodiffusion du plancton et des particules; des sonars d'établissement de profils glaciaires pour mesurer l'épaisseur des glaces marines, la topographie sous les glaces et pour évaluer les vagues et les ondes de tempête; des instruments de mesure de la qualité de l'eau pour en déterminer la salinité, la température, la turbidité, la composition en chlorophylle et en oxygène dissous; et des collecteurs de sédiment automatisés recueillant les particules qui coulent pour mesurer les flux biogéochimiques. Des travaux sur le terrain en vue de récupérer et de redéployer les corps d'amarrage ont été effectués par le brise-glace de recherche NGCC Amundsen en 2015 et en 2016, puis par le NGCC Sir Wilfrid Laurier en 2017 et en 2018. Il convient de noter qu'en 2018, en raison de conditions de glace épaisse, cinq des sept corps d'amarrage de l'OIB n'ont pas pu être récupérés par le NGCC Sir Wilfrid Laurier. Ces corps d'amarrage seront récupérés en septembre 2019.

Voici les principales observations découlant de l'ensemble complet des données :

- Les taux élevés de récupération des données (supérieurs à 90 % en moyenne) témoignent du succès du programme sur le terrain de l'OIB. L'attention portée aux

détails en matière de contrôle de la qualité et l'application continue des leçons retenues ont donné lieu à un ensemble de données quasi ininterrompu aux sept emplacements de 2014 à 2018, malgré quelques lacunes.

- Les conditions de la glace marine dans le sud de la mer de Beaufort de 2015 à 2018 se caractérisent par des débâcles plus tôt que la normale au printemps et par une couverture de glace saisonnière, en septembre de chaque année, de taille similaire à l'étendue minimale enregistrée (à l'exception de 2018). Les résultats accessibles provenant de l'ensemble de données IPS de l'OIB traduisent une tendance similaire, soit des saisons libres de glace de plus longue durée et des glaces légèrement plus minces.
- Les profileurs de courant et les débitmètres actuels situés aux sept emplacements des corps d'arrimage ont fourni les mesures du courant océanique traversant la colonne d'eau de 2014 à 2018 et ont été utilisés pour caractériser les courants traversant la plate-forme continentale, la rupture de la plate-forme continentale et le talus. Ces instruments fournissent des données scientifiques sur les schémas de circulation à grande et à petite échelle et en offrent un aperçu. Les vitesses de courant sont constantes d'une année à l'autre; des schémas de circulation à grande et à petite échelle similaires ont été observés d'une année à l'autre, malgré certaines variations temporelles et spatiales.
- Les séries chronologiques de 2014 à 2018 ayant trait à la température et à la salinité indiquent de façon constante que la variabilité relative aux propriétés physiques de la masse d'eau se produit en grande partie dans les 200 m sous la surface. Chaque année, plusieurs changements se produisant dans la masse d'eau située dans les 200 m sous la surface en raison de la remontée et de la plongée des eaux ont été relevés principalement en ce qui concerne les corps d'amarrage dans le talus. Sous les 200 m, les diagrammes représentant la température et la salinité affichent peu de variabilité d'une année à l'autre quant aux propriétés physiques de la masse d'eau.
- L'ensemble de données quasi ininterrompu sur quatre ans fournit des renseignements précieux sur l'environnement physique marin de la mer de Beaufort. Un premier examen des ensembles de données est présenté dans les rapports techniques annuels et indique les caractéristiques clés de l'environnement physique. L'ensemble de données offre la possibilité d'approfondir la recherche et de comprendre les processus océan-glace dans le sud de la mer de Beaufort.

En 2018, l'équipe de l'OIB a amorcé un travail de synthèse intitulé « Variability of the Beaufort Ice-Ocean Environment Synthesis: A Synthesis Report » (synthèse de la variabilité de l'environnement glace-océan de la mer de Beaufort : rapport de synthèse), lequel sera élaboré de 2018 à 2021. Le rapport de synthèse constituera un élément fondamental de l'Évaluation environnementale stratégique régionale dans la mer de Beaufort (EESMB) d'Affaires autochtones et du Nord Canada (AANC). L'objectif de ce travail de synthèse consiste à élaborer un document instructif résumant l'environnement physique marin en combinant l'analyse et l'examen des données actuelles et nouvelles obtenues au moyen des observatoires de corps

d'amarrage et de produits de modélisation de pointe. Le projet vise à poursuivre la liaison et la coordination avec les intervenants pertinents parmi les Inuvialuits et les acteurs de l'industrie dans la mer de Beaufort en vue de communiquer et de réaliser les produits de recherche et de données. Le rapport fournira un point de vue intégré sur l'ensemble de données de l'OIB en une synthèse des huit années (de 2009 à 2017) d'observations améliorées de l'environnement physique marin dans le sud de la mer de Beaufort.

En somme, le programme de l'OIB consistait en la prolongation de quatre années d'une série chronologique sur la glace marine et l'océan en des emplacements de longue durée dans la mer de Beaufort : la dérive, l'épaisseur et l'encrêtement de la glace, les courants, la température et la salinité de l'océan, les vagues et les ondes de tempête, la présence de plancton en fonction de la diffusion acoustique et autres variables étudiées. Le projet a contribué à l'amélioration de la climatologie des océans et de la glace marine (moyennes, extrêmes, cycles saisonniers, covariation, etc.) établies par l'analyse statistique des observations des corps d'amarrage. Le projet a permis d'améliorer la description de la circulation océanique au-dessus du talus de la mer de Beaufort, y compris la remontée et de la plongée des eaux, les trajectoires de l'eau par rapport à celle des transports, les caractéristiques et la propagation des remous, ainsi que l'échelle de cohérence des mouvements océaniques. De nouveaux types de données ont été acquis (sur le cycle biogéochimique, le flux de particules vers le bas) qui sont appropriés pour orienter les procédés d'ingénierie permettant d'atténuer les répercussions prévues des activités de mise en valeur au large dans la mer de Beaufort.

Le programme de l'OIB prouve que la surveillance à long terme est essentielle pour évaluer et en fin de compte prédire les variations interannuelles dans les processus océanographiques d'importance pour la mise en valeur des ressources au large, y compris le rôle du changement climatique et de la variabilité naturelle. Une fois établie, la valeur des observatoires à long terme, tels que ceux qui ont été fournis par le projet de l'OIB, s'accroît exponentiellement chaque année. Or, en raison du modèle de financement de durée relativement courte au Canada et de l'évolution rapide des priorités dans la mer de Beaufort, il faudrait élaborer une approche multipartite pour assurer la viabilité à long terme des observations.

Executive Summary

This report describes the 2015-2016 activities of the integrated Beaufort Observatory (iBO), a four-year program (2015-2018) managed by ArcticNet in partnership with Fisheries and Oceans Canada and Golder Associates Ltd. iBO is supported by the Environmental Study Research Funds and Imperial Oil Resources Ventures Limited. iBO aims to contribute key oceanographic information required for decisions on development and regulations in the offshore Canadian Beaufort Sea by extending existing time-series measurements and integrating regional understanding of the shelf and slope environment through year-round measurements acquired through subsurface moorings.

The activities described in this report focus on the turnaround of 7 moorings initially deployed in 2014 which constitute the backbone of the iBO observational program and aim to provide a regionally-integrated ice and ocean dataset. The main goal of this report is to provide an initial review of the dataset acquired during 2014 -2015 through these 7 moorings. Only the dataset processed thus far is presented, which includes all current meter and current profiler data, temperature-salinity data at 4 out of 7 moorings, and preliminary biogeochemical flux data from one sediment trap and from the near-bottom particle-size analyzer. Data from Ice Profiling Sonars 2014-2015 and additional sediment trap data still in process are expected to be presented as an addendum of the present report to be delivered by March 31, 2017.

For each presented dataset, the spatial and temporal variability is discussed and events of interest that warrant further investigation are identified. An initial analysis of the mean current patterns near the surface and near the bottom during the operational season is provided. The concluding remarks provide a summary of oceanographic phenomena that could be targeted for further studies. Lessons learned stemming from the 2015 operations as well as objectives and milestones for iBO in 2016-2017 are also defined.

Table of Contents

1.0	INTRODUCTION.....	1
1.1	Report Organization.....	2
1.2	Physical Setting of the Study Area.....	3
2.0	MATERIAL AND METHODS	4
2.1	Taut-line Mooring Design.....	4
2.1.1	Slope Moorings	4
2.1.2	Shelf Moorings	5
2.2	Compass Calibration and Verification.....	6
2.3	Mooring Recovery and Deployment.....	7
2.3.1	Shipboard Operations.....	8
2.4	Data Processing and QA/QC	10
2.4.1	Current Meters and Current Profilers.....	10
2.4.2	Temperature-Salinity Loggers	12
2.4.3	Ice Profiling Sonars and Ice velocity.....	13
2.4.4	Sediment Traps	13
2.4.5	Particle Size Analyzer.....	13
3.0	RESULTS AND DISCUSSION	15
3.1	Ocean Currents	15
3.1.1	Mooring BR-1	17
3.1.2	Mooring BR-3	29
3.1.3	Mooring BR-G	40
3.1.4	Mooring BR-K.....	52
3.1.5	Mooring DFO-2.....	58
3.1.6	Mooring DFO-1.....	63
3.1.7	Mooring DFO-9.....	67
3.1.8	Spatial Variability of Surface and Bottom Currents in Open Water.....	71
3.2	Temperature and Salinity.....	74
3.3	Biogeochemical Fluxes	88
4.0	CONCLUSIONS.....	90
4.1	Concluding Remarks on the 2014-2015 Dataset	90
4.2	2015 Fieldwork Lessons Learned and Recommendations	91

4.3	Objectives and Milestones for 2016-2017.....	92
-----	--	----

5.0	REFERENCES.....	94
------------	------------------------	-----------

TABLES

Table 1:	Summary of Post-calibration Compass Errors of TRDI ADCPs for BR Moorings.....	7
Table 2:	Mean Error of Recovered Nortek Compasses (10 Degree Increment) of BR moorings.	7
Table 3:	2014-2015 Mooring Recovery Summary.....	7
Table 4:	2015-2016 Mooring Deployment Summary.....	8
Table 5:	Magnetic declination values for 2014-2015 iBO Moorings	10
Table 6:	Angles chosen to describe the along-slope/shelf current component for each iBO mooring.....	15
Table 7:	Selected bin depths to characterize circulation patterns throughout the water column.	15
Table 8:	Summary of current profilers and current meters clock drift, first and last good record, and percentage of raw data return on iBO moorings from 2014 to 2015.	16
Table 9:	Annual statistics of current speed and direction at BR-1-14 from selected bin depths representative of water mass variability in the Beaufort Sea (see Table 7 for water mass description).....	22
Table 10:	Annual statistics of current speed and direction at BR-3-14 from selected bin depths representative of water mass variability in the Beaufort Sea (see Table 7 for water mass description).....	33
Table 11:	Annual statistics of current speed and direction at BR-G-14 from selected bin depths representative of water mass variability in the Beaufort Sea (see Table 7 for water mass description).....	45
Table 12:	Annual statistics of current speed and direction at BR-K-14 from selected bin depths representative of water mass variability in the Beaufort Sea (see Table 7 for water mass description).....	55
Table 13:	Annual statistics of current speed and direction at DFO-2-14 from selected bin depths representative of water mass variability in the Beaufort Sea (see Table 7 for water mass description).....	60
Table 14:	Annual statistics of current speed and direction at DFO-1-14 from a selected bin depth representative of the Polar-mixed layer (see Table 7 for water mass description).....	65
Table 15:	Annual statistics of current speed and direction at DFO-9-14 from a selected bin depth representative of the Polar-mixed layer (see Table 7 for water mass description).....	69
Table 16:	Summary of CT data logger clock drift and percentage of raw data return on iBO moorings from 2014 to 2015.....	76
Table 17:	Summary of valid and flagged data from CT loggers deployed on the BR slope moorings from 2014 to 2015. See Table 16 for the instrument model associated with each serial number.....	77
Table 18:	2016-2017 iBO Milestones	92
Table 19:	Summary statistics of current speed, vector-averaged direction and number of valid records by bin depth at BR-1-14 based on the data acquired with the QM ADCP #12699 from 2014 to 2015. Bin depths flagged manually as part of the QA/QC are highlighted in red.....	110
Table 20:	Summary statistics of current speed, vector-averaged direction and number of valid records by bin depth at BR-1-14 based on the data acquired with the LR ADCP #12943 from 2014 to 2015.	111
Table 21:	Summary statistics of current speed, vector-averaged direction and number of valid records at 591.1 and 733.1 m depth at BR-1-14 as based on the data acquired with the Aquadopp DW #6270 and #8414 from 2014 to 2015.	112
Table 22:	Summary statistics of current speed, vector-averaged direction and number of valid records by bin depth at BR-3-14 based on the data acquired with the LR ADCP #18785 from 2014 to 2015. Bin depths flagged manually as part of the QA/QC are highlighted in red.....	112

Table 23: Summary statistics of current speed, vector-averaged direction and number of valid records at 553.1 and 677.6 m depth at BR-3-14 as based on the data acquired with the Aquadopp DW #8418 and #2756 from 2014 to 2015. 113

Table 24: Summary statistics of current speed, vector-averaged direction and number of valid records by bin depth at BR-G-14 based on the data acquired with the QM ADCP #8784 from 2014 to 2015. Bin depths flagged manually as part of the QA/QC are highlighted in red. 113

Table 25: Summary statistics of current speed, vector-averaged direction and number of valid records by bin depth at BR-G-14 based on the data acquired with the LR ADCP #13079 from 2014 to 2015. 114

Table 26: Summary statistics of current speed, vector-averaged direction and number of valid records at 585.3 and 692.5 m depth at BR-G-14 as based on the data acquired with the Aquadopp DW #9473 and #9847 from 2014 to 2015. 115

Table 27: Summary statistics of current speed, vector-averaged direction and number of valid records by bin depth at BR-K-14 based on the data acquired with the WHS ADCP #2646 from 2014 to 2015. 115

Table 28: Summary statistics of current speed, vector-averaged direction and number of valid records by bin depth at BR-K-14 based on the data acquired with the Aquadopp Profiler #11147 from 2014 to 2015. Bin depths flagged manually as part of the QA/QC are highlighted in red. 116

Table 29: Summary statistics of current speed, vector-averaged direction and number of valid records by bin depth at DFO-2-14 based on the data acquired with the NB ADCP #586 from 2014 to 2015. 117

Table 30: Summary statistics of current speed, vector-averaged direction and number of valid records by bin depth at DFO-1-14 based on the data acquired with the NB ADCP #318 from 2014 to 2015. 118

Table 31: Summary statistics of current speed, vector-averaged direction and number of valid records by bin depth at DFO-9-14 based on the data acquired with the WHS ADCP #18318 from 2014 to 2015. 118

FIGURES

Figure 1: Bathymetric map of the Canadian Beaufort Sea showing the location of iBO moorings.2

Figure 2: Time-series of current speed, current direction and along-slope current component at mooring BR-1-14 as obtained with the QM ADCP #12699. The black line depicts the instrument depth. 18

Figure 3: Time-series of current speed, current direction and along-slope current component at mooring BR-1-14 as obtained with the LR ADCP #12943. The black line depicts the instrument depth. 19

Figure 4: Time-series of current speed, current direction and along-slope current component at 591 m at mooring BR-1-14 as obtained with the Aquadopp #6270.20

Figure 5: Time-series of current speed, current direction and along-slope current component at 733 m at mooring BR-1-14 as obtained with the Aquadopp #8414.21

Figure 6: Seasonal current roses at 28 m depth at BR-1-14 as based on low-pass filtered data from bin cell #21 acquired with the QM ADCP #12699. Roses point toward where the currents are going. Seasons are defined following the meteorological convention (Fall: October-December; Winter: January-March; Spring: April-June; Summer: July-September).23

Figure 7: Seasonal current roses at 132 m depth at BR-1-14 as based on low-pass filtered data from bin cell #8 acquired with the QM ADCP #12699. Roses point toward where the currents are going. Seasons are defined following the meteorological convention (Fall: October-December; Winter: January-March; Spring: April-June; Summer: July-September).24

Figure 8: Seasonal current roses at 223 m depth at BR-1-14 as based on low-pass filtered data from bin cell #14 acquired with the LR ADCP #12943. Roses point toward where the currents are going. Seasons are defined following the meteorological convention (Fall: October-December; Winter: January-March; Spring: April-June; Summer: July-September).25

Figure 9: Seasonal current roses at 351 m depth at BR-1-14 as based on low-pass filtered data from bin cell #6 acquired with the LR ADCP #12943. Roses point toward where the currents are going. Seasons are defined following the meteorological convention (Fall: October-December; Winter: January-March; Spring: April-June; Summer: July-September).26

Figure 10: Seasonal current roses at 591 m depth at BR-1-14 as based on data acquired with the Aquadopp #6270. Roses point toward where the currents are going. Seasons are defined following the meteorological convention (Fall: October-December; Winter: January-March; Spring: April-June; Summer: July-September).27

Figure 11: Seasonal current roses at 733 m depth at BR-1-14 as based on data acquired with the Aquadopp #8414. Roses point toward where the currents are going. Seasons are defined following the meteorological convention (Fall: October-December; Winter: January-March; Spring: April-June; Summer: July-September).28

Figure 12: Time-series of current speed, current direction and along-slope current component at mooring BR-3-14 as obtained with the LR ADCP #18785. The black line depicts the instrument depth.30

Figure 13: Time-series of current speed, current direction and along-slope current component at 553 m at mooring BR-3-14 as obtained with the Aquadopp #8418.31

Figure 14: Time-series of current speed, current direction and along-slope current component at 678 m at mooring BR-3-14 as obtained with the Aquadopp #2756.32

Figure 15: Seasonal current roses at 53 m depth at BR-3-14 as based on low-pass filtered data from bin cell #24 acquired with the LR ADCP #18785. Roses point toward where the currents are going. Seasons are defined following the meteorological convention (Fall: October-December; Winter: January-March; Spring: April-June; Summer: July-September).34

Figure 16: Seasonal current roses at 133 m depth at BR-3-14 as based on low-pass filtered data from bin cell #19 acquired with the LR ADCP #18785. Roses point toward where the currents are going. Seasons are defined following the meteorological convention (Fall: October-December; Winter: January-March; Spring: April-June; Summer: July-September).35

Figure 17: Seasonal current roses at 213 m depth at BR-3-14 as based on low-pass filtered data from bin cell #14 acquired with the LR ADCP #18785. Roses point toward where the currents are going. Seasons are defined following the meteorological convention (Fall: October-December; Winter: January-March; Spring: April-June; Summer: July-September).36

Figure 18: Seasonal current roses at 341 m depth at BR-3-14 as based on low-pass filtered data from bin cell #6 acquired with the LR ADCP #18785. Roses point toward where the currents are going. Seasons are defined following the meteorological convention (Fall: October-December; Winter: January-March; Spring: April-June; Summer: July-September).37

Figure 19: Seasonal current roses at 553 m depth at BR-3-14 as based on data acquired with the Aquadopp #8418. Roses point toward where the currents are going. Seasons are defined following the meteorological convention (Fall: October-December; Winter: January-March; Spring: April-June; Summer: July-September).38

Figure 20: Seasonal current roses at 678 m depth at BR-3-14 as based on data acquired with the Aquadopp #2756. Roses point toward where the currents are going. Seasons are defined following the meteorological convention (Fall: October-December; Winter: January-March; Spring: April-June; Summer: July-September).39

Figure 21: Time-series of current speed, current direction and along-slope current component at mooring BR-G-14 as obtained with the QM ADCP #8784. The black line depicts the instrument depth.41

Figure 22: Time-series of current speed, current direction and along-slope current component at mooring BR-G-14 as obtained with the LR ADCP #13079. The black line depicts the instrument depth.42

Figure 23: Time-series of current speed, current direction and along-slope current component at 585 m at mooring BR-G-14 as obtained with the Aquadopp #9473.43

Figure 24: Time-series of current speed, current direction and along-slope current component at 693 m at mooring BR-G-14 as obtained with the Aquadopp #9847.44

Figure 25: Seasonal current roses at 26 m depth at BR-G-14 as based on low-pass filtered data from bin cell #20 acquired with the QM ADCP #8784. Roses point toward where the currents are going. Seasons are defined following the meteorological convention (Fall: October-December; Winter: January-March; Spring: April-June; Summer: July-September).46

Figure 26: Seasonal current roses at 130 m depth at BR-G-14 as based on low-pass filtered data from bin cell #7 acquired with the QM ADCP #8784. Roses point toward where the currents are going. Seasons are defined following the meteorological convention (Fall: October-December; Winter: January-March; Spring: April-June; Summer: July-September).47

Figure 27: Seasonal current roses at 219 m depth at BR-G-14 as based on low-pass filtered data from bin cell #14 acquired with the LR ADCP #13079.48

Figure 28: Seasonal current roses at 347 m depth at BR-G-14 as based on low-pass filtered data from bin cell #6 acquired with the LR ADCP #13079. Roses point toward where the currents are going. Seasons are defined following the meteorological convention (Fall: October-December; Winter: January-March; Spring: April-June; Summer: July-September).49

Figure 29: Seasonal current roses at 585 m depth at BR-G-14 as based on data acquired with the Aquadopp #9473. Roses point toward where the currents are going. Seasons are defined following the meteorological convention (Fall: October-December; Winter: January-March; Spring: April-June; Summer: July-September).50

Figure 30: Seasonal current roses at 693 m depth at BR-G-14 as based on data acquired with the Aquadopp #9847. Roses point toward where the currents are going. Seasons are defined following the meteorological convention (Fall: October-December; Winter: January-March; Spring: April-June; Summer: July-September).51

Figure 31: Time-series of current speed, current direction and along-slope current component at mooring BR-K-14 as obtained with the WHS ADCP #2646. The black line depicts the instrument depth.53

Figure 32: Time-series of current speed, current direction and along-slope current component at 140 m at mooring BR-K-14 as obtained with the Aquadopp Profiler #11147.54

Figure 33: Seasonal current roses at 22 m depth at BR-K-14 as based on low-pass filtered data from bin cell #14 acquired with the WHS ADCP #2646. Roses point toward where the currents are going. Seasons are defined following the meteorological convention (Fall: October-December; Winter: January-March; Spring: April-June; Summer: July-September).56

Figure 34: Seasonal current roses at 126 m depth at BR-K-14 as based on low-pass filtered data from bin cell #1 acquired with the WHS ADCP #2646. Roses point toward where the currents are going. Seasons are defined following the meteorological convention (Fall: October-December; Winter: January-March; Spring: April-June; Summer: July-September).57

Figure 35: Time-series of current speed, current direction and along-slope current component at mooring DFO-2-14 as obtained with the NB ADCP #586. The black line depicts the instrument depth.59

Figure 36: Seasonal current roses at 20 m depth at DFO-2-14 as based on low-pass filtered data from bin cell #21 acquired with the SC-ADCP #586. Roses point toward where the currents are going. Seasons are defined following the meteorological convention (Fall: October-December; Winter: January-March; Spring: April-June; Summer: July-September).61

Figure 37: Seasonal current roses at 102 m depth at DFO-2-14 as based on low-pass filtered data from bin cell #1 acquired with the SC-ADCP #586. Roses point toward where the currents are going. Seasons are defined following the meteorological convention (Fall: October-December; Winter: January-March; Spring: April-June; Summer: July-September).62

Figure 38: Time-series of current speed, current direction and along-slope current component at mooring DFO-1-14 as obtained with the NB ADCP #318. The black line depicts the instrument depth.64

Figure 39: Seasonal current roses at 23 m depth at DFO-1-14 as based on low-pass filtered data from bin cell #7 acquired with the SC-ADCP #318. Roses point toward where the currents are going. Seasons are defined following the meteorological convention (Fall: October-December; Winter: January-March; Spring: April-June; Summer: July-September).66

Figure 40: Time-series of current speed, current direction and along-slope current component at mooring DFO-9-14 as obtained with the WHS ADCP #18318. The black line depicts the instrument depth.68

Figure 41: Seasonal current roses at 22 m depth at DFO-9-14 as based on low-pass filtered data from bin cell #7 acquired with the WHS ADCP #18318. Roses point toward where the currents are going. Seasons are defined following the meteorological convention (Fall: October-December; Winter: January-March; Spring: April-June; Summer: July-September).70

Figure 42: Near-surface currents for the open water season as based on low-pass filtered current velocity data from the nearest bin depth to 20 m. All data between June 15 and October 15 over 2014-2015 were used to construct the current roses. Please note that the rose of DFO-2 is slightly displaced to the east of the mooring location for visual purpose.72

Figure 43: Near-bottom currents for the open water season as based on low-pass filtered current velocity data from the bin depth nearest to bottom at each location. All data between June 15 and October 15 over 2014-2015 were used to construct the current roses. Roses indicate toward where the current is flowing.73

Figure 44: Temperature time-series recorded at BR-1-14 over 2014-2015. The legend shows the serial number and depth of each CT logger.78

Figure 45: Temperature time-series recorded at BR-3-14 over 2014-2015. The legend shows the serial number and depth of each CT logger.79

Figure 46: Temperature time-series recorded at BR-G-14 over 2014-2015. The legend shows the serial number and depth of each CT logger.....80

Figure 47: Temperature time-series recorded at BR-K-14 over 2014-2015. The legend shows the serial number and depth of each CT logger.....81

Figure 48: Salinity time-series recorded at BR-1-14 over 2014-2015. The legend shows the serial number and depth of each CT logger.82

Figure 49: Salinity time-series recorded at BR-3-14 over 2014-2015. The legend shows the serial number and depth of each CT logger.83

Figure 50: Salinity time-series recorded at BR-G-14 over 2014-2015. The legend shows the serial number and depth of each CT logger.84

Figure 51: Salinity time-series recorded at BR-K-14 over 2014-2015. The legend shows the serial number and depth of each CT logger.85

Figure 52: Temperature-salinity diagram constructed upon all data acquired with the CT loggers attached to the slope moorings BR-1, BR-3, BR-G and BR-K over 2014-2015. CTD profile data taken at mooring locations during the CCGS Amundsen cruise in 2014 are depicted by the 4 black lines.86

Figure 53: Zoom on the temperature-salinity diagram constructed upon data acquired with the deep CT loggers (>400 m) attached to the slope moorings BR-1, BR-3 and BR-G over 2014-2015. CTD profile data taken at mooring locations during the CCGS Amundsen cruise in 2014 are depicted by the 3 black lines.87

Figure 54: Phytoplankton cell fluxes collected by the upper sediment trap deployed at BR-G-14 along with satellite-derived ice concentrations in the area above the mooring during the 2014-2015 deployment period.88

Figure 55: Time-series of particle size distribution and particle volume concentration as recorded with the LISST 100X deployed near the bottom at BR-K-14.89

APPENDICES

Appendix A. 2014-2015 Final Mooring Diagrams

Appendix B. Technical Advisory Committee Meeting 2015

Appendix C. Beaufort Sea Collaborations 2015 Meeting Summary

Appendix D. Data deliverable

Appendix E. Summary Statistics of Ocean Currents

1.0 INTRODUCTION

The beginning of ice and ocean monitoring in the Canadian Beaufort Sea can be traced back to the 1980's when oceanographic moorings were deployed by Fisheries and Oceans Canada (DFO) in partnership with the oil and gas industry to understand ice, wave and surge hazards and ocean current variability. During the next two decades, programs that involved government, industry and indigenous peoples injected funding to maintain year-round observations through DFO moorings that focused primarily on the shallow shelf region. In the mid-2000's, ArcticNet Inc. established the Long-Term Oceanic Observatories (LTOO) project to maintain additional moorings in the southeastern Beaufort Sea that were initially deployed as part of the Canadian Arctic Shelf Exchange Study (CASES: 2002-2004) and targeting the offshore slope environment. The LTOO project has been sustained since then through collaborations with different programs, such as partnerships with the oil and gas industry (2009-2011) and through the Beaufort Regional Environmental Assessment (BREA: 2011-2015).

With the momentum reached after decades of observations, the need to foster synergy between the different mooring programs in the Beaufort Sea became urgent. Within this context, the integrated Beaufort Observatory (iBO) was developed to maintain key time-series and to integrate the datasets collected over the last 30 years. This technical report describes the activities undertaken as part of the first year of iBO from April 1, 2015 to March 31, 2016. iBO is a four-year program (2015-2018) managed by ArcticNet in partnership with DFO and Golder Associates Ltd. (Golder). The program is supported by the Environmental Study Research Funds (ESRF) and Imperial Oil Resources Ventures Limited (IORVL). iBO aims to contribute key oceanographic information required for decisions on development and regulations in the offshore Canadian Beaufort Sea by extending existing time-series measurements and integrating regional understanding of the shelf and slope environment through year-round measurements acquired by autonomous instruments on submerged moorings.

The iBO program will contribute to the development of regional syntheses of ocean circulation, sea ice observations and biogeochemical fluxes that will include:

- Information on the magnitude, duration and return period of extreme ice features;
- Ice and ocean datasets to document and interpret inter-annual variability of ice circulation, ocean circulation and particulate matter fluxes in relation to various environmental forcing factors;
- Data to support the development and evaluation of accurate numerical prediction models for operational ocean forecasting and the validation/verification of regional research models for simulating ice, seawater and oil spill trajectories.

The activities conducted under the umbrella of the iBO program during 2015-2016 include the turnaround of 4 slope moorings initially deployed in 2014 from the CCGS Amundsen as part of the Beaufort Marine Observatories project of BREA and 3 shelf moorings deployed in 2014 from the CCGS Sir Wilfrid Laurier (Laurier) as part of the DFO-PERD Beaufort Marine Hazards program. Together, these 7 moorings (Figure 1) constitute the backbone of the Integrated Beaufort Observatory (iBO), providing an ice and ocean dataset of regional scope. In a larger context, iBO activities in 2015-16 also included the organization of two side-meetings at the ArcticNet Annual Scientific Meeting: (1) an annual meeting of the Technical Advisory Committee (TAC) to review field operations and data recovery; and (2) a first Beaufort Sea Collaborations meeting to initiate bilateral exchange of data and joint studies that would feed into the iBO scientific framework.

The main goal of this technical report is to provide an initial review of the dataset acquired during the transition year of 2014-2015 as based on the 7 iBO installations that prolong key time-series initiated through ArcticNet/BREA and DFO over the last years. Only the datasets processed thus far are presented, which include all current meter, current profiler, and temperature-salinity data and part of the biogeochemical flux data. Data sets

from the Ice Profiling Sonars (IPS) currently being processed will be added to constitute the final 2014-2015 data record. Salient oceanographic features and events of interest during 2014-15 are discussed in relation to both long-term observations and recent process-oriented studies. In conclusion, we identify lessons learned stemming from the 2015 operations and define objectives and priorities for 2016-2017.

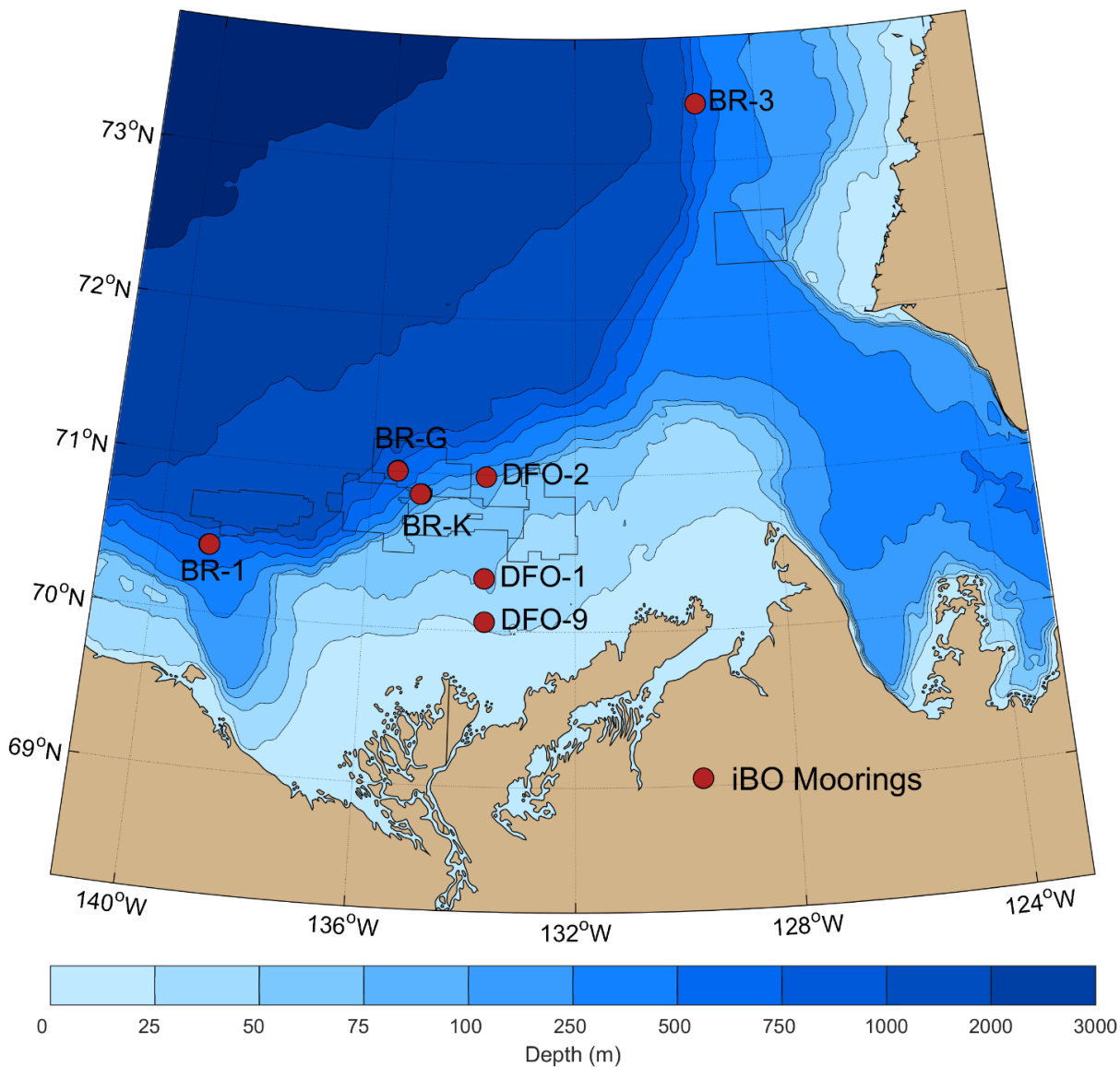


Figure 1: Bathymetric map of the Canadian Beaufort Sea showing the location of iBO moorings.

1.1 Report Organization

This report provides an overview of the physical setting of the study area in section 1.2. A summary of iBO mooring design, field calibration activities, and shipboard mooring operations conducted onboard the CCGS Amundsen and CCGS Laurier in 2015 are provided in sections 2.1 through 2.3. Description of the post-processing and QA/QC procedures applied to the recovered data and samples is presented in section 2.4. Section 3.0 provides a review of the processed datasets for the 7 moorings shown in Figure 1, with the exception of the data from the IPS for which the QA/QC is underway (target availability date is December 31, 2016; see section 4.3). Data are presented by parameters: section 3.1 provides a detailed overview of the ocean current speed and direction recorded throughout the water column at all 7 moorings; section 3.1.8 provides a review of water mass variability based on

temperature and salinity records; and section 3.3 presents preliminary data from sediment traps and from the particle-size analyzer deployed near the shelf edge. Section 4.0 summarizes initial observations on the 2014-2015 dataset, lessons learned from the fieldwork and objectives for 2016-2017. The appendices provide the final mooring diagrams for 2014-2015 (Appendix A) and summaries of the TAC and Beaufort Sea Collaboration meetings (Appendix B and Appendix C) hosted as part of the ArcticNet Annual Scientific Meeting, Vancouver, in December 2015. Appendix D lists the electronic files provided as a data deliverable in addition of this report. Appendix E provides a tabular summary of descriptive statistics pertaining to ocean currents measured at the 7 iBO moorings in 2014-2015.

1.2 Physical Setting of the Study Area

The Canadian Beaufort Shelf (Figure 1) is a narrow Arctic shelf (120 km width × 530 km length) comprised of a series of plateaus separated by shallow channels (Blasco et al., 2013). The shelf break is located at 80-100 m water depth where the slope angle increases to 2-6° toward the deep Canada Basin. The region is largely influenced by the Mackenzie River, which is the largest Arctic river in terms of sediment load (~127 × 10⁶ t per year) and the fourth largest for freshwater discharge (330 km³ yr⁻¹) (Macdonald et al. 1998).

Ice cover in the region exhibits a pronounced seasonal cycle with considerable inter-annual variability. Galley et al. (2013) recently documented that no significant trends in summer sea ice concentration on the mid-to upper slope of the central shelf has been measured from 1996 to 2010, although off the shelf to the northwest, a decrease in old sea ice concentration compensated by an increase in first-year sea ice was detected. Typically, seasonal sea ice over the Canadian Beaufort Shelf begins to form in October in the coastal sector and by December the ice cover is consolidated over the region (Carmack and Macdonald, 2002). In winter, landfast ice forms in the nearshore out to about the 20 m isobath and an ice rubble field (i.e. the *stamukhi*; Giovando and Herlinveaux 1981), which includes grounded ice, develops at the outer edge of the landfast ice. Beyond the *stamukhi*, an intermittently open flaw lead separates the landfast ice from the moving pack ice extending over the outer shelf that typically drifts westward with the Beaufort Gyre (Macdonald et al. 1995). The flaw lead is part of the Cape Bathurst Polynya system centered at the mouth of the Amundsen Gulf (Barber and Hanesiak 2004). The summer retreat of the ice usually begins with the widening of this polynya in June when easterly winds and/or the anticyclonic (clockwise) surface circulation in the Beaufort Sea moves sea ice away.

On the inner to mid-shelf, ice drift, ocean circulation, and the trajectory of the Mackenzie River plume, are highly variable and linked to wind dynamics (Melling, 1993; Melling and Riedel 1994; O'Brien et al. 2006). Over the outer shelf and on the slope, large-scale surface circulation (upper 50 m) is dominated by westward-flowing currents from the Beaufort Gyre (Ingram et al. 2008). The water mass that occupies the upper 50 m is the Polar mixed-layer with salinity of ~30-31 on average (practical scale), which is largely influenced by seasonality, river inputs and ice growth/melt cycles. From 50 to 200 m depth near the shelfbreak, the mean currents reflect the propagation of an eastward shelfbreak jet in the Canadian Beaufort Sea (Forest et al. 2015; Dmitrenko et al. 2016) as observed in the Alaskan Beaufort Sea (Pickart 2004; von Appen and Pickart 2012). This current can be defined as a narrow flow (10-15 km width) trapped to the shelf break and carrying Pacific Water (salinity ~33). This current is subject to frequent reversals to the west which are normally associated with upwelling (Aagaard, 1984; Pickart et al. 2013). At 20-30 km from the shelf edge, the eastward shelfbreak jet is no longer present and the mean current vectors in the upper 200 m are progressively directed to the west in the opposite direction than near the shelf edge, following again the anti-cyclonic motion of the Beaufort Gyre (Forest et al. 2015). Below 200 m depth on the mid- to lower slope, currents are bathymetrically steered and flow along the slope to the northeast (Aagaard 1984). Atlantic Water (salinity 34.8) occupies the 200-800 m water interval. Mesoscale eddies are known to populate the region especially near the shelf edge, where currents are expected to be the strongest and where shelf-slope exchanges take place (e.g. Kulikov et al. 1998; Williams et al. 2008).

2.0 MATERIAL AND METHODS

This section of the report provides detailed information on the tautline mooring design and instrumentation of iBO moorings (section 2.1), on calibration activities related to current meters and current profiler compasses (section 2.2), as well as on mooring recovery and deployment operations aboard the CCGS Amundsen and CCGS Laurier (section 2.3). A description of the QA/QC processing chains for each moored instrument is provided in section 2.4.

2.1 Taut-line Mooring Design

2.1.1 Slope Moorings

The slope moorings array consists of 3 similarly designed long moorings (BR-1, BR-G and BR-3) located on the middle continental slope (~700-750 m depth) and one short mooring (BR-K) located on the upper slope near the shelf edge (~150 m water depth in 2014-2015, ~170 m in 2015-2016; Figure 1). Final mooring diagrams for 2014-2015 can be found in Appendix A.

The longer moorings on the lower slope consist of the following key components:

- ASL Ice Profiling Sonar (IPS) was used at approximately 60 m depth to measure ice draft and non-directional waves during intervals of open water. IPS were mounted in 30-inch spherical syntactic foam floats (Mooring Systems Inc. - MSI).
- 150 kHz Teledyne RD Instruments (TRDI) Quarter Master Acoustic Doppler Current Profiler (QM ADCP) were used at approximately 200 m (2014-2015) or 180 m (2015-2016) water depth to profile upper water column currents at 8 m (2014-2015) or 4 m (2015-2016) vertical resolution and measure ice velocity using a Bottom-Track feature. The QM ADCPs were mounted up-looking in 40-inch syntactic foam floats (Flotation Technologies - DeepWater Buoyancy).
- 75 kHz TRDI Long Ranger ADCP (LR ADCP) were used at approximately 450 m water depth to measure water velocity profiles at a coarser 16 m resolution. The LR ADCPs were mounted up-looking in 40-inch syntactic foam floats (Flotation Technologies).
- Two high frequency short-range (<1 m) Nortek Aquadopp DW (AQD) single point current meters were used to measure water velocity at approximately 600 m and 10 m above the bottom. Each Nortek AQD was equipped with a vane to hold the heading nearly constant for the duration of each ensemble interval.
- Two Technicap PPS 3/3-24S 24 cup sequential sediment traps were deployed between the IPS, QM ADCP and LR ADCP to record the annual cycle in vertical particle flux.
- RBR Conductivity and Temperature (CT) loggers were installed at approximately 60 m, 130 m (2015-2016 only), 180 m, and 450 m water depth, as well as 10 m above the bottom. These instruments measure water temperature and salinity and are used to compute sound speed to improve IPS and ADCP processing.
- Various smaller syntactic foam floats were distributed along the mooring as required.
- Tandem ORE Edgetech acoustic releases were used as the primary locating and recovery devices.

The shallow (upper slope) mooring consisted of the following key components:

- A 300 kHz TRDI Workhorse Sentinel ADCP (WHS ADCP) was used at approximately 140 m water depth to profile currents with a vertical resolution of 8 m, as well as to measure ice velocity using the Bottom-Track feature. The WHS ADCPs were mounted upward looking in 33-inch syntactic foam ellipsoid floats manufactured by MSI.

- A RBR CT logger with auxiliary sensors to measure turbidity, dissolved oxygen, and chlorophyll fluorescence was installed at approximately 18 m above the bed.
- A Sequoia LISST 100X laser diffraction systems was located 18 m above the seafloor to provide measurements of particle size distributions and associated volume concentrations in the lower water column. The LISST measurements help to better quantify the seasonal and annual variability of vertical and horizontal fluxes of inorganic solids.
- A 1 MHz Nortek Aquadopp profiling current meter (AQP) was mounted down-looking below the LISST instrument to provide details of the flow and acoustic backscatter structure near the seafloor on the upper slope. The AQP's measure three-dimensional current velocities and provide a measure of acoustic backscatter intensity in 2 m range bins from the bottom to about 16 m above seabed. Combined with the velocity profile information from upward looking ADCP's the profilers provide a detailed and near complete view of the water column vertical structure.
- An additional syntactic foam ellipsoid float was located above the LISST cage to provide floatation for the lower portion of the mooring.
- Tandem ORE Edgetech (Model CART) acoustic releases were used as the primary recovery device.

As described above, a number of improvements were made in 2015 to the iBO moorings with respect to the previous BREA 2014 mooring designs. This included a fifth CT logger added at approximately 130 m to monitor variability in the core of the Pacific Halocline water mass. The QM ADCP was raised from 200 m to approximately 180 m to allow a better resolution of currents in the upper water column. Bin size of this instrument was also reduced from 8 to 4 m. TRDI ADCP settings were also adjusted to improve the overall data quality and quantity. Finally, the polypropylene drop line at the three offshore moorings was reduced from 10 m to 5 m to allow a better resolution of the near-bottom flow and water properties.

2.1.2 Shelf Moorings

The moorings at all three shelf locations (DFO-9, DFO-1, and DFO-2; Figure 1) have similar design (Appendix A). They are located in this sequence at approximately the 30 m, 55 m and 110 m isobaths; the last location is actually just off the shelf at the top of the continental slope. Recording instruments at the two shallower sites (DFO-9 and DFO-1) are actually placed on two separate nearby (50-150 m separation) moorings so as to keep the equipment close to the seabed safe from drifting ice and to avoid interference between the two sonar used for observations. The depth at the third site is sufficient that the recording instruments, one above the other, on a single mooring.

The installations at all three sites support the following instrument:

- ASL IPS was used at 30-50 m depth to measure ice draft and non-directional waves during intervals of open water. IPS of three types are in use: original IPS4 units operating at 200-kHz acoustic frequency; updated W-IPS4 units operating at 420 kHz and measuring wave height as well as ice draft; IPS5 units operating at 420 kHz with increased data storage capacity. IPS were mounted in light-weight stainless steel frames each supported by a collar of four 14-inch spherical plastic floats (Viny Inc. Model 12B3).
- 300-kHz TRDI ADCP was operated from about 4 m above the seabed to measure ocean current velocity at depths incrementing by 4 m between about 8-m elevation to about 15-m depth, plus ice velocity. ADCP of two types are in use: old model narrow-band ADCP (NB ADCP) and new model broad-band WHS ADCP. The former NB ADCPs operating with higher signal-noise ratio and better magnetic compasses are favoured for Arctic use. ADCPs were mounted in light-weight stainless steel frames each supported by a collar of four 14-inch spherical plastic floats (Viny Inc. Model 12B3).The frames were coupled into the mooring above a

swivel and equipped with vanes so that the ADCP was not prone to rapid spinning and remained aligned with local current.

- CT recorders (Seacat SBE37: Sea Bird Electronics Inc.) were installed on the frame of each ADCP, about 3 m above the seabed. They record the temperature and salinity of water within the bottom boundary layer as an indicator of cross-shelf up-welling and down-welling.
- Acoustic transponder releases (Model CART: ORE Edgetech) were mounted in tandem 1 m above the mooring's deadweight anchor. The CART is the device used to locate each mooring and to enable its recovery by unhooking the buoyant part of the mooring from its heavy anchor. Two transponding releases are used in parallel for redundancy in this essential function.

2.2 Compass Calibration and Verification

Compass calibration is an important consideration for current meters deployed in the Canadian Beaufort Sea due to the reduced magnitude of the horizontal component of the Earth's magnetic field in the Canadian Arctic, about one third of its value in southern Canada. Calibration and verification of the current meter compasses near the approximate geomagnetic latitude where they will be deployed is advisable prior to deployment. Moreover care must be taken to eliminate all sources of magnetic interference from the instrument-supporting cages on the mooring and similarly also in the immediate vicinity of the calibration activities. For this reason, calibration activities cannot take place onboard the Amundsen or Laurier.

Compasses in the instruments recording data during 2014-15 were (in most cases) calibrated before deployment in 2014. In 2015, three compass calibration/verification activities took place as part of iBO. The first activity was conducted from June 8 to 10 by Golder personnel at the BBE Expediting compound next to the airport at Inuvik and consisted of the compass calibration of 8 TRDI ADCPs for BR moorings. The second activity took place from September 5 to 7 following the ArcticNet 2015 Leg 3a expedition aboard the Amundsen and was conducted by Golder and ArcticNet personnel. This task consisted in the compass verification of Nortek current meters as a follow-up activity to the factory calibration conducted by Nortek in 2014. Unfortunately in 2015, three Nortek instruments recovered by the Laurier could not be verified due to logistical constraints.

The third activity on Herschel Island on September 29 was supported from the Laurier. DFO would normally have two such shore visits during its Arctic annual campaign so that recovered instruments requiring re-calibration could be evaluated. Compass calibration only before deployment has been the customary DFO practice for the ADCPs used at the shelf sites. Moreover because the batteries within the NB ADCPs used at DFO-1 and DFO-2 are widely separated from the compass, these instruments are not calibrated annually. The residual root-mean-square departure from linearity in the Beaufort area is 0.7° for NB ADCP #318 used at DFO-1 and 0.5° for NB ADCP #0586 used at DFO-2. That for WHS ADCP #18318 used at DFO-9, and measured in September 2014, was 0.8° . In all cases a polynomial approximation to the small residual non-linearity has been applied to the indicated magnetic headings during data processing (see section 2.4.1).

The TRDI ADCP compasses for BR moorings were successfully calibrated to within the acceptable Arctic limits suggested by the manufacturer (± 5 degrees). Table 1 provides a summary of the post-calibration compass errors reported by the manufacturer's software for each TRDI ADCP. The compass readings in increments of 10 degrees were verified against True North after correction for magnetic declination. The TRDI ADCP compasses provided consistent results with a constant declination accurate to ± 4 degrees in all directions. No polynomial correction was applied to the indicated headings of TRDI ADCPs from BR moorings during post-processing. This is because the polynomial fit calculated at Inuvik might not be directly applicable to offshore locations over the slope. The compass reading verification at Inuvik from June 8 to 10, 2015 represented a control test of the compass accuracy rather than an additional calibration to be applied over the one recommended by the manufacturer (Table 1). Also,

ADCP WHS ADCP #3778 that does not have the Bottom-Track feature was kept as a spare instrument during field operations and was not deployed.

Table 1: Summary of Post-calibration Compass Errors of TRDI ADCPs for BR Moorings

Instrument	Serial Number	Mooring	Error from TRDI Software (degrees)
WHS 300 kHz	102	BR-K-15	1.4
WHS 300 kHz	3778	Not deployed	0.8
QM 150 kHz	12698	BR-1-15	1.7
QM 150 kHz	12824	BR-3-15	1.8
QM 150 kHz	12841	BR-G-15	0.3
LR 75 kHz	12942	BR-3-15	1.3
LR 75 kHz	12884	BR-1-15	1.5
LR 75 kHz	12892	BR-G-15	1.7

The Nortek instrument compasses were successfully verified to within acceptable Arctic limits recommended by RDI (± 5 degrees). Table 2 provides a summary of the post-verification compass errors calculated from readings in 10 degree increments over 360 degrees. It is recommended that the two Nortek instruments recovered from the Laurier (#6270 and #8414) should be further verified before redeployment as an effort to complete the summary provided in Table 2.

Table 2: Mean Error of Recovered Nortek Compasses (10 Degree Increment) of BR moorings.

Instrument	Serial Number	Mooring	Mean Calculated Error \pm Standard Deviation around the Compass (degrees)
Aquadopp Profiler	11147	BR-K-14	0.9 \pm 0.7
Aquadopp DeepWater	2756	BR-3-14	0.9 \pm 0.5
Aquadopp DeepWater	8418	BR-3-14	3.7 \pm 1.8
Aquadopp DeepWater	9743	BR-G-14	2.0 \pm 1.0
Aquadopp DeepWater	9847	BR-G-14	1.6 \pm 1.1

2.3 Mooring Recovery and Deployment

This section of the report provides details on iBO mooring recovery and deployment operations conducted aboard the CCGS Amundsen and CCGS Sir Wilfrid-Laurier (section 2.3.1) during the 2015 field campaigns. Coordinates and depths of the mooring at their recovery and re-deployment are provided in Table 3 and Table 4.

Table 3: 2014-2015 Mooring Recovery Summary

Mooring	Latitude (WGS84)	Longitude (WGS84)	Water Depth (m)	2014 Deployment Date and Time (UTC)	2015 Recovery Date and Time (UTC)
BR-K-14	70° 51.747'N	135° 01.198'W	156	Aug-22-2014 16:05	Aug-26-2015 14:10
BR-G-14	71° 00.128'N	135° 30.565'W	701	Aug-23-2014 23:30	Aug-26-2015 21:00
BR-1-14	70° 25.909'N	139° 01.370'W	757	Sep-01-2014 21:25	Sep-29-2015 19:40
BR-3-14	73° 24.516'N	129° 21.390'W	700	Aug-27-2014 13:35	Aug-31-2015 17:11
DFO-2-14	70° 59.357'N	133° 44.636'W	111	Sep-30-2014 16:23	Sep-26-2015 15:07
DFO-1-14 (IPS)	70° 20.030'N	133° 44.371'W	55	Sep-30-2014 22:17	Sep-27-2015 14:44
DFO-1-14 (ADCP)	70° 20.035'N	133° 44.459'W	55	Sep-30-2014 22:14	Sep-27-2015 15:03

DFO-9-14 (IPS)	70° 03.537'N	133° 42.922'W	35	Oct-01-2014 02:04	Sep-27-2015 17:44
DFO-9-14 (ADCP)	70° 03.501'N	133° 42.942'W	35	Oct-01-2014 01:53	Sep-27-2015 18:02

Notes: BR-1-14 and DFO moorings were recovered from the Laurier, while other moorings were recovered from the Amundsen.

Table 4: 2015-2016 Mooring Deployment Summary

Mooring	Latitude (WGS84)	Longitude (WGS84)	Water Depth (m)	2015 Deployment Date and Time (UTC)
BR-K-15	70° 51.763'N	135° 1.706'W	170	Aug-27-2015 14:29
BR-G-15	71° 00.122'N	135° 29.612'W	700	Aug-28-2015 18:53
BR-1-15	70° 25.9435'N	139° 01.2347'W	753	Sep-30-2015 22:33
BR-3-15	73° 24.566'N	129° 21.224'W	690	Aug-31-2015 21:15
DFO-2-15	70° 59.361'N	133° 44.627'W	110	Sep-26-2015 23:30
DFO-9-15 (IPS)	70° 20.029'N	133° 44.371'W	55	Sep-27-2015 15:41
DFO-9-15 (ADCP)	70° 20.035'N	133° 44.459'W	55	Sep-27-2015 15:34
DFO-1-15 (IPS)	70° 03.501'N	133° 42.941'W	35	Sep-27-2015 21:46
DFO-1-15 (ADCP)	70° 03.537'N	133° 42.922'W	35	Sep-27-2015 21:40

Notes: BR-1-15 and DFO moorings were deployed from the Laurier, while other moorings were deployed from the Amundsen.

2.3.1 Shipboard Operations

Steps for mooring recovery aboard the CCGS Amundsen and CCGS Laurier generally included:

- pre-operations Job Safety Assessment (JSA) meeting, an operational planning meeting, and a toolbox meeting (on deck);
- confirm mooring presence and orientation with the multibeam sonar and interrogate the mooring to determine range; multi-beam sonar not used on the Laurier;
- maneuver ship into position depending on prevailing drift, wind and sea state;
- conduct a conductivity, temperature and depth (CTD) cast to provide overlapping water column data for data processing; relative timing of CTD cast varies with logistic constraints on Sir Wilfrid Laurier
- enable the acoustic release and send a command to release the mooring;
- launch the fast rescue craft (FRC, or zodiac) and recover the mooring using the FRC and tow alongside the port bow;
- lift mooring elements onto the foredeck and take instruments off the mooring as they are brought on deck, then take the mooring apart (i.e., a complete disassembly of the mooring);
- inspect and rinse instruments with freshwater and stow in plastic bins;
- transfer of equipment onto the 600 level (moonpool area and mooring lab 610) on the Amundsen; equipment transferred to seacon lab spaces on the Laurier – fore deck and boat deck
- download data from the instruments, as schedule permits unless re-using an instrument;
- perform preliminary review and visual inspection of the data, as schedule permits unless re-using an instrument;
- store and secure the instruments on board the ship, and

- service and maintain the instruments, including any required trouble-shooting or field repair.

A safety incident related to a Benthos Locator Model ALP-364/EL (serial #4774) that was recovered from BR-3 occurred during Leg 3a aboard the Amundsen. The incident involved the over-pressurization of the instrument through the exposure of the internal lithium batteries to seawater and the subsequent blowout of the pinger's end cap following hydrogen gas formation. This blowout resulted in the spillage of seawater and lithium hydroxide into mooring laboratory 610. It also injured the left hand of one of the science personnel that was standing in the laboratory next to the pinger at the time of the blowout. Details on the incident can be found in the memorandum prepared by Golder on September 2, 2015 (Golder, 2015).

Servicing of the mooring instruments involved the following steps:

- opening the housing (if required) and inspecting interior for corrosion, and other damage;
- changing the batteries (if required), and replacing desiccant (if applicable);
- cleaning the o-ring surfaces and re-greasing and replacing or cleaning all o-rings;
- running a trial delayed-start deployment using instrument's internal power with computer disconnected, followed by upload and inspection of data record;
- programming the instrument for deployment;
- completing a record of programming (screenshots and paper record sheets).

Before programming and deployment of instruments on the moorings, standard manufacturer procedures and pre-deployment tests were followed to provide verification of instrument operation. Instruments were generally programmed for a 1-year deployment, except for instruments at BR-3 for which a 2-year programming was used given its remote location north of Banks Island, which might pose challenges for future recovery operations. This mooring was also equipped with the more robust 8242XS Edgetech acoustic releases that have an extended battery life of at least 2 years. A contingency phase was implemented for all Ice Profilers in order to continue measurements in the case that the mooring is not recovered in the fall of 2016.

Steps in the mooring deployment were as follows:

- confirm the design of the mooring particulars to meet the site constraints;
- review lifting plan and JSA;
- assemble the mooring on deck (using the original configuration or a modified configuration, as appropriate);
- toolbox meeting on-deck;
- deploy the mooring;
- enable and interrogate the acoustic release;
- perform triangulation to determine the location of the mooring on the bottom;
- disable the acoustic release;
- perform multibeam survey of the mooring to confirm position in water column (Amundsen only); and
- perform CTD cast.

Multibeam data collected after deployment confirmed that all moorings deployed from the Amundsen were oriented vertically in a proper position. Multibeam interpretation concerning moored instrument depth was done by experienced multibeam professionals whom helped locate approximate instrument depths. The interpretation of the acoustic data identified the majority of the large instruments except for instruments from the longer mooring BR-G-15, where some uncertainty concerning some instruments' depths was noticed. The signal provided by the M40 floats of the TRDI ADCPs from this mooring was apparently at least 10 m shallower than expected. Although this should not have any impact on mooring reliability, inspection of existing ropes to confirm their actual length (and their potential replacement) is warranted. It is also possible that this apparent discrepancy might be due to the precision\ interpretation of the water column software of the multibeam sonar.

2.4 Data Processing and QA/QC

2.4.1 Current Meters and Current Profilers

This section of the report provides a summary of QA/QC procedure applied to current meters and current profilers deployed on both BR and DFO moorings. The QA/QC procedure of current profilers on BR mooring differs slightly from that applied to DFO instruments (see details below). Further harmonization of both processing chains is planned for 2016-2017. For all moorings, pressure sensors on the TRDI ADCPs were zeroed at the time of setup in order to account for atmospheric pressure in the depth calculation performed by the instrument. Processing routines were used to convert pressure measured by the Nortek AQDs, to water depth; pressure measurements in air before and after the instrument deployment were averaged to account for atmospheric pressure. For BR moorings, processing of the ASCII files from Nortek AQDs or MATLAB® binary files TRDI ADCPs was completed using MATLAB® software. For DFO moorings, data was processed using the in-house software and routines (the IOS SHELL suite) from DFO, which produce ASCII multi-line header files and multiple ASCII data files. These DFO ASCII files were converted into the BR mooring file format (MATLAB® binary and Text files) for plotting, analyses and to be provided as a data deliverable.

Processing and quality-checking of the current time-series data consisted of the following steps:

- 1) Measurements made by the instrument while it was out of the water, as determined from pressure readings, were removed.
- 2) East and North horizontal components of velocities were corrected to true north based on local magnetic declination. An annual average magnetic declination was used for the deployment period based on the Natural Resources Canada numerical model for the International Geomagnetic Reference Field 2012 (IGRF-12; <http://www.geomag.nrcan.gc.ca/calc/mdcal-eng.php>). The summary of magnetic declination values each for each mooring is listed in Table 5.

Table 5: Magnetic declination values for 2014-2015 iBO Moorings

Mooring	Magnetic Declination [degrees East]
BR-G-14	23.6
BR-K-14	23.7
BR-3-14	24.4
BR-1-14	22.8
DFO-2-14	24.4
DFO-1-14	24.2
DFO-9-14	24.2

- 3) Compass readings from the ADCPs at the DFO moorings were further corrected using a polynomial fit calculated from the output of the compass at precise increments of the geomagnetic heading as measured at Hershel Island during the DFO calibration activity (section 2.2). This additional correction compensates for the small residual non-linearity (0.5-0.7°) that remains in the ADCP compass' response to heading. The Hershel Island calibration site is considered close enough to the deployment locations of the shelf moorings so that a polynomial correction can be applied. No polynomial correction was applied to the indicated directions of TRDI ADCPs from BR moorings during post-processing. This is because the polynomial fit calculated at Inuvik (section 2.2) might not be directly applicable to offshore locations over the slope. The compass reading verification at Inuvik however showed a constant declination accurate to ± 4 degrees in all directions, which is considered as an acceptable error for TRDI instruments (TRDI 2014).
 - 4) Acoustic amplitude was plotted for each beam to check the quality of the instrument signal return and filtered for amplitudes below the noise floor for the respective instrument (Nortek 2013; TRDI 2014).
 - 5) Nominal depths of echo intensity and velocity data from TRDI ADCPs deployed at the DFO sites were calculated using a spline interpolation along each beam that corrects for the effects of changing pitch and roll. Nominal depths from the TRDI ADCPs deployed at the BR moorings were calculated using the default bin mapping method (nearest vertical bin) for TRDI ADCPs (TRDI 2014) that uses the 20° beam slant angle. The latter approach provides similar results to the spline interpolation method in the cases that the tilt is lower than 10° (>99.5% of time for each time series).
 - 6) For ADCPs deployed at the BR moorings, the following steps were applied to filter data and to identify and flag data that were considered as suspicious:
 - a) Data were filtered for sidelobe interference using the beam slant angle of the instrument. For the Nortek Aquadopp profiler at BR-K, this value was 25° (Nortek 2013) and for the TRDI ADCPs this value was 20° (for all LR, QM and WHS ADCPs) or 30° (for NB ADCPs on DFO-2 and DFO-1). The filter correction was calculated as the product of the instrument depth and the cosine of the slant angle plus one range bin. The filtered range approximately corresponds to the top 10% of the range to surface or bottom depending on whether the instrument was up-looking or down-looking, respectively. Within iBO, only the Nortek Aquadopp profiler at BR-K is down-looking.
 - b) For TRDI instruments, data with corresponding Percent Good (PG) 4 plus PG1 values less than 25% (TRDI 2014; IOOS 2015) were removed. The PG value is a data-quality indicator that reports the percentage (0 to 100) of valid data collected for each depth cell of the velocity profile using the four beams (PG4) and three beams (PG3). It is an indicator of the following criteria: low correlation, large error velocity and fish detection (false target threshold) (TRDI 2006).
 - c) Time series data from ancillary sensors on the current profilers were inspected for QA/QC purposes. Nortek recommends that the instrument tilt not exceed a maximum of 10° for measurement of currents (Nortek 2013) and TRDI recommends a maximum tilt limit of 15° (TRDI 2014). Data when tilt was exceeding the respective thresholds were flagged as part of the QA/QC.
 - d) Data were further filtered using the error velocity (TRDI instruments only) and maximum vertical velocity thresholds. The error velocity is a measure of the homogeneity of the water mass that is measured. The data from TRDI ADCPs on BR slope moorings were filtered for vertical velocities greater than 0.1 m/s and error velocities greater than 0.15 m/s (i.e. arbitrary values based on error velocity thresholds developed as part of the BREA program).
 - e) Additional visual inspection guided the flagging of (subjectively) suspicious bin values.
 - 7) For ADCPs deployed at the DFO sites, a multi-stage decision tree was applied to identify and flag data judged to be of little value by a variety of criteria. These criteria include:
-

- a) Surface interference: Ensemble values masked because they lie in the side-lobe shadow of the least zenith-pointing beam.
- b) Beam-to-beam differences: Ensemble values masked if more than three differences between beams exceed 8 counts.
- c) Extreme strong echo: Ensemble values masked because at least one beam differs from the others by more than 25 counts.
- d) Extr+Diffs: ensemble values masked due to combined conditions of 2 & 3.
- e) PercentGood < 25: Ensemble values masked because fewer than 25% of the ping data yielded 3 or 4 beam solutions.
- f) Low Amplitude: Ensemble values masked because 1 or more beams have amplitude of less than 1 counts.
- g) Error Velocity: Ensemble values masked because the so-called error velocity (actually the difference between independent values of vertical velocity) exceeded 2.8 times the standard deviation of the time series (approximately the 99th percentile).
- h) VertVel: Ensemble values masked because the vertical velocity exceeded 2.8 times the standard deviations of the time series (approximately the 99th percentile).

Final QA/QC time-series data from ADCPs are usually gappy and can be difficult to use in some applications. To generate continuous time series of data at sub-tidal frequencies, the final processing step processing might include the complex demodulation of the time-series within over-lapping 12-hour windows (e.g. Melling et al. 2001). This additional step was not applied to the current data delivered as part of Appendix D. However, a low-pass filter (PL66TN, Beardsley and Rosenfeld 1983) was applied to selected bin depth time-series for each instrument data (interpolated linearly to 1-hour intervals for consistency) in order to construct seasonal current roses (16 directions, 22.5° bins) of the sub-tidal current component as presented in section 3.1.

2.4.2 Temperature-Salinity Loggers

Data were extracted from the RBR sensors using Ruskin® software (RBR, 2016) and from Sea Bird sensors using Sea Bird Electronics software. Time-series from BR moorings were processed and plotted using MATLAB® scripts, whereas the same task was accomplished by DFO using in-house IOS SHELL routines. QA/QC data of DFO CT sensors is still underway and is not presented as part of this report.

Time series were clipped for out-of-water values and evaluated visually for data quality. In addition, an automated filter is applied to the conductivity and temperature data to flag potential spikes from the data time-series using a seven-sample moving window. All values outside of ± 1.5 standard deviations about the moving window mean that could be considered spikes are flagged; spikes in conductivity are far more common than spikes in temperature. Any spikes identified in the temperature or conductivity time-series cause the corresponding salinity values also to be flagged because salinity is temperature and conductivity dependent.

In addition, the temperature and salinity data from all moorings were verified for accuracy against nearby CTD casts acquired at the times of deployment and recovery of the associated moorings. Since appreciable drift in sensor calibration rarely occurs for temperature, the assessment of calibration drift is normally carried out for conductivity; it is done on the basis of potential temperature versus salinity plots. Data from the reference CTD and from the in situ sensor within one week of the CTD cast. For Sea Bird sensors, drift in conductivity calibration is usually associated with silting or bio-fouling, For the RBR sensors it is most likely associated with interference from local support structures, electrically conductive or otherwise. .

At the time of writing, data from the moored CT loggers have yet to be corrected for any offset or drift in the sensor data. Such correction will be implemented when both conductivity data from the 2014 mission will be available in a processed format (only temperature and salinity were available thus far) as well as when the site-specific CTD casts from the 2015 mission will be available in order to assess the drift.

2.4.3 Ice Profiling Sonars and Ice velocity

The time-consuming QA/QC process for IPS data is currently underway. The derivation of ice draft from IPS signal data employs well-established methods that have been developed during the processing many dozens of IPS datasets over the past three decades (Melling et al. 1995; Melling and Riedel, 2004; Fissel et al. 2008).

There are many steps in the processing of IPS signal data to ice draft. The procedures for detection of erroneous target data and for calibration of zero ice draft in particular are meticulous and require considerable experience. It is not useful to document the process here in detail. The interested reader is referred to Melling et al. (1995) and Melling and Riedel (2004).

Ice velocity is derived from data provided by TRDI's patented bottom-track firmware in the WHS and QM ADCPs (see section 2.1). It can also be derived from binned water-column data recorded by LR ADCPs if certain conditions are met. The procedures for deriving reliable estimates of ice velocity from ADCP data are quite involved. Moreover a certain level of subjectivity must be tolerated in the analysis because greatly varying conditions at the target (rough or smooth ice; continuous or broken ice cover; rough seas or calm seas; other targets yielding plausible echoes; etc.) generate ambiguity. The interested reader is referred to more thorough discussions provided by Melling and Riedel (2004) and ASL (2015).

2.4.4 Sediment Traps

Each longer slope mooring is equipped with two automated sediment traps (at approximately 125 and 310 m depth) to record the annual cycle in vertical particle flux (inorganic sediments, organic carbon and particulate nitrogen) and plankton community composition in the upper water column. Sediment trap samples from BR-G-14 and BR-3-14 moorings were recovered aboard Amundsen and were retrieved at the ship demobilization in Québec City in November. Sediment trap samples from BR-1-14 were recovered aboard the Laurier and were shipped to Québec City from in January 2016. All traps functioned properly and provided a complete time-series, except for the upper trap at BR-1-14 (~120 m) that was affected by a failure in the rotating mechanisms of the motor. No samples were recovered from this trap.

Analyses on the sediment trap samples are underway at Université Laval. As a first step, sediment trap samples were splitted to prepare a subsample for the measurements of total particulate matter (TPM), particulate organic carbon (POC), and particulate nitrogen (PN). In the coming weeks, subsamples will be filtered, weighed and processed on the CHN elemental analyzer for TPM, POC and PN values. In addition, zooplankton actively entering the sediment traps (named "swimmers") and that are present in the subsample were removed. Zooplankton organisms collected at the upper trap at mooring BR-G-14 trap were identified to the lowest species possible to monitor the seasonal and inter-annual fluctuation in the zooplankton community structure. Aliquots of the upper trap at BR-G-14 were also used for the enumeration and identification of phytoplankton cells to indirectly assess the magnitude, timing, and composition of the phytoplankton spring bloom.

2.4.5 Particle Size Analyzer

Post-processing of the LISST 100X data from BR-K-14 was done using MATLAB® following Sequoia (2008). The raw data (binaries) were first read and extracted. Scattering inversion and volume concentration calculations were performed using both the spherical and random mathematical models. The spherical model assumes that particles that scattered light are all spheres (Mie solution); while the random model assumes that particles are randomly (or

irregularly) shaped. These steps were performed following Sequoia (2008) processing routines and guidelines. In situ background scattering measurements that correspond to periods of very low particle volume concentration were used instead of the background scattering obtained when the instrument was out of the water. This approach compensates for biases introduced within the background scattering measurements over a long term-period (~1 year) due to dirt or biofilms that can accumulate on the sensor despite the use of a BioBlock (Sequoia, pers. comm. 2016). The following QA/QC filtering was also performed on the corrected data:

- Data with laser reference equal to 0 were removed;
- Data with associated laser transmission less than 0.1 (10%) or superior to 0.995 (99.5%) were removed; and
- Additional manual filtering was done to remove erroneous data (spikes).

Statistics and characteristic parameters for each model (including total volume concentration, mean particle size, standard deviation and silt density) were calculated using Sequoia's MATLAB® routines (Sequoia, 2008). Total volume concentration represents the cumulative volume concentration of particles measured in all 32 size classes. The mean particle size and standard deviations are weighted with the volume concentrations of all 32 class sizes. Silt density is the estimated volume concentration ratio of silt particles (particles smaller than 64 µm) to the total volume concentration.

3.0 RESULTS AND DISCUSSION

This section of the report provides detailed summaries of the available QA/QC datasets from current profilers and current meters (section 3.1), CT loggers (section 3.2), as well as from sediment traps and the particle-size-analyzer (section 3.3) deployed on iBO moorings during 2014-2015. Processing of IPS data (from all moorings) and CT logger data (from shelf moorings DFO 2, 1 and 9) was still in progress at the time of completion of this report and is not presented here. It should be noted, however, that all the IPS at the 7 iBO moorings and all CT loggers at the DFO moorings functioned properly and provided complete datasets over 2014-2015 with a total of 100% of raw data return. Processing and QA/QC data from IPS 2014-2015 are expected to be presented as part of upcoming complementary reports provided by ASL Environment.

3.1 Ocean Currents

Processed data for all current profilers and current meters from the 7 iBO moorings 2014-2015 are presented in this section of the report. For each instrument, a time-series plot of current speed, current direction and along-slope/shelf current component is presented. The along-slope component was chosen based on the angle of the bathymetric contours at each mooring location (Table 6) with respect to True North. It was also chosen for consistency with previous mooring studies that described the along-slope/shelf flow, the current component that typically dominates current variability in the offshore Beaufort Sea (Williams et al. 2008; Forest et al. 2015; Dmitrenko et al. 2016). Annual statistics of current speed and direction for selected bin depths (nearest available bins to those listed in Table 7) are also provided to characterize the net behaviour of ocean currents with depth.

Seasonal current roses based on the sub-tidal component of current velocity were constructed for the same selected bin depths (Table 7) to contrast the temporal variability of ocean circulation patterns in relation to the distinct water masses and water mass boundaries. The sub-tidal component was obtained by applying a low-pass filter with a half-amplitude period of 33 hours to each selected time-series linearly interpolated over 1-hour intervals (PL66TN, Beardsley and Rosenfeld 1983). In addition, a complete tabular summary of current speed descriptive statistics, vector-averaged direction and number of valid records is provided for every bin depth of each instrument in Appendix E. Meta-data for each instrument (i.e. serial number, mean instrument depth, date and time of first and last good record, and percentage of raw data return) is provided in Table 8.

Table 6: Angles chosen to describe the along-slope/shelf current component for each iBO mooring.

Mooring	Angle, degrees True North (TN)
BR-1	78
BR-3	0
BR-G, BR-K, DFO-2, DFO-1, DFO-9	52

Table 7: Selected bin depths to characterize circulation patterns throughout the water column.

Approximative Bin Depth (m)	Rationale (based on Lansard et al. 2012)
20	Near-surface circulation within the Polar-Mixed Layer (salinity \approx 31-32)
130	Core of the Pacific Halocline water mass (salinity \approx 33)
220	Boundary between the Pacific Halocline and Atlantic water
350	Mid-depth of the water column over the slope, core of the Atlantic Water mass (salinity \approx 34.8)
550	Deep circulation over the slope, lower portion of the Atlantic water mass
700	Near-bottom circulation at the boundary between the Atlantic water and Canada Basin deep water mass (salinity \approx 34.9)

Table 8: Summary of current profilers and current meters clock drift, first and last good record, and percentage of raw data return on iBO moorings from 2014 to 2015.

Mooring	Instrument	Serial number	Depth (m)	Clock Drift (mm:ss)	First Good Record (UTC)	Last Good Record (UTC)	Raw Data Return ¹
BR-1-14	TRDI QM ADCP 150kHz	12699	199.8	00:10 fast	Sep-01-2014 21:33:00	Sep-29-2015 19:36:00	100.0%
BR-1-14	TRDI LR ADCP 75kHz	12943	455.8	02:20 fast	Sep-01-2014 21:30:00	Sep-29-2015 19:30:00	100.0%
BR-1-14	Nortek Aquadopp DW 2MHz	6270	591.1	00:20 fast	Sep-01-2014 22:00:00	Sep-28-2015 13:30:00	99.7%
BR-1-14	Nortek Aquadopp DW 2MHz	8414	733.1	00:27 fast	Sep-01-2014 22:00:00	Sep-28-2015 13:30:00	99.7%
BR-3-14	TRDI QM ADCP 150kHz	12823	179.2	00:13 slow	Aug-27-2014 13:50:05	Sep-14-2014 6:18:40	4.8%
BR-3-14	TRDI LR ADCP 75kHz	18785	445.6	00:37 slow	Aug-27-2014 15:15:00	Aug-31-2015 16:45:00	100.0%
BR-3-14	Nortek Aquadopp DW 2MHz	8418	553.1	00:12 fast	Aug-27-2014 14:00:00	Aug-31-2015 17:30:00	100.0%
BR-3-14	Nortek Aquadopp DW 2MHz	2756	677.6	01:20 fast	Aug-27-2014 14:00:00	Aug-20-2015 20:30:00	97.1%
BR-G-14	TRDI QM ADCP 150kHz	8784	190.0	09:08 slow	Aug-23-2014 23:57:00	Aug-26-2015 20:37:52	100.0%
BR-G-14	TRDI LR ADCP 75kHz	13079	451.5	00:18 fast	Aug-24-2014 1:15:00	Aug-26-2015 20:15:00	100.0%
BR-G-14	Nortek Aquadopp DW 2MHz	9473	585.3	00:35 fast	Aug-24-2014 0:00:00	Aug-26-2015 21:30:00	100.0%
BR-G-14	Nortek Aquadopp DW 2MHz	9847	692.5	00:49 fast	Aug-24-2014 0:00:00	Aug-26-2015 21:30:00	100.0%
BR-K-14	TRDI WHS ADCP 300kHz	2646	136.1	06:03 slow	Aug-22-2014 17:45:00	Aug-26-2015 13:00:00	100.0%
BR-K-14	Nortek Aquadopp Profiler 1Mhz	11147	140.0	00:23 fast	Aug-22-2014 17:00:00	Aug-26-2015 14:00:00	100.0%
DFO-2-14	TRDI NB ADCP 300kHz	586	108.0	08:17 slow	Sep-30-2014 16:40:04	Sep-26-2015 13:28:07	100.0%
DFO-1-14	TRDI NB ADCP 300kHz	318	51.0	10:04 slow	Sep-26-2015 22:30:09	Sep-6-2015 4:39:22	81.5% ²
DFO-9-14	TRDI WHS ADCP 300kHz	18318	31.0	10:02 slow	Oct-01-2014 01:53:00	Sep-27-2015 17:09:52	100.0%

¹Note: The raw data return is based on the number of records (including bad data) during the period from the mooring deployment to the mooring recovery.

²Note: Data loss at site DFO-1-14 was caused by intermittent failure of the data recorder

3.1.1 Mooring BR-1

Time-series plots of current speed, direction, and along-slope current component from the QM ADCP, LR ADCP and the two Aquadopp DW deployed at BR-1 over 2014-2015 are provided in Figure 2 through Figure 5. The data in the QM and LR ADCP plots are filtered for bins with PG4+PG1 values less than 25%, bins affected by sidelobe interference and for error velocity thresholds as described in section 2.4.1. The first valid bin depth for the QM ADCP at BR-1-14 after removing sidelobe interference was 19.5 m (bin cell 22), although this bin depth contains only 8% of valid data (Appendix E). Bin depths 123.5 and 131.5 m (bin cells 8 and 9) of the QM ADCP were affected by the presence of the upper Technicap sediment trap, which resulted in reflection observed in the echo intensity (not shown) and a general decrease in current speed at these depths. Accordingly, bin cells 8, 9 and 22 of QM ADCP #1299 were manually flagged as part of the QA/QC and data from these bin depths should be treated carefully before being used in further analyses.

The LR ADCP #12943 did not show any suspicious bin cells due to interference with other parts of the mooring (Figure 3). The first valid bin depth for this instrument was 47.1 m (bin cell 25) with a percentage of valid data of 96.6% (Appendix E). The percentage of valid records was slightly less than 90% at bin depths 95.1 and 79.1 m for this instrument (bin cells 22 and 23) due to partial loss of data in the fall 2014 and during spring-summer 2015 (Figure 3). This data loss has been linked to high intensity of ambient sound generated at the surface due to ice floes passing over the mooring, although it is not clear yet why this phenomenon did not affect bin cells 24 and 25 (47.1 and 63.1 m) to the same extent as cells 22 and 23. The deep Aquadopp current meters #6270 (591.1 m) and #8414 (733.1 m) provided complete time-series with a percentage of valid data return of 96.8% for each instrument (Figure 4, Figure 5 and Appendix E).

Mean current speeds at BR-1-14 ranged from 9 to 14 cm/s in the upper 200 m of the water column; and from 4 to 8 cm/s below 200 m (Table 9, Appendix E). Vector-averaged directions were typically to the west-southwest (220-250°TN) for all bin depths down to 431 m. However, both lowermost Aquadopps at 591 and 733 m showed an averaged direction to the east-southeast (210-130°TN). Maximum current speed for un-flagged bins was 87 cm/s on October 7, 2014 at 27.5 m depth. Strong current speeds (>60 cm/s) were generally detected over October 4-7, 2014 throughout the upper 200 m. Periods of stronger currents approaching 50 cm/s were also recorded over October 17-20, 2014 and April 24-26, 2015. These strong current events corresponded to strong negative along-slope currents, meaning a westward flow (i.e. upwelling conditions) presumably driven by strong easterly winds. Moderate to strong eastward-directed currents (up to ~30 cm/s, confined to the upper 200 m) were primarily detected in late February/early March 2015 and early August 2015. Both events appear to correspond to the passage of eddy-like features with noticeable reversals in the current direction from the north-northeast to the south-southeast over a 10-14 day period (Figure 2 and Figure 3).

Seasonal current roses (low-pass filtered) for selected bin depths at mooring BR-1-14 are provided in Figure 6 through Figure 11. The strong westward current events (>50 cm/s) detected in the upper water column in October 2014 (fall) and April 2015 (spring) are particularly visible when looking at the current roses for the Pacific Halocline (132 m, Figure 7). Also at this depth, the presence of moderate north-eastward currents in summer 2015 reflects the passage of eddy-like features mentioned above. In the Atlantic water mass at 223 and 351 m depth, low-pass filtered currents were generally weak (<10 cm/s) and variable around the compass (Figure 9 and Figure 10). In the lowermost layers of the water column at 591 and 733 m, currents were also weak, but showed more variability in their dominant direction over time. Near the bottom at 733 m, most frequent currents were in fact repeatedly directed to the south (across the slope toward the shelf; Figure 11), a pattern that contrasts with what has been recorded at all the other depths at BR-1 over 2014-2015.

BR-1; Quartermaster Broadband 153.6 kHz; 70.4318 N, 139.0228 W; 2014-2015; Instr. #12699; 199.8 m depth

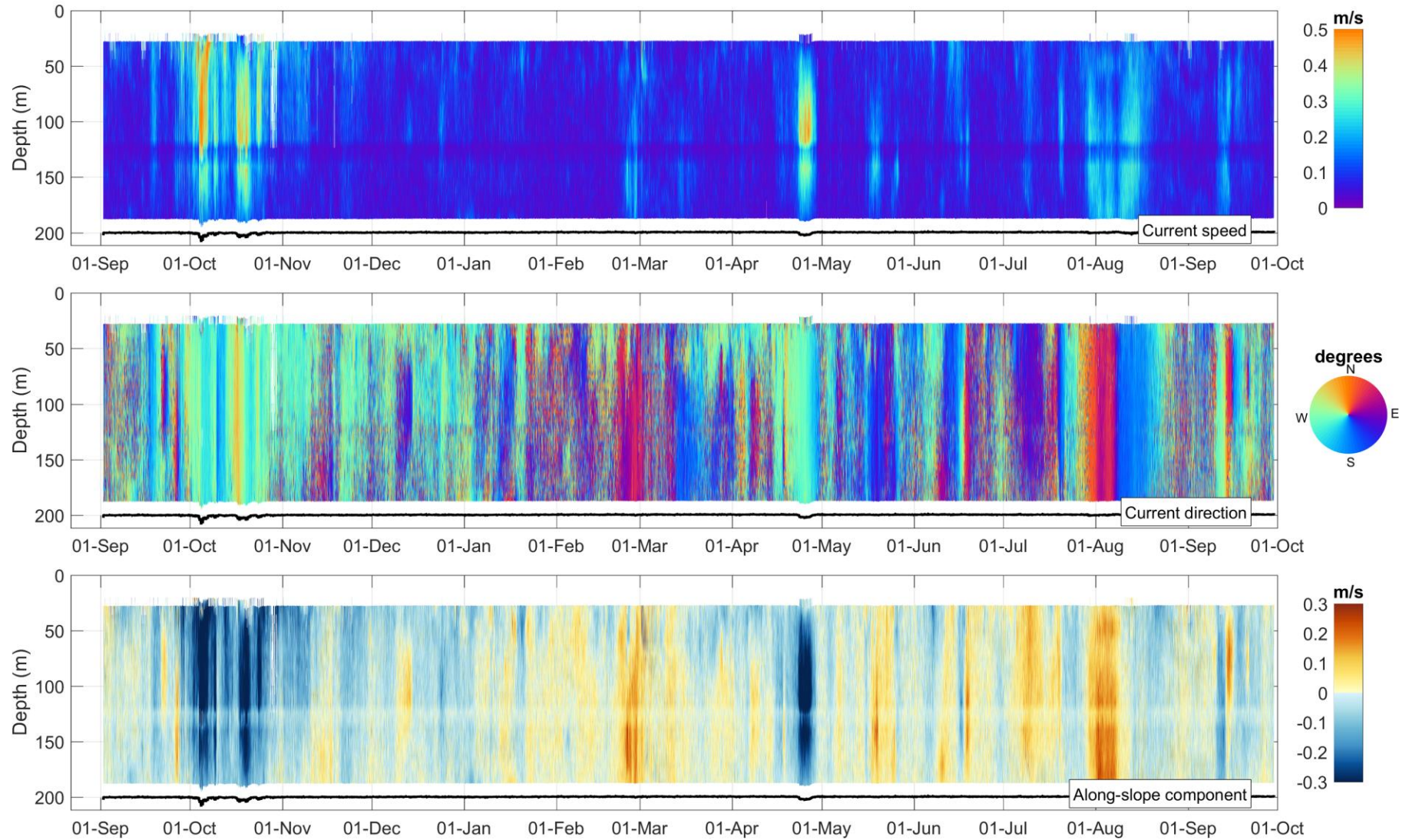


Figure 2: Time-series of current speed, current direction and along-slope current component at mooring BR-1-14 as obtained with the QM ADCP #12699. The black line depicts the instrument depth.

BR-1; Long Ranger Broadband 76.8 kHz; 70.4318 N, 139.0228 W; 2014-2015; Instr. #12943; 455.8 m depth

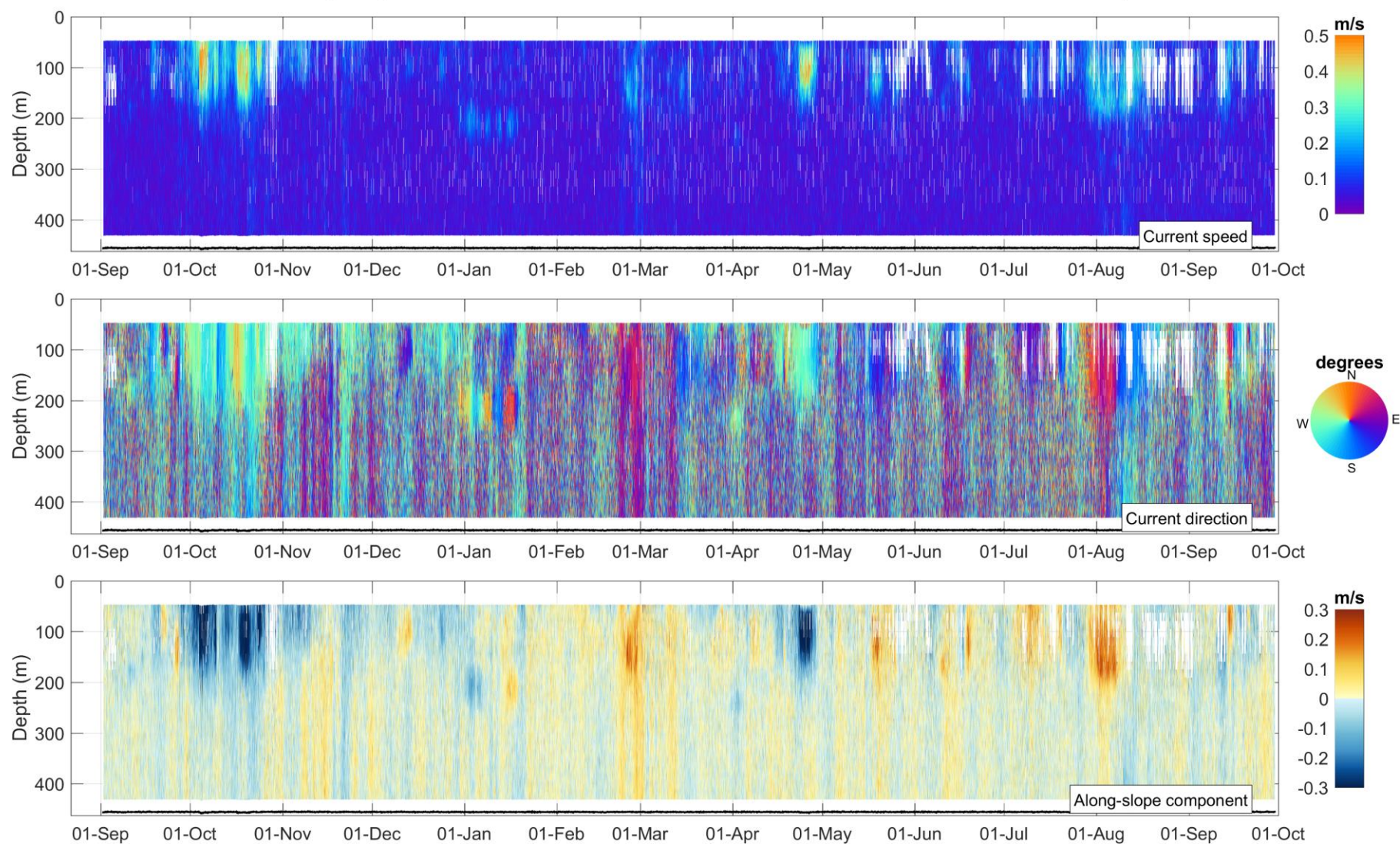


Figure 3: Time-series of current speed, current direction and along-slope current component at mooring BR-1-14 as obtained with the LR ADCP #12943. The black line depicts the instrument depth.

BR-1; Aquadopp DeepWater 2-MHz; 70.4318 N, 139.0228 W; 2014-2015; AQD. #AQD 6270; 591.1 m depth

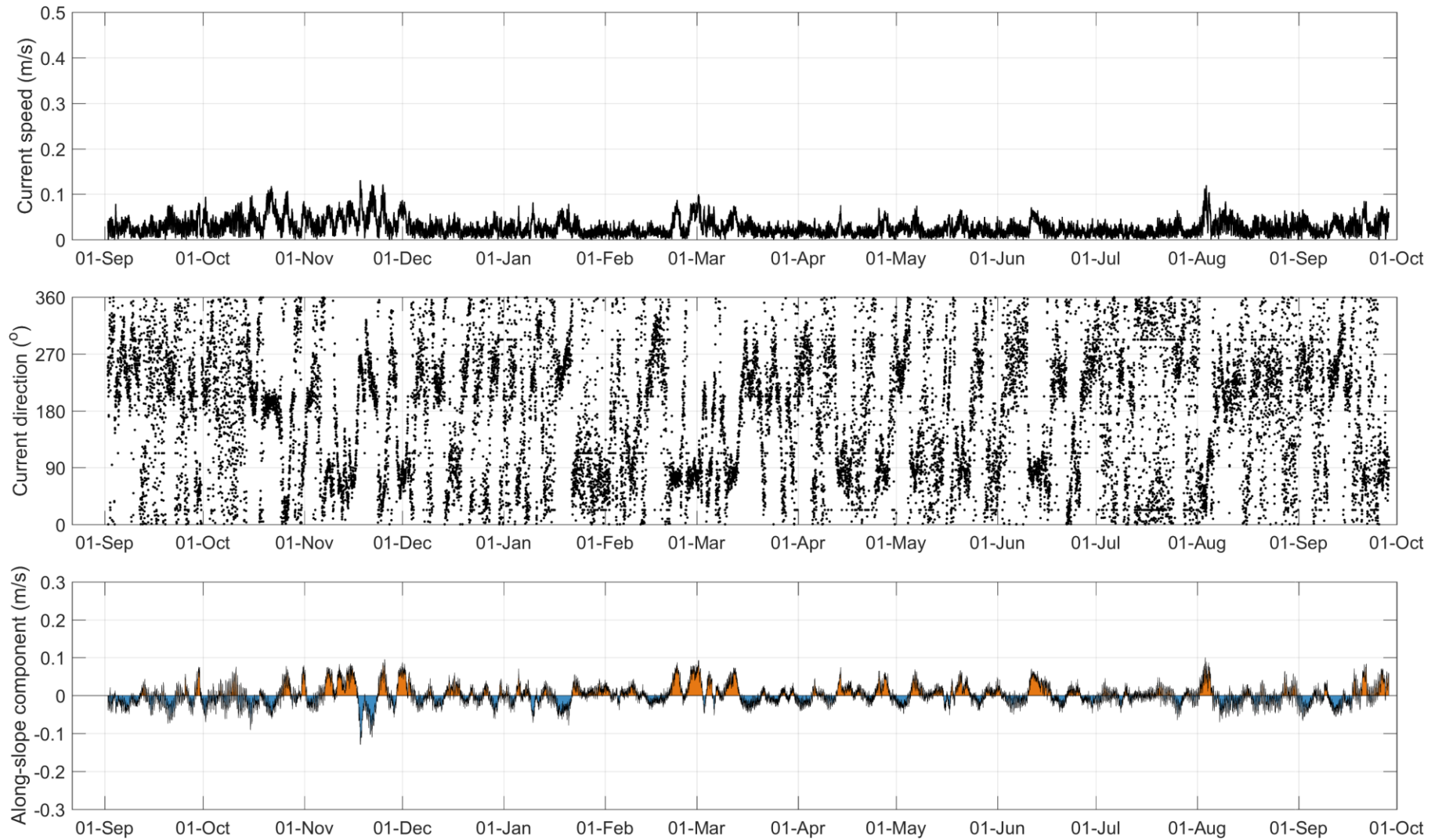


Figure 4: Time-series of current speed, current direction and along-slope current component at 591 m at mooring BR-1-14 as obtained with the Aquadopp #6270.

BR-1; Aquadopp DeepWater 2-MHz; 70.4318 N, 139.0228 W; 2014-2015; AQD. #AQD 8414; 733.1 m depth

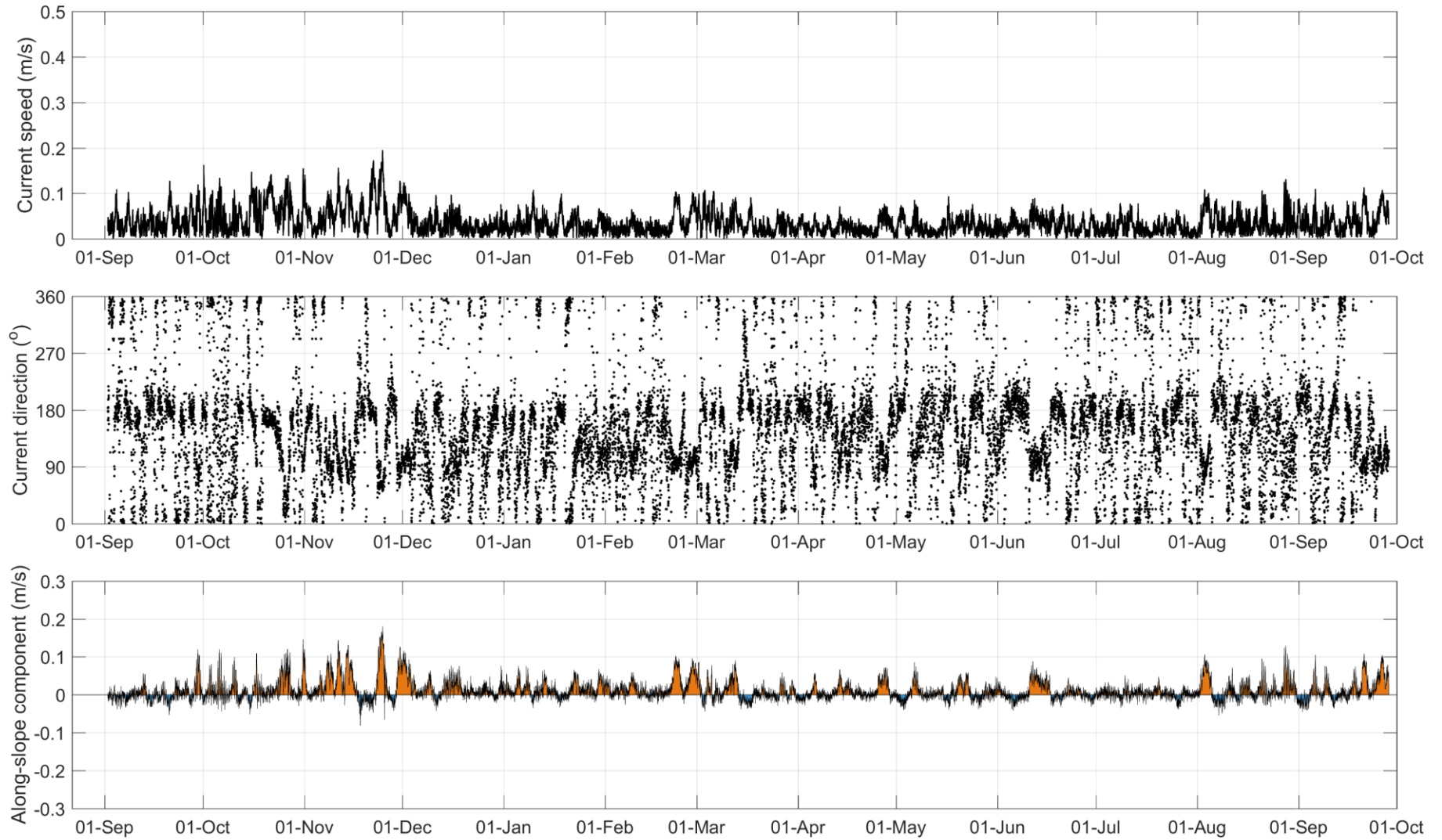


Figure 5: Time-series of current speed, current direction and along-slope current component at 733 m at mooring BR-1-14 as obtained with the Aquadopp #8414.

Table 9: Annual statistics of current speed and direction at BR-1-14 from selected bin depths representative of water mass variability in the Beaufort Sea (see Table 7 for water mass description).

Bin Depth (m)	Median Speed (m/s)	Mean Speed (m/s)	75%ile Speed (m/s)	95%ile Speed (m/s)	99%ile Speed (m/s)	Max Speed (m/s)	Standard Deviation Speed (m/s)	Vector-Averaged Direction (deg TN)
27.5	0.09	0.11	0.14	0.26	0.41	0.87	0.08	251.7
132.5	0.07	0.10	0.12	0.26	0.36	0.53	0.08	233.4
223.1	0.05	0.06	0.08	0.13	0.17	0.30	0.04	250.9
351.1	0.05	0.05	0.07	0.11	0.14	0.43	0.03	194.4
591.1	0.02	0.03	0.04	0.06	0.09	0.13	0.02	128.6
733.1	0.03	0.04	0.05	0.09	0.12	0.20	0.03	108.7

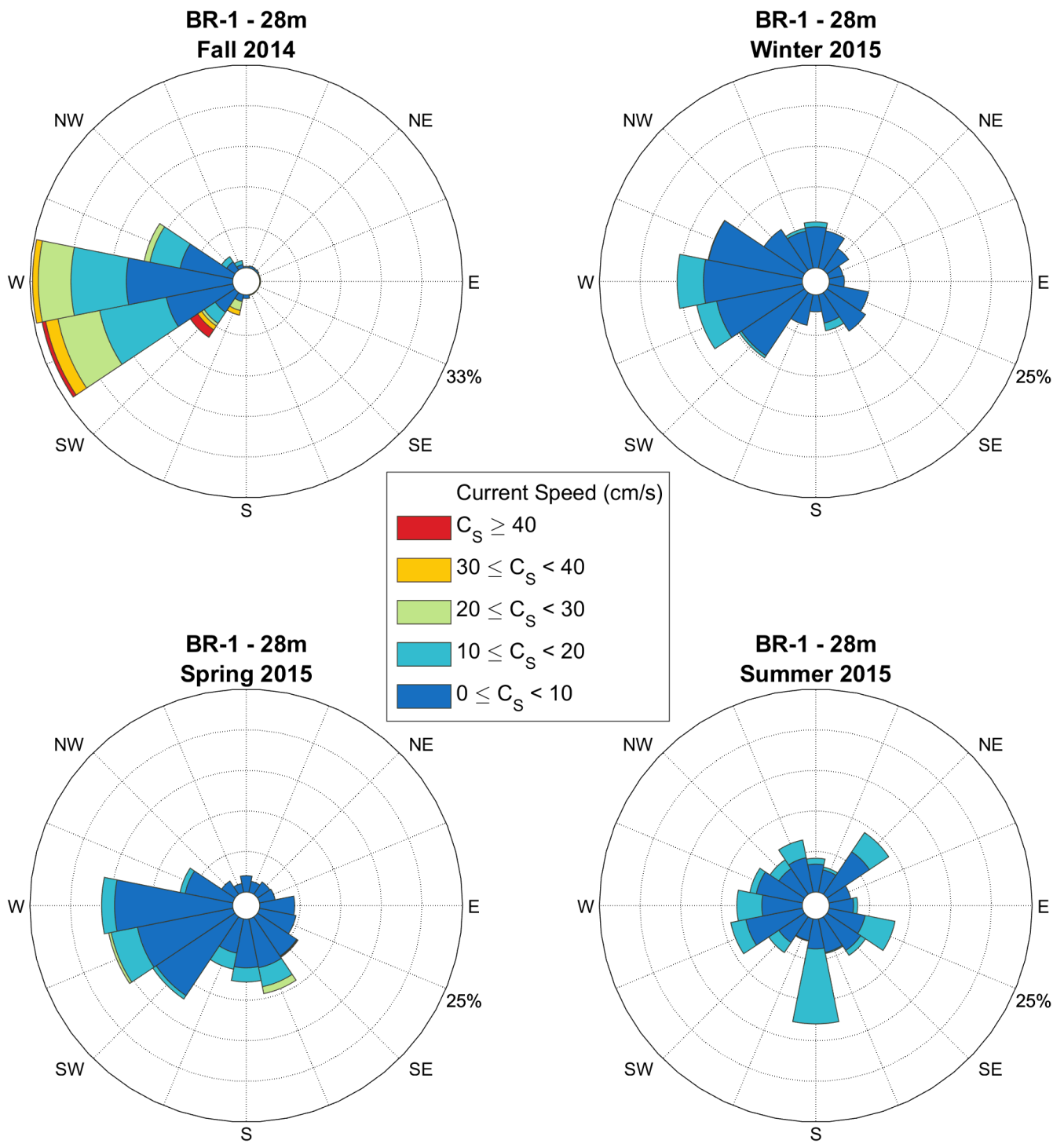


Figure 6: Seasonal current roses at 28 m depth at BR-1-14 as based on low-pass filtered data from bin cell #21 acquired with the QM ADCP #12699. Roses point toward where the currents are going. Seasons are defined following the meteorological convention (Fall: October-December; Winter: January-March; Spring: April-June; Summer: July-September).

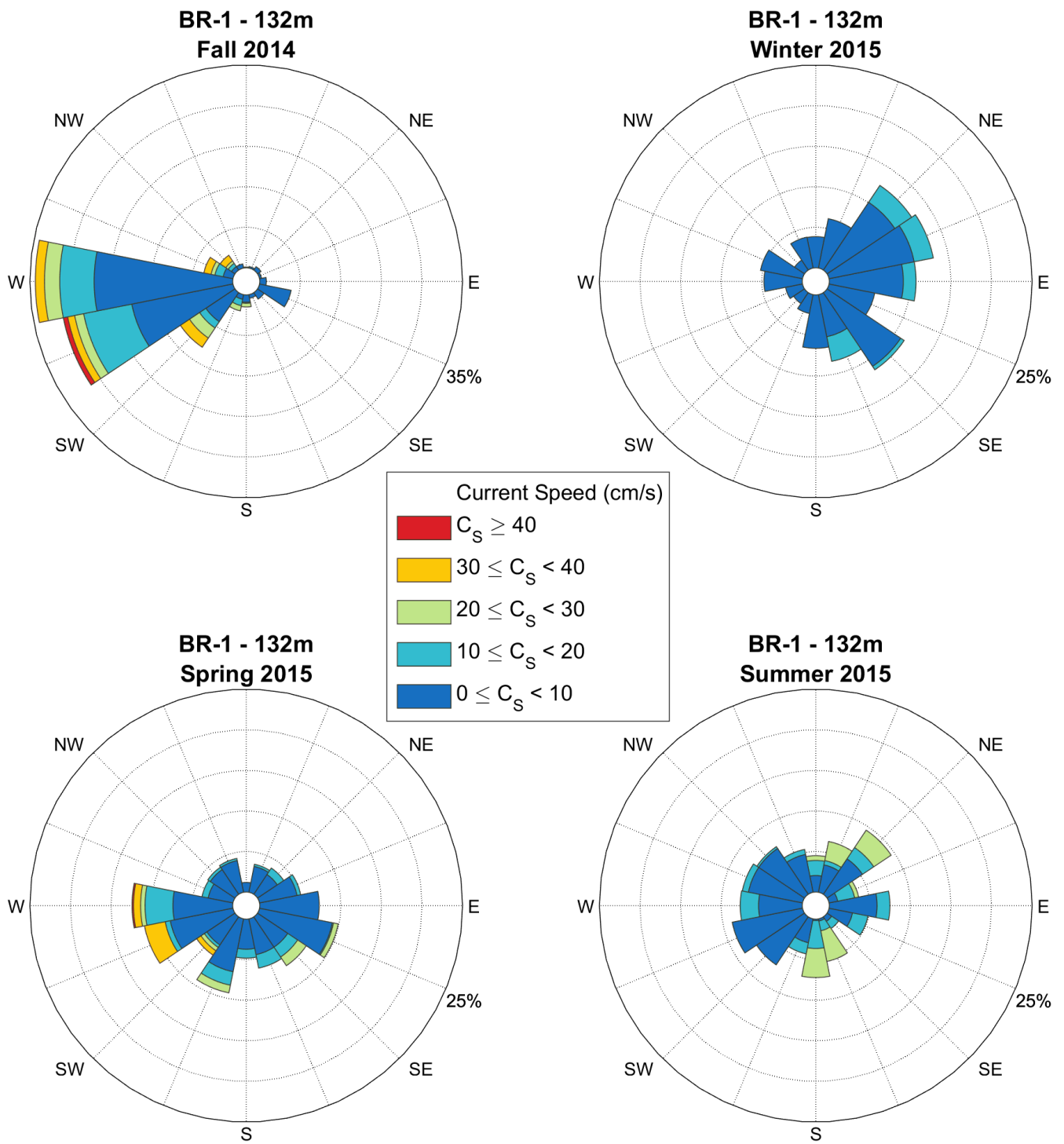


Figure 7: Seasonal current roses at 132 m depth at BR-1-14 as based on low-pass filtered data from bin cell #8 acquired with the QM ADCP #12699. Roses point toward where the currents are going. Seasons are defined following the meteorological convention (Fall: October-December; Winter: January-March; Spring: April-June; Summer: July-September).

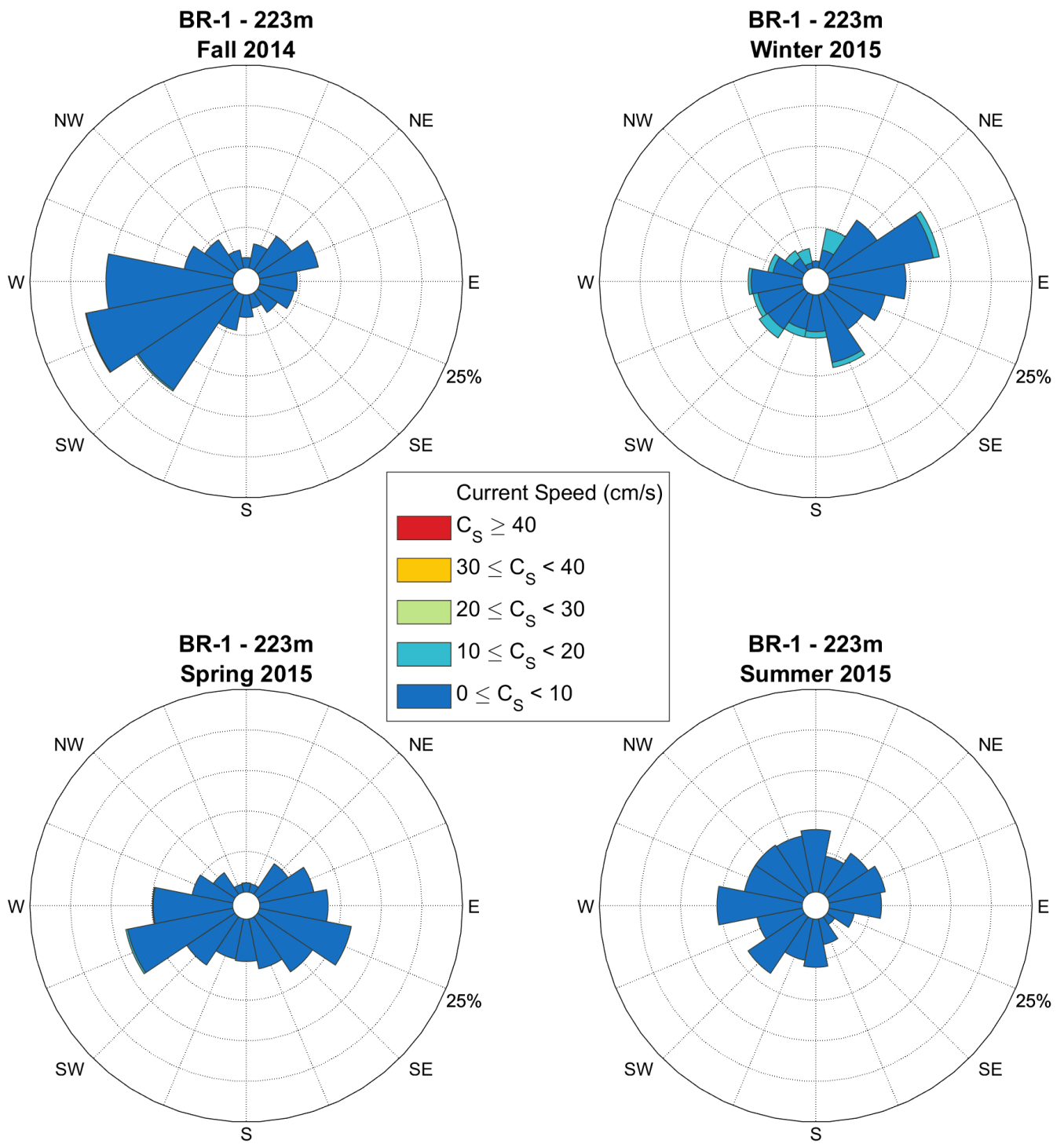


Figure 8: Seasonal current roses at 223 m depth at BR-1-14 as based on low-pass filtered data from bin cell #14 acquired with the LR ADCP #12943. Roses point toward where the currents are going. Seasons are defined following the meteorological convention (Fall: October-December; Winter: January-March; Spring: April-June; Summer: July-September).

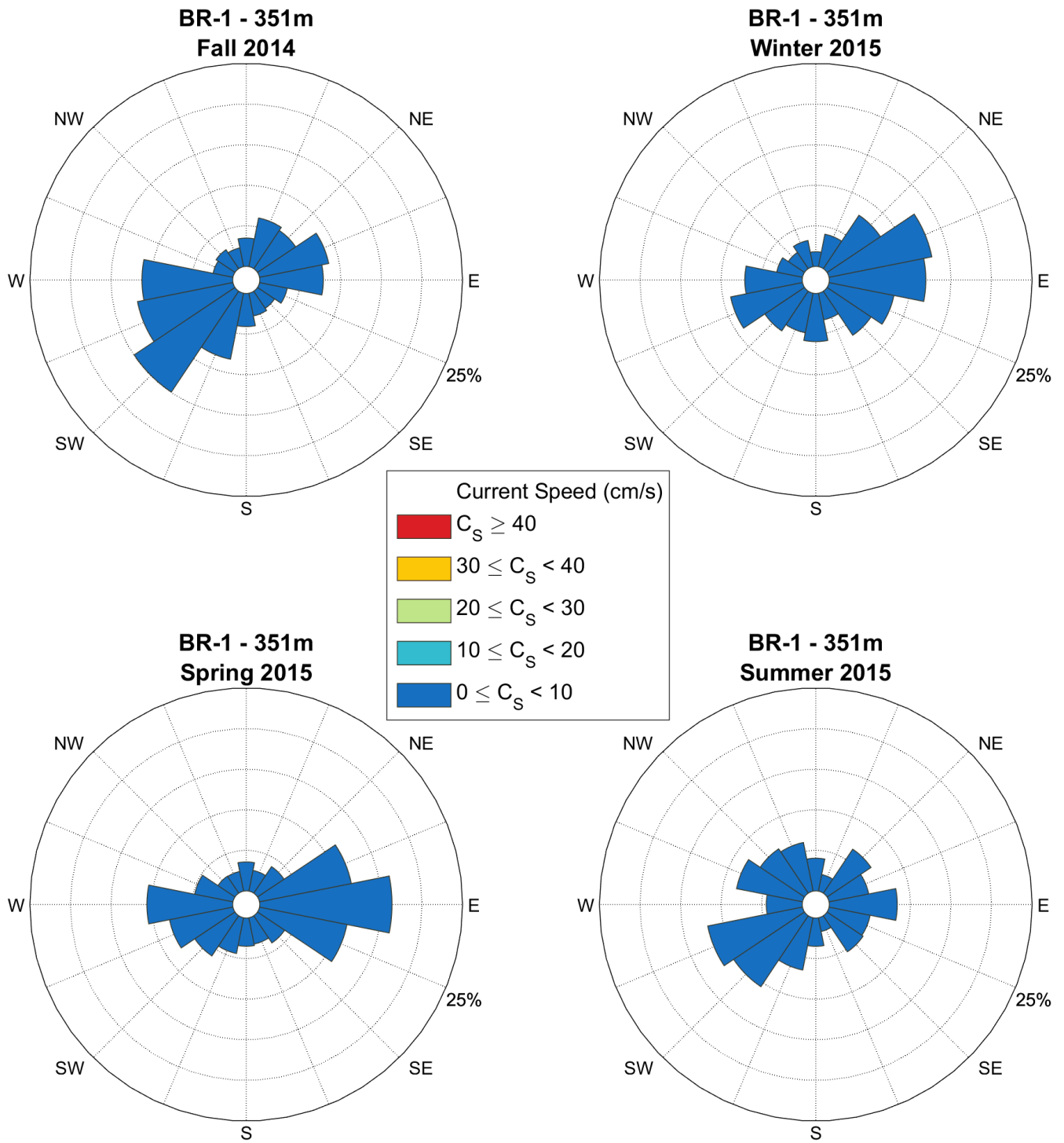


Figure 9: Seasonal current roses at 351 m depth at BR-1-14 as based on low-pass filtered data from bin cell #6 acquired with the LR ADCP #12943. Roses point toward where the currents are going. Seasons are defined following the meteorological convention (Fall: October-December; Winter: January-March; Spring: April-June; Summer: July-September).

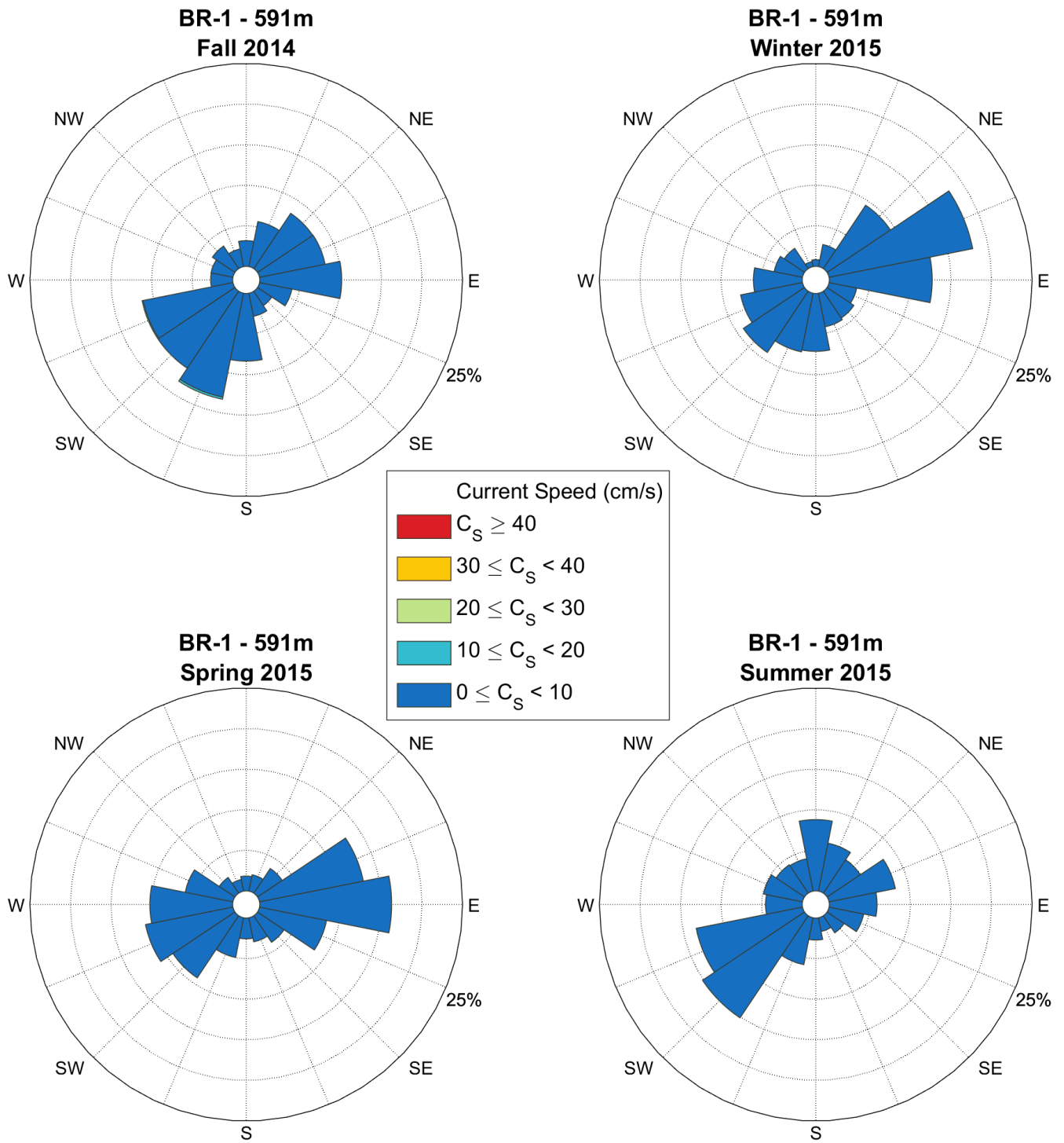


Figure 10: Seasonal current roses at 591 m depth at BR-1-14 as based on data acquired with the Aquadopp #6270. Roses point toward where the currents are going. Seasons are defined following the meteorological convention (Fall: October-December; Winter: January-March; Spring: April-June; Summer: July-September).

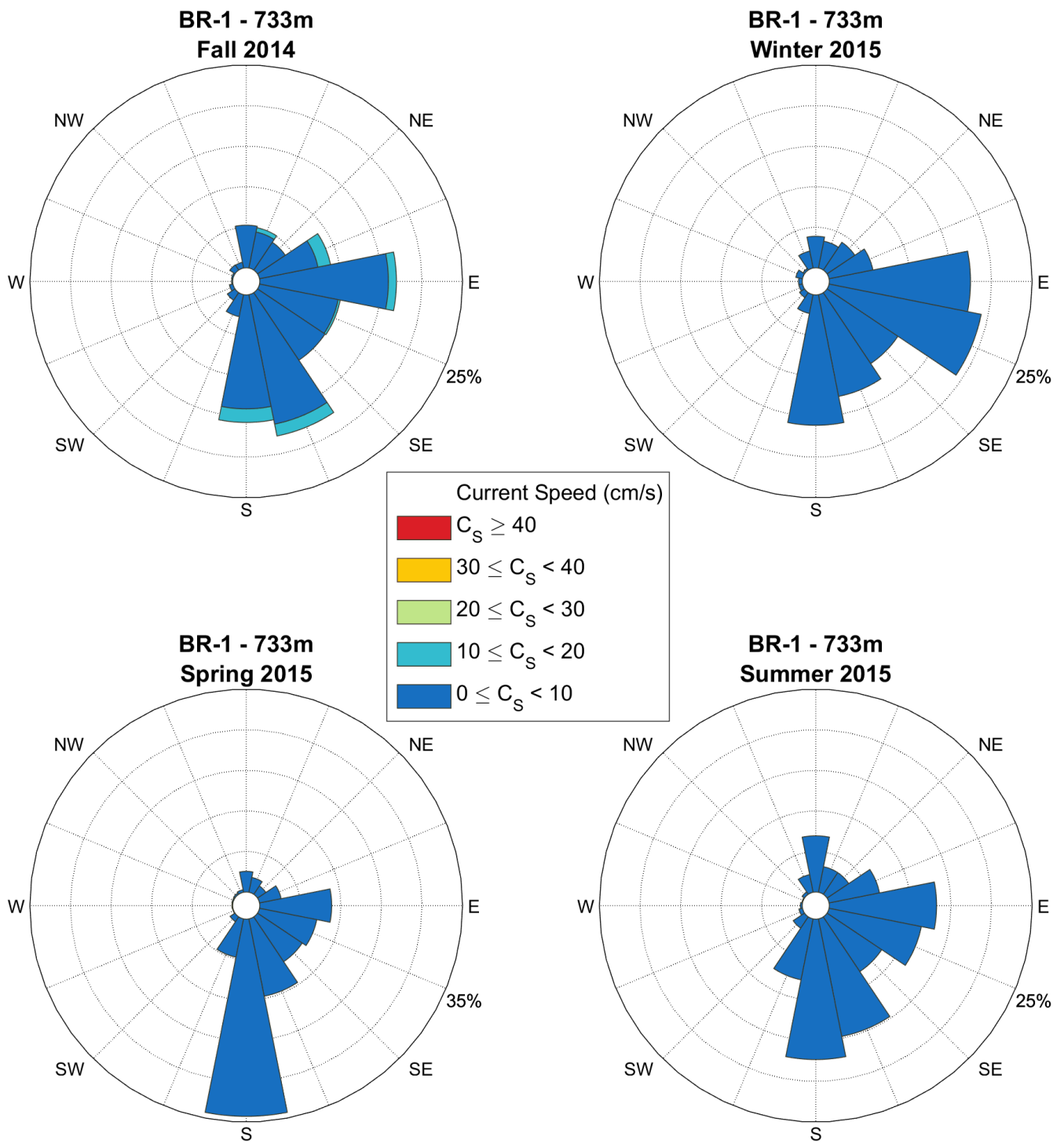


Figure 11: Seasonal current roses at 733 m depth at BR-1-14 as based on data acquired with the Aquadopp #8414. Roses point toward where the currents are going. Seasons are defined following the meteorological convention (Fall: October-December; Winter: January-March; Spring: April-June; Summer: July-September).

3.1.2 Mooring BR-3

Time-series plots of current speed, direction, and along-slope current component from the LR ADCP and the two Aquadopp DW deployed at BR-3 over 2014-2015 are provided in Figure 12 through Figure 14. Data from the QM ADCP #12823 at BR-3-14 are not presented since this instrument stopped recording on September 8, 2014 due to water leakage in the external battery housing. Investigation revealed that the leakage likely occurred through the connector on the dummy plug side of the housing. This unexpected leakage should not be confounded with previous corrosion problems (identified over 2010-2011) that affected the impulse bulkhead connectors that connect the housing to the transducer on TRDI ADCPs, a problem that has since been resolved.

The data in the LR ADCP plots are filtered for bins with PG4+PG1 values less than 25%, bins affected by sidelobe interference and for error velocity thresholds as described in section 2.4.1. The LR ADCP #18785 at BR-3-14 provided a complete annual dataset, although a suspicious bin cell at 326 m depth (bin cell 7) was manually flagged as part of the QA/QC process (Figure 12, Appendix E). This bin depth was likely affected by the presence of the lower Technicap sediment trap, which resulted in reflection observed in the echo intensity and a general decrease in current speed at this depth. However, it is not clear why the lower Technicap trap interfered with the signal of the LR ADCP #12785 at BR-3, whereas this was not detected at the other slope moorings BR-1 (Figure 3) and BR-G (Figure 22). The first valid bin depth for the LR ADCP #18785 at BR-3 was 54.0 m (bin cell 24) with a percentage of valid data of 99.2% (Appendix E). The percentage of valid records remained near 99% at all bin depths for this instrument. Partial data loss possibly linked to high intensity of ambient sound generated by sea ice at the surface was observed only briefly in early October 2014 at this location (Figure 12). The deep Aquadopp current meters #8418 (553.1 m) and #2756 (677.6 m) provided complete time-series with a percentage of valid data return of 98.3% for each instrument (Figure 13, Figure 14 and Appendix E).

Mean current speeds at BR-3-14 ranged from 5 to 8 cm/s throughout the water column, taking into account that the near surface layer above 50 m remains unresolved (Table 10, Appendix E). Vector-averaged directions were uniformly to the south (160-190°TN) from 54 to 150 m depth, but rapidly veered to the east and to north in the interval between 150 and 198 m. At the bin depth of 198 m and below, mean currents were consistently to the north (between 330 and 30°TN), as also showed by the data recorded by both lowermost Aquadopps at 551 and 678 m depth. Maximum current speed at BR-3-14 was 48 cm/s on October 13, 2014 as recorded at 310 m depth (Appendix E). Another brief event of 47 cm/s was recorded at 54 m depth on May 15, 2015. These elevated current speed events were however of very brief duration each (<30 minutes) and should be evaluated with caution. Less than 1% of the entire current speed dataset at BR-3-14 was greater than 20 cm/s (Appendix E).

Seasonal current roses (low-pass filtered) for selected bin depths at mooring BR-3-14 are provided in Figure 15 through Figure 20. The current roses further illustrate that current speed at this location is steadily weak (typically less than 10 cm/s). However, current direction at BR-3 is more variable over time than what the annually-averaged vector direction showed. In particular, a discernable pattern in the lower portion of the water column (341 to 678 m) is that northward currents are more frequent in winter and spring than during the summer and fall when more southward currents are recorded. Another event of interest was the recording of relatively strong northward currents (slightly above 30 cm/s) recorded near the bottom at 678 m depth on March 2, 2015. This event was seen throughout the water column (Figure 12), but was strongest at the lowermost depth monitored. It also occurred approximately 6 days after a similarly along-slope current pulse measured at BR-1, which was strongest around 150 m depth and linked to an eddy-like feature (Figure 3).

BR-3; Long Ranger Broadband 76.8 kHz; 73.4086 N, 129.3565 W; 2014-2015; Instr. #18785; 445.6 m depth

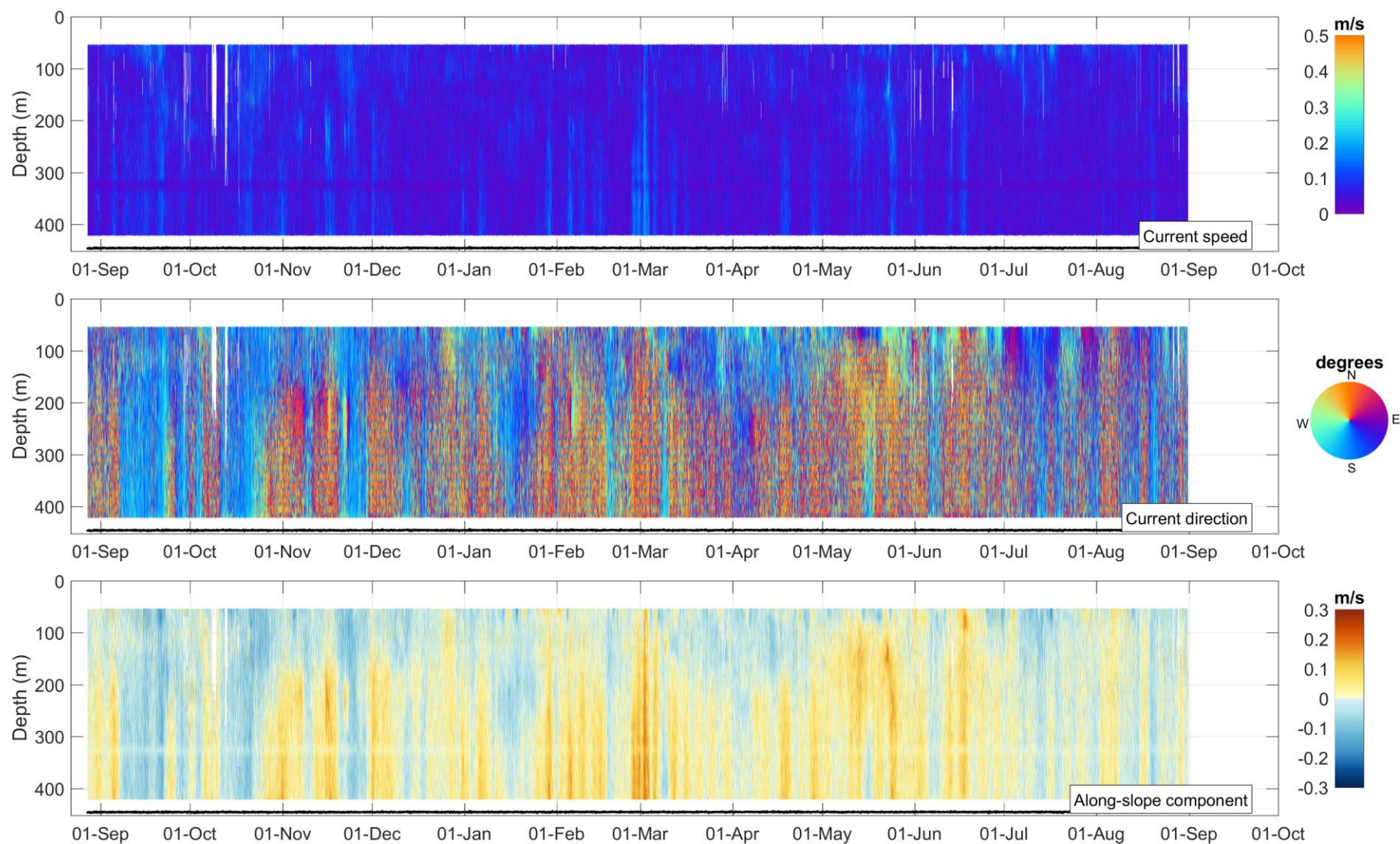


Figure 12: Time-series of current speed, current direction and along-slope current component at mooring BR-3-14 as obtained with the LR ADCP #18785. The black line depicts the instrument depth.

BR-3; Aquadopp DeepWater 2-MHz; 73.4086 N, 129.3565 W; 2014-2015; AQD. #AQD 8418; 553.1 m depth

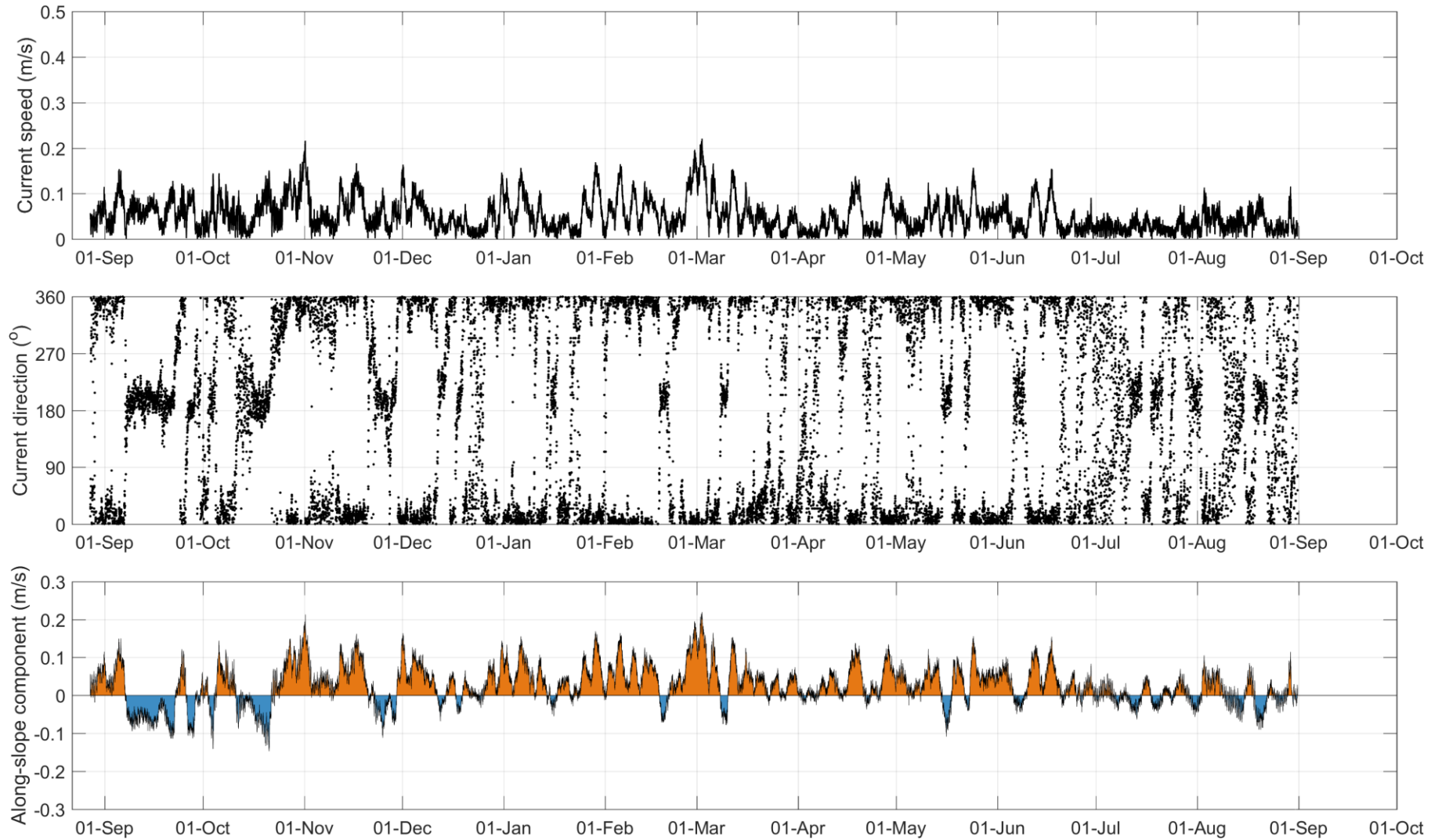


Figure 13: Time-series of current speed, current direction and along-slope current component at 553 m at mooring BR-3-14 as obtained with the Aquadopp #8418.

BR-3; Aquadopp DeepWater 2-MHz; 73.4086 N, 129.3565 W; 2014-2015; AQD. #AQD 2756; 677.6 m depth

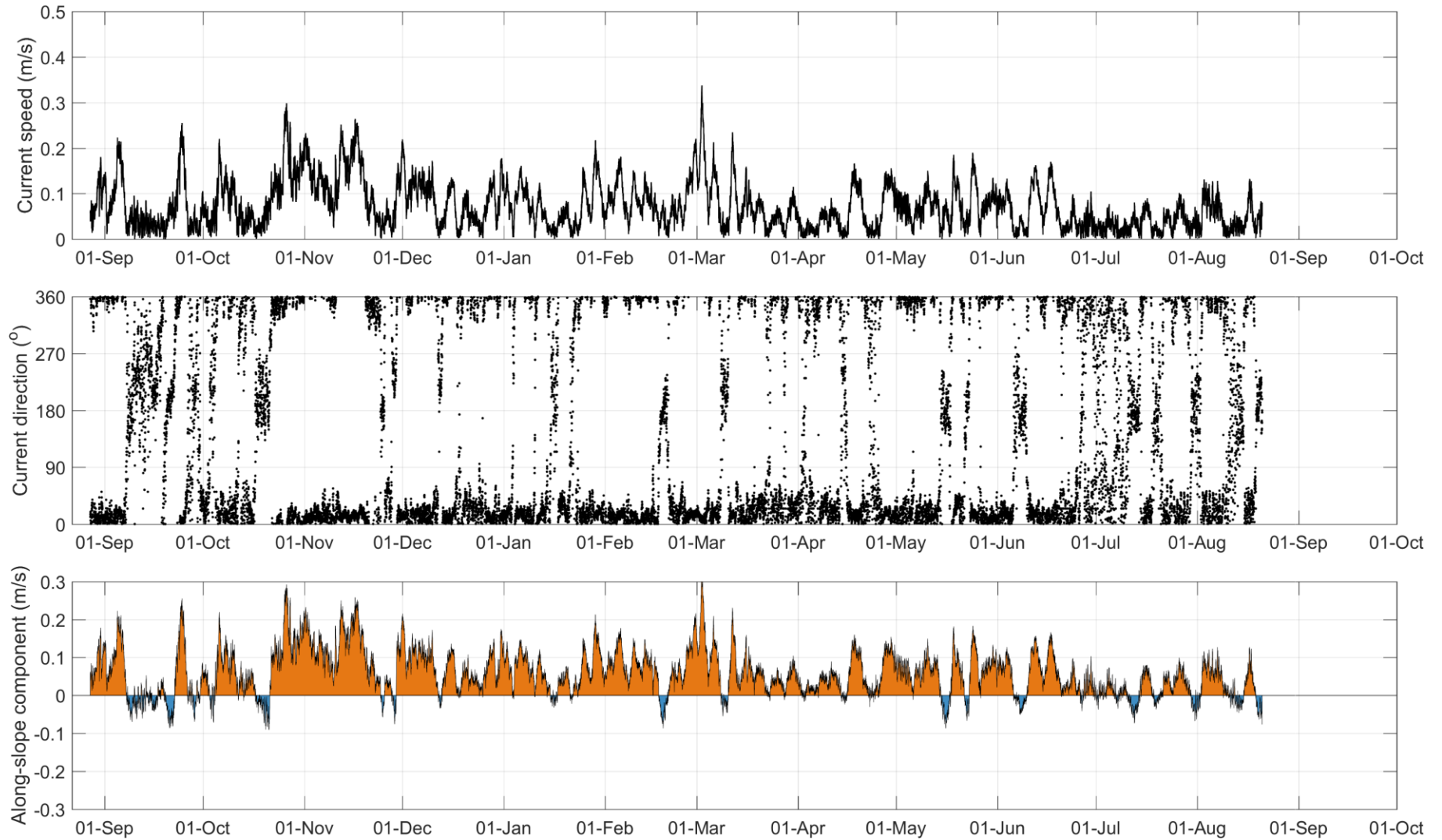


Figure 14: Time-series of current speed, current direction and along-slope current component at 678 m at mooring BR-3-14 as obtained with the Aquadopp #2756.

Table 10: Annual statistics of current speed and direction at BR-3-14 from selected bin depths representative of water mass variability in the Beaufort Sea (see Table 7 for water mass description).

Bin Depth (m)	Median Speed (m/s)	Mean Speed (m/s)	75%ile Speed (m/s)	95%ile Speed (m/s)	99%ile Speed (m/s)	Max Speed (m/s)	Standard Deviation Speed (m/s)	Vector-Averaged Direction (deg TN)
53.0	0.07	0.08	0.10	0.15	0.20	0.47	0.04	186.5
133.0	0.06	0.06	0.08	0.13	0.17	0.33	0.03	171.0
213.0	0.05	0.06	0.08	0.12	0.16	0.33	0.03	16.3
341.0	0.05	0.06	0.08	0.12	0.15	0.26	0.03	350.4
553.1	0.04	0.05	0.07	0.12	0.16	0.22	0.04	332.1
677.6	0.06	0.07	0.10	0.17	0.23	0.34	0.05	346.7

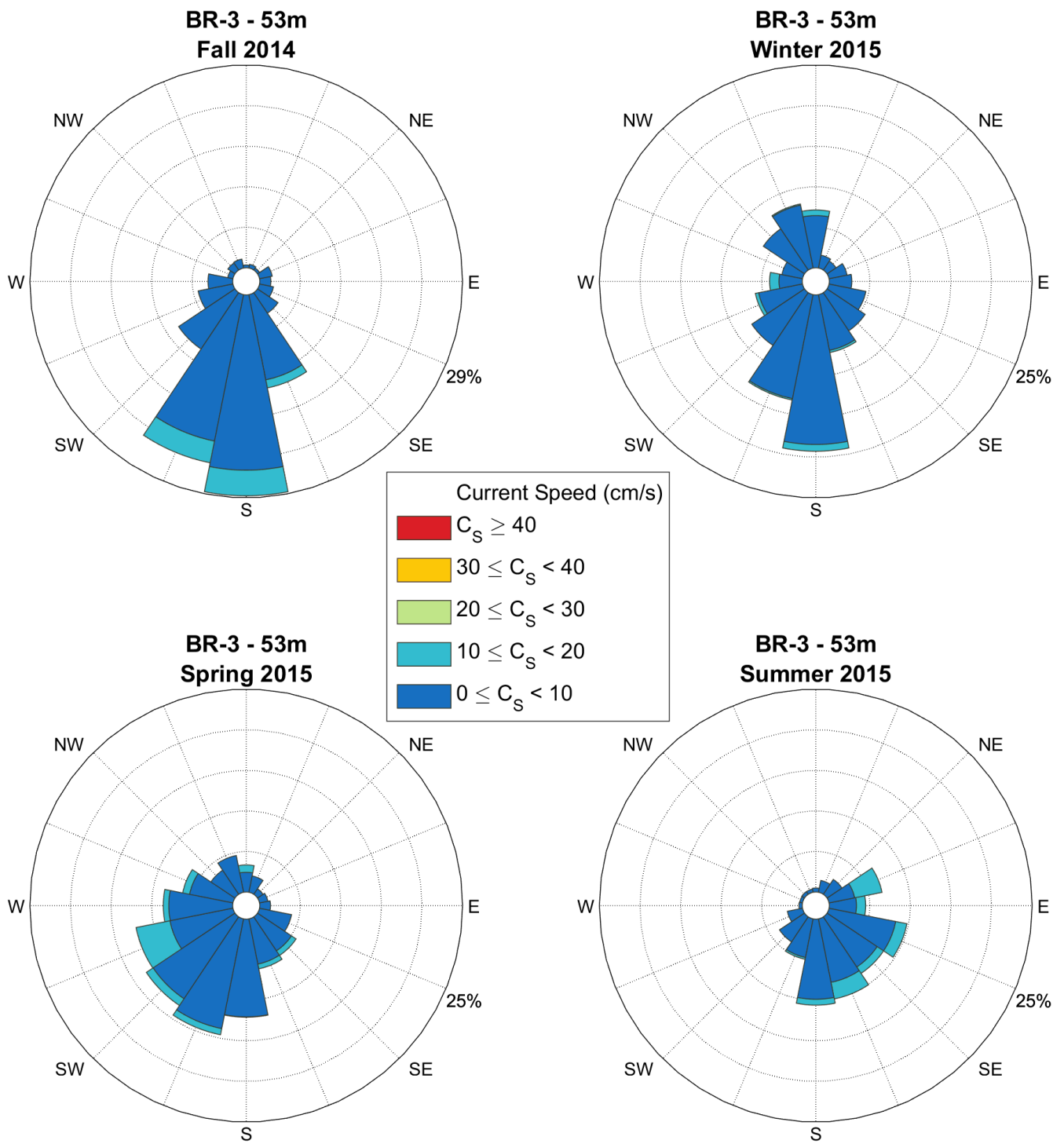


Figure 15: Seasonal current roses at 53 m depth at BR-3-14 as based on low-pass filtered data from bin cell #24 acquired with the LR ADCP #18785. Roses point toward where the currents are going. Seasons are defined following the meteorological convention (Fall: October-December; Winter: January-March; Spring: April-June; Summer: July-September).

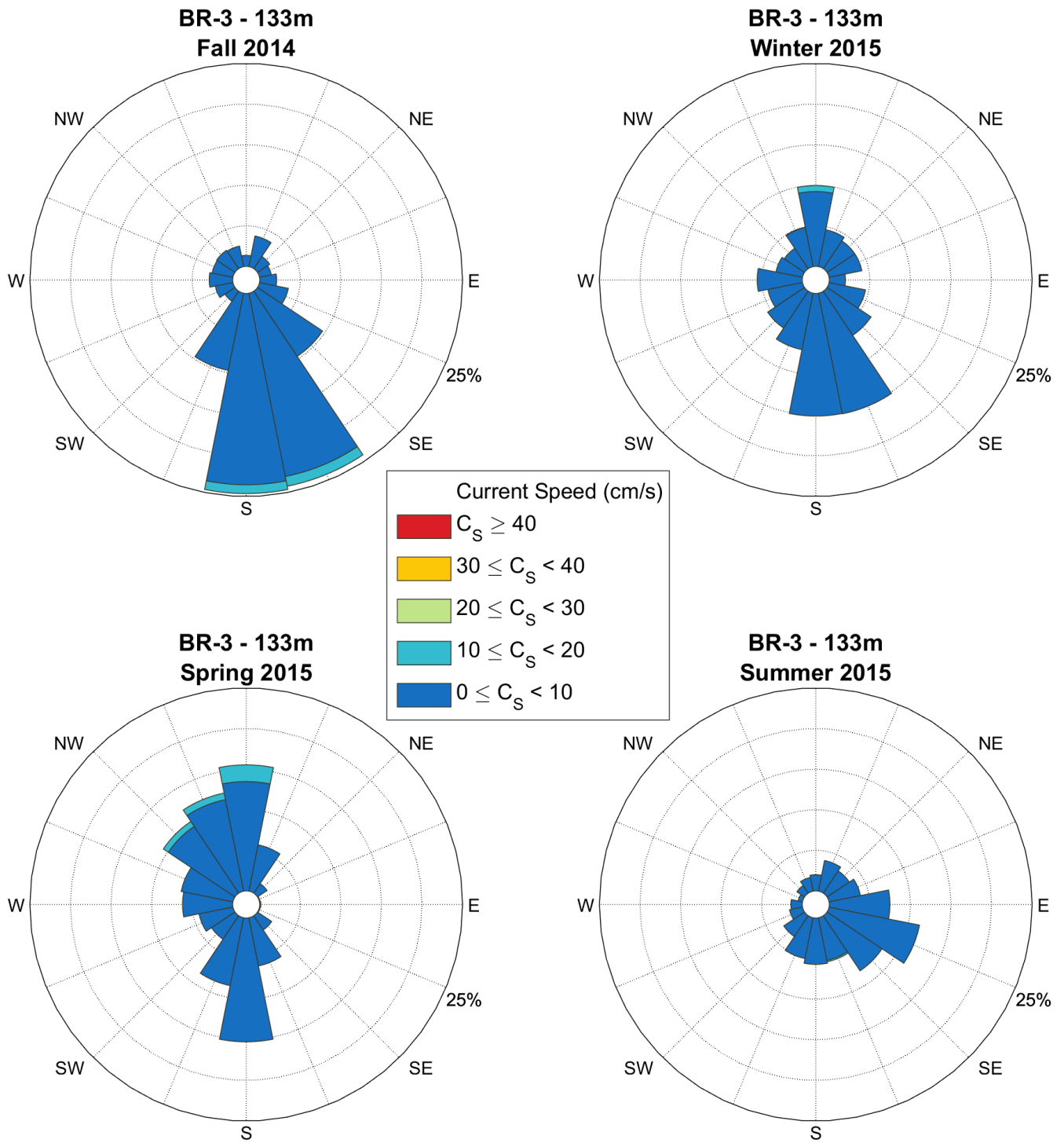


Figure 16: Seasonal current roses at 133 m depth at BR-3-14 as based on low-pass filtered data from bin cell #19 acquired with the LR ADCP #18785. Roses point toward where the currents are going. Seasons are defined following the meteorological convention (Fall: October-December; Winter: January-March; Spring: April-June; Summer: July-September).

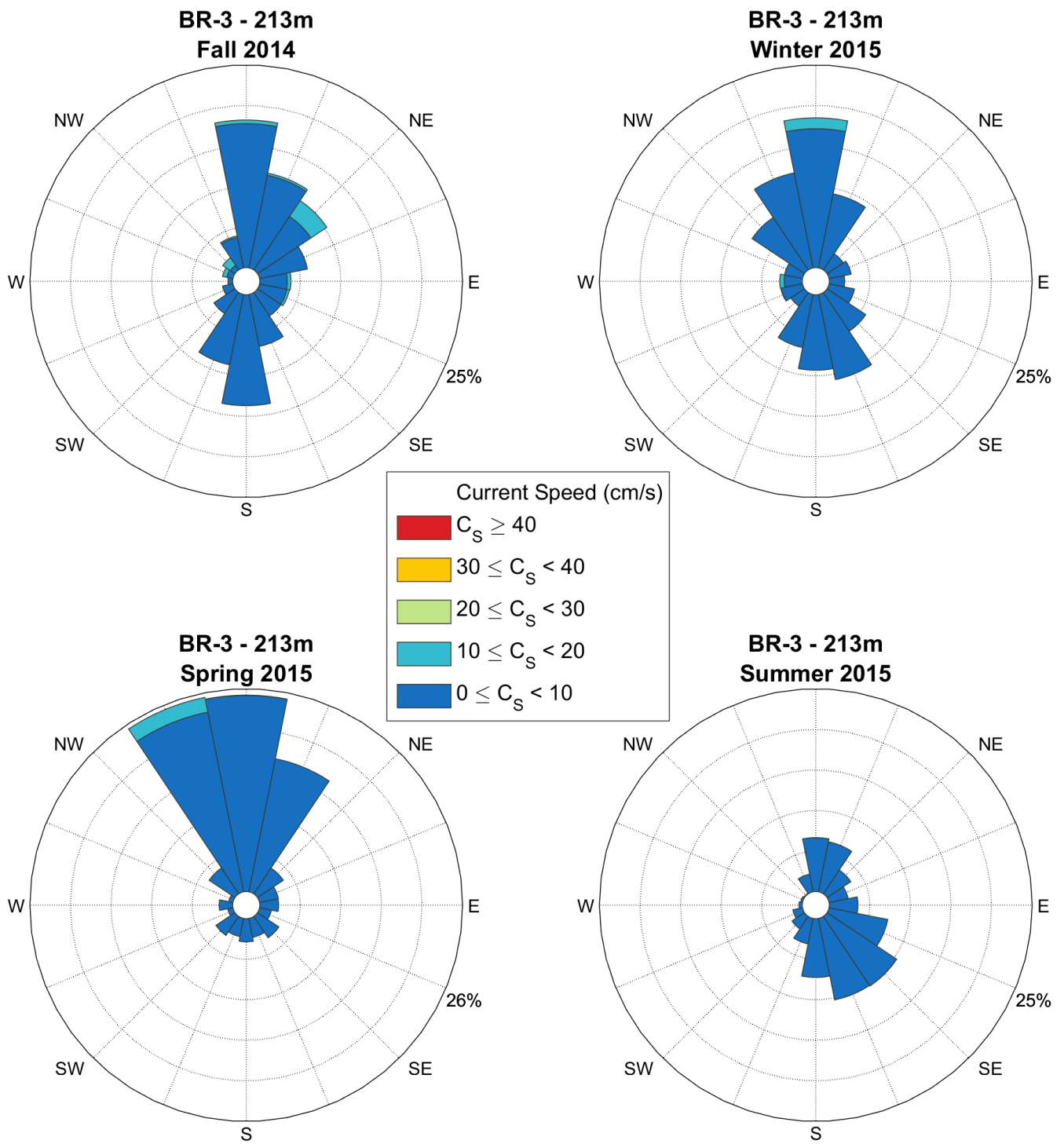


Figure 17: Seasonal current roses at 213 m depth at BR-3-14 as based on low-pass filtered data from bin cell #14 acquired with the LRADCP #18785. Roses point toward where the currents are going. Seasons are defined following the meteorological convention (Fall: October-December; Winter: January-March; Spring: April-June; Summer: July-September).

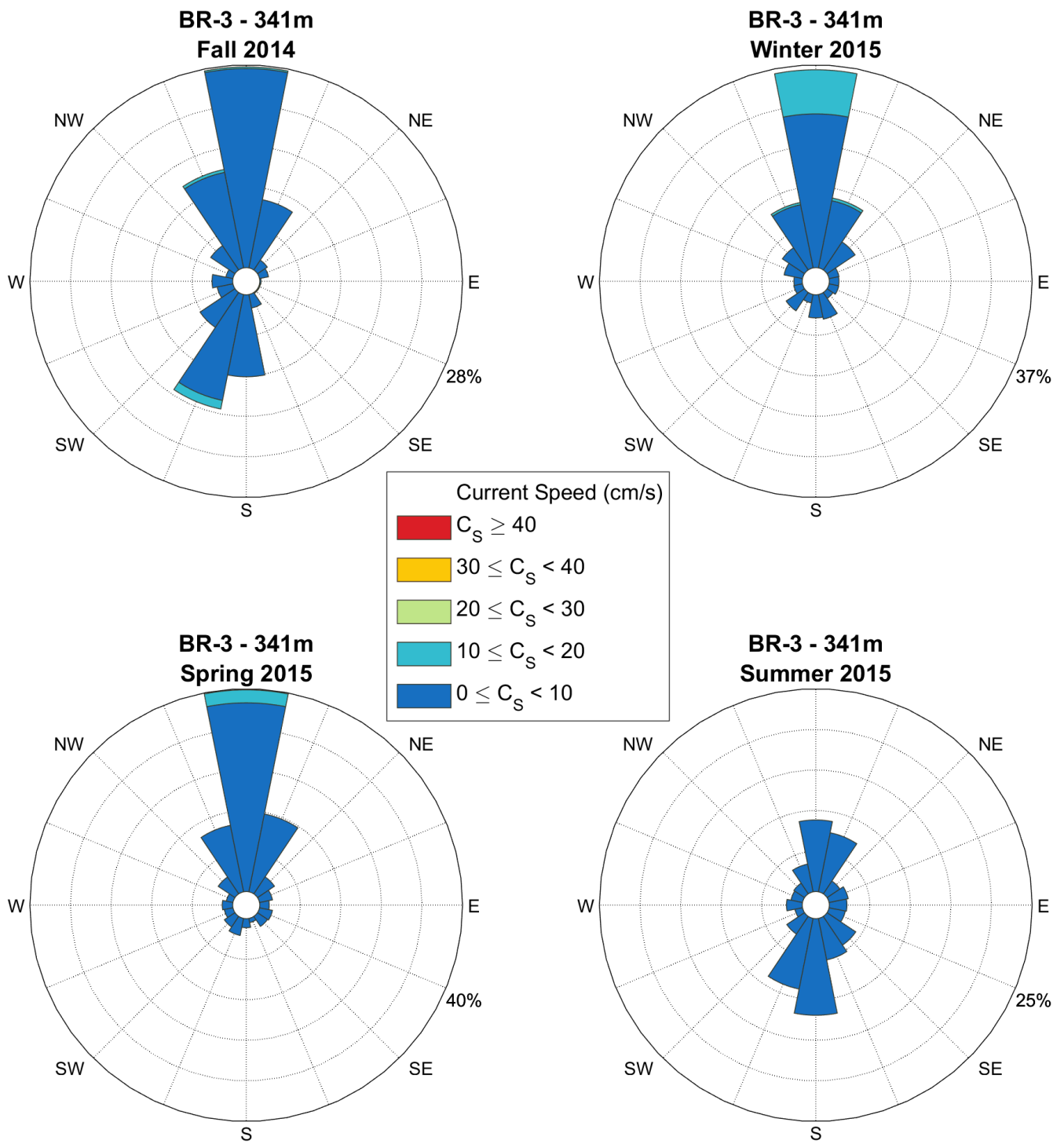


Figure 18: Seasonal current roses at 341 m depth at BR-3-14 as based on low-pass filtered data from bin cell #6 acquired with the LR ADCP #18785. Roses point toward where the currents are going. Seasons are defined following the meteorological convention (Fall: October-December; Winter: January-March; Spring: April-June; Summer: July-September).

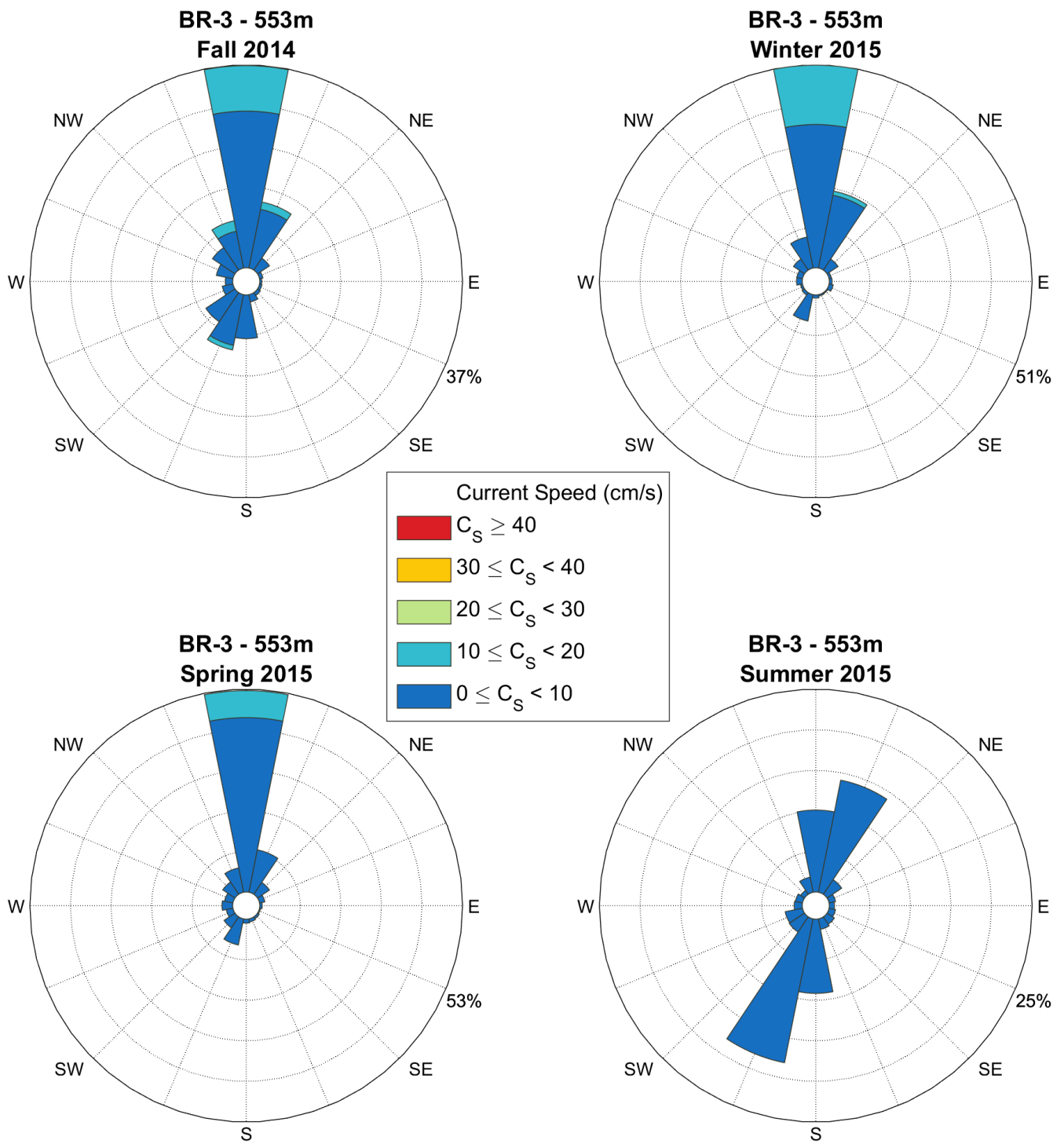


Figure 19: Seasonal current roses at 553 m depth at BR-3-14 as based on data acquired with the Aquadopp #8418. Roses point toward where the currents are going. Seasons are defined following the meteorological convention (Fall: October-December; Winter: January-March; Spring: April-June; Summer: July-September).

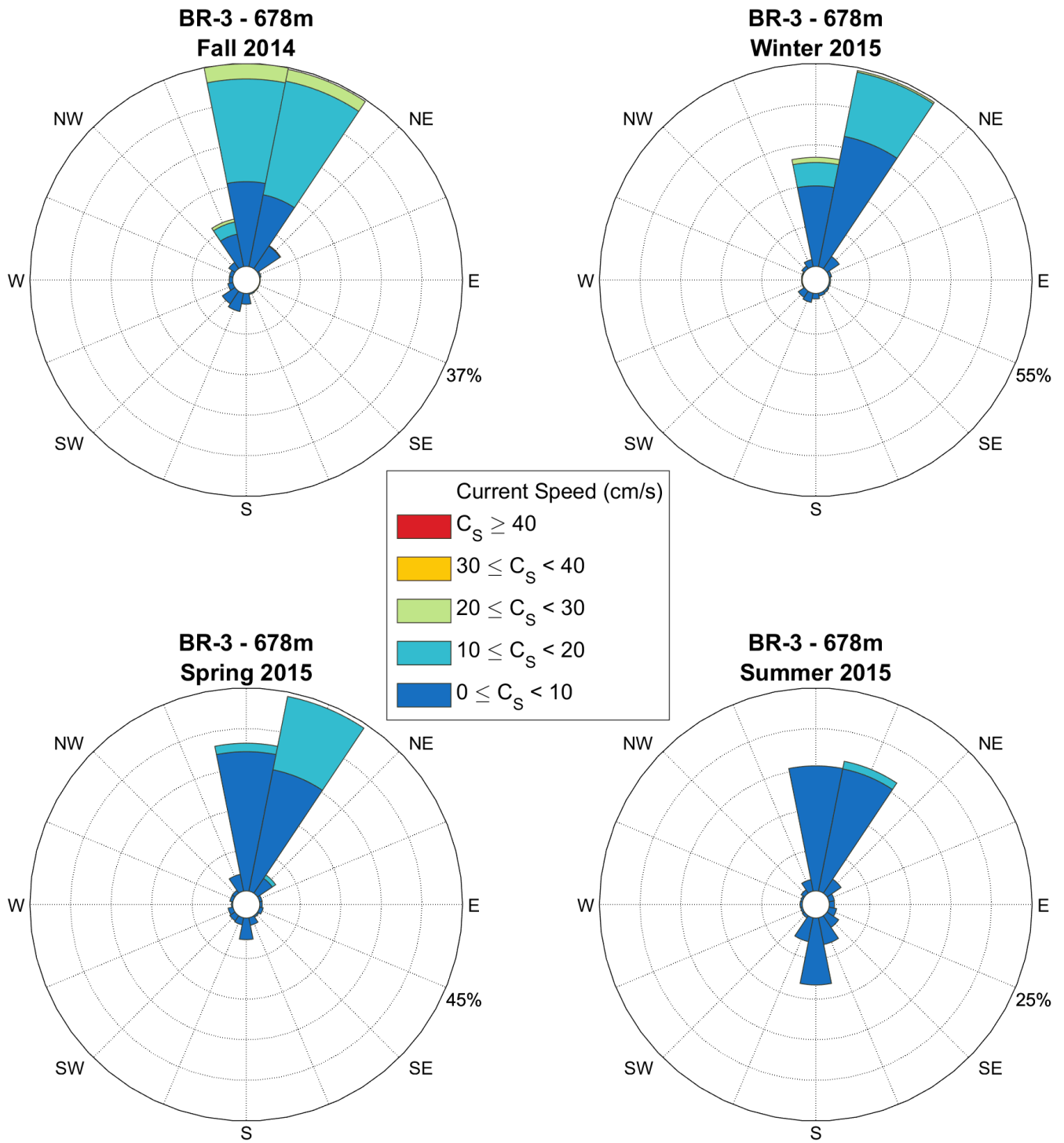


Figure 20: Seasonal current roses at 678 m depth at BR-3-14 as based on data acquired with the Aquadopp #2756. Roses point toward where the currents are going. Seasons are defined following the meteorological convention (Fall: October-December; Winter: January-March; Spring: April-June; Summer: July-September).

3.1.3 Mooring BR-G

Time-series plots of current speed, direction, and along-slope current component from the QM ADCP, LR ADCP and the two Aquadopp DW deployed at BR-G over 2014-2015 are provided in Figure 21 through Figure 24. The data in the QM and LR ADCP plots are filtered for bins with PG4+PG1 values less than 25%, bins affected by sidelobe interference and for error velocity thresholds as described in section 2.4.1. The first valid bin depth for the QM ADCP #8784 at BR-G-14 after removing sidelobe interference was 25.9 m (bin cell 20) with a percentage of valid data of 97.9% (Appendix E). Bin depths 113.9 and 121.9 m (bin cells 8 and 9) were affected by the presence of the upper Technicap sediment trap (as at BR-1), which resulted in reflection observed in the echo intensity (not shown) and a general decrease in current speed at these depths. Accordingly, bin cells 8 and 9 QM ADCP #8784 were manually flagged as part of the QA/QC and data from these bin depths should be treated carefully before being used in further analyses.

The LR ADCP #13079 did not show any sign of suspicious bins due to interference with other parts of the mooring (Figure 22). The first valid bin depth for this instrument was 43.1 m (bin cell 25) with a percentage of valid data of 47% (Appendix E). Data from this bin depth were of high quality and did not show any suspicious spikes in the speed or echo intensity. Partial data loss possibly linked to high intensity of ambient sound generated by sea ice at the surface was observed only briefly in spring and early summer 2015 (Figure 22). The deep Aquadopp current meters #9473 (585.3 m) and #9847 (692.5 m) provided complete time-series with a percentage of valid data return of 99.0% for each instrument (Figure 23, Figure 24 and Appendix E).

Mean current speeds at BR-G-14 ranged from 9 to 14 cm/s in the upper 200 m of the water column; and from 5 to 8 cm/s below 200 m (Table 11, Appendix E). Vector-averaged directions were typically to the southwest (200-245°TN) for all bins down to 187 m depth. Beginning at 203 m, currents veer progressively to the south, southeast and east until 427 m depth. Further down below in the water column, data from the deep Aquadopps at 585 and 692 m showed that the annually-averaged direction was to the northeast along the slope (37-42°TN). Maximum current speed at BR-G-14 was 92 cm/s on October 9, 2014 at 19.5 m depth. This maximum current speed at BR-G-14 occurred exactly 2 days after the maximum current speed recorded at BR-1 (see section 3.1.1). Strong current speeds (>60 cm/s) were generally detected over October 8-10, 2014 throughout the upper 100 m. Periods of stronger currents of ~50 cm/s were recorded near the surface over October 20-21, 2014. Within the 100-200 m water interval, strong currents were also recorded in late December 2014, early January 2015 and late February 2015 (e.g. Figure 21). The December-January event was associated with a sustained current direction to the southeast (across the slope toward the shelf) whereas the late February event was to the west (although current direction is marked by several reversals around this period). In the first half of April 2015, a large eddy-like feature was detected at BR-G between 50 and 250 m depth with rotating currents of 20-30 cm/s (Figure 22).

Seasonal current roses (low-pass filtered) for selected bin depths at mooring BR-1-14 are provided in Figure 25 through Figure 30. A seasonal pattern in current speed can be first identified with stronger near surface currents (26 m, Figure 25) in summer and fall and stronger subsurface currents (130 m, Figure 26) occurring in winter and spring under ice cover. Current direction is also variable on a monthly basis and strong current speeds (>40 cm/s) cannot be directly related to one particular direction at these depths. Below 200 m, currents are relatively weak and below 10 cm/s, although episodic increases in December 2014 and January 2015 were characterized by cross-slope currents approaching 30 cm/s around 200 m depth (Figure 22). Current speed and direction in the lowermost section of the water column (585 and 692 m, Figure 29 and Figure 30) were generally similar, although they were more uniformly to the east-northeast than at mid-depth (347 m, Figure 28) where no clear trend in the current direction can be identified.

BR-G; Quarter Master Broadband 153.6 kHz; 71.0021 N, 135.5094 W; 2014-2015; Instr. #8784; 190.0 m depth

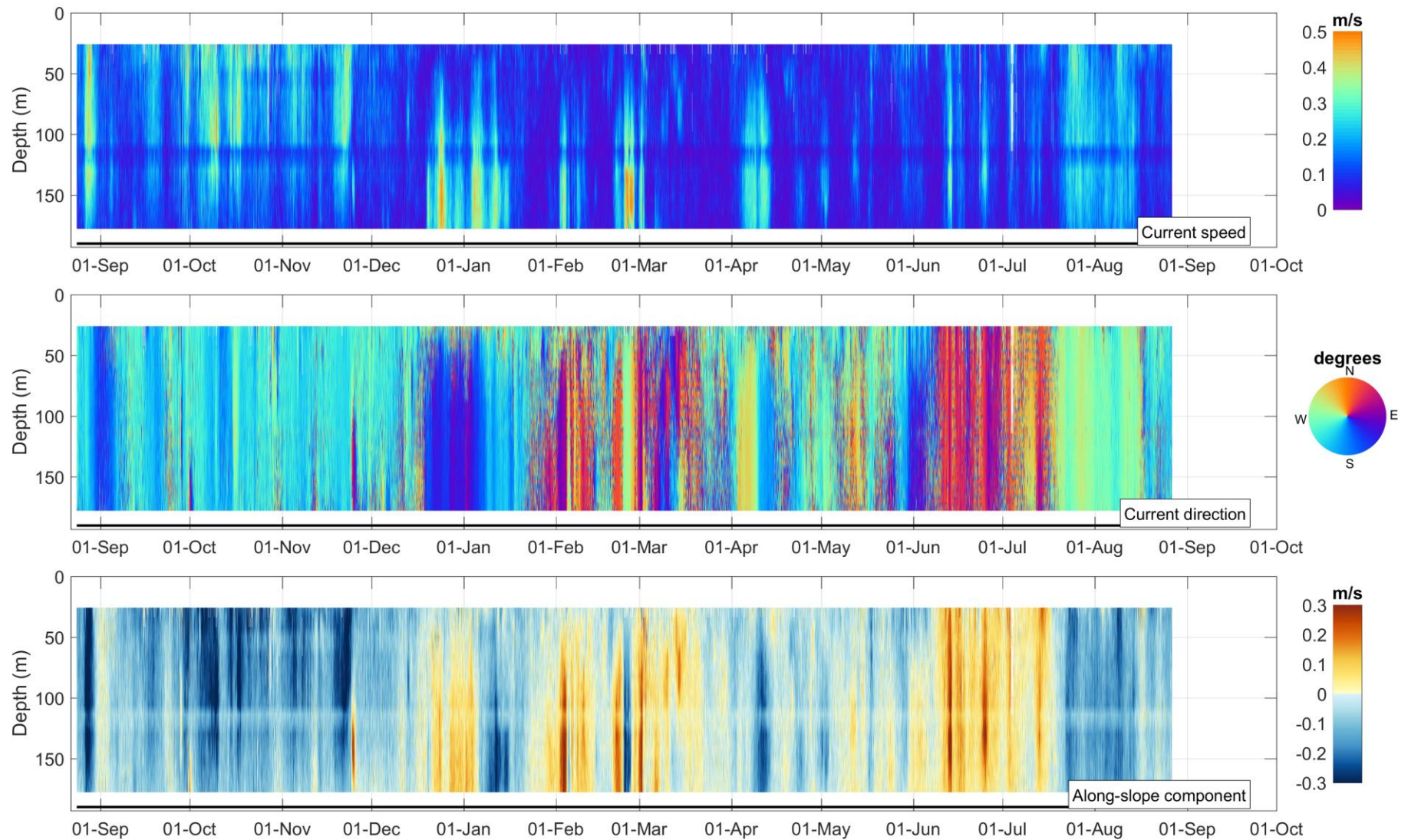


Figure 21: Time-series of current speed, current direction and along-slope current component at mooring BR-G-14 as obtained with the QM ADCP #8784. The black line depicts the instrument depth.

BR-G; Long Ranger Broadband 76.8 kHz; 71.0021 N, 135.5094 W; 2014-2015; Instr. #13079; 451.5 m depth

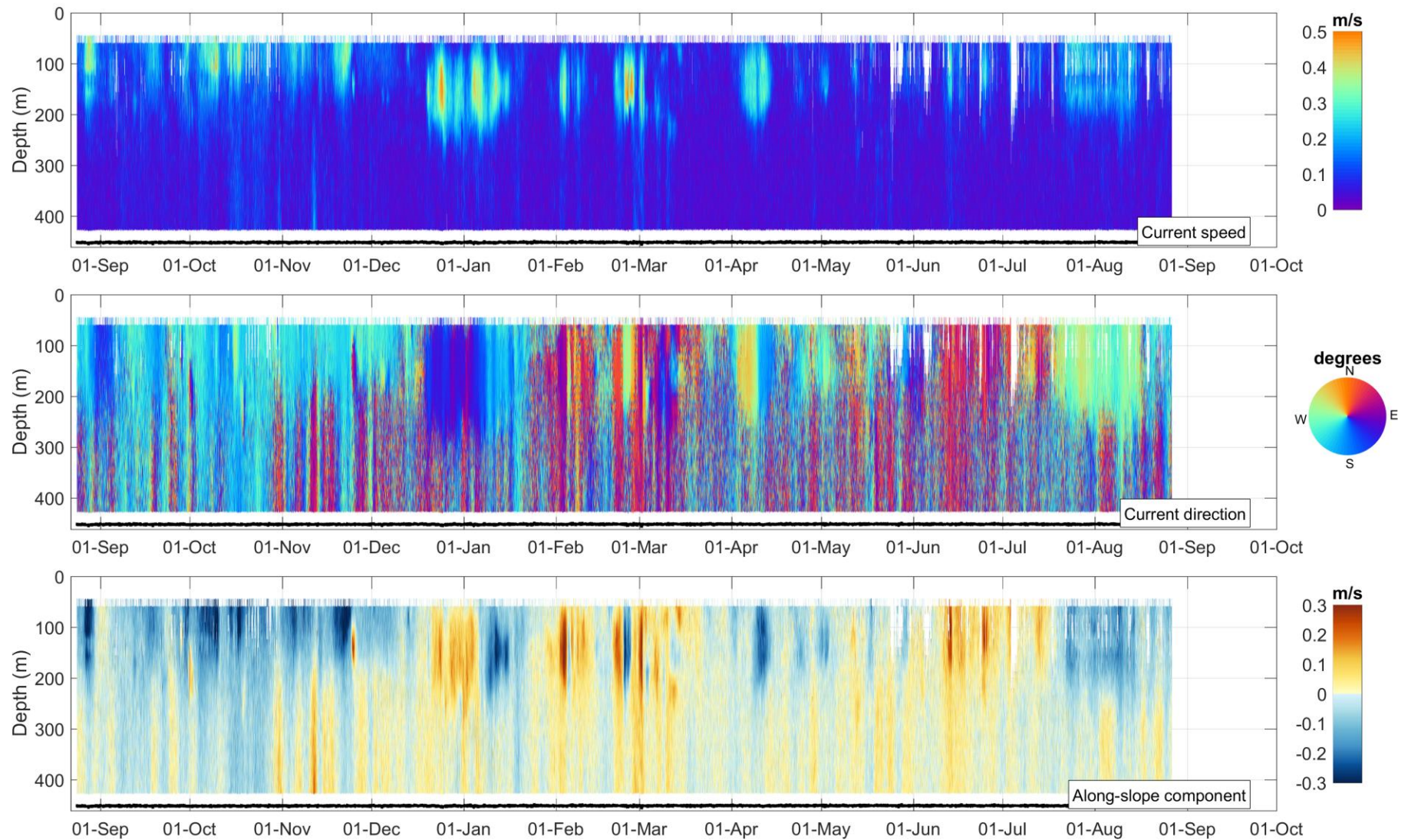


Figure 22: Time-series of current speed, current direction and along-slope current component at mooring BR-G-14 as obtained with the LR ADCP #13079. The black line depicts the instrument depth.

BR-G; Aquadopp DeepWater 2-MHz; 71.0021 N, 135.5094 W; 2014-2015; AQD. #AQD 9473; 585.3 m depth

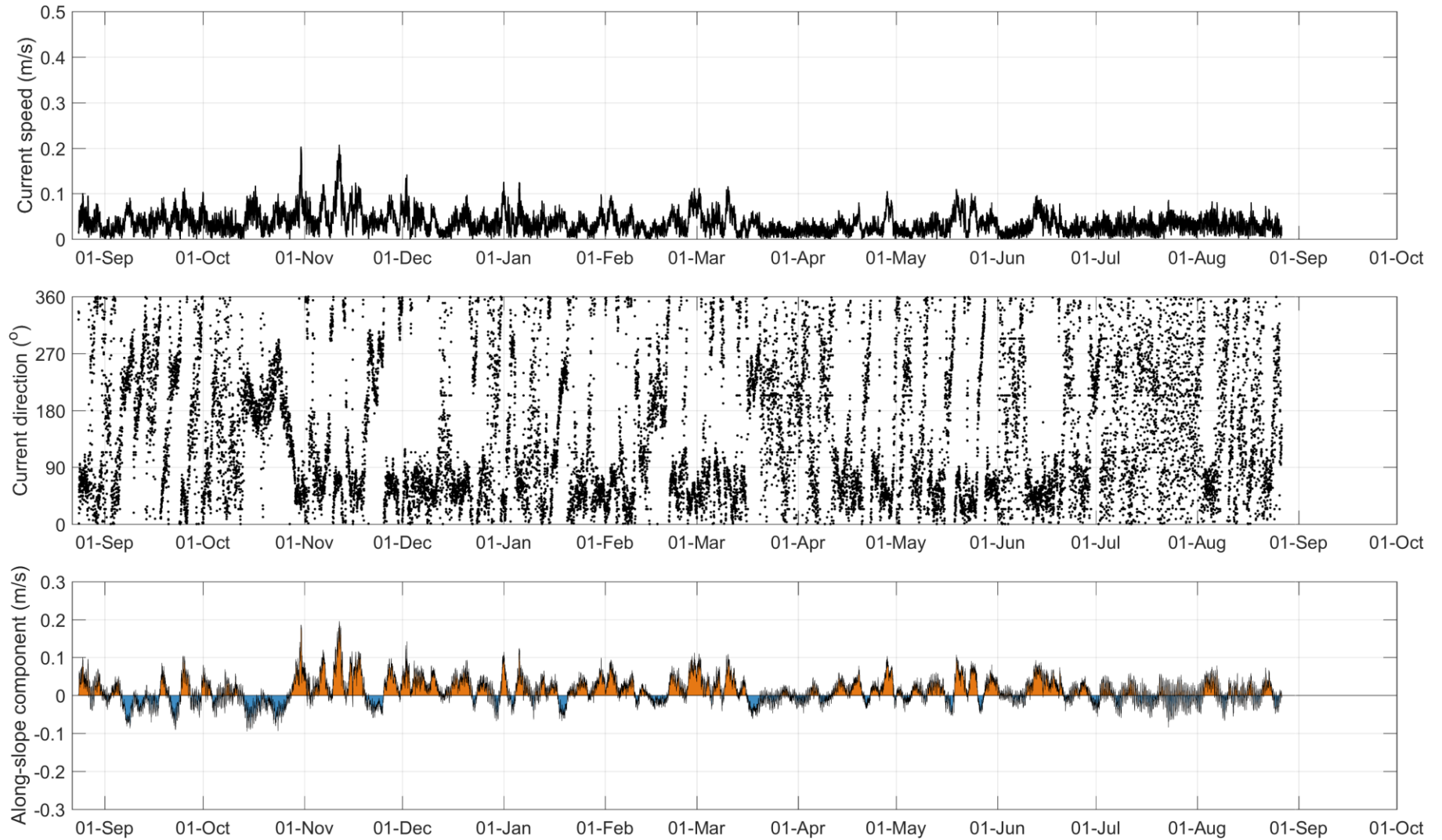


Figure 23: Time-series of current speed, current direction and along-slope current component at 585 m at mooring BR-G-14 as obtained with the Aquadopp #9473.

BR-G; Aquadopp DeepWater 2-MHz; 71.0021 N, 135.5094 W; 2014-2015; AQD. #AQD 9847; 692.5 m depth

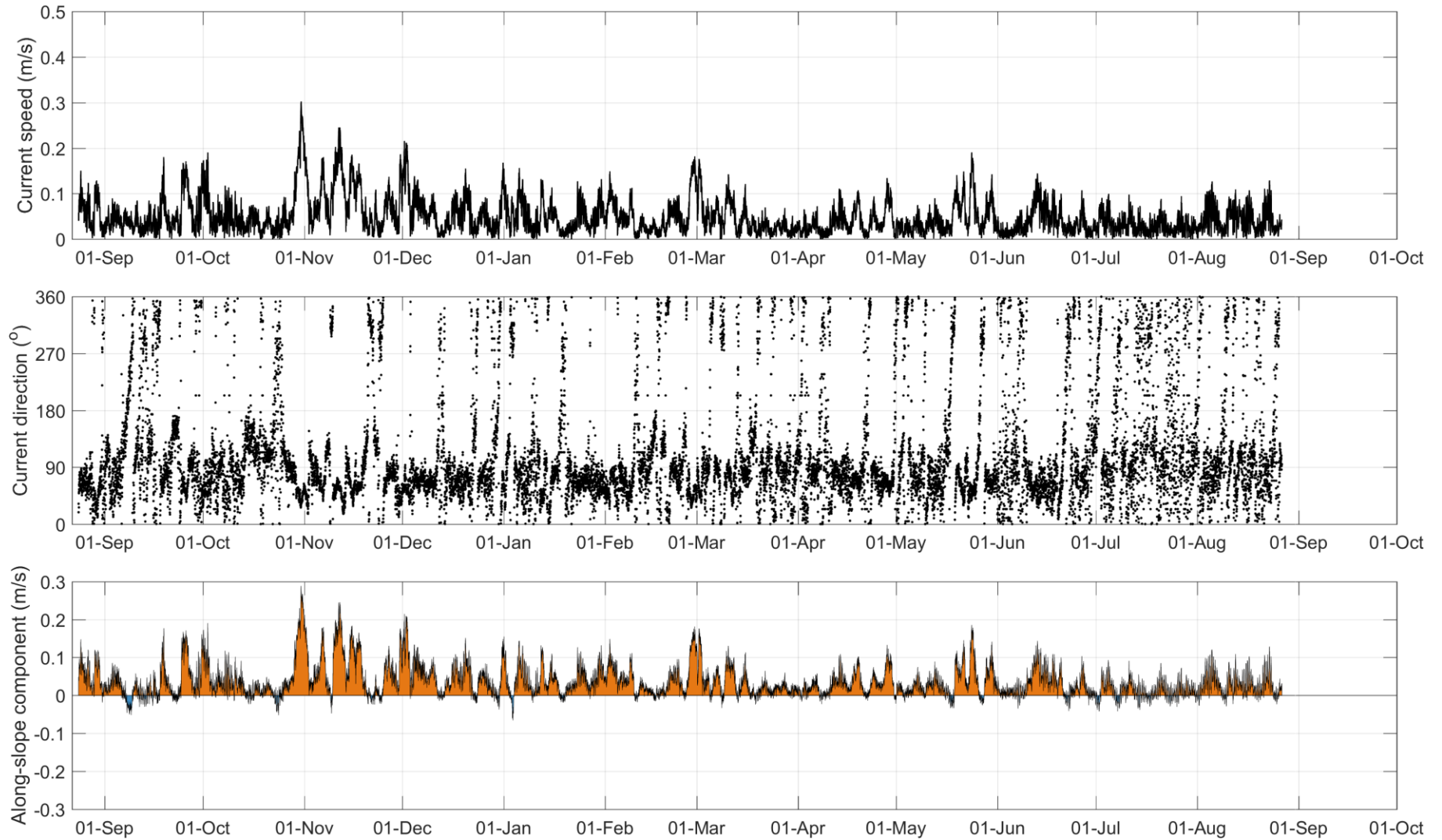


Figure 24: Time-series of current speed, current direction and along-slope current component at 693 m at mooring BR-G-14 as obtained with the Aquadopp #9847.

Table 11: Annual statistics of current speed and direction at BR-G-14 from selected bin depths representative of water mass variability in the Beaufort Sea (see Table 7 for water mass description).

Bin Depth (m)	Median Speed (m/s)	Mean Speed (m/s)	75%ile Speed (m/s)	95%ile Speed (m/s)	99%ile Speed (m/s)	Max Speed (m/s)	Standard Deviation Speed (m/s)	Vector-Averaged Direction (deg TN)
25.9	0.11	0.13	0.18	0.30	0.39	0.92	0.09	245.9
129.9	0.12	0.14	0.19	0.32	0.41	0.55	0.09	230.6
219.1	0.06	0.08	0.10	0.18	0.25	0.35	0.05	182.8
347.1	0.05	0.05	0.07	0.10	0.14	0.21	0.03	128.9
585.3	0.03	0.04	0.05	0.08	0.11	0.21	0.02	37.3
692.5	0.04	0.05	0.07	0.13	0.18	0.30	0.04	42.6

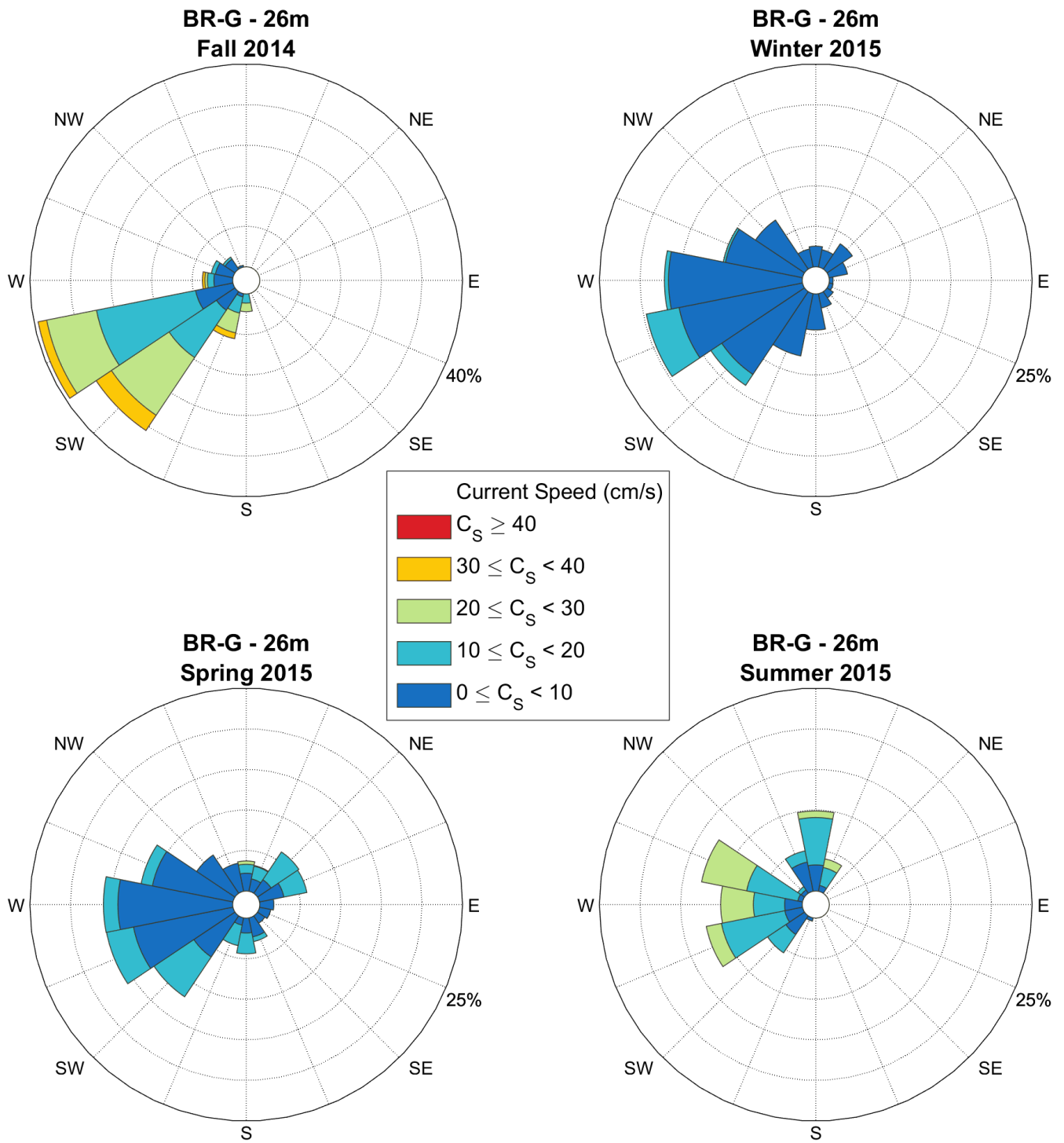


Figure 25: Seasonal current roses at 26 m depth at BR-G-14 as based on low-pass filtered data from bin cell #20 acquired with the QM ADCP #8784. Roses point toward where the currents are going. Seasons are defined following the meteorological convention (Fall: October-December; Winter: January-March; Spring: April-June; Summer: July-September).

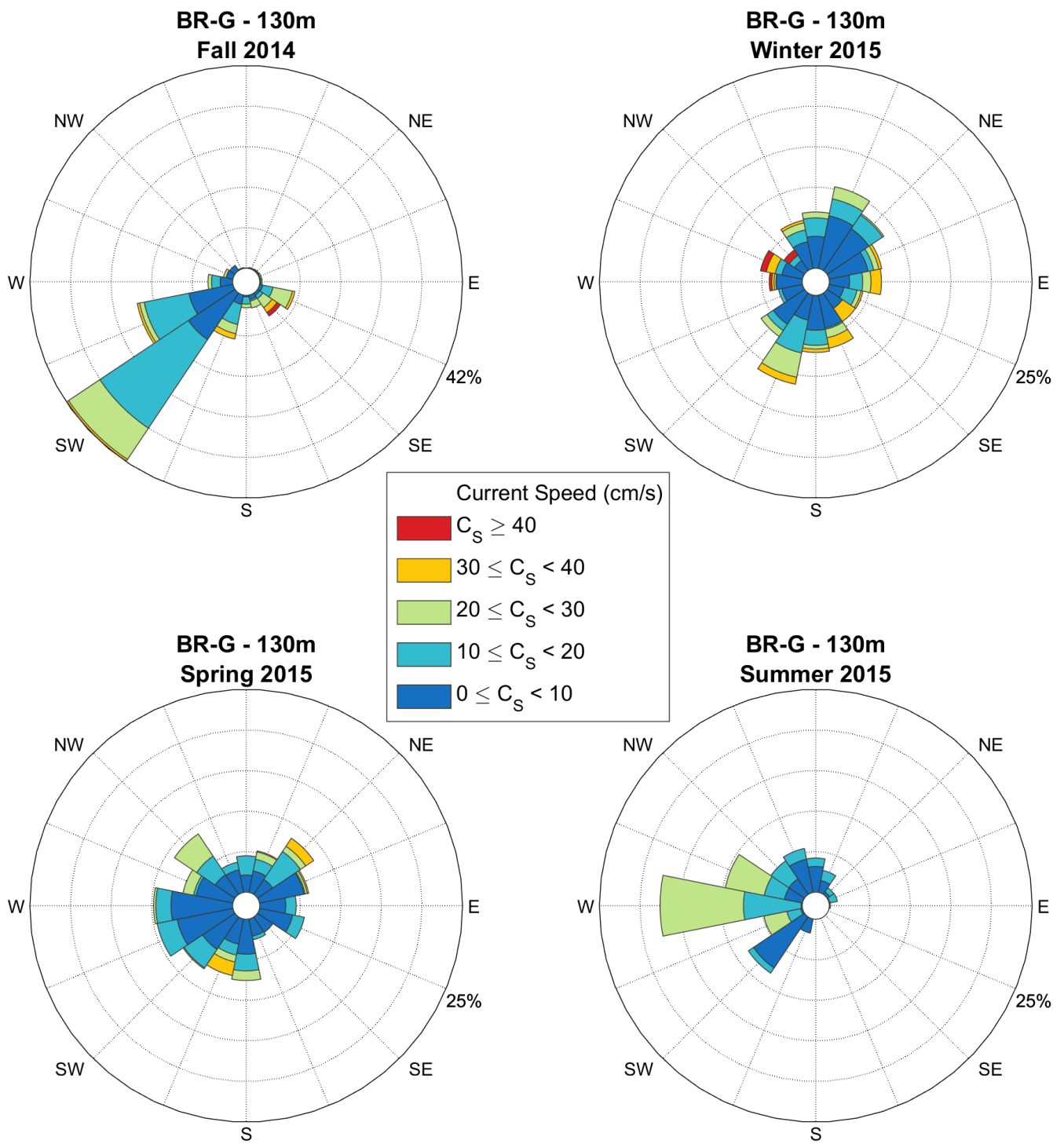


Figure 26: Seasonal current roses at 130 m depth at BR-G-14 as based on low-pass filtered data from bin cell #7 acquired with the QM ADCP #8784. Roses point toward where the currents are going. Seasons are defined following the meteorological convention (Fall: October-December; Winter: January-March; Spring: April-June; Summer: July-September).

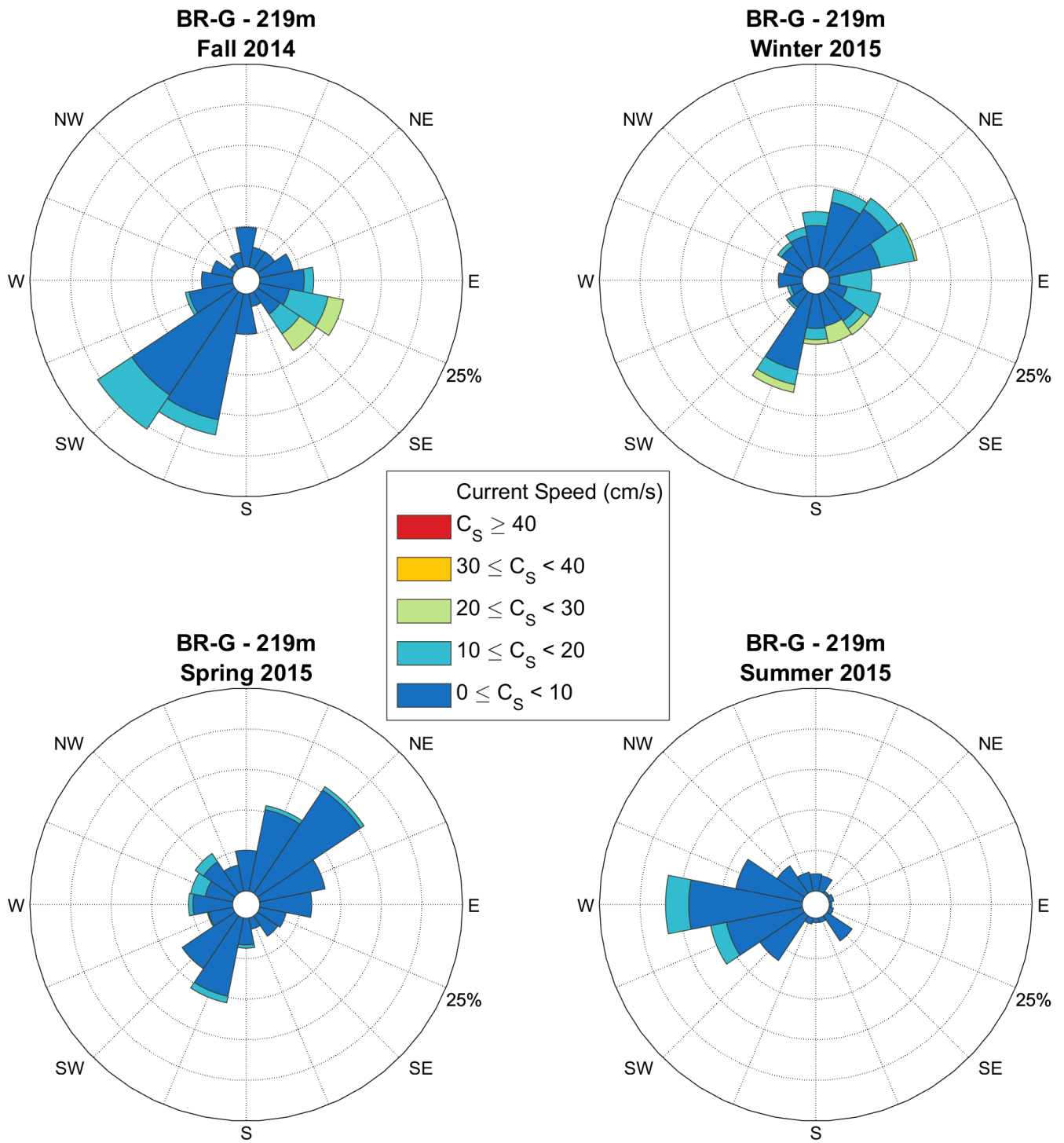


Figure 27: Seasonal current roses at 219 m depth at BR-G-14 as based on low-pass filtered data from bin cell #14 acquired with the LR ADCP #13079.

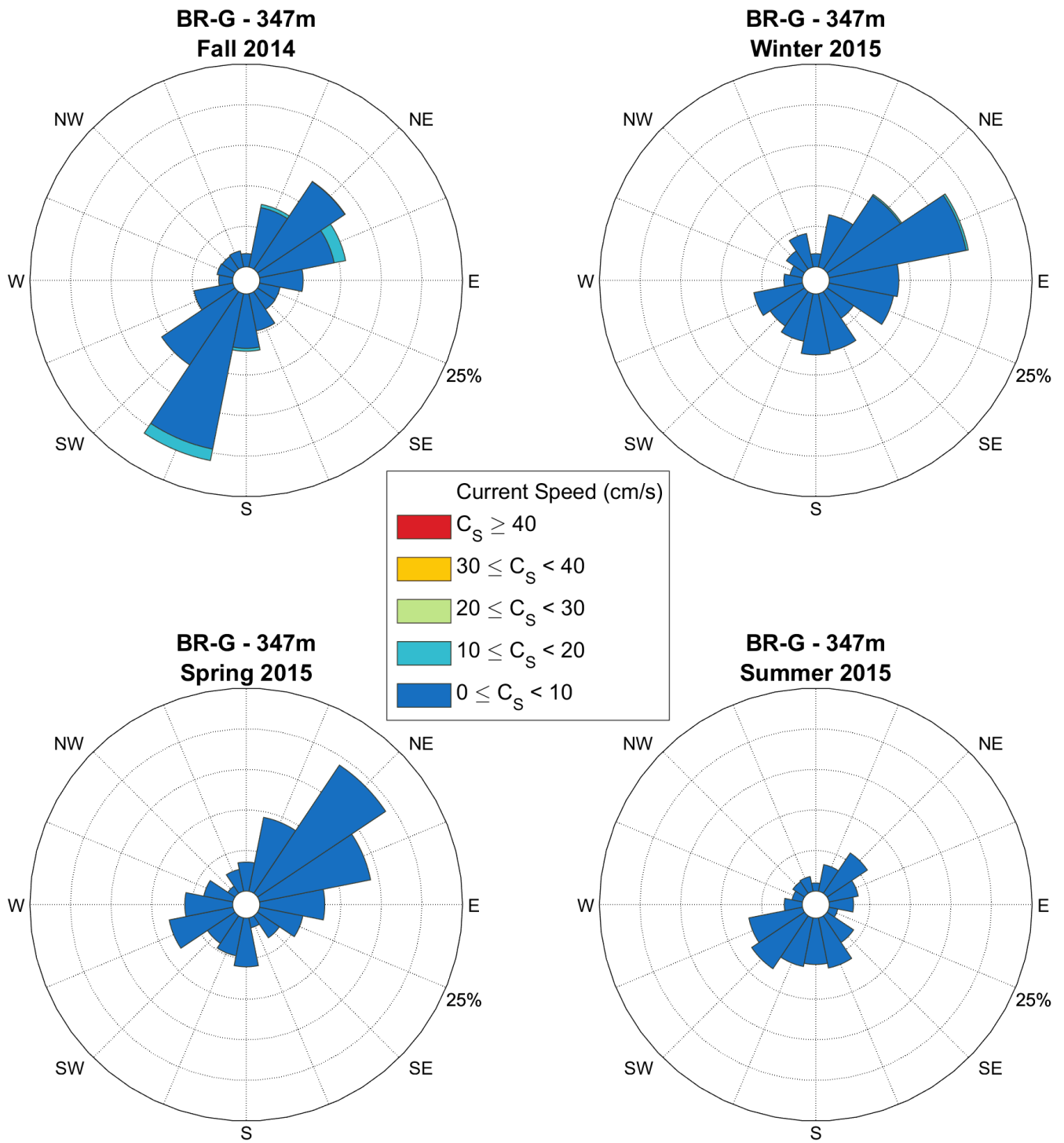


Figure 28: Seasonal current roses at 347 m depth at BR-G-14 as based on low-pass filtered data from bin cell #6 acquired with the LR ADCP #13079. Roses point toward where the currents are going. Seasons are defined following the meteorological convention (Fall: October-December; Winter: January-March; Spring: April-June; Summer: July-September).

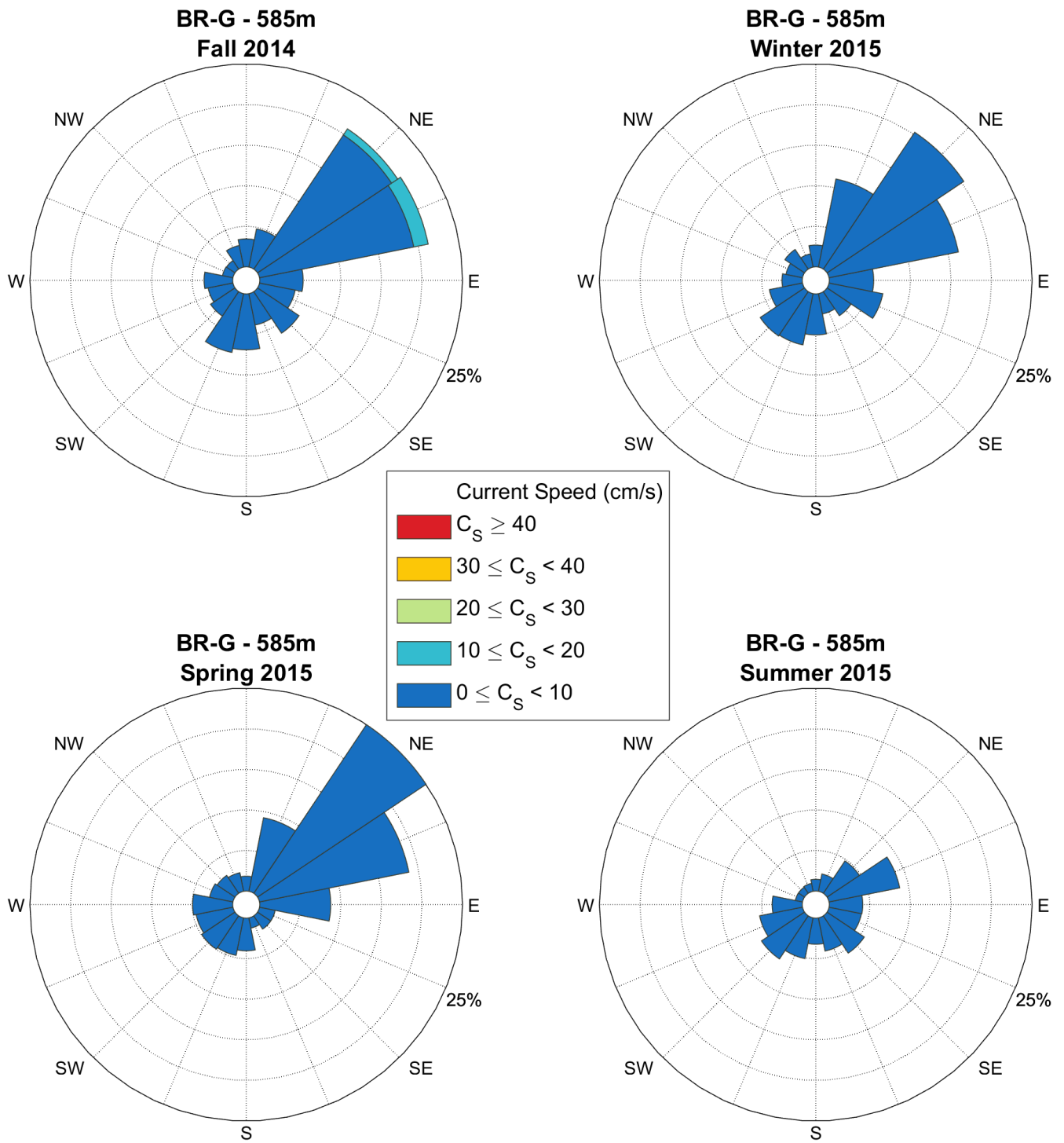


Figure 29: Seasonal current roses at 585 m depth at BR-G-14 as based on data acquired with the Aquadopp #9473. Roses point toward where the currents are going. Seasons are defined following the meteorological convention (Fall: October-December; Winter: January-March; Spring: April-June; Summer: July-September).

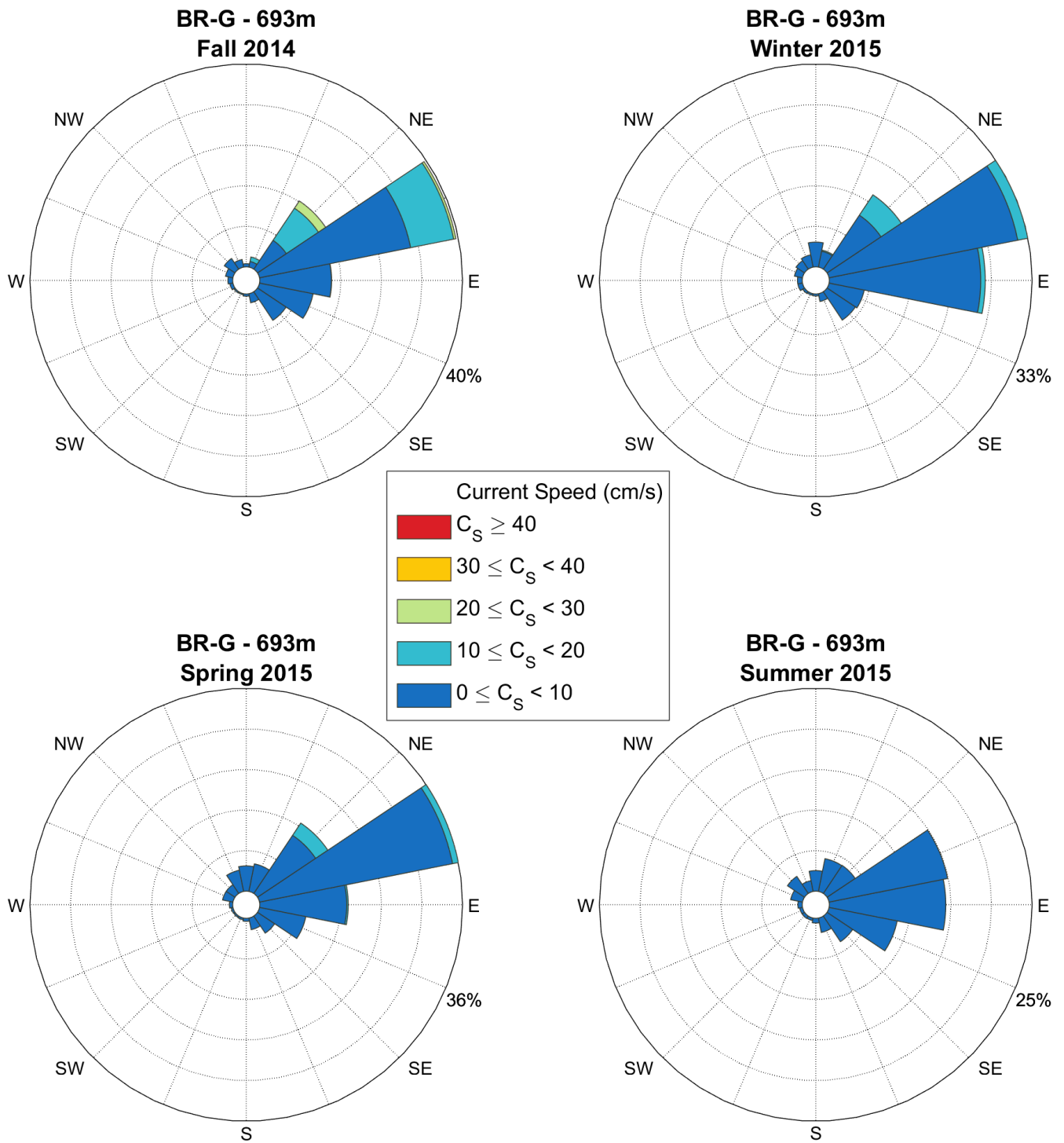


Figure 30: Seasonal current roses at 693 m depth at BR-G-14 as based on data acquired with the Aquadopp #9847. Roses point toward where the currents are going. Seasons are defined following the meteorological convention (Fall: October-December; Winter: January-March; Spring: April-June; Summer: July-September).

3.1.4 Mooring BR-K

Time-series plots of current speed, direction, and along-slope current component from the WHS ADCP and the Aquadopp Profiler deployed at the upper slope mooring BR-K over 2014-2015 are provided in Figure 31 through Figure 32. The data in the WHS ADCP plot are filtered for bins with PG4+PG1 values less than 25%, bins affected by sidelobe interference and for error velocity thresholds as described in section 2.4.1. The first valid bin depth for the WHS ADCP #2646 at BR-K-14 after removing sidelobe interference was 22.2 m (bin cell 14) with a percentage of valid data of 85.7% (Appendix E). Percentage of valid data below the uppermost valid bin depth ranged from 96.8 to 99.7%. No bin depth was manually flagged due to possible interference with other parts of the mooring for this instrument as part of the QA/QC procedure.

The down-looking Aquadopp Profiler #11147 at BR-K-14 provided a complete annual dataset of bottom currents on the upper slope (Figure 32), although a suspicious bin cell at 142.4 m depth (bin cell 2) was manually flagged as part of the QA/QC process (Appendix E). This bin depth was likely affected by the presence of the acoustic release tandem kit located approximately 2 m below the Aquadopp, which resulted in reflection observed in the echo intensity and suspicious current direction at this depth (Figure 32). The data from other bin depths down to the bottom were of high quality with a percentage of valid data of 99.5% for all bin cells.

Mean current speeds at BR-K-14 ranged from 12 to 16 cm/s throughout the water column (Appendix E, Table 12, which represents the strongest ensemble of mean currents recorded throughout the 7 iBO moorings over 2014-2015. Vector-averaged directions were uniformly to the west-southwest (256-271°TN) from 22 to 46 m depth. Between 54 and 78 m, a rapid transition from a westward current to a northward current and eventually a north-eastward current can be identified in the mean vectors (Appendix E). From 86 m (the approximative depth of the shelf break) down to the bottom (153 m), currents are uniformly to the northeast along the slope.

Maximum current speed at BR-K-14 was 84 cm/s on October 29, 2014 as recorded at 38 m depth. Numerous relatively strong current speed events (>50 cm/s) were recorded at BR-K in the fall of 2014 and at other occasions from winter to summer 2015. Most of the strong current speeds during the fall of 2014 were typically surface-intensified while the other events were depth-intensified with stronger speeds around 80-100 m (Figure 31). The strongest current speed that was recorded near the bottom at BR-K was 54 cm/s on October 11, 2014, similarly to other slope moorings that recorded strong currents around this date (see section 3.1.1 to 3.1.3). Another strong event of 45 cm/s was detected on March 2, 2015 just above the seafloor at the same time as an along-slope current pulse appeared to have propagated to the northeast.

Seasonal current roses (low-pass filtered) for selected bin depths at mooring BR-K-14 are provided in Figure 33 and Figure 34. The differences in the most frequent current directions between the upper (22 m) and lower bin depths (126 m) at this location demonstrates the existence of a narrow and steady north-eastward current along the upper slope up to the shelf break depth (i.e. consistent with the presence of a shelfbreak jet propagating to the northeast on average, see section 1.2). In particular, please note the maximum frequency percentage of occurrence associated with each monthly current rose at 126 m, which is around 60% (Figure 34). This provides evidence that the most unidirectional currents recorded throughout the 7 iBO moorings were recorded in the lower portion of the water column at BR-K. By contrast, current directions are much more variable in the upper water column above the depth of the shelf break (Figure 33), although they also generally follow the along-slope geographical axis.

BR-K; WorkHorse Sentinel Broadband 307.2 kHz; 70.8624 N, 135.0199 W; 2014-2015; Instr. #2646; 136.1 m depth

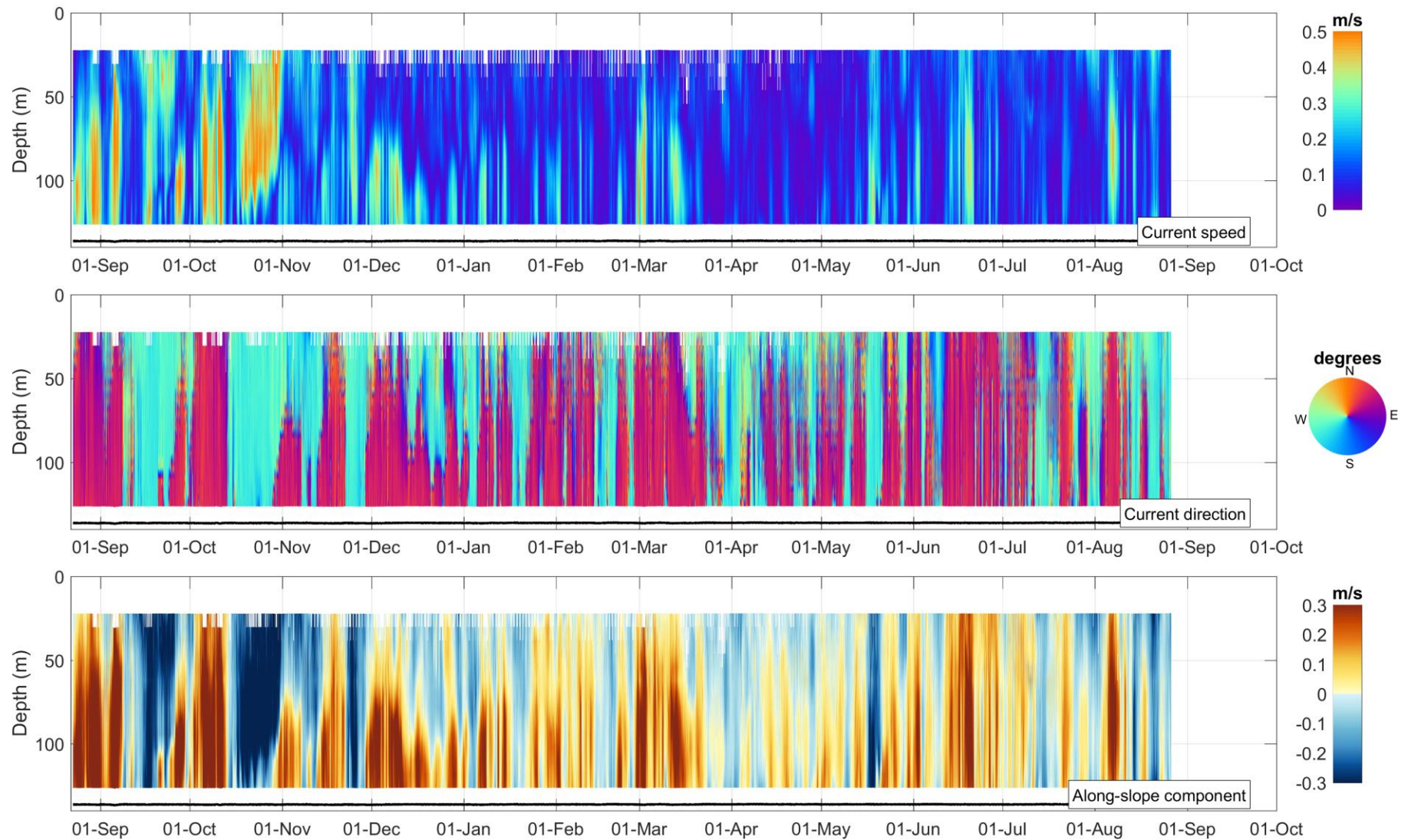


Figure 31: Time-series of current speed, current direction and along-slope current component at mooring BR-K-14 as obtained with the WHS ADCP #2646. The black line depicts the instrument depth.

BR-K; Aquadopp Profiler 1-MHz; 70.8624 N, 135.0199 W; 2014-2015; AQD. #AQD11147; 140.0 m depth

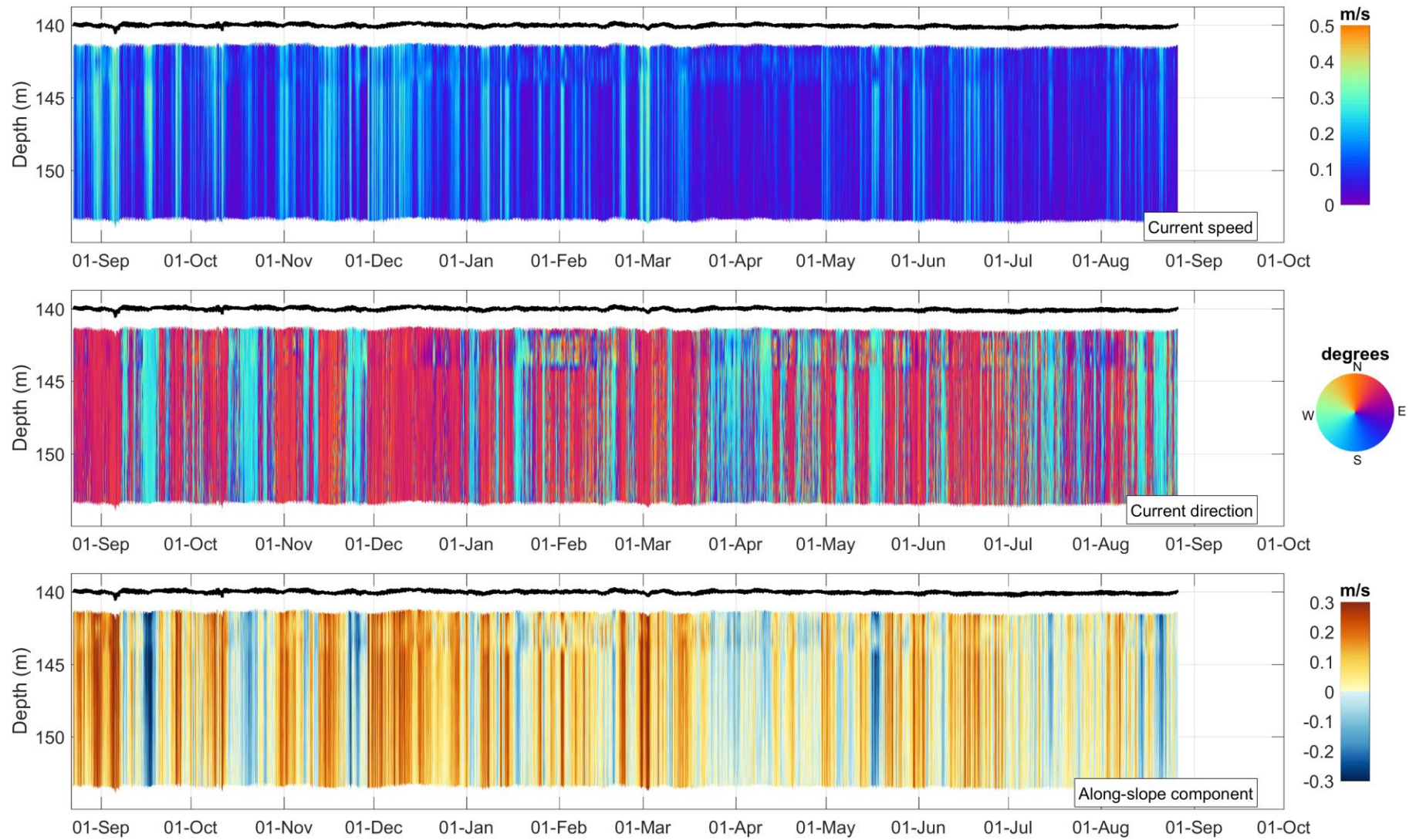


Figure 32: Time-series of current speed, current direction and along-slope current component at 140 m at mooring BR-K-14 as obtained with the Aquadopp Profiler #11147.

Table 12: Annual statistics of current speed and direction at BR-K-14 from selected bin depths representative of water mass variability in the Beaufort Sea (see Table 7 for water mass description).

Bin Depth (m)	Median Speed (m/s)	Mean Speed (m/s)	75%ile Speed (m/s)	95%ile Speed (m/s)	99%ile Speed (m/s)	Max Speed (m/s)	Standard Deviation Speed (m/s)	Vector-Averaged Direction (deg TN)
22.2	0.10	0.12	0.17	0.30	0.43	0.71	0.09	256.2
126.2	0.12	0.14	0.20	0.34	0.43	0.69	0.10	38.8

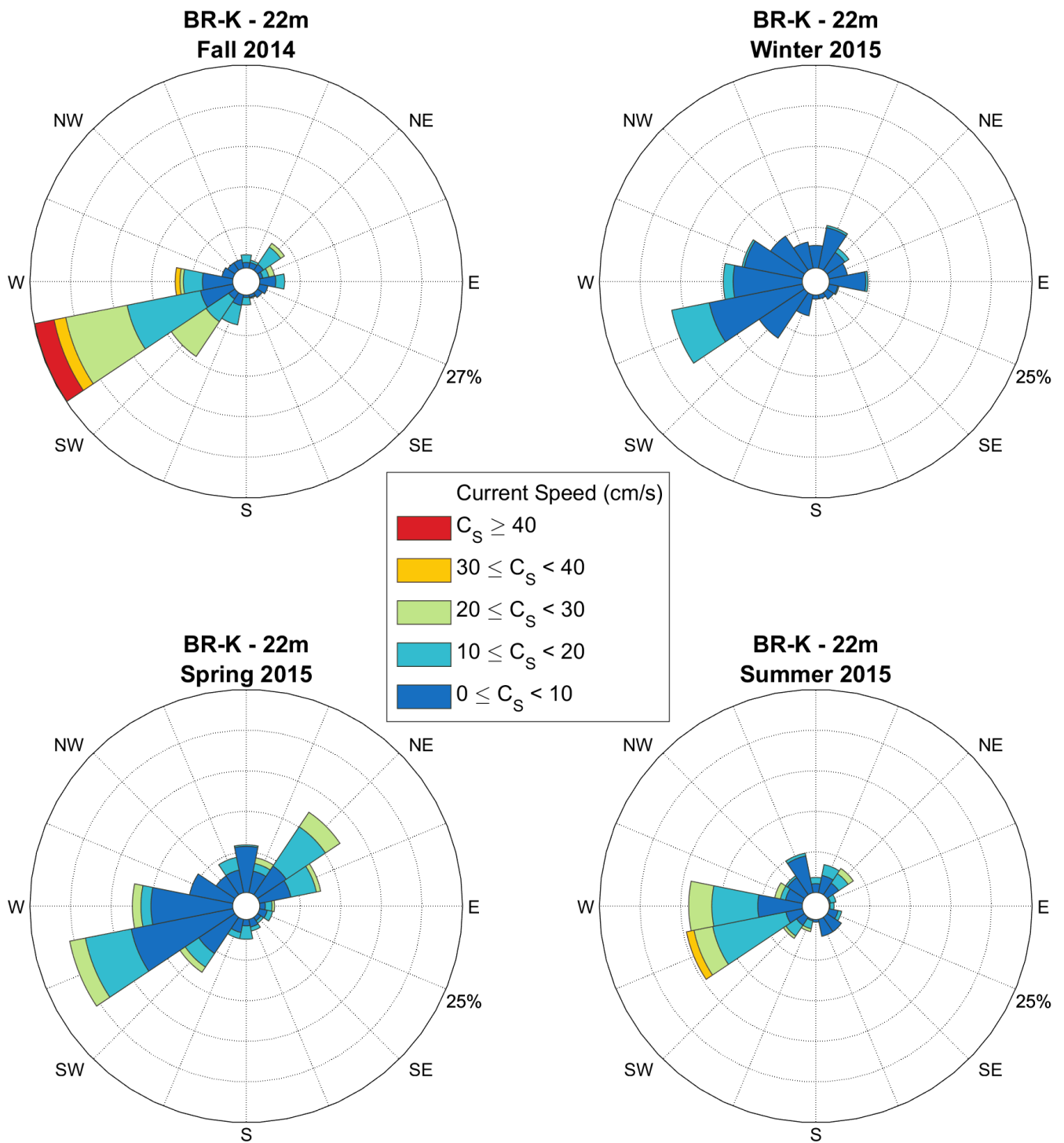


Figure 33: Seasonal current roses at 22 m depth at BR-K-14 as based on low-pass filtered data from bin cell #14 acquired with the WHS ADCP #2646. Roses point toward where the currents are going. Seasons are defined following the meteorological convention (Fall: October-December; Winter: January-March; Spring: April-June; Summer: July-September).

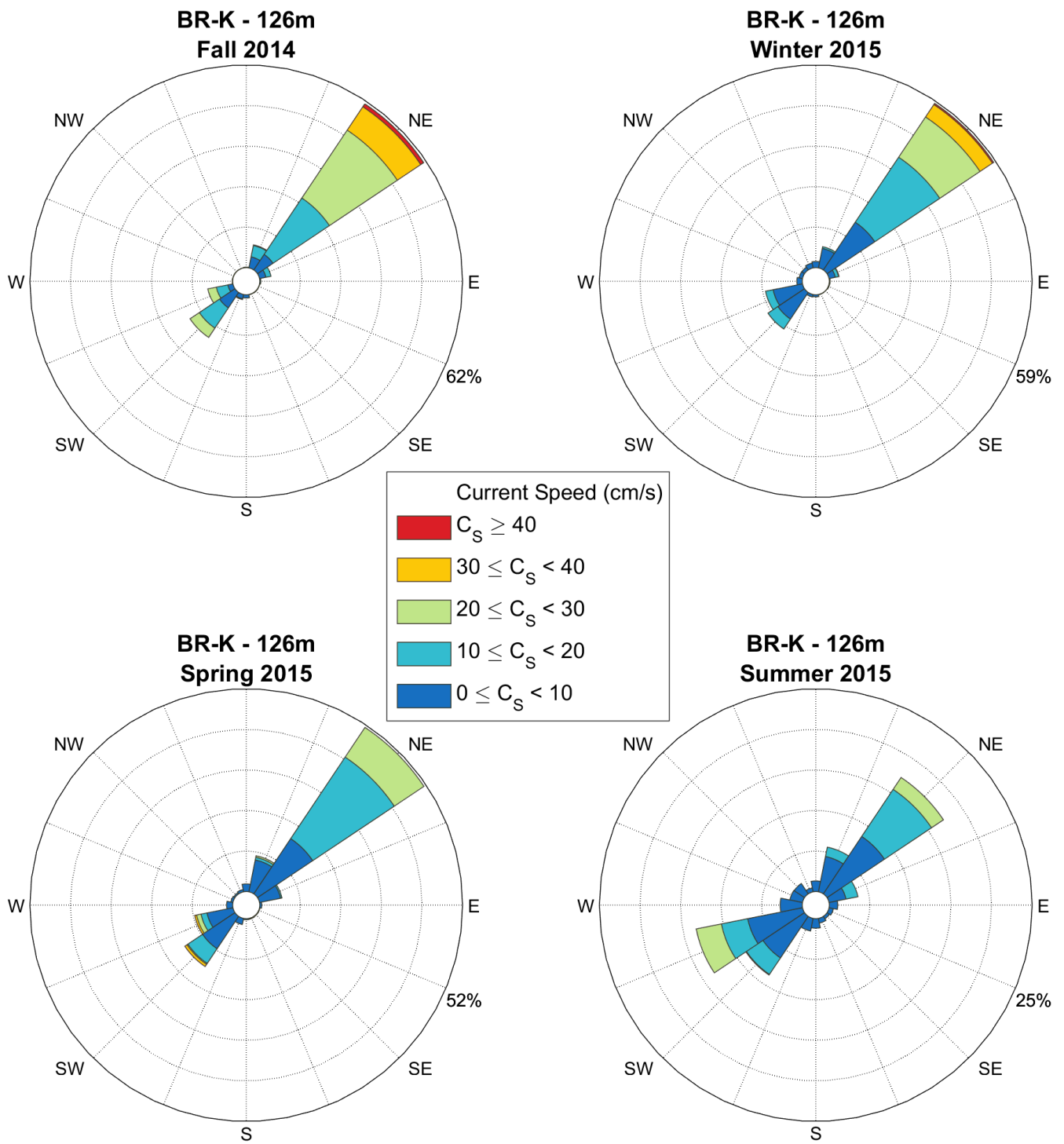


Figure 34: Seasonal current roses at 126 m depth at BR-K-14 as based on low-pass filtered data from bin cell #1 acquired with the WHS ADCP #2646. Roses point toward where the currents are going. Seasons are defined following the meteorological convention (Fall: October-December; Winter: January-March; Spring: April-June; Summer: July-September).

3.1.5 Mooring DFO-2

A time-series plot of current speed, direction, and along-slope current component from the NB ADCP deployed at the outer shelf mooring DFO-2 over 2014-2015 is provided in Figure 35. The data in the NB ADCP plot are filtered for bins with PG4 values less than 25%, bins affected by sidelobe interference and for error velocity thresholds and other masks as described in section 2.4.1. The first valid bin depth for the NB ADCP #586 at DFO-2-14 after removing sidelobe interference was 20.0 m (bin cell 22) with a percentage of valid data of 91.0% (Appendix E). Percentage of valid data below the uppermost valid bin depth ranged from 97.5 to 100.0%. No bin depth was manually flagged for this instrument as part of the QA/QC procedure.

Mean current speeds at DFO-2-14 ranged from 7 to 12 cm/s throughout the water column, with the stronger mean currents typically near the surface (Appendix E, Table 13). Similarly to the pattern observed at BR-K-14, vector-averaged directions were uniformly to the southwest ($246\text{-}254^\circ\text{TN}$) from 20 to 74.8 m depth, followed by a rapid shift to the northeast at the lower bin depths. In the case of DFO-2-14, the transition between the southwest and northeast mean currents is very sharp and takes place within a 4-m water interval only. Already at 78.7 m, the mean current had veered to the northeast (45°TN) and remains steadily in this direction ($49\text{-}54^\circ\text{TN}$) until the lowermost bin depth located 10 m above the bottom (102 m water depth).

Maximum current speed at DFO-2-14 was 76 cm/s on October 26, 2014 as recorded from 32 to 40 m depth (Appendix E). This strong current speed event is part of the general increase in current speed observed at DFO-2-14 over October 2014. This period was characterized by strong negative along-shelf current component (to the southwest) throughout the water column (Figure 35). A similarly strong current event to the southwest was also detected in late September 2015. Both events that occurred in open water were typified by a surface-intensified flow. Depth-intensified flow was recorded at times at DFO-2-14, such as on March 3, 2015 at midnight UTC when a marked, but relatively quick, increase in the along-slope component (~ 40 cm/s, to the northeast) was recorded. This event is consistent with similar north-eastward-directed current pulses recorded at depth a few hours earlier on March 2 at both moorings BR-K and BR-G (Figure 21 and Figure 31).

Seasonal current roses (low-pass filtered) for selected bin depths at mooring DFO-2-14 are provided in Figure 36 and Figure 37. The differences in the most frequent current directions between the upper (20 m) and lower bin depths (102 m) at this location further illustrates the general circulation pattern at the outer shelf/upper slope that is characterized by south-westward currents near the surface and north-eastward currents at depth. The current roses at 102 m at DFO-2-14 were however not as narrow and unidirectionally-directed as at BR-K-14 where the shelfbreak jet steered by the bottom topography of the upper slope is centered. At DFO-2, it is possible to surmise that the subsurface circulation is looser and less trapped to the bottom due to the gentler slope topography at this site when compared to BR-K, thus less prone to the generation of a jet. As a result, current speed is also less intense near the bottom at DFO-2 than at BR-K.

DFO-2; NB ADCP 300kHz; 70.9893 N, 133.7439 W; 2014-2015; Instr. #586; 108 m depth

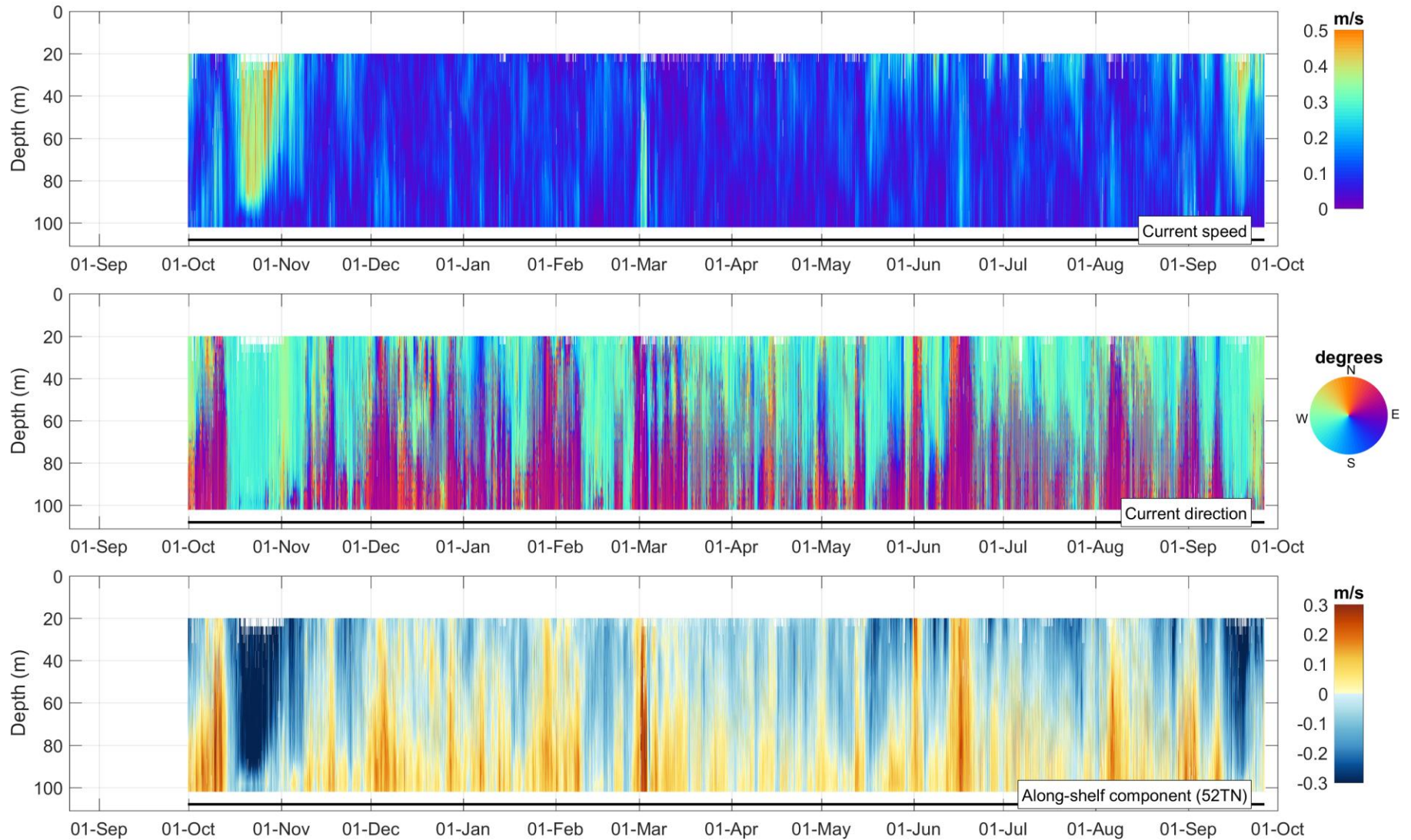


Figure 35: Time-series of current speed, current direction and along-slope current component at mooring DFO-2-14 as obtained with the NB ADCP #586. The black line depicts the instrument depth.

Table 13: Annual statistics of current speed and direction at DFO-2-14 from selected bin depths representative of water mass variability in the Beaufort Sea (see Table 7 for water mass description).

Bin Depth (m)	Median Speed (m/s)	Mean Speed (m/s)	75%ile Speed (m/s)	95%ile Speed (m/s)	99%ile Speed (m/s)	Max Speed (m/s)	Standard Deviation Speed (m/s)	Vector-Averaged Direction (deg TN)
20.0	0.10	0.12	0.17	0.30	0.39	0.56	0.09	253.71
102.1	0.06	0.07	0.10	0.17	0.22	0.41	0.05	49.85

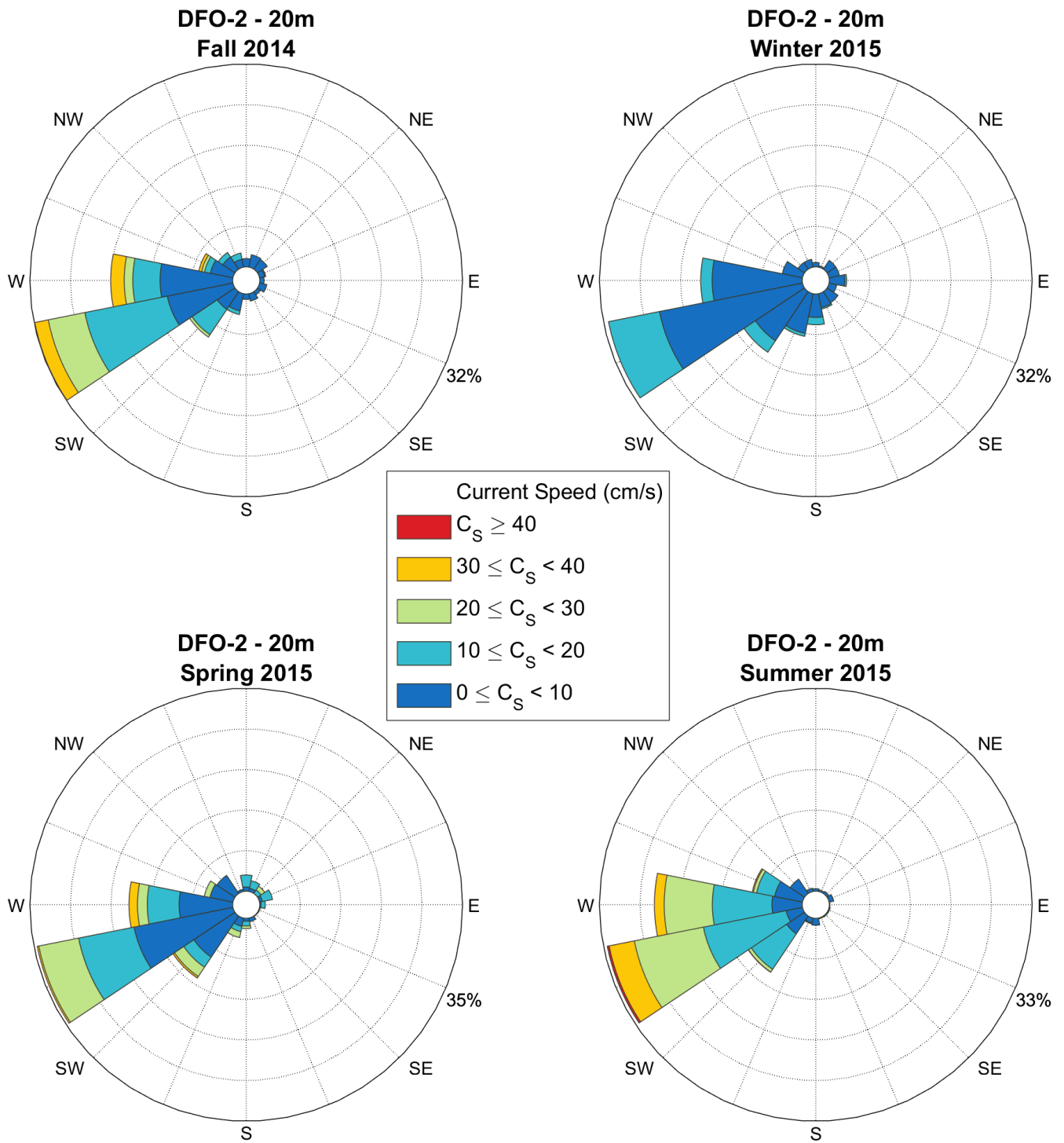


Figure 36: Seasonal current roses at 20 m depth at DFO-2-14 as based on low-pass filtered data from bin cell #21 acquired with the SC-ADCP #586. Roses point toward where the currents are going. Seasons are defined following the meteorological convention (Fall: October-December; Winter: January-March; Spring: April-June; Summer: July-September).

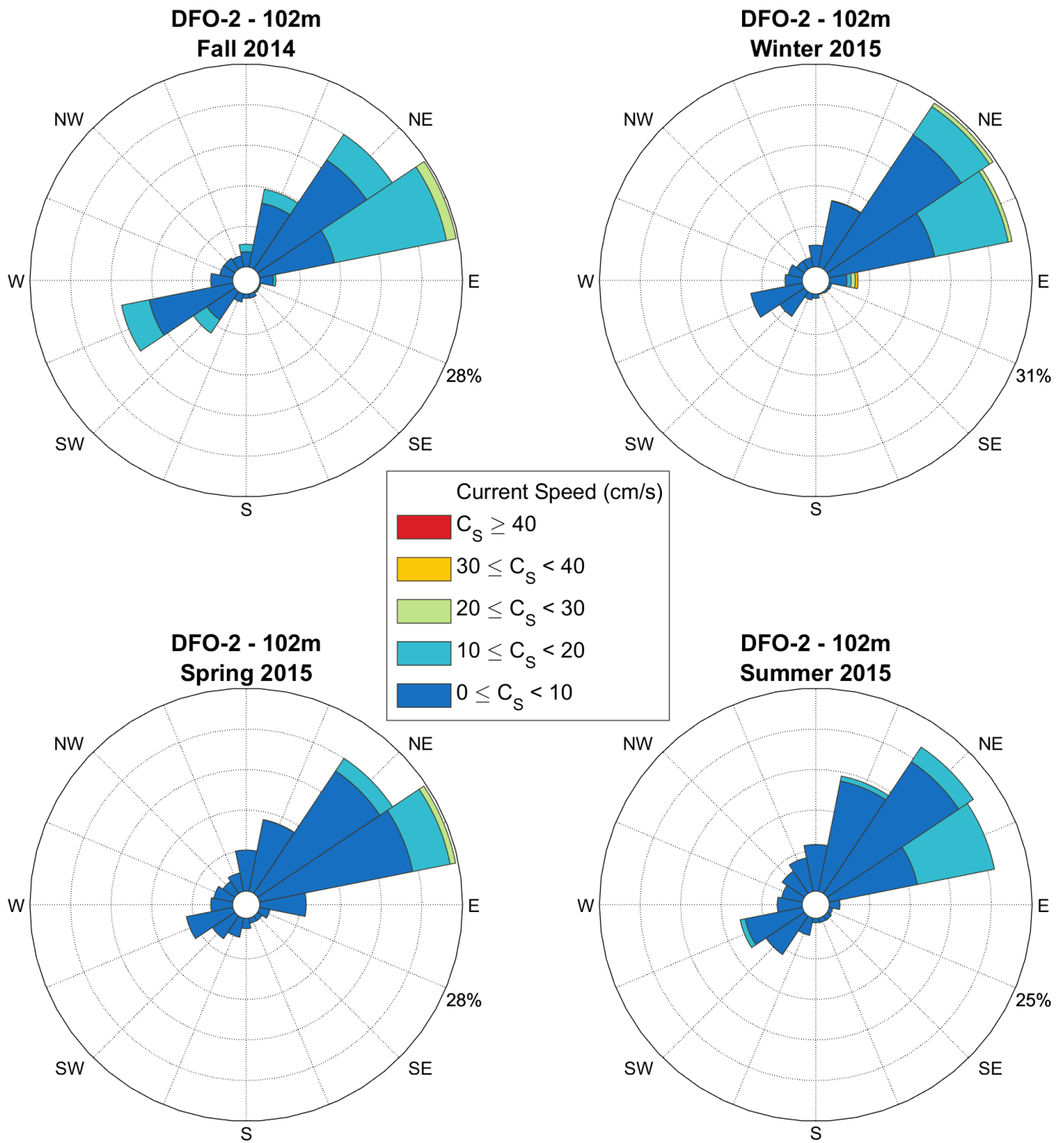


Figure 37: Seasonal current roses at 102 m depth at DFO-2-14 as based on low-pass filtered data from bin cell #1 acquired with the SC-ADCP #586. Roses point toward where the currents are going. Seasons are defined following the meteorological convention (Fall: October-December; Winter: January-March; Spring: April-June; Summer: July-September).

3.1.6 Mooring DFO-1

A time-series plot of current speed, direction, and along-slope current component from the NB ADCP deployed at the mid-shelf mooring DFO-1 over 2014-2015 is provided in Figure 38. The data in the NB ADCP plot are filtered for bins with PG4 values less than 25%, bins affected by sidelobe interference and for error velocity thresholds and other masks as described in section 2.4.1. The first valid bin depth for the NB ADCP #318 at DFO-1-14 after removing sidelobe interference was 11.0 m (bin cell 10) with a percentage of valid data of 58.8% (Appendix E). Percentage of valid data below the uppermost valid bin depth ranged from 84.8 to 86.3%. Approximately 14% of the dataset at DFO-1-14 was lost due to an intermittent malfunction of the NB ADCP internal data recorder for 47 days between May 7 02:36:05 to June 23 01:37:20 and again for the last 20 days of the deployment. However, no bin depth was manually flagged for this instrument as part of the QA/QC procedure.

Mean current speeds at the mid-shelf site DFO-1-14 is about 8-9 cm/s throughout the water column, with no discernable vertical pattern in current speed intensity (Appendix E, Table 14). Vector-averaged directions are also steadily oriented to the south (160-188°TN) at all bin depths. Maximum current speed at this site was 53 cm/s on February 25, 2015, as recorded in the lower portion of the water column at 42 m depth (Appendix E). This relatively strong current speed event appears to be related to the general increase in north-eastward currents observed at depth at several mooring locations around late February and early March 2015.

Seasonal current roses (low-pass filtered) for one bin depth (23 m) in the middle of the water column at mooring DFO-1-14 are provided in Figure 39. These plots show that currents over the mid-shelf are typically weak to moderate (<20 cm/s) and that stronger currents in 2014-2015 occurred primarily in fall. It should be noted however that the current rose for spring 2015 does not reflect the actual range of current speeds and directions prevailing during that season due to the bad data recorded by the NB ADCP #318 in May-June 2015.

DFO-1; NB ADCP 300kHz; 70.3339 N, 133.741 W; 2014-2015; Instr. #318; 51 m depth

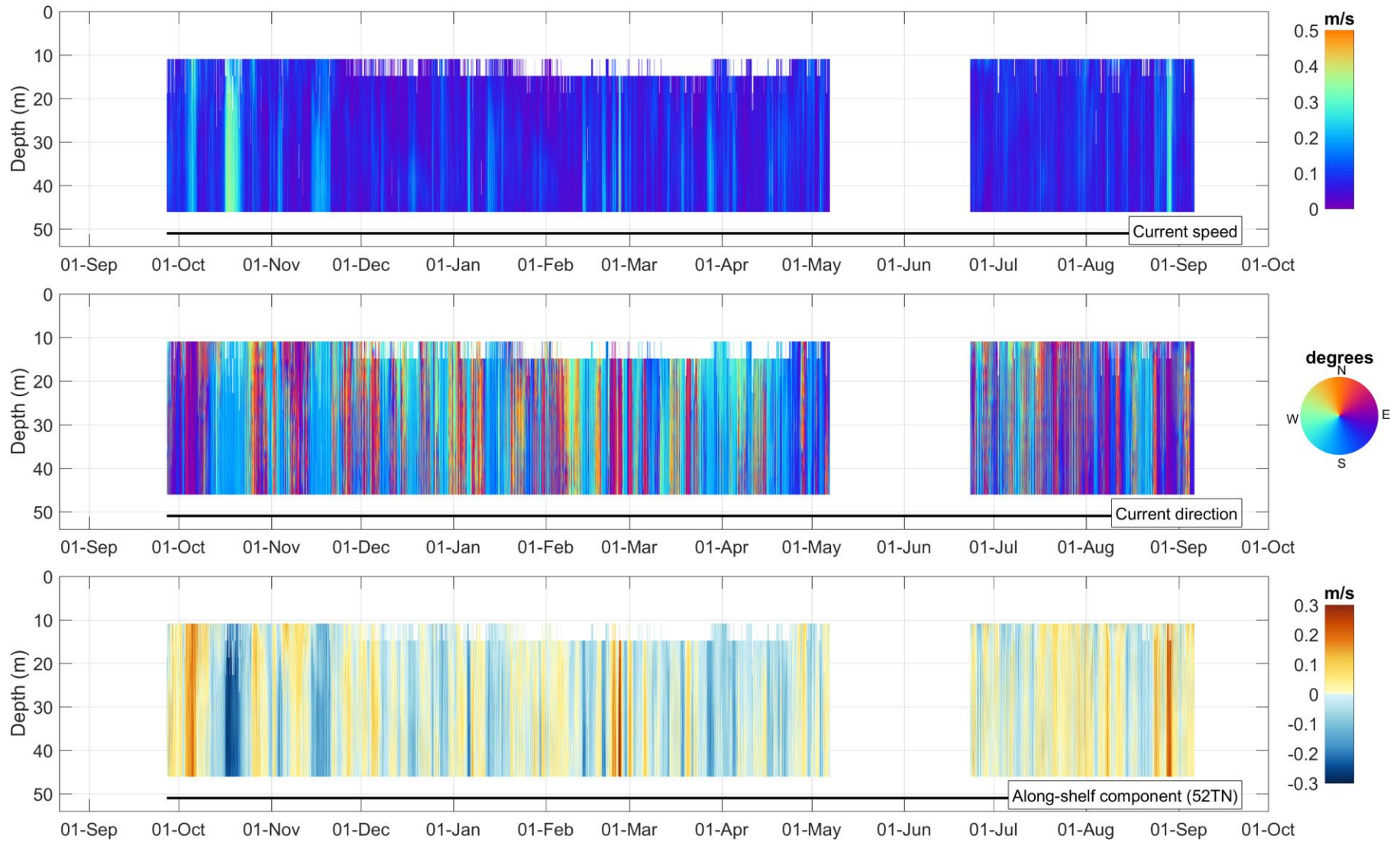


Figure 38: Time-series of current speed, current direction and along-slope current component at mooring DFO-1-14 as obtained with the NB ADCP #318. The black line depicts the instrument depth.

Table 14: Annual statistics of current speed and direction at DFO-1-14 from a selected bin depth representative of the Polar-mixed layer (see Table 7 for water mass description).

Bin Depth (m)	Median Speed (m/s)	Mean Speed (m/s)	75%ile Speed (m/s)	95%ile Speed (m/s)	99%ile Speed (m/s)	Max Speed (m/s)	Standard Deviation Speed (m/s)	Vector-Averaged Direction (deg TN)
23.0	0.07	0.08	0.10	0.17	0.30	0.42	0.05	176.94

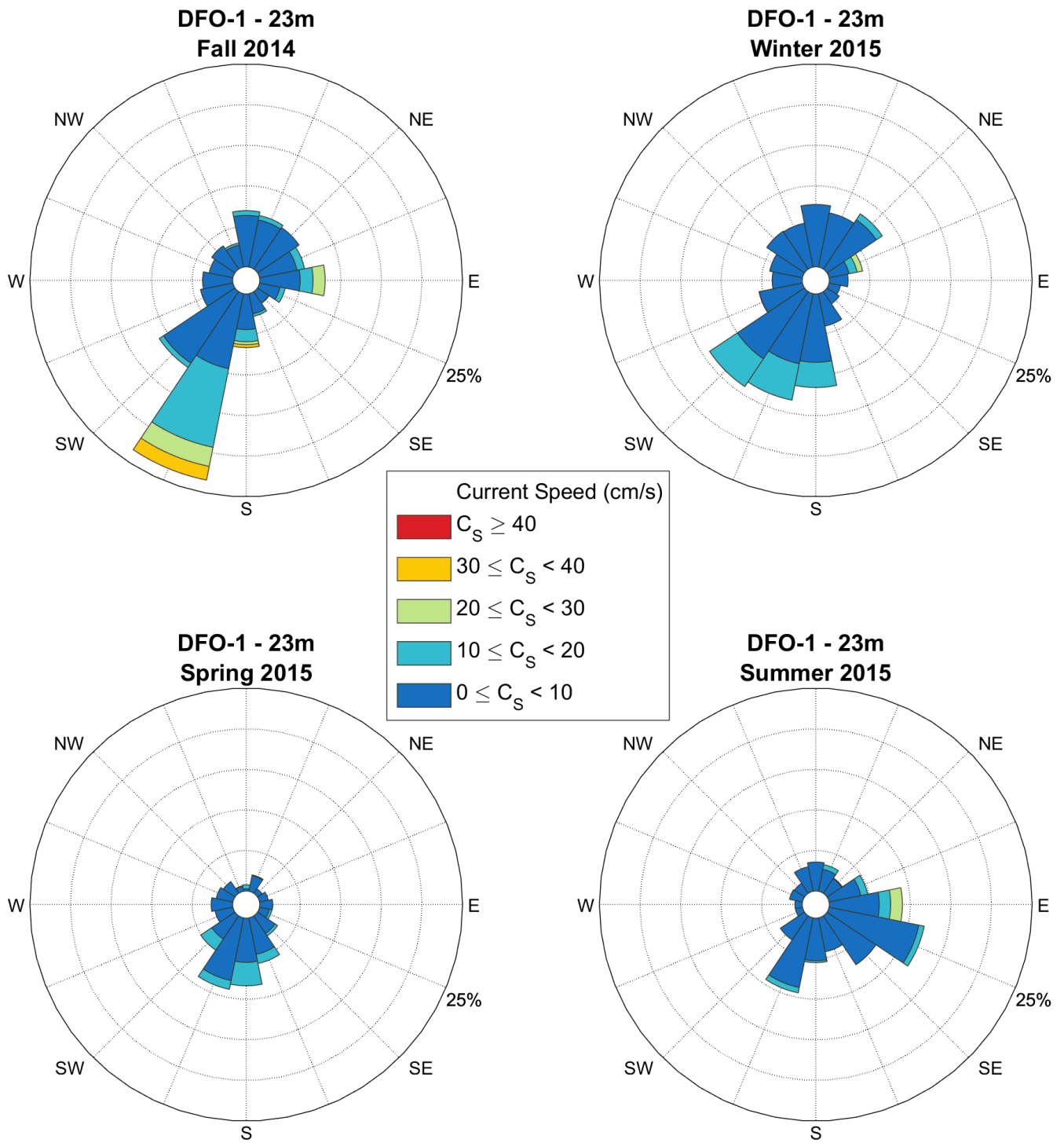


Figure 39: Seasonal current roses at 23 m depth at DFO-1-14 as based on low-pass filtered data from bin cell #7 acquired with the SC-ADCP #318. Roses point toward where the currents are going. Seasons are defined following the meteorological convention (Fall: October-December; Winter: January-March; Spring: April-June; Summer: July-September).

3.1.7 Mooring DFO-9

A time-series plot of current speed, direction, and along-slope current component from the WHS ADCP deployed at the inner shelf mooring DFO-9 over 2014-2015 is provided in Figure 40. The data in the WHS ADCP plot are filtered for bins with PG4 values less than 25%, bins affected by sidelobe interference and for error velocity thresholds and other masks as described in section 2.4.1. The first valid bin depth for the WHS ADCP #18318 at DFO-9-14 after removing sidelobe interference was 3.8 m (bin cell 25) with a percentage of valid data of 40.8% (Appendix E). Percentage of valid data below the uppermost valid bin depth ranged from 45 to 96%. The relatively low percentage of valid data at DFO-9-14 is primarily related to low echo intensity between beams and abnormally-high vertical velocity and error velocity, a measure of the consistency of current velocity across the ADCP beams. Investigation is ongoing to determine what caused the low echo and high vertical/error velocity in this dataset, something that has not been seen in earlier deployments at this site.

Based on the valid data collected at DFO-9-14, mean current speeds at this site range from 7 to 14 cm/s throughout the water column, with the stronger mean currents typically near the surface (Table 15, Appendix E). Vector-averaged directions were all in the south-eastern quadrant (101-172°TN) from 3.8 to 27.8 m depth. Maximum current speed at DFO-9-14 was 100 cm/s on September 1-2, 2015 as recorded from 4.8 to 8.8 m depth (Appendix E). The direction of this strong current was to the east-southeast (106-127°TN) throughout the water column. Similar strong current events to the east-southeast were detected on November 11, 2014 and on March 1, 2015. The early March event is consistent with similar eastward-directed current pulses recorded at BR-G, BR-K, DFO-1 and DFO-2 (Figure 21, Figure 31, Figure 35, and Figure 38).

Seasonal current roses (low-pass filtered) for one bin depth (22 m) at mooring DFO-9-14 are provided in Figure 41. This bin depth was selected to provide a representative overview of current speed and direction at this location since the percentage of valid data at this depth was greater than 90% (Appendix E). The rose plots show that currents over the inner-shelf are typically weak to moderate (<20 cm/s) and that stronger currents in 2014-2015 occurred primarily fall 2014 and summer 2015.

DFO-9; WHS 300 307.2kHz; 70.0584 N, 133.7157 W; 2014-2015; Instr. #18318; 31.0 m depth

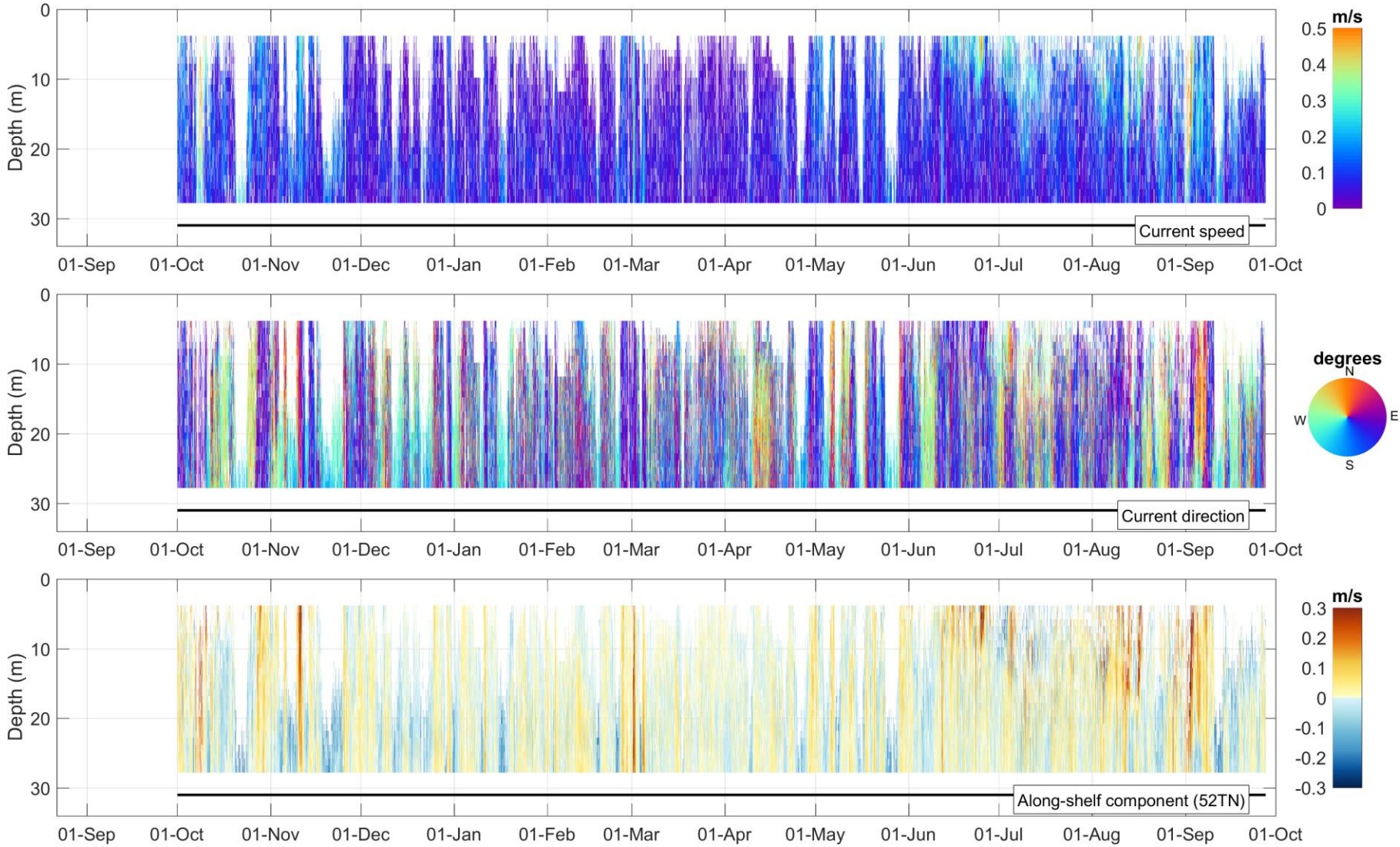


Figure 40: Time-series of current speed, current direction and along-slope current component at mooring DFO-9-14 as obtained with the WHS ADCP #18318. The black line depicts the instrument depth.

Table 15: Annual statistics of current speed and direction at DFO-9-14 from a selected bin depth representative of the Polar-mixed layer (see Table 7 for water mass description).

Bin Depth (m)	Median Speed (m/s)	Mean Speed (m/s)	75%ile Speed (m/s)	95%ile Speed (m/s)	99%ile Speed (m/s)	Max Speed (m/s)	Standard Deviation Speed (m/s)	Vector-Averaged Direction (deg TN)
21.8	0.07	0.08	0.11	0.18	0.27	0.61	0.06	168.0

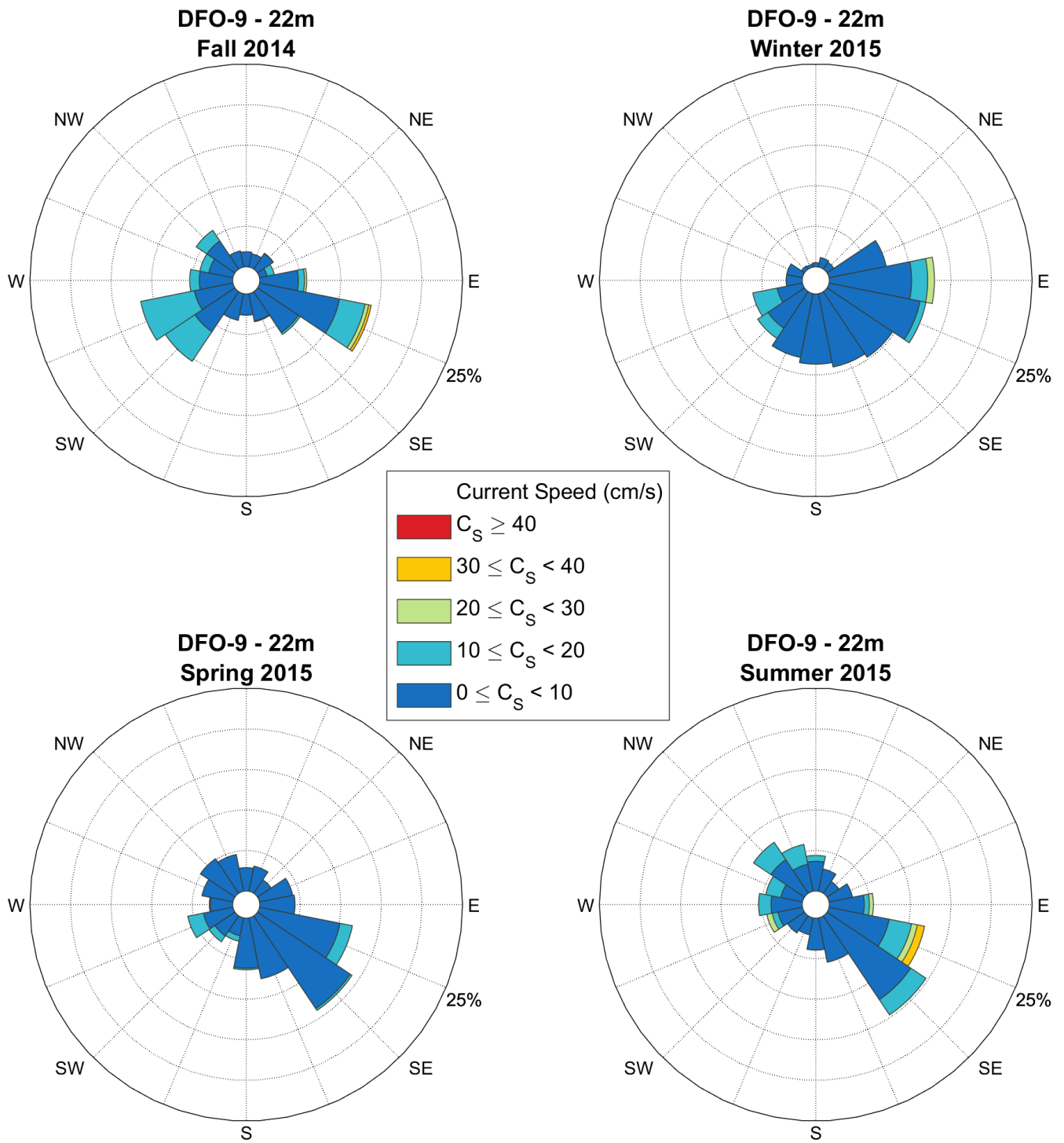


Figure 41: Seasonal current roses at 22 m depth at DFO-9-14 as based on low-pass filtered data from bin cell #7 acquired with the WHS ADCP #18318. Roses point toward where the currents are going. Seasons are defined following the meteorological convention (Fall: October-December; Winter: January-March; Spring: April-June; Summer: July-September).

3.1.8 Spatial Variability of Surface and Bottom Currents in Open Water

Near-surface and near-bottom currents (low-pass filtered) during the open water season (June 15 to October 15, from both 2014 and 2015) were mapped as current roses in Figure 42 and Figure 43 to provide an overview of ocean circulation patterns during the operational season in the southeastern Beaufort Sea. The currents roses illustrate that the dominant surface circulation pattern over the outer shelf and on the slope (BR moorings and DFO-2) is in accord with the anti-cyclonic (clockwise) motion of the Beaufort Gyre. Moorings BR-3 and DFO-2 provides compelling evidence for the predominance of a south-southwest surface current along the slope and outer shelf. By contrast, near-bottom currents along the slope flow generally to the east, while over the mid- to inner shelf bottom currents are similar to surface currents.

Near-surface currents during the open water season at BR-1, BR-G and BR-K were more variable than at BR-3 and DFO-2 (Figure 42). Currents at BR-K were aligned with the bathymetric contours, but frequent reversals of the south-westward flow to the northeast can be discerned in this dataset. This contrasts with what was measured at the nearby DFO-2 mooring. At BR-G, episodes of northward currents were detected in addition of the predominant south-westward flow. Ocean circulation at BR-1 in the outer Mackenzie Trough is the most variable, with a spreading of the current rose in various directions although the westward component still dominates at this location. The presence of southward and northward currents at this location is symptomatic of the enhanced eddy activity that apparently developed in the Mackenzie Trough in summer 2015 when compared to other moorings (see section 3.1.1).

Near-bottom currents at DFO-2, BR-G, and BR-K were similar to each other with a flow predominantly toward the northeast and a few reversals to the southwest recorded at BR-K (Figure 43). As seen previously, currents at BR-K are also stronger than at BR-G and DFO-2 on the average. Near-bottom currents at BR-1 and BR-3 follow the bathymetric contours at their respective location, with a dominant flow to the south at BR-1 up the Mackenzie Canyon, and a dominant current to the north at BR-3 along the slope near Banks Island. More frequent stronger currents (>10 cm) were measured near the bottom at BR-3 when compared to BR-1.

On the mid- to inner shelf at DFO-2 and DFO-9, surface and near-bottom circulation during the open water season is relatively weak and variable, with more frequent currents to the east-southeast toward the coast throughout the water column. This may be related to the wind conditions observed during the sampling period as westerly winds in the region are known to advect surface toward the coast (e.g. Dmitrenko et al. 2016) which generate downwelling-favorable conditions. The environmental context of 2014-2015 (i.e. wind, large-scale ice conditions, storm activities) remains however to be investigated to confirm any trend.

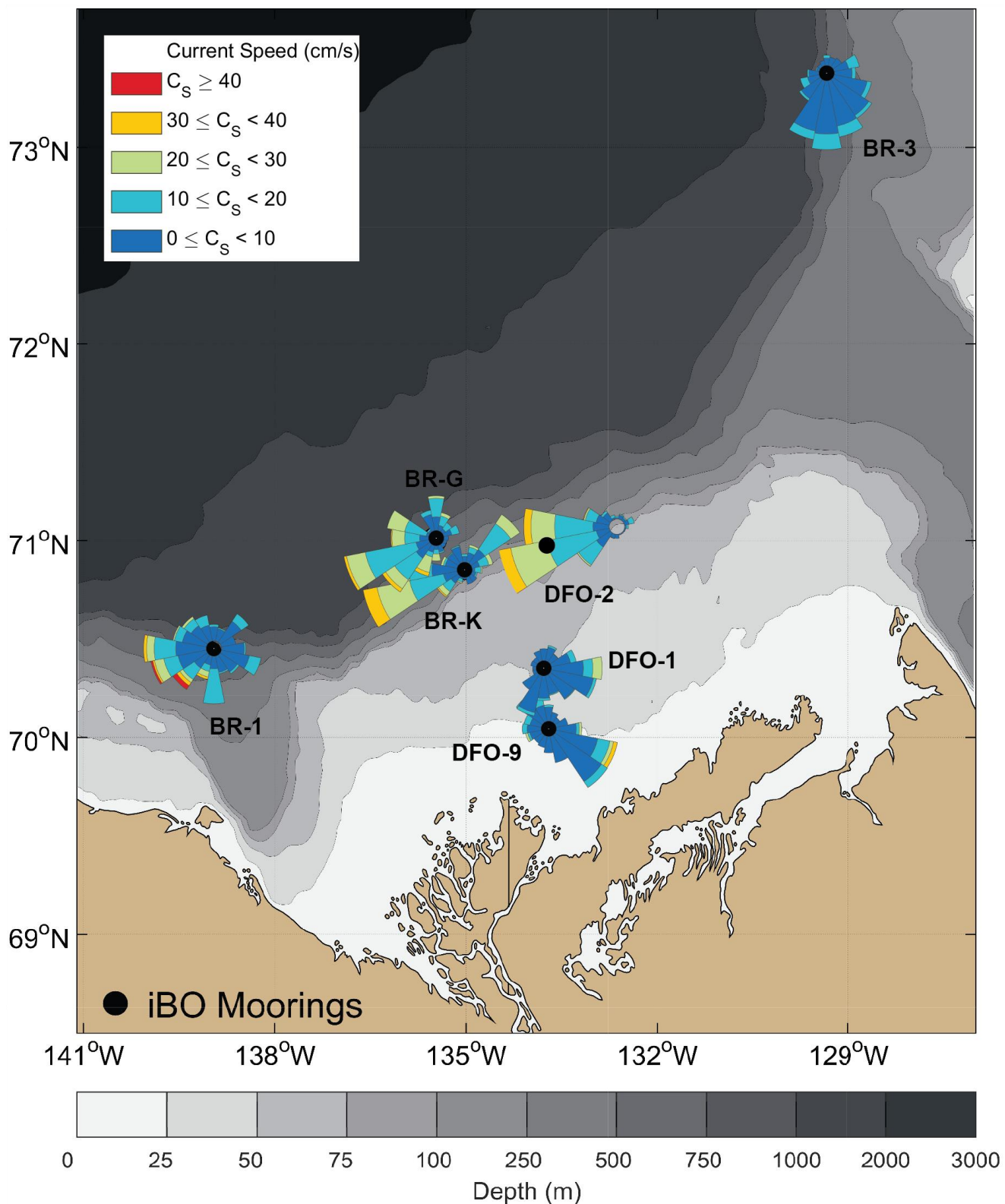


Figure 42: Near-surface currents for the open water season as based on low-pass filtered current velocity data from the nearest bin depth to 20 m. All data between June 15 and October 15 over 2014-2015 were used to construct the current roses. Please note that the rose of DFO-2 is slightly displaced to the east of the mooring location for visual purpose.

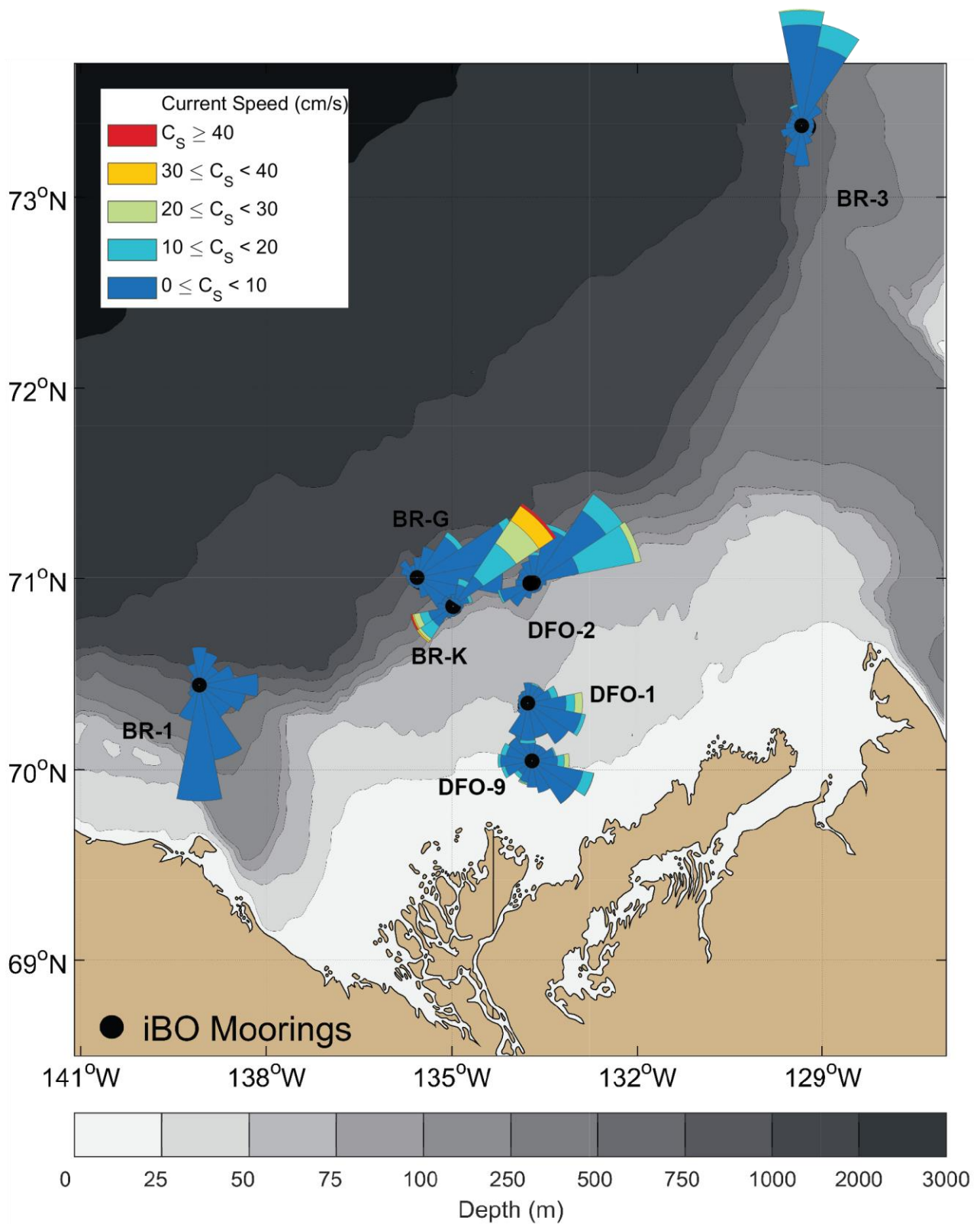


Figure 43: Near-bottom currents for the open water season as based on low-pass filtered current velocity data from the bin depth nearest to bottom at each location. All data between June 15 and October 15 over 2014-2015 were used to construct the current roses. Roses indicate toward where the current is flowing.

3.2 Temperature and Salinity

The summary of CT logger data recovery success on iBO moorings 2014-2015 is provided in Table 16. All CT loggers provided a complete dataset, except for the RBR CT-FI-Tu-DO #22044 attached at 141 m depth on BR-K-14. This instrument stopped recording on September 7, 2014 due to a battery failure possibly linked to short-circuiting (unidentified cause). This instrument was sent to the manufacturer for further inspection. Data processing for DFO CT logger is still in progress and is not presented here. Summary of valid and flagged data (suspicious spikes) for each processed CT sensor is provided in Table 17.

Processed temperature and salinity data from all CT loggers deployed on BR moorings over 2014-2015 are presented using time-series plots of temperature and salinity at each mooring. Temperature time-series recorded at moorings BR-1, BR-3, BR-G and BR-K are presented in Figure 44 through Figure 47. Salinity time-series for the same moorings are provided in Figure 48 through Figure 51. Data from temperature-salinity time-series presented below were filtered for spike-like values that were detected using the method described in section 2.4.2. Missing data were replaced by linearly-interpolated values in the time-series plots. A temperature-salinity diagram is also provided in Figure 52, which combines all QA/QC data from the moored CT loggers (also filtered for spikes, but not interpolated for missing values) as well as water column profile data from CTD casts conducted at mooring deployment in 2014 aboard the Amundsen.

The temperature time-series recorded at discrete depths varying from 38 to 693 m on the slope illustrate the typical vertical layering in temperature in the Beaufort Sea (e.g. Lansard et al. 2012 and references therein), although marked temporal variability was observed, especially at BR-G (Figure 46). Temperature was most variable in the upper 200 m of the water column, with temperature varying from around 0°C down to around -1.7°C. Rapid transitions from relatively warm to relatively cold (and vice-versa) temperature were often detected in this water interval. For example, a sudden increase from -1.4 to 0.4°C was recorded at 96 m at BR-K in late October 2014 (Figure 47). At BR-G, marked decreases in temperature (from -0.8 to -1.5°C) were successively measured at 192 m from January to April 2015, concomitantly with modest increases (from -1.7 to -1.5°C) at 43.1 m (Figure 46). These events when the upper 200 m of the water column was quasi-homogenized in terms of temperature correspond apparently to the passage of eddy-like features over the mooring (see section Mooring BR-G). Warmest waters (near 0.5°C) were recorded at the deep moorings with the ~450 m CT loggers located in the Atlantic water mass. At the lowermost CT logger depths (about 600-700 m), temperature was approximately 0.5°C colder than at ~450 m due to the progressive transition to Canada Basin deep water that occupies depths below 800 m in the region (Lansard et al. 2012).

Likewise temperature, salinity time-series showed that most of the variability in terms of water mass physical properties occurs in the upper 200 m (Figure 48 through Figure 51). Contrary to temperature, salinity is monotonically increasing with depth in the Beaufort Sea. Over the slope in 2014-2015, salinity from 450 to 700 m depth occupied a very narrow range from 34.7 to 34.9, while salinity in the upper 200 m ranged from 29.5 (BR-3, 39 m in early July 2015) up to 34.8 (BR-K, 96 m in late October 2014). The rapid increase in salinity observed at the upper slope mooring BR-K at both 96 m and 59 m in late October and November 2014 (Figure 51) is likely a sign of upwelling of deep waters taking place at the shelf break. The general trend of negative along-slope current component observed at moorings BR-K and DFO moorings in October-November 2014 is also consistent with upwelling conditions (see section 3.1.3). The successive eddy-like features observed at BR-G from January to April 2015 are also well depicted by the salinity time-series at this location (Figure 50). The pinching of salinity time-series (toward salinity \approx 33) seen at this location during winter possibly illustrates the successive passage of cold-core anti-cyclonic eddies filled with water of Pacific origin (Figure 50). Such a phenomenon was also observed at BR-1 in early August 2015 (Figure 48), although the deployment of two additional CT sensors between the IPS and QM-ADCP at BR-G in 2014 (at 83 and 150 m) provided key data that enabled better resolving the moving

eddy-like features. In 2015, all lower slope moorings were equipped with a CT logger between the IPS and QM ADCP at deployment (at approximately 130 m). This decision was taken on the basis of a trade-off between equipment availability and a wish to better resolve the upper water column temperature-salinity structure, including eddy dynamics.

The temperature-salinity diagram combining all data from the CT loggers provides a further way to characterize the different water masses occupying the water column at mooring locations over 2014-2015 (Figure 52). This diagram provides compelling evidence that most of the variability in the water column is taking place in the upper 200 m. It also illustrates that all datasets from CT sensors deployed in the upper 100 m contain at least some periods when seawater was near the freezing point (as a result of winter processes). The visual comparison between CTD cast data from 2014 and the moored CT sensor data provides a preliminary assessment of the accuracy of the CT sensor data. It is reminded that no CT logger data was corrected yet for drift or instrument offset, since processed CTD cast data from 2015 are not available yet. However, instruments in the upper 200 m did not appear to be affected by any visible bias given their consistency with respect to the freezing line and the expected variability in the shape of the halocline (i.e. between ~32.0 and 34.7 salinity) that changes over time due to upwelling/downwelling and other mixing processes. Further examination of the CTD casts data collected in 2015 will enable confirming if these instruments were affected by any bias.

However, the deeper CT logger instruments (>400 m) do show already some offsets with respect to the CTD cast data collected in 2014. A zoom on the narrow domain of the temperature-salinity variability in the lower portion of the Atlantic water mass is shown in Figure 53. Although such a zoom exaggerates the discrepancy between the moored CT data and the CTD cast data, it illustrates that the deep CT sensors might be affected by individual instrument-specific offsets (e.g. temperature sensor of CT #15272, to be verified) or miscalculation in the relationship linking pressure to conductivity and potential temperature. It is reminded that the RBR CT loggers do not have their own pressure sensor. Depth of RBR CT sensors needs to be estimated on the basis of other nearby instruments. Such miscalculations are likely to be the case of the observed biases and investigation is underway to resolve them.

Table 16: Summary of CT data logger clock drift and percentage of raw data return on iBO moorings from 2014 to 2015.

Mooring	Instrument	Serial number	Depth (m)	Clock Drift (mm:ss)	First Good Record (UTC)	Last Good Record (UTC)	Raw Data Return (%)
BR-1-14	RBR XR420 CT	15262	51.8	00:22 fast	Sep-01-2014 21:40:00	Sep-29-2015 19:40:00	100.0%
BR-1-14	RBR XR420 CT	15279	201.8	00:32 fast	Sep-01-2014 21:40:00	Sep-29-2015 19:40:00	100.0%
BR-1-14	RBR XR420 CT	15267	457.8	00:01 slow	Sep-01-2014 21:40:00	Sep-29-2015 19:40:00	100.0%
BR-1-14	RBR XR420 CT	15268	591.1	00:42 fast	Sep-01-2014 21:40:00	Sep-29-2015 19:40:00	100.0%
BR-3-14	RBR XR420 CT	15264	38.7	00:38 fast	Aug-27-2014 13:50:00	Aug-31-2015 17:10:00	100.0%
BR-3-14	RBR XR420 CT	15263	181.2	01:17 fast	Aug-27-2014 13:40:00	Aug-31-2015 17:10:00	100.0%
BR-3-14	RBR XR420 CT	15281	447.6	00:51 fast	Aug-27-2014 13:50:00	Aug-31-2015 17:10:00	100.0%
BR-3-14	RBR XR420 CT	15275	677.6	00:25 fast	Aug-27-2014 13:50:00	Aug-31-2015 17:10:00	100.0%
BR-G-14	SBE 37SM Microcat	12236	43.1	00:13 fast	Aug-23-2014 23:50:00	Aug-26-2015 21:00:00	100.0%
BR-G-14	RBR XR420 CTD	17352	82.7	00:53 fast	Aug-23-2014 23:45:00	Aug-26-2015 20:45:00	100.0%
BR-G-14	RBR XR420 CT	15273	150.0	01:08 fast	Aug-23-2014 23:40:00	Aug-26-2015 21:00:00	100.0%
BR-G-14	RBR XR420 CT	15280	192.0	01:22 fast	Aug-23-2014 23:40:00	Aug-26-2015 21:00:00	100.0%
BR-G-14	RBR XR420 CT	15266	453.5	00:23 fast	Aug-23-2014 23:40:00	Aug-26-2015 21:00:00	100.0%
BR-G-14	RBR XR420 CT	15272	692.5	00:51 fast	Aug-23-2014 23:40:00	Aug-26-2015 21:00:00	100.0%
BR-K-14	SBE 37SM Microcat	12235	58.6	00:18 fast	Aug-21-2014 16:20:00	Aug-25-2015 14:10:00	100.0%
BR-K-14	RBR XR420 CTD-Tu-DO	10419	95.9	01:10 fast	Aug-22-2014 18:00:00	Aug-26-2015 14:00:00	100.0%
BR-K-14	RBR XR420 CT-FI-Tu-DO	22044	140.8	Not available	Aug-22-2014 18:00:00	Sep-07-2014 4:00:00	4.2%
DFO-2-14	SBE 37SM Microcat	05890	105	01:52 slow	Sep-30 2014 16:30	Sep-26-2015 15:02	100.0%
DFO-1-14	SBE 37SM Microcat	04992	52	01:31 fast	Sep-30-2014 22:15	Sep-27-2015 14:49	100.0%
DFO-9-14	SBE 37SM Microcat	09973	31	02:31 fast	Oct-01-2014 02:15	Sep-27-2015 17:45	100.0%

¹Note: Data from DFO CT loggers is still in process and QA/QC dataset from these instruments is not presented here.

Table 17: Summary of valid and flagged data from CT loggers deployed on the BR slope moorings from 2014 to 2015. See Table 16 for the instrument model associated with each serial number.

Mooring	Serial number	Depth (m)	Number of Valid Conductivity Records	Number of Flagged Conductivity Records	% of Valid and Un-flagged Conductivity Records (%)	Number of Valid Temperature Records	Number of Flagged Temperature Records	% of Valid and Un-flagged Temperature Records (%)
BR-1-14	15262	51.8	56,580	26	99.95	56,580	83	99.95
BR-1-14	15279	201.8	56,580	0	100.00	56,580	0	100.00
BR-1-14	15267	457.8	56,580	1	100.00	56,580	0	100.00
BR-1-14	15268	591.1	56,580	0	100.00	56,580	0	100.00
BR-3-14	15264	38.7	53,155	9	99.98	53,155	34	99.98
BR-3-14	15263	181.2	53,157	3	99.99	53,157	2	99.99
BR-3-14	15281	447.6	53,157	1	100.00	53,157	0	100.00
BR-3-14	15275	677.6	53,157	1	100.00	53,157	1	100.00
BR-G-14	12236	43.1	52,976	22	99.96	52,976	58	99.96
BR-G-14	17352	82.7	35,316	0	100.00	35,316	66	100.00
BR-G-14	15273	150.0	52,976	0	100.00	52,976	0	100.00
BR-G-14	15280	192.0	52,976	0	100.00	52,976	0	100.00
BR-G-14	15266	453.5	52,976	13	99.98	52,976	1	99.98
BR-G-14	15272	692.5	52,975	0	100.00	52,975	0	100.00
BR-K-14	12235	58.6	53,124	34	99.94	53,124	47	99.94
BR-K-14	10419	95.9	17,707	13	99.93	17,707	13	99.93
BR-K-14	22044	140.8	371	0	100.00	371	1	100.00

¹Note: The percentage of valid data is based on the total number of records returned by the instrument from deployment to recovery.

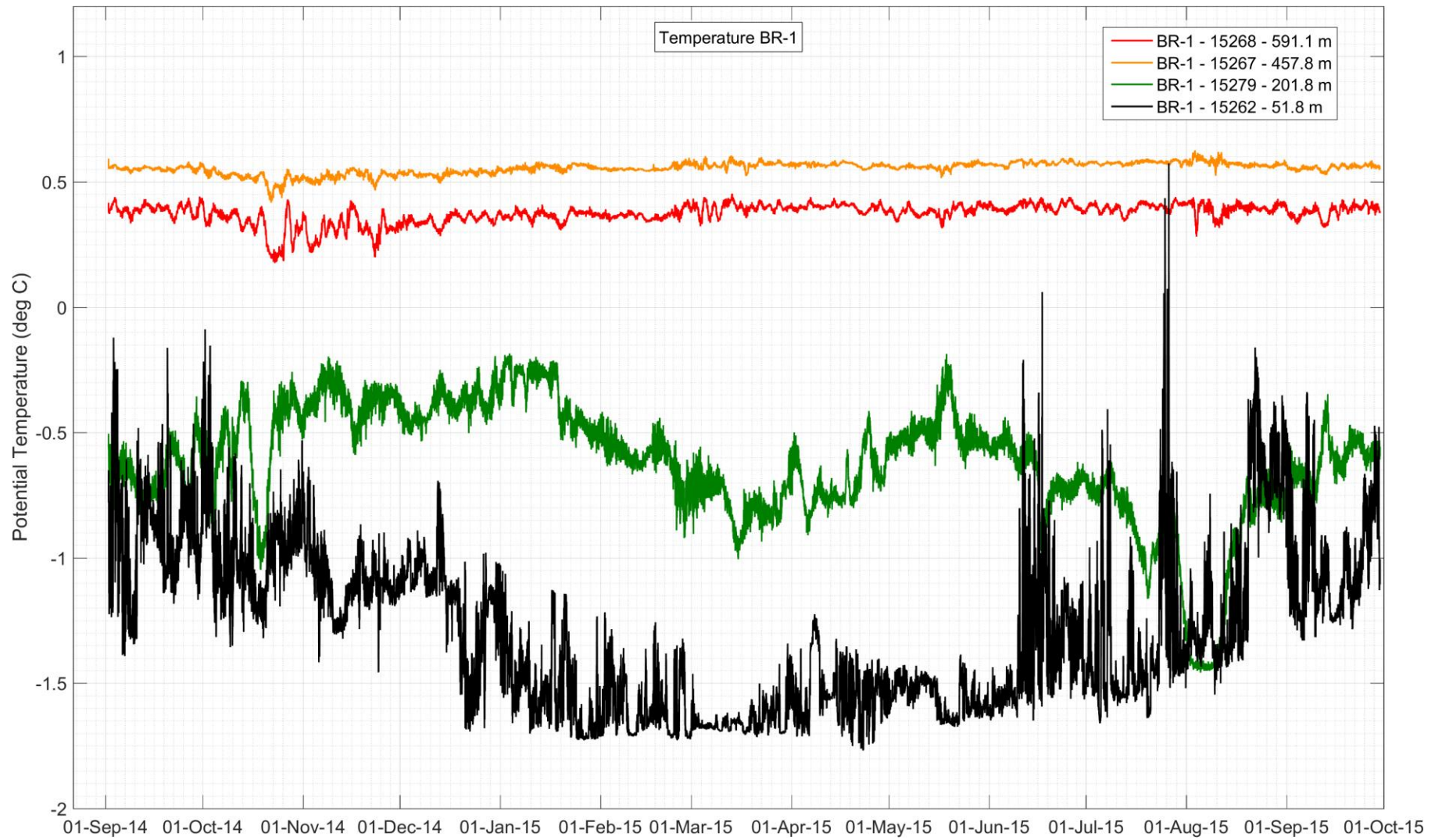


Figure 44: Temperature time-series recorded at BR-1-14 over 2014-2015. The legend shows the serial number and depth of each CT logger.

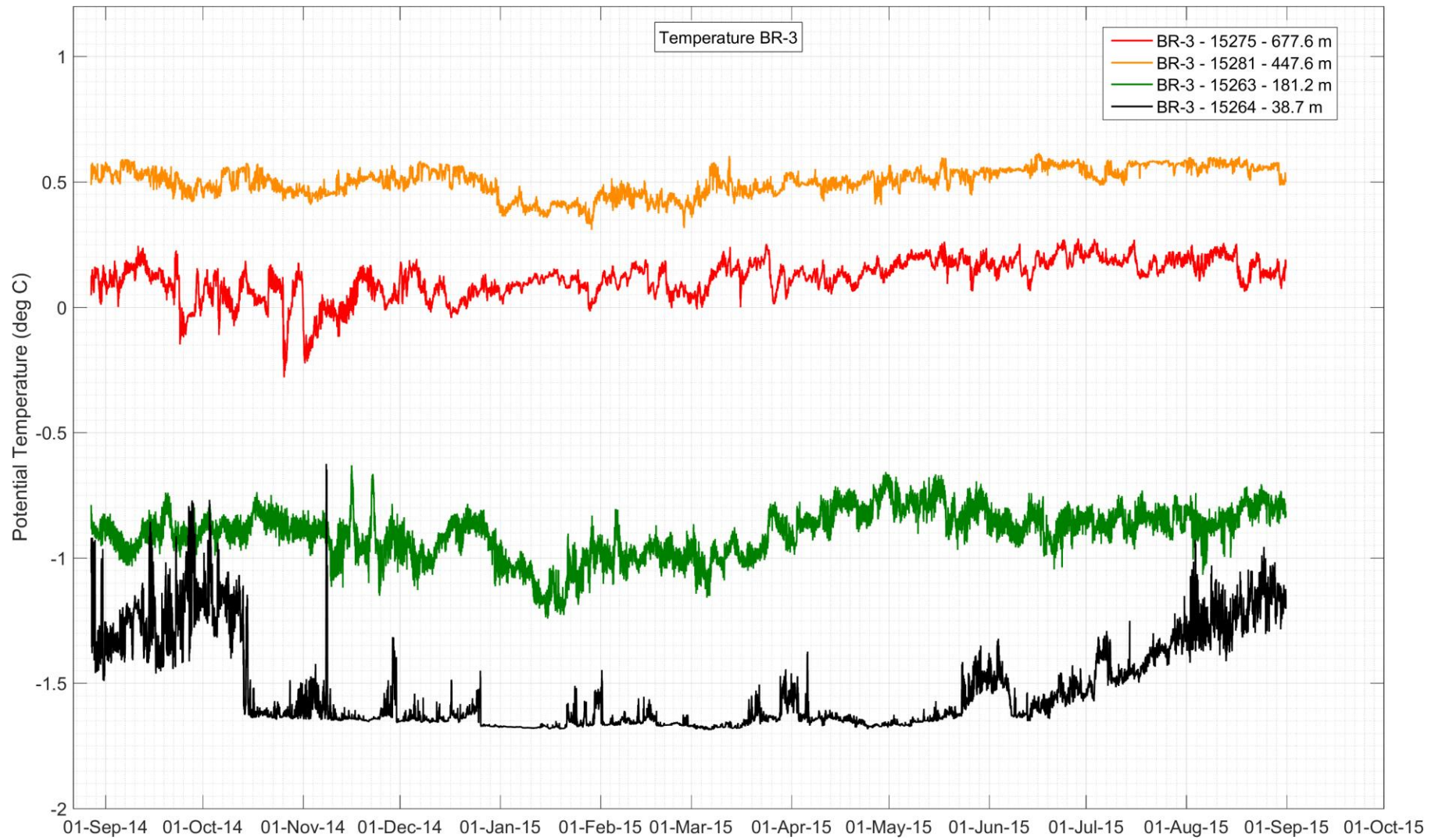


Figure 45: Temperature time-series recorded at BR-3-14 over 2014-2015. The legend shows the serial number and depth of each CT logger.

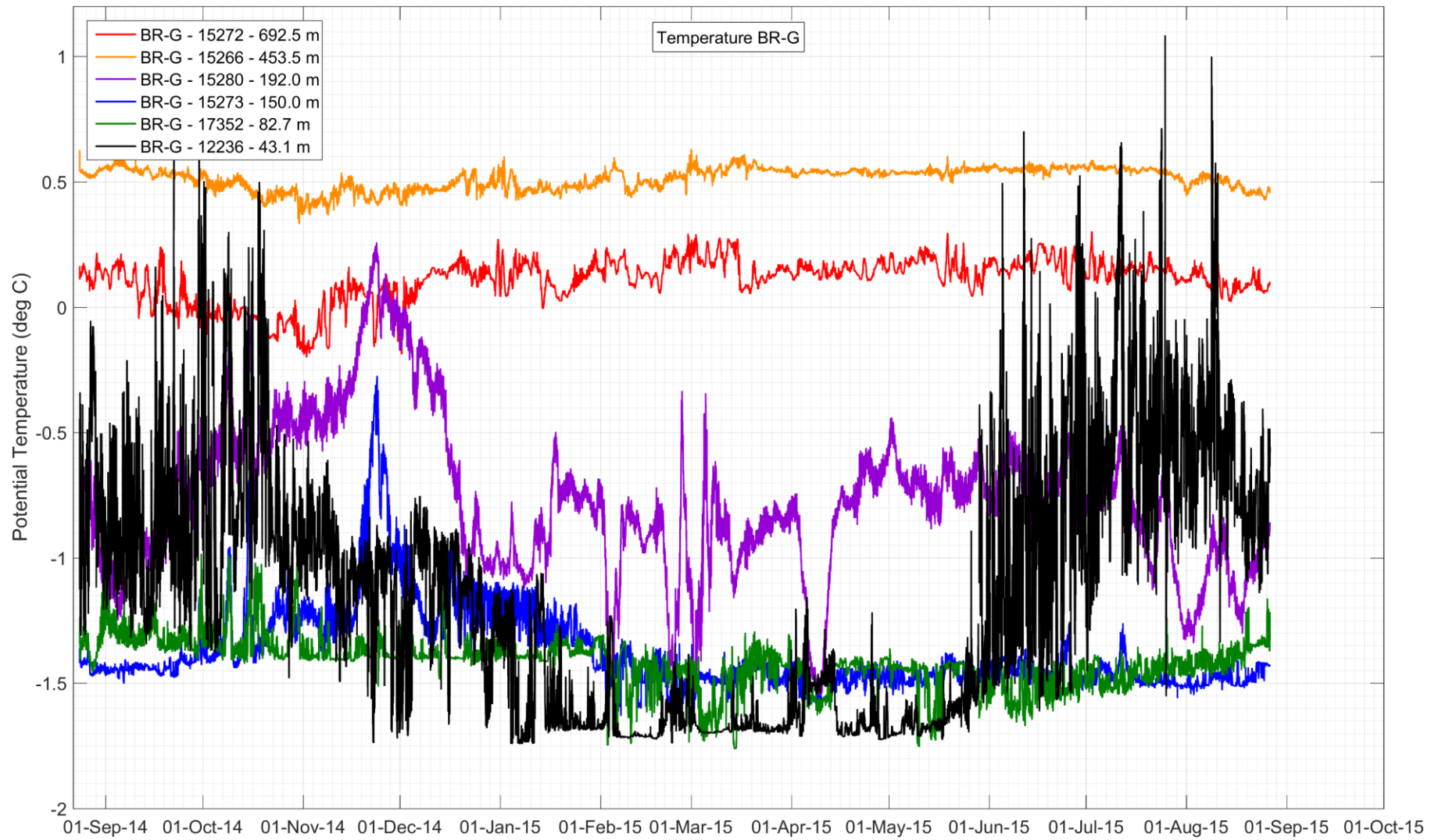


Figure 46: Temperature time-series recorded at BR-G-14 over 2014-2015. The legend shows the serial number and depth of each CT logger.

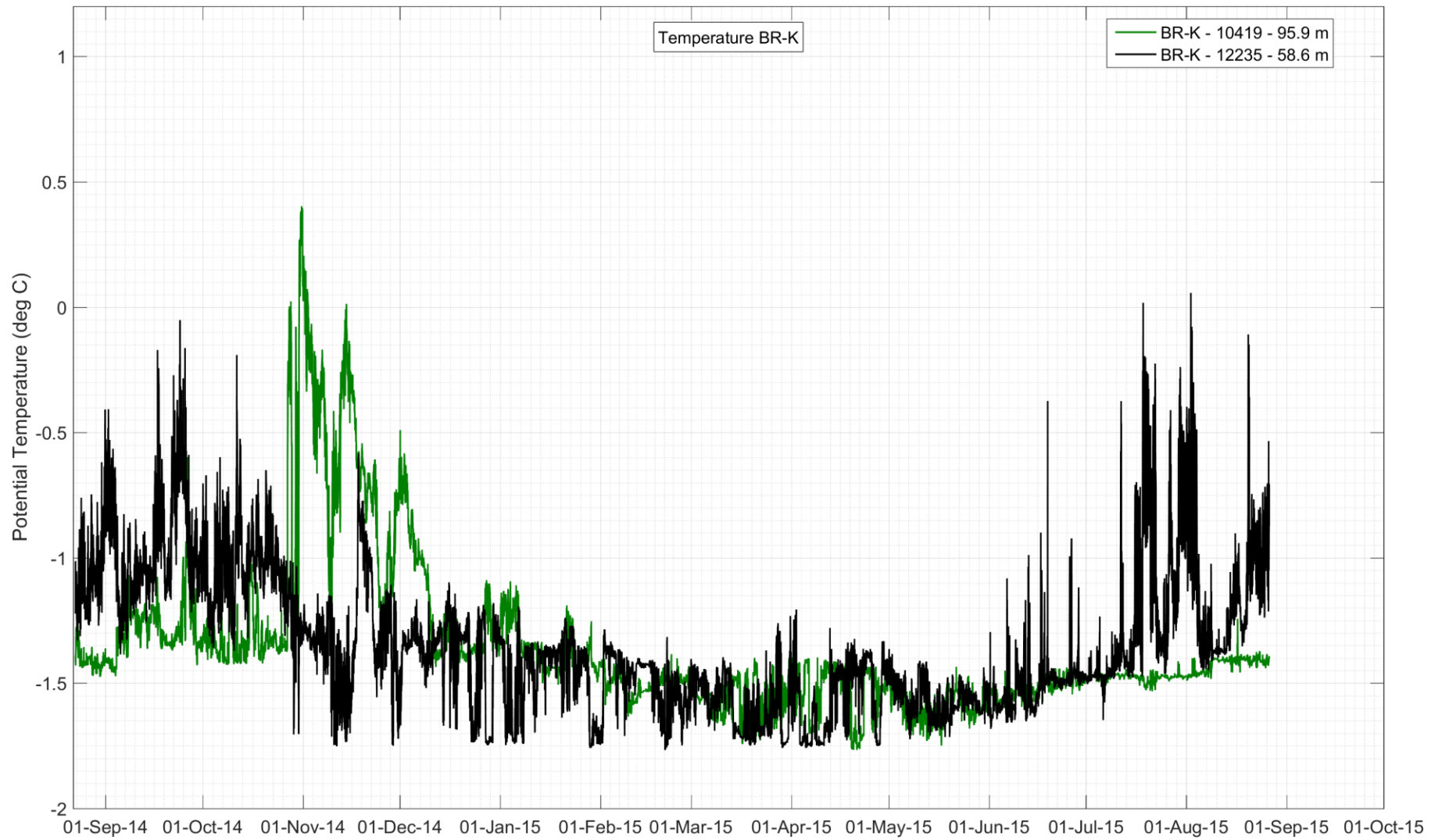


Figure 47: Temperature time-series recorded at BR-K-14 over 2014-2015. The legend shows the serial number and depth of each CT logger.



Figure 48: Salinity time-series recorded at BR-1-14 over 2014-2015. The legend shows the serial number and depth of each CT logger.



Figure 49: Salinity time-series recorded at BR-3-14 over 2014-2015. The legend shows the serial number and depth of each CT logger.

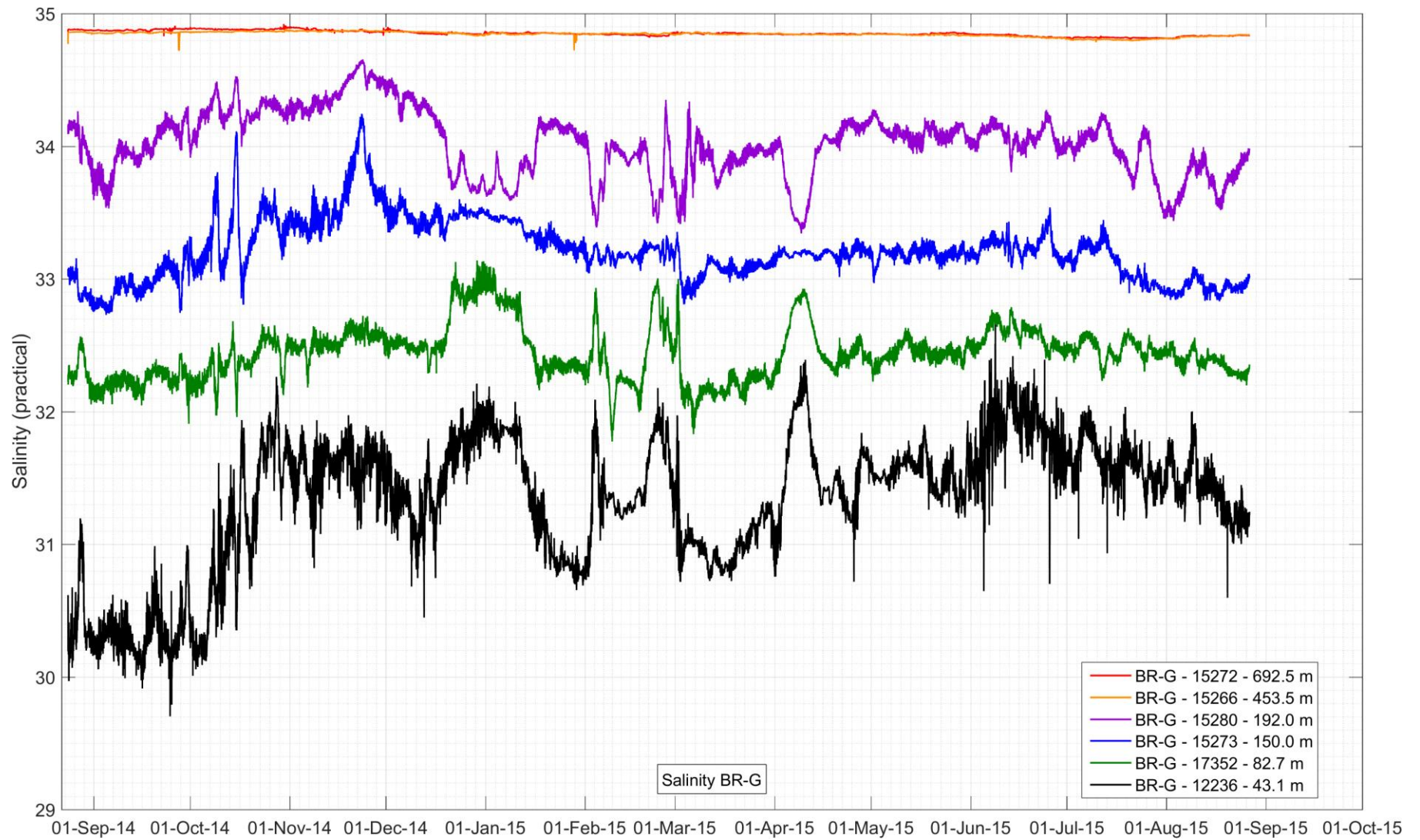


Figure 50: Salinity time-series recorded at BR-G-14 over 2014-2015. The legend shows the serial number and depth of each CT logger.



Figure 51: Salinity time-series recorded at BR-K-14 over 2014-2015. The legend shows the serial number and depth of each CT logger.

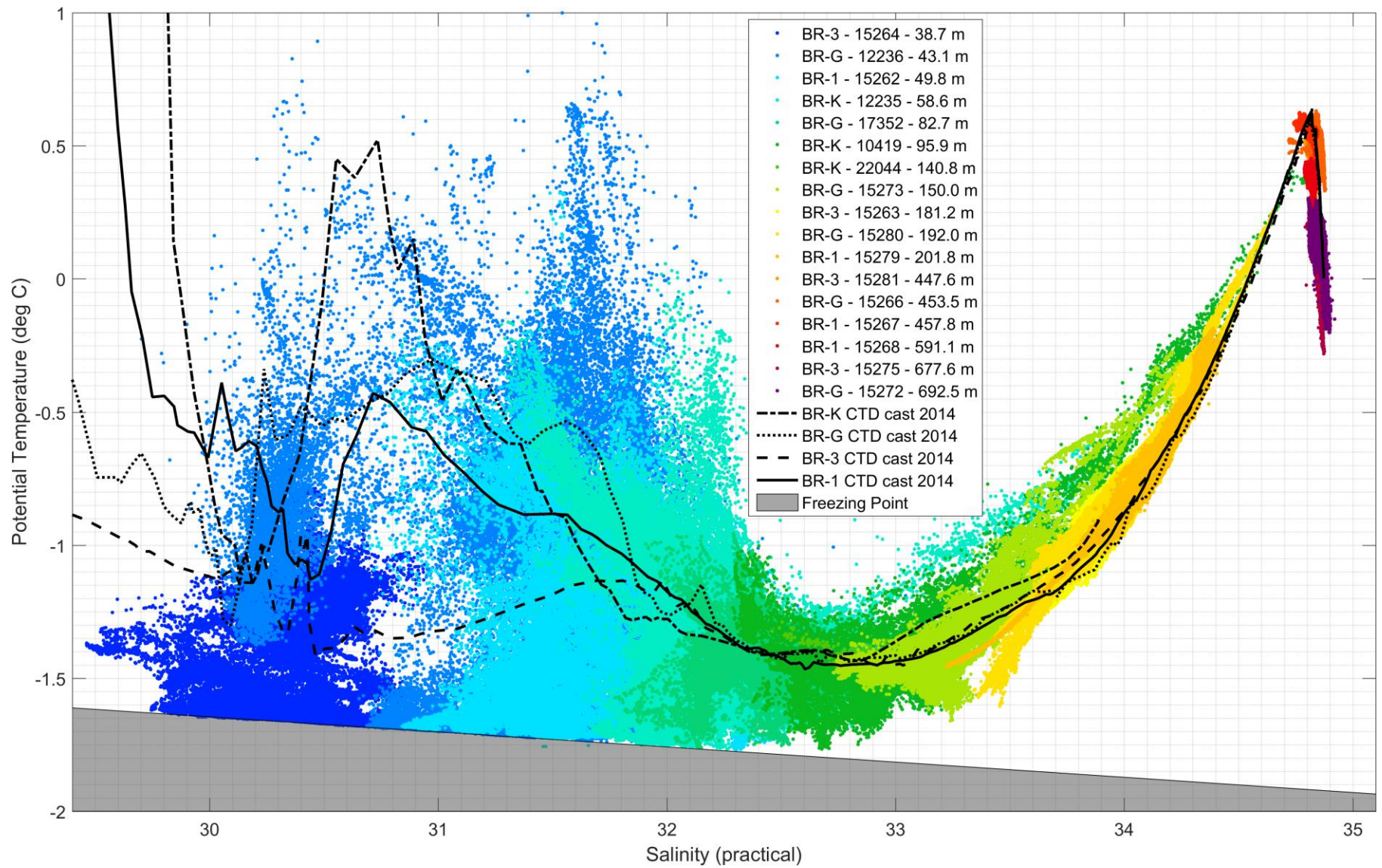


Figure 52: Temperature-salinity diagram constructed upon all data acquired with the CT loggers attached to the slope moorings BR-1, BR-3, BR-G and BR-K over 2014/2015. CTD profile data taken at mooring locations during the CCGS Amundsen cruise in 2014 are depicted by the 4 black lines.

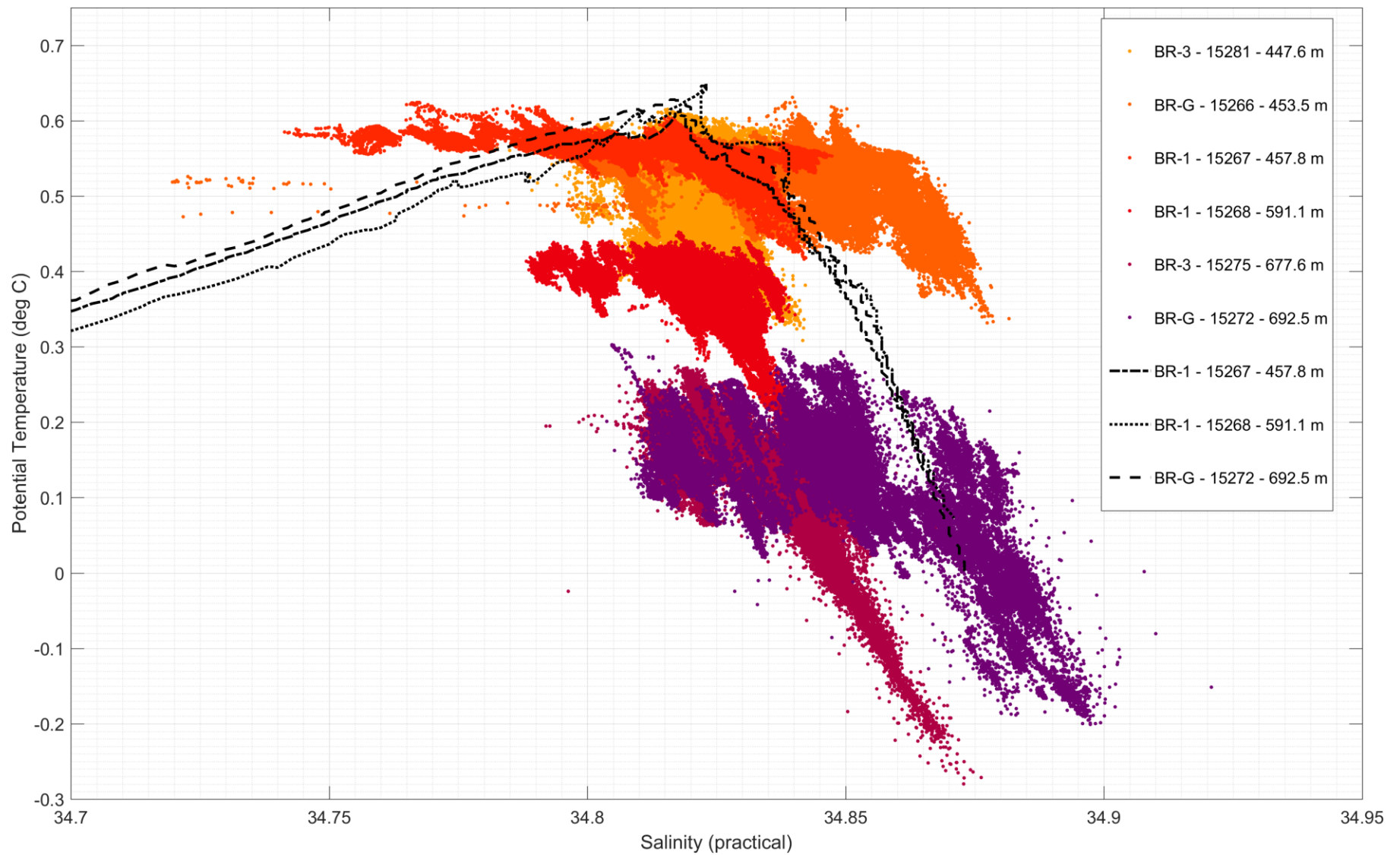


Figure 53: Zoom on the temperature-salinity diagram constructed upon data acquired with the deep CT loggers (>400 m) attached to the slope moorings BR-1, BR-3 and BR-G over 2014-2015. CTD profile data taken at mooring locations during the CCGS Amundsen cruise in 2014 are depicted by the 3 black lines.

3.3 Biogeochemical Fluxes

This section of the report provides a preliminary assessment of biogeochemical implications of the physical oceanography setting presented in the sections above. Within iBO, automated sediment traps are deployed at 2 depths on the longer slope moorings (see section 2.1.1) to provide insights on the biological regime and cycle of marine productivity in the offshore domain of the southeastern Beaufort Sea. This includes the export of organic carbon as well as information on the planktonic food web, the community of small organisms that supports upper trophic levels, such as fish and marine mammals. The particle size analyzer LISST 100X deployed at BR-K-14 is rather used to report on lateral sediment transport events and seabed erosion near the shelf edge.

Phytoplankton cells (millions cells $m^{-2} d^{-1}$) collected in the sediment trap deployed at 125 m on the BR-G-14 mooring indicated the onset of phytoplankton production and export in early May (Figure 54), with a peak in phytoplankton export (almost exclusively diatoms) in early June. Phytoplankton export remained relatively high for the remainder of the ice-free season. Zooplankton (swimmers, individual's $m^{-2} d^{-1}$) mainly carnivorous copepods, were abundant at the beginning of the deployment in October (data not shown). This peak possibly reflected the descent of copepods for overwintering, with the carnivorous copepods following the herbivorous copepods down even though the latter were not found in high numbers. No clear patterns were observed in spring and summer, but further investigation will be done at the species level.

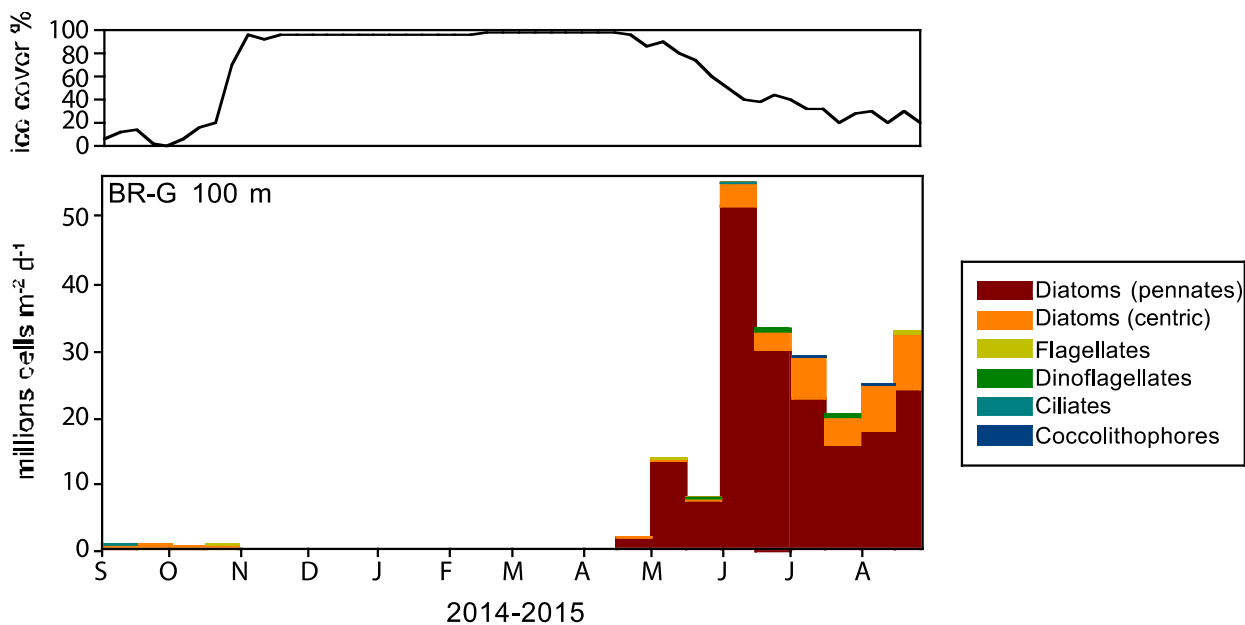


Figure 54: Phytoplankton cell fluxes collected by the upper sediment trap deployed at BR-G-14 along with satellite-derived ice concentrations in the area above the mooring during the 2014-2015 deployment period.

Particle size distribution and particle volume concentration recorded with the LISST 100X deployed near the bottom at BR-K-14 are provided in Figure 55. The valid size range for this time-series was identified as being from 10 to 100 μm (equivalent spherical diameter), which corresponds to silty-clay particles and fine sand that typically dominate bed sediment composition at the outer shelf edge. Peaks in particle volume concentration were observed primarily in fall 2014 and spring-summer 2015, but an unusual mid-winter peak in early March 2015 was also detected. This event corresponds to the widespread eastward current intensification noticed with the current profilers at the central shelf moorings over late February-early March 2015. Further investigation of the changing patterns of the particle size distribution over time should provide additional insights on horizontal and vertical sediment transport at the shelf edge in relationship to the ocean circulation regime.

BR-K-14; Particle Size Distribution and Volume Concentration; Sequoia LISST #1473; 139 m depth

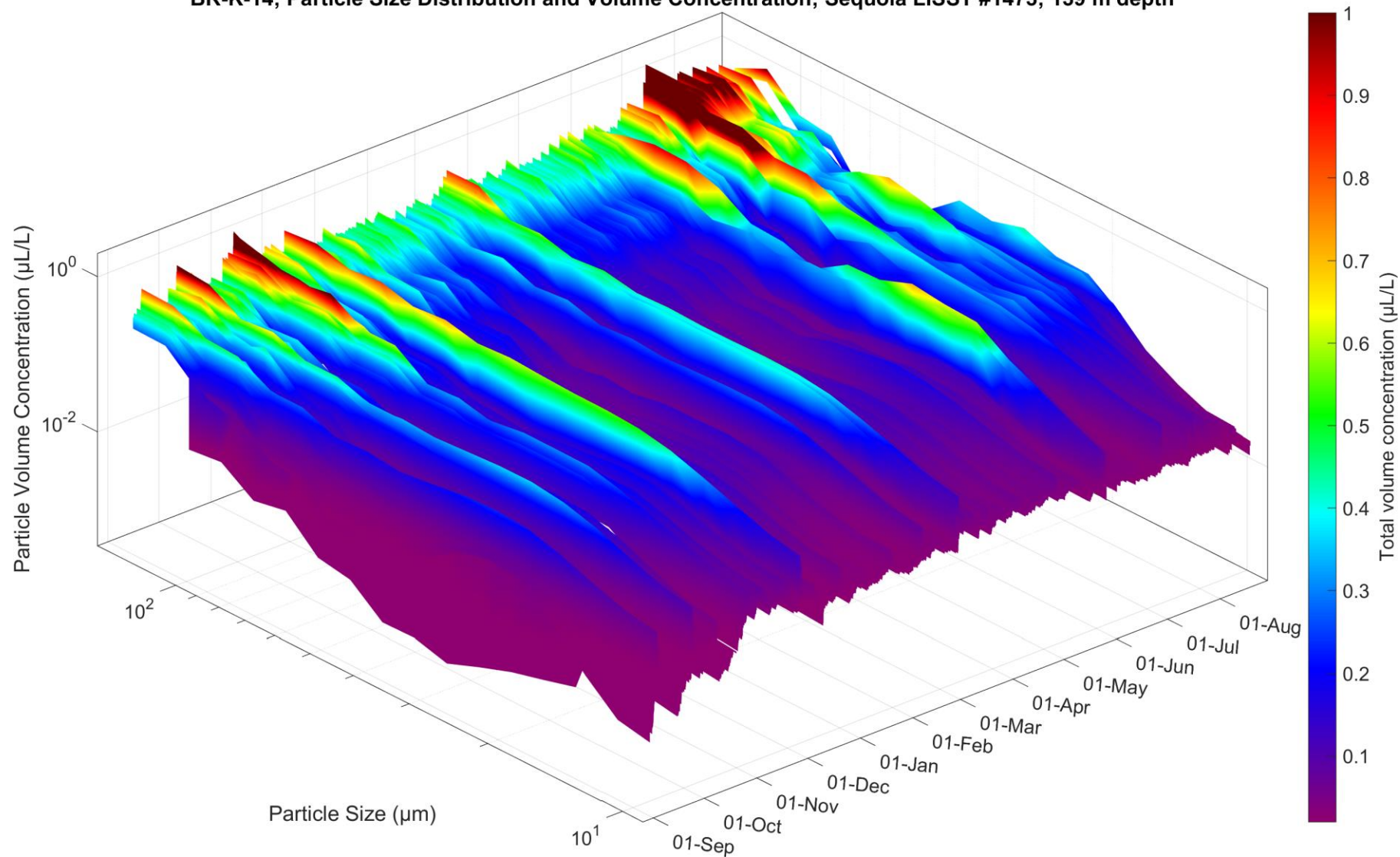


Figure 55: Time-series of particle size distribution and particle volume concentration as recorded with the LISST 100X deployed near the bottom at BR-K-14.

4.0 CONCLUSIONS

This section of the report provides additional discussion on the 2014-2015 QA/QC dataset available thus far. Concluding remarks on features of interest are provided in section 4.1. Lessons learned from the 2015 field operations are listed in section 4.2. At this stage of the project, the lessons learned and recommendations are currently being addressed to make more robust and secure future mooring deployments in 2016; and to increase the overall quality of the dataset. Objectives and priorities for 2016-2017 are also presented in section 4.3, including an outlook of the foreseeable milestones for the second year of the iBO scientific program.

4.1 Concluding Remarks on the 2014-2015 Dataset

The core of this report aimed at providing an initial review of the available QA/QC data from the 7 iBO moorings recovered in 2015. Valid data and various quality indicators have been presented for current meters and current profilers deployed at all moorings; as well as CT loggers from the BR moorings. The QA/QC dataset for these instruments is readily available as formatted Text files (ASCII) provided as a data deliverable (see Appendix D). In addition, an initial outlook on sediment fluxes (particle size distribution) and plankton community structure over the slope was presented using the preliminary LISST 100X dataset from BR-K and part of the sediment trap data. A number of features of interest were recorded that warrant further investigation:

- A consistent pattern of stronger currents flowing to the west-southwest (typically stronger at the surface than at depth, up to ~0.8 m/s at DFO-2 and BR-K) was generally measured at all moorings in October 2014. Variability of temperature-salinity recorded concomitantly suggests that shelf-break upwelling occurred during this period. Data should be investigated further to determine the chronology of this event regionally and to understand the larger physical context, including the atmospheric forcing factors.
 - A general increase in the along-slope current component was recorded around late February/early March 2015 at all moorings. This general increase was seen as a depth-intensified current (up to 0.4-0.5 m/s at BR-K at ~100 m) flowing to the east-northeast. At BR-3, stronger currents during this event were recorded in the lower portion of the water column (>300 m), suggesting a vertical dissipation of the along-slope velocity component as this current propagated northward. Further investigation of this phenomenon could be undertaken to decipher its nature and determine its characteristics (period, amplitude).
 - Eddy-like features were identified visually in the current speed/direction and temperature-salinity time-series, especially at BR-G-14. This latter dataset could be used to further characterize and investigate the dynamics of these features and discuss their implications in terms of vertical and horizontal transport.
 - Current speed and direction data at BR-K-14 provide evidence for the occurrence of a unique narrow jet-like current trapped to the shelf break and characterized by relatively elevated mean current speeds (~13-16 cm/s) not measured at any other mooring. The variability of this narrow and energetic current should be investigated, including his possible role in eddy formation and its impact on seawater trajectories and particulate matter fluxes.
 - Temperature-salinity and current speed time-series showed small-scale high-frequency fluctuations (<1 day) that resemble internal tide oscillations that could be analyzed using power spectral density estimates. Such processes are important to understand the oceanic variability occurring within the mesoscale frequency band, encompassing periods of one hour to one day.
 - The strong peak in phytoplankton cells observed at the upper sediment trap at BR-G-14 in early June 2015 appears to be unusually early for the onset of the productive season in the offshore domain of the Beaufort Sea. This peak should be analyzed in a larger spatial and temporal context to identify if 2015 was an unusual year in terms of vernal ice melt and biological activity.
-

4.2 2015 Fieldwork Lessons Learned and Recommendations

This section of the report identifies lessons learned and recommendations from work on the Amundsen and Laurier during the 2015 iBO Program that are currently being addressed to improve future mooring deployments and recoveries. The list of recommendations has been finalized following the iBO TAC Meeting that was hosted as part of the ArcticNet Annual Scientific Meeting, Vancouver, on December 7, 2015 (see Appendix B).

- Following the overpressure and spillage of a benthos pinger during leg 3a onboard the Amundsen, it is recommended that the benthos pingers should not be redeployed as part of any further redeployment of iBO moorings. Alternative location devices, such as Sonotronics pingers should be evaluated to replace the Benthos pingers. Extra care should be taken in the handling of any pingers to be recovered in 2016.
- Although sediment trap motors have proven to be robust and reliable instruments over the years, the unexpected failure of one of them at BR-1-14 underscores the need to carry spare trap motors as part of every future expedition.
- The damaged TRDI battery housing from the TRDI QM ADCPs that stopped recording prematurely require complete refurbishing before further usage. Inspection of the connector on the dummy plug side of all TRDI housings in stock should be inspected and replaced to prevent future leaks. However, the use of silicone grease and duct tape to protect impulse bulkhead connectors from corrosion of the power pin on RDI ADCPs appears to be effective and should be continued.
- Battery packs for the TRDI ADCPs and Benthos acoustic releases fabricated by *Batteries Experts* and provided by *Crobel Electronique* were found to have a very poor fit in their respective housings. It is advised that proper batteries from the manufacturer should be bought in future years.
- Given the discrepancy between some target instrument depths and instrument depths measured in situ by upper instruments on the lower slope moorings (e.g. the IPS at BR-1-14 was 10 m shallower; the SBE 37SM at BR-G-14 was ~15 m shallower; and the TRDI QM ADCP at BR-3-14 was ~20 m shallower than expected), the lengths of the Kevlar rope segments dedicated to the longer offshore moorings should be thoroughly verified before being reutilized in 2016. In place, the progressive replacement of ropes for longer BR moorings in 2016 is recommended given that some of them have been used since 2011 or possibly earlier.
- It has been noticed that the calibration date of RBR CT instruments is outdated (3 years old). All recovered RBR CT loggers and SBE 37SM CTD should be calibrated before re-deployment in 2016. RBR instrument #22044 (that stopped recording prematurely) should be particularly inspected for any problem as the cause of the battery failure within this instrument was not identified.
- Changing the galvanized steel shackles above RDI & Nortek ADCPs for stainless steel shackles (316 grade) should be considered to minimize perturbations of the magnetic field near the ADCP compasses. Alternatively, the effect of the galvanized steel shackle above the ADCP could be verified by testing the compass accuracy with and without the shackle above it (as part of the routine maintenance activities conducted at Laval University for example).
- Consider buying additional M40 floats or stainless steel cages from Squarewave Marine Technologies to duplicate TRDI ADCPs floats for longer slope moorings and facilitate turn-around at sea (i.e. in the case that the Laurier is used to turnaround lower slope moorings).
- Titanium bars should be preferred to stainless steel bars on sediment traps to avoid corrosion with shackles. An inventory of the amount of traps with stainless steel bars is needed before considering changing the bars. In place, changing the stainless steel bars for in-line ropes could be evaluated.

- Nortek instruments on BR-1-14 that could not be verified as part of the compass verification activity conducted in Inuvik in the wake of the Amundsen expedition should be verified at Laval University for consistency with other equipment.

4.3 Objectives and Milestones for 2016-2017

Objectives of iBO for 2016-2017 are centered on the recovery and redeployment of the 7 iBO moorings from the Amundsen and Laurier icebreakers. Foreseeable milestones for 2016-2017 are listed in Table 18. This includes the finalization of the QA/QC for 2014-2015 data and the upcoming processing of 2015-2016 datasets. Ancillary activities like the verification of ADCP compasses and several TAC meetings to address field logistic and operations are planned to ensure a timely development of the project in 2016-2017. Outreach activities to disseminate the results of the program (peer-reviewed publications and conference presentations) and to foster collaborations with the larger Beaufort Sea community will also be undertaken assuming that iBO will be supported by ESRF and industry partners in 2016-2017 at least to the same extent as in 2015-2016. In addition of the milestones listed in Table 18, we aim at pursuing a certain number of secondary objectives, which also depends on the total funding available for data processing and analyses within iBO. These include:

- A further harmonization of the QA/QC methodology used to process data from current profilers and CT loggers from the shelf moorings (processed by DFO) and slope moorings (processed by Golder/ArcticNet). Bin depth mapping, bad data masking and filtering as well compass correction represent key elements to be addressed.
- Potential development of a common data format aligned with the NetCDF format and conventions, including the development of a conversion tool between DFO and Golder/ArcticNet respective ASCII formats. This would allow iBO data to be better aligned with international conventions, thus providing an improved archiving approach.
- Topical studies that would specifically address the iBO science objectives, including the documentation of poorly resolved processes (e.g. mesoscale eddies) or extreme ice and ocean features (e.g. storm surges) and their impact on the marine environment and biogeochemical fluxes.
- Initiation of a “Status of the Beaufort Sea” report that would build on published studies and results, existing data (but unpublished), as well as newly-acquired datasets to review the ice-ocean setting and provides new knowledge on the functioning and seasonality of the region. The timeline and scope of this status report remain to be established.

Table 18: 2016-2017 iBO Milestones

Milestone	Date
Pre-field 2016 Operational Conference Call Meeting	April 29, 2016
Instrumentation maintenance completed at DFO and ArcticNet	May 15, 2016
Presentation of the iBO program and preliminary results as part of the session “Monitoring marine ecosystems and climate” of CMOS 2016, Fredericton	June 1, 2016
Finalization of 2014-2015 CT logger dataset, including correction for offset and drift	August 1, 2016
Technical Advisory Committee Conference Call - Summer Meeting	August 10, 2016
Recovery and redeployment of slope moorings onboard the Amundsen	September 15, 2016
Post-field verification of Nortek and TRDI ADCP compasses in Inuvik	September 20, 2016

Finalization of 2014-2015 current meter and current profiler QA/QC dataset	December 1, 2016
Recovery and redeployment of shelf moorings onboard the Laurier	October 20, 2016
Publication of iBO paper (project description) as part of the Arctic Journal	November 1, 2016
Annual Technical Advisory Committee Meeting, ArcticNet Science Meeting, Winnipeg	December 5, 2016
2 nd Beaufort Collaborations Meeting, ArcticNet Science Meeting, Winnipeg	December 6, 2016
Publication of iBO paper as part of the project update section of the Eos Journal	January 15, 2017
Finalization of data processing of IPS 2014-2015 and related reporting	January 31, 2017
QA/QC of ADCP and CT logger 2015-2016 data	March 31, 2017
iBO Technical Report 2016-2017 Submitted	March 31, 2017

5.0 REFERENCES

- Aagaard, K., 1984. The Beaufort Undercurrent. In: Barnes, P.W., Schell, D.M., Reimnitz, E. (Eds.), *The Alaskan Beaufort Sea: Ecosystems and Environments*. Academic Press, New York, pp. 47–74.
- ASL Environmental Sciences Inc. 2015. *IPS Processing Toolbox User's Guide*. Report by ASL Environmental Sciences Inc., Victoria BC, Canada, 136 pp.
- Barber, D.G., Hanesiak, J.M., 2004. Meteorological forcing of sea ice concentrations in the southern Beaufort Sea over the period 1979 to 2000. *J. Geophys. Res. (C Oceans)* 109, C06014.
- Blasco, S., Bennett, R., Brent, T., Burton, M., Campbell, P., Carr, E., Covill, R., Dallimore, S., Davies, E., Hughes-Clarke, J., Issler, D., Leonard, L., MacKillop, K., Mazzotti, S., Patton, E., Rogers, G., Shearer, J. and White, M., 2013. 2010 State of Knowledge: Beaufort Sea Seabed Geohazards Associated with Offshore Hydrocarbon Development; Geological Survey of Canada, Open File 6989, 340 p. doi:10.4095/292616
- Carmack, E.C., MacDonald, R.W., 2002. Oceanography of the Canadian Shelf of the Beaufort Sea: a Setting for Marine Life. *Arctic* 55, suppl. 1, 29-45.
- Dmitrenko, I. A., Kirillov, S. A., Forest, A., Gratton, Y., Volkov, D. L., Williams, W. J., Lukovich, J. V., Belanger, C. and Barber, D. G. 2016, Shelfbreak current over the Canadian Beaufort Sea continental slope: Wind-driven events in January 2005. *J. Geophys. Res. Oceans*. Accepted Author Manuscript. doi:10.1002/2015JC011514
- Fissel, D. B., Marko, J. R., Melling, H. 2008, (July). Advances in marine ice profiling for oil and gas applications. In *Proceedings of the Ictech 2008 Conference*.
- Forest, A., Osborne, P. D., Fortier, L., Sampei, M., and Lowings, M. G. 2015. Physical forcings and intense shelf–slope fluxes of particulate matter in the halocline waters of the Canadian Beaufort Sea during winter. *Continental Shelf Research*, 101, 1-21.
- Galley, R. J., Else, B. G. T., Prinsenber, S. J., Babb, D., Barber, D. G. 2013. Summer Sea Ice Concentration, Motion, and Thickness Near Areas of Proposed Offshore Oil and Gas Development in the Canadian Beaufort Sea—2009. *Arctic*, 105-116.
- Giovando, L.F., Herlinveaux, R.H., 1981. A discussion of factors influencing dispersion of pollutants in the Beaufort Sea. *Pacific Marine Science Report* 81-4, p. 198.
- Golder 2015. *ArcticNet 2015 Leg 3a Safety Incident Report: Benthos Locator Overpressure*. Memorandum
- Integrated Ocean Observing System (IOOS). 2015. *Manual for Real-Time Quality Control of In-Situ Current Observations: A Guide to Quality Control and Quality Assurance of Acoustic Doppler Current Profiler Observations*. Version 2.0 October 2015.
- Kulikov, E.A., Carmack, E.C., Macdonald, R.W., 1998. Flow variability at the continental shelf break of the Mackenzie Shelf in the Beaufort Sea. *Journal of Geophysical Research. C. Oceans* 103, 12,725-712,741.
- Lansard, B., Mucci, A., Miller, L. A., Macdonald, R. W., Gratton, Y. 2012. Seasonal variability of water mass distribution in the southeastern Beaufort Sea determined by total alkalinity and $\delta^{18}\text{O}$. *J. Geophys. Res. (C Oceans)* 117(C3).
- Macdonald, R.W., Paton, D.W., Carmack, E.C., Omstedt, A., 1995. The freshwater budget and under-ice spreading of Mackenzie River water in the Canadian Beaufort Sea based on salinity and $\delta^{18}\text{O}/\delta^{16}\text{O}$ measurements in water and ice. *J. Geophys. Res. (C Oceans)* 100, 895-919.

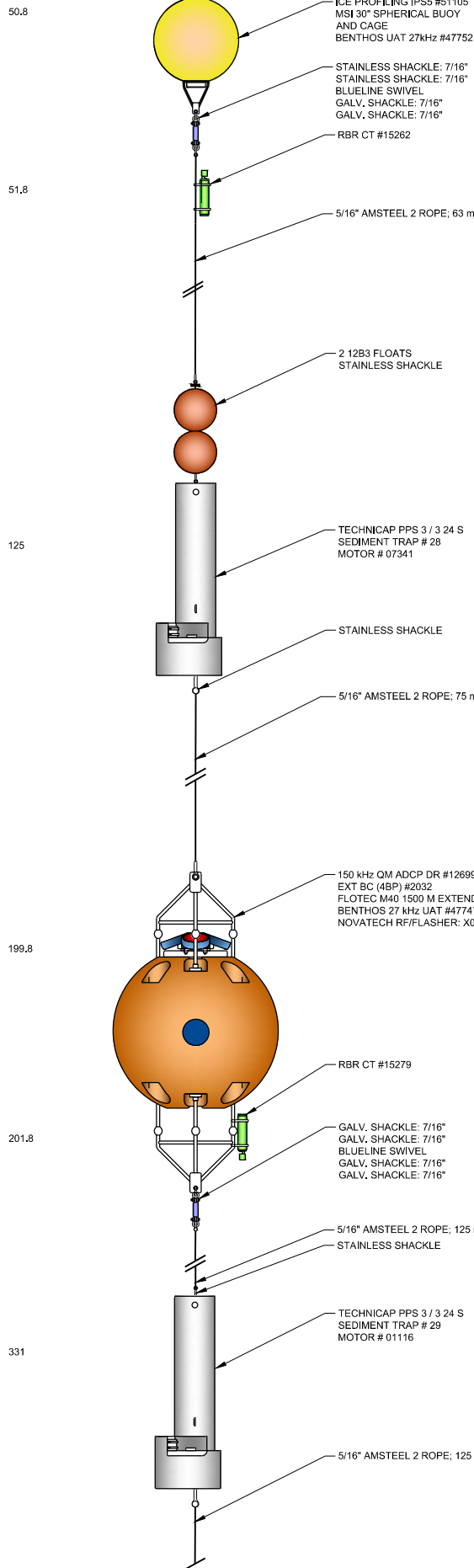
- Macdonald, R.W., Solomon, S.M., Cranston, R.E., Welch, H.E., Yunker, M.B., Gobeil, C., 1998. A sediment and organic carbon budget for the Canadian Beaufort Shelf. *Marine Geology* 144, 255-273.
- Melling, H., 1993. The formation of a haline shelf front in wintertime in an ice-covered arctic sea. *Continental Shelf Research* 13, 1123–1147.
- Melling, H., Riedel, D.A. 2004. Draft and Movement of Pack Ice in the Beaufort Sea: A Time-Series Presentation April 1990 - August 1999. Canadian Technical Report of Hydrography and Ocean Sciences 238, v + 24 pp.
- Melling, H., Johnston, P. H., Riedel, D.A. 1995. Measurements of the underside topography of sea ice by moored subsea sonar. *Journal of Atmospheric and Oceanic Technology*, 12(3), 589-602.
- Melling, H., Gratton, Y., Ingram, G. 2001. Ocean circulation within the North Water polynya of Baffin Bay. *Atmosphere-Ocean*, 39(3), 301-325.
- Nortek AS (Nortek). 2013. Comprehensive Manual. December 2013.
- O'Brien, M.C., Macdonald, R.W., Melling, H., Iseki, K., 2006. Particle fluxes and geochemistry on the Canadian Beaufort Shelf: Implications for sediment transport and deposition. *Continental Shelf Research* 26, 41-81.
- Pickart, R.S., 2004. Shelfbreak circulation in the Alaskan Beaufort Sea: Mean structure and variability. *J. Geophys. Res. (C Oceans)* 109, C04024.
- Pickart, R.S., Schulze, L.M., Moore, G.W.K., Charette, M.A., Arrigo, K.R., van Dijken, G., Danielson, S.L., 2013. Long-term trends of upwelling and impacts on primary productivity in the Alaskan Beaufort Sea. *Deep Sea Research Part I: Oceanographic Research Papers* 79, 106-121.
- RBR-Global (RBR). 2016. Ruskin User Guide. Latest version available at: <https://rbr-global.com/support/software>.
- Beardsley, R. C., and L. K. Rosenfeld 1983, Introduction to the CODE-1 moored array and large-scale data report, in CODE-1: Moored Array and Large-Scale Data Report, edited by L. K. Rosenfeld, Tech. Rep. WHOI-83-23, CODE Tech. Rep. 21, pp. 1216, Woods Hole Oceanogr. Inst., Woods Hole, Mass.
- Sequoia Scientific. 2008. Processing LISST-100 and LISST-100X Data in MATLAB. Online Article (last update: 11 July 2012). <http://www.sequoiasci.com/article/processing-lisst-100-and-lisst-100x-data-in-matlab/>.
- Teledyne RDI (TRDI). 2014. Monitor, Sentinel, Mariner, Long Ranger, and Quartermaster Commands and Output Data Format. P/N 957-6156-00. Revised March 2014.
- Teledyne RDI (TRDI). 2006. Acoustic Doppler Current Profiler Principles of Operation: A Practical Primer. P/N 951-6069-00. December 2006.
- von Appen, W. J., Pickart, R. S. 2012. Two configurations of the western Arctic shelfbreak current in summer. *Journal of Physical Oceanography*, 42(3), 329-351.
- Williams, W. J., Melling, H., Carmack, E. C., & Ingram, R. G. 2008. Kugmallit Valley as a conduit for cross-shelf exchange on the Mackenzie Shelf in the Beaufort Sea. *Journal of Geophysical Research: Oceans*, 113(C2).

Appendix A. 2014-2015 Final Mooring Diagrams

The final mooring diagrams 2014-2015 are provided below. Instrument depths correspond to the mean depths measured (for instruments equipped with a pressure sensor) or estimated for each instrument throughout the deployment period.

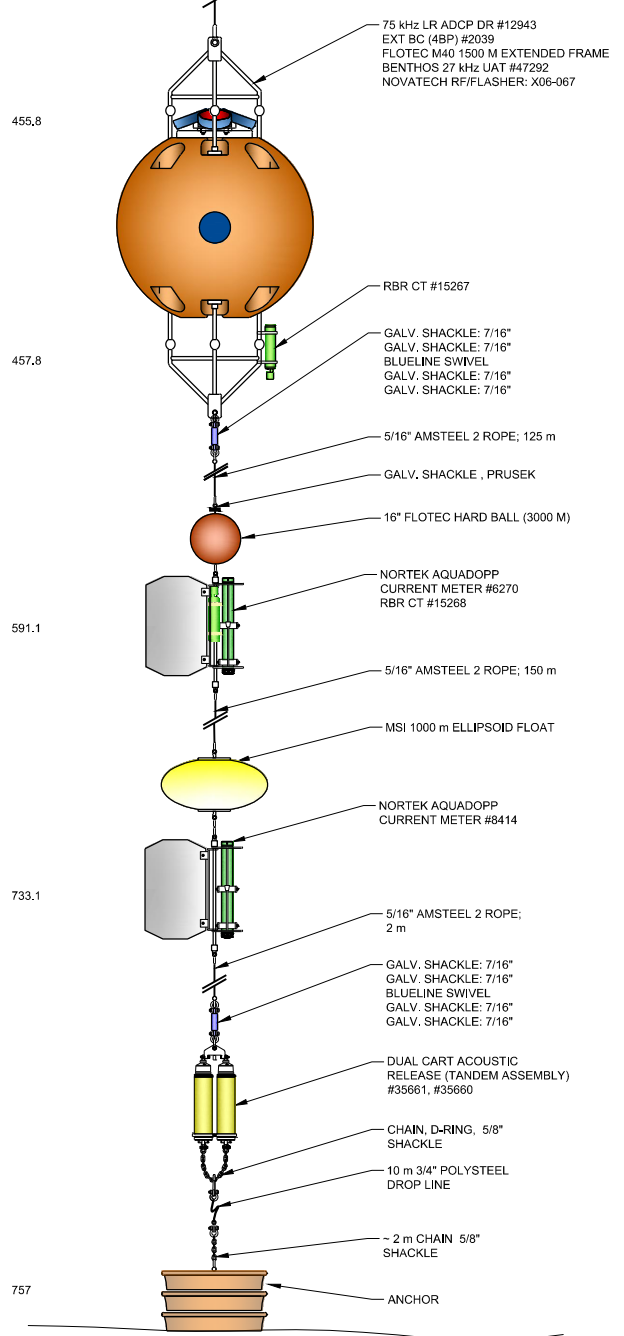
DEPTH (m)

COMPONENT



DEPTH (m)

COMPONENT



NOT TO SCALE

CLIENT
ARCTICNET

PROJECT
BREA \ IBO

TITLE
2014-2015 MOORING DIAGRAM BR-1

CONSULTANT

YYYY-MM-DD 2016-03-16

PREPARED GC

DESIGN GC

REVIEW AF

APPROVED ---



PROJECT No.
1406102

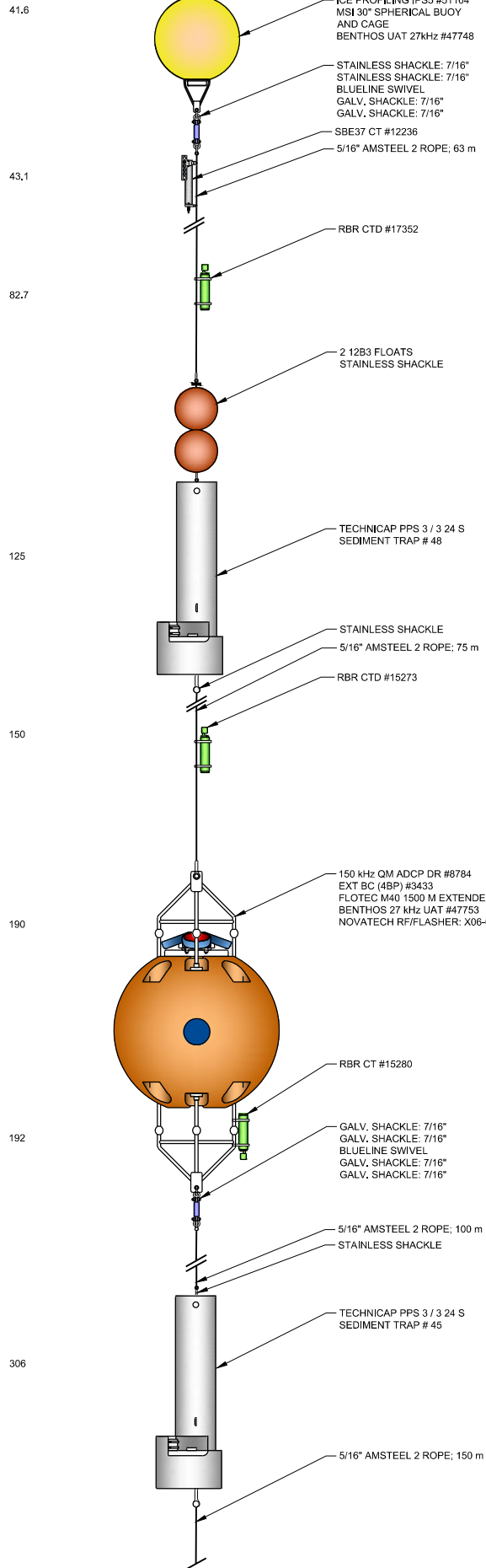
CONTROL

Rev.

FIGURE
3

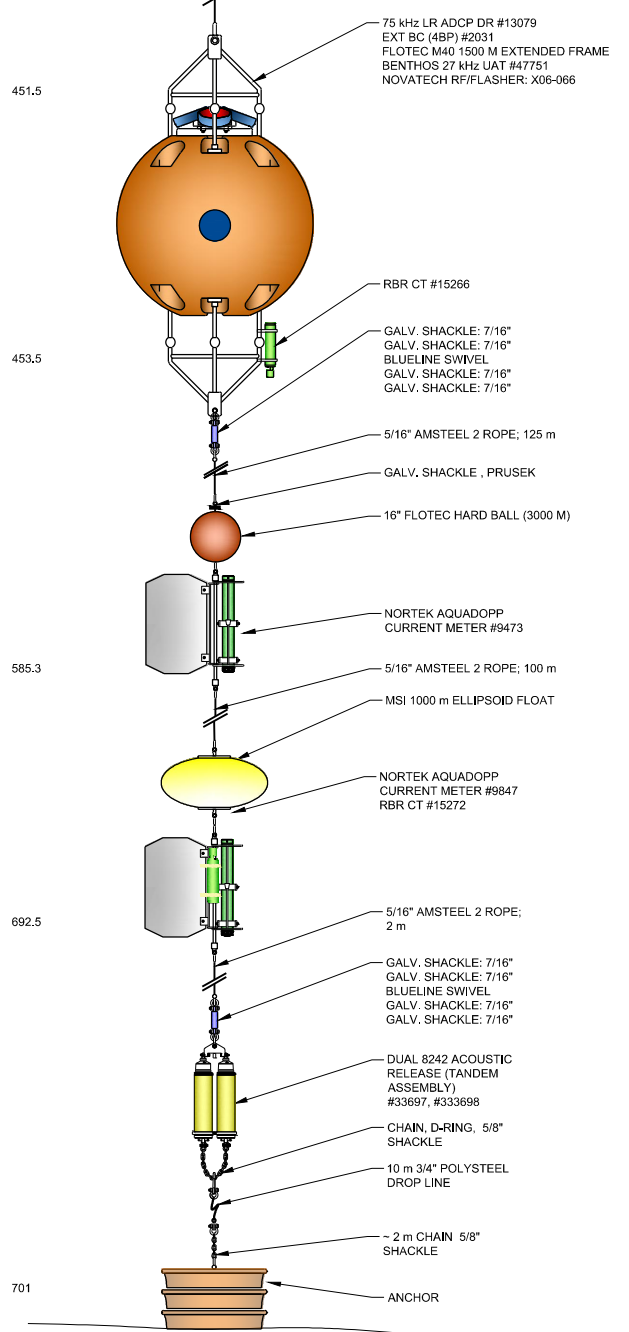
DEPTH (m)

COMPONENT



DEPTH (m)

COMPONENT



NOT TO SCALE

CLIENT
ARCTICNET

PROJECT
BREA \ IBO

TITLE
2014-2015 MOORING DIAGRAM BR-G

CONSULTANT

YYYY-MM-DD 2016-03-14

PREPARED GC

DESIGN GC

REVIEW AF

APPROVED ---



PROJECT No.
1406102

CONTROL

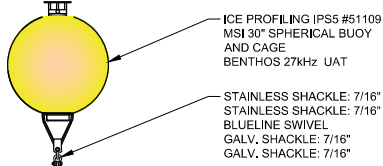
Rev.

FIGURE
2

DEPTH (m)

COMPONENT

37.6



38.7

SPMD

39.6

5/16" AMSTEEL 2 ROPE; 63 m

2 12B3 FLOATS
STAINLESS SHACKLE

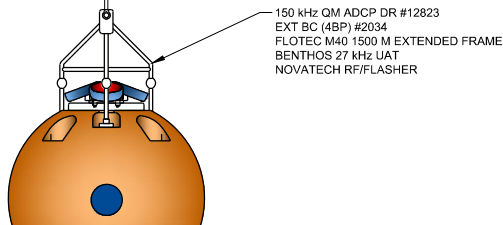
125

TECHNICAP PPS 3 / 3 24 S
SEDIMENT TRAP # 39
MOTOR # 09-845

STAINLESS SHACKLE

5/16" AMSTEEL 2 ROPE; 70 m

179.2



181.2

SPMD

182.2

5/16" AMSTEEL 2 ROPE; 125 m

STAINLESS SHACKLE

326

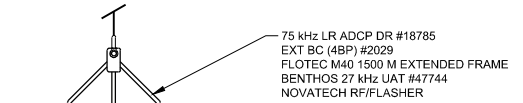
TECHNICAP PPS 3 / 3 24 S
SEDIMENT TRAP # 47
MOTOR # 12-25

5/16" AMSTEEL 2 ROPE; 125 m

DEPTH (m)

COMPONENT

445.6



447.6

RBR CT #15281

GALV. SHACKLE: 7/16"
GALV. SHACKLE: 7/16"
BLUELINE SWIVEL
GALV. SHACKLE: 7/16"
GALV. SHACKLE: 7/16"

553.1

5/16" AMSTEEL 2 ROPE; 125 m

GALV. SHACKLE, PRUSEK

16" FLOTEC HARD BALL (3000 M)

NORTEK AQUADOPP
CURRENT METER #8418

677.6

5/16" AMSTEEL 2 ROPE; 100 m

MSI 1000 m ELLIPSOID FLOAT

NORTEK AQUADOPP
CURRENT METER #2756
RBR CT #15275

700

5/16" AMSTEEL 2 ROPE;
2 m

GALV. SHACKLE: 7/16"
GALV. SHACKLE: 7/16"
BLUELINE SWIVEL
GALV. SHACKLE: 7/16"
GALV. SHACKLE: 7/16"

DUAL CART ACOUSTIC
RELEASE (TANDEM ASSEMBLY)
#33749, #33748

CHAIN, D-RING, 5/8"
SHACKLE

10 m 3/4" POLYSTEEL
DROP LINE

~ 2 m CHAIN 5/8"
SHACKLE

ANCHOR

NOT TO SCALE

CLIENT
ARCTICNET

PROJECT
BREA | IBO

TITLE
2014-2015 MOORING DIAGRAM BR-3

CONSULTANT

YYYY-MM-DD 2016-03-16

PREPARED GC

DESIGN GC

REVIEW AF

APPROVED ---

PROJECT No.
1406102

CONTROL

Rev.

FIGURE
4



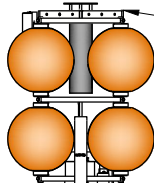
Path: \\fredmond\geomat\geomat\GOLDER\COSTAL_GROU..._PROJECTS\13340031_..._PRODUCTION\DWG... | File Name: 13340031_4000_4001-HC-006.dwg

IF THIS MEASUREMENT DOES NOT MATCH WHAT IS SHOWN, THE SHEET SIZE HAS BEEN MODIFIED FROM ANSII A

DEPTH (m)

COMPONENT

57.4



ICE PROFILING SONAR IPS5 #51108
 ASL DUAL CAGE
 8 12B3 FLOATS
 NOVATECH RF/FLASHER: X06-061
 XR420CTm+Tu+FI+DO #22043
 BENTHOS 27KHz UAT #47745

GALV. SHACKLE: 1/2"
 GALV. SHACKLE: 7/16"
 BLUELINE SWIVEL
 GALV. SHACKLE: 7/16"
 GALV. SHACKLE: 7/16"

58.6

SBE37 CT #12235

5/16" AMSTEEL 2 ROPE; 74 m

95.9

RBR CTD +Tu + DO #10419

136.1

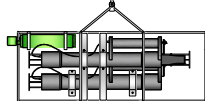
300KHz WH ADCP #2646
 EXT BC FOR ADCP #3835
 MSI 300 m ELLIPSOID FLOAT & STEEL CAGE
 BENTHOS 27KHz UAT #47873

GALV. SHACKLE: 5/8"
 GALV. SHACKLE: 7/16"
 BLUELINE SWIVEL
 GALV. SHACKLE: 7/16"
 GALV. SHACKLE: 7/16"

MSI 300 m ELLIPSOID FLOAT

5/16" AMSTEEL 2 ROPE; 2 m

139.2



XR420CT + Tu + FI + DO #22044
 LISST-100X PARTICLE ANALYZER # 1473
 STAINLESS STEEL INSTRUMENT FRAME

GALV. SHACKLE: 7/16"
 GALV. SHACKLE: 7/16"
 BLUELINE SWIVEL
 GALV. SHACKLE: 7/16"
 GALV. SHACKLE: 7/16"

1MHz NORTEK AQUADOPP
 CURRENT PROFILER AQD #11147

140.0

GALV. SHACKLE: 7/16"
 GALV. SHACKLE: 7/16"
 BLUELINE SWIVEL
 GALV. SHACKLE: 7/16"
 GALV. SHACKLE: 7/16"

5/16" AMSTEEL 2 ROPE; 2 m

DUAL CART ACOUSTIC
 RELEASE (TANDEM
 ASSEMBLY)
 #33737, #33738

D-RING SHACKLE: 3/4"
 10 m 3/4" POLYSTEEL
 DROP LINE

~ 2 m CHAIN

GALV. SHACKLE: 7/8"

155



ANCHOR

NOT TO SCALE

CLIENT
 ARCTICNET

PROJECT
 BREA \ IBO

TITLE
 2014-2015 MOORING DIAGRAM BR-K

CONSULTANT



YYYY-MM-DD 2016-03-07

PREPARED GC

DESIGN GC

REVIEW AF

APPROVED

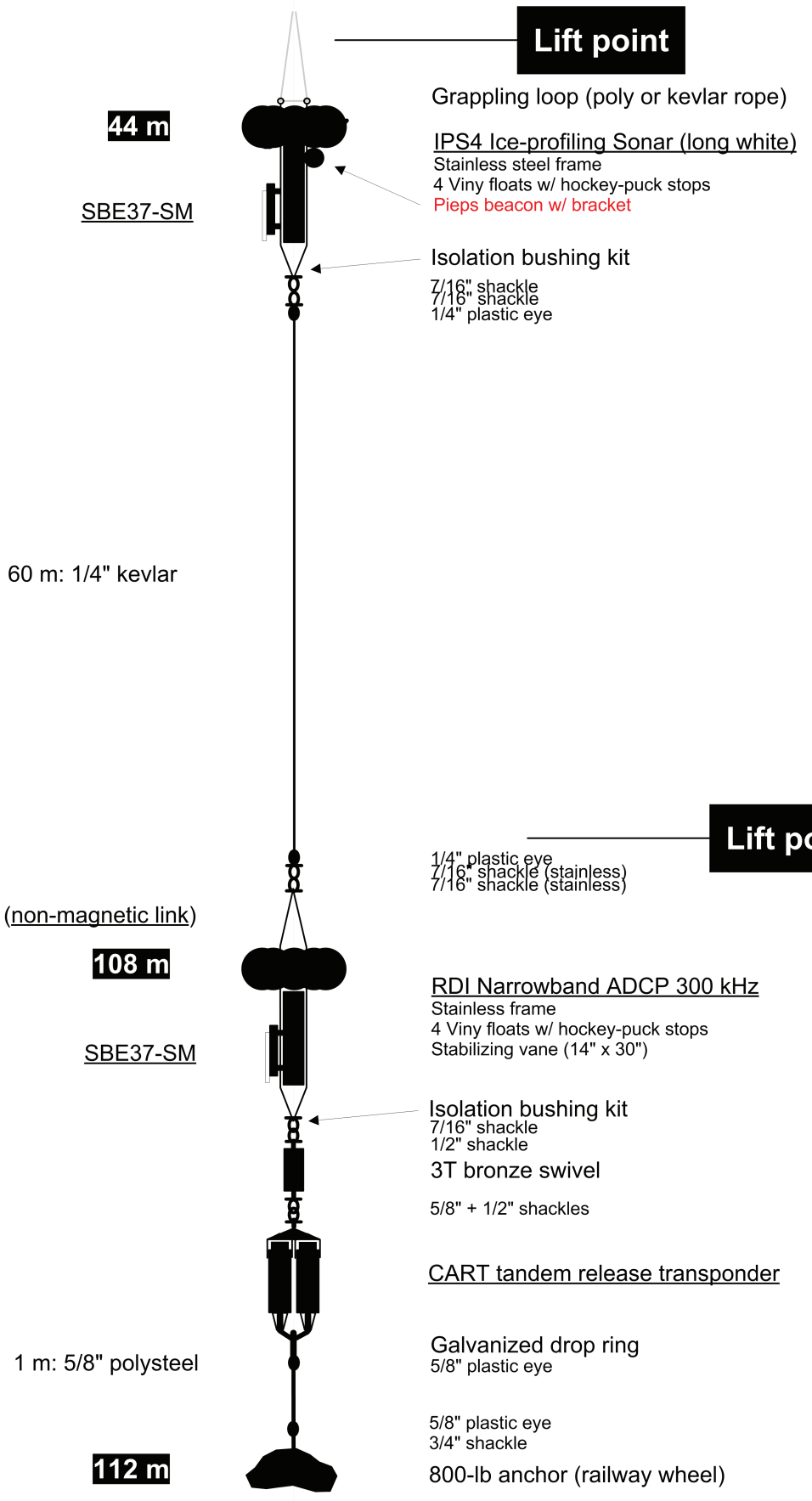
PROJECT No.
 1406102

Rev.

FIGURE
 1

Path: \\vesmond\geomat\geomat\GOLDER\COSTAL_GROUP_REDMOND\99_PROJECTS\13340031_ArcticNet\4000_4001\02_PROD\DUCTION\DWG\13340031_4000_4001-HC-001.dwg

IF THIS MEASUREMENT DOES NOT MATCH WHAT IS SHOWN, THE SHEET SIZE HAS BEEN MODIFIED FROM ANSI A



Lift point

Use a kevlar loop tied to the hook
The cut end should pull through the lugs
on deployment

44 m

SBE37-SM

Grappling loop (poly or kevlar rope)
IPS4 Ice-profiling Sonar (long white)
Stainless steel frame
4 Viny floats w/ hockey-puck stops
Pieps beacon w/ bracket

Isolation bushing kit
7/16" shackle
7/16" shackle
1/4" plastic eye

60 m: 1/4" kevlar

Site 2 Mooring
2014-2015 Beaufort Sea
71° 00' N, 133° 45' W
Declination: 24.4°
Inclination: 83.1°
H = 7078 nT

Lift point

Use a kevlar loop tied to frame.
The cut end should pull through the
opening

(non-magnetic link)

108 m

SBE37-SM

1/4" plastic eye
7/16" shackle (stainless)
7/16" shackle (stainless)

RDI Narrowband ADCP 300 kHz
Stainless frame
4 Viny floats w/ hockey-puck stops
Stabilizing vane (14" x 30")

Isolation bushing kit
7/16" shackle
1/2" shackle
3T bronze swivel
5/8" + 1/2" shackles

1 m: 5/8" polysteel

CART tandem release transponder

Galvanized drop ring
5/8" plastic eye

112 m

5/8" plastic eye
3/4" shackle
800-lb anchor (railway wheel)

Twinned Moorings at Sites 1 & 9

2014-2015 Beaufort Sea

70° 20'N 133° 45'W & 70° 05'N 133° 45'W

Depth: 55 m & Depth: 35 m

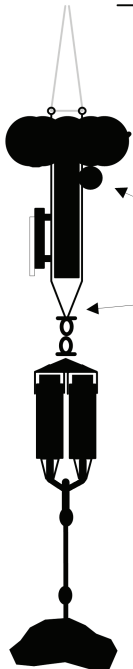
Declination: 23.6° Inclination: 82.7° H = 7380 nT

Use a kevlar loop tied to the hook
The cut end should pull through the
lugs on deployment

Lift point

X-3 m

SBE37-SM



Grappling loop (poly or kevlar rope)

IPS4/5 Ice-profiling Sonar (long white)

Stainless steel frame
4 Vinyl floats w/ hockey-puck stops
Pieps beacon w/ bracket

Isolation bushing kit

5/8" + 7/16" shackles

CART tandem release transponder

Galvanized drop ring
5/8" plastic eye

5/8" plastic eye
3/4" shackle

450-lb anchor (chain clump)

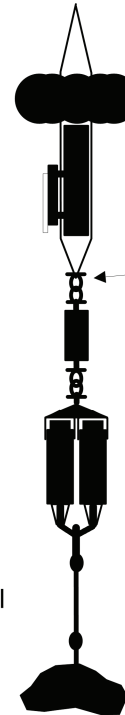
1 m: 5/8" polysteel

X m

Lift point

X-4 m

SBE37-SM



RDI NB or WH ADCP 300 kHz

Stainless frame
4 Vinyl floats w/ hockey-puck stops
Stabilizing vane (14" x 30")

Isolation bushing kit

7/16" shackle
1/2" shackle

3T bronze swivel

5/8" + 1/2" shackles

CART tandem release transponder

Galvanized drop ring
5/8" plastic eye

5/8" plastic eye
3/4" shackle

450-lb anchor (chain clump)

1 m: 5/8" polysteel

X m

October 2, 2014

**integrated Beaufort Observatory (iBO) 2015 Annual Meeting
Technical Advisory Committee Meeting Minutes**

ArcticNet Annual Scientific Meeting
Westin Bayshore Vancouver, Room Coquitlam
7 December 2015, 13:00 – 17:00

Agenda and summary of discussion

13:00 to 13:10 Welcome and introduction

**Approval of agenda
Meeting objectives**

- *Review 2015 field activities and lessons learned*
- *Review 2014-2015 data recovery success*
- *Coordinate ESRF reporting (due 31 March 2016)*
- *Early planning of 2016 field campaigns*

13:10 to 14:00 Review of 2015 field activities and lessons learned

- *Debrief on planning and field mobilization*
 1. **Timeline:** Planning went smoothly. Calibration of TRDI ADCPs in Inuvik successful. Satellite compass required for 2016 calibration activities. Conference calls helped to coordinate between teams. Agreement on mooring modifications and instrument settings was reached. Work instructions and record sheets helped to be ready at sea.
- *CCGS Amundsen recoveries and deployments*
 1. **Recovery:** A total of 7 moorings were successfully recovered from the CCGS *Amundsen*. However, mooring BS-1 was only recovered using a homemade grappling device made on board and after 2-3 attempts. Although the reason for the failed release of mooring BS-1 from its anchor is unknown, it is suggested that shorter chains be used between the releases to avoid a situation where the chains get pinched or stuck. A Norwegian grapple should always be on board.
 2. **Deployment:** Adjustments should be made with the upper line to get the right length/depth of moorings. Drop lines should be a minimum of 5 m long (when deployed from the *Amundsen*). Humfrey uses 1 m drop lines because on the *Laurier* the mooring is held from the top of the acoustic release and releases and anchors are lifted together from the boom crane (unlike using the A-Frame on *Amundsen*).
 3. **Batteries:** Better to buy original batteries from manufacturer to avoid poor fit (e.g. TRDI)
 4. **Offset of mooring length:** Humfrey suggests that the offset may be due to the measuring device, but could also be due to the precision of the water column software of the *Amundsen's* multibeam. A section is marked on the concrete to get accurate lengths at IOS.
 5. **On board documentation:** need to take photos of each instrument as they come out of the water
- *CCGS Laurier recoveries and deployments*
 1. **Operations:** CCGS *Laurier* was in a multitask/Arctic patrol mode with a schedule mostly constrained by fueling in Dutch Harbor. The budgeted iBO time (2.5 days) worked overall but was difficult due to the multitask program.
- *Health and safety*
 1. **CCGS Amundsen:** The explosion of a Pinger resulted in a hand injury. This was due to a problem of pressurization or a leak combined with a weak cap (titanium cap would have been ok). There is still one pinger to be recovered by the CCGS *Laurier* next year so use caution. As this could happen with other suspicious/risky instruments, procedures must be reviewed to restrict access to the mooring laboratory 610 on CCGS *Amundsen*.

14:00 to 15:00 Review of 2014-2015 data recovery success

- *Instrumentation performance – causes and implications*
 1. ASL Ice profilers
 - Overall ASL ice profilers were successful. New settings were useful.
 2. TRDI ADCP
 - Problems with batteries
 - All ADCP housings and instrument hardware returned on Amundsen and Laurier should be subject to routine maintenance
 - Sentinel = short-circuit on BR-4 (BR-4 was not redeployed so no further consequences)
 3. Nortek AQD and Continental
 - Aquadopp = some small battery problems but overall success
 - Compass = overall good results except for one Continental. Shawn needs to make a follow-up with Nortek regarding the large error.
 - The magnetic influence of shackles should be tested with the compass.
 4. RBR and SBE CT loggers
 - Only 1 CT sensor failed after one week = short-circuit in one CR battery. The instrument has already been shipped back to RBR to be recalibrated.
 5. Sediment traps and LISST
 - Everything worked except the lower Technicap PPS/3 trap on BR-1; no samples were collected. The pinion was going sideways so it stalled on a sharp corner. Shawn needs to talk to someone at Technicap about it.
 - Titanium bars should replace stainless steel bars on sediment traps to avoid corrosion with shackles. An inventory of the amount of traps with stainless steel bars is needed before considering changing the bars. Humfrey suggests saving money by changing the bars and using a line instead.
 - Biofouling on the LISST apparently affected data quality at the end of the year.
 6. Acoustic releases
 - Be careful regarding steel on steel shackles. evaluate whether galvanized shackles can be used instead – e.g. confirm potential metal to metal corrosion potential and interference with magnetic compasses
 7. Other technical issues (CCGS Laurier)
 - One large TRDI face-seal O-ring was squished.
 - Spare CART release: wire was crushed, or maybe it was a problem with the battery, this needs to be checked.
 - Titanium bolts that appeared to have no grease needed to be cut, which was time-consuming. Maybe BlueGoop was not used on the titanium bolts = when in doubt, use a lot of grease.
 - Shackle pins were also not greased.
 - Over-anoding is always good.
 - All instruments should be shipped in purpose built boxes to avoid potential damage during transport
 - ADCP compasses calibration was impossible due to bad weather = needs to be calibrated next year on Herschel Island

 - *Mooring robustness and reliability: what to improve for 2016 and other lessons learned*
 1. Add iridium beacons (3000\$): Humfrey doubts the necessity of iridium beacons as they are useless if they come up under-ice and may just cause anguish as you know that the mooring is up but you cannot do much about it. Such investment needs to be thoroughly considered.
-

2. Replacing M40 by cages: Consider buying Jo Poole's cages in case of duplicate moorings. 1 cage = 5000\$, 2 cages would be needed for the CCGS Laurier
3. Shawn suggests changing drop lines from Polysteel to Dyneema or Kevlar for improved strength. Phil noted the difference is that Polysteel can stretch somewhat and this is helpful to provide some spring in the line for heavy anchors to avoid potential damage to components on release of the anchor. Martin suggests: If it ain't broke, don't fix it. Shawn should evaluate the costs and benefits, and also verify the ropes' lengths.
4. Dummy plugs and dummy plug connectors on ADCP battery housings need to be verified.
5. Include 1 (or 2) sediment trap spare motors to the IOS shipment next year.
6. Mooring turnover was too long = Need more duplicate gear to improve efficiency.
7. Update Amundsen calibration kit (compass, table)
8. Include LISST comm cable and Benthos deck box in kits for both Amundsen and Laurier

15:00 to 15:15 Break

15:15 to 16:00 Coordinate ESRF reporting

- *Update on ongoing data QA/QC: preliminary figures and datasets*
 1. It is agreed that the datasets from the iBO project need to be made available in a similar format and efforts must be made to coordinate QA/QC procedures. Humfrey's ASCII files could be converted with Matlab to create a single file for each parameter. Humfrey could provide an example file and Alex or Phil will work on a script and assess the effort needed to change the format.
 2. An agreement on a QA/QC protocol must be sorted by the end of January = discussion should start as early as possible. A discussion on the action list is also needed: Share processing steps (filtering, flagging), verify if steps are similar, and if QA/QC rejections are based on the same criteria.
 3. Preliminary data = Need to explore apparent problems with long beam data.
 4. Pressure sensor of Quarter Master at BR-G provided erratic data (needs to adjust depth)
- *Review reporting objectives and plan ESRF report due 31 March 2016 (format, contributors, tasks, timeline)*
 1. The ESRF report due on 31 March is a deliverable of the iBO project (and not a requirement of ESRF). This report will be used by the iBO project members as a reference document to track progress and will also be available to collaborators. There is no template; we just need to agree on a format. Check if an interactive PDF report would be time-manageable.
 2. There are still no IOS-ESRF and IOS-ArcticNet agreements. This will delay the QA/QC schedule. If no ArcticNet – IOS agreement is in place early in the New Year, we may need to consider having ArcticNet pay ASL directly for the IPS analyses (Humfrey to inquire about cost with ASL if done through this route).
 3. Extremely tight reporting schedule with other reports due in February (financial and progress reports).
 4. Data to be included in the technical report (not necessarily what was recovered this year but as much as possible):
 - iBO moorings (7)
 - All TRDI ADCPs (10)
 - IPS
 - CT sensors (15 to 20) including Seabird
 - Traps results if possible (at least pictures of sediment trap cups)
 - LISST
 - All Nortek Aquadopp (7)
 5. Existence of all data must be mentioned in the report even if it is not presented.
 6. Alex, Keith and Catherine will brainstorm and suggest a structure for the report (integrative report with links?)

16:00 to 17:00 Early planning of Beaufort Sea campaigns 2016

- *Overview of CCGS Amundsen and Laurier cruise plans 2016*

1. CCGS Laurier

- Similar cruise in 2016 than in 2015: starting in late September in the Beaufort Sea until the first or second week of October.
- Loading in Victoria during the third week of June.
- There will probably be a participation of the Geological Survey and MBARI with their ROV.
- The new DBO8 line will be sampled.
- There is a possibility that 4-5 days will be available for iBO operations.
- It is agreed that the recovery and deployment of BR-1 will be done on the Laurier once again.

2. CCGS Amundsen

- Mooring activities in August 2015 were at a perfect time regarding weather; it will most probably not be the case in 2016 due to a later expedition date. Timeline:
 - February 9 = Amundsen planning meeting Montreal and mooring design
 - Early May = ADCP calibration
 - May 21-26 = Mobilization
 - May 27-29 = Sea Trials
 - June 3 = Departure
 - September 29 to October 16 = Leg 4 = Beaufort Sea / ArcticNet ESRF
 - 5 moorings to recover and redeploy = CA05-CA08 + BR-G and BR-K in the blocks + BR-3 off Banks Island.
 - October 30 – Nov 4 = Demobilization
- *Overview of the BOEM-MARES program (Francis Wiese, invited)*
 1. Umbrella funding organism over 5 years
 2. 45 PIs – 8 institutions
 3. Emphasis on Mackenzie plume and marine mammals
 4. Potential Healy cruise in June/July leaving from Barrow and sampling DBO lines (funding approval for Healy in mid-January)
 5. Possibility of a drone to measure heat flux
 6. Data deposited at AOOS
 7. Conceptual framework based on alpha-beta oceans (Carmack and Wassmann)
 8. Marine mammal tagging
 9. No moorings in the water at the moment (next year hopefully)
- *Discussion on operational and scientific concerted efforts between iBO and BOEM-MARES*
 1. Interest to develop a Beaufort Collaborative for sharing data and logistics.
 2. Request for the opportunity to send people and deploy gear on board the Amundsen and/or the Laurier. Probably some flexibility for the Amundsen. Quite limited for the Laurier depending on the participation of the Geological Survey; must also be on a collaborative agreement basis.

17:00

Meeting adjourned

**Beaufort Observatory (iBO)
Canadian Beaufort Sea Collaborations Meeting Summary**

ArcticNet Annual Scientific Meeting (ASM)
Westin Bayshore Vancouver, Room Coquitlam
8 December 2015, 8:45-12:00

The first iBO collaborations meeting was held on December 8, 2015 as part of the ArcticNet Annual Scientific Meeting (ASM 2015, Vancouver) to discuss opportunities for bilateral exchange of data, resources and expertise that would help achieve the iBO objectives. The meeting included 21 participants from academia, government, consulting services and the oil and gas industry. It represented the first iBO meeting to discuss enhanced collaborations and identify relevant applications of the past and new mooring datasets that would relate to the perspective and challenges of hydrocarbon development in the Canadian Beaufort Sea.

The meeting agenda included a series of focus presentations summarizing past and ongoing research activities in the Beaufort Sea followed by an open discussion on the need for iBO studies to address questions relevant to stakeholder needs. The central need to have access to long-term and high-quality data on sea ice and on the oceanography of the Beaufort Sea environment was underscored.

The following key questions were identified:

- Can we develop a decision framework on sea ice variability and trends for the operational season and predict local sea ice conditions to inform industry stakeholders and regulators?
- What is the variability of ocean circulation patterns that needs to be taken into account for the development of realistic probabilistic scenarios of seawater/oil spill trajectories over the slope, including under-ice oil spill and its propagation across national boundaries?
- What are the duration and return period of extreme ice thickness features, significant wave heights and ocean currents locally and regionally, including those associated with mesoscale eddies, storm surges and downwelling/upwelling events?

Given the scientific challenges associated with these questions, a strategy is needed to transpose them into specific goals and lines of investigation in order to generate observational case-studies, modelling analyses or concept papers making use of iBO data and/or addressing iBO objectives.

Examples of such studies could include (but are not restricted to):

- Characterization of the inter-annual variability of general ice cover motion/thickness and ocean circulation as a function of different atmospheric patterns;
- Analyses of moored ice and current profiler datasets to document the severity and frequency of occurrence of extreme ice features, waves and ocean currents;
- Detailed investigations of specific oceanographic processes (e.g. up/down-welling, mesoscale eddies, mixed-layer depth, stratification) that could influence oil spill trajectories and fate of surfacing of submerged blowout products;
- Modelling studies on the timing of ice retreat and open water persistence in relation to initial sea ice conditions and atmospheric driver scenarios to develop three-month forecast of ice-season severity;
- Concept paper tying industrial needs with fundamental marine research through the development of innovative scientific objectives;
- Studies to assess rise of blowout plumes (gas, oil, sediment, water) and depth of neutral buoyancy for rising plume emulsions under Arctic conditions of temperature and salinity;

- Data-model analyses to understand containment of pollutant under drifting ice, trajectory of drift with ice following containment, or trajectory of drift with ocean currents at various depths for subsurface plumes.

Within this context, data from iBO will be made available to Canadian and international collaborators. The initiative will not provide new funding, but will rather represent an umbrella to bring together scientists from diverse horizons and industry stakeholders that have an interest in the oceanography of the Canadian Beaufort Sea and its adjacent environments in the primary context of hydrocarbon development.

At this stage, iBO is currently probing the larger community to assess interests to develop specific studies and study goals that could be aligned with the lines of investigation presented above. An approach will be developed to facilitate bilateral exchange of data. A primary step toward the development of an iBO collaborative framework will also be to compile the meta-data from ancillary projects in addition to the meta-data from iBO itself and those from closely related mooring programs (e.g. Fisheries and Oceans Canada, ArcticNet) already available through the Polar Data Catalogue (<https://www.polardata.ca/>).

A preliminary list of iBO collaborators, meta-data, research studies and specific lines of investigation is expected to be completed during fall 2016. This list will be used to develop a hands-on Beaufort Sea collaborations workshop to be hosted at the ArcticNet ASM 2016 in Winnipeg in December 2016. New knowledge and the integration of unpublished data with ongoing records and models generated through the iBO collaborative framework are expected to provide the basis for a *Status of the Beaufort Sea* report.

Appendix D. Data deliverable

In addition to this report, we issue the available oceanographic data that was processed and quality checked following the methods described in section 2.4. The data is provided electronically. This data is provided as a draft and could be subject to further revisions. The data are provided as Matlab and ASCII files for the following instruments:

Mooring	Mooring depth (m)	Instrument	Serial Number	Instrument depth (m)
BR-1-14	757	RBR XR-420 CT	15262	51.8
		TRDI QM ADCP 150 kHz	12699	199.8
		RBR XR-420 CT	15279	201.8
		TRDI LR ADCP 75 kHz	12943	455.8
		RBR XR-420 CT	15267	457.8
		Aquadopp DW 2 MHz	6270	591.1
		RBR XR-420 CT	15268	591.1
		Aquadopp DW 2 MHz	8414	733.1
BR-3-14	700	RBR XR-420 CT	15264	38.7
		TRDI QM ADCP 150 kHz	12823	179.2
		RBR XR-420 CT	15263	181.2
		TRDI LR ADCP 75 kHz	18785	445.6
		RBR XR-420 CT	15281	447.6
		Aquadopp DW 2 MHz	8418	553.1
		Aquadopp DW 2 MHz	2756	677.6
		RBR XR-420 CT	15275	677.6
BR-G-14	701	SBE 37SM (Microcat)	12236	43.1
		RBR XR-420 CTD	17352	82.7
		RBR XR-420 CT	15273	150.0
		TRDI QM ADCP 150 kHz	8784	190.0
		RBR XR-420 CT	15280	192.0
		TRDI LR ADCP 75 kHz	13079	451.5
		RBR XR-420 CT	15266	453.5
		Aquadopp DW 2 MHz	9473	585.3
		Aquadopp DW 2 MHz	9847	692.5
		RBR XR-420 CT	15272	692.5
BR-K-14	155	SBE 37SM (Microcat)	12235	58.6
		RBR XR-420 CTD-Tu-DO	10419	95.9
		TRDI WHS ADCP 300 kHz	2646	136.1
		Aquadopp Profiler 1 MHz	11147	140.0
		RBR XR-420 CT-Tu-FI-DO	22044	140.8
DFO-2-14	112	TRDI NB ADCP 300kHz	586	108.0
DFO-1-14	55	TRDI NB ADCP 300kHz	318	51.0
DFO-9-14	36	TRDI WHS ADCP 300kHz	18318	31.0

Appendix E. Summary Statistics of Ocean Currents

Table 19: Summary statistics of current speed, vector-averaged direction and number of valid records by bin depth at BR-1-14 based on the data acquired with the QM ADCP #12699 from 2014 to 2015. Bin depths flagged manually as part of the QA/QC are highlighted in red.

Bin Depth (m)	Min Speed (m/s)	1%ile Speed (m/s)	5%ile Speed (m/s)	25%ile Speed (m/s)	Median Speed (m/s)	Mean Speed (m/s)	75%ile Speed (m/s)	95%ile Speed (m/s)	99%ile Speed (m/s)	Max Speed (m/s)	Standard Deviation Speed (m/s)	Vector-Averaged Direction (deg TN)	Number of Valid Records	% of Valid Data (%)
19.5	0.00	0.01	0.03	0.07	0.14	0.19	0.27	0.48	0.71	1.58	0.15	241.8	15,503	8.21
27.5	0.00	0.01	0.02	0.05	0.09	0.11	0.14	0.26	0.41	0.87	0.08	251.7	186,750	98.86
35.5	0.00	0.01	0.02	0.06	0.09	0.11	0.14	0.26	0.41	0.66	0.08	250.5	187,810	99.42
43.5	0.00	0.01	0.02	0.06	0.09	0.11	0.14	0.26	0.38	0.61	0.08	249.4	188,080	99.56
51.5	0.00	0.01	0.02	0.06	0.09	0.11	0.14	0.26	0.39	0.59	0.08	248.6	188,070	99.56
59.5	0.00	0.01	0.02	0.05	0.09	0.11	0.14	0.26	0.39	0.65	0.08	247.3	188,050	99.55
67.5	0.00	0.01	0.02	0.05	0.08	0.10	0.13	0.25	0.39	0.69	0.08	244.8	188,040	99.54
75.5	0.00	0.01	0.02	0.05	0.08	0.10	0.13	0.27	0.40	0.66	0.08	242.4	188,020	99.53
83.5	0.00	0.01	0.02	0.05	0.08	0.10	0.13	0.27	0.41	0.65	0.08	241.0	188,060	99.56
91.5	0.00	0.01	0.02	0.05	0.08	0.10	0.13	0.27	0.42	0.63	0.08	240.6	188,120	99.59
99.5	0.00	0.01	0.02	0.05	0.08	0.10	0.13	0.27	0.43	0.60	0.08	240.1	188,210	99.63
107.5	0.00	0.01	0.02	0.05	0.08	0.10	0.13	0.27	0.43	0.59	0.08	240.2	188,300	99.68
115.5	0.00	0.01	0.02	0.05	0.08	0.10	0.13	0.27	0.43	0.59	0.08	239.6	188,380	99.73
123.5	0.00	0.00	0.01	0.03	0.04	0.06	0.07	0.16	0.28	0.56	0.06	241.7	188,550	99.82
131.5	0.00	0.01	0.01	0.03	0.05	0.07	0.09	0.19	0.28	0.47	0.06	236.7	188,600	99.84
139.5	0.00	0.01	0.02	0.05	0.07	0.10	0.12	0.26	0.36	0.53	0.08	233.4	188,590	99.83
147.5	0.00	0.01	0.02	0.04	0.07	0.09	0.12	0.25	0.34	0.54	0.07	231.2	188,600	99.84
155.5	0.00	0.01	0.02	0.04	0.07	0.09	0.11	0.24	0.31	0.49	0.07	231.3	188,600	99.84
163.5	0.00	0.01	0.02	0.04	0.07	0.08	0.11	0.22	0.29	0.45	0.06	231.3	188,600	99.84
171.5	0.00	0.01	0.02	0.04	0.06	0.08	0.10	0.21	0.27	0.43	0.06	232.6	188,600	99.84
179.5	0.00	0.01	0.02	0.04	0.06	0.07	0.10	0.19	0.25	0.38	0.05	234.0	188,600	99.84
187.5	0.00	0.01	0.02	0.04	0.06	0.07	0.09	0.17	0.24	0.37	0.05	236.4	188,600	99.84

Table 20: Summary statistics of current speed, vector-averaged direction and number of valid records by bin depth at BR-1-14 based on the data acquired with the LR ADCP #12943 from 2014 to 2015.

Bin Depth (m)	Min Speed (m/s)	1%ile Speed (m/s)	5%ile Speed (m/s)	25%ile Speed (m/s)	Median Speed (m/s)	Mean Speed (m/s)	75%ile Speed (m/s)	95%ile Speed (m/s)	99%ile Speed (m/s)	Max Speed (m/s)	Standard Deviation Speed (m/s)	Vector-Averaged Direction (deg TN)	Number of Valid Records	% of Valid Data (%)
47.1	0.00	0.01	0.02	0.06	0.09	0.11	0.14	0.25	0.35	0.59	0.07	248.1	36,498	96.60
63.1	0.00	0.01	0.02	0.05	0.09	0.11	0.14	0.27	0.40	0.73	0.08	243.2	35,372	93.62
79.1	0.00	0.01	0.02	0.05	0.09	0.11	0.14	0.30	0.43	0.75	0.09	240.8	33,783	89.42
95.1	0.00	0.01	0.02	0.05	0.09	0.11	0.14	0.30	0.44	0.72	0.09	240.4	33,441	88.51
111.1	0.00	0.01	0.02	0.05	0.08	0.11	0.14	0.29	0.44	0.65	0.09	237.1	34,089	90.23
127.1	0.00	0.01	0.02	0.05	0.08	0.10	0.13	0.27	0.41	0.57	0.08	231.9	34,915	92.41
143.1	0.00	0.01	0.02	0.05	0.08	0.10	0.12	0.24	0.34	0.51	0.07	227.7	35,816	94.80
159.1	0.00	0.01	0.02	0.04	0.07	0.09	0.11	0.22	0.30	0.58	0.06	226.3	36,594	96.86
175.1	0.00	0.01	0.02	0.04	0.07	0.08	0.10	0.19	0.26	0.45	0.05	227.8	37,158	98.35
191.1	0.00	0.01	0.02	0.04	0.06	0.07	0.09	0.16	0.21	0.36	0.04	237.2	37,299	98.72
207.1	0.00	0.01	0.01	0.04	0.06	0.06	0.08	0.14	0.19	0.38	0.04	246.9	37,341	98.84
223.1	0.00	0.01	0.01	0.03	0.05	0.06	0.08	0.13	0.17	0.30	0.04	250.9	37,393	98.97
239.1	0.00	0.01	0.01	0.03	0.05	0.06	0.07	0.12	0.15	0.27	0.03	251.8	37,479	99.20
255.1	0.00	0.01	0.01	0.03	0.05	0.05	0.07	0.11	0.14	0.23	0.03	248.3	37,483	99.21
271.1	0.00	0.01	0.01	0.03	0.05	0.05	0.07	0.11	0.14	0.34	0.03	224.7	37,479	99.20
287.1	0.00	0.01	0.01	0.03	0.05	0.05	0.07	0.11	0.14	0.26	0.03	221.8	37,455	99.14
303.1	0.00	0.01	0.01	0.03	0.05	0.05	0.07	0.11	0.14	0.38	0.03	207.3	37,459	99.15
319.1	0.00	0.01	0.01	0.03	0.05	0.05	0.07	0.11	0.13	0.43	0.03	206.4	37,408	99.01
335.1	0.00	0.01	0.01	0.03	0.05	0.05	0.07	0.10	0.13	0.42	0.03	202.4	37,446	99.11
351.1	0.00	0.01	0.01	0.03	0.05	0.05	0.07	0.11	0.14	0.43	0.03	194.4	37,431	99.07
367.1	0.00	0.01	0.01	0.03	0.05	0.05	0.07	0.10	0.13	0.32	0.03	207.9	37,694	99.77
383.1	0.00	0.01	0.01	0.03	0.05	0.05	0.07	0.10	0.13	0.23	0.03	220.5	37,691	99.76
399.1	0.00	0.01	0.01	0.03	0.05	0.05	0.07	0.10	0.13	0.34	0.03	220.8	37,695	99.77
415.1	0.00	0.01	0.01	0.03	0.05	0.05	0.07	0.10	0.13	0.22	0.03	222.8	37,692	99.76

431.1	0.00	0.01	0.01	0.03	0.05	0.05	0.07	0.11	0.14	0.25	0.03	223.1	37,699	99.78
-------	------	------	------	------	------	------	------	------	------	------	------	-------	--------	-------

Table 21: Summary statistics of current speed, vector-averaged direction and number of valid records at 591.1 and 733.1 m depth at BR-1-14 as based on the data acquired with the Aquadopp DW #6270 and #8414 from 2014 to 2015.

Bin Depth (m)	Min Speed (m/s)	1%ile Speed (m/s)	5%ile Speed (m/s)	25%ile Speed (m/s)	Median Speed (m/s)	Mean Speed (m/s)	75%ile Speed (m/s)	95%ile Speed (m/s)	99%ile Speed (m/s)	Max Speed (m/s)	Standard Deviation Speed (m/s)	Vector-Averaged Direction (deg TN)	Number of Valid Records	% of Valid Data (%)
591.1	0.00	0.00	0.01	0.01	0.02	0.03	0.04	0.06	0.09	0.13	0.02	128.6	18,800	96.80
733.1	0.00	0.00	0.01	0.02	0.03	0.04	0.05	0.09	0.12	0.20	0.03	108.7	18,800	96.80

Table 22: Summary statistics of current speed, vector-averaged direction and number of valid records by bin depth at BR-3-14 based on the data acquired with the LR ADCP #18785 from 2014 to 2015. Bin depths flagged manually as part of the QA/QC are highlighted in red.

Bin Depth (m)	Min Speed (m/s)	1%ile Speed (m/s)	5%ile Speed (m/s)	25%ile Speed (m/s)	Median Speed (m/s)	Mean Speed (m/s)	75%ile Speed (m/s)	95%ile Speed (m/s)	99%ile Speed (m/s)	Max Speed (m/s)	Standard Deviation Speed (m/s)	Vector-Averaged Direction (deg TN)	Number of Valid Records	% of Valid Data (%)
53.0	0.00	0.01	0.02	0.04	0.07	0.08	0.10	0.15	0.20	0.47	0.04	186.5	35,264	99.20
69.0	0.00	0.01	0.02	0.04	0.07	0.07	0.10	0.15	0.20	0.36	0.04	179.6	35,092	98.71
85.0	0.00	0.01	0.02	0.04	0.06	0.07	0.09	0.13	0.17	0.51	0.04	176.0	34,983	98.41
101.0	0.00	0.01	0.02	0.04	0.06	0.06	0.08	0.13	0.16	0.35	0.03	174.6	34,864	98.07
117.0	0.00	0.01	0.02	0.04	0.06	0.06	0.08	0.12	0.16	0.30	0.03	173.9	34,891	98.15
133.0	0.00	0.01	0.02	0.04	0.06	0.06	0.08	0.13	0.17	0.33	0.03	171.0	34,945	98.30
149.0	0.00	0.01	0.02	0.04	0.06	0.06	0.08	0.13	0.17	0.31	0.03	162.2	34,972	98.37
165.0	0.00	0.01	0.01	0.03	0.05	0.06	0.08	0.12	0.16	0.44	0.03	144.1	35,075	98.66
181.0	0.00	0.01	0.01	0.03	0.05	0.06	0.08	0.12	0.15	0.36	0.03	82.8	35,154	98.89
197.0	0.00	0.01	0.01	0.03	0.05	0.06	0.08	0.12	0.16	0.33	0.03	32.4	35,226	99.09
213.0	0.00	0.01	0.01	0.03	0.05	0.06	0.08	0.12	0.16	0.33	0.03	16.3	35,278	99.24
229.0	0.00	0.01	0.01	0.03	0.05	0.06	0.08	0.12	0.16	0.37	0.03	8.1	35,330	99.38
245.0	0.00	0.01	0.01	0.03	0.05	0.06	0.08	0.12	0.15	0.26	0.03	1.5	35,362	99.47
261.0	0.00	0.01	0.01	0.03	0.05	0.06	0.07	0.12	0.15	0.28	0.03	359.6	35,388	99.54

277.0	0.00	0.01	0.01	0.03	0.05	0.06	0.07	0.11	0.15	0.24	0.03	355.8	35,391	99.55
293.0	0.00	0.01	0.01	0.03	0.05	0.06	0.07	0.11	0.15	0.34	0.03	352.8	35,405	99.59
309.0	0.00	0.01	0.01	0.03	0.05	0.06	0.08	0.12	0.15	0.48	0.03	351.4	35,406	99.60
325.0	0.00	0.00	0.01	0.02	0.04	0.04	0.05	0.09	0.12	0.37	0.02	350.2	35,430	99.66
341.0	0.00	0.01	0.01	0.03	0.05	0.06	0.08	0.12	0.15	0.26	0.03	350.4	35,417	99.63
357.0	0.00	0.01	0.01	0.03	0.05	0.06	0.08	0.12	0.15	0.25	0.03	351.0	35,424	99.65
373.0	0.00	0.01	0.01	0.03	0.05	0.06	0.08	0.12	0.16	0.33	0.03	351.2	35,428	99.66
389.0	0.00	0.01	0.01	0.03	0.05	0.06	0.08	0.12	0.16	0.28	0.03	350.4	35,431	99.67
405.0	0.00	0.01	0.01	0.03	0.05	0.06	0.08	0.12	0.16	0.32	0.03	350.9	35,431	99.67
421.0	0.00	0.01	0.01	0.03	0.06	0.06	0.08	0.13	0.16	0.28	0.03	349.9	35,431	99.67

Table 23: Summary statistics of current speed, vector-averaged direction and number of valid records at 553.1 and 677.6 m depth at BR-3-14 as based on the data acquired with the Aquadopp DW #8418 and #2756 from 2014 to 2015.

Bin Depth (m)	Min Speed (m/s)	1%ile Speed (m/s)	5%ile Speed (m/s)	25%ile Speed (m/s)	Median Speed (m/s)	Mean Speed (m/s)	75%ile Speed (m/s)	95%ile Speed (m/s)	99%ile Speed (m/s)	Max Speed (m/s)	Standard Deviation Speed (m/s)	Vector-Averaged Direction (deg TN)	Number of Valid Records	% of Valid Data (%)
553.1	0.00	0.00	0.01	0.02	0.04	0.05	0.07	0.12	0.16	0.22	0.04	332.1	17,719	98.30
677.6	0.00	0.01	0.01	0.03	0.06	0.07	0.10	0.17	0.23	0.34	0.05	346.7	17,201	98.33

Table 24: Summary statistics of current speed, vector-averaged direction and number of valid records by bin depth at BR-G-14 based on the data acquired with the QM ADCP #8784 from 2014 to 2015. Bin depths flagged manually as part of the QA/QC are highlighted in red.

Bin Depth (m)	Min Speed (m/s)	1%ile Speed (m/s)	5%ile Speed (m/s)	25%ile Speed (m/s)	Median Speed (m/s)	Mean Speed (m/s)	75%ile Speed (m/s)	95%ile Speed (m/s)	99%ile Speed (m/s)	Max Speed (m/s)	Standard Deviation Speed (m/s)	Vector-Averaged Direction (deg TN)	Number of Valid Records	% of Valid Data (%)
25.9	0.00	0.01	0.03	0.07	0.11	0.13	0.18	0.30	0.39	0.92	0.09	245.9	173,930	97.86
33.9	0.00	0.01	0.03	0.07	0.11	0.13	0.18	0.30	0.39	0.71	0.09	244.0	175,660	98.83
41.9	0.00	0.01	0.03	0.07	0.12	0.13	0.18	0.30	0.38	0.57	0.08	243.0	175,960	99.00
49.9	0.00	0.01	0.03	0.07	0.11	0.12	0.16	0.28	0.36	0.58	0.08	242.6	176,130	99.10
57.9	0.00	0.01	0.03	0.07	0.11	0.12	0.16	0.27	0.36	0.52	0.07	241.6	176,040	99.05
65.9	0.00	0.01	0.03	0.07	0.12	0.13	0.18	0.28	0.36	0.51	0.08	240.7	175,910	98.97

73.9	0.00	0.01	0.03	0.07	0.12	0.13	0.18	0.28	0.36	0.58	0.08	240.2	175,870	98.95
81.9	0.00	0.01	0.03	0.07	0.12	0.13	0.18	0.29	0.37	0.63	0.08	239.2	175,910	98.97
89.9	0.00	0.01	0.03	0.07	0.12	0.14	0.19	0.29	0.38	0.64	0.08	237.2	175,970	99.01
97.9	0.00	0.01	0.03	0.07	0.12	0.14	0.19	0.30	0.38	0.66	0.08	235.4	176,050	99.05
105.9	0.00	0.01	0.03	0.07	0.12	0.14	0.19	0.31	0.39	0.61	0.09	233.9	176,190	99.13
113.9	0.00	0.01	0.02	0.05	0.08	0.09	0.12	0.21	0.35	0.60	0.07	232.2	176,460	99.28
121.9	0.00	0.01	0.02	0.06	0.10	0.11	0.15	0.25	0.33	0.53	0.07	232.1	176,450	99.28
129.9	0.00	0.01	0.03	0.07	0.12	0.14	0.19	0.32	0.41	0.55	0.09	230.6	176,490	99.30
137.9	0.00	0.01	0.03	0.07	0.12	0.14	0.19	0.31	0.42	0.59	0.09	229.2	176,520	99.32
145.9	0.00	0.01	0.03	0.06	0.11	0.13	0.18	0.31	0.42	0.61	0.09	228.0	176,540	99.33
153.9	0.00	0.01	0.03	0.06	0.11	0.13	0.18	0.30	0.43	0.65	0.09	226.5	176,560	99.34
161.9	0.00	0.01	0.02	0.06	0.10	0.12	0.17	0.30	0.43	0.60	0.09	224.6	176,570	99.34
169.9	0.00	0.01	0.02	0.06	0.09	0.12	0.16	0.29	0.41	0.59	0.09	221.7	176,560	99.34
177.9	0.00	0.01	0.02	0.05	0.09	0.11	0.15	0.28	0.39	0.61	0.08	218.2	176,570	99.34

Table 25: Summary statistics of current speed, vector-averaged direction and number of valid records by bin depth at BR-G-14 based on the data acquired with the LR ADCP #13079 from 2014 to 2015.

Bin Depth (m)	Min Speed (m/s)	1%ile Speed (m/s)	5%ile Speed (m/s)	25%ile Speed (m/s)	Median Speed (m/s)	Mean Speed (m/s)	75%ile Speed (m/s)	95%ile Speed (m/s)	99%ile Speed (m/s)	Max Speed (m/s)	Standard Deviation Speed (m/s)	Vector-Averaged Direction (deg TN)	Number of Valid Records	% of Valid Data (%)
43.1	0.00	0.01	0.03	0.07	0.12	0.13	0.18	0.30	0.36	0.64	0.08	236.5	16,696	46.98
59.1	0.00	0.01	0.03	0.07	0.11	0.13	0.17	0.28	0.35	0.49	0.08	237.4	34,665	97.55
75.1	0.00	0.01	0.03	0.07	0.12	0.13	0.18	0.28	0.37	0.67	0.08	235.1	33,709	94.86
91.1	0.00	0.01	0.03	0.07	0.12	0.14	0.19	0.30	0.38	0.81	0.08	230.3	33,314	93.75
107.1	0.00	0.01	0.03	0.07	0.12	0.14	0.19	0.32	0.40	0.63	0.09	226.9	33,664	94.73
123.1	0.00	0.01	0.03	0.07	0.12	0.13	0.18	0.29	0.40	0.54	0.08	221.4	34,212	96.27
139.1	0.00	0.01	0.03	0.07	0.11	0.13	0.18	0.29	0.42	0.55	0.09	220.7	34,545	97.21
155.1	0.00	0.01	0.02	0.06	0.10	0.13	0.17	0.30	0.43	0.61	0.09	219.1	34,755	97.80

171.1	0.00	0.01	0.02	0.05	0.09	0.11	0.15	0.29	0.40	0.57	0.08	213.2	34,957	98.37
187.1	0.00	0.01	0.02	0.05	0.08	0.10	0.13	0.26	0.35	0.52	0.07	204.4	35,111	98.80
203.1	0.00	0.01	0.02	0.04	0.07	0.09	0.11	0.22	0.29	0.45	0.06	194.5	35,196	99.04
219.1	0.00	0.01	0.02	0.04	0.06	0.08	0.10	0.18	0.25	0.35	0.05	182.8	35,241	99.17
235.1	0.00	0.01	0.02	0.04	0.06	0.07	0.09	0.15	0.20	0.35	0.04	175.9	35,275	99.27
251.1	0.00	0.01	0.02	0.03	0.06	0.06	0.08	0.13	0.17	0.31	0.04	172.3	35,294	99.32
267.1	0.00	0.01	0.01	0.03	0.05	0.06	0.08	0.12	0.15	0.26	0.03	162.5	35,298	99.33
283.1	0.00	0.01	0.01	0.03	0.05	0.05	0.07	0.11	0.14	0.23	0.03	152.2	35,303	99.34
299.1	0.00	0.01	0.01	0.03	0.05	0.05	0.07	0.10	0.13	0.21	0.03	146.6	35,308	99.36
315.1	0.00	0.01	0.01	0.03	0.05	0.05	0.07	0.10	0.13	0.23	0.03	137.5	35,308	99.36
331.1	0.00	0.01	0.01	0.03	0.05	0.05	0.07	0.10	0.14	0.23	0.03	133.2	35,309	99.36
347.1	0.00	0.01	0.01	0.03	0.05	0.05	0.07	0.10	0.14	0.21	0.03	128.9	35,309	99.36
363.1	0.00	0.01	0.01	0.03	0.05	0.05	0.07	0.10	0.14	0.27	0.03	117.2	35,309	99.36
379.1	0.00	0.01	0.01	0.03	0.05	0.05	0.07	0.10	0.14	0.29	0.03	113.3	35,309	99.36
395.1	0.00	0.01	0.01	0.03	0.04	0.05	0.06	0.10	0.14	0.28	0.03	100.5	35,309	99.36
411.1	0.00	0.01	0.01	0.03	0.04	0.05	0.06	0.10	0.14	0.38	0.03	93.0	35,308	99.36
427.1	0.00	0.01	0.01	0.03	0.04	0.05	0.06	0.10	0.14	0.27	0.03	86.7	35,308	99.36

Table 26: Summary statistics of current speed, vector-averaged direction and number of valid records at 585.3 and 692.5 m depth at BR-G-14 as based on the data acquired with the Aquadopp DW #9473 and #9847 from 2014 to 2015.

Bin Depth (m)	Min Speed (m/s)	1%ile Speed (m/s)	5%ile Speed (m/s)	25%ile Speed (m/s)	Median Speed (m/s)	Mean Speed (m/s)	75%ile Speed (m/s)	95%ile Speed (m/s)	99%ile Speed (m/s)	Max Speed (m/s)	Standard Deviation Speed (m/s)	Vector-Averaged Direction (deg TN)	Number of Valid Records	% of Valid Data (%)
585.3	0.00	0.00	0.01	0.02	0.03	0.04	0.05	0.08	0.11	0.21	0.02	37.3	17,658	99.06
692.5	0.00	0.00	0.01	0.02	0.04	0.05	0.07	0.13	0.18	0.30	0.04	42.6	17,658	99.06

Table 27: Summary statistics of current speed, vector-averaged direction and number of valid records by bin depth at BR-K-14 based on the data acquired with the WHS ADCP #2646 from 2014 to 2015.

Bin Depth (m)	Min Speed (m/s)	1%ile Speed (m/s)	5%ile Speed (m/s)	25%ile Speed (m/s)	Median Speed (m/s)	Mean Speed (m/s)	75%ile Speed (m/s)	95%ile Speed (m/s)	99%ile Speed (m/s)	Max Speed (m/s)	Standard Deviation Speed (m/s)	Vector-Averaged Direction (deg TN)	Number of Valid Records	% of Valid Data (%)
---------------	-----------------	-------------------	-------------------	--------------------	--------------------	------------------	--------------------	--------------------	--------------------	-----------------	--------------------------------	------------------------------------	-------------------------	---------------------

22.2	0.00	0.01	0.02	0.06	0.10	0.12	0.17	0.30	0.43	0.71	0.09	256.2	30,464	85.74
30.2	0.00	0.01	0.02	0.06	0.10	0.13	0.17	0.32	0.44	0.80	0.10	258.4	34,383	96.77
38.2	0.00	0.01	0.02	0.06	0.10	0.13	0.17	0.33	0.45	0.84	0.10	262.3	35,137	98.89
46.2	0.00	0.01	0.02	0.06	0.10	0.13	0.16	0.34	0.47	0.81	0.10	271.1	35,345	99.47
54.2	0.00	0.01	0.02	0.06	0.10	0.13	0.17	0.35	0.48	0.78	0.10	295.1	35,399	99.63
62.2	0.00	0.01	0.02	0.05	0.09	0.13	0.16	0.37	0.49	0.78	0.11	336.5	35,402	99.63
70.2	0.00	0.01	0.02	0.05	0.10	0.14	0.18	0.40	0.50	0.79	0.12	19.6	35,403	99.64
78.2	0.00	0.01	0.02	0.06	0.10	0.14	0.20	0.42	0.53	0.77	0.12	37.1	35,404	99.64
86.2	0.00	0.01	0.02	0.06	0.11	0.15	0.21	0.42	0.53	0.75	0.13	42.6	35,404	99.64
94.2	0.00	0.01	0.02	0.06	0.11	0.16	0.22	0.43	0.54	0.76	0.13	44.5	35,404	99.64
102.2	0.00	0.01	0.02	0.06	0.11	0.16	0.23	0.42	0.53	0.80	0.13	44.7	35,406	99.65
110.2	0.00	0.01	0.02	0.06	0.12	0.15	0.22	0.41	0.51	0.76	0.12	44.3	35,406	99.65
118.2	0.00	0.01	0.02	0.06	0.12	0.15	0.22	0.38	0.48	0.74	0.11	42.3	35,406	99.65
126.2	0.00	0.01	0.02	0.06	0.12	0.14	0.20	0.34	0.43	0.69	0.10	38.8	35,406	99.65

Table 28: Summary statistics of current speed, vector-averaged direction and number of valid records by bin depth at BR-K-14 based on the data acquired with the Aquadopp Profiler #11147 from 2014 to 2015. Bin depths flagged manually as part of the QA/QC are highlighted in red.

Bin Depth (m)	Min Speed (m/s)	1%ile Speed (m/s)	5%ile Speed (m/s)	25%ile Speed (m/s)	Median Speed (m/s)	Mean Speed (m/s)	75%ile Speed (m/s)	95%ile Speed (m/s)	99%ile Speed (m/s)	Max Speed (m/s)	Standard Deviation Speed (m/s)	Vector-Averaged Direction (deg TN)	Number of Valid Records	% of Valid Data (%)
141.4	0.00	0.01	0.02	0.05	0.10	0.12	0.17	0.28	0.36	0.53	0.08	31.1	8,853	99.58
142.4	0.00	0.01	0.03	0.06	0.10	0.11	0.15	0.24	0.31	0.56	0.07	32.4	8,853	99.58
143.4	0.00	0.01	0.03	0.06	0.10	0.12	0.16	0.24	0.31	0.52	0.07	32.9	8,853	99.58
144.4	0.00	0.01	0.02	0.05	0.09	0.11	0.16	0.27	0.35	0.52	0.08	31.8	8,853	99.58
145.4	0.00	0.01	0.02	0.05	0.09	0.11	0.15	0.27	0.34	0.54	0.08	32.4	8,853	99.58
146.4	0.00	0.01	0.02	0.04	0.08	0.11	0.15	0.26	0.34	0.54	0.08	33.2	8,853	99.58
147.4	0.00	0.01	0.02	0.04	0.08	0.10	0.15	0.26	0.33	0.51	0.08	33.7	8,853	99.58
148.4	0.00	0.01	0.02	0.04	0.08	0.10	0.14	0.25	0.33	0.53	0.08	34.2	8,853	99.58
149.4	0.00	0.01	0.01	0.04	0.08	0.10	0.14	0.25	0.32	0.51	0.07	33.9	8,853	99.58

150.4	0.00	0.01	0.01	0.04	0.07	0.09	0.13	0.24	0.31	0.48	0.07	32.8	8,853	99.58
151.4	0.00	0.01	0.01	0.04	0.07	0.09	0.13	0.23	0.31	0.52	0.07	32.4	8,853	99.58
152.4	0.00	0.01	0.01	0.03	0.06	0.09	0.12	0.23	0.30	0.46	0.07	30.8	8,853	99.58
153.4	0.00	0.01	0.01	0.03	0.06	0.08	0.12	0.22	0.29	0.45	0.07	28.9	8,853	99.58

Table 29: Summary statistics of current speed, vector-averaged direction and number of valid records by bin depth at DFO-2-14 based on the data acquired with the NB ADCP #586 from 2014 to 2015.

Bin Depth (m)	Min Speed (m/s)	1%ile Speed (m/s)	5%ile Speed (m/s)	25%ile Speed (m/s)	Median Speed (m/s)	Mean Speed (m/s)	75%ile Speed (m/s)	95%ile Speed (m/s)	99%ile Speed (m/s)	Max Speed (m/s)	Standard Deviation Speed (m/s)	Vector-Averaged Direction (deg TN)	Number of Valid Records	% of Valid Data (%)
20	0.00	0.01	0.02	0.06	0.10	0.12	0.17	0.30	0.39	0.56	0.09	253.71	11,831	91.06
23.9	0.00	0.01	0.03	0.06	0.11	0.13	0.17	0.33	0.47	0.67	0.10	252.81	12,672	97.54
27.8	0.00	0.01	0.03	0.07	0.11	0.13	0.17	0.34	0.46	0.65	0.10	252.25	12,803	98.55
31.8	0.00	0.01	0.03	0.07	0.11	0.13	0.17	0.33	0.45	0.76	0.09	252.14	12,966	99.80
35.7	0.00	0.01	0.03	0.06	0.11	0.13	0.16	0.32	0.44	0.76	0.09	251.69	12,977	99.89
39.6	0.00	0.01	0.03	0.06	0.10	0.12	0.16	0.30	0.44	0.76	0.09	250.95	12,976	99.88
43.5	0.00	0.01	0.02	0.06	0.10	0.12	0.15	0.28	0.44	0.75	0.08	250.49	12,980	99.91
47.4	0.00	0.01	0.02	0.06	0.10	0.11	0.14	0.28	0.42	0.74	0.08	249.67	12,978	99.89
51.3	0.00	0.01	0.02	0.06	0.09	0.11	0.13	0.27	0.42	0.71	0.08	248.83	12,961	99.76
55.2	0.00	0.01	0.02	0.06	0.09	0.11	0.13	0.27	0.42	0.72	0.08	248.14	12,982	99.92
59.1	0.00	0.01	0.02	0.06	0.09	0.11	0.13	0.27	0.41	0.70	0.08	247.49	12,984	99.94
63	0.00	0.01	0.02	0.06	0.09	0.11	0.13	0.26	0.41	0.67	0.08	247.24	12,987	99.96
66.9	0.00	0.01	0.02	0.06	0.09	0.10	0.13	0.25	0.40	0.63	0.07	246.76	12,987	99.96
70.9	0.00	0.01	0.03	0.06	0.09	0.10	0.13	0.24	0.40	0.59	0.07	246.61	12,985	99.95
74.8	0.00	0.01	0.02	0.05	0.08	0.10	0.12	0.24	0.39	0.56	0.07	247.57	12,986	99.95
78.7	0.00	0.01	0.02	0.05	0.08	0.10	0.12	0.23	0.38	0.56	0.07	44.73	12,985	99.95
82.6	0.00	0.01	0.02	0.05	0.08	0.10	0.12	0.22	0.38	0.55	0.07	53.51	12,984	99.94
86.5	0.00	0.01	0.02	0.05	0.08	0.09	0.12	0.22	0.35	0.48	0.07	54.33	12,982	99.92
90.4	0.00	0.01	0.02	0.05	0.07	0.09	0.12	0.21	0.30	0.45	0.06	54.14	12,969	99.82

94.3	0.00	0.01	0.02	0.04	0.07	0.08	0.11	0.19	0.25	0.43	0.05	54.39	12,976	99.88
98.2	0.00	0.01	0.02	0.04	0.07	0.08	0.11	0.18	0.24	0.42	0.05	54.48	12,961	99.76
102.1	0.00	0.01	0.02	0.04	0.06	0.07	0.10	0.17	0.22	0.41	0.05	49.85	12,992	100.00

Table 30: Summary statistics of current speed, vector-averaged direction and number of valid records by bin depth at DFO-1-14 based on the data acquired with the NB ADCP #318 from 2014 to 2015.

Bin Depth (m)	Min Speed (m/s)	1%ile Speed (m/s)	5%ile Speed (m/s)	25%ile Speed (m/s)	Median Speed (m/s)	Mean Speed (m/s)	75%ile Speed (m/s)	95%ile Speed (m/s)	99%ile Speed (m/s)	Max Speed (m/s)	Standard Deviation Speed (m/s)	Vector-Averaged Direction (deg TN)	Number of Valid Records	% of Valid Data (%)
11.0	0.00	0.01	0.02	0.04	0.07	0.08	0.11	0.18	0.27	0.41	0.05	179.68	9,710	58.76
15.0	0.00	0.01	0.02	0.04	0.07	0.08	0.10	0.16	0.27	0.46	0.05	188.09	14,012	84.79
19.0	0.00	0.01	0.02	0.04	0.07	0.08	0.10	0.17	0.29	0.44	0.05	180.17	14,218	86.04
23.0	0.00	0.01	0.02	0.04	0.07	0.08	0.10	0.17	0.30	0.42	0.05	176.94	14,253	86.25
27.0	0.00	0.01	0.02	0.04	0.07	0.08	0.11	0.18	0.30	0.41	0.06	173.25	14,261	86.30
31.0	0.00	0.01	0.02	0.05	0.07	0.08	0.11	0.19	0.31	0.42	0.06	169.75	14,264	86.32
34.0	0.00	0.01	0.02	0.05	0.07	0.09	0.11	0.19	0.31	0.45	0.06	167.00	14,264	86.32
38.0	0.00	0.01	0.02	0.05	0.07	0.09	0.11	0.20	0.31	0.49	0.06	164.34	14,263	86.31
42.0	0.00	0.01	0.02	0.05	0.07	0.09	0.11	0.20	0.32	0.53	0.06	161.52	14,266	86.33
46.0	0.00	0.01	0.02	0.04	0.07	0.08	0.10	0.19	0.32	0.51	0.06	159.88	14,269	86.35

Table 31: Summary statistics of current speed, vector-averaged direction and number of valid records by bin depth at DFO-9-14 based on the data acquired with the WHS ADCP #18318 from 2014 to 2015.

Bin Depth (m)	Min Speed (m/s)	1%ile Speed (m/s)	5%ile Speed (m/s)	25%ile Speed (m/s)	Median Speed (m/s)	Mean Speed (m/s)	75%ile Speed (m/s)	95%ile Speed (m/s)	99%ile Speed (m/s)	Max Speed (m/s)	Standard Deviation Speed (m/s)	Vector-Averaged Direction (deg TN)	Number of Valid Records	% of Valid Data (%)
3.8	0.00	0.01	0.02	0.05	0.11	0.14	0.20	0.40	0.57	0.97	0.13	106.0	7,084	40.81
4.8	0.00	0.01	0.02	0.05	0.10	0.13	0.19	0.38	0.54	0.99	0.12	105.9	7,821	45.05
5.8	0.00	0.01	0.02	0.04	0.09	0.12	0.17	0.35	0.52	1.01	0.11	105.7	8,797	50.68
6.8	0.00	0.01	0.01	0.04	0.08	0.11	0.15	0.31	0.50	1.08	0.11	105.1	9,597	55.29
7.8	0.00	0.01	0.01	0.04	0.08	0.11	0.15	0.29	0.47	1.04	0.10	104.4	10,433	60.10
8.8	0.00	0.01	0.01	0.04	0.07	0.10	0.14	0.27	0.44	1.00	0.10	103.8	11,173	64.36

9.8	0.00	0.01	0.01	0.04	0.07	0.10	0.13	0.27	0.44	0.95	0.09	104.5	11,756	67.72
10.8	0.00	0.01	0.01	0.04	0.07	0.10	0.12	0.26	0.44	0.92	0.09	102.8	12,429	71.60
11.8	0.00	0.01	0.02	0.04	0.07	0.09	0.12	0.24	0.42	0.88	0.09	101.1	12,944	74.57
12.8	0.00	0.01	0.02	0.04	0.07	0.09	0.12	0.23	0.40	0.89	0.08	101.7	13,241	76.28
13.8	0.00	0.01	0.02	0.04	0.07	0.09	0.11	0.22	0.39	0.82	0.08	103.5	13,632	78.53
14.8	0.00	0.01	0.02	0.04	0.07	0.09	0.11	0.21	0.37	0.82	0.07	107.2	13,997	80.63
15.8	0.00	0.01	0.02	0.04	0.07	0.09	0.11	0.20	0.36	0.82	0.07	111.9	14,333	82.57
16.8	0.00	0.01	0.02	0.04	0.07	0.09	0.11	0.20	0.34	0.78	0.07	120.8	14,679	84.56
17.8	0.00	0.01	0.02	0.04	0.07	0.09	0.11	0.19	0.33	0.78	0.07	132.5	14,981	86.30
18.8	0.00	0.01	0.02	0.05	0.07	0.09	0.11	0.19	0.31	0.69	0.06	143.4	15,297	88.12
19.8	0.00	0.01	0.02	0.05	0.07	0.08	0.11	0.19	0.29	0.70	0.06	154.3	15,567	89.68
20.8	0.00	0.01	0.02	0.05	0.07	0.08	0.11	0.19	0.28	0.70	0.06	163.1	15,810	91.08
21.8	0.00	0.01	0.02	0.04	0.07	0.08	0.11	0.18	0.27	0.61	0.06	168.0	15,904	91.62
22.8	0.00	0.01	0.02	0.04	0.07	0.08	0.10	0.18	0.26	0.61	0.05	171.0	16,010	92.23
23.8	0.00	0.01	0.02	0.04	0.07	0.08	0.10	0.18	0.26	0.61	0.05	171.9	16,275	93.76
24.8	0.00	0.01	0.02	0.04	0.06	0.08	0.10	0.17	0.26	0.59	0.05	170.4	16,312	93.97
25.8	0.00	0.01	0.01	0.04	0.06	0.07	0.09	0.17	0.25	0.58	0.05	167.0	16,361	94.25
26.8	0.00	0.01	0.01	0.03	0.06	0.07	0.09	0.16	0.23	0.58	0.05	165.3	16,335	94.10
27.8	0.00	0.01	0.01	0.03	0.06	0.07	0.09	0.16	0.24	0.56	0.05	165.6	16,832	96.96

Executive Summary

This report describes the 2015-2016 activities of the integrated Beaufort Observatory (iBO), a four-year program (2015-2018) managed by ArcticNet in partnership with Fisheries and Oceans Canada and Golder Associates Ltd. iBO is supported by the Environmental Studies Research Fund and Imperial Oil Resources Ventures Limited. iBO aims to contribute key oceanographic information required for decisions on development and regulations in the offshore Canadian Beaufort Sea by extending existing time-series measurements and integrating regional understanding of the shelf and slope environment through year-round measurements acquired by autonomous measuring systems on subsurface moorings.

The activities described in this report focus on the turnaround of 7 moorings which constitute the backbone of the iBO observational program, initially deployed in 2014. These provide the means to obtain a regionally-integrated ice and ocean dataset. The main goal of this report is to provide an initial review of the dataset acquired during 2015 -2016 through the operation of these 7 moorings. Only the data components processed thus far are presented; these include all current meter and current profiler data, temperature-salinity data, and preliminary biogeochemical flux data from one sediment trap. Data acquired using ice-profiling sonar and sediment traps during 2014 to 2016 are still in the process stage; summaries of these data will be presented as an addendum to the present report at a later date.

For each presented dataset, the spatial and temporal variability is discussed and events of interest that warrant further investigation are identified. A statistical analysis of the mean current patterns near the surface and near the bottom is provided, including a comparison of the 2014-2015 and 2015-2016 observing periods. The concluding remarks provide a summary of oceanographic phenomena that could be targeted for further study. Lessons learned stemming from the 2016 operations as well as objectives and milestones for iBO in 2017-2018 are also summarized. The last section of the report presents a framework for the potential development of a State of the Beaufort Sea Report that would synthesize past and present mooring datasets in order to support a broader Strategic Regional Environmental Assessment for the Beaufort Sea.

Table of Contents

1.0	INTRODUCTION.....	1
1.1	Report Organization.....	2
1.2	Physical Setting of the Study Area	3
2.0	MATERIAL AND METHODS	5
2.1	Taut-line Mooring Design.....	5
2.1.1	Slope Moorings	5
2.1.2	Shelf Moorings	6
2.2	Compass Calibration and Verification.....	7
2.3	Mooring Recovery and Deployment	8
2.3.1	Shipboard Mooring Operations.....	9
2.4	Data Processing and QA/QC.....	11
2.4.1	Current Meters and Current Profilers.....	11
2.4.2	Temperature-Salinity Loggers	13
2.4.3	Ice Profiling Sonars and Ice velocity.....	14
2.4.4	Sediment Traps	14
3.0	RESULTS AND DISCUSSION	16
3.1	Sea Ice Conditions	16
3.2	Ocean Currents	18
3.2.1	Mooring BR-1	20
3.2.2	Mooring BR-3	32
3.2.3	Mooring BR-G	43
3.2.4	Mooring BR-K.....	55
3.2.5	Mooring DFO-2.....	60
3.2.6	Mooring DFO-1.....	65
3.2.7	Mooring DFO-9.....	69
3.2.8	Spatial Variability of Surface and Bottom Currents in Open Water.....	73
3.3	Temperature and Salinity.....	77
3.4	Biogeochemical Fluxes.....	93
4.0	CONCLUSIONS.....	95
4.1	Concluding Remarks on the 2015-2016 Dataset.....	95
4.2	2016 Fieldwork Lessons Learned and Recommendations	96
4.3	Objectives and Milestones for 2017-2018.....	97
5.0	REFERENCES.....	100

TABLES

Table 1: Mean Error of Recovered Nortek and TRDI Compasses (10 Degree Increment).....	8
Table 2: 2015-2016 Mooring Recovery Summary.....	8
Table 3: 2016-2017 Mooring Deployment Summary.....	8
Table 4: Magnetic declination values for 2015-2016 iBO Moorings	11
Table 5: Angles chosen to describe the along-slope/shelf current component for each iBO mooring.....	18
Table 6: Selected bin depths to characterize circulation patterns throughout the water column.	18
Table 7: Summary of current profilers and current meters clock drift, first and last good record, and percentage of raw data return on iBO moorings from 2015 to 2016.	19
Table 8: Annual statistics of current speed and direction at BR-1-15 from selected bin depths representative of water mass variability in the Beaufort Sea (see Table 6 for water mass description).....	25
Table 9: Annual statistics of current speed and direction at BR-3-15 from selected bin depths representative of water mass variability in the Beaufort Sea (see Table 6 for water mass description).....	36
Table 10: Annual statistics of current speed and direction at BR-G-15 from selected bin depths representative of water mass variability in the Beaufort Sea (see Table 6 for water mass description).....	48
Table 11: Annual statistics of current speed and direction at BR-K-15 from selected bin depths representative of water mass variability in the Beaufort Sea (see Table 6 for water mass description).....	57
Table 12: Annual statistics of current speed and direction at DFO-2-15 from selected bin depths representative of water mass variability in the Beaufort Sea (see Table 6 for water mass description).....	62
Table 13: Annual statistics of current speed and direction at DFO-1-15 from a selected bin depth representative of the Polar-mixed layer (see Table 6 for water mass description).....	67
Table 14: Annual statistics of current speed and direction at DFO-9-15 from a selected bin depth representative of the Polar-mixed layer (see Table 6 for water mass description).....	71
Table 15: Summary of CT data logger clock drift and percentage of raw data return on iBO moorings from 2015 to 2016.....	79
Table 16: Summary of valid and flagged data from CT loggers deployed on the BR slope moorings from 2015 to 2016. See Table 15 for the instrument model associated with each serial number.	80
Table 17: 2017-2018 iBO Milestones	97
Table 18: Summary statistics of current speed, vector-averaged direction and number of valid records by bin depth at BR-1-15 based on the data acquired with the QM ADCP #12698 from 2015 to 2016. Bin depths flagged manually as part of the QA/QC are highlighted in red.....	117
Table 19: Summary statistics of current speed, vector-averaged direction and number of valid records by bin depth at BR-1-15 based on the data acquired with the LR ADCP #12884 from 2015 to 2016.	118
Table 20: Summary statistics of current speed, vector-averaged direction and number of valid records at 595.6 and 757.3 m depth at BR-1-15 as based on the data acquired with the Aquadopp DW #2792 and #2701 from 2015 to 2016.	119
Table 21: Summary statistics of current speed, vector-averaged direction and number of valid records by bin depth at BR-3-15 based on the data acquired with the LR ADCP #12942 from 2015 to 2016. Bin depths flagged manually as part of the QA/QC are highlighted in red.....	120
Table 22: Summary statistics of current speed, vector-averaged direction and number of valid records at 574.7 and 685.2 m depth at BR-3-15 as based on the data acquired with the Aquadopp DW #6109 and #8541 from 2015 to 2016.	121
Table 23: Summary statistics of current speed, vector-averaged direction and number of valid records by bin depth at BR-G-15 based on the data acquired with the QM ADCP #12841 from 2015 to 2016. Bin depths flagged manually as part of the QA/QC are highlighted in red.	121

Table 24: Summary statistics of current speed, vector-averaged direction and number of valid records by bin depth at BR-G-15 based on the data acquired with the LR ADCP #12892 from 2015 to 2016. 122

Table 25: Summary statistics of current speed, vector-averaged direction and number of valid records at 580.9 and 690.8 m depth at BR-G-15 as based on the data acquired with the Aquadopp DW #9846 and #8434 from 2015 to 2016. 123

Table 26: Summary statistics of current speed, vector-averaged direction and number of valid records by bin depth at BR-K-15 based on the data acquired with the WHS ADCP #102 from 2015 to 2016. 124

Table 27: Summary statistics of current speed, vector-averaged direction and number of valid records by bin depth at DFO-2-15 based on the data acquired with the NB ADCP #464 from 2015 to 2016. 124

Table 28: Summary statistics of current speed, vector-averaged direction and number of valid records by bin depth at DFO-1-15 based on the data acquired with the NB ADCP #506 from 2015 to 2016. 125

Table 29: Summary statistics of current speed, vector-averaged direction and number of valid records by bin depth at DFO-9-15 based on the data acquired with the WHS ADCP #12414 from 2015 to 2016. 126

FIGURES

Figure 1: Bathymetric map of the Canadian Beaufort Sea showing the location of iBO moorings (in red). Moorings from partner projects (ArcticNet, DFO, MARES/BOEM) are also shown on the map but are not detailed in the present report).2

Figure 2: Weekly ice coverage by stage of development for the season 2016 (March – September 2016) as based on daily ice charts from Canadian Ice services. Brown: old ice. Green: first-year ice. Pink/purple: New/Young ice. Red line: average sea ice concentration 1992-2015. Data source: Ice graph 2.5, <http://iceweb1.cis.ec.gc.ca/IceGraph/>. 16

Figure 3: Sea ice concentration (% coverage) for a 12.5 X 12.5 km pixel area over each iBO mooring during 2015-2016 as derived from SSM/I satellite imagery. The black line shows the mean ice concentration over 1992-2015 within each pixel. ...17

Figure 4: Time-series of current speed, current direction and along-slope current component at mooring BR-1-15 measured by the QM ADCP #12698. The black line depicts the instrument depth.21

Figure 5: Time-series of current speed, current direction and along-slope current component at mooring BR-1-15 measured by the LR ADCP #12884. The black line depicts the instrument depth.22

Figure 6: Time-series of current speed, current direction and along-slope current component at 596 m at mooring BR-1-15 measured by the Aquadopp #2792.23

Figure 7: Time-series of current speed, current direction and along-slope current component at 757 m at mooring BR-1-15 measured by the Aquadopp #2701.24

Figure 8: Seasonal current roses at 20 m depth (bin cell #11) at BR-1-15 measured by the QM ADCP #12698. Data are low-pass filtered. Roses indicate the direction toward which currents flow. Seasons are defined following the meteorological convention (Fall: October-December; Winter: January-March; Spring: April-June; Summer: July-September).26

Figure 9: Seasonal current roses at 132 m depth (bin cell #39) at BR-1-15 measured by the QM ADCP #12698. Data are low-pass filtered. Roses indicate the direction toward which currents flow. Seasons are defined following the meteorological convention (Fall: October-December; Winter: January-March; Spring: April-June; Summer: July-September).27

Figure 10: Seasonal current roses at 213 m depth (bin cell #15) at BR-1-15 measured by the LR ADCP #12884. Data are low-pass filtered. Roses indicate the direction toward which currents flow. Seasons are defined following the meteorological convention (Fall: October-December; Winter: January-March; Spring: April-June; Summer: July-September).28

Figure 11: Seasonal current roses at 357 m depth (bin cell #6) at BR-1-15 measured by the LR ADCP #12884. Data are low-pass filtered. Roses indicate the direction toward which currents flow. Seasons are defined following the meteorological convention (Fall: October-December; Winter: January-March; Spring: April-June; Summer: July-September).29

Figure 12: Seasonal current roses at 596 m depth at BR-1-15 measured by the Aquadopp #2792. Data are low-pass filtered. Roses indicate the direction toward which currents flow. Seasons are defined following the meteorological convention (Fall: October-December; Winter: January-March; Spring: April-June; Summer: July-September).30

Figure 13: Seasonal current roses at 757 m depth at BR-1-15 measured by the Aquadopp #2701. Data are low-pass filtered. Roses indicate the direction toward which currents flow. Seasons are defined following the meteorological convention (Fall: October-December; Winter: January-March; Spring: April-June; Summer: July-September)..... 31

Figure 14: Time-series of current speed, current direction and along-slope current component at mooring BR-3-15 measured by the LR ADCP #12942. The black line depicts the instrument depth. 33

Figure 15: Time-series of current speed, current direction and along-slope current component at 575 m at mooring BR-3-15 as obtained with the Aquadopp #6109. 34

Figure 16: Time-series of current speed, current direction and along-slope current component at 685 m at mooring BR-3-15 as obtained with the Aquadopp #8541. 35

Figure 17: Seasonal current roses at 54 m depth (bin cell #24) at BR-3-15 measured by the LR ADCP #12942. Data are low-pass filtered. Roses point toward where the currents are going. Seasons are defined following the meteorological convention (Fall: October-December; Winter: January-March; Spring: April-June; Summer: July-September)..... 37

Figure 18: Seasonal current roses at 134 m depth (bin cell #19) at BR-3-15 measured by the LR ADCP #12942. Data are low-pass filtered. Roses indicate the direction toward which currents flow. Seasons are defined following the meteorological convention (Fall: October-December; Winter: January-March; Spring: April-June; Summer: July-September). 38

Figure 19: Seasonal current roses at 214 m depth (bin cell #14) at BR-3-15 measured by the LR ADCP #12942. Data are low-pass filtered. Roses indicate the direction toward which currents flow. Seasons are defined following the meteorological convention (Fall: October-December; Winter: January-March; Spring: April-June; Summer: July-September). 39

Figure 20: Seasonal current roses at 342 m depth (bin cell #6) at BR-3-15 measured by the LR ADCP #12942. Data are low-pass filtered. Roses indicate the direction toward which currents flow. Seasons are defined following the meteorological convention (Fall: October-December; Winter: January-March; Spring: April-June; Summer: July-September). 40

Figure 21: Seasonal current roses at 575 m depth at BR-3-15 measured by the Aquadopp #6109. Data are low-pass filtered. Roses indicate the direction toward which currents flow. Seasons are defined following the meteorological convention (Fall: October-December; Winter: January-March; Spring: April-June; Summer: July-September)..... 41

Figure 22: Seasonal current roses at 685 m depth at BR-3-15 measured by the Aquadopp #8541. Data are low-pass filtered. Roses indicate the direction toward which currents flow. Seasons are defined following the meteorological convention (Fall: October-December; Winter: January-March; Spring: April-June; Summer: July-September)..... 42

Figure 23: Time-series of current speed, current direction and along-slope current component at mooring BR-G-15 measured by the QM ADCP #12841. The black line depicts the instrument depth. 44

Figure 24: Time-series of current speed, current direction and along-slope current component at mooring BR-G-15 measured by the LR ADCP #12892. The black line depicts the instrument depth. 45

Figure 25: Time-series of current speed, current direction and along-slope current component at 581 m at mooring BR-G-15 measured by the Aquadopp #9846. 46

Figure 26: Time-series of current speed, current direction and along-slope current component at 691 m at mooring BR-G-15 measured by the Aquadopp #8434. 47

Figure 27: Seasonal current roses at 20 m depth (bin cell #34) at BR-G-15 measured by the QM ADCP #12841. Data are low-pass filtered. Roses indicate the direction toward which currents flow. Seasons are defined following the meteorological convention (Fall: October-December; Winter: January-March; Spring: April-June; Summer: July-September). 49

Figure 28: Seasonal current roses at 132 m depth (bin cell #6) at BR-G-15 measured by the QM ADCP #12841. Data are low-pass filtered. Roses indicate the direction toward which currents flow. Seasons are defined following the meteorological convention (Fall: October-December; Winter: January-March; Spring: April-June; Summer: July-September). 50

Figure 29: Seasonal current roses at 220 m depth (bin cell #14) at BR-G-15 measured by the LR ADCP #12892. Data are low-pass filtered. Roses indicate the direction toward which currents flow. Seasons are defined following the meteorological convention (Fall: October-December; Winter: January-March; Spring: April-June; Summer: July-September). 51

Figure 30: Seasonal current roses at 348 m depth (bin cell #6) at BR-G-15 measured by the LR ADCP #12892. Data are low-pass filtered. Roses indicate the direction toward which currents flow. Seasons are defined following the meteorological convention (Fall: October-December; Winter: January-March; Spring: April-June; Summer: July-September). 52

Figure 31: Seasonal current roses at 581 m depth at BR-G-15 measured by the Aquadopp #9846. Data are low-pass filtered. Roses indicate the direction toward which currents flow. Seasons are defined following the meteorological convention (Fall: October-December; Winter: January-March; Spring: April-June; Summer: July-September).....53

Figure 32: Seasonal current roses at 691 m depth at BR-G-15 measured by the Aquadopp #8434. Data are low-pass filtered. Roses indicate the direction toward which currents flow. Seasons are defined following the meteorological convention (Fall: October-December; Winter: January-March; Spring: April-June; Summer: July-September).....54

Figure 33: Time-series of current speed, current direction and along-slope current component at mooring BR-K-15 measured by the WHS ADCP #102. The black line depicts the instrument depth.56

Figure 34: Seasonal current roses at 23 m depth (bin cell #15) at BR-K-15 measured by the WHS ADCP #102. Data are low-pass filtered. Roses indicate the direction toward which currents flow. Seasons are defined following the meteorological convention (Fall: October-December; Winter: January-March; Spring: April-June; Summer: July-September).58

Figure 35: Seasonal current roses at 127 m depth (bin cell #2) at BR-K-15 measured by the WHS ADCP #102. Data are low-pass filtered. Roses indicate the direction toward which currents flow. Seasons are defined following the meteorological convention (Fall: October-December; Winter: January-March; Spring: April-June; Summer: July-September).59

Figure 36: Time-series of current speed, current direction and along-slope current component at mooring DFO-2-15 measured the NB ADCP #506. The black line depicts the instrument depth.61

Figure 37: Seasonal current roses at 23 m depth at DFO-2-15 as based on low-pass filtered data from bin cell #20 measured by the NB ADCP #506. Roses indicate the direction toward which currents flow. Seasons are defined following the meteorological convention (Fall: October-December; Winter: January-March; Spring: April-June; Summer: July-September).63

Figure 38: Seasonal current roses at 101 m depth at DFO-2-15 as based on low-pass filtered data from bin cell #1 measured by the NB ADCP #506. Roses indicate the direction toward which currents flow. Seasons are defined following the meteorological convention (Fall: October-December; Winter: January-March; Spring: April-June; Summer: July-September).64

Figure 39: Time-series of current speed, current direction and along-slope current component at mooring DFO-1-15 measured by the NB ADCP #464. The black line depicts the instrument depth.....66

Figure 40: Seasonal current roses at 19 m depth at DFO-1-15 as based on low-pass filtered data from bin cell #8 measured by the NB ADCP #464. Roses indicate the direction toward which currents flow. Seasons are defined following the meteorological convention (Fall: October-December; Winter: January-March; Spring: April-June; Summer: July-September).68

Figure 41: Time-series of current speed, current direction and along-slope current component at mooring DFO-9-15 measured by the WHS ADCP #18414. The black line depicts the instrument depth.70

Figure 42: Seasonal current roses at 21 m depth at DFO-9-15 as based on low-pass filtered data from bin cell #8 measured by the WHS ADCP #18414. Roses indicate the direction toward which currents flow. Seasons are defined following the meteorological convention (Fall: October-December; Winter: January-March; Spring: April-June; Summer: July-September).72

Figure 43: Near-surface currents for the open water season for low-pass filtered current velocity data from the bin depth nearest bin depth to 50 m at all moorings except DFO-1 and DFO-9 which are closest to a bin depth of 20 m. Data when sea ice was present (winter-spring) were filtered out. Roses indicate toward where the current is flowing.74

Figure 44: Near-bottom currents for the open water season for low-pass filtered current velocity data from the bin depth nearest to bottom at each location. Data when sea ice was present (winter-spring) were filtered out. Roses indicate toward where the current is flowing.75

Figure 45: Surface zonal wind composite in summer 2015 and 2016 (June to August) in the western Arctic as based on NCEP/NCAR reanalysis data. Following the NCEP convention, positive values indicate westerly wind, whereas negative values indicate easterly wind (data source: <https://www.esrl.noaa.gov/psd/data/composites/hour/>)76

Figure 46: Temperature time-series measured at BR-1-15 from 2015 to 2016. The legend shows the serial number and depth of each CT logger.....81

Figure 47: Temperature time-series recorded at BR-3-15 from 2015 to 2016. The legend shows the serial number and depth of each CT logger.....	82
Figure 48: Temperature time-series recorded at BR-G-15 from 2015 to 2016. The legend shows the serial number and depth of each CT logger.....	83
Figure 49: Temperature time-series recorded at BR-K-15 from 2015 to 2016. The legend shows the serial number and depth of each CT logger.....	84
Figure 50: Temperature time-series recorded at DFO-2-15, DFO-1-15, and DFO-9-15 from 2015 to 2016. The legend shows the serial number and depth of each CT logger.	85
Figure 51: Salinity time-series recorded at BR-1-15 from 2015 to 2016. The legend shows the serial number and depth of each CT logger.	86
Figure 52: Salinity time-series recorded at BR-3-15 from 2015 to 2016. The legend shows the serial number and depth of each CT logger.	87
Figure 53: Salinity time-series recorded at BR-G-15 from 2015 to 2016. The legend shows the serial number and depth of each CT logger.	88
Figure 54: Salinity time-series recorded at BR-K-15 from 2015 to 2016. The legend shows the serial number and depth of each CT logger.	89
Figure 55: Salinity time-series recorded at DFO-2-15, DFO-1-15, and DFO-9-15 from 2015 to 2016. The legend shows the serial number and depth of each CT logger.	90
Figure 56: Temperature-salinity diagram constructed upon all data acquired with the CT loggers attached to the moorings BR-1, BR-3, BR-G, BR-K, DFO-2, DFO-1, and DFO-9 from 2015 to 2016. CTD profile data taken at mooring locations during the CCGS Amundsen and Laurier cruises in 2015 are depicted by the 4 black lines.....	91
Figure 57: Zoom on the temperature-salinity diagram constructed upon data acquired with the deep CT loggers (>400 m) attached to the slope moorings BR-1, BR-3 and BR-G from 2015 to 2016. CTD profile data taken at mooring locations during the CCGS Amundsen and Laurier cruises in 2015 are depicted by the 3 black lines.....	92
Figure 58: Time-series of diatom fluxes in 2015-2016 in the Beaufort Sea.....	93
Figure 59: Time-series of the ice algae <i>Nitzschia frigida</i> fluxes in 2015-2016 in the Beaufort Sea	94
Figure 60: General roadmap for the potential development of the State of the Beaufort Sea Report over 2017-2019, pending the availability of additional manpower and financial resources to support the development of this product over 2017-2019.	99

APPENDICES

Appendix A.	2015-2016 Final Mooring Diagrams
Appendix B.	Technical Advisory Committee Meeting 2016
Appendix C.	Data deliverable
Appendix D.	Summary Statistics of Ocean Currents

1.0 INTRODUCTION

The beginning of ice and ocean monitoring in the Canadian Beaufort Sea can be traced back to the 1980's when oceanographic moorings were deployed by Fisheries and Oceans Canada (DFO) in partnership with the oil and gas industry to document ice, wave and surge hazards and ocean current variability. During the next two decades, programs that involved government, industry and indigenous peoples injected funding to maintain year-round observations through DFO moorings that focused primarily on the continental shelf and the deep Canada Basin. In the mid-2000's, ArcticNet Inc. established the Long-Term Oceanic Observatories (LTOO) project to maintain moorings in the southeastern Beaufort Sea that were first deployed as part of the Canadian Arctic Shelf Exchange Study (CASES: 2002-2004); these brought a focus on the intervening continental slope which had received little prior attention. The LTOO project has been sustained since then through collaborations with different programs, such as partnerships with the oil and gas industry (2009-2011) and through the Beaufort Regional Environmental Assessment (BREA: 2011-2015).

The integrated Beaufort Observatory (iBO) was conceived as a means of fostering synergy among the primary long term mooring programs in the Beaufort Sea, enabling: 1) continuation of the time series at key locations; 2) synthesis of observations collected over the past three decades. This technical report describes the activities undertaken as part of the second year of iBO from April 1, 2016 to March 31, 2017. iBO is a four-year program (2015-2018) managed by ArcticNet in partnership with DFO and Golder Associates Ltd. (Golder). The program is supported by the Environmental Study Research Funds (ESRF) and Imperial Oil Resources Ventures Limited (IORVL). iBO aims to contribute key oceanographic information and understanding required for decisions on environmental stewardship and on industrial development and its regulation in the Canadian Beaufort Sea.

The iBO program contributes to the development of regional syntheses of ocean circulation, sea ice observations and biogeochemical fluxes that will include:

- Information on the magnitude, extent and return period of extreme ice features and of hazardous sea conditions – waves, surge and strong current;
- Ice and ocean datasets to document and interpret inter-annual variability of ice circulation, ocean circulation and particulate matter fluxes in relation to various environmental forcing factors;
- Data to support the development and evaluation of accurate numerical prediction models for operational ocean forecasting and the validation/verification of regional research models for simulating ice, seawater and oil spill trajectories.

The activities conducted under the umbrella of the iBO program during 2016-2017 include the turnaround of moorings deployed in 2015, four on the continental slope from CCGS Amundsen and three on the continental shelf CCGS Sir Wilfrid Laurier (Laurier). Together, these 7 moorings (Figure 1) constitute the backbone of iBO, providing an ice and ocean dataset of regional scope. In a larger context, iBO activities in 2016 also included the organization of two activities at the ArcticNet Annual Scientific Meeting: (1) a meeting of the Technical Advisory Committee (TAC) to review field operations and data recovery; and (2) a special science session on the Beaufort Sea ice and ocean regime that gathered iBO TAC members and other colleagues interested in the physical oceanography of the Canadian Beaufort Sea. This session aimed to review recent advances in the understanding of the regional variability to set the stage for a potential State of the Beaufort Sea report to be developed over 2017-2018.

The goal of this technical report is to provide a summary of the data acquired from the 7 iBO installations in 2015 to 2016 which represent an extension of key time-series initiated through ArcticNet/BREA and DFO over the preceding years. Only the 2015-2016 data that have been processed thus far are presented in this report; such

include all current meter, current profiler, and temperature-salinity data and part of the biogeochemical flux data. Data sets from the ice profiling sonars (IPS) currently being processed will be added to constitute the final 2015-2016 data record, since the availability of processed IPS data is delayed by about a year relative to processed ADCP and CT sensor data. Salient oceanographic features and events of interest during 2015-16 are discussed in relation to both long-term observations and recent process-oriented studies. In conclusion, we identify lessons learned stemming from the 2016 operations and define objectives and priorities for 2017-2018.

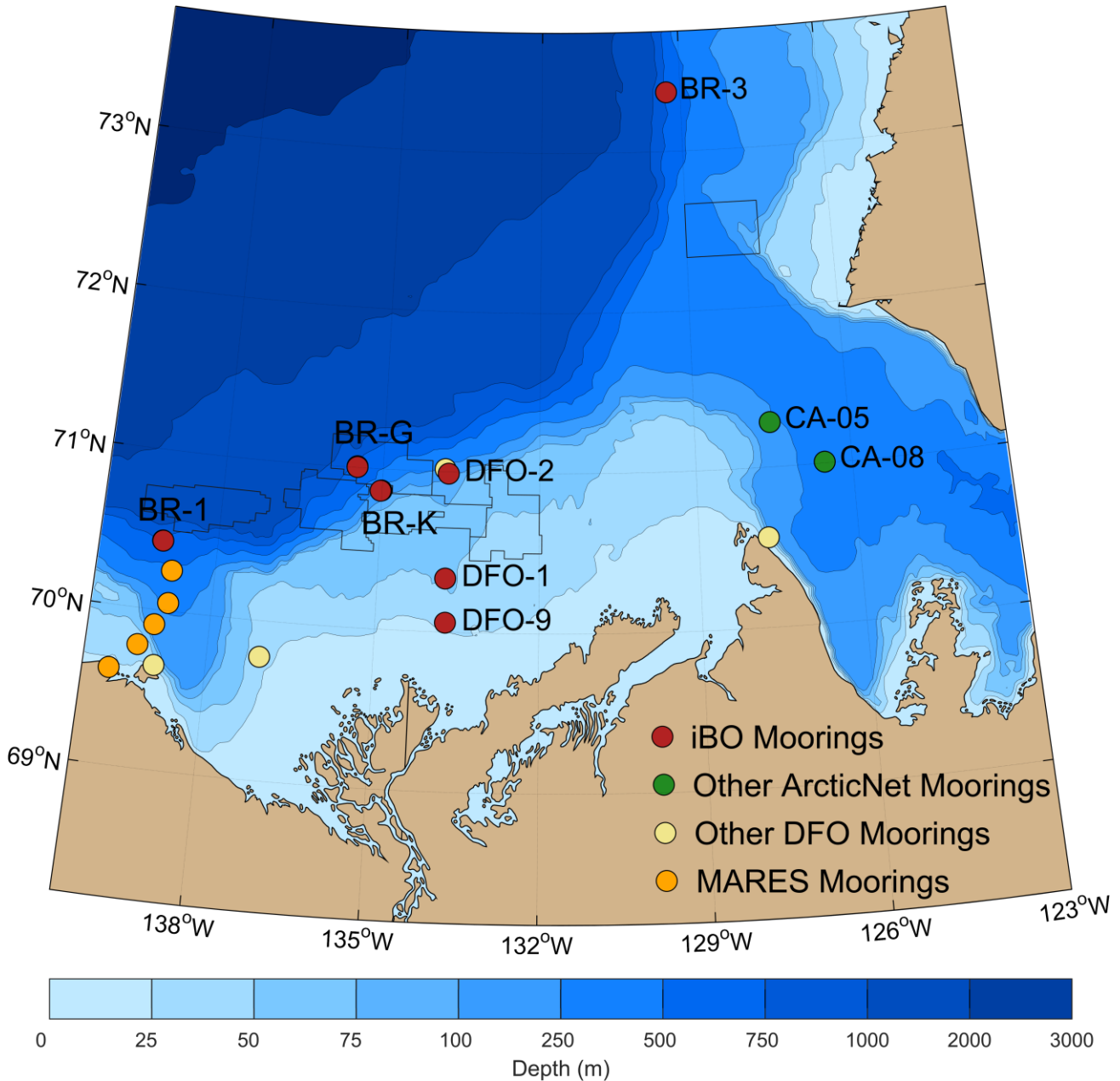


Figure 1: Bathymetric map of the Canadian Beaufort Sea showing the location of iBO moorings (in red). Moorings from partner projects (ArcticNet, DFO, MARES/BOEM) are also shown on the map but are not detailed in the present report.

1.1 Report Organization

This report provides an overview of the physical setting of the study area in section 1.2. A summary of iBO mooring design, field calibration activities, and shipboard mooring operations conducted onboard the CCGS Amundsen

and CCGS Laurier in 2016 are provided in sections 2.1 through 0. Description of the post-processing and QA/QC procedures applied to the recovered data and samples is presented in section 2.4. Section 3.0 provides a review of the processed datasets for the 7 moorings shown in Figure 1, with the exception of the data from the IPS for which the QA/QC is underway and the particle-size analyzer which is not currently being completed. Data are grouped by parameter: section 3.2 provides a detailed overview of the ocean current speed and direction recorded throughout the water column at all 7 moorings; section 3.2.8 provides a review of water mass variability based on temperature and salinity records; and section 3.4 presents preliminary data from sediment traps. Section 4.0 summarizes initial observations on the 2015-2016 dataset, lessons learned from the fieldwork and sets objectives for 2017-2018, including the potential development of a State of the Beaufort Sea Report. The appendices provide the final mooring diagrams for 2015-2016 (Appendix A) and summaries of the TAC and Beaufort Sea Collaboration meetings (Appendix B) hosted as part of the ArcticNet Annual Scientific Meeting, Winnipeg, in December 2016. Appendix C lists the electronic files provided as a data deliverable with this report. Appendix D provides a tabular summary of descriptive statistics pertaining to ocean currents measured at the 7 iBO moorings in 2015-2016.

1.2 Physical Setting of the Study Area

The Canadian Beaufort Shelf (Figure 1) is a narrow Arctic shelf (120 km width × 530 km length) comprised of a series of plateaus separated by shallow channels (Blasco et al., 2013). The shelfbreak is located at 80-100 m depth where the slope angle increases to 2-6° toward the deep Canada Basin. The region is greatly influenced by the Mackenzie River, which is the largest Arctic river in terms of sediment load (~127 × 10⁶ t per year) and the fourth largest in terms of freshwater discharge (330 km³ yr⁻¹) (Macdonald et al. 1998).

Ice cover in the region undergoes a seasonal cycle with considerable inter-annual variability. Galley et al. (2013) recently documented that no significant trend in summer sea ice concentration on the mid-to upper slope of the central shelf has been measured from 1996 to 2010, although off the shelf to the northwest, a decrease in old sea ice concentration compensated by an increase in first-year sea ice is apparent. Typically, seasonal sea ice begins to form in October in the coastal sector and by early to mid-November the ice cover is consolidated over the entire region¹ (Carmack and Macdonald, 2002). In winter, landfast ice forms in the nearshore out to about the 20 m isobath and an ice rubble field (i.e. the *stamukhi*; Giovando and Herlinveaux 1981), which includes grounded ice, develops at the outer edge of the landfast ice. Beyond the *stamukhi*, a recurrent flaw lead separates the landfast ice from the moving pack ice that typically drifts westward driven by [prevailing wind (Macdonald et al. 1995). The Cape Bathurst Polynya centered at the mouth of the Amundsen Gulf is part of the flaw lead system that borders the Beaufort Sea (Barber and Hanesiak 2004). The summer retreat of the ice to the north-west driven by the seasonal increase in east wind¹ causes widening of the flaw lead typically in June, but sometimes as much as 6 weeks earlier.

On the inner to mid-shelf, ice drift, ocean circulation, and the trajectory of the Mackenzie River plume, are highly variable and linked to wind dynamics (Melling, 1993; Melling and Riedel 1994; O'Brien et al. 2006). Over the outer shelf and on the slope, large-scale surface circulation (upper 50 m) is dominated by westward-flowing current of the Beaufort Gyre (Ingram et al. 2008). The water mass that occupies the upper 50 m (polar mixed-layer) is the Arctic Surface Water with salinity of ~30-31 (practical scale) on average in winter, but this value changes markedly with river input and the growth and melt of ice. From 50 to 200 m depth near the shelfbreak, a submerged stream of north-eastward flow delineates the Beaufort under-current (Forest et al. 2015; Dmitrenko et al. 2016), the eastward continuation of a feature first described in the Alaskan Beaufort Sea (Aagaard 1984; Pickart 2004; von Appen and Pickart 2012). This current is 10-15 km in width and topographically steered along the upper slope; it predominately transports Arctic water of Pacific origin (salinity ~33), but some water of Atlantic origin (salinity 34.0-

¹ <http://iceweb1.cis.ec.gc.ca/30Atlas/page1.xhtml?region=WA&lang=en>

34.9) which typically dominates the 200-1000 m layer of the water column is entrained at times. This under-current is subject to frequent wind-forced reversals to the west which are commonly associated with upwelling (Aagaard, 1984; Pickart et al. 2013). The under-current is the strongest circulation feature in the area and intrinsic to shelf-slope exchange of water in the Beaufort (e.g. Kulikov et al. 1998; Williams et al. 2008). At 20-30 km from the shelf edge, the eastward shelfbreak jet is no longer present and the mean current in the upper 200 m is westward within the anti-cyclonic motion of the Beaufort Gyre (Forest et al. 2015). Mesoscale eddies frequent the region beyond the shelf edge.

2.0 MATERIAL AND METHODS

This section of the report provides detailed information on the tautline mooring design and instrumentation of iBO moorings (section 2.1), compass calibration activities for current meters and current profilers (section 2.2), and mooring recovery and deployment operations aboard the CCGS Amundsen and CCGS Laurier (section 2.3). A description of the QA/QC processing steps for each moored instrument is provided in section 2.4.

2.1 Taut-line Mooring Design

2.1.1 Slope Moorings

The slope moorings array consists of 3 similarly designed long moorings (BR-1, BR-G and BR-3) located on the middle continental slope (~700-750 m depth) and one short mooring (BR-K) located on the upper slope near the shelf edge (~170 m depth; Figure 1). Mooring diagrams (as deployed) for 2015-2016 are included in Appendix A.

The longer moorings on the lower slope consist of the following key components:

- ASL Ice Profiling Sonar (IPS) was used at approximately 60 m depth to measure ice draft and non-directional waves during intervals of open water. IPS were mounted in 30-inch spherical syntactic foam floats (Mooring Systems Inc. - MSI).
- 150 kHz Teledyne RD Instruments (TRDI) Quarter Master Acoustic Doppler Current Profiler (QM ADCP) were used at approximately 180 m water depth to profile upper water column currents at 4 m vertical resolution and measure ice velocity using a Bottom-Track feature. The QM ADCPs were mounted up-looking in 40-inch syntactic foam floats (Flotation Technologies - DeepWater Buoyancy).
- 75 kHz TRDI Long Ranger ADCP (LR ADCP) were used at approximately 450 m water depth to measure water velocity profiles at 16 m vertical resolution. The LR ADCPs were mounted up-looking in 40-inch syntactic foam floats (Flotation Technologies).
- Two high frequency short-range (<1 m) Nortek Aquadopp DW (AQD) single point current meters were used to measure water velocity at approximately 10 m and 110 m above the bottom. Each Nortek AQD was equipped with a vane to hold the heading nearly constant for the duration of each ensemble interval.
- Two Technicap PPS 3/3-24S 24 cup sequential sediment traps were deployed between the IPS, QM ADCP and LR ADCP to record the annual cycle in vertical particle flux.
- RBR Conductivity and Temperature (CT) loggers were installed at approximately 60 m, 130 m, 180 m, and 450 m water depth, as well as 10 m above the bottom. These instruments measure water temperature and salinity and are used to compute sound speed to improve IPS and ADCP processing.
- Various smaller syntactic foam floats were distributed along the mooring as required.
- Tandem Edgetech CART acoustic releases were used as the primary locating and recovery devices.

The shallow (upper slope) mooring consisted of the following key components:

- A 300 kHz TRDI Workhorse Sentinel ADCP (WHS ADCP) was used at approximately 140 m water depth to profile currents with a vertical resolution of 8 m, as well as to measure ice velocity using the Bottom-Track feature. The WHS ADCPs were mounted upward looking in 33-inch syntactic foam ellipsoid floats manufactured by MSI.
 - A RBR CT logger with auxiliary sensors to measure turbidity, dissolved oxygen, and chlorophyll fluorescence was installed at approximately 18 m above the bed.
-

- A Sequoia LISST 100X laser diffraction system was located 18 m above the seafloor to provide measurements of particle size distributions and associated volume concentrations in the lower water column. The LISST measurements help to better quantify the seasonal and annual variability of vertical and horizontal fluxes of inorganic solids.
- A 1 MHz Nortek Aquadopp profiling current meter (AQP) was mounted down-looking below the LISST to provide details of the flow and acoustic backscatter structure near the seafloor on the upper slope. The AQP's measure three-dimensional current velocities and provide a measure of acoustic backscatter intensity in 2 m range bins from the bottom to about 16 m above seabed. Combined with the velocity profile information from upward looking ADCP's the profilers provide a detailed and near complete view of the water column vertical structure.
- An additional syntactic foam ellipsoid float was located above the LISST cage to provide floatation for the lower portion of the mooring.
- Edgetech (Model CART) acoustic releases in tandem were used as the primary recovery device.

Improvements made in 2015 to the iBO moorings with respect to the previous BREA 2014 mooring designs were maintained for 2016-2017. This included a fifth CT logger added at 130 m to monitor variability in the core of the Pacific halocline. The QM ADCP was deployed at 180 m to allow a better resolution of currents in the upper water column with bin sizes of 4 m. Also, TRDI ADCP settings were further adjusted in 2016 to improve the overall data quality and quantity following a change from alkaline to lithium battery packs. Finally, all BR moorings on the slope in 2016 were assembled using new Amsteel II ropes (Golder 2016b).

2.1.2 Shelf Moorings

The moorings at all three shelf locations (DFO-9, DFO-1, and DFO-2; Figure 1) have similar design (Appendix A). They are located at approximately the 28 m, 55 m and 110 m isobaths, respectively; DFO-2 is on the upper continental slope and DFO-2 and DFO-9 lie within the Kugmallit sea valley. Recording instruments at the two shallower sites (DFO-9 and DFO-1) are placed on two separate nearby (50-150 m separation) moorings so as to keep the equipment near the seabed safe from drifting ice and to avoid interference between the two sonars used for observations. The depth at the third site is sufficient that the instruments are located one above the other on a single mooring.

The installations at all three sites support the following instruments:

- ASL IPS are located at 30-50 m depth to measure ice draft and non-directional waves during intervals of open water. IPS of three types are in use: original IPS4 units operating at 200-kHz acoustic frequency; updated W-IPS4 units operating at 420 or 895 kHz and measuring wave height as well as ice draft; IPS5 units operating at 420 kHz with increased data storage capacity. IPS are mounted in light-weight stainless steel frames each supported by a collar of four 14-inch spherical plastic floats (Viny Inc. Model 12B3).
- 300-kHz TRDI ADCPs are located about 4 m above the seabed to measure ocean current at 4 m vertical resolution between about 6-m elevation above the seabed to about 15-m depth below the surface, plus ice velocity. ADCPs of two types are in use: original narrow-band ADCPs (NB-ADCP) and newer broad-band WHS-ADCPs. The NB ADCPs operating with higher signal-noise ratio and better magnetic compasses are favoured for Arctic use. ADCPs are mounted in light-weight stainless steel frames each supported by a collar of four 14-inch spherical plastic floats (Viny Inc. Model 12B3) and equipped with vane so that the ADCP heading remains stable throughout a measurement interval. The frame is coupled into the mooring through a swivel.

- CT recorders (Seacat SBE37: Sea Bird Electronics Inc.) are installed on the frame with each ADCP, about 3 m above the seabed. They record the temperature and salinity of water within the bottom boundary layer and provide sensitive indication of up-welling and down-welling motions.
- Acoustic transponder releases (Model CART: ORE Edgetech) were mounted in tandem 1 m above the mooring's deadweight anchor. The CART is the device used to locate each mooring and to enable its recovery by unhooking the buoyant part of the mooring from its heavy anchor. Two transponding releases are used in parallel for redundancy in this essential function.

2.2 Compass Calibration and Verification

Compass calibration is an important consideration for current meters deployed in the Canadian Beaufort Sea due to the reduced magnitude of the horizontal component of the Earth's magnetic field in the Canadian Arctic, less than one third of its value in southern Canada. Calibration and verification of the current meter compasses near the approximate geomagnetic latitude where they will be deployed is advisable prior to deployment. Moreover, care must be taken to eliminate all sources of magnetic interference from the instrument-supporting cages on the mooring and similarly also in the immediate vicinity of the calibration activities. For this reason, calibration activities cannot take place onboard the Amundsen or Laurier.

The compass calibration procedure for TRDI current meters corrects for both soft iron effect (i.e. distortion of the Earth's magnetic field by local ferrous metal) and hard iron effects (i.e. magnetic influence from magnetic material in the vicinity of the instrument, such as mooring hardware and batteries). Nortek's compass calibration for Aquadopp and Continental instruments only corrects for hard iron effects and not for soft iron effects.

Summaries of compass calibration and verification activity are provided in the iBO 2016 field reports from the Amundsen and Laurier expeditions (Golder 2016b; IOS-DFO, 2016). In 2016, compass verification from Nortek and TRDI instruments deployed from the Amundsen took place on August 24, 2016 at Kugluktuk during crew change and from September 18 to 20 following the ArcticNet 2016 Leg 3a expedition also at Kugluktuk. This task consisted of the compass verification of one WHS TRDI ADCP (#7844) and eight Nortek instruments, with three of them recovered from BR-1-14; the latter could not be verified in 2015 due to logistical constraints. Compasses were verified against True North after correction for magnetic declination at Kugluktuk again in August-September 2016 (17° 55' East). Calibrations of DFO instruments deployed from Laurier were conducted at Herschel Island on October 3, 2015.

Table 1 provides a summary of the post-verification compass errors (calculated from readings made in 10 degree increments) for the verification activities conducted in August-September 2016. In the last column of Table 1, the mean calculated error is the accuracy of the compass; this value has been used in processing to correct the compass reading. For the instruments deployed from Amundsen, where stabilizing vanes were not used with the current meters, the value of standard deviation in the same column represents the precision of that correction; the largest value of 4° indicates that uncorrected errors ranged over $\pm 6^\circ$ (for a sine wave) as the heading of the instrument varied. For instruments deployed from Laurier which were equipped with stabilizing vanes, the residual non-linearity – summarized as a standard deviation Table 1 – was used in calibration so that the precision in all cases is approximately 1°.

The Nortek instrument compasses were successfully verified to within the acceptable Arctic limits recommended by the manufacturer (<5 degrees). However, the TRDI WHS #102 post-verification displayed a mean error of 7.6 degrees suggesting a higher variability (sensitivity) at Arctic latitudes. Re-calibration of the instrument was also attempted in September 2016 in Kugluktuk by ArcticNet personnel after Leg 3a, but was unsuccessful due to the unit's Arctic sensitivity. This unit will not be re-used on future iBO moorings.

Table 1: Mean Error of Recovered Nortek and TRDI Compasses (10 Degree Increment).

Instrument	Serial Number	Mooring	Mean Calculated Error \pm Standard Deviation around the Compass (degrees)
Aquadopp DeepWater	6270	BR-01-14	0.8 \pm 0.6
Aquadopp DeepWater	8414	BR-01-14	3.6 \pm 2.0
Aquadopp DeepWater	2792	BR-01-15	3.6 \pm 2.1
Aquadopp DeepWater	2701	BR-01-15	2.2 \pm 1.3
Aquadopp DeepWater	9846	BR-G-15	2.1 \pm 1.1
Aquadopp DeepWater	8434	BR-G-15	3.2 \pm 1.9
Aquadopp DeepWater	8541	BR-03-15	0.8 \pm 0.7
Aquadopp Profiler	9711	BR-K-15	5.2 \pm 2.9
TRDI WHS ADCP	0102	BR-K-15	7.6 \pm 4.0
TRDI NB-ADCP	0505	DFO-2	0.9 \pm 0.7
TRDI NB-ADCP	0464	DFO-1	0.7 \pm 1.4
TRDI WHS ADCP	12414	DFO-9	1.4 \pm 3.1

2.3 Mooring Recovery and Deployment

This section of the report provides details on iBO mooring recovery and deployment operations conducted aboard the CCGS Amundsen and CCGS Sir Wilfrid-Laurier (section 2.3.1) during the 2016 field campaigns. Coordinates and depths of the mooring at their recovery and re-deployment are provided in Table 2 and Table 3.

Table 2: 2015-2016 Mooring Recovery Summary

Mooring	Latitude (WGS84)	Longitude (WGS84)	Water Depth (m)	2015 Deployment Date and Time (UTC)	2016 Recovery Date and Time (UTC)
BR-K-15	70° 51.763' N	135° 1.706' W	168.9	Aug-27-2015 14:29	Sep-01-2016 02:40
BR-G-15	71° 00.122' N	135° 29.612' W	700.3	Aug-28-2015 18:53	Sep-01-2016 00:26
BR-1-15	70° 25.9435' N	139° 01.2347' W	753.0	Sep-30-2015 22:33	Sep-01-2016 15:50
BR-3-15	73° 24.566' N	129° 21.224' W	689.4	Aug-31-2015 21:15	Sep-07-2016 22:59
DFO-2-15	70° 59.3608' N	133° 44.6272' W	110.8	Sep-26-2015 23:30	Sep-30-2016 14:52
DFO-1a-15	70° 20.0348' N	133° 44.4586' W	54.8	Sep-27-2015 15:41	Sep-25-2016 20:07
DFO-1b-15	70° 20.0294' N	133° 44.3711 W	54.8	Sep-27-2015 15:34	Sep-25-2016 20:15
DFO-9a-15	70° 03.5370' N	133° 42.9223' W	31.0	Sep-27-2015 21:40	Sep-25-2015 16:53
DFO-9b-15	70° 03.5007' N	133° 42.9405' W	31.0	Sep-27-2015 21:46	Sep-25-2015 16:45

Notes: DFO moorings were recovered from the Laurier, while other moorings were recovered from the Amundsen.

Table 3: 2016-2017 Mooring Deployment Summary

Mooring	Latitude (WGS84)	Longitude (WGS84)	Water Depth (m)	2016 Deployment Date and Time (UTC)
BR-K-16	70° 51.795' N	135° 01.449' W	166	Sep-05-2016 00:18
BR-G-16	71° 00.128' N	135° 29.447' W	699	Sep-06-2016 17:58
BR-1-16	70° 25.986' N	139° 01.620' W	754	Sep-03-2016 02:49
BR-3-16	73° 24.610' N	129° 21.760' W	719	Sep-09-2016 00:39
BR-3b-16	73° 24.057' N	129° 21.240' W	690	Sep-05-2016 00:18

DFO-2-16	70° 59.3590' N	133° 44.6363' W	111	Sep-30-2016 15:42
DFO-1a-16 ¹	70° 20.0310' N	133° 44.3690' W	55	Sep-25-2016 21:53
DFO-1b-16 ¹	70° 20.0350' N	133° 44.4520' W	55	Sep-25-2016 21:55
DFO-9a-16 ¹	70° 03.5339' N	133° 42.9176' W	31 ²	Sep-25-2016 18:17
DFO-9b-16 ¹	70° 03.5013' N	133° 42.9369' W	31 ²	Sep-25-2016 18:13

Notes: ¹ DFO moorings were deployed from the Laurier, while other moorings were deployed from the Amundsen.

² This mooring was deployed in a dredged borrow pit for protection from ice. The tabulated depth is that of the surrounding seabed, not that of the pit.

2.3.1 Shipboard Mooring Operations

Steps for mooring recovery aboard the CCGS Amundsen and CCGS Laurier generally included:

- pre-operations Job Safety Assessment (JSA) meeting, an operational planning meeting, and a toolbox meeting (on deck);
- confirm mooring presence and orientation with the multibeam sonar and interrogate the mooring to determine range; multi-beam sonar not used on the Laurier;
- maneuver ship into position depending on prevailing drift, wind and sea state;
- conduct a conductivity, temperature and depth (CTD) cast to provide overlapping water column data for data processing; relative timing of CTD cast varies with logistic constraints on Sir Wilfrid Laurier
- enable the acoustic release and send a command to release the mooring;
- mooring positioned relative to the bow of the ship for recovery;
- lift mooring elements onto the foredeck and take instruments off the mooring as they are brought on deck, then take the mooring apart (i.e., a complete disassembly of the mooring);
- inspect and rinse instruments with freshwater and stow in plastic bins;
- transfer of equipment lab spaces for inspection and data recovery;
- immediately download data from the instruments if re-using, otherwise as schedule permits;
- perform preliminary review and graphical inspection of the data if re-using the instrument, otherwise as schedule permits;
- store and secure the instruments on board the ship, and
- service and maintain the instruments, including any required trouble-shooting or field repair.

All mooring recovery operations were conducted safely and successfully on the foredeck and from the FRC, when involved. Particular attention was given to the handling of the remaining Benthos Locator Model ALP-364/EL deployed in 2015 to ensure that these problematic instruments were manipulated correctly. Details on a safety incident related to a Benthos Locator that was recovered from BR-3-14 during Leg 3a in 2014 aboard the Amundsen can be found in a technical memorandum (Golder, 2015). The incident involved the over-pressurization of the instrument through the exposure of the internal lithium batteries to seawater and the subsequent blowout of the pinger's end cap following hydrogen gas formation.

Servicing of the mooring instruments involved the following steps:

- opening the housing (if required) and inspecting interior for corrosion, and other damage;
- changing the batteries (if required), and replacing desiccant (if applicable);
- cleaning the o-ring surfaces and re-greasing and replacing or cleaning all o-rings;
- running a trial delayed-start deployment using instrument's internal power with computer disconnected, followed by upload and inspection of data record;
- programming the instrument for deployment;
- completing a record of programming (screenshots and paper record sheets).

Before programming and deployment of instruments on the moorings, standard manufacturer procedures and pre-deployment tests were followed to provide verification of instrument operation. Instruments were generally programmed for a 1-year deployment. However, those at BR-3 were programmed for two years' operations because at this northerly location west of Banks Island ice can in some years preclude mooring recovery operations. This mooring was also equipped with Edgetech 8242XS acoustic releases that have an extended battery life of at least 2 years. A contingency phase was implemented for all Ice Profilers in order to continue measurements in the event that the mooring might not be recovered in the fall of 2016.

Steps in the mooring deployment were as follows:

- confirm the design of the mooring particulars to meet the site's constraints;
- review the lifting plan and JSA;
- assemble the mooring on deck (using the original configuration or a modified configuration, as appropriate);
- conduct a toolbox meeting on-deck;
- deploy the mooring;
- enable and interrogate the acoustic release;
- perform triangulation to determine the actual location of the mooring, as distinct from the drop point;
- disable the acoustic release;
- perform multibeam survey of the mooring to confirm position in water column (Amundsen only); and
- perform CTD cast.

Multibeam data collected after deployment of each mooring from Amundsen was examined by experienced analysts to establish that the mooring was positioned on the correct isobath and that the resting depths of the instruments after deployment were as planned; most of the large instruments can be detected by the multi-beam sonar. Instruments were at their target depths at all sites except BR-3-16, where a depth discrepancy was noticed. Although the anchor of this mooring was dropped over the target 690 m isobath, the mooring drifted during descent and landed in water approximately 29 meters deeper than expected. The mishap is linked to the presence of a steep slope adjacent to the narrow (1-km width) ledge which was the target for the mooring. The *Amundsen* was apparently too close to the edge of the ledge when the mooring was dropped; a long swell from the west-southwest posed challenge to the maneuvering of the ship to the intended drop point, despite prolonged effort on the bridge.

As a result of the deeper bottom depth at BR-3-16, the ASL IPS was estimated to be located around 87-89 m depth, which is 2-4 m beyond the maximum target range of 85 m programmed for this instrument. The ASL IPS

only find targets within the specified maximum range, so this situation would result in missing the thinner part (0-5 m) of the ice thickness distribution, although the deeper ridge keels would be detected. Since the ice measurements are a priority of iBO, it was decided to design a complementary mooring (named BR-3b-16) that consisted of an ASL IPS and CT sensor only and deployed at the correct depth of 60 m. This mooring was deployed 1-km south of BR-3-16 along the ice drift route on a wider region of the small plateau where BR-3 has been located since 2014. This would fortuitously provide dual measurements of thicker ice keels (>5 m) nearby Banks Island over 2016-2018. The data quality and quantity from other instruments (e.g. ADCPs, CT sensors) at BR-3-16 will not be affected by the discrepancy from the planned deployment depth.

2.4 Data Processing and QA/QC

2.4.1 Current Meters and Current Profilers

This section of the report provides a summary of QA/QC procedure applied to current meters and current profilers deployed on both BR and DFO moorings. The QA/QC procedure of current profilers on BR mooring differs slightly from that applied to DFO instruments (see details below). Further harmonization of both processing chains is planned for 2017-2018. For all moorings, pressure sensors on the TRDI ADCPs were zeroed at the time of setup in order to account for atmospheric pressure in the depth calculation performed by the instrument. Processing routines were used to convert pressure measured by the Nortek AQDs, to water depth; pressure measurements in air before and after the instrument deployment were averaged to represent mean atmospheric pressure. For BR moorings, processing of the ASCII files from Nortek AQDs or MATLAB® binary files from TRDI ADCPs was completed using MATLAB® software. For DFO moorings, data was processed using the in-house software and routines (the IOS SHELL suite) from DFO, which produce ASCII multi-line header files and multiple ASCII data files. These DFO ASCII files were converted into the BR mooring file format (MATLAB® binary and Text files) for plotting, analyses and to be provided as a data deliverable.

Processing and quality-checking of the current time-series data consisted of the following steps:

- 1) Measurements made by the instrument while it was out of the water, as determined from pressure readings, were removed.
- 2) East and North horizontal components of velocities were corrected to true north based on local magnetic declination. An annual average magnetic declination was used for the deployment period based on the Natural Resources Canada numerical model for the International Geomagnetic Reference Field 2012 (IGRF-12; <http://www.geomag.nrcan.gc.ca/calc/mdcal-eng.php>). The summary of magnetic declination values each for each mooring is listed in Table 4.

Table 4: Magnetic declination values for 2015-2016 iBO Moorings

Mooring	Magnetic Declination [degrees East]
BR-G-15	22.9
BR-K-15	23.0
BR-3-15	24.4
BR-1-15	23.5
DFO-2-15	23.1
DFO-1-15	23.0
DFO-9-15	22.9

- 3) Compass readings from the ADCPs at the DFO moorings were further corrected for compass non-linearity using a polynomial approximation to compass response as a function of instrument geomagnetic heading (section 2.2). This can span a range that exceeds 10° peak to peak, depending on the instrument and its battery. The geomagnetic field near the Beaufort coast is considered close enough to the locations of moorings so that the measured polynomial correction is applicable offshore². No polynomial correction was applied to the indicated directions of TRDI ADCPs at the BR sites because the ±4-degree root-mean-square non-linearity was considered acceptable (TRDI 2014).
- 4) Acoustic amplitude was plotted for each beam to check the quality of the instrument signal return and filtered for amplitudes below the noise floor for the respective instrument (Nortek 2013; TRDI 2014).
- 5) Nominal depths of echo intensity and velocity data from TRDI ADCPs deployed at the DFO sites were calculated using a spline interpolation along each beam that corrects for the effects of changing pitch and roll. Nominal depths from the TRDI ADCPs deployed at the BR moorings were calculated using the default bin mapping method (nearest vertical bin) for TRDI ADCPs (TRDI 2014) that uses the 20° beam slant angle. The latter approach provides similar results to the spline interpolation method in the cases that the tilt is lower than 10° (>99.5% of time for each time series).
- 6) For ADCPs deployed at the BR moorings, the following steps were applied to filter data and to identify and flag data that were considered as suspicious:
 - a) Data were filtered for sidelobe interference using the beam slant angle of the instrument. For the Nortek Aquadopp profiler at BR-K, this value was 25° (Nortek 2013) and for the TRDI ADCPs this value was 20° (for all LR, QM and WHS ADCPs) or 30° (for NB ADCPs on DFO-2 and DFO-1). At BR moorings the filter correction was calculated as the product of the instrument depth and the cosine of the slant angle plus one range bin. The filtered range approximately corresponds to the top 10% of the range to surface or bottom depending on whether the instrument was up-looking or down-looking (only the Aquadopp profiler at BR-K).
 - b) For TRDI instruments, datasets were filtered using the Percent Good (PG) values. Data points with a combined PG4 and PG1 value of less than 25% (TRDI 2014; IOS 2015) were removed from the dataset. The PG value is a data-quality indicator that reports the percentage (0 to 100) of valid data collected for each depth cell of the velocity profile using the four beams (PG4) and three beams (PG3). It is an indicator of the following criteria: low correlation, large error velocity and fish detection (false target threshold) (TRDI 2006).
 - c) Time series data from ancillary sensors on the current profilers were inspected for QA/QC purposes. Nortek recommends that the instrument tilt not exceed a maximum of 10° for measurement of currents (Nortek 2013) and TRDI recommends a maximum tilt limit of 15° (TRDI 2014). Data when tilt was exceeding the respective thresholds were flagged as part of the QA/QC.
 - d) Data were further filtered using the error velocity (TRDI instruments only) and maximum vertical velocity thresholds. The error velocity is a measure of the homogeneity of water movement across the span of the 4 inclined sonar beams. The data from TRDI ADCPs on BR slope moorings were filtered for vertical velocities greater than 0.1 m/s and error velocities greater than 0.15 m/s (i.e. arbitrary values based on error velocity thresholds developed as part of the BREA program).
 - e) Additional visual inspection guided the flagging of (subjectively) suspicious bin values.

² The strengths of the horizontal component and the declination angles of geomagnetic field at Inuvik, Herschel Island and site BR-G at the time of writing were respectively: 8505, 8413 & 7147 nT and 81.5°, 81.6° & 82.9°.

- f) Bottom track ranges (WHS and QM) are corrected for pitch and roll following the methodology of Woodgate and Holroyd (2011).
- 7) For ADCPs deployed at the DFO sites, a multi-stage decision tree was applied to identify and flag data judged to be of little value by a variety of criteria. These criteria include:
- a) Surface interference: Eliminating surface interference at the DFO sites used the same methodology as at BR sites, except that the ADCP-measured range to the surface (water-ice or water-air) was used in place of the ADCP's depth.
 - b) Beam-to-beam differences: Ensemble values masked if more than three differences between beams exceed 8 counts.
 - c) Extreme strong echo: Ensemble values masked because at least one beam differs from the others by more than 25 counts.
 - d) Extr+Diffs: ensemble values masked due to combined conditions of 2 & 3.
 - e) PercentGood < 25: Ensemble values masked because fewer than 25% of the ping data yielded 3 or 4 beam solutions.
 - f) Low Amplitude: Ensemble values masked because 1 or more beams have amplitude of less than 1 counts.
 - g) Error Velocity: Ensemble values masked because the so-called error velocity (actually the difference between independent values of vertical velocity) exceeded 2.8 times the standard deviation of the time series (approximately the 99th percentile). The editing threshold here and in the next step were not fixed but set adaptively.
 - h) VertVel: Ensemble values masked because the vertical velocity exceeded 2.8 times the standard deviations of the time series (approximately the 99th percentile).

Final QA/QC time-series data from ADCPs are usually gappy and can be difficult to use in some applications. To generate continuous time series of data at sub-tidal frequencies, the final processing step for DFO was the complex demodulation of the time-series within over-lapping 12-hour windows (e.g. Melling et al. 2001). This additional step was not applied to the current data delivered as part of Appendix D. Instead a low-pass filter (PL66TN, Beardsley and Rosenfeld 1983) was applied to selected bin depth time-series for each instrument data (interpolated linearly to 1-hour intervals for consistency) in order to construct seasonal current roses (16 directions, 22.5° bins) of the sub-tidal current component as presented in section 3.2.

2.4.2 Temperature-Salinity Loggers

Data were extracted from the RBR sensors using Ruskin® software (RBR, 2016) and from Sea Bird sensors using Sea Bird Electronics software. Time-series from BR moorings were processed and plotted using MATLAB® scripts, whereas the same task was accomplished by DFO using in-house IOS SHELL routines.

For CT sensors on the BR moorings time series were clipped for out-of-water values and evaluated visually for data quality. In addition, an automated filter is applied to the conductivity and temperature data to flag potential spikes from the data time-series using a seven-sample moving window. All values outside of ± 1.5 standard deviations about the moving window mean that could be considered spikes are flagged; spikes in conductivity are far more common than spikes in temperature. Any spikes identified in the temperature or conductivity time-series cause the corresponding salinity values also to be flagged because salinity is temperature and conductivity dependent.

In addition, the temperature and salinity data from all moorings were verified and corrected for accuracy against nearby CTD casts acquired at the time of deployment in 2015. Since appreciable drift in sensor calibration rarely occurs for temperature, the assessment of calibration drift is normally carried out for conductivity; it is done on the basis of potential temperature versus salinity plots. For Sea Bird sensors, drift in conductivity calibration is usually associated with silting or bio-fouling. For the RBR sensors a calibration shift from laboratory values can occur via intrusion of mooring components (conducting or non-conducting lines, support structure, etc.) into the (20-cm diameter) sensing volume for conductivity.

2.4.3 Ice Profiling Sonars and Ice velocity

Processing and QA/QC data from IPS 2014-2015 and IPS 2015-2016 is currently underway and results are expected to be presented as part of upcoming complementary reports provided by DFO and ASL Environmental (ASL). It should be noted, however, that all the IPS at the 7 iBO moorings and all CT loggers at the DFO moorings functioned properly and provided complete datasets from 2015 to 2016 with a total of 100% of raw data return. The derivation of ice draft from IPS signal data employs well-established methods that have been developed during the processing of many dozens of IPS datasets over the past three decades (Melling et al. 1995; Melling and Riedel, 2004; Fissel et al. 2008).

There are many steps in the processing of IPS signal data to ice draft. The procedures for detection of erroneous target data and for calibration of zero ice draft in particular are meticulous and require considerable experience. It is not useful to document the process here in detail. The interested reader is referred to Melling et al. (1995) and Melling and Riedel (2004).

Ice velocity is derived from data provided by TRDI's patented bottom-track firmware in the WHS and QM ADCPs (see section 2.1). It can also be derived from binned water-column data recorded by LR ADCPs if certain conditions are met. The ASL procedures for deriving reliable estimates of ice velocity from ADCP data are numerous. Moreover, a certain level of subjectivity must be tolerated in the analysis because greatly varying conditions at the target (rough or smooth ice; continuous or broken ice cover; rough seas or calm seas; other targets yielding plausible echoes; etc.) generate ambiguity. The interested reader is referred to more thorough discussions provided by Melling and Riedel (2004) and ASL (2015).

2.4.4 Sediment Traps

Each of the BR moorings on the middle continental slope was equipped with two automated sediment traps (at approximately 125 and 310 m depth) to record the annual cycle in vertical particle flux (inorganic sediments, organic carbon and particulate nitrogen) and plankton community composition in the upper water column. All traps provided complete particle flux time-series as expected. However, two anomalies were observed: (1) the trap carousel at BR-01-15 rotated in the wrong direction, but completed a full-year sequence; and (2) the lower trap at BR-G-15 completed full sampling from 2015 to 2016, but some sample cups did not rotate and collected more particles than expected. This was the case for mid-September to mid-October 2015 (1 month), June 2016 (1 month), and mid-July to September (47 days in the same cup). Possible causes for the inversion of the motor at BR-1-15 and stalling of the carousel at various dates at BR-G-15 are currently being investigated by the manufacturer.

Analyses on the sediment trap samples are underway at Université Laval. As a first step, sediment trap samples were split to prepare a subsample for the measurements of total particulate matter (TPM), particulate organic carbon (POC), and particulate nitrogen (PN). In the coming weeks, subsamples will be filtered, weighed and processed on the CHN elemental analyzer for TPM, POC and PN values. In addition, zooplankton actively entering the sediment traps (named "swimmers") and that are present in the subsample were removed. Zooplankton organisms will be identified to the lowest species possible to monitor the seasonal and inter-annual fluctuation in

the zooplankton community structure. Aliquots are also used for the enumeration and identification of phytoplankton cells to indirectly assess the magnitude, timing, and composition of the phytoplankton spring bloom.

3.0 RESULTS AND DISCUSSION

This section of the report summarizes measurements of currents, salinity, temperature, and sediment trap data collected in the 2015-2016 deployment interval. A description of sea ice conditions is provided for context.

3.1 Sea Ice Conditions

The southern Beaufort was characterised by a very early sea ice breakup in 2016, approximately 6 weeks ahead of normal according to Canadian Ice Services (CIS, 2016). Weekly ice coverage by stage of development for the season 2016 is provided in Figure 2. Open water was already present in the region by May and throughout the summer ice coverage remained near record lows in the Beaufort Sea. Sea ice concentration over each mooring location as obtained from SSM/I satellite imagery (12.5 x 12.5 km pixel resolution) is provided in Figure 3. The data show that sea ice growth in the fall was close to normal. However, the wind-driven exit of sea ice from the southern Canadian Beaufort started in late April and continued progressively through the rest of spring. This was the case for each site except BR-03 where sea ice persisted near the average in June-July. Regional seasonal ice coverage minimum in September 2016 was near 4.9%, the second lowest coverage on record just behind 2012 (2.2%).

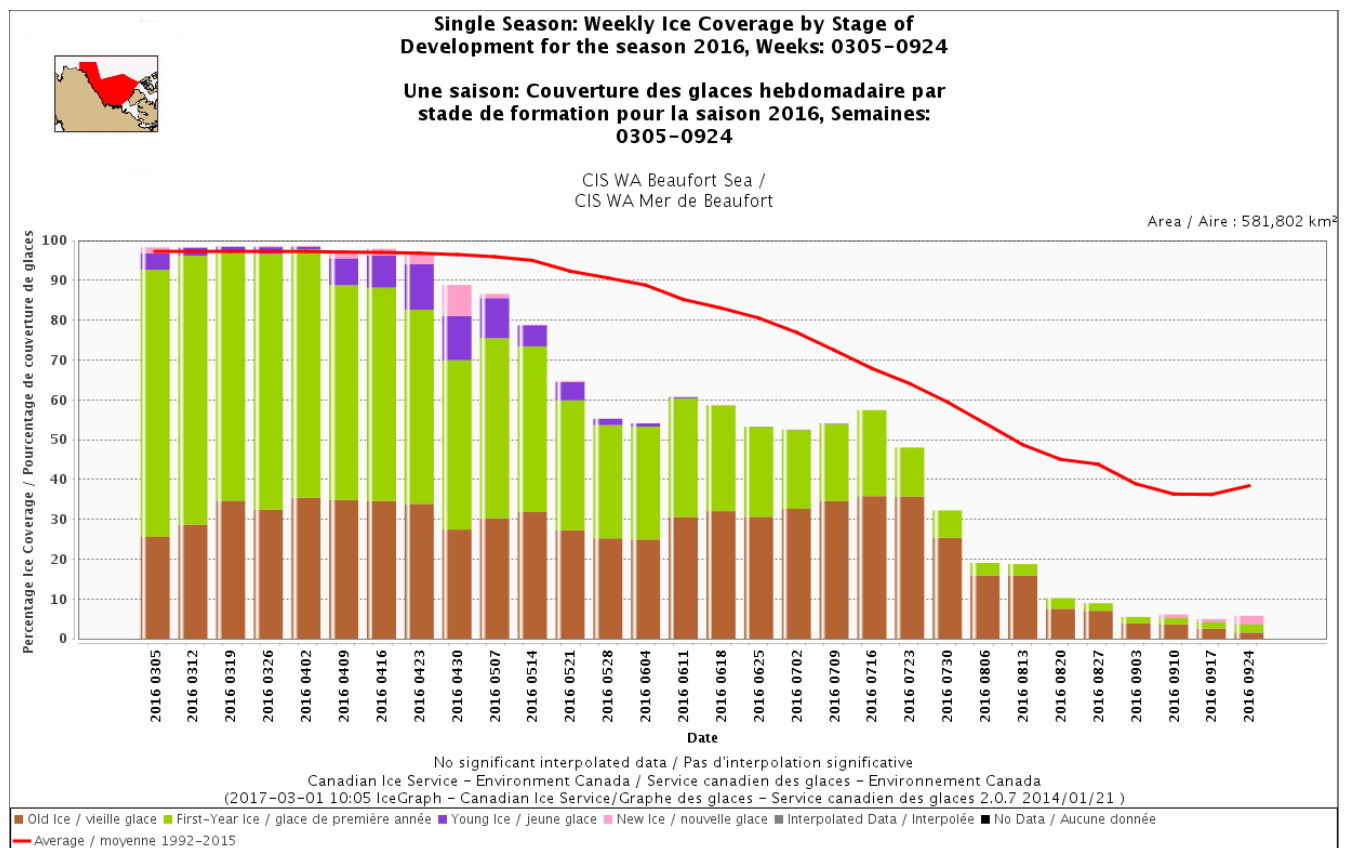


Figure 2: Weekly ice coverage by stage of development for the season 2016 (March – September 2016) as based on daily ice charts from Canadian Ice services. Brown: old ice. Green: first-year ice. Pink/purple: New/Young ice. Red line: average sea ice concentration 1992-2015. Data source: Ice graph 2.5, <http://iceweb1.cis.ec.gc.ca/IceGraph/>.

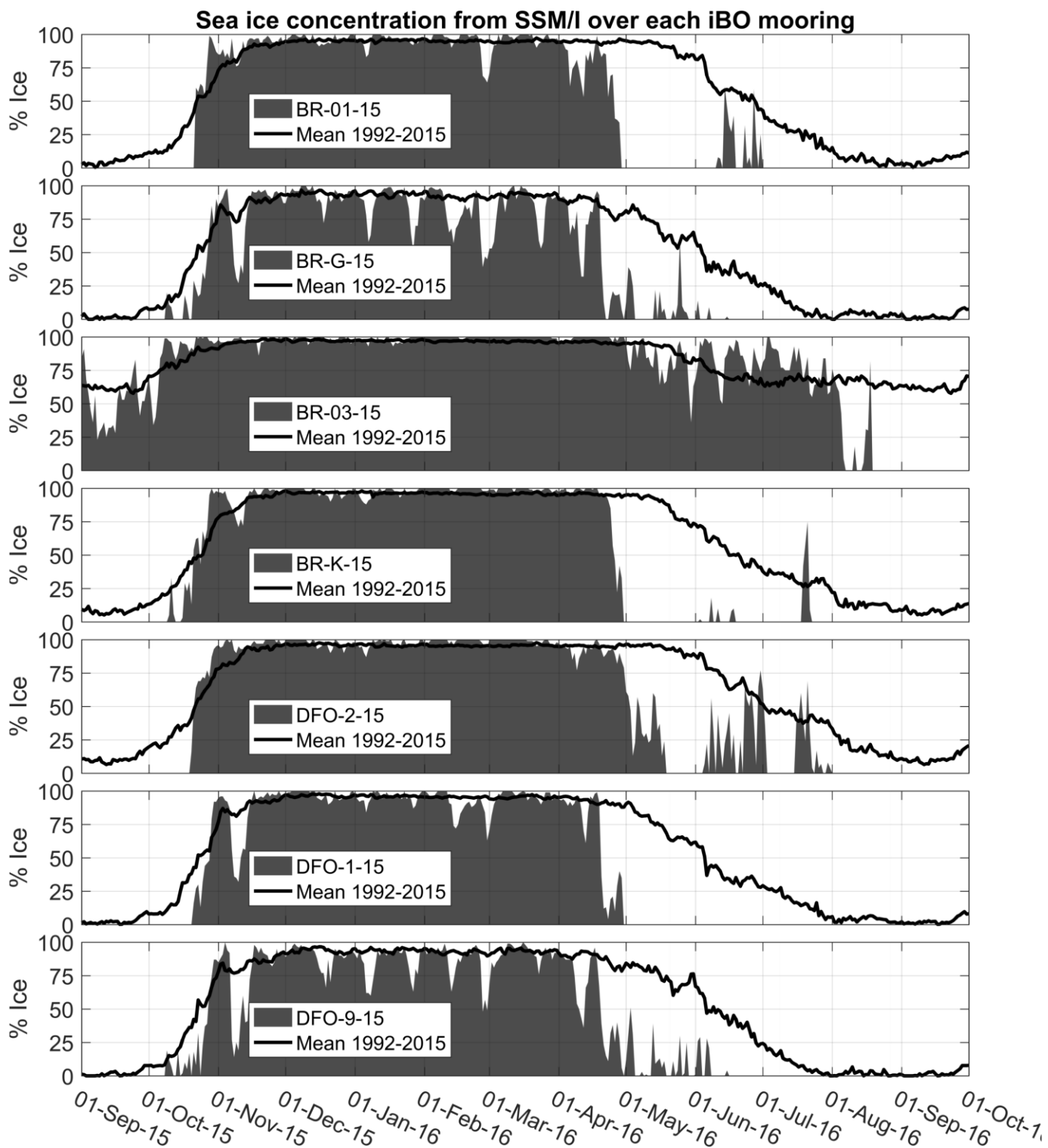


Figure 3: Sea ice concentration (% coverage) for a 12.5 X 12.5 km pixel area over each iBO mooring during 2015-2016 as derived from SSM/I satellite imagery. The black line shows the mean ice concentration over 1992-2015 within each pixel.

3.2 Ocean Currents

Processed data for all current profilers and current meters from the 7 iBO moorings for 2015 to 2016 are presented in this section of the report. For each instrument, a time-series plot of current speed, current direction and along-isobath current speed is presented. The along-isobath component of current typically dominates current variability over the continental slope (Williams et al. 2008; Forest et al. 2015; Dmitrenko et al. 2016). The along-isobath direction was estimated as the heading of the bathymetric contour at each mooring location (Table 5) with respect to true North; this is consistent with previous mooring studies that described the along-isobath flow. Annual statistics of current speed and direction for selected bin depths (nearest available bins to those listed in Table 6) are also provided to characterize the net behaviour of ocean currents with depth.

Seasonal current roses based on the sub-tidal component of current velocity were constructed for the same selected bin depths (Table 6) to contrast the temporal variability of ocean circulation patterns in relation to the distinct water masses and water mass boundaries. The sub-tidal component was obtained by applying a low-pass filter with a half-amplitude period of 33 hours to each selected time-series linearly interpolated over 1-hour intervals (PL66TN, Beardsley and Rosenfeld 1983). In addition, a complete tabular summary of current speed descriptive statistics, vector-averaged direction and number of valid records is provided for every bin depth of each instrument in Appendix D. Meta-data for each instrument (i.e. serial number, mean instrument depth, date and time of first and last good record, and percentage of raw data return) is provided in Table 7.

Table 5: Angles chosen to describe the along-slope/shelf current component for each iBO mooring.

Mooring	Angle, degrees True North (TN)
BR-1	78
BR-3	0
BR-G, BR-K, DFO-2	52
DFO-9 ¹	90
DFO-1 ¹	10

¹Note: DFO-1 and DFO-9 sit in the Kugmallit sea valley where the isobaths are sharply bent. The angles at these two sites were adjusted for the expected flow conditions across the valley.

Table 6: Selected bin depths to characterize circulation patterns throughout the water column.

Approximate Bin Depth (m)	Rationale (based on Lansard et al. 2012)
20	Near-surface circulation within the Polar-Mixed Layer (salinity \approx 31-32)
130	Core of the Pacific Halocline water mass (salinity \approx 33)
220	Boundary between the Pacific Halocline and Atlantic water
350	Mid-depth of the water column over the slope, core of the Atlantic Water mass (salinity \approx 34.8)
550	Deep circulation over the slope, lower portion of the Atlantic water mass
700	Near-bottom circulation at the boundary between the Fram Strait and Barents Sea branches of Atlantic water (salinity \approx 34.9)

Table 7: Summary of current profilers and current meters clock drift, first and last good record, and percentage of raw data return on iBO moorings from 2015 to 2016.

Mooring	Instrument	Serial number	Depth (m)	Clock Drift (mm:ss)	First Good Record (UTC)	Last Good Record (UTC)	Raw Data Return ¹
BR-1-15	TRDI QM ADCP 150 kHz	12698	180.0	03:50 slow	Sep-30-2015 22:45:00	Sep-01-2016 15:30:00	100%
BR-1-15	TRDI LR ADCP 75 kHz	12884	460.0	02:49 slow	Sep-30-2015 23:00:00	Sep-01-2016 15:30:00	100%
BR-1-15	Nortek Aquadopp DW	2792	595.5	00:31 slow	Sep-30-2015 23:00:00	Sep-01-2016 15:30:00	100%
BR-1-15	Nortek Aquadopp DW	2701	757.3	00:17 slow	Sep-30-2015 23:00:00	Aug-25-2016 6:56:32	98%
BR-3-15	TRDI QM ADCP 150 kHz	12824	171.7	N/A	N/A	N/A	0%
BR-3-15	TRDI LR ADCP 75 kHz	12942	446.7	01:43 slow	Aug-31-2015 23:00:00	Sep-07-2016 22:00:00	100%
BR-3-15	Nortek Aquadopp DW	6109	574.7	N/A	Aug-31-2015 23:00:00	Jan-31-2016 1:00:00	41%
BR-3-15	Nortek Aquadopp DW	8541	685.2	19:04 slow	Aug-31-2015 23:00:00	Sep-07-2016 22:00:00	100%
BR-G-15	TRDI QM ADCP 150 kHz	12841	160.7	04:02 slow	Aug-28-2015 19:00:00	Sep-01-2016 0:15:00	100%
BR-G-15	TRDI LR ADCP 75 kHz	12892	452.7	03:30 fast	Aug-28-2015 19:00:00	Aug-31-2016 23:30:00	100%
BR-G-15	Nortek Aquadopp DW	9846	580.9	00:58 fast	Aug-28-2015 19:00:00	Sep-01-2016 0:00:00	100%
BR-G-15	Nortek Aquadopp DW	8434	690.8	01:02 slow	Aug-28-2015 19:00:00	Sep-01-2016 0:00:00	100%
BR-K-15	TRDI WHS ADCP 300 kHz	102	145.0	02:15 slow	Aug-27-2015 14:30:00	Sep-01-2016 2:38:36	100%
BR-K-15	Nortek Aquadopp Profiler ²	9711	152.2	00:45 fast	Aug-27-2015 15:00:00	Sep-01-2016 2:00:00	100%
DFO-2-15	TRDI NB ADCP 300 kHz	506	107.0	09:33 slow	Sep-27-2015 23:30:00	Sep-30-2016 14:30:00	100%
DFO-1-15	TRDI NB ADCP 300 kHz	464	51.0	07:16 slow	Sep-27-2015 16:00:00	Sep-25-2016 19:30:00	100%
DFO-9-15	TRDI WHS ADCP 300 kHz	12414	32.0	08:43 slow	Sep-27-2015 22:00:00	Sep-25-2016 16:00:00	100%

N/A = not available due to instrument failure

¹Note: The raw data return is based on the number of records (including bad data) during the period from the mooring deployment to the mooring recovery.

²Note: All data from the Nortek Aquadopp Profiler at BR-K was flagged as questionable due to an error in the deployment. The data are not presented in this report as a result.

3.2.1 Mooring BR-1

Time-series plots of current speed, direction, and along-slope current component from the QM ADCP, LR ADCP and the two Aquadopp DW deployed at BR-1 from 2015 to 2016 are provided in Figure 4 through Figure 7. The data in the QM and LR ADCP plots are filtered for bins with PG4+PG1 values less than 25%, bins affected by sidelobe interference and for error velocity thresholds as described in section 2.4.1. The first valid bin depth for QM ADCP #12698 at BR-1-15 after removing sidelobe interference was 14.8 m (bin cell 40), although this bin depth contains only 84% valid data (Appendix D). Bin depths 67.8 and 71.8 m (bin cells 26 and 27) of the QM ADCP were affected by the presence of the IPS float and cage, which resulted in reflection observed in the echo intensity (not shown) and a general decrease in current speed at these depths. A reflection was also observed at bin depth 131.8 (bin cell 11) due to the CT sensor and frame located at this depth. Accordingly, bin cells 11, 26, and 27 of QM ADCP #12698 were manually flagged as part of the QA/QC and data from these bin depths should be treated carefully before being used in further analyses.

The LR ADCP #12884 measured currents at BR-1-15 did not appear to have been impacted by interference with other parts of the mooring (Figure 5). The first valid bin depth for this instrument was 52.6 m (bin cell 25) with 67.8% valid data (Appendix D). The percentage of valid data was less than 90% in the upper water column at bin depths 180.6 and shallower (bin cells 17 to 25) due to a partial loss of data in the fall 2015 and during spring-summer 2016 (Figure 5). This data loss was observed during periods when the level of ambient noise (by wind, waves and sea ice) was greater than the echo from scatterers (plankton) in the water column. The incapacity of the LR ADCP #12884 to cope with high level of ambient noise was likely linked to the selection of the Low Power mode in the setup of this instrument as an attempt to increase battery life in 2015. This issue is not expected to occur again since all LR ADCPs could be programmed with the High Power mode in 2016 due to an upgrade from standard alkaline to high-capacity Lithium battery packs. The deep Aquadopp current meters #2792 (595.5 m) and #2701 (757.3 m) provided complete time-series with a percentage of valid data return of 100% for each instrument (Figure 6, Figure 7 and Appendix D).

Mean current speeds at BR-1-15 ranged from 9 to 15 cm/s in the upper 200 m of the water column; and from 3 to 8 cm/s below 200 m (Table 8, Appendix D). Vector-averaged directions were typically to the west-southwest (210-270°TN) for all bin depths down to 245 m. Below 245 m the direction transitions from southerly to east-southeast (115-210°TN). Aquadopps at 596 m and 757 m measured an average direction to the east of 75°TN and 107°TN, respectively. The maximum current speed measured for un-flagged bins was 62 cm/s on August 12, 2016 at 144 m depth. Strong current speeds within the upper 200 m (>50 cm/s, with stronger values centered around 150 m) were detected during a westward current event from August 11-13, 2016. Intermittent intervals of stronger currents to the west-northwest were generally measured from May through August 2016 when the region was ice free. The resulting strong negative along-slope currents were presumably driven by strong easterly winds, although their depth-intensified patterns (e.g. Figure 4) suggest that the wind forcing was not local. Moderate to strong eastward-directed currents (up to ~30 cm/s, confined to the upper 200 m) were primarily detected in December 2015 and January and May 2016.

Seasonal current roses (low-pass filtered) for selected bin depths at mooring BR-1-15 are provided in Figure 8 through Figure 13. The strong westward current events (>50 cm/s) detected in the upper water column from May through August (spring and summer) are particularly visible in the summer current roses for the Pacific Halocline (132 m, Figure 9). Lower in the water column, at the depths of Atlantic water mass, low-pass filtered currents were generally weak (<10 cm/s) and variable around the compass (Figure 11 and Figure 12). Near the bottom at 757 m, most frequent currents were directed to the south (across the slope toward the shelf; Figure 13), a pattern that contrasts with what has been recorded at all the other depths at BR-1.

BR-1; QM Broadband 153.6 kHz; 70.43239 N, 139.02058 W; 2015-2016; Instr. #12698

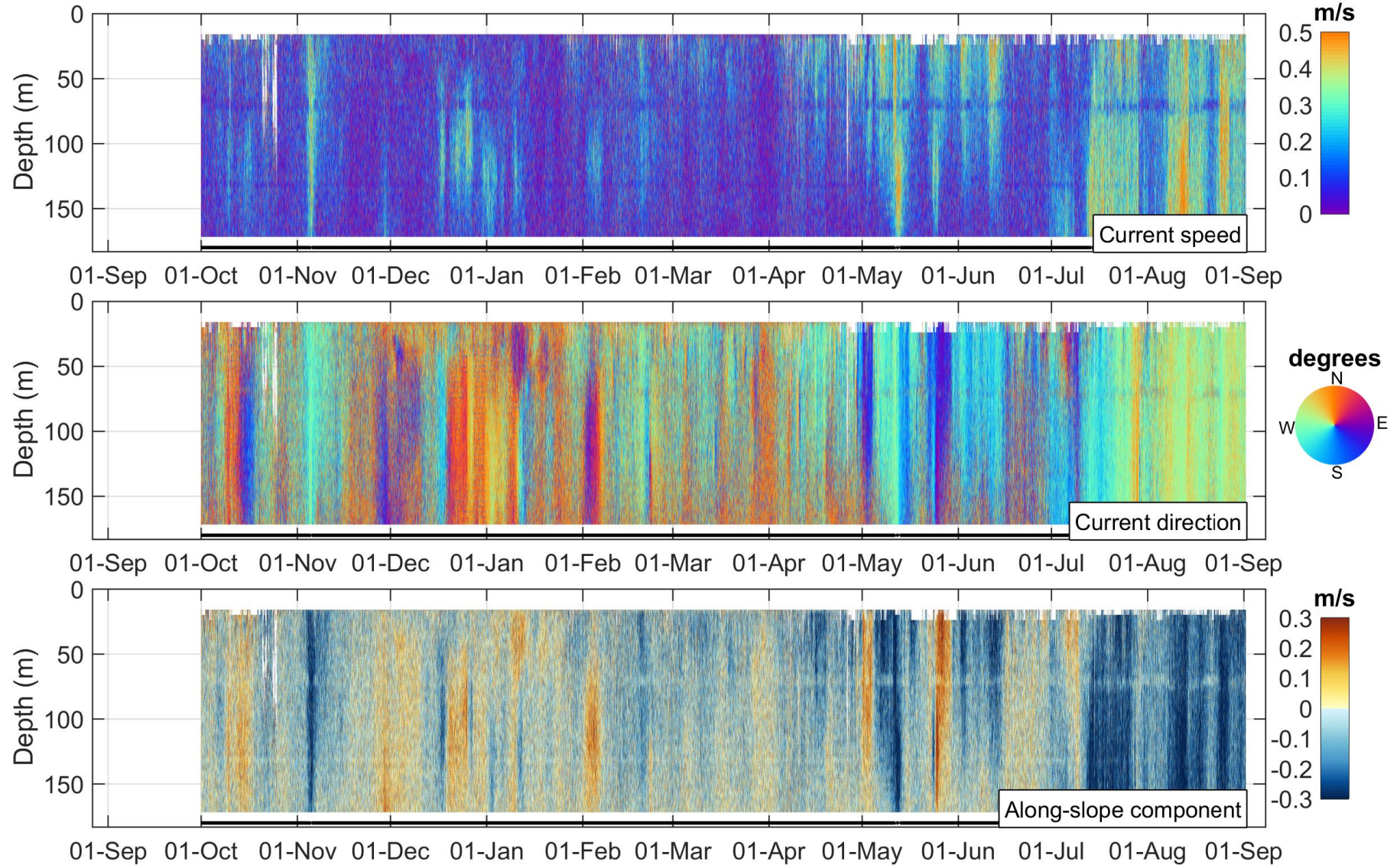


Figure 4: Time-series of current speed, current direction and along-slope current component at mooring BR-1-15 measured by the QM ADCP #12698. The black line depicts the instrument depth.

BR-1; LR Broadband 76.8 kHz; 70.43239 N, 139.02058 W; 2015-2016; Instr. #12884

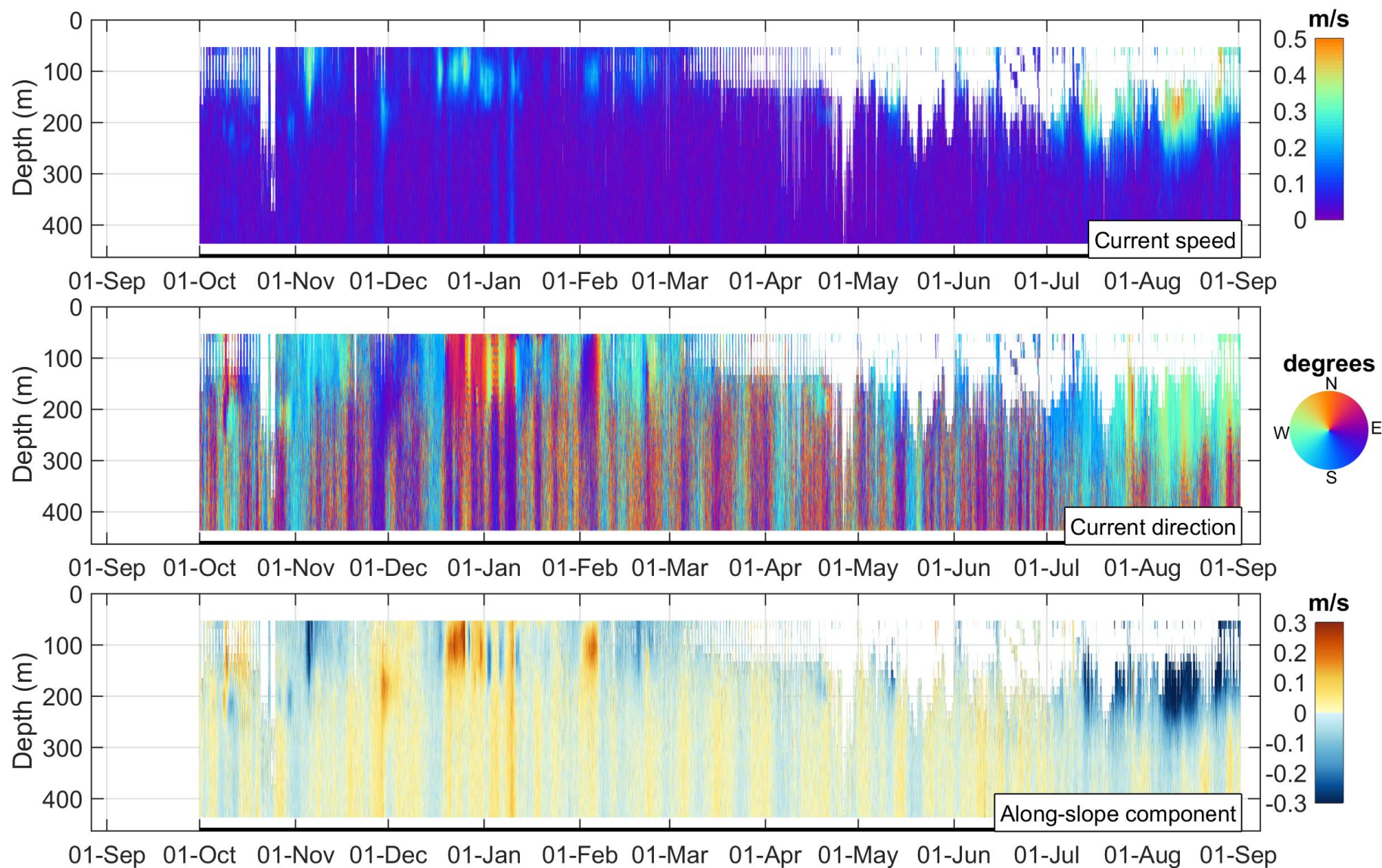


Figure 5: Time-series of current speed, current direction and along-slope current component at mooring BR-1-15 measured by the LR ADCP #12884. The black line depicts the instrument depth.

BR-1; Aquadopp DeepWater 2-MHz; 70.43239 N, 139.02058 W; 2015-2016; Instr. #2792

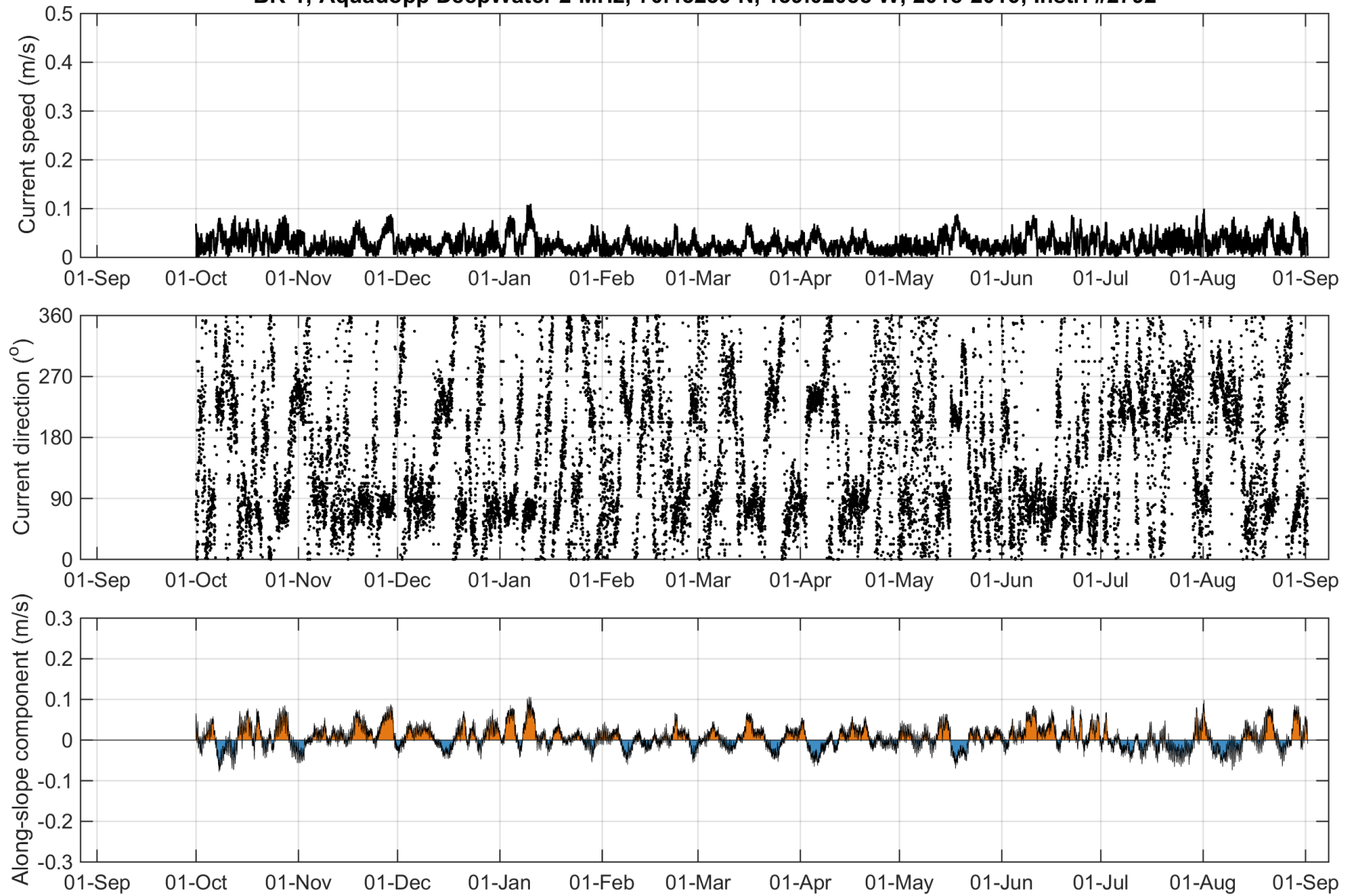


Figure 6: Time-series of current speed, current direction and along-slope current component at 596 m at mooring BR-1-15 measured by the Aquadopp #2792.

BR-1; Aquadopp DeepWater 2-MHz; 70.43239 N, 139.02058 W; 2015-2016; Instr. #2701

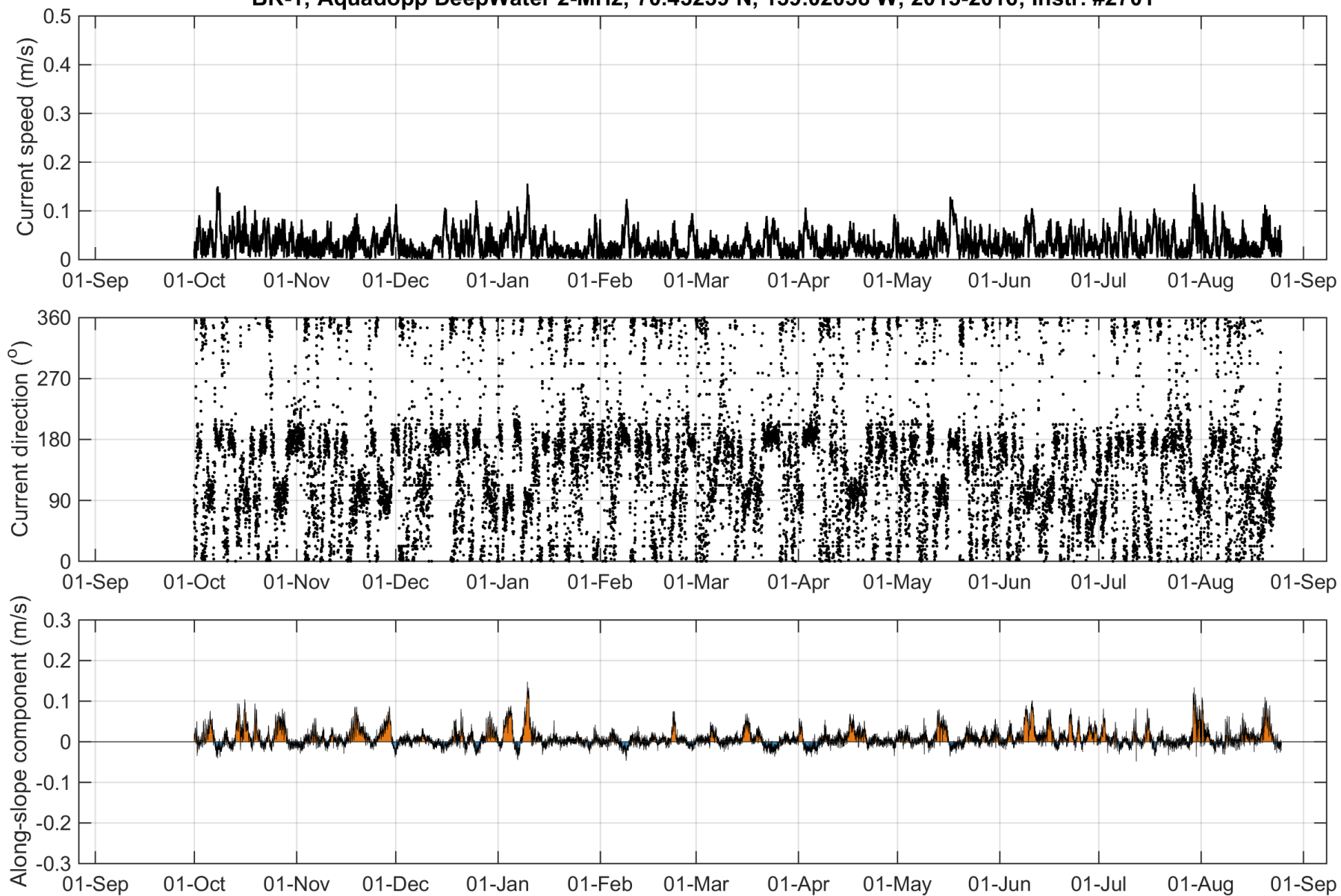


Figure 7: Time-series of current speed, current direction and along-slope current component at 757 m at mooring BR-1-15 measured by the Aquadopp #2701.

Table 8: Annual statistics of current speed and direction at BR-1-15 from selected bin depths representative of water mass variability in the Beaufort Sea (see Table 6 for water mass description).

Bin Depth (m)	Median Speed (m/s)	Mean Speed (m/s)	75%ile Speed (m/s)	95%ile Speed (m/s)	99%ile Speed (m/s)	Max Speed (m/s)	Standard Deviation Speed (m/s)	Vector-Averaged Direction (deg TN)
19.8	0.13	0.15	0.21	0.36	0.46	0.61	0.10	266.8
131.8	0.08	0.11	0.15	0.34	0.45	0.59	0.10	262.2
212.6	0.04	0.07	0.07	0.25	0.34	0.41	0.07	224.7
356.6	0.03	0.03	0.04	0.06	0.08	0.14	0.02	140.9
595.5	0.03	0.03	0.04	0.06	0.08	0.11	0.02	75.7
757.3	0.03	0.03	0.04	0.08	0.11	0.16	0.02	106.5

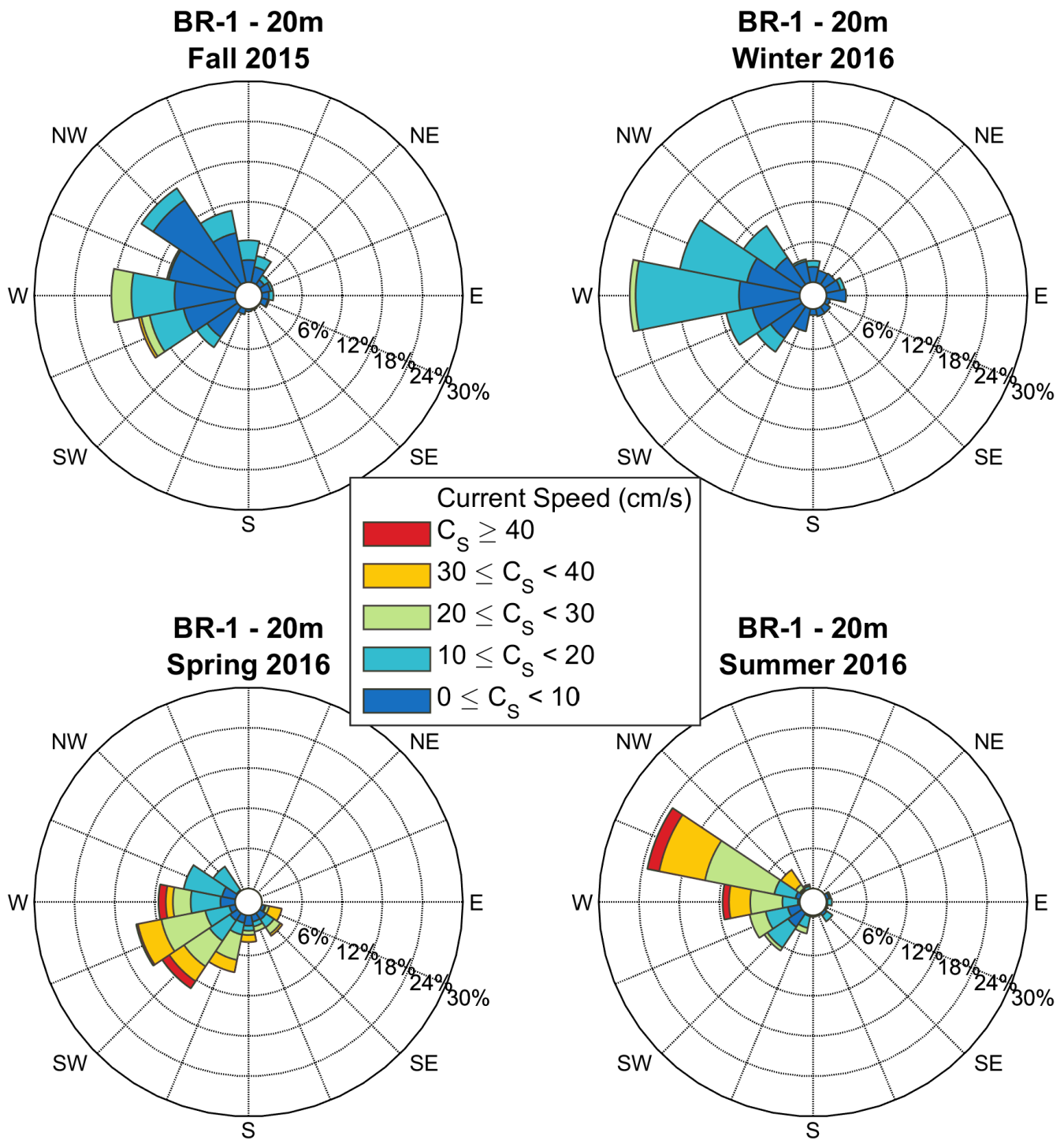


Figure 8: Seasonal current roses at 20 m depth (bin cell #11) at BR-1-15 measured by the QM ADCP #12698. Data are low-pass filtered. Roses indicate the direction toward which currents flow. Seasons are defined following the meteorological convention (Fall: October-December; Winter: January-March; Spring: April-June; Summer: July-September).

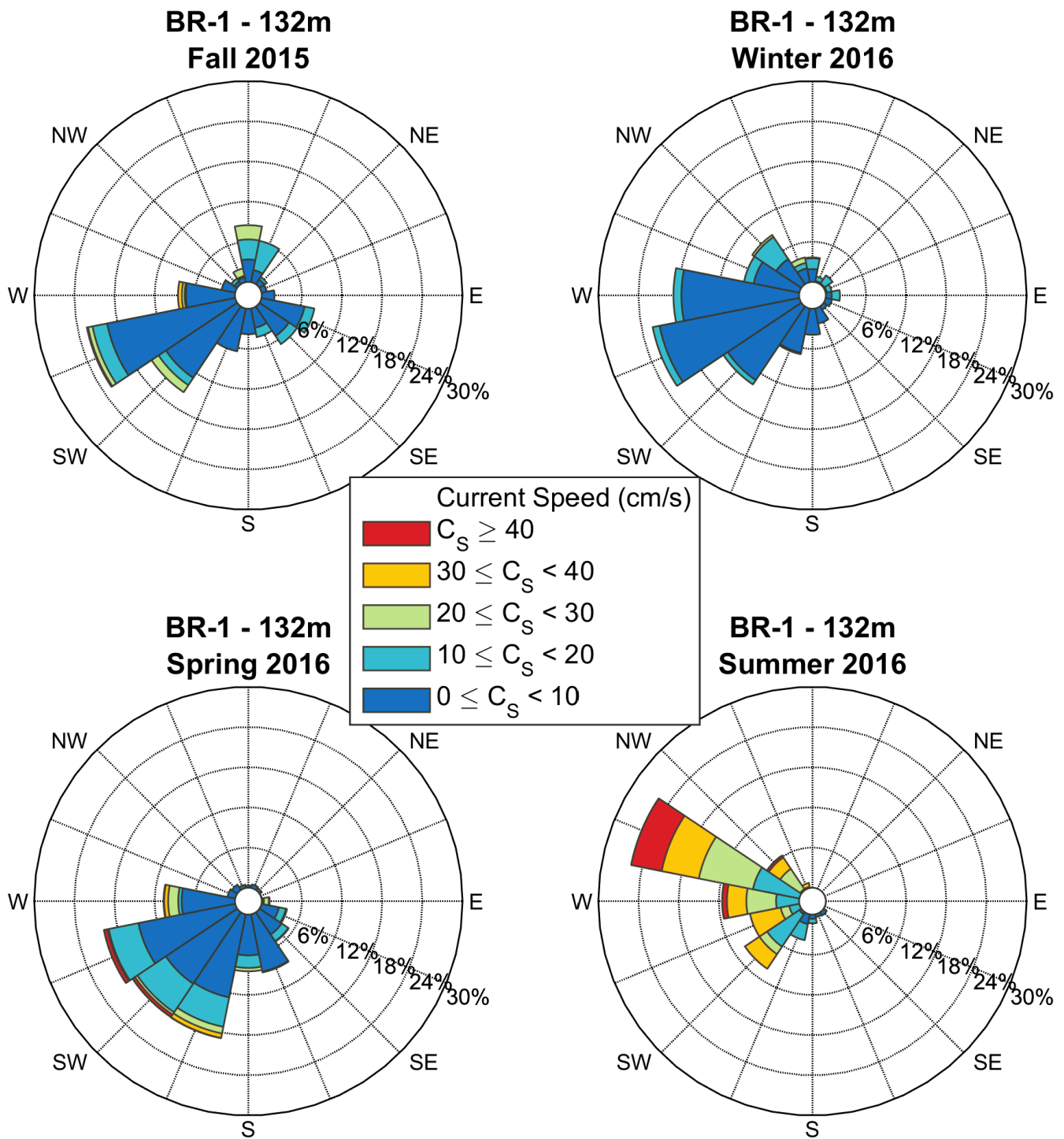


Figure 9: Seasonal current roses at 132 m depth (bin cell #39) at BR-1-15 measured by the QM ADCP #12698. Data are low-pass filtered. Roses indicate the direction toward which currents flow. Seasons are defined following the meteorological convention (Fall: October-December; Winter: January-March; Spring: April-June; Summer: July-September).

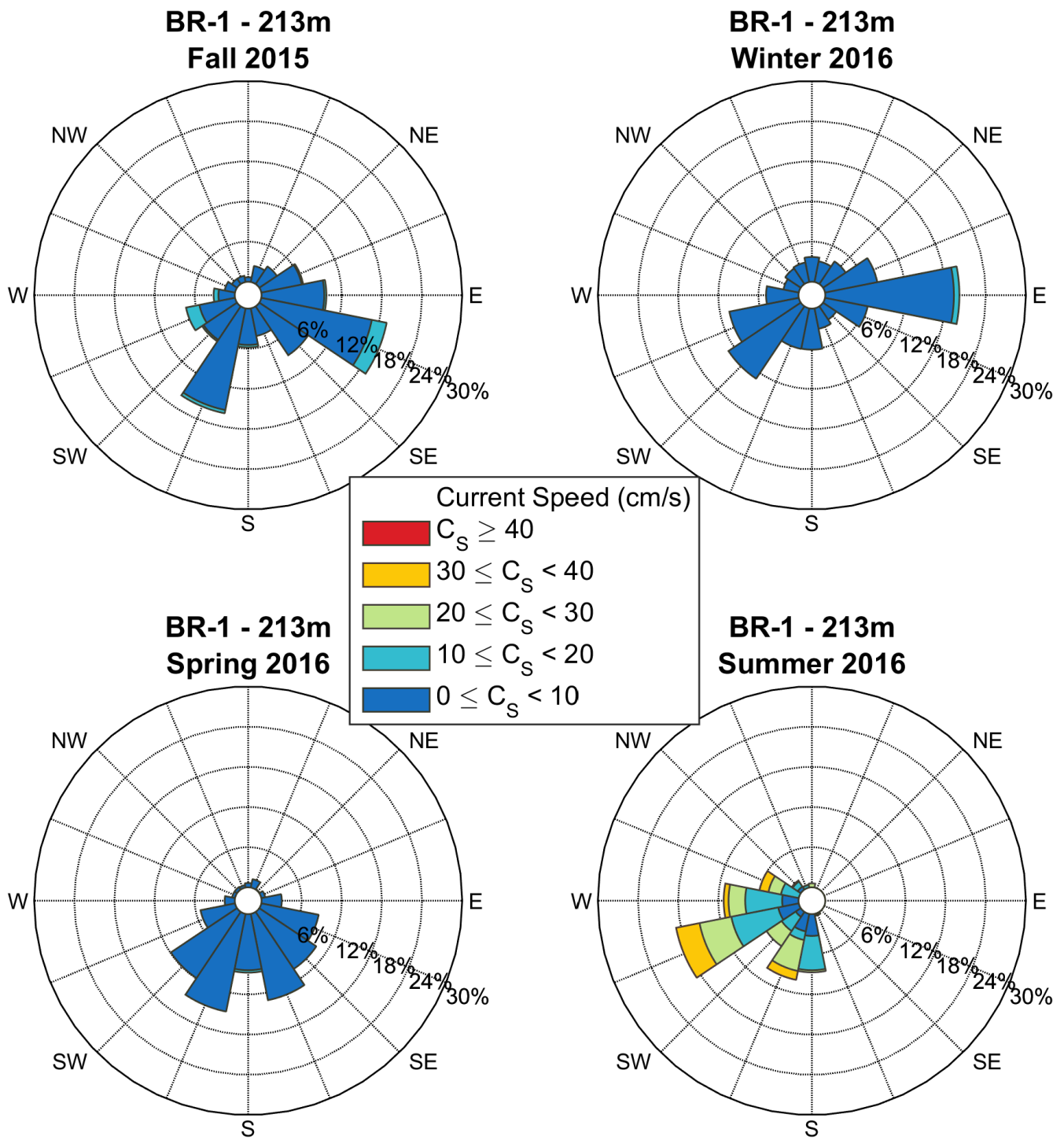


Figure 10: Seasonal current roses at 213 m depth (bin cell #15) at BR-1-15 measured by the LR ADCP #12884. Data are low-pass filtered. Roses indicate the direction toward which currents flow. Seasons are defined following the meteorological convention (Fall: October-December; Winter: January-March; Spring: April-June; Summer: July-September).

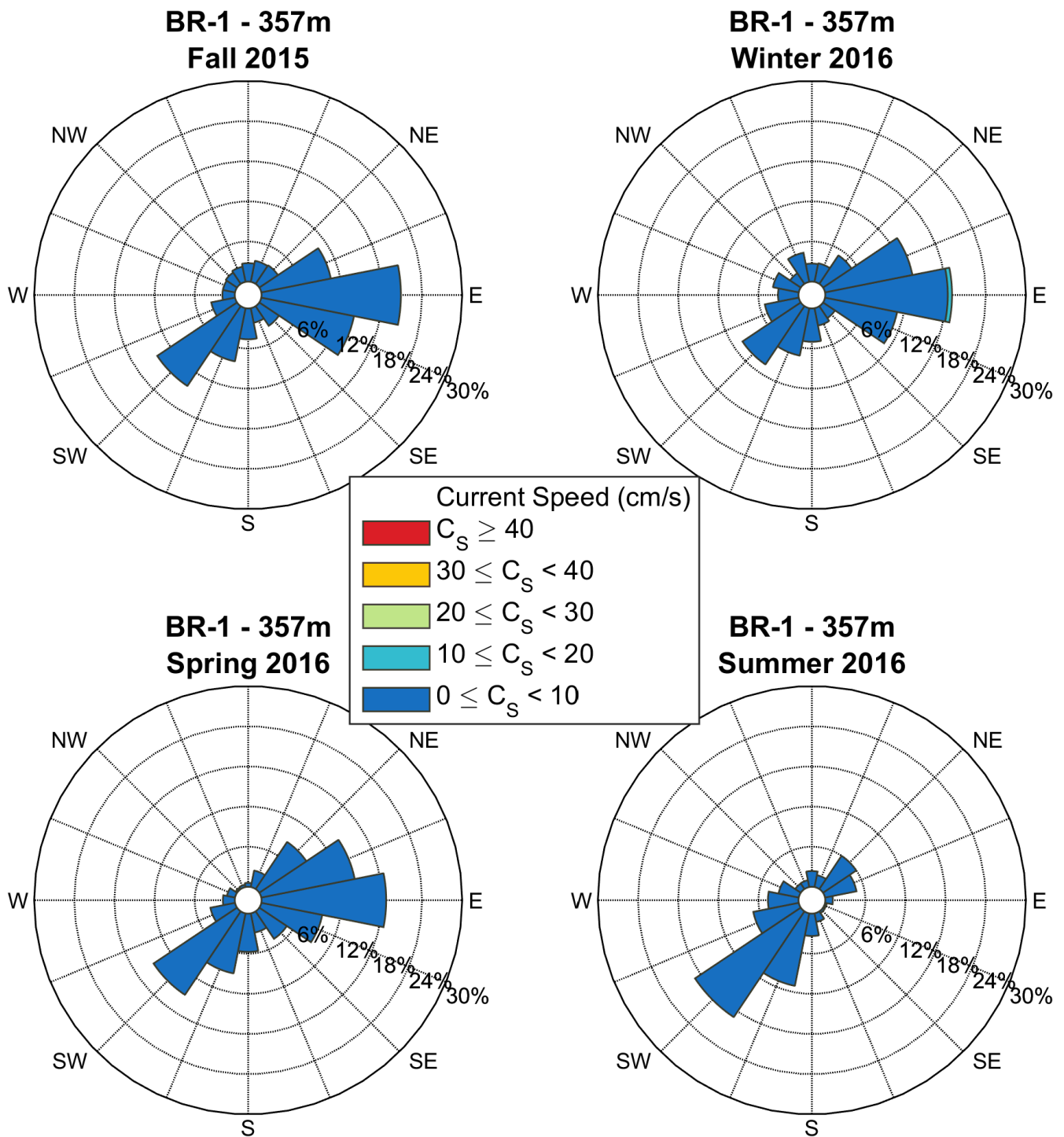


Figure 11: Seasonal current roses at 357 m depth (bin cell #6) at BR-1-15 measured by the LR ADCP #12884. Data are low-pass filtered. Roses indicate the direction toward which currents flow. Seasons are defined following the meteorological convention (Fall: October-December; Winter: January-March; Spring: April-June; Summer: July-September).

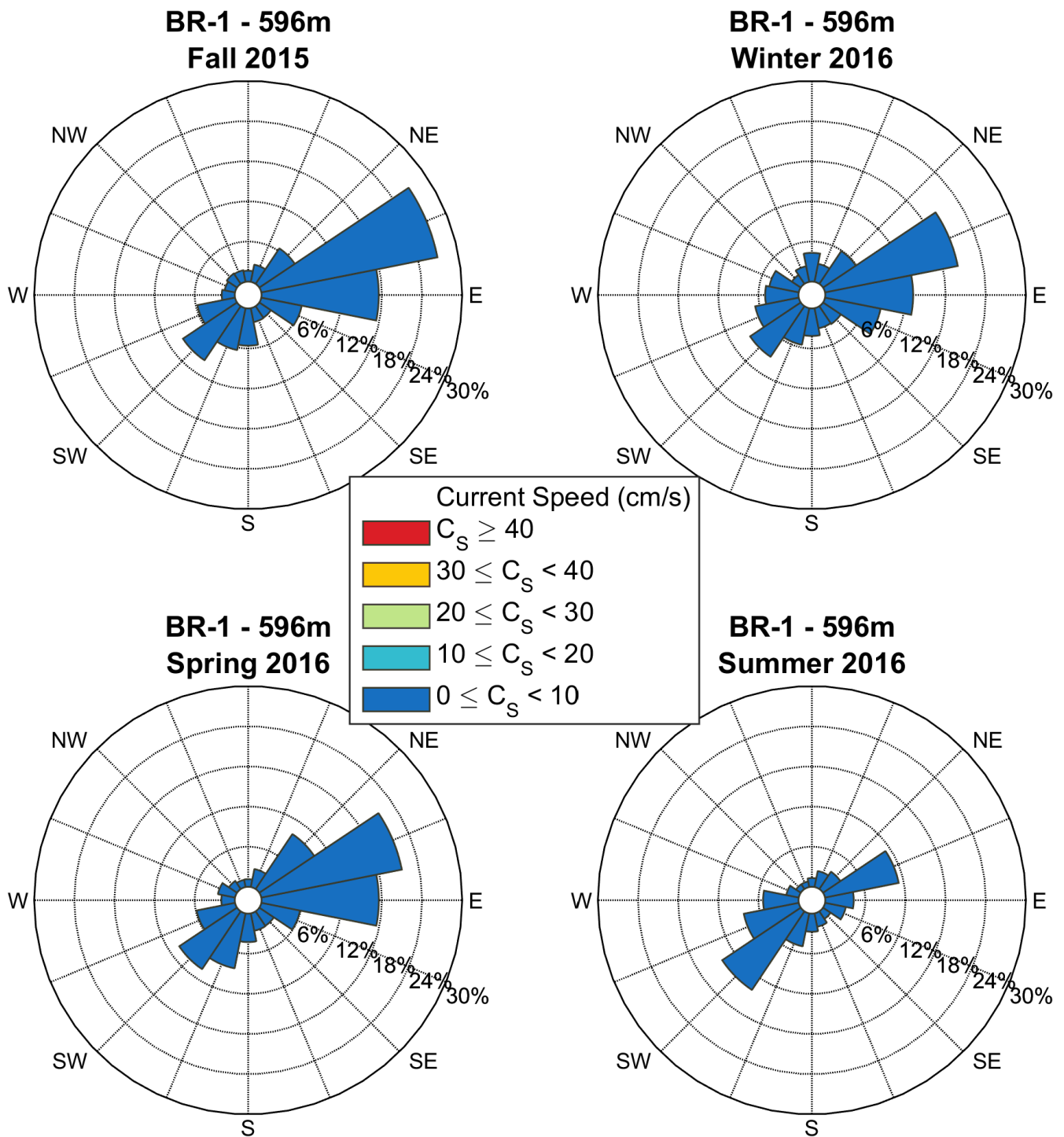


Figure 12: Seasonal current roses at 596 m depth at BR-1-15 measured by the Aquadopp #2792. Data are low-pass filtered. Roses indicate the direction toward which currents flow. Seasons are defined following the meteorological convention (Fall: October-December; Winter: January-March; Spring: April-June; Summer: July-September).

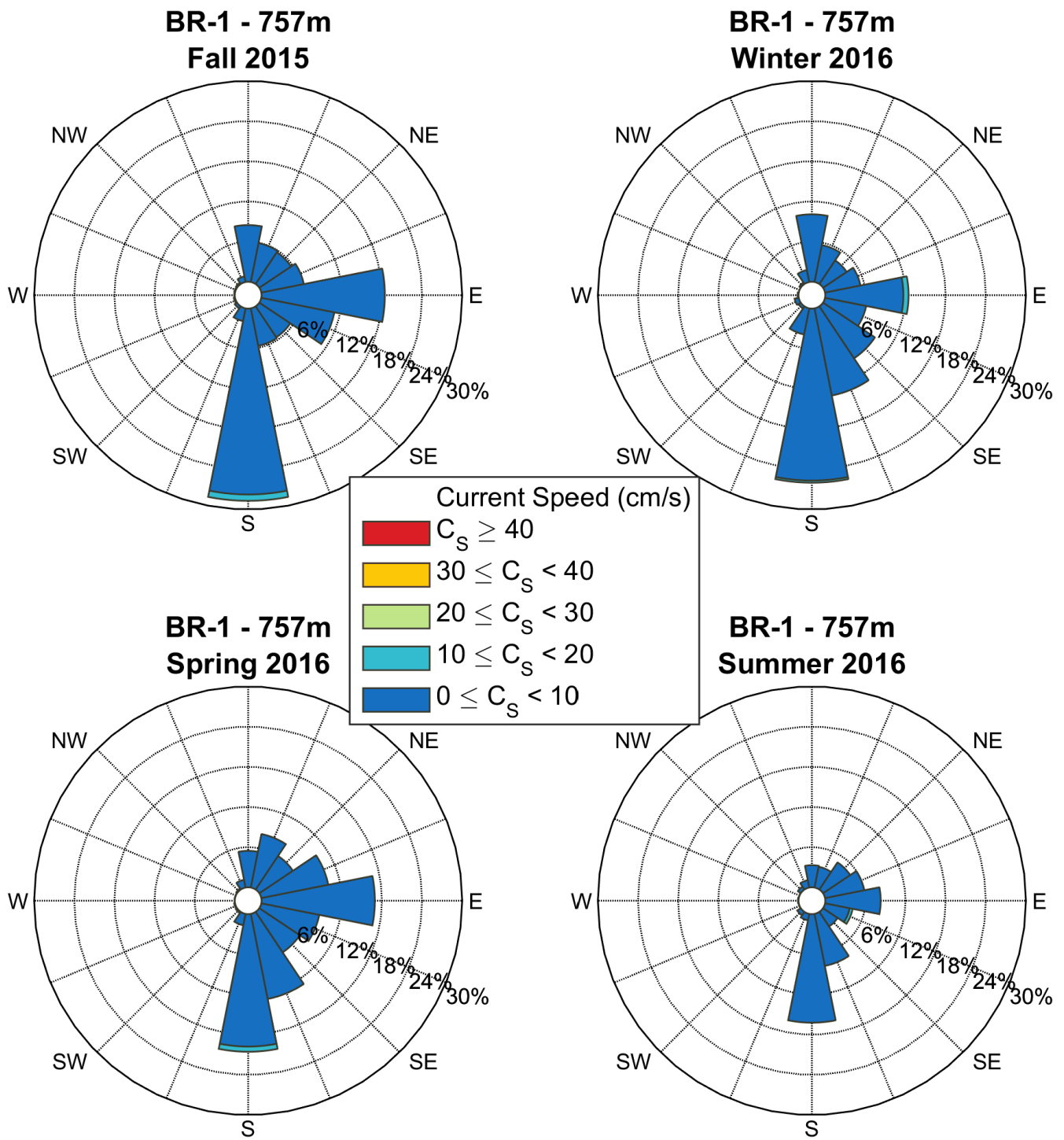


Figure 13: Seasonal current roses at 757 m depth at BR-1-15 measured by the Aquadopp #2701. Data are low-pass filtered. Roses indicate the direction toward which currents flow. Seasons are defined following the meteorological convention (Fall: October-December; Winter: January-March; Spring: April-June; Summer: July-September).

3.2.2 Mooring BR-3

Time-series plots of current speed, direction, and along-slope current component from the LR ADCP and the two Aquadopp DW deployed at BR-3 from 2015 to 2016 are provided in Figure 14 through Figure 16. No data were available from the QM ADCP #12824 at BR-3-15 due to water leakage in the external battery housing. The follow-up investigation revealed that the leakage likely occurred due to a failure of end cap o-ring.

The data in the LR ADCP plots are filtered for bins with PG4+PG1 values less than 25%, bins affected by sidelobe interference and for error velocity thresholds as described in section 2.4.1. The LR ADCP #12942 at BR-3-15 provided a complete annual dataset, although a suspicious bin cell at 310 m depth (bin cell 8) was manually flagged as part of the QA/QC process (Figure 14, Appendix D). This bin depth was likely affected by the presence of the lower Technicap sediment trap, which resulted in reflection observed in the echo intensity and a general decrease in current speed at this depth. However, it is not clear why the lower Technicap trap interfered with the signal of the LR ADCP #12942 at BR-3, and not at the other slope moorings BR-1 (Figure 5) and BR-G (Figure 24). The first valid bin depth for the LR ADCP #12942 at BR-3 was 54.4 m (bin cell 24) with 98.7% valid data (Appendix D). The percentage of valid records was above 97% at all bin depths for this instrument. Partial data loss possibly linked to high intensity of ambient sound generated by sea ice or wind/waves at the surface was observed only briefly in early October 2015 and mid-August 2016 at this location (Figure 14). The deep Aquadopp current meter #6109 at 574.7 m provided only a partial dataset due to water leakage as a result of a corroded connector. The instrument provided data until January 31, 2016; 100% of the available data was valid (Figure 15 and Appendix D). The deep Aquadopp current meter #8541 at 685.2 m provided a complete time-series with a 100% valid data (Figure 16 and Appendix D).

Mean current speeds at BR-3-15 ranged from 5 to 8 cm/s throughout the water column, taking into account that the near surface layer above 50 m remains unresolved (Table 9, Appendix D). The strongest mean currents were measured at the deepest bin depth by the deep Aquadopp. Vector-averaged directions were uniformly to the south (160-190°TN) from 54 to 150 m depth, but rapidly veered to the east and to north in the interval between 150 and 214 m. At the bin depth of 230 m and below, mean currents were consistently to the north (between 330 and 30°TN), including at both lowermost Aquadopps at 575 and 685 m depth. The maximum current speed measured for un-flagged bins at BR-3-15 was 34 cm/s on August 20, 2016 at 246 m depth (Appendix D). Another event of greater than 15 to 20 cm/s magnitude was measured throughout the water column below 100 m depth and above 420 m depth from January 9 to 14, 2016. Less than 1% of the entire LR ADCP current speed dataset at BR-3-15 was greater than 20 cm/s (Appendix D).

Seasonal current roses (low-pass filtered) for selected bin depths at mooring BR-3-15 are provided in Figure 17 through Figure 22. The current roses illustrate that the dominate flow direction in the upper water column (54 m to 134 m) is southward, particularly during the winter. In the lower portion of the water column (214 m to 685 m) northward currents are more frequent however there is some bi-directionality in the currents at 214 m water depth.

BR-3; LR Broadband 76.8 kHz; 73.40943 N, 129.35373 W; 2015-2016; Instr. #12942

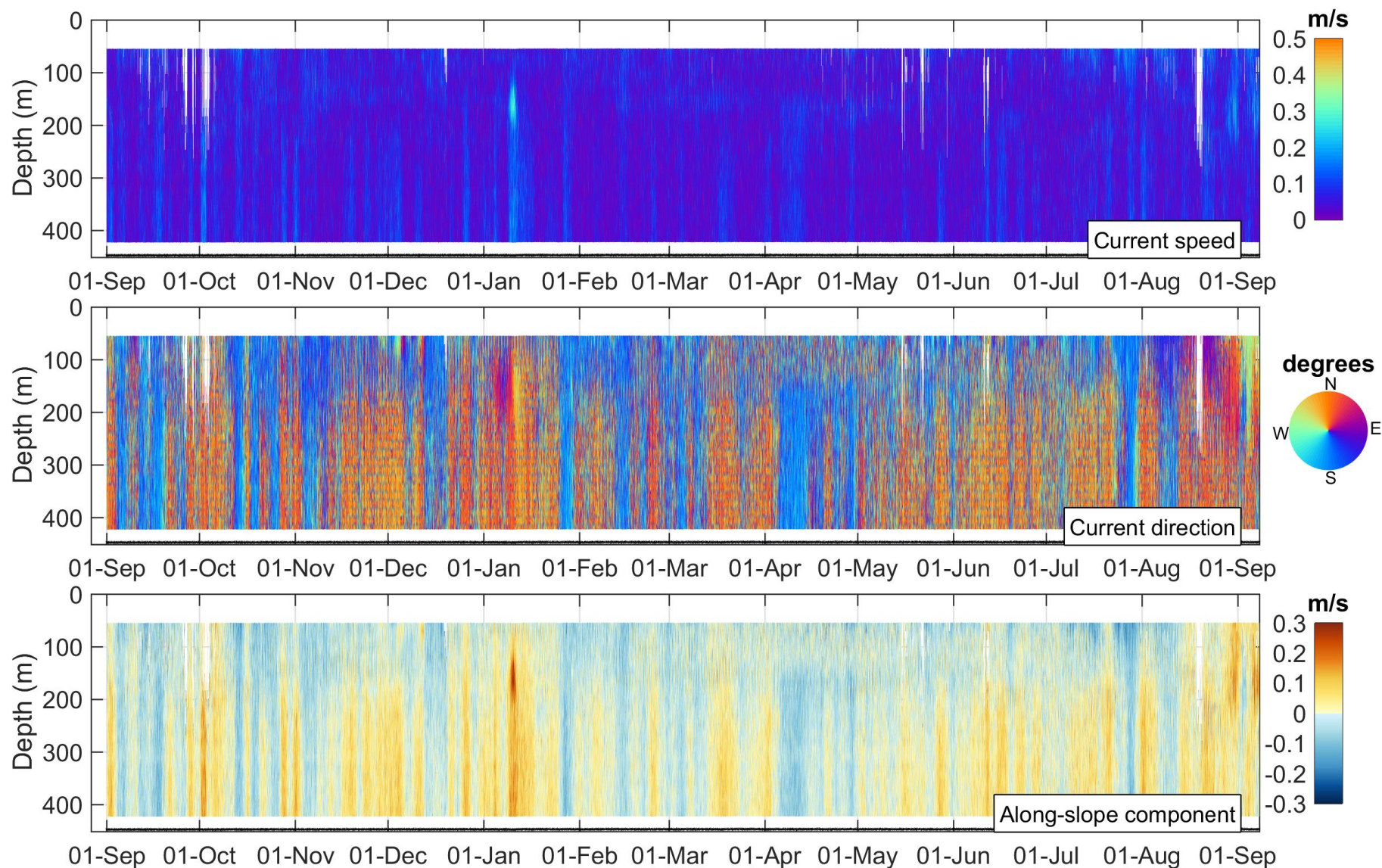


Figure 14: Time-series of current speed, current direction and along-slope current component at mooring BR-3-15 measured by the LR ADCP #12942. The black line depicts the instrument depth.

BR-3; Aquadopp DeepWater 2-MHz; 73.40943 N, 129.35373 W; 2015-2016; Instr. #6109

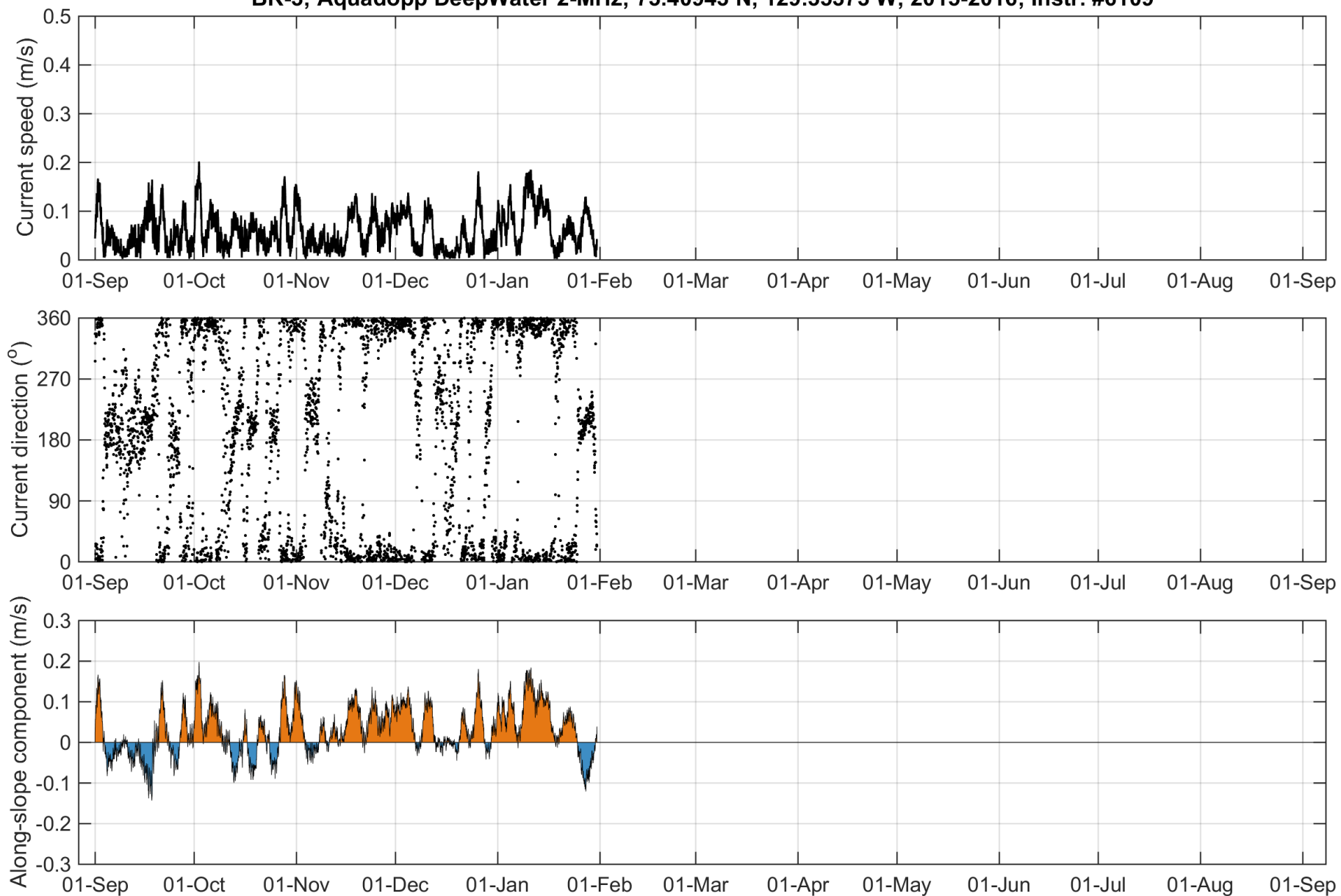


Figure 15: Time-series of current speed, current direction and along-slope current component at 575 m at mooring BR-3-15 as obtained with the Aquadopp #6109.

BR-3; Aquadopp DeepWater 2-MHz; 73.40943 N, 129.35373 W; 2015-2016; Instr. #8541

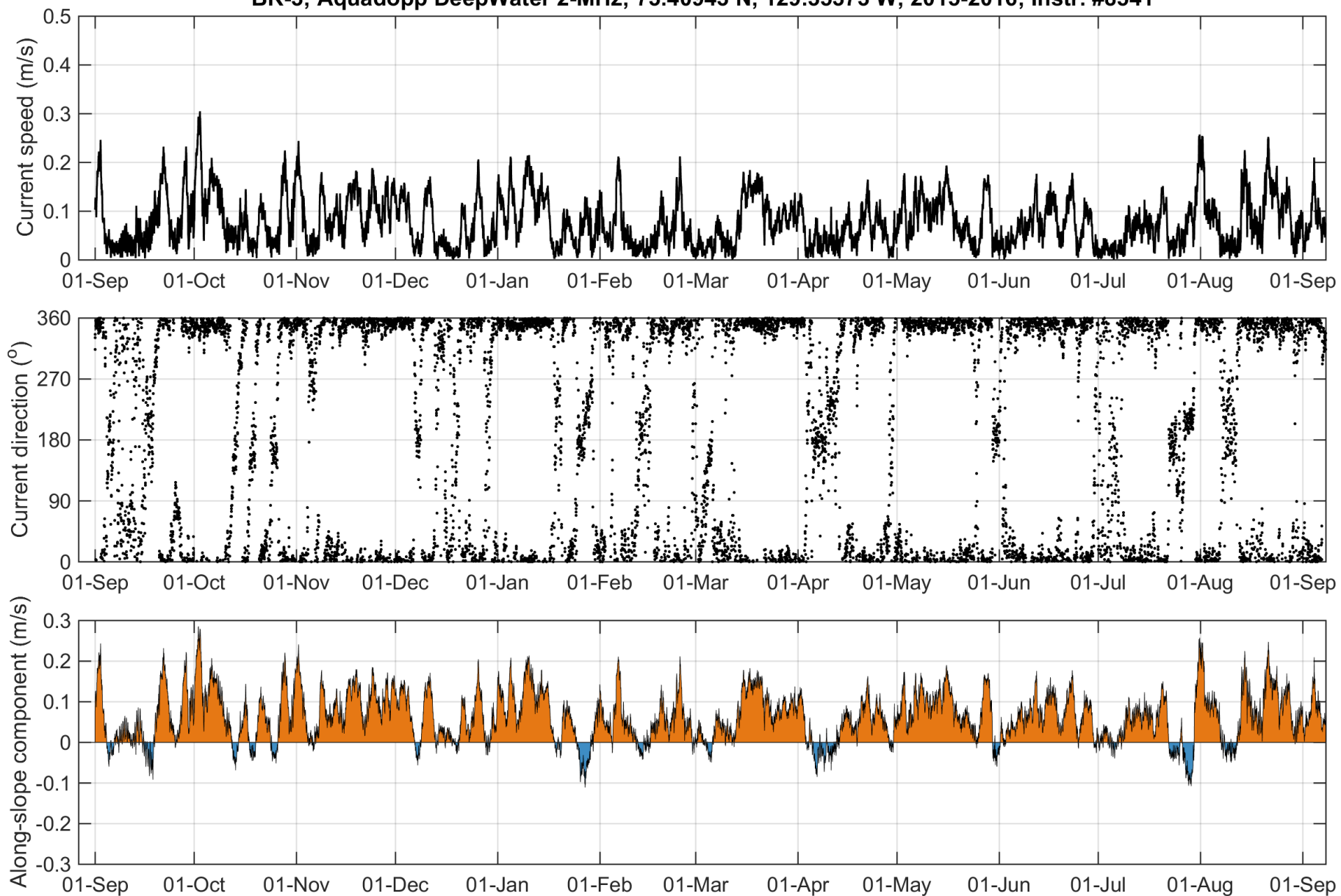


Figure 16: Time-series of current speed, current direction and along-slope current component at 685 m at mooring BR-3-15 as obtained with the Aquadopp #8541.

Table 9: Annual statistics of current speed and direction at BR-3-15 from selected bin depths representative of water mass variability in the Beaufort Sea (see Table 6 for water mass description).

Bin Depth (m)	Median Speed (m/s)	Mean Speed (m/s)	75%ile Speed (m/s)	95%ile Speed (m/s)	99%ile Speed (m/s)	Max Speed (m/s)	Standard Deviation Speed (m/s)	Vector-Averaged Direction (deg TN)
54.4	0.07	0.07	0.10	0.15	0.19	0.29	0.04	175.0
134.4	0.05	0.06	0.07	0.11	0.15	0.30	0.03	164.2
214.4	0.05	0.05	0.07	0.11	0.15	0.28	0.03	40.9
342.4	0.05	0.05	0.07	0.11	0.14	0.20	0.03	352.7
574.7	0.05	0.06	0.09	0.13	0.16	0.20	0.04	325.5
685.2	0.07	0.08	0.11	0.17	0.21	0.31	0.05	331.5

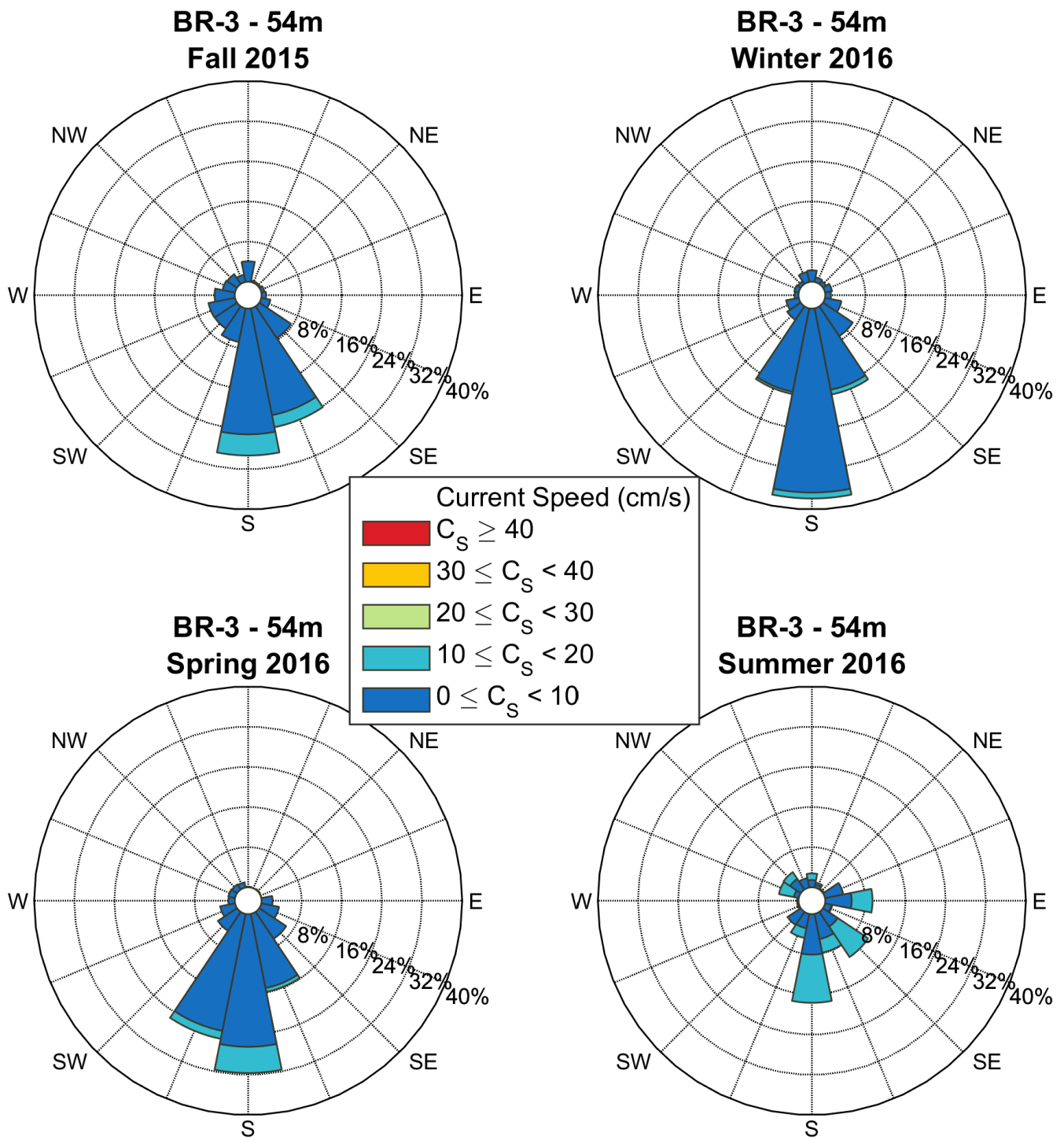
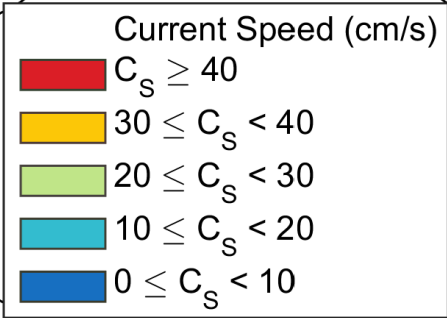
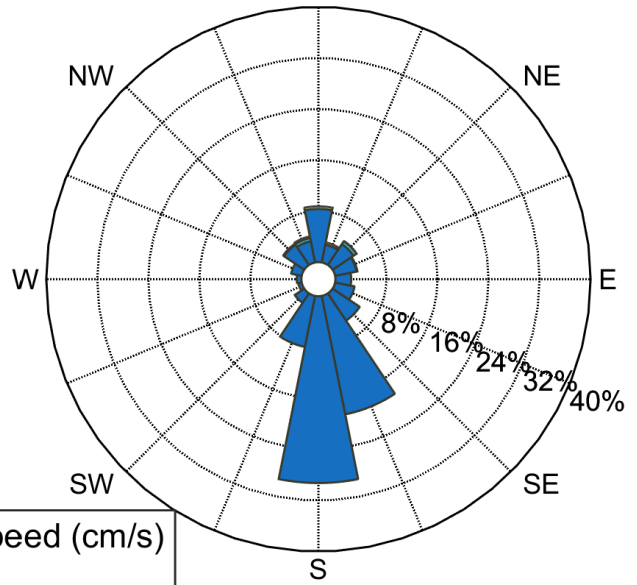
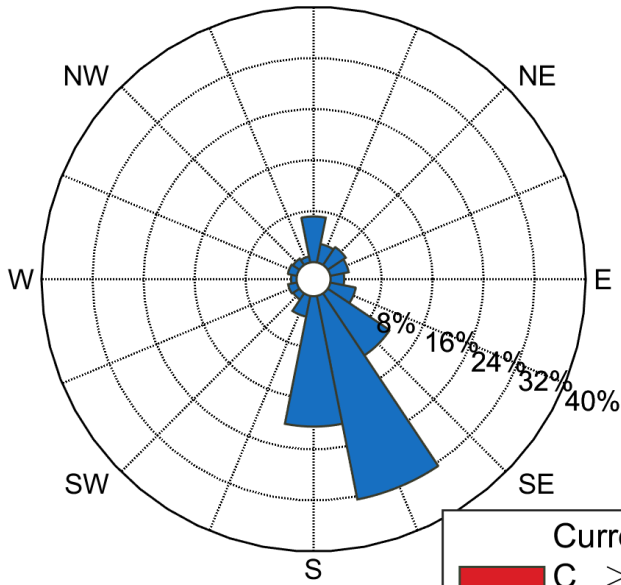


Figure 17: Seasonal current roses at 54 m depth (bin cell #24) at BR-3-15 measured by the LR ADCP #12942. Data are low-pass filtered. Roses point toward where the currents are going. Seasons are defined following the meteorological convention (Fall: October-December; Winter: January-March; Spring: April-June; Summer: July-September).

**BR-3 - 134m
Fall 2015**

**BR-3 - 134m
Winter 2016**



**BR-3 - 134m
Spring 2016**

**BR-3 - 134m
Summer 2016**

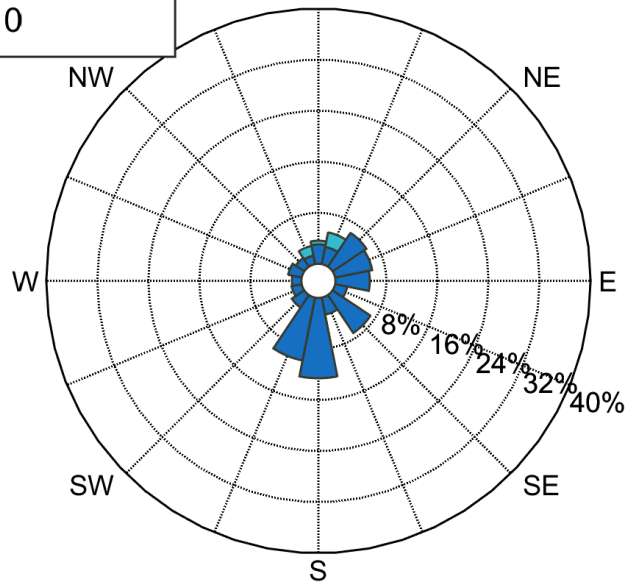
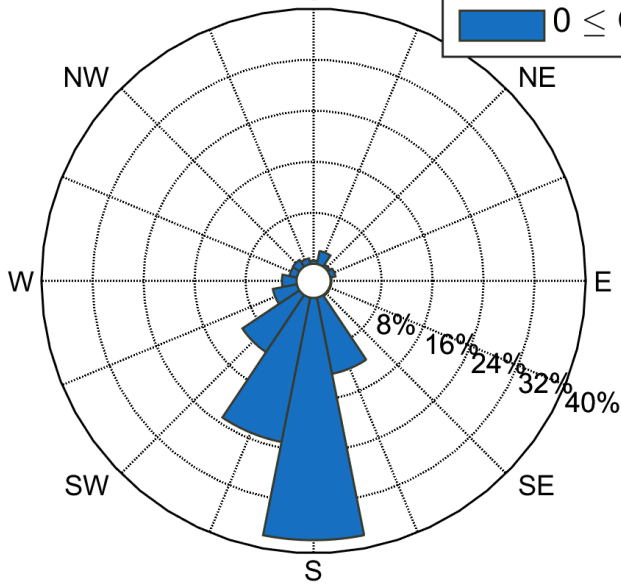


Figure 18: Seasonal current roses at 134 m depth (bin cell #19) at BR-3-15 measured by the LR ADCP #12942. Data are low-pass filtered. Roses indicate the direction toward which currents flow. Seasons are defined following the meteorological convention (Fall: October-December; Winter: January-March; Spring: April-June; Summer: July-September).

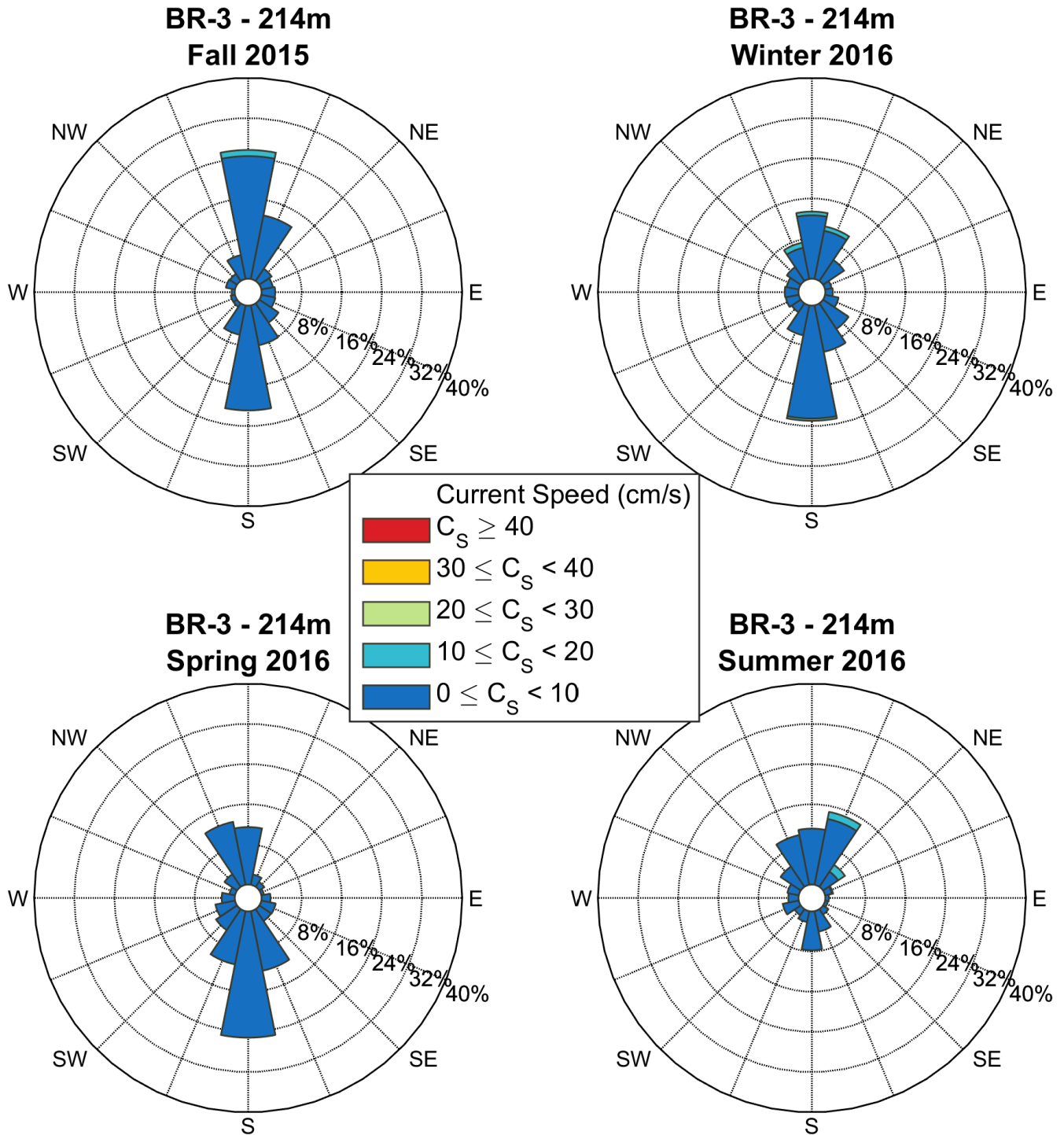


Figure 19: Seasonal current roses at 214 m depth (bin cell #14) at BR-3-15 measured by the LR ADCP #12942. Data are low-pass filtered. Roses indicate the direction toward which currents flow. Seasons are defined following the meteorological convention (Fall: October-December; Winter: January-March; Spring: April-June; Summer: July-September).

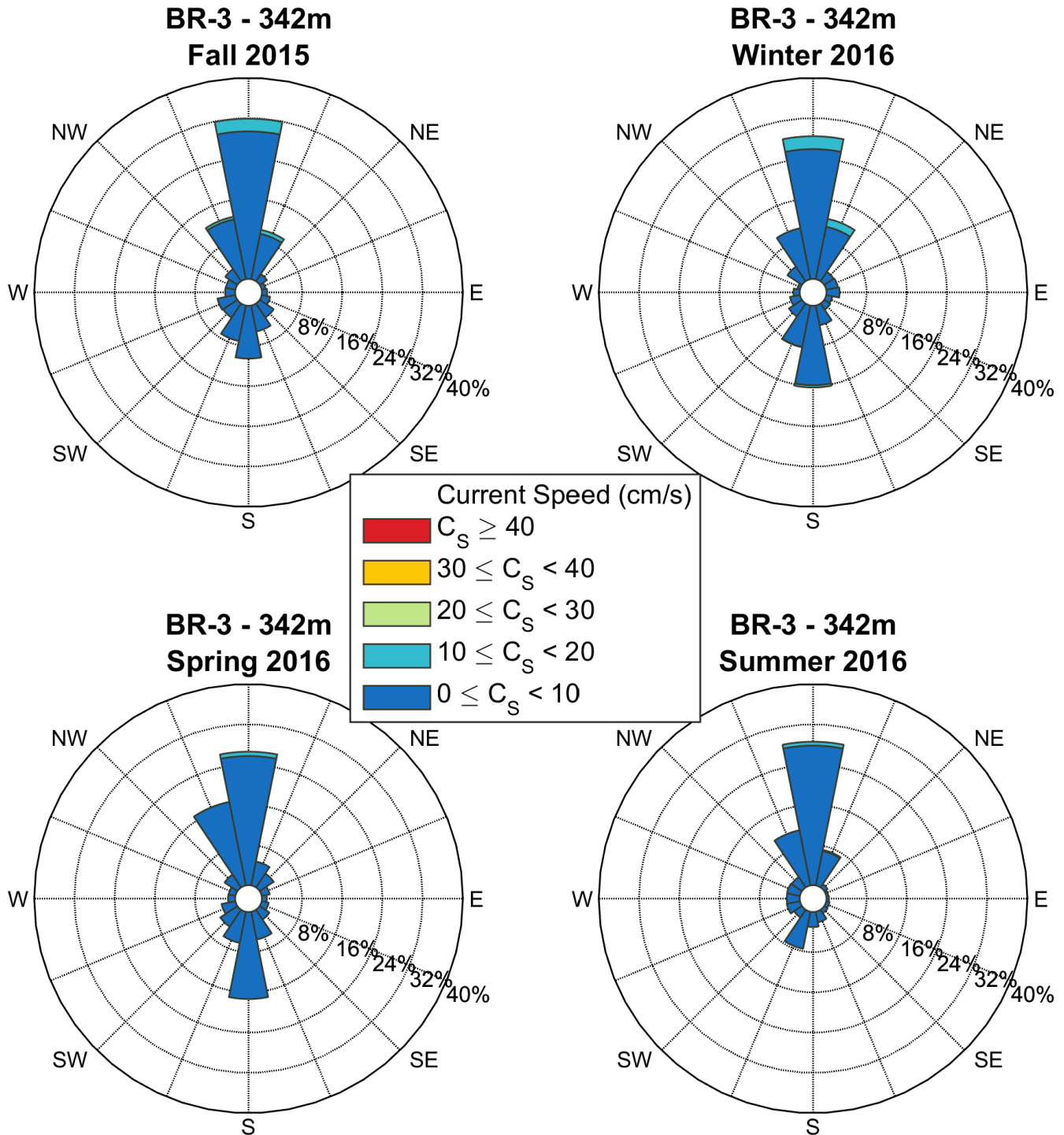


Figure 20: Seasonal current roses at 342 m depth (bin cell #6) at BR-3-15 measured by the LR ADCP #12942. Data are low-pass filtered. Roses indicate the direction toward which currents flow. Seasons are defined following the meteorological convention (Fall: October-December; Winter: January-March; Spring: April-June; Summer: July-September).

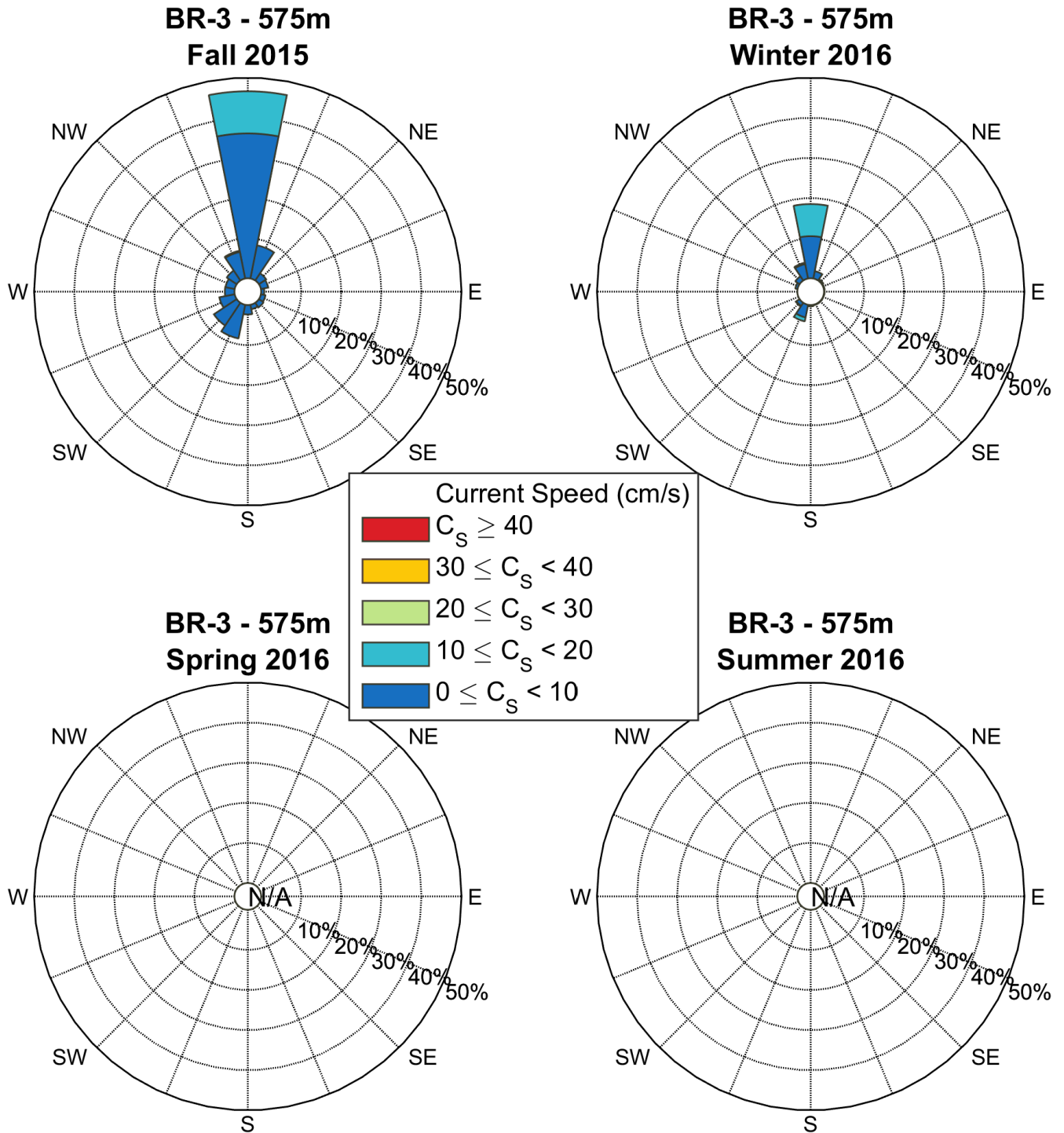


Figure 21: Seasonal current roses at 575 m depth at BR-3-15 measured by the Aquadopp #6109. Data are low-pass filtered. Roses indicate the direction toward which currents flow. Seasons are defined following the meteorological convention (Fall: October-December; Winter: January-March; Spring: April-June; Summer: July-September).

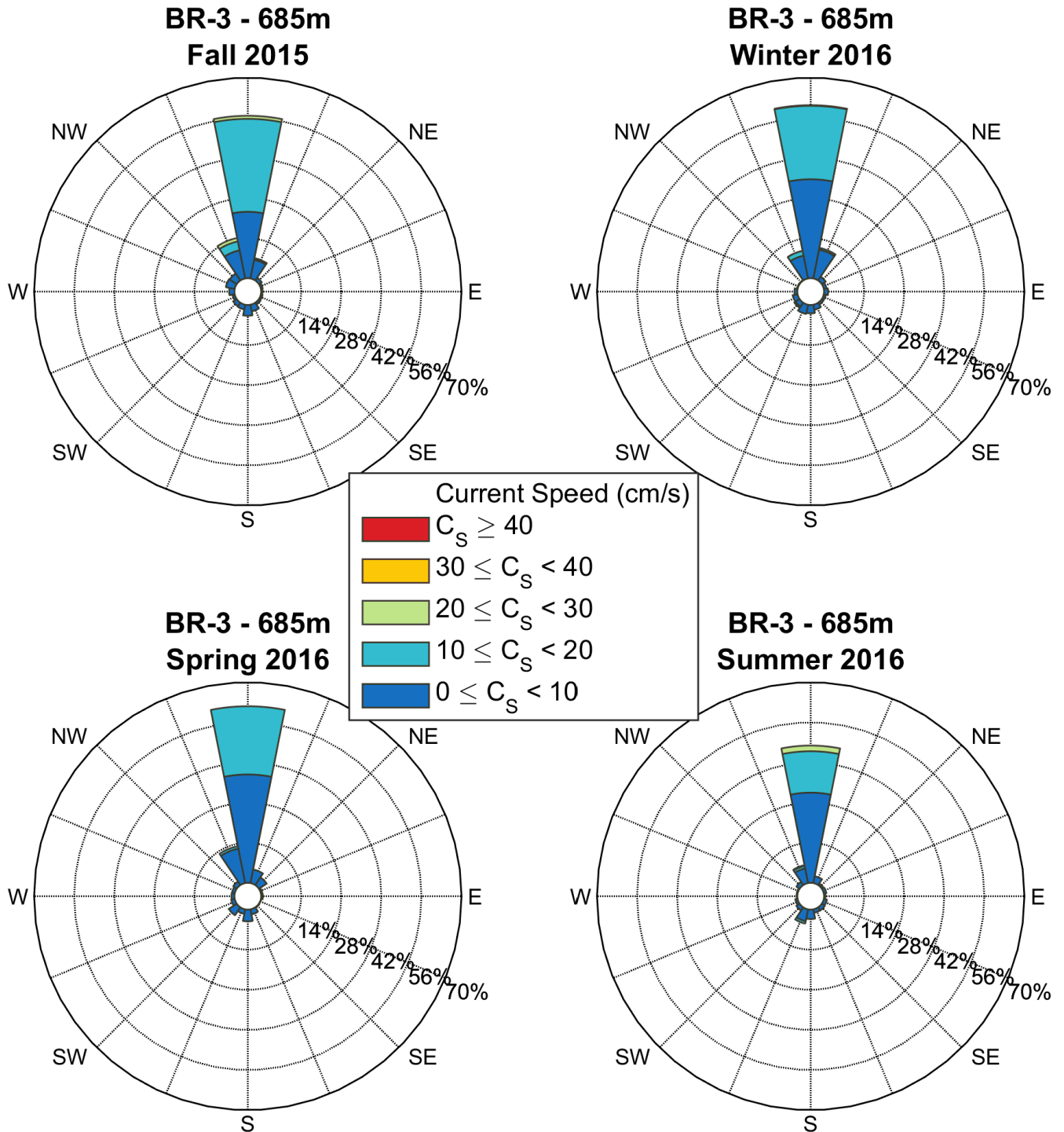


Figure 22: Seasonal current roses at 685 m depth at BR-3-15 measured by the Aquadopp #8541. Data are low-pass filtered. Roses indicate the direction toward which currents flow. Seasons are defined following the meteorological convention (Fall: October-December; Winter: January-March; Spring: April-June; Summer: July-September).

3.2.3 Mooring BR-G

Time-series plots of current speed, direction, and along-slope current component from the QM ADCP, LR ADCP and the two Aquadopp DW deployed at BR-G from 2015 to 2016 are provided in Figure 23 through Figure 26. The data in the QM and LR ADCP plots are filtered for bins with PG4+PG1 values less than 25%, bins affected by sidelobe interference and for error velocity thresholds as described in section 2.4.1. The first valid bin depth for the QM ADCP #12841 at BR-G-15 after removing sidelobe interference was 16.5 m (bin cell 35) with 88.8% valid data (Appendix D). Bin depths 104.5 and 108.5 m (bin cells 12 and 13) were affected by the presence of the upper Technicap sediment trap (as at BR-1), which resulted in reflection observed in the echo intensity (not shown) and a general decrease in current speed at these depths. Accordingly, bin cells 12 and 13 for QM ADCP #12841 were manually flagged as part of the QA/QC and data from these bin depths should be treated carefully before being used in further analyses.

The LR ADCP #12892 did not show any sign of suspicious bins due to interference with other parts of the mooring (Figure 24). The first valid bin depth for this instrument was 44.7 m (bin cell 25) with 88.4% valid data (Appendix D). Data from this bin depth were of high quality and did not show any suspicious spikes in the speed or echo intensity. Partial data loss possibly linked to high intensity of ambient sound generated by sea ice at the surface was observed briefly in fall 2015 and in spring and early summer 2016 (Figure 24). The deep Aquadopp current meters #9846 (580.9 m) and #8432 (690.8 m) provided complete time-series with 100% valid data for each instrument (Figure 25, Figure 26 and Appendix D).

Mean current speeds at BR-G-15 ranged from 8 to 19 cm/s in the upper 200 m of the water column; and from 4 to 7 cm/s below 200 m (Table 10, Appendix D). Vector-averaged directions were typically to the west-southwest (255-280°TN) for all bins down to 220 m depth. Beginning at 236 m, currents veer progressively to the northwest (285-340°TN) until 428 m depth. Further down below in the water column, data from the deep Aquadopps at 581 and 691 m showed that the annually-averaged direction was to the northeast along the slope (34-52°TN). The maximum current speed at BR-G-15 was 110 cm/s on October 18, 2015 at 44 m depth, measured by the LR ADCP. A strong event to the northwest was also detected from June 19 to 24, 2016 during which current speeds exceeded 50 cm/s. The instrument tilt also exceeded the 15-degree threshold for reliable measurements during this event.

Seasonal current roses (low-pass filtered) for selected bin depths at mooring BR-G-15 are provided in Figure 27 through Figure 32. A seasonal pattern in current speed can be identified with stronger near surface currents (20 m, Figure 27) in fall, spring, and summer. Stronger subsurface currents (130 m, Figure 28) occur in the late fall. At both depths the current direction shows a reversal from southwestward in the fall, winter, and spring to northeastward in the summer. Below 200 m, currents are relatively weak and are typically less than 10 to 15 cm/s, with variable directions at 220 and 348 m. A cross-slope current was measured at both depths in the spring and summer. Current speed and direction in the lowermost section of the water column (581 and 691 m, Figure 31 and Figure 32) were generally similar and uniformly to the east-northeast along the slope.

BR-G; QM Broadband 153.6 kHz; 71.00203 N, 135.49353 W; 2015-2016; Instr. #12841

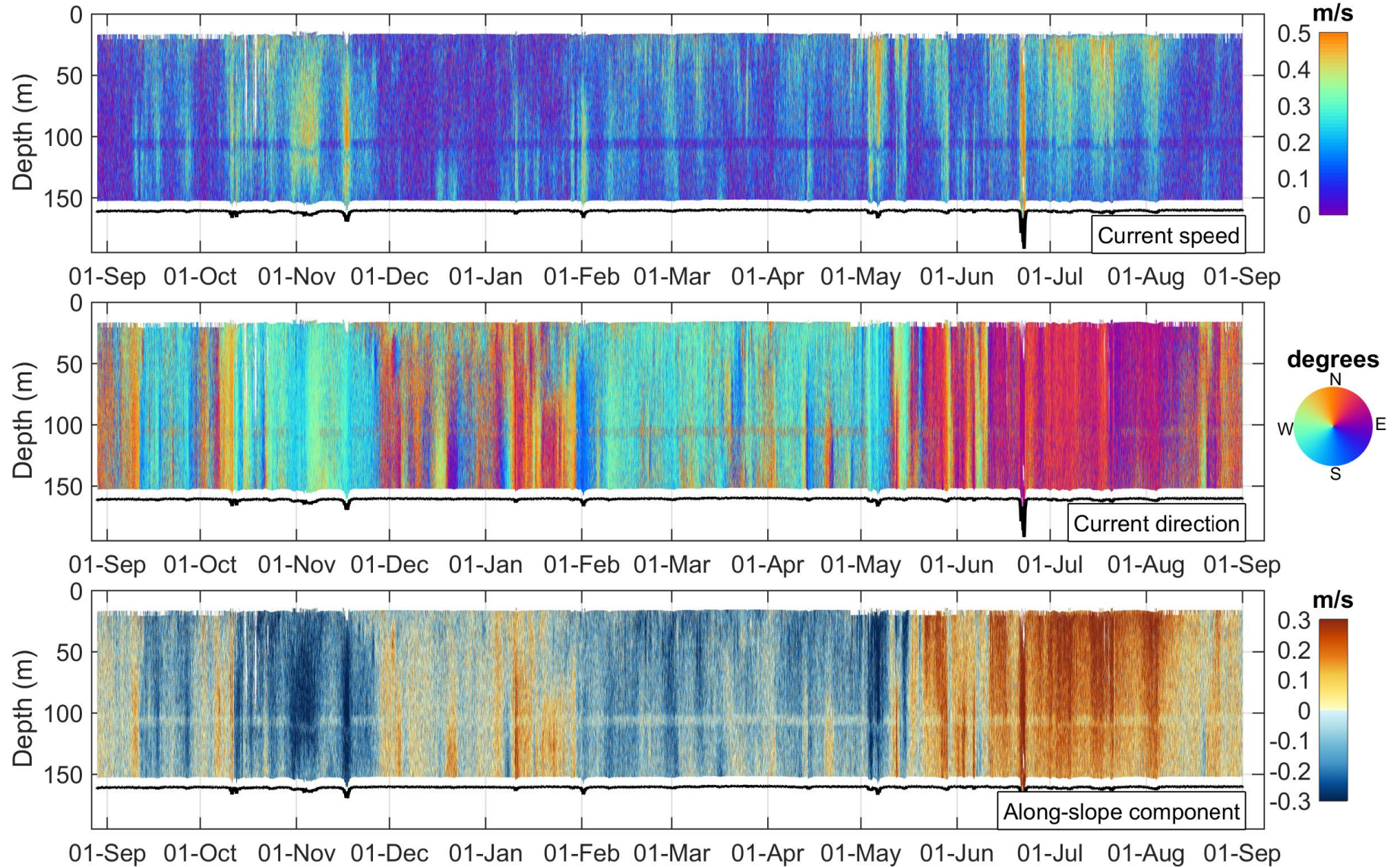


Figure 23: Time-series of current speed, current direction and along-slope current component at mooring BR-G-15 measured by the QM ADCP #12841. The black line depicts the instrument depth.

BR-G; LR Broadband 76.8 kHz; 71.00203 N, 135.49353 W; 2015-2016; Instr. #12892

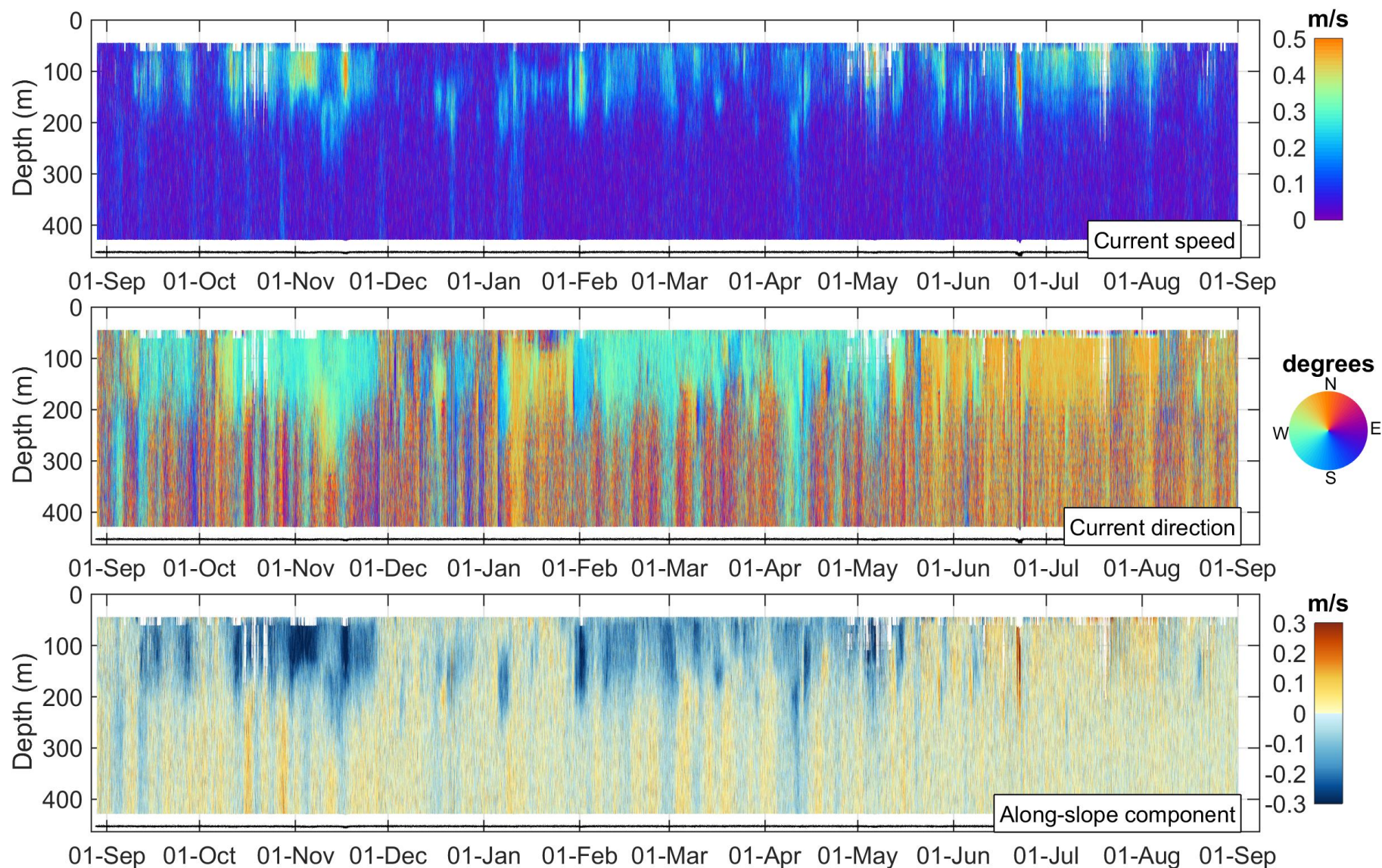


Figure 24: Time-series of current speed, current direction and along-slope current component at mooring BR-G-15 measured by the LR ADCP #12892. The black line depicts the instrument depth.

BR-G; Aquadopp DeepWater 2-MHz; 71.00203 N, 135.49353 W; 2015-2016; Instr. #9846

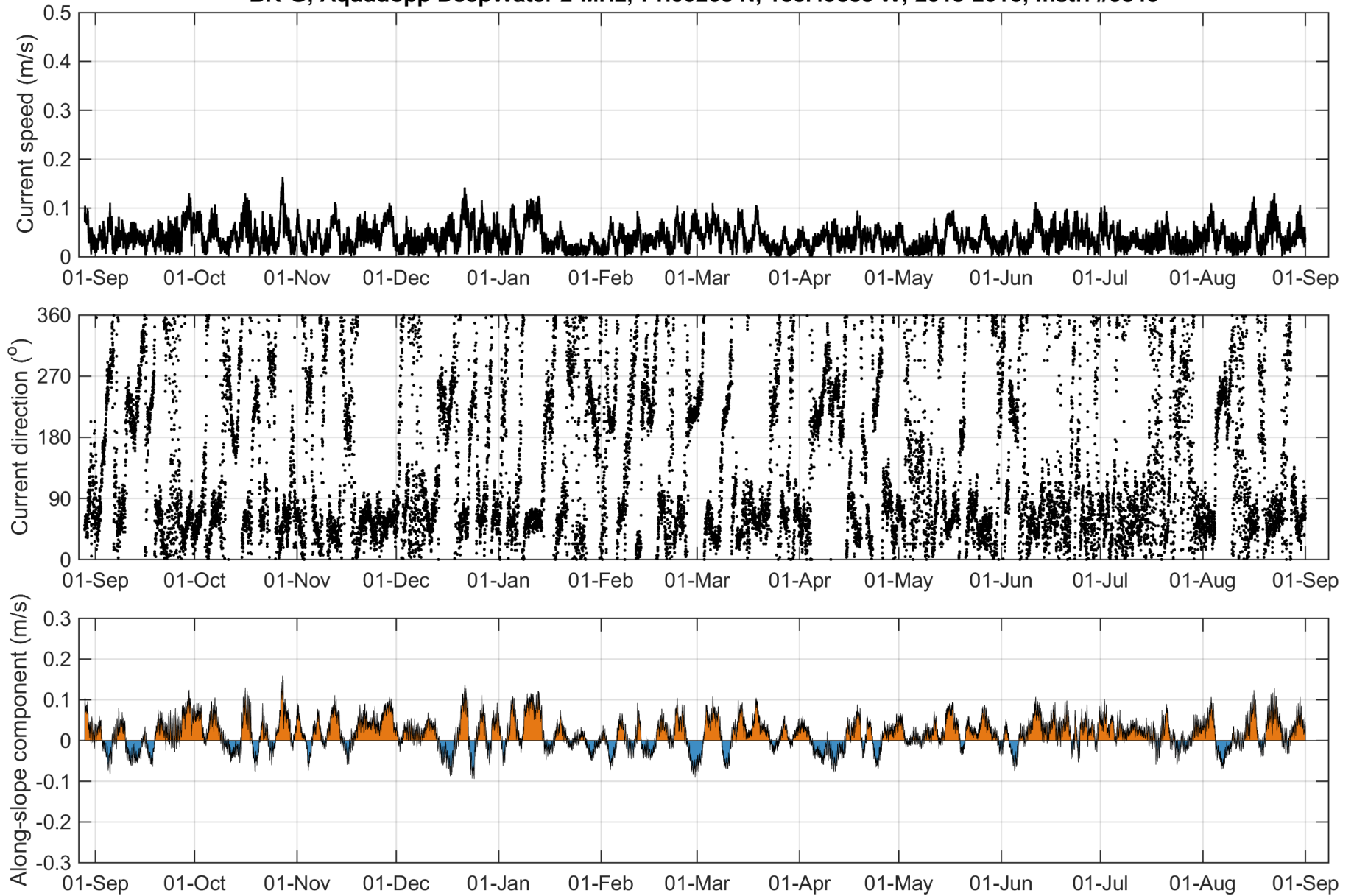


Figure 25: Time-series of current speed, current direction and along-slope current component at 581 m at mooring BR-G-15 measured by the Aquadopp #9846.

BR-G; Aquadopp DeepWater 2-MHz; 71.00203 N, 135.49353 W; 2015-2016; Instr. #8434

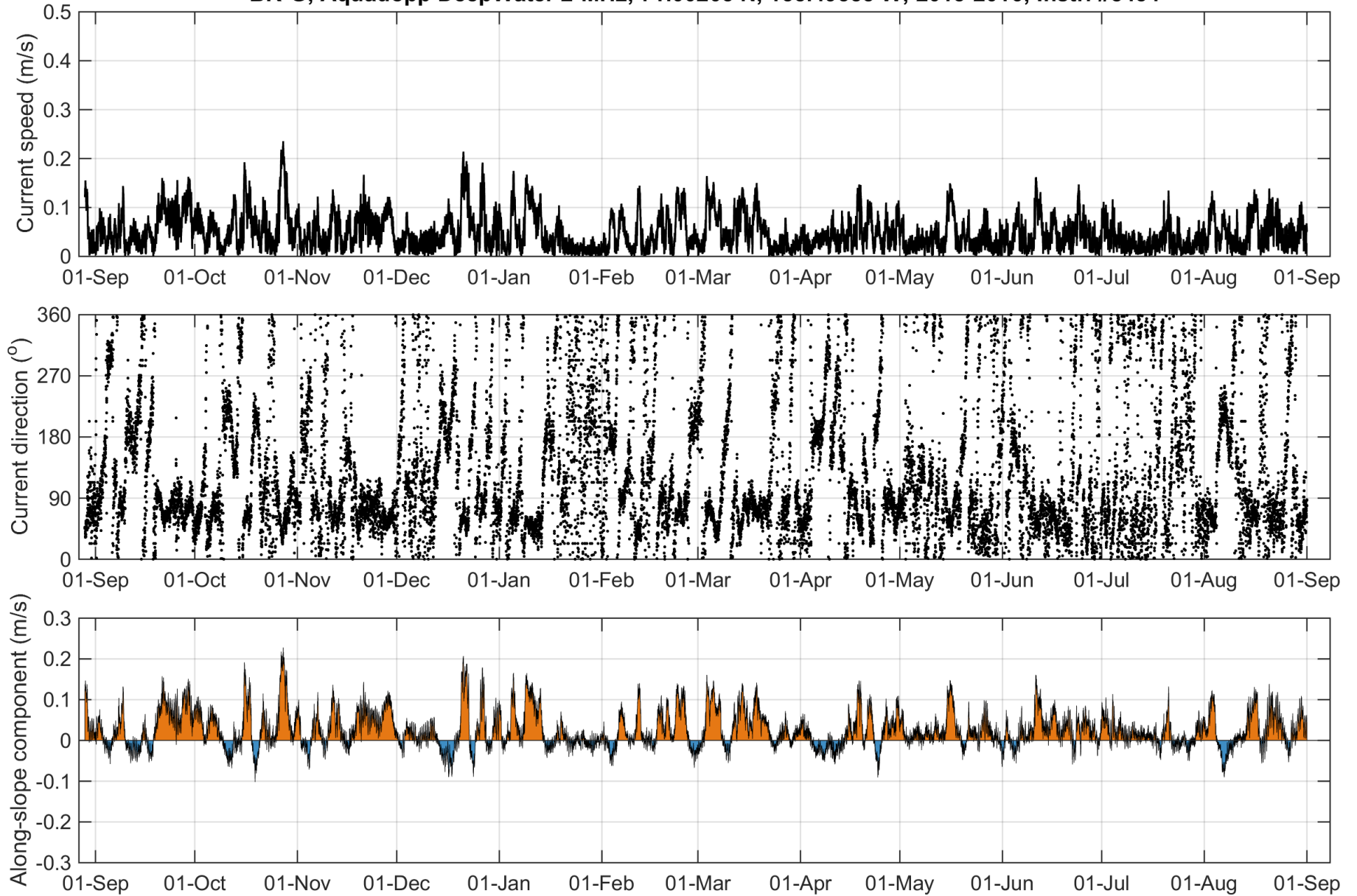


Figure 26: Time-series of current speed, current direction and along-slope current component at 691 m at mooring BR-G-15 measured by the Aquadopp #8434.

Table 10: Annual statistics of current speed and direction at BR-G-15 from selected bin depths representative of water mass variability in the Beaufort Sea (see Table 6 for water mass description).

Bin Depth (m)	Median Speed (m/s)	Mean Speed (m/s)	75%ile Speed (m/s)	95%ile Speed (m/s)	99%ile Speed (m/s)	Max Speed (m/s)	Standard Deviation Speed (m/s)	Vector-Averaged Direction (deg TN)
20.5	0.17	0.19	0.26	0.40	0.47	0.60	0.11	272.8
132.5	0.13	0.14	0.19	0.28	0.38	0.69	0.08	263.3
220.7	0.06	0.06	0.08	0.14	0.19	0.30	0.04	279.8
348.7	0.04	0.04	0.06	0.09	0.12	0.18	0.02	316.4
580.9	0.04	0.04	0.05	0.09	0.11	0.16	0.02	33.7
690.8	0.04	0.05	0.07	0.12	0.16	0.24	0.04	52.2

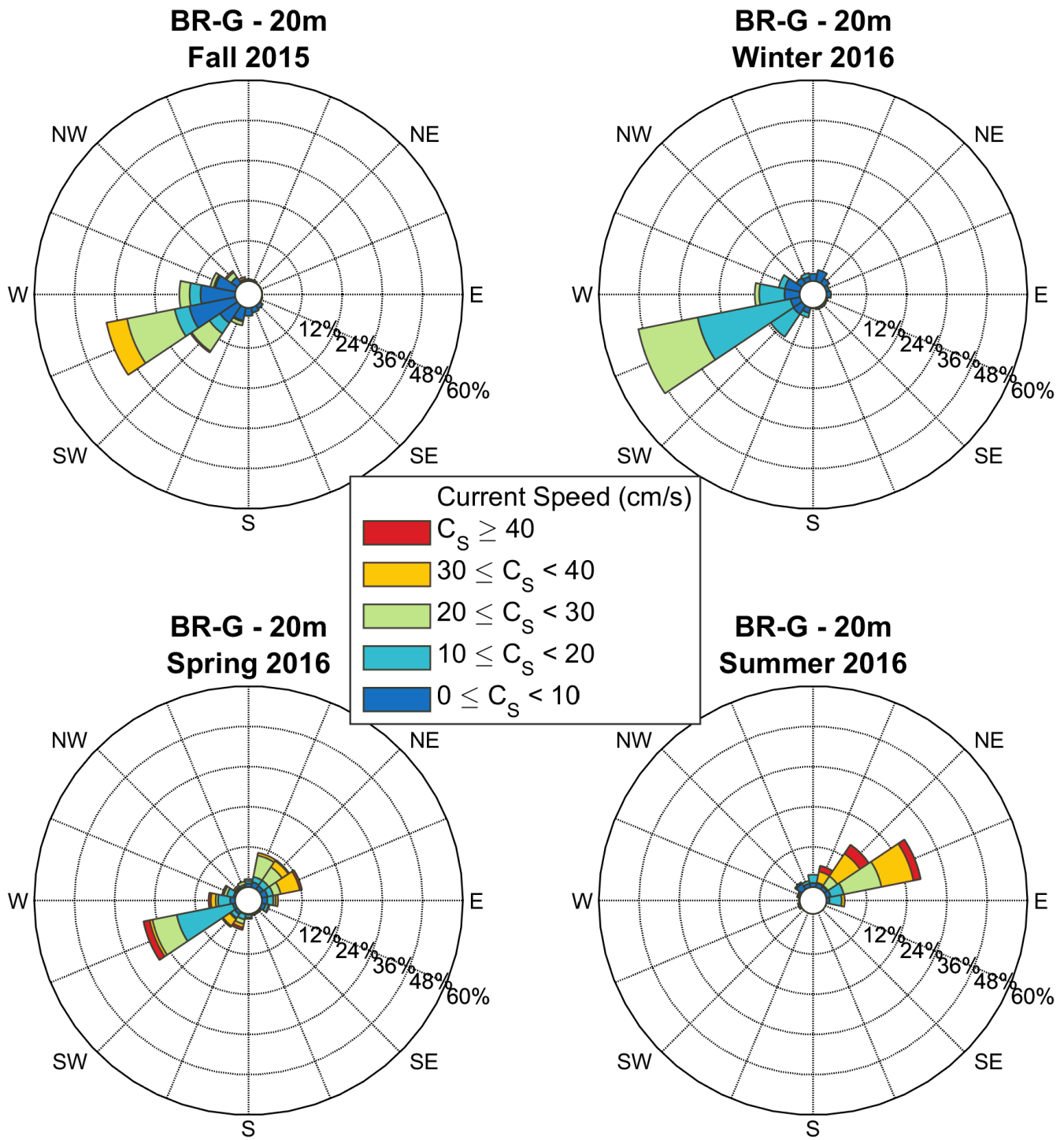


Figure 27: Seasonal current roses at 20 m depth (bin cell #34) at BR-G-15 measured by the QM ADCP #12841. Data are low-pass filtered. Roses indicate the direction toward which currents flow. Seasons are defined following the meteorological convention (Fall: October-December; Winter: January-March; Spring: April-June; Summer: July-September).

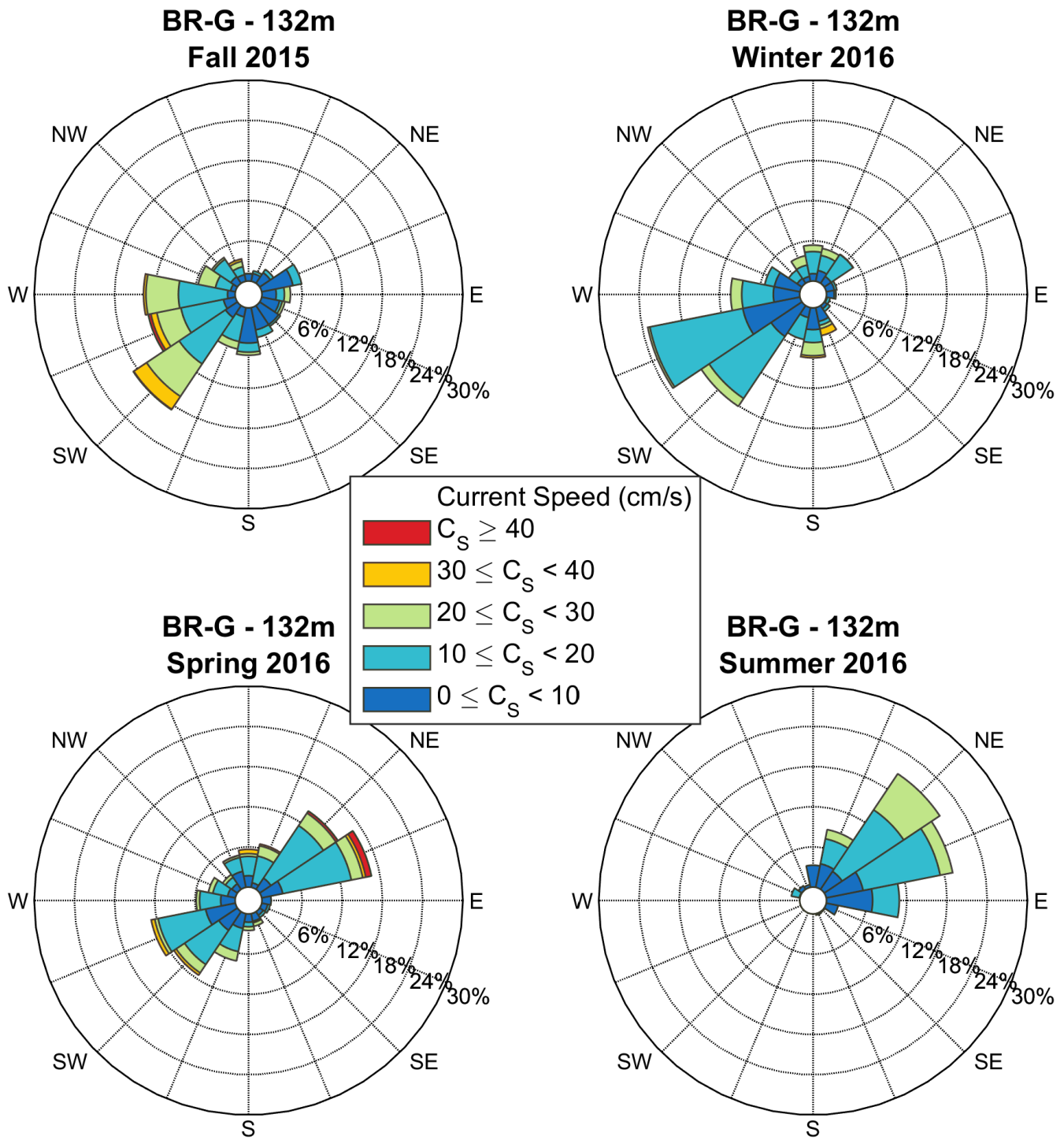


Figure 28: Seasonal current roses at 132 m depth (bin cell #6) at BR-G-15 measured by the QM ADCP #12841. Data are low-pass filtered. Roses indicate the direction toward which currents flow. Seasons are defined following the meteorological convention (Fall: October-December; Winter: January-March; Spring: April-June; Summer: July-September).

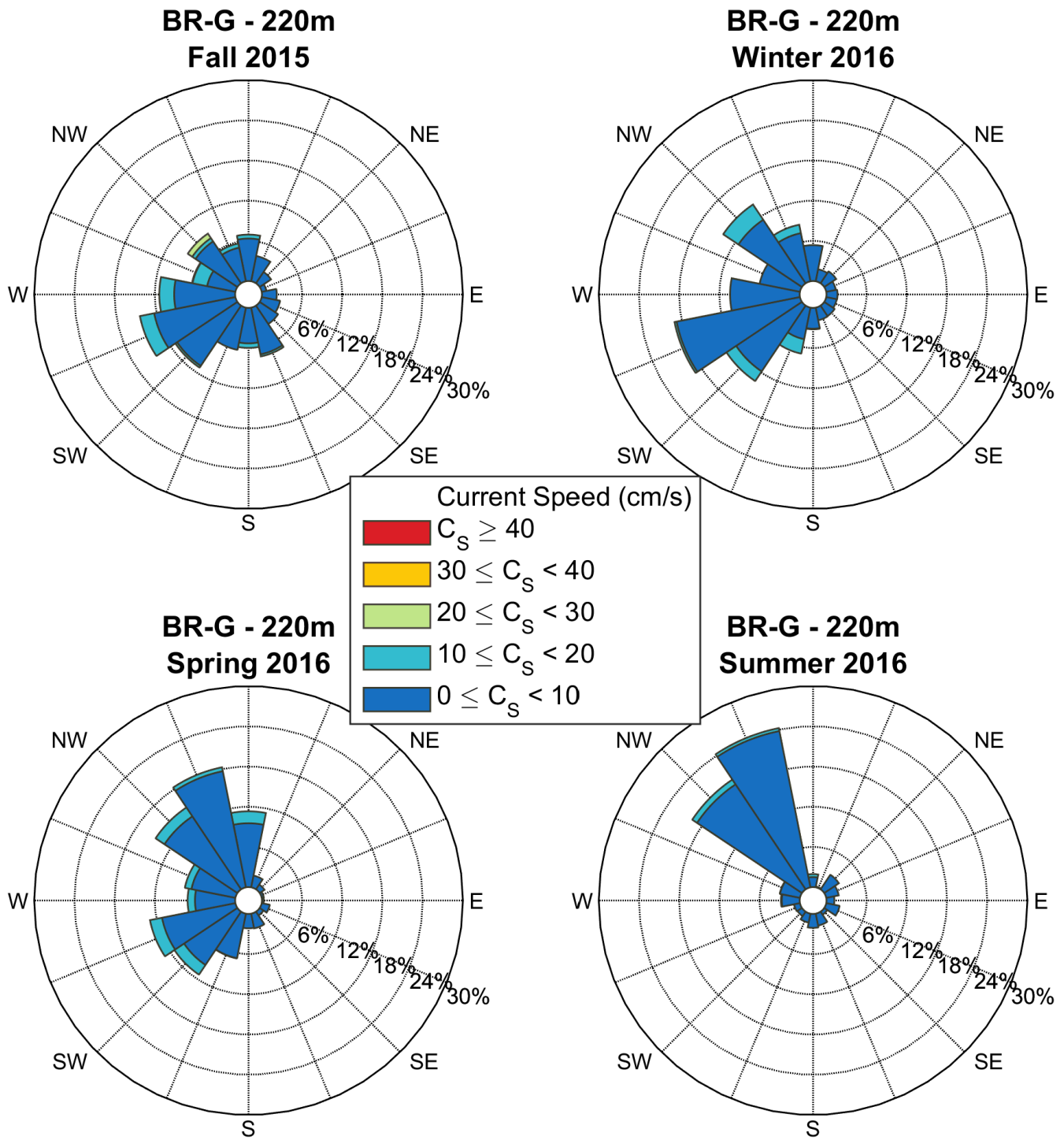


Figure 29: Seasonal current roses at 220 m depth (bin cell #14) at BR-G-15 measured by the LR ADCP #12892. Data are low-pass filtered. Roses indicate the direction toward which currents flow. Seasons are defined following the meteorological convention (Fall: October-December; Winter: January-March; Spring: April-June; Summer: July-September).

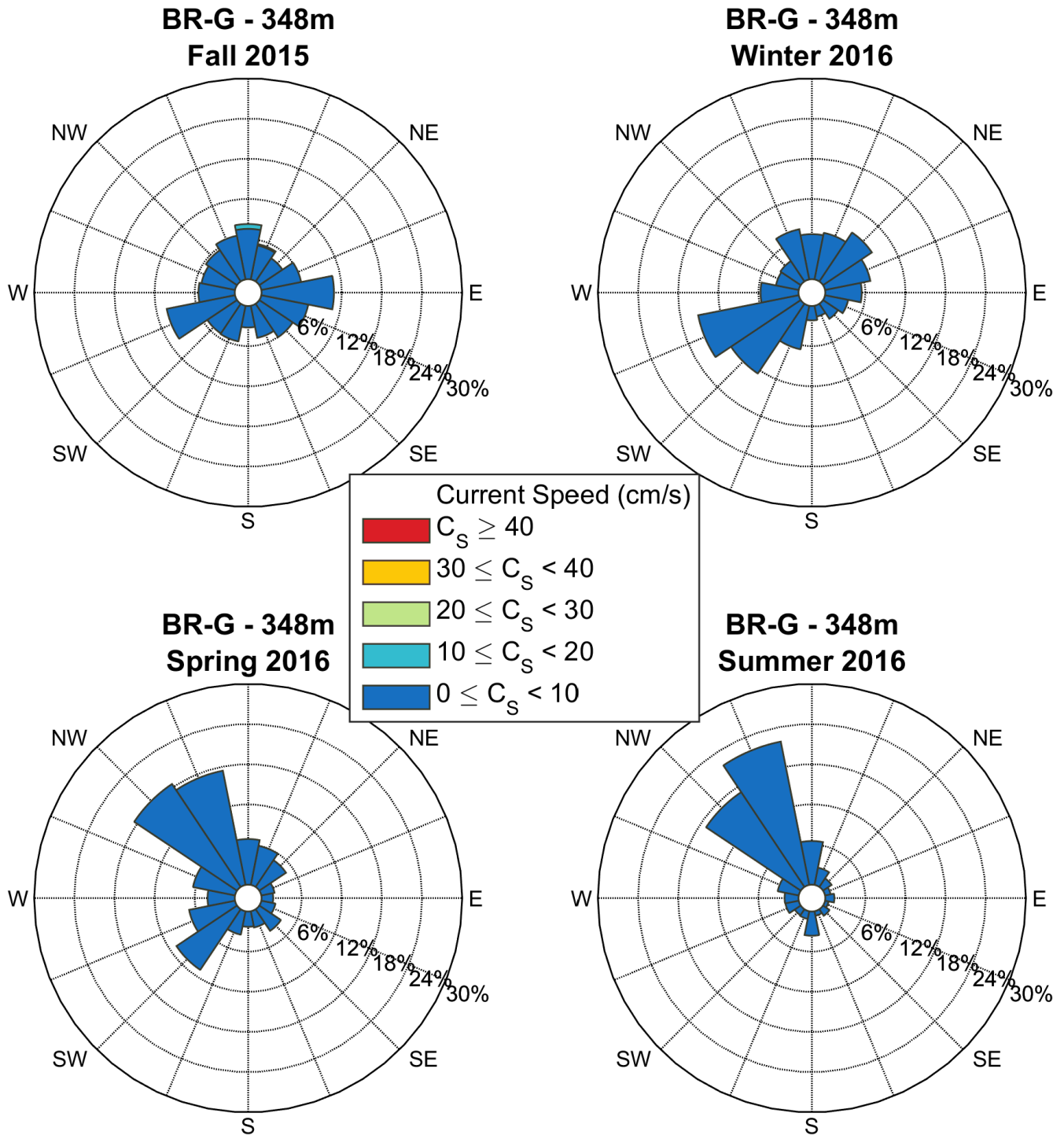


Figure 30: Seasonal current roses at 348 m depth (bin cell #6) at BR-G-15 measured by the LR ADCP #12892. Data are low-pass filtered. Roses indicate the direction toward which currents flow. Seasons are defined following the meteorological convention (Fall: October-December; Winter: January-March; Spring: April-June; Summer: July-September).

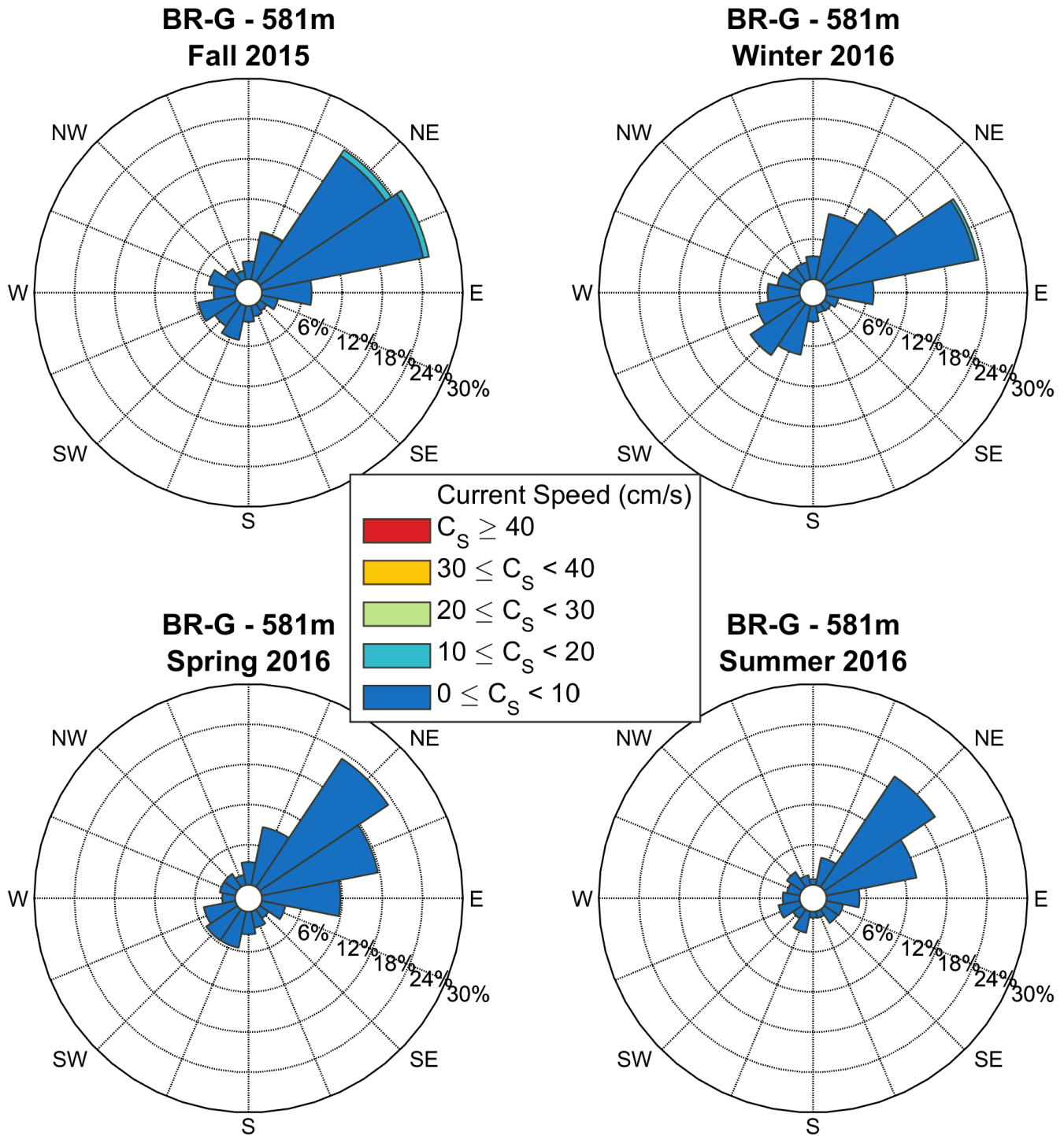


Figure 31: Seasonal current roses at 581 m depth at BR-G-15 measured by the Aquadopp #9846. Data are low-pass filtered. Roses indicate the direction toward which currents flow. Seasons are defined following the meteorological convention (Fall: October-December; Winter: January-March; Spring: April-June; Summer: July-September).

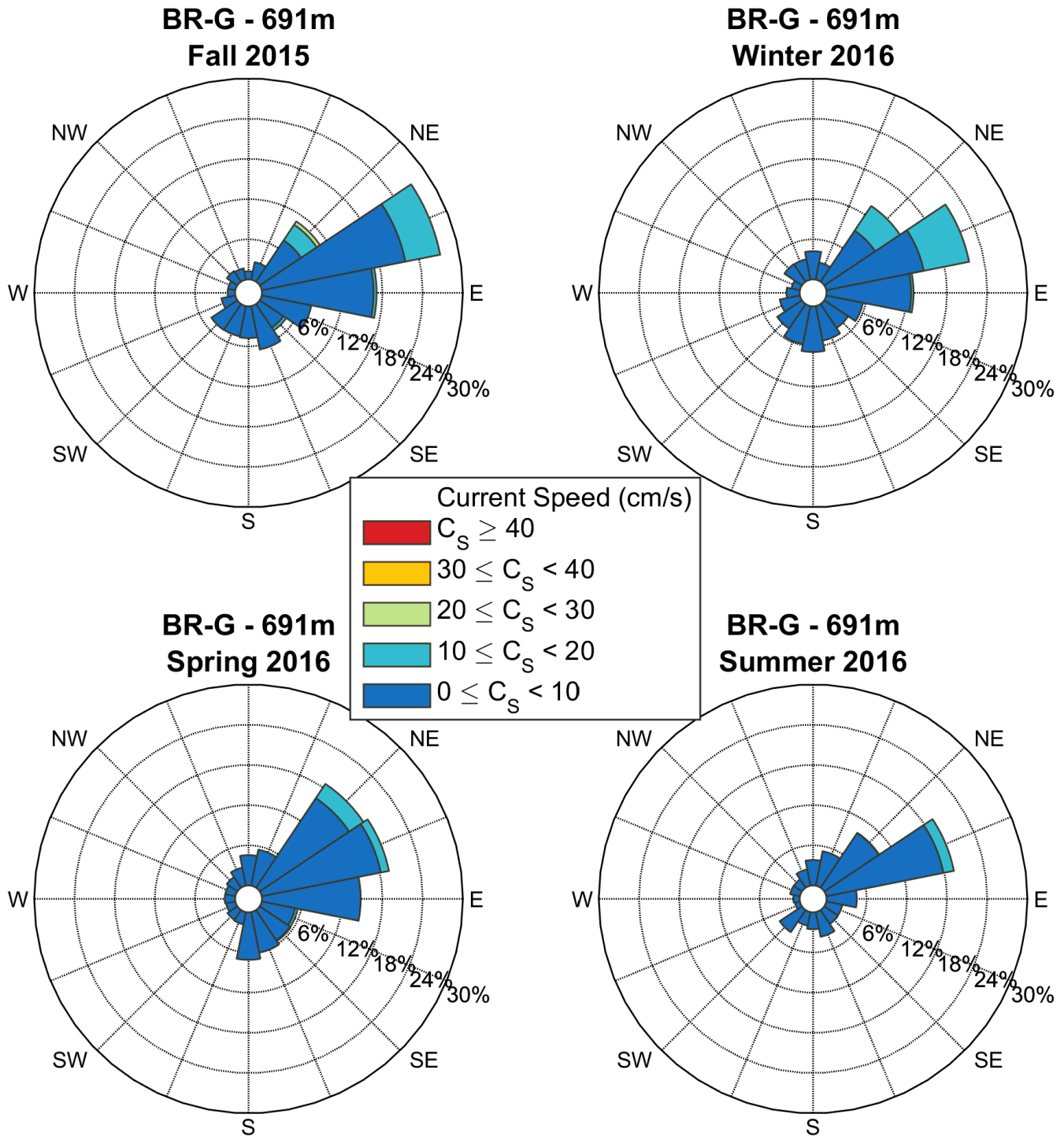


Figure 32: Seasonal current roses at 691 m depth at BR-G-15 measured by the Aquadopp #8434. Data are low-pass filtered. Roses indicate the direction toward which currents flow. Seasons are defined following the meteorological convention (Fall: October-December; Winter: January-March; Spring: April-June; Summer: July-September).

3.2.4 Mooring BR-K

Time-series plots of current speed, direction, and along-slope current component from the WHS ADCP deployed at the upper slope mooring BR-K from 2015 to 2016 are provided in Figure 33. The Nortek Aquadopp profiler was deployed incorrectly on the mooring and the data is not considered reliable as a result. The data in the WHS ADCP plot are filtered for bins with PG4+PG1 values less than 25%, bins affected by sidelobe interference and for error velocity thresholds as described in section 2.4.1. The first valid bin depth for the WHS ADCP #102 at BR-K-15 after removing sidelobe interference was 22.9 m (bin cell 15) with 74.3% valid data (Appendix D). The percentage of valid data below the uppermost valid bin depth ranged from 87.0 to 100%. No bin depth was manually flagged due to possible interference with other parts of the mooring for this instrument as part of the QA/QC procedure.

Mean current speeds at BR-K-15 measured by the WHS ADCP ranged from 16 to 20 cm/s throughout the water column (Appendix D, Table 11). Vector-averaged directions were uniformly to the northeast (50-65°TN) from 38 to 135 m depth; the uppermost two bins were more variable with vector-averaged directions of 253°TN and 342°TN.

Maximum current speed measured at BR-K-15 was 95 cm/s on July 20, 2016 at 79 m depth. Current magnitudes were elevated at all depths measured the WHS ADCP at BR-K. Current direction during the event was uniformly to the northeast (50-65°TN) in the upper water column measured by the WHS ADCP, consistent with an intensification of the Beaufort shelfbreak jet flowing within 10-15 km of the shelf edge on the upper slope (see section 1.2). Numerous other relatively strong current speed events (>50 cm/s) were recorded at BR-K from the fall of 2015 to spring 2016 and are characterized by a strong negative along-slope current component to the southwest, in the opposite direction than the mean current. Conditions during these events are consistent with the development of an upwelling jet and transport of deeper waters up the shelf (see section 3.3 for more).

Seasonal current roses (low-pass filtered) for selected bin depths at mooring BR-K-15 are provided in Figure 34 and Figure 35. The differences in the most frequent current directions between the upper (23 m) and lower bin depths (127 m) at this location reflects the presence of the shelfbreak jet. The currents at 126 m are unidirectional to the northeast while the currents measured at 23 m depth are more variable (but still along the slope), particularly outside of the summer season.

BR-K; WH Broadband 307.2 kHz; 70.86272 N, 135.02843 W; 2015-2016; Instr. #102

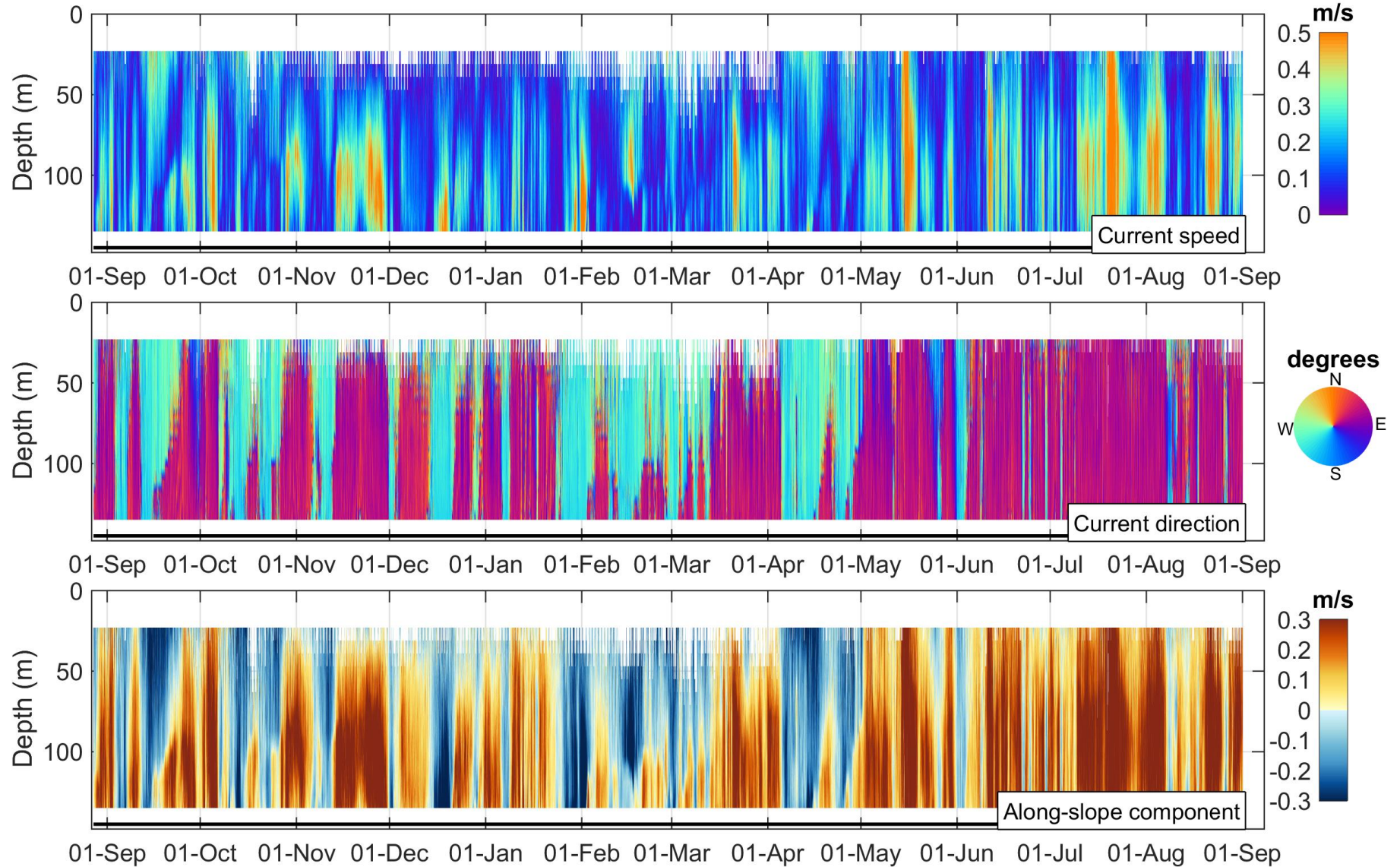


Figure 33: Time-series of current speed, current direction and along-slope current component at mooring BR-K-15 measured by the WHS ADCP #102. The black line depicts the instrument depth.

Table 11: Annual statistics of current speed and direction at BR-K-15 from selected bin depths representative of water mass variability in the Beaufort Sea (see Table 6 for water mass description).

Bin Depth (m)	Median Speed (m/s)	Mean Speed (m/s)	75%ile Speed (m/s)	95%ile Speed (m/s)	99%ile Speed (m/s)	Max Speed (m/s)	Standard Deviation Speed (m/s)	Vector-Averaged Direction (deg TN)
22.9	0.14	0.16	0.22	0.35	0.54	0.85	0.11	253.4
126.9	0.18	0.20	0.28	0.44	0.56	0.75	0.13	58.6

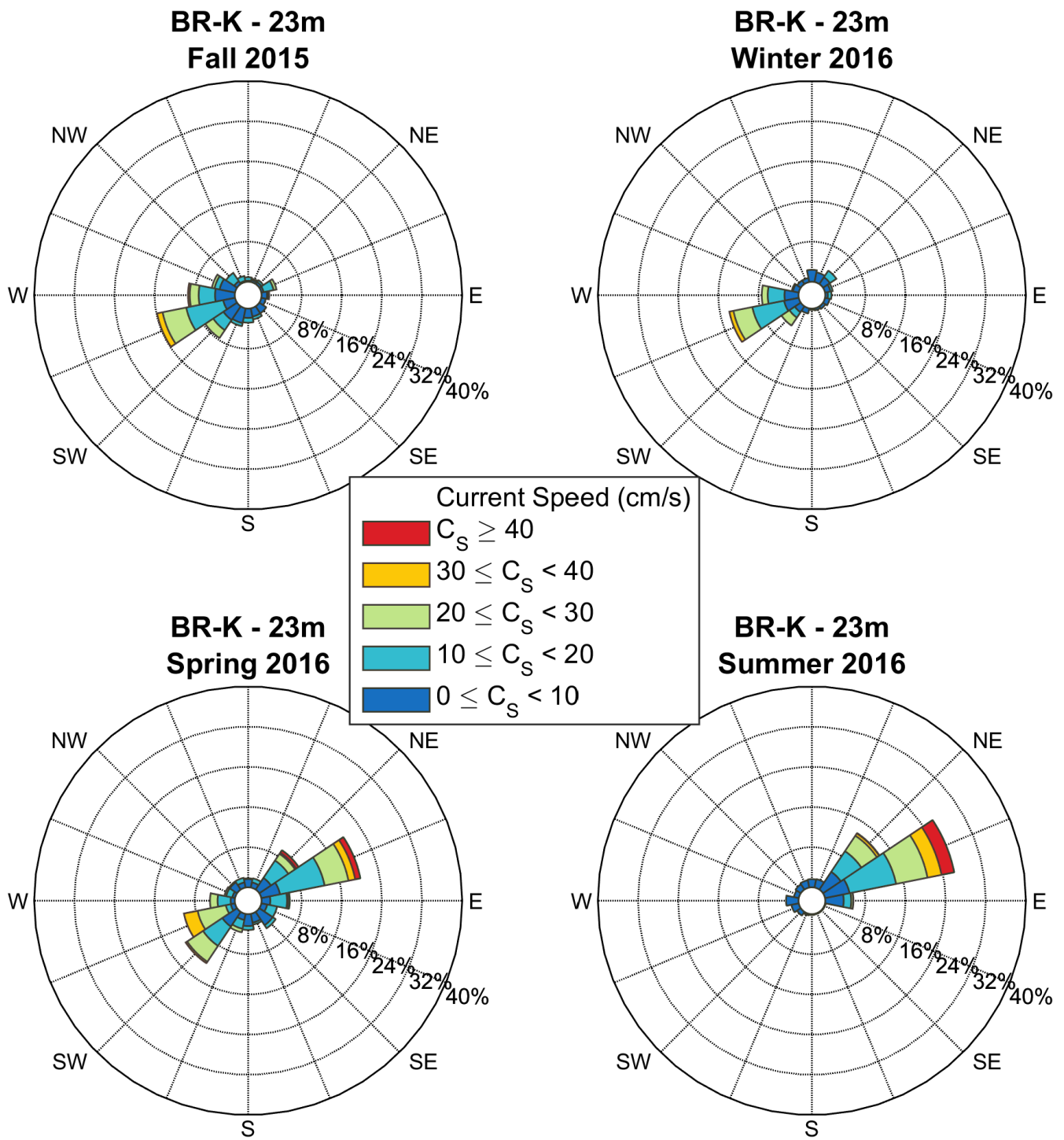


Figure 34: Seasonal current roses at 23 m depth (bin cell #15) at BR-K-15 measured by the WHS ADCP #102. Data are low-pass filtered. Roses indicate the direction toward which currents flow. Seasons are defined following the meteorological convention (Fall: October-December; Winter: January-March; Spring: April-June; Summer: July-September).

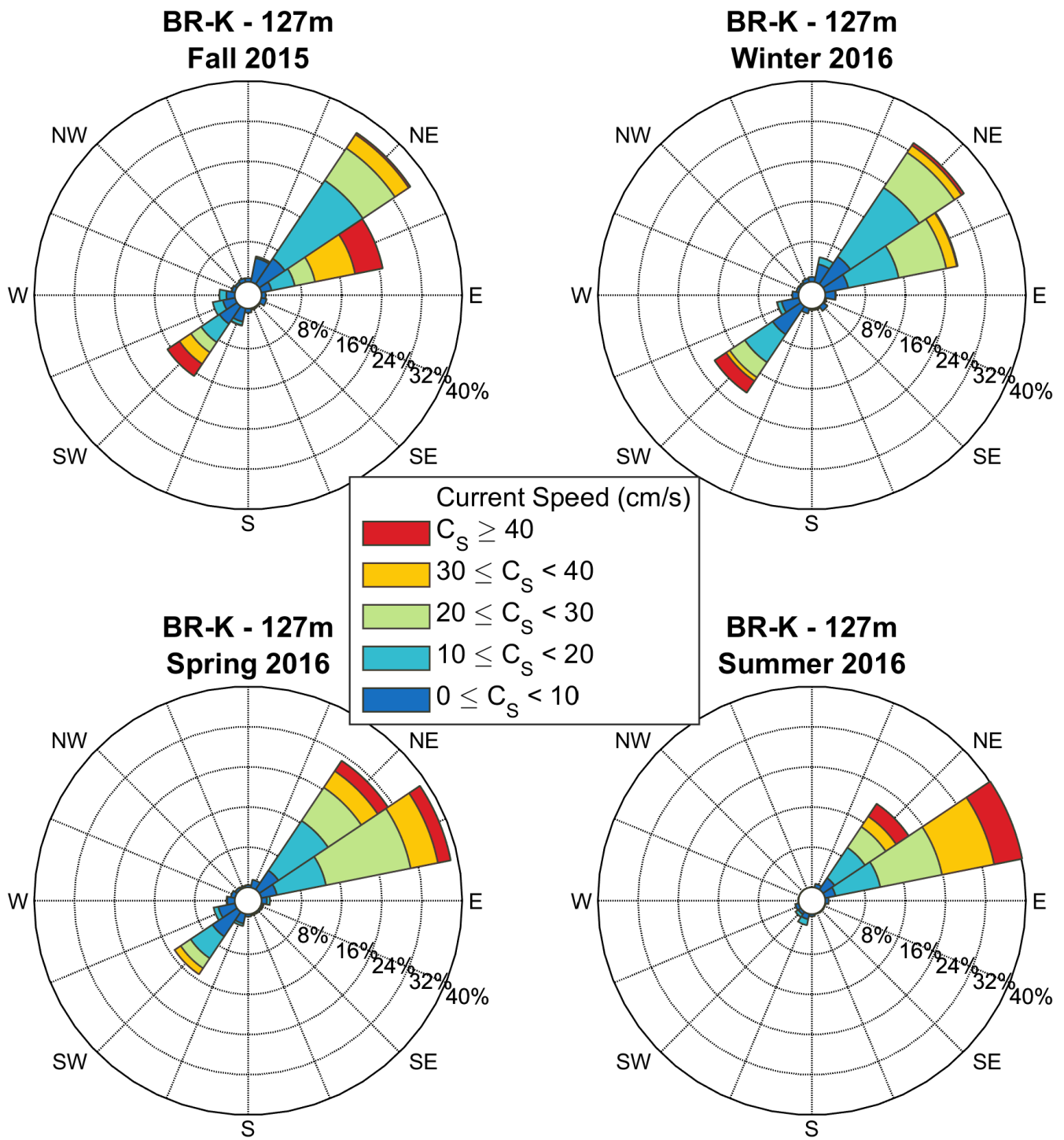


Figure 35: Seasonal current roses at 127 m depth (bin cell #2) at BR-K-15 measured by the WHS ADCP #102. Data are low-pass filtered. Roses indicate the direction toward which currents flow. Seasons are defined following the meteorological convention (Fall: October-December; Winter: January-March; Spring: April-June; Summer: July-September).

3.2.5 Mooring DFO-2

A time-series plot of current speed, direction, and along-slope current component from the NB ADCP deployed at the outer shelf mooring DFO-2 from 2015 to 2016 is provided in Figure 36. The data in the NB ADCP plot are filtered for bins with PG4 values less than 25%, bins affected by sidelobe interference and for error velocity thresholds and other masks as described in section 2.4.1. The first valid bin depth for the NB ADCP #506 at DFO-2-15 after removing sidelobe interference was 19.3 m (bin cell 21) with a percentage of valid data of 33% (Appendix D). The percentage of valid data below the uppermost valid bin depth ranged from 68.8% to 100.0%. No bin depth was manually flagged for this instrument as part of the QA/QC procedure.

Mean current speeds at DFO-2-15 ranged from 9 to 14 cm/s throughout the water column, with the stronger mean currents typically near the surface (Appendix D, Table 12). Vector-averaged directions in the upper water column are towards the southwest (210-245°TN) from 20 to 51 m depth, followed by a rapid shift to the northeast (55-75°TN) at the lower bin depths from 60 to 100 m. The direction of the currents in the lower bin depths are comparable to those measured by nearby BR-K-15 and are aligned parallel to the slope.

Maximum current speed at DFO-2-15 was 64 cm/s on October 26, 2015 at the 23 m depth bin (Appendix D). Currents at DFO-2 were stronger in October and the majority of fall 2015 in comparison to the remainder of the measurement interval. Currents during October were characterized by a strong negative along-shelf current component to the southwest throughout the water column (Figure 36). A surface-intensified current event (>30 cm/s) was measured from June 15-19, 2016 from 20 to 60 m depth and is also characterized by a strong negative along-shelf current.

Seasonal current roses (low-pass filtered) for selected bin depths at mooring DFO-2-15 are provided in Figure 37 and Figure 38. The depth bin at 23 m (bin cell 20) was chosen rather than the depth bin at 20 m because of the low percentage of valid data in the uppermost bin. The current roses at the upper (23 m) and lower bin depths (101 m) at this location illustrate the general circulation pattern at the outer shelf/upper slope that is characterized by south-westward currents near the surface, although during summer surface currents are more variable with more frequent northeastward currents. At depth, north-eastward currents dominate during all seasons. The current at 101 m is smaller in magnitude and less unidirectional in comparison to BR-K-15 where the shelfbreak jet, steered by the bottom topography of the upper slope, is centered. A similar pattern was observed in the 2014-2015 data and it was hypothesized that at DFO-2, the subsurface circulation is looser and less trapped to the bottom due to the gentler slope topography at this site when compared to BR-K, thus less prone to the generation of a jet.

DFO-2; NB ADCP 300kHz; 70.9893 N, 133.7438 W; 2015-2016; Instr. #506; 107 m depth

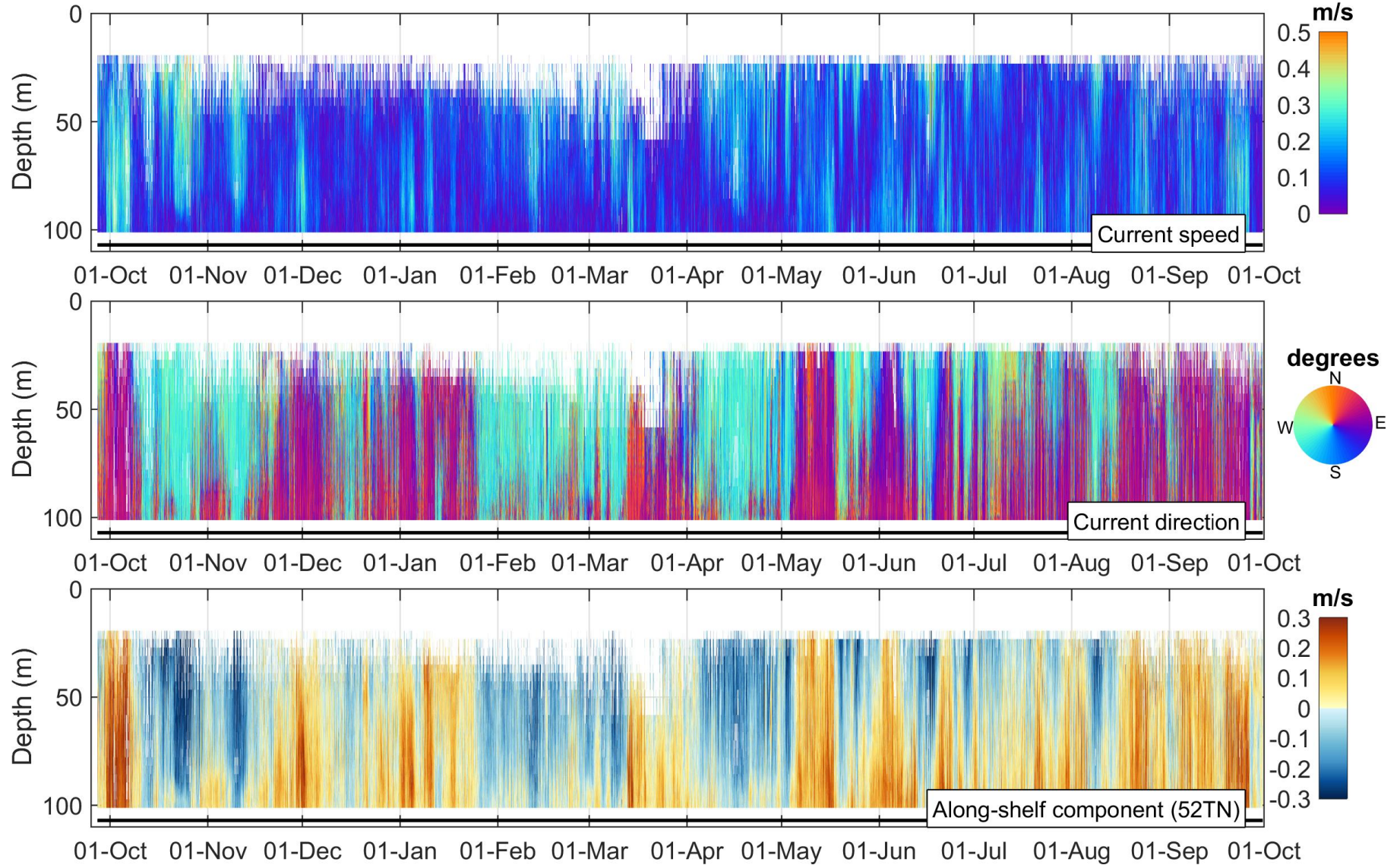


Figure 36: Time-series of current speed, current direction and along-slope current component at mooring DFO-2-15 measured the NB ADCP #506. The black line depicts the instrument depth.

Table 12: Annual statistics of current speed and direction at DFO-2-15 from selected bin depths representative of water mass variability in the Beaufort Sea (see Table 6 for water mass description).

Bin Depth (m)	Median Speed (m/s)	Mean Speed (m/s)	75%ile Speed (m/s)	95%ile Speed (m/s)	99%ile Speed (m/s)	Max Speed (m/s)	Standard Deviation Speed (m/s)	Vector-Averaged Direction (deg TN)
23.2	0.11	0.13	0.17	0.29	0.38	0.64	0.08	237.1
101.2	0.08	0.09	0.13	0.21	0.27	0.38	0.06	55.8

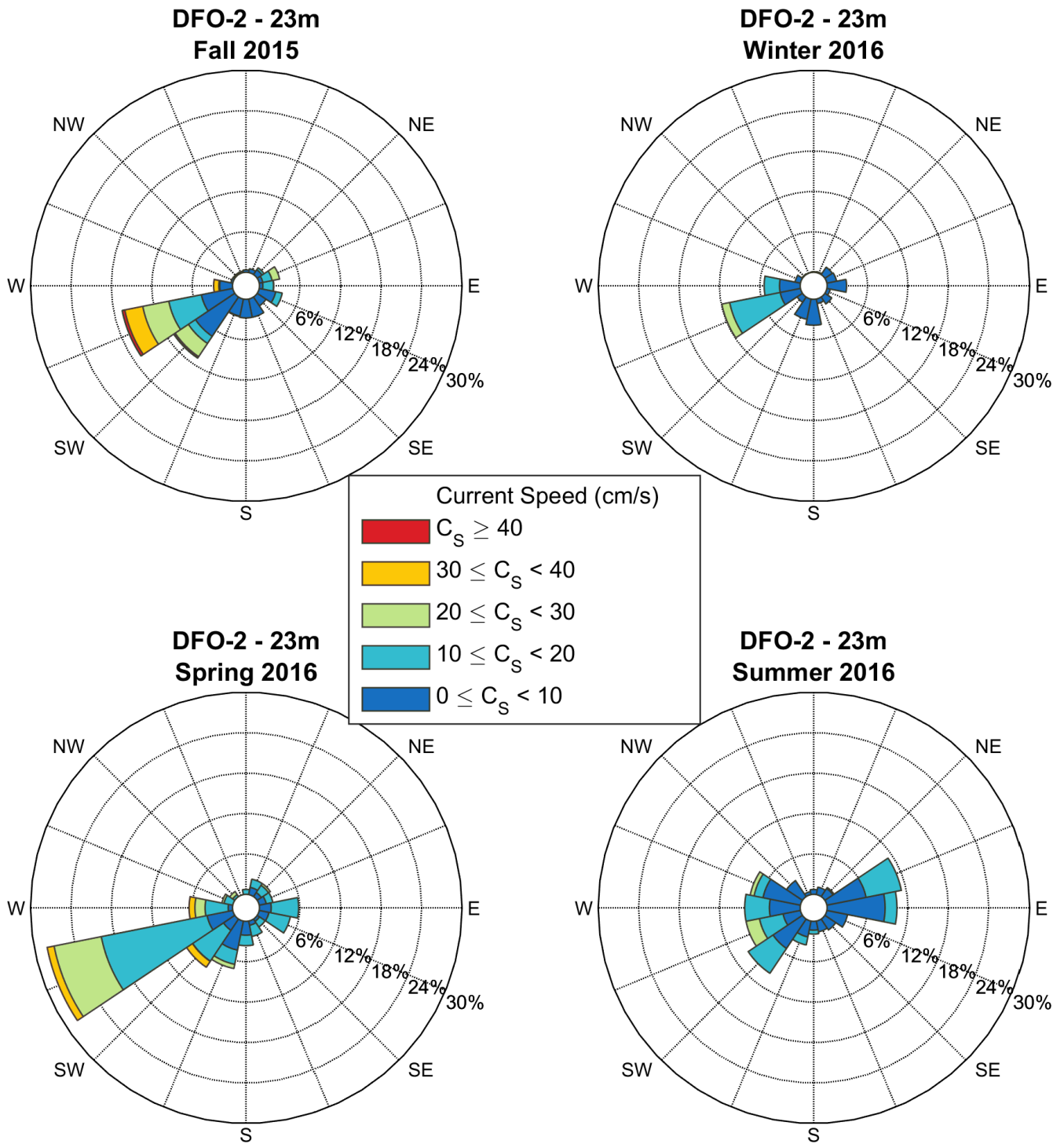


Figure 37: Seasonal current roses at 23 m depth at DFO-2-15 as based on low-pass filtered data from bin cell #20 measured by the NB ADCP #506. Roses indicate the direction toward which currents flow. Seasons are defined following the meteorological convention (Fall: October-December; Winter: January-March; Spring: April-June; Summer: July-September).

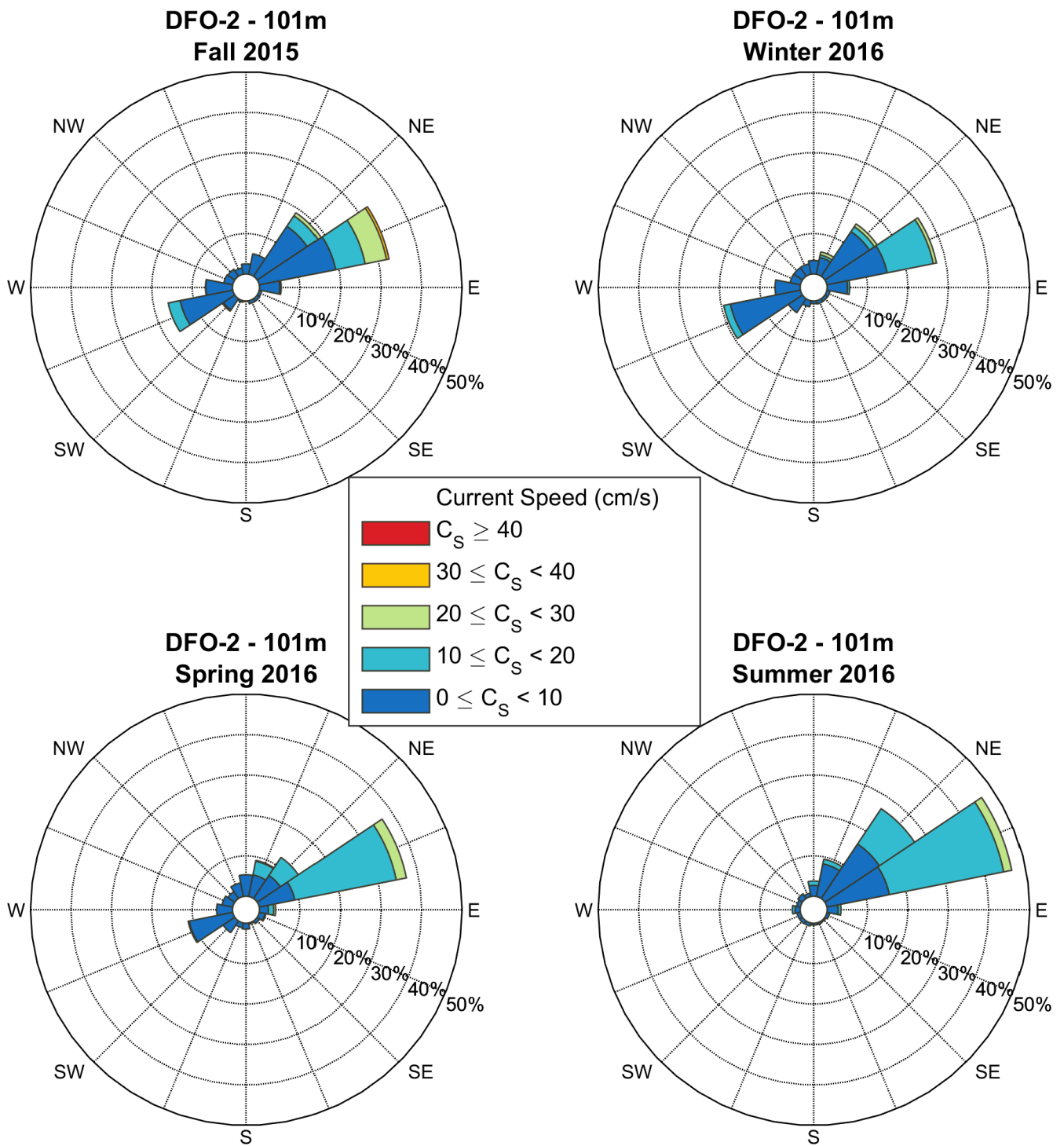


Figure 38: Seasonal current roses at 101 m depth at DFO-2-15 as based on low-pass filtered data from bin cell #1 measured by the NB ADCP #506. Roses indicate the direction toward which currents flow. Seasons are defined following the meteorological convention (Fall: October-December; Winter: January-March; Spring: April-June; Summer: July-September).

3.2.6 Mooring DFO-1

A time-series plot of current speed, direction, and along-slope current component from the NB ADCP deployed at the mid-shelf mooring DFO-1 from 2015 to 2016 is provided in Figure 39. The data in the NB ADCP plot are filtered for bins with PG4 values less than 25%, bins affected by sidelobe interference and for error velocity thresholds and other masks as described in section 2.4.1. The first valid bin depth for the NB ADCP #318 at DFO-1-15 after removing sidelobe interference was 11.1 m (bin cell 10) with 81.5% valid data (Appendix D). Percentage of valid data below the uppermost valid bin depth ranged from 99.1% to 100.0%. No bin depth was manually flagged for this instrument as part of the QA/QC procedure.

Mean current speeds at the mid-shelf site DFO-1-15 is 10 cm/s throughout the water column, with no discernable vertical pattern in current speed intensity (Appendix D, Table 13). Vector-averaged directions are consistently oriented to the south (155-170°TN) at all bin depths. Maximum current speed at this site was 51 cm/s on October 24, 2015, measured in the upper portion of the water column at 11 m depth (Appendix D). This relatively strong current speed event appears to be related to the increase in north-eastward currents observed the mooring.

Seasonal current roses (low-pass filtered) for one bin depth (19 m) in the middle of the water column at mooring DFO-1-15 are provided in Figure 40. These plots show that currents over the mid-shelf are typically weak to moderate (<20 cm/s) and that stronger currents occurred primarily in winter and spring.

DFO-1; NB ADCP 300kHz; 70.3339 N, 133.741 W; 2015-2016; Instr. #464; 51 m depth

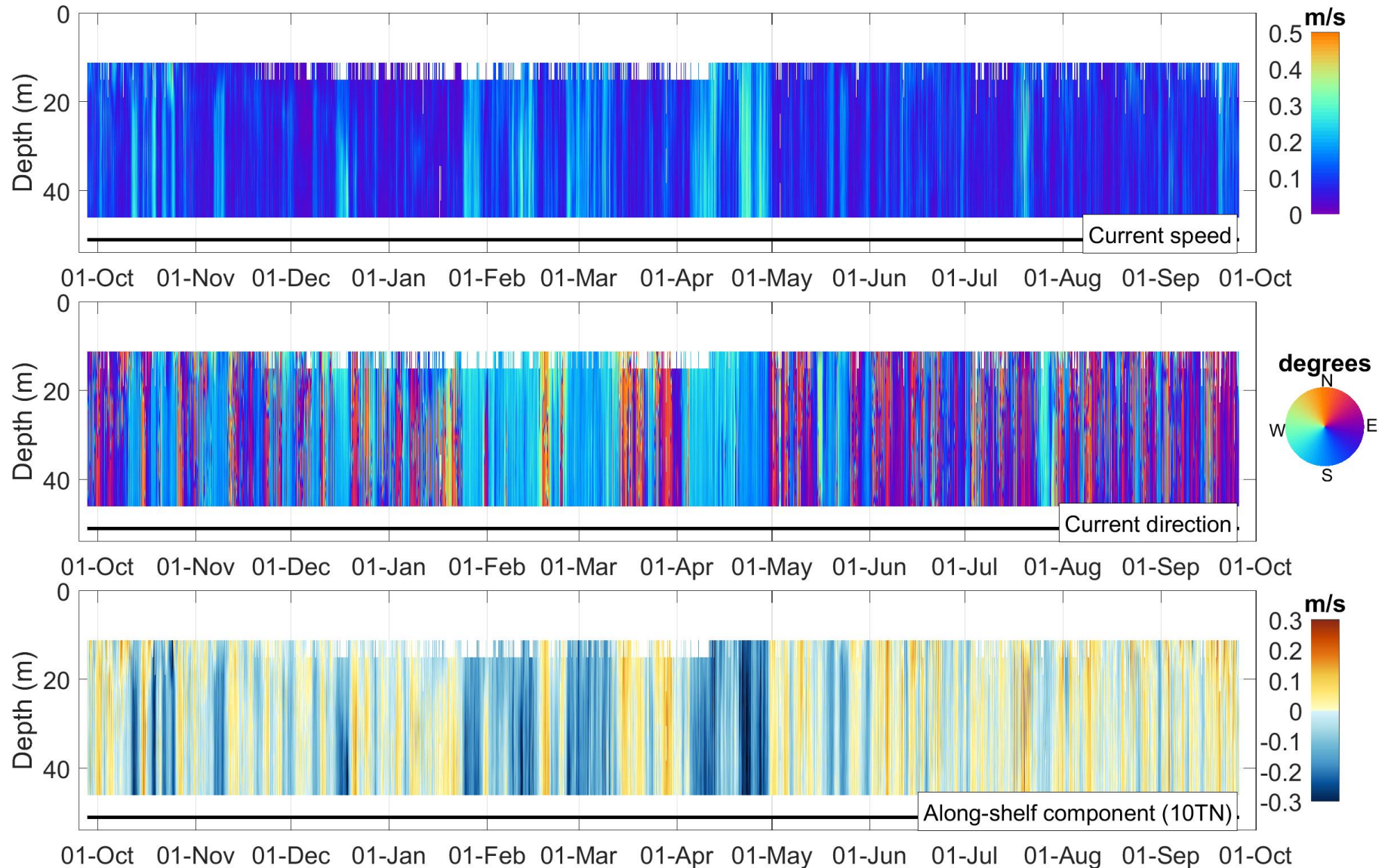


Figure 39: Time-series of current speed, current direction and along-slope current component at mooring DFO-1-15 measured by the NB ADCP #464. The black line depicts the instrument depth.

Table 13: Annual statistics of current speed and direction at DFO-1-15 from a selected bin depth representative of the Polar-mixed layer (see Table 6 for water mass description).

Bin Depth (m)	Median Speed (m/s)	Mean Speed (m/s)	75%ile Speed (m/s)	95%ile Speed (m/s)	99%ile Speed (m/s)	Max Speed (m/s)	Standard Deviation Speed (m/s)	Vector-Averaged Direction (deg TN)
18.9	0.09	0.10	0.13	0.21	0.28	0.40	0.06	171.1

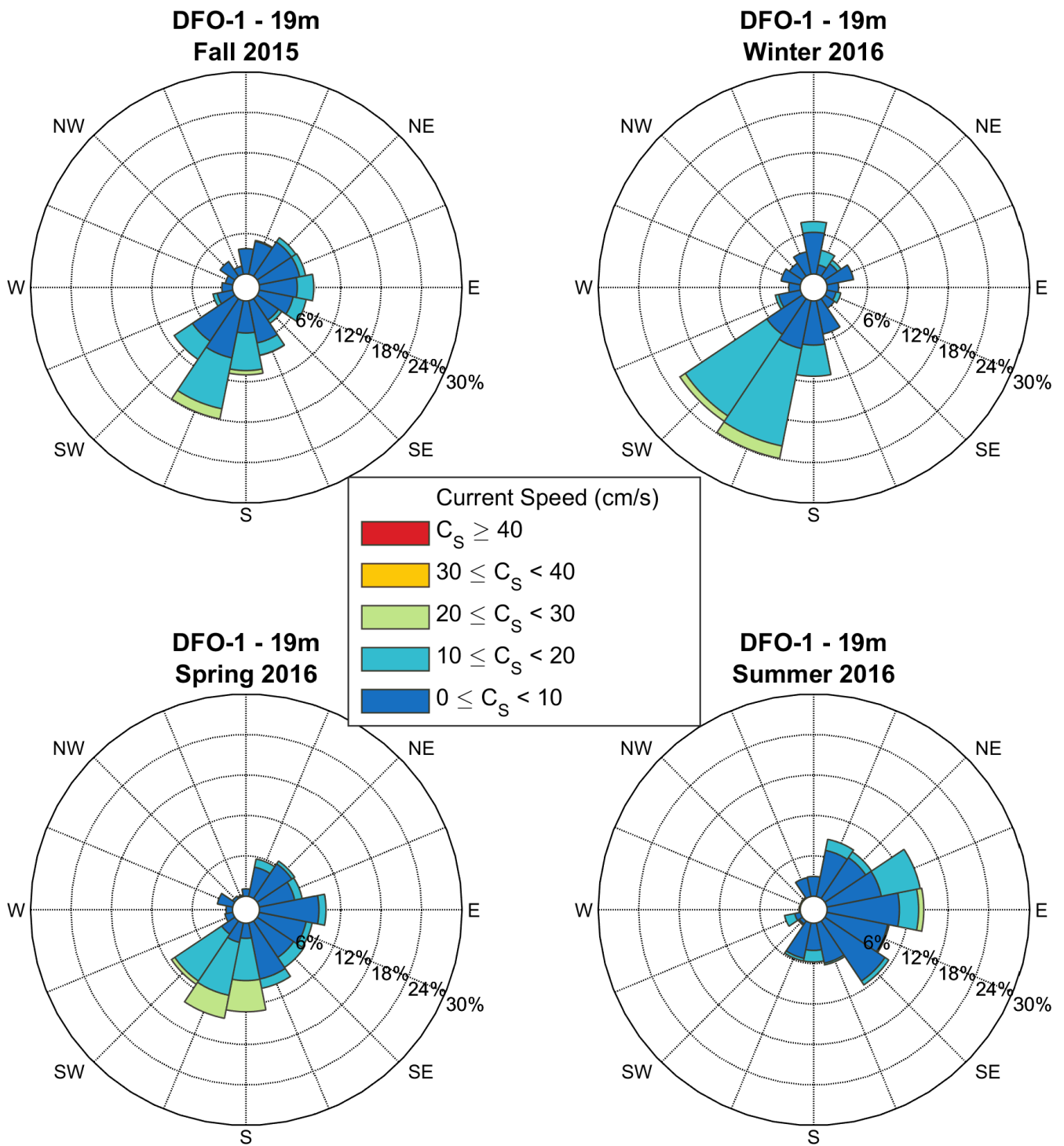


Figure 40: Seasonal current roses at 19 m depth at DFO-1-15 as based on low-pass filtered data from bin cell #8 measured by the NB ADCP #464. Roses indicate the direction toward which currents flow. Seasons are defined following the meteorological convention (Fall: October-December; Winter: January-March; Spring: April-June; Summer: July-September).

3.2.7 Mooring DFO-9

A time-series plot of current speed, direction, and along-slope current component from the WHS ADCP deployed at the inner shelf mooring DFO-9 from 2015 to 2016 is provided in Figure 41. The data in the WHS ADCP plot are filtered for bins with PG4 values less than 25%, bins affected by sidelobe interference and for error velocity thresholds and other masks as described in section 2.4.1. The first valid bin depth for the WHS ADCP #12414 at DFO-9-15 after removing sidelobe interference was 2.8 m (bin cell 26) with a percentage of valid data of 60.7% (Appendix D). Percentage of valid data below the uppermost valid bin depth ranged from 85.8 to 100.0%.

Based on the valid data collected at DFO-9-15, mean current speeds at this site range from 8 to 18 cm/s throughout the water column, with the stronger mean currents typically near the surface (Table 14, Appendix D). Vector-averaged directions were all in the south-western quadrant (200-270°TN) from 2.8 to 27.8 m depth with a minor change in direction with depth from west toward the south. Maximum current speed at DFO-9-15 was 100 cm/s on October 1, 2015 at the uppermost depth bin (2.8 m). The direction of this strong current was to the west-northwest. Current speeds were also strong (>30 cm/s) around July 19-21, 2016. A similar event was also measured at mooring BR-K, BR-G, and DFO-1. At DFO-2, intensified currents in the lower water column were measured beginning July 20, 2016 (Figure 36), slightly delayed from the event measured at the previously mentioned moorings.

Seasonal current roses (low-pass filtered) for one bin depth (21 m) at mooring DFO-9-15 are provided in Figure 42. The rose plots show that currents over the inner-shelf are typically weak to moderate (<30 cm/s) and bi-directional, orientated along the shelf break. The strongest currents (>30 cm/s) were measured in fall 2015.

DFO-9; WHS 300 307200kHz; 70.0589 N, 133.7154 W; 2015-2016; Instr. #12414; 31 m depth

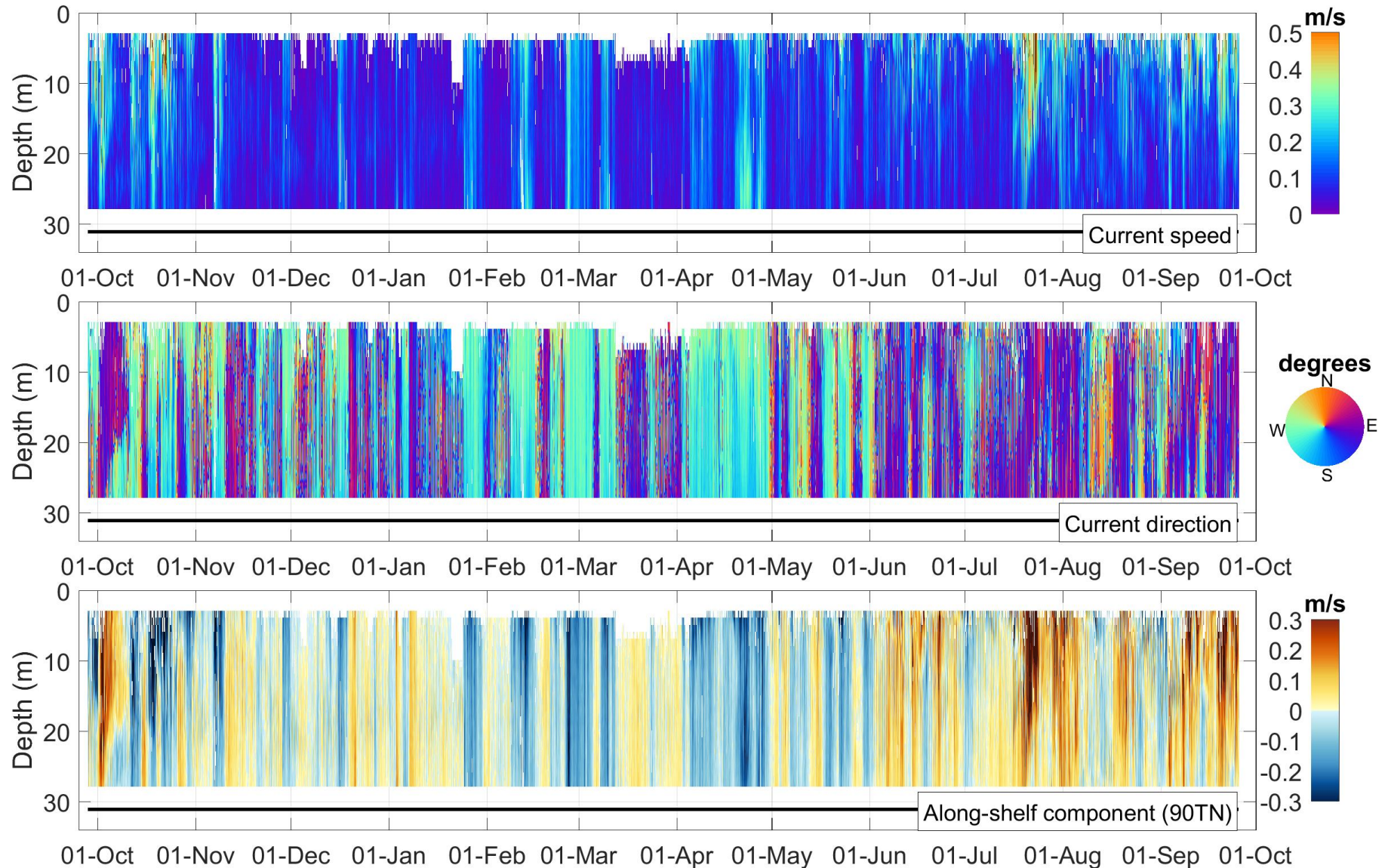


Figure 41: Time-series of current speed, current direction and along-slope current component at mooring DFO-9-15 measured by the WHS ADCP #18414. The black line depicts the instrument depth.

Table 14: Annual statistics of current speed and direction at DFO-9-15 from a selected bin depth representative of the Polar-mixed layer (see Table 6 for water mass description).

Bin Depth (m)	Median Speed (m/s)	Mean Speed (m/s)	75%ile Speed (m/s)	95%ile Speed (m/s)	99%ile Speed (m/s)	Max Speed (m/s)	Standard Deviation Speed (m/s)	Vector-Averaged Direction (deg TN)
20.8	0.09	0.10	0.13	0.22	0.31	0.55	0.06	202.5

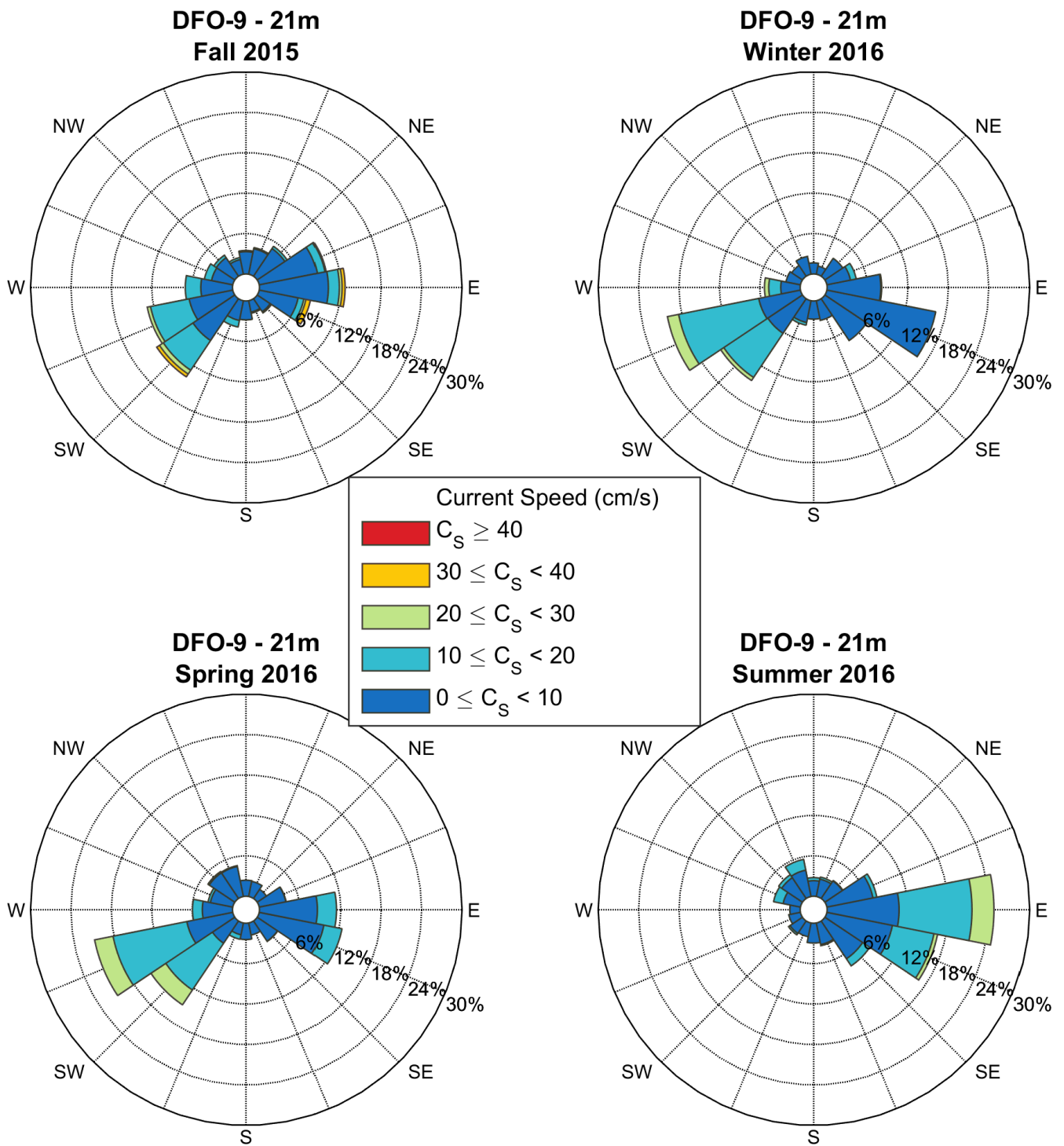


Figure 42: Seasonal current roses at 21 m depth at DFO-9-15 as based on low-pass filtered data from bin cell #8 measured by the WHS ADCP #18414. Roses indicate the direction toward which currents flow. Seasons are defined following the meteorological convention (Fall: October-December; Winter: January-March; Spring: April-June; Summer: July-September).

3.2.8 Spatial Variability of Surface and Bottom Currents in Open Water

Near-surface and near-bottom currents (low-pass filtered) during the open water season (June to October) were mapped as current roses in Figure 43 and Figure 44 to provide an overview of ocean circulation variability during the operational season in the southeastern Beaufort Sea. The analysis is based on data acquired through iBO since 2014, thus comprising data presented as part of the 2015-2016 technical report (ArcticNet et al., 2016). Each map represents current variability during a composite open water season, which is based on the initial (fall) and final (summer) sampling period of a given deployment year. Merging of multi-annual datasets and generation of actual current patterns per year is planned at a later stage of the iBO program as part of the planned State of the Beaufort Sea report (see section 4.3).

The currents roses illustrate that the dominant surface circulation pattern in open water during 2014-2015 at the four BR moorings and at DFO-2 was in accord with the anti-cyclonic (clockwise) motion of the Beaufort Gyre. These moorings provide evidence for the predominance of a south-southwest surface current along the slope and shelf break. By contrast, surface currents in 2015-2016 during open water conditions showed a different pattern, with dominance of northeastward currents at BR-G, BR-K, and DFO-2 and northwestward currents at BR-1. Surface currents at BR-3 were relatively similar in both 2015-2016 and 2014-2015. The currents along the slope of the Mackenzie Shelf showed less directional variability in 2015-2016 than the year before (Figure 43).

The difference in surface current patterns between the two sampling years appears related to the difference in prevailing wind over the western Arctic during the summers of 2015 and 2016 (Figure 45). Average wind conditions in summer 2015 over the entire Beaufort Sea were marked by weak easterlies, which generate surface stress that drives the typical anti-cyclonic circulation of the Beaufort Gyre. By contrast, a deep cyclone dominating the central Arctic Ocean during the summer of 2016 maintained westerly air flow in the Beaufort Sea north of about 71°N (the latitude of DFO-2), confining easterly wind to the Mackenzie and Alaskan shelves. This wind pattern may explain why surface currents were primarily flowing to the west at BR-1, while they were directed to the east at BR-G, -K and DFO-2. Stronger wind speed on the average in 2016 also offers an explanation for the more unidirectional currents patterns seen during this year, especially since the region was particularly ice free in 2016.

Near-bottom currents during summer and fall (Figure 44) showed much less inter-annual variability than surface currents. Near-bottom currents at DFO-2, BR-G, and BR-K were similar to each other in both 2014-2015 and 2015-2016, with a flow predominantly toward the northeast. Reversals to the southwest were however more frequent at BR-K than at DFO-2 and BR-G. Near-bottom currents are also stronger at BR-K than at BR-G and DFO-2 on average, which is related to the shelf-break jet that occupies a narrow 10-15 km corridor on the upper slope. Near-bottom currents at BR-1 and BR-3 during both sampling years follow the bathymetric contours at their respective location, with a dominant flow to the south at BR-1, and a dominant current to the north at BR-3 near Banks Island. More frequent stronger currents (>10 cm) were measured near the bottom at BR-3 when compared to BR-1.

On the mid- to inner shelf at DFO-2 and DFO-9, surface and near-bottom circulation during the open water season was relatively weak and variable during both 2014-2015 and 2015-2016. More frequent currents to the east-southeast along the bathymetric contours toward the coast were measured throughout the water column during both years. Currents at these locations thus appear to be less driven by surface wind patterns than at the other iBO mooring locations. This may be related to the presence of a coastal current primarily driven by buoyancy gradients likely triggered by the Mackenzie River run-off. The interplay between wind, river discharge and circulation patterns remains however to be better investigated to confirm any primary forcing factor at these locations.

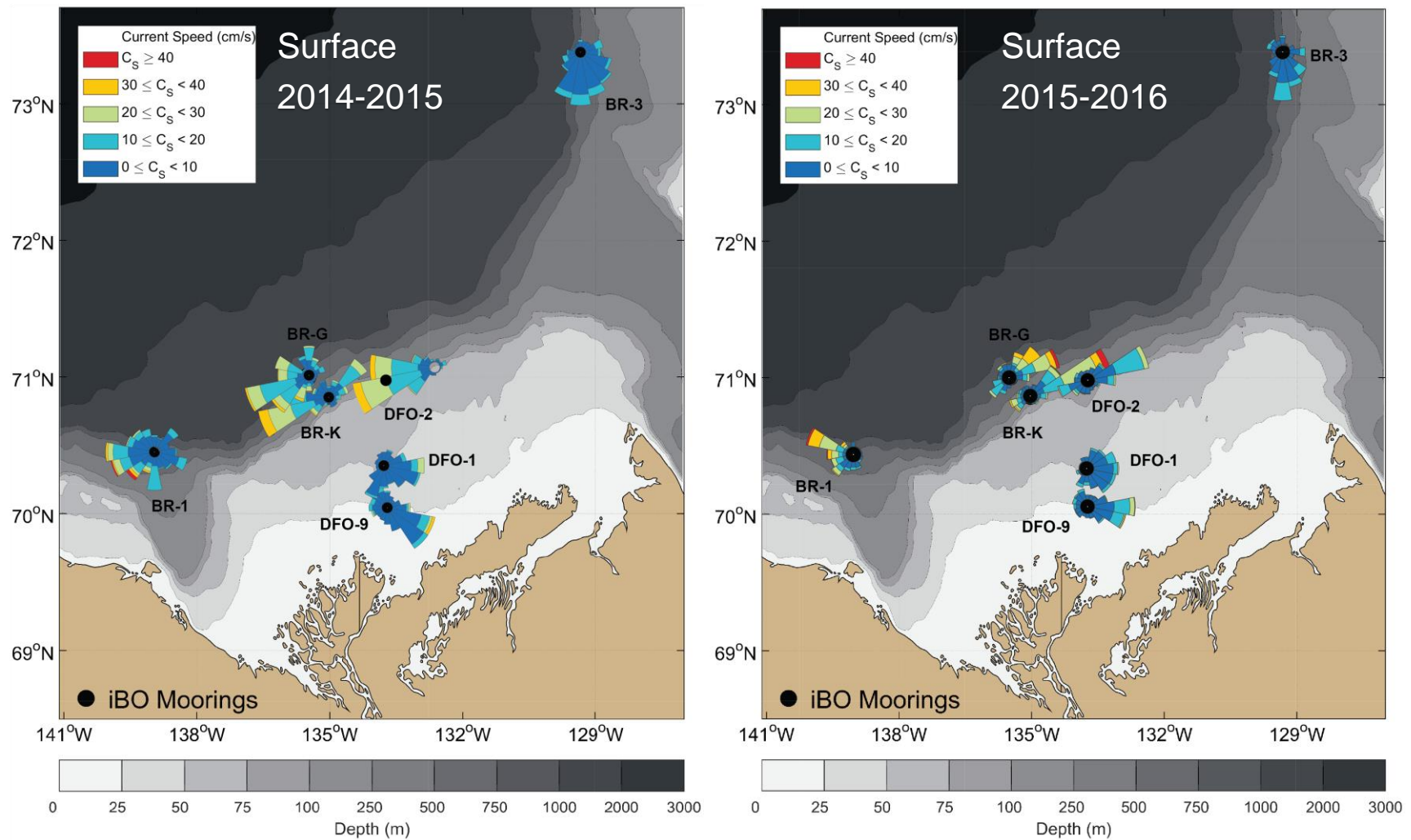


Figure 43: Near-surface currents for the open water season for low-pass filtered current velocity data from the bin depth nearest bin depth to 50 m at all moorings except DFO-1 and DFO-9 which are closest to a bin depth of 20 m. Data when sea ice was present (winter-spring) were filtered out. Roses indicate toward where the current is flowing.

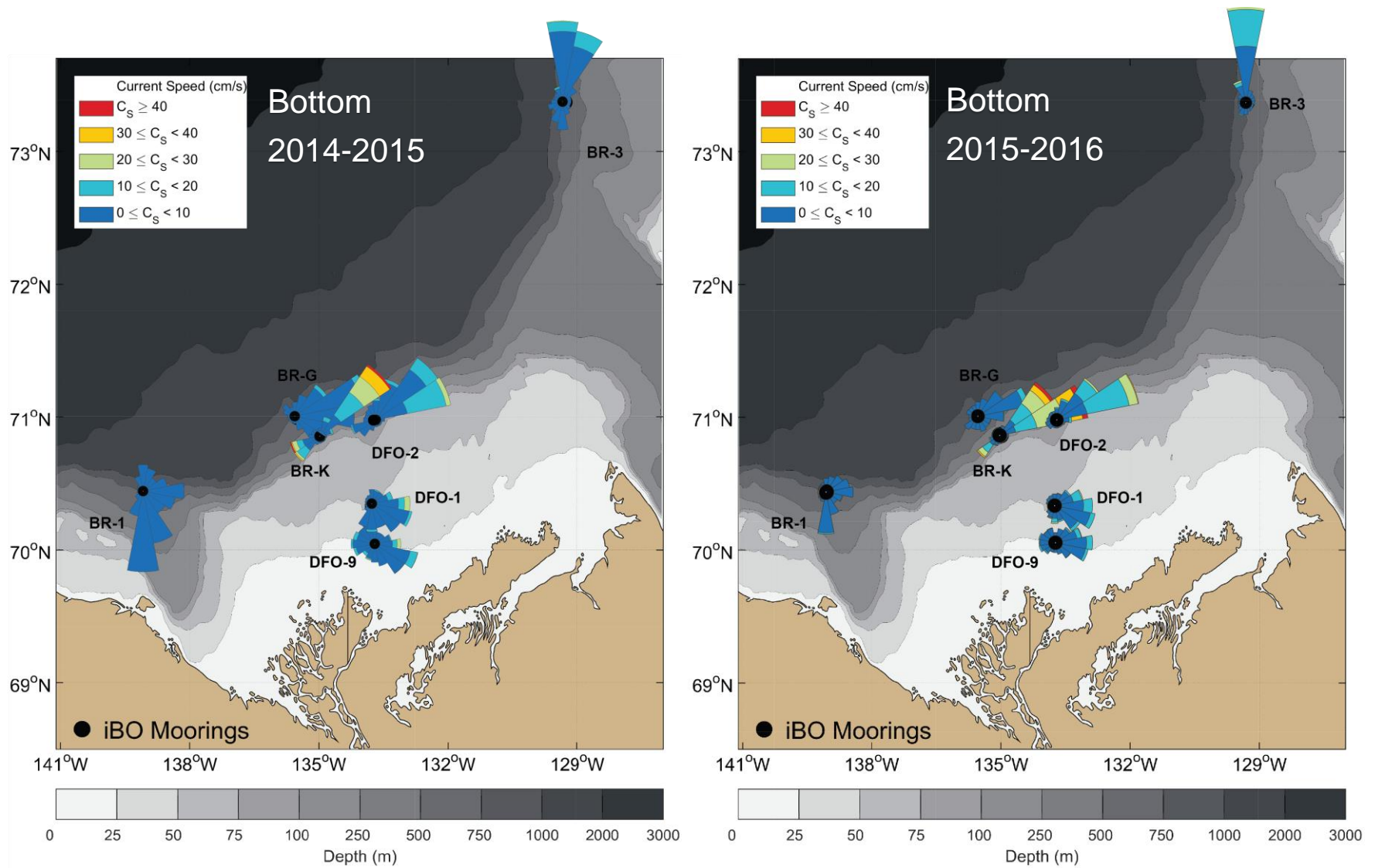
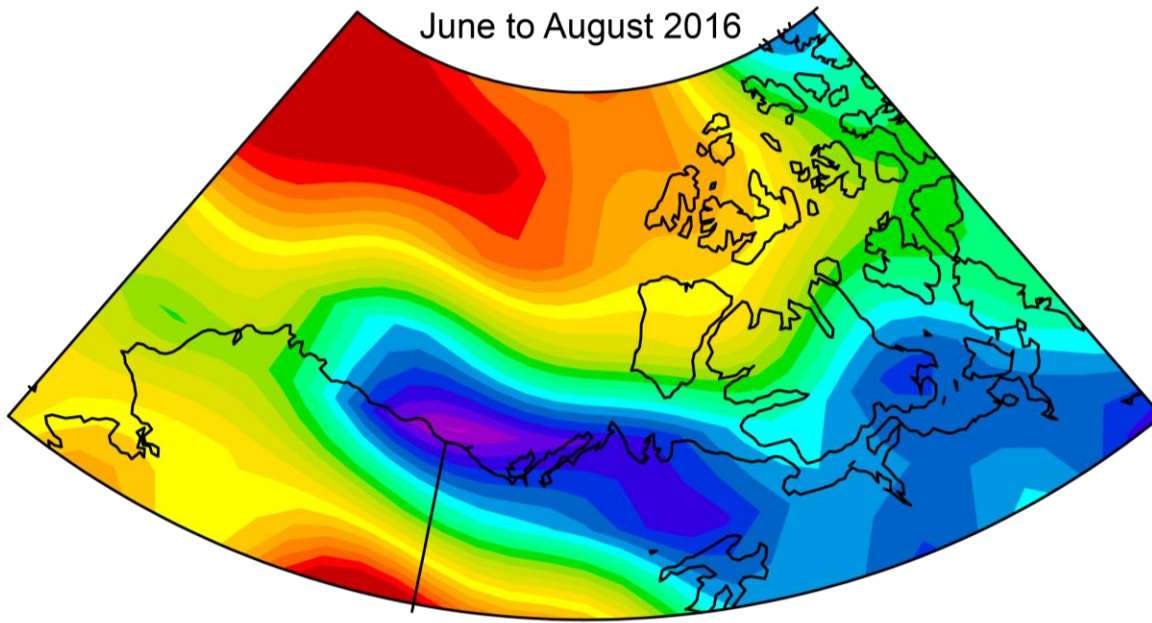
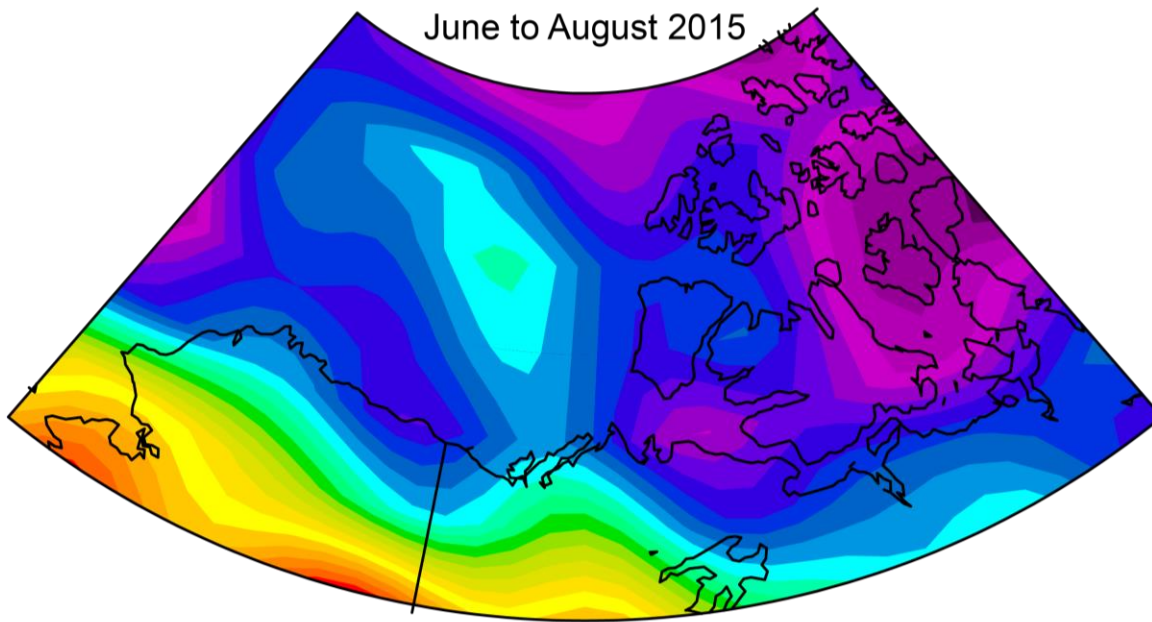


Figure 44: Near-bottom currents for the open water season for low-pass filtered current velocity data from the bin depth nearest to bottom at each location. Data when sea ice was present (winter-spring) were filtered out. Roses indicate toward where the current is flowing.



Mean zonal wind in m/s [positive is westerly; negative is easterly]

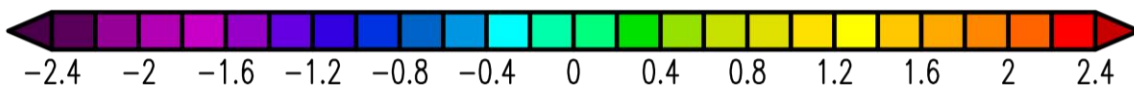


Figure 45: Surface zonal wind composite in summer 2015 and 2016 (June to August) in the western Arctic as based on NCEP/NCAR reanalysis data. Following the NCEP convention, positive values indicate westerly wind, whereas negative values indicate easterly wind (data source: <https://www.esrl.noaa.gov/psd/data/composites/hour/>)

3.3 Temperature and Salinity

The summary of CT logger data recovery success on iBO moorings from 2015 to 2016 is provided in Table 15. A summary of valid and flagged data (suspicious spikes) for each processed CT sensor is provided in Table 16 for the BR moorings. Statistics are not presented for the DFO moorings due to differences in the QA/QC processing methodology.

Processed temperature and salinity data from all CT loggers deployed on BR moorings from 2015 to 2016 are presented using time-series plots of temperature and salinity at each mooring. Temperature time-series recorded at moorings BR-1, BR-3, BR-G and BR-K are presented in Figure 46 through Figure 49. Salinity time-series for the same moorings are provided in Figure 51 through Figure 54. Temperature and salinity time-series for DFO moorings are combined into two plots in Figure 50 and Figure 55. Data from temperature-salinity time-series presented below were filtered for spike-like values that were detected using the method described in section 2.4.2. Missing data were replaced by linearly-interpolated values in the time-series plots. A temperature-salinity diagram is also provided in Figure 56, which combines all QA/QC data from the moored CT loggers (also filtered for spikes, but not interpolated for missing values) as well as water column profile data from CTD casts conducted at mooring deployment in 2015 aboard the Amundsen and Laurier.

The temperature time-series recorded at discrete depths varying from 32 to 762 m on the slope illustrate the typical vertical layering in temperature in the Beaufort Sea (e.g. Lansard et al. 2012 and references therein), although marked temporal variability was observed, especially at BR-G (Figure 48) and BR-1 (Figure 46). Temperature was most variable in the upper 200 m of the water column, with temperature varying from around 0°C down to around -1.8°C with the exception of the shelf mooring DFO-9 which varies from -1.8°C to as warm as 4.2°C in summer 2016. Rapid transitions from relatively cold to relatively warm (and vice-versa) temperature were often detected in the upper 200 m. For example, a sudden increase from -1.3 to 2°C was recorded at 36 m at BR-3 in late July 2016 (Figure 47). This sudden increase occurred when sea ice coverage was still around 50% at the BR-3 location (Figure 3) and is even more pronounced than the temperature increase measured at the same depth at BR-G to the south in late summer (~1°C; Figure 48).

At BR-K near the bottom on the upper slope, approximately five notable increases in temperature (from -1.4 to 0.4°C) were measured at 151 m from September 2015 to May 2016; each fluctuation occurring over 1 to 2 week intervals and may correspond to upwelling events (see below). At BR-1 a concomitant increase in temperature (of 1 to 1.5°C) was also measured at the three CT sensors in the upper 200 m of the water column over a one-week interval in mid-December (Figure 46). This event of short duration appears to correspond to the passage of an eddy-like feature over the mooring.

Likewise temperature, salinity time-series showed that most of the variability in terms of water mass physical properties occurs in the upper 200 m (Figure 51 through Figure 54). Contrary to temperature, salinity is monotonically increasing with depth in the Beaufort Sea. Over the slope in 2015 to 2016, salinity from 450 to 760 m depth occupied a very narrow range from 34.8 to 34.9, while salinity in the upper 200 m ranged from 28 (DFO-9, 32 m in October 2015) up to 34.8 (BR-K, 151 m in late April 2015). The rapid increase in salinity and temperature observed at the upper slope mooring BR-K over five different intervals from September 2015 through May 2016 (Figure 54) is likely a sign of upwelling of deep waters taking place at the shelf break. The general trend of negative along-slope current component observed at moorings BR-K and DFO moorings at the same intervals is also consistent with upwelling conditions. Similarly, salinity increases were also observed at BR-1 in mid-December concurrent with increases in temperature at the same depth, with the exception of the surface CT sensor (62 m) which recorded a simultaneous decrease in salinity. Currents at BR-1 during this interval are cross-slope to the north, consistent with upwelling conditions.

The temperature-salinity diagram combining all data from the CT loggers provides a further way to characterize the different water masses occupying the water column at mooring locations from 2015 to 2016 (Figure 56). This diagram provides evidence that most of the variability in the water column is taking place in the upper 200 m. It also illustrates that all datasets from CT sensors deployed in the upper 100 m contain at least some periods when seawater was near the freezing point (as a result of winter processes). The visual comparison between CTD cast data from 2015 and the moored CT sensor data provides a preliminary assessment of the accuracy of the CT sensor data. Instruments in the upper 200 m did not appear to be affected by any visible bias given their consistency with respect to the freezing line and the expected variability in the shape of the halocline (i.e. between ~32.0 and 34.7 salinity) that changes over time due to upwelling/downwelling and other mixing processes.

The deeper CT logger instruments (>400 m) did show some offset with respect to the CTD cast data collected in 2015. A zoom on the narrow domain of the temperature-salinity variability in the lower portion of the Atlantic water mass is shown in Figure 57. These instruments were visually corrected to the CTD cast data to address individual instrument-specific offsets or miscalculation in the relationship linking pressure to conductivity and potential temperature. It should be noted that the RBR CT loggers do not include an integrated pressure sensor. Depth of RBR CT sensors needs to be estimated on the basis of other nearby instruments which is a likely a source of the observed biases.

Table 15: Summary of CT data logger clock drift and percentage of raw data return on iBO moorings from 2015 to 2016.

Mooring	Instrument	Serial number	Depth (m)	Clock Drift (mm:ss)	First Good Record (UTC)	Last Good Record (UTC)	Raw Data Return (%)
BR-1-15	RBR XR420 CT	15262	62.1	01:01 slow	Sep-30-2015 22:40:00	Sep-01-2016 15:50:00	100%
BR-1-15	RBR XR420 CT	15268	130.0	01:15 fast	Sep-30-2015 22:40:00	Sep-01-2016 15:50:00	100%
BR-1-15	RBR XR420 CT	15279	182.0	01:45 fast	Sep-30-2015 22:40:00	Sep-01-2016 15:50:00	100%
BR-1-15	RBR XR420 CT	15267	461.0	00:41 fast	Sep-30-2015 22:40:00	Sep-01-2016 15:50:00	100%
BR-1-15	RBR Concerto CTD	60270	762.0	00:09 slow	Sep-30-2015 22:40:00	Sep-01-2016 15:50:00	100%
BR-3-15	RBR XR420 CT	15270	36.0	00:33 slow	Aug-31-2015 22:20:00	Sep-07-2016 22:00:00	100%
BR-3-15	RBR XR420 CTD	17351	104.6	00:38 fast	Aug-31-2015 22:20:00	Sep-07-2016 22:30:00	100%
BR-3-15	RBR XR420 CT	15269	173.7	00:28 fast	Aug-31-2015 22:20:00	Sep-07-2016 22:00:00	100%
BR-3-15	RBR XR420 CT	15272	448.7	00:36 fast	Aug-31-2015 22:20:00	Sep-07-2016 22:00:00	100%
BR-3-15	RBR XR420 CT	15278	685.2	09:55 slow	Aug-31-2015 22:20:00	Sep-07-2016 22:00:00	100%
BR-G-15	RBR XR420 CT	15273	34.5	00:55 fast	Aug-28-2015 19:00:00	Sep-01-2016 0:00:00	100%
BR-G-15	RBR XR420 CT-Tu-DO	10419	106.4	01:20 fast	Aug-28-2015 19:30:00	Sep-01-2016 0:00:00	100%
BR-G-15	RBR XR420 CT	15258	162.7	01:06 fast	Aug-28-2015 19:00:00	Sep-01-2016 0:00:00	100%
BR-G-15	RBR XR420 CT	15266	454.7	00:27 fast	Aug-28-2015 19:00:00	Sep-01-2016 0:00:00	100%
BR-K-15	RBR XR420 CT-Tu-DO-FI	22043	150.8	00:51 fast	Aug-27-2015 15:00:00	Sep-01-2016 2:00:00	100%
DFO-2-15	SBE37 CTD	05081	106	00:00	Sep-26-2015 23:45:00	Sep-30-2016 14:45:00	100%
DFO-1-15	SBE37 CTD	06764	50.2	00:06 slow	Sep-27-2015 17:00:00	Sep-25-2016 20:00:00	100%
DFO-9-15	SBE37 CTD	06759	32.1	00:01 fast	Sep-27-2015 22:00:00	Sep-25-2016 16:45:00	100%

Table 16: Summary of valid and flagged data from CT loggers deployed on the BR slope moorings from 2015 to 2016. See Table 15 for the instrument model associated with each serial number.

Mooring	Serial number	Depth (m)	Number of Valid Conductivity Records	Number of Flagged Conductivity Records	% of Valid and Un-flagged Conductivity Records (%)	Number of Valid Temperature Records	Number of Flagged Temperature Records	% of Valid and Un-flagged Temperature Records (%)
BR-1-15	15262	62.1	48,488	10	100.0%	48,488	2	100.0%
BR-1-15	15268	130.0	17,905	7	100.0%	17,905	22	100.0%
BR-1-15	15279	182.0	53,169	7	100.0%	53,169	8	100.0%
BR-1-15	15267	461.0	48,361	151	99.7%	48,361	22	99.7%
BR-1-15	60270	762.0	53,169	9	100.0%	53,169	4	100.0%
BR-3-15	15270	36.0	48,488	17	100.0%	48,488	4	100.0%
BR-3-15	17351	104.6	48,488	7	100.0%	48,488	119	100.0%
BR-3-15	15269	173.7	26,858	8	100.0%	26,858	7	100.0%
BR-3-15	15272	448.7	26,858	22	99.9%	26,858	63	99.9%
BR-3-15	15278	685.2	26,858	49	99.8%	26,858	42	99.8%
BR-G-15	15273	34.5	53,169	9	100.0%	53,169	19	100.0%
BR-G-15	10419	106.4	26,858	9	100.0%	26,858	4	100.0%
BR-G-15	15258	162.7	48,488	7	100.0%	48,488	7	100.0%
BR-G-15	15266	454.7	53,169	8	100.0%	53,169	3	100.0%
BR-G-15	15280	690.8	8,892	7	99.9%	8,892	7	99.9%
BR-K-15	22043	150.8	17,722	12	99.9%	17,722	107	99.9%

Note: The percentage of valid data is based on the total number of records returned by the instrument from deployment to recovery. Data from DFO moorings are not presented here due to the difference in methodology for data processing.

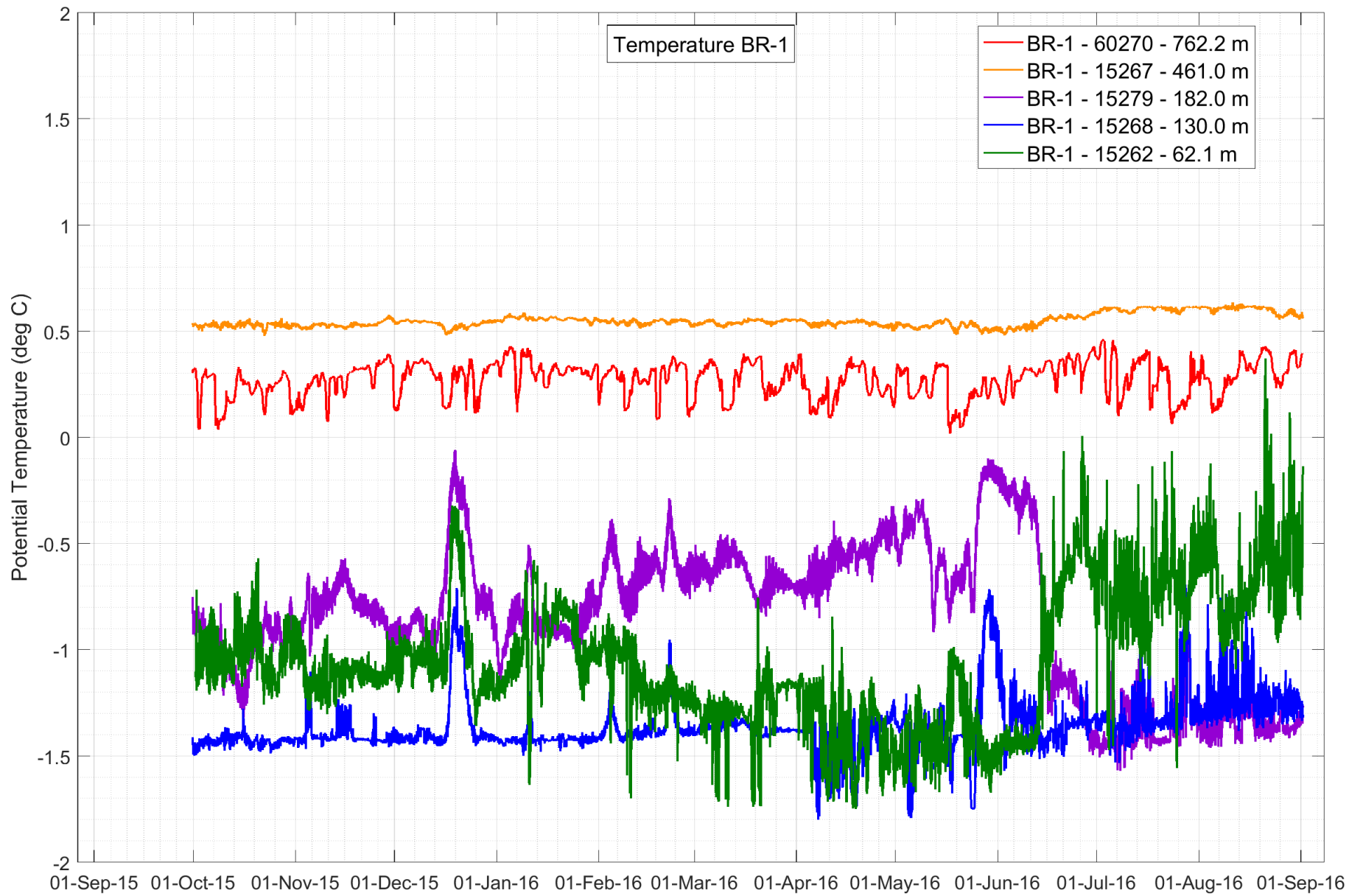


Figure 46: Temperature time-series measured at BR-1-15 from 2015 to 2016. The legend shows the serial number and depth of each CT logger.

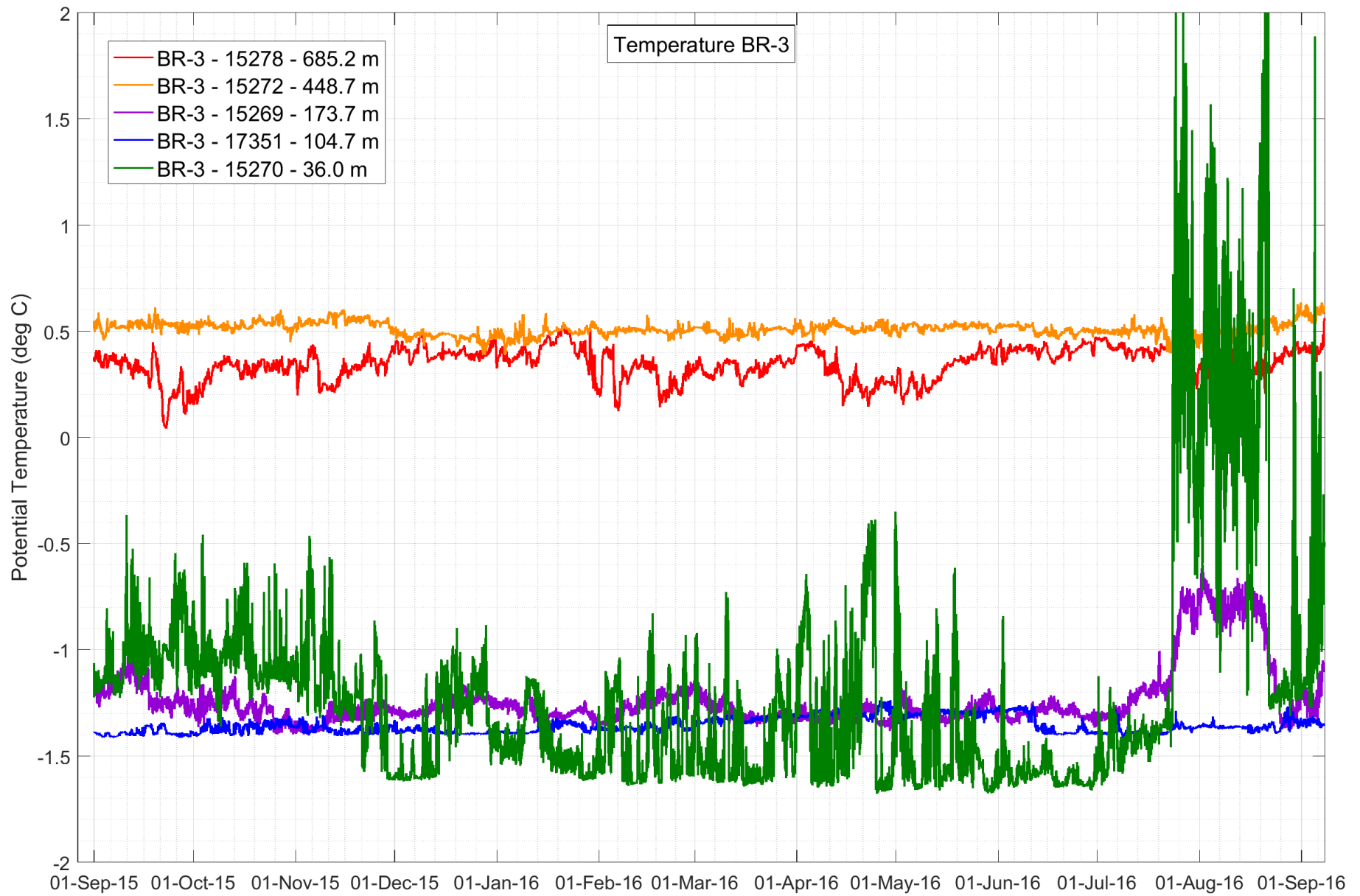


Figure 47: Temperature time-series recorded at BR-3-15 from 2015 to 2016. The legend shows the serial number and depth of each CT logger.

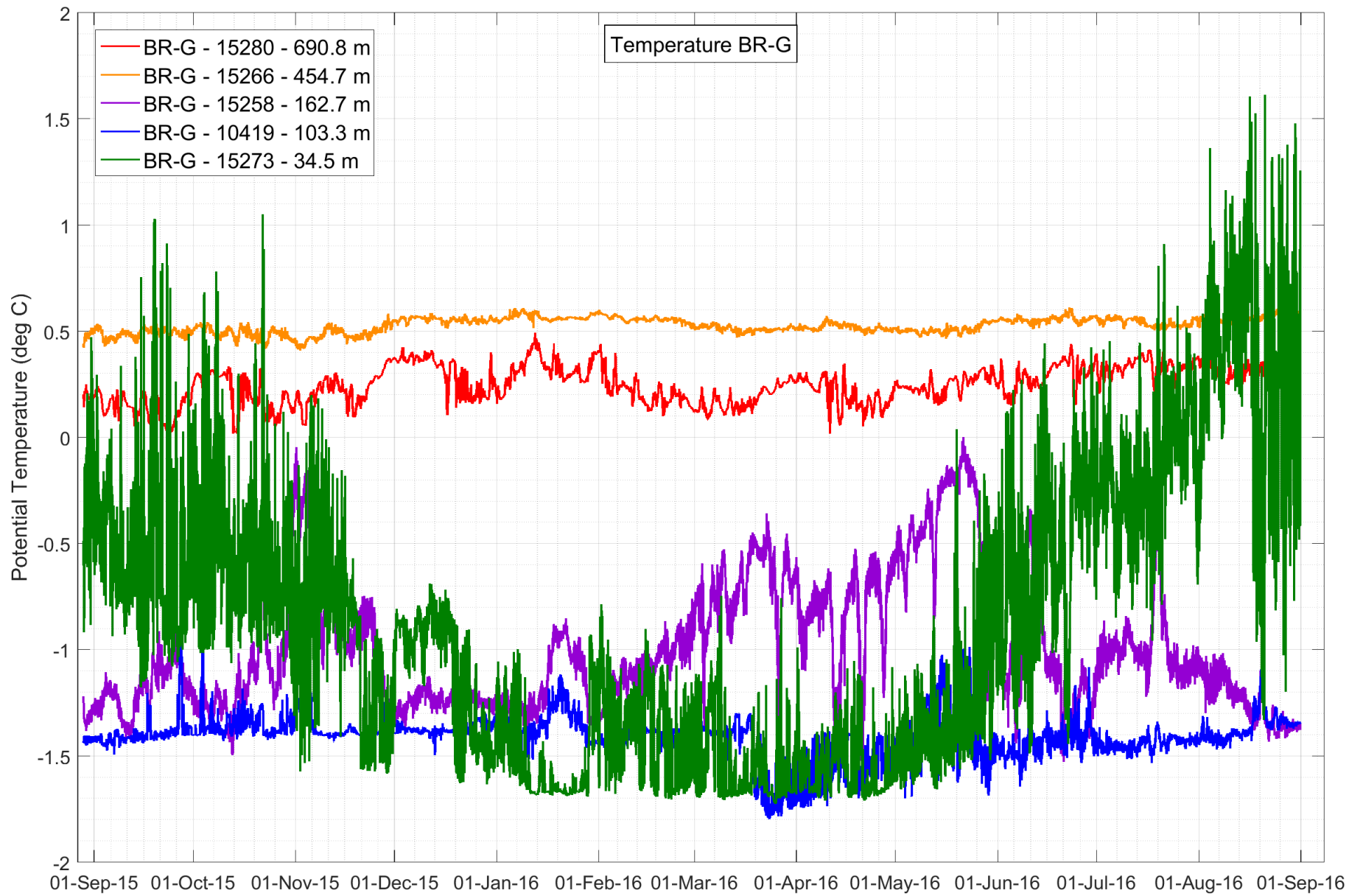


Figure 48: Temperature time-series recorded at BR-G-15 from 2015 to 2016. The legend shows the serial number and depth of each CT logger.

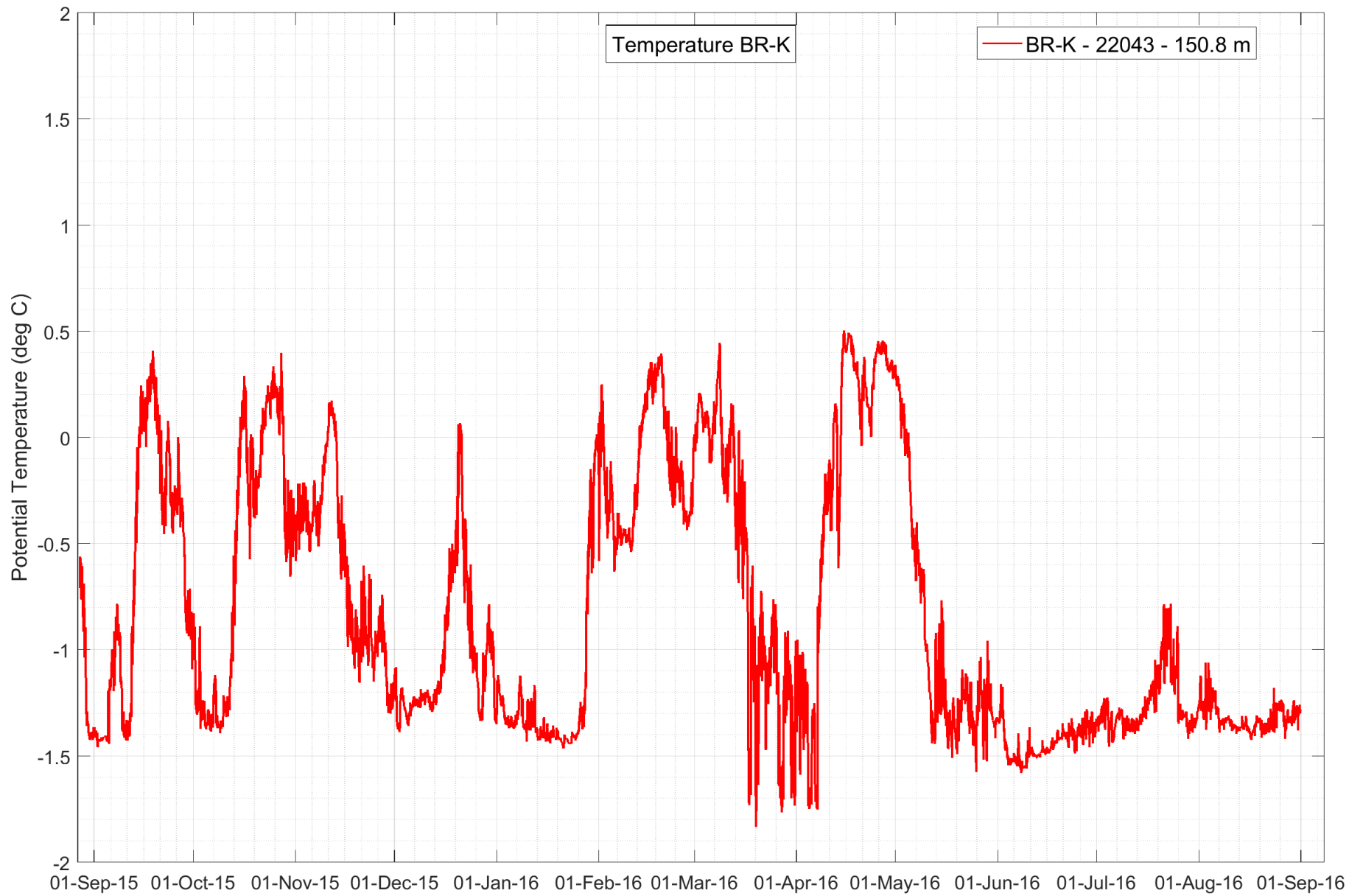


Figure 49: Temperature time-series recorded at BR-K-15 from 2015 to 2016. The legend shows the serial number and depth of each CT logger.

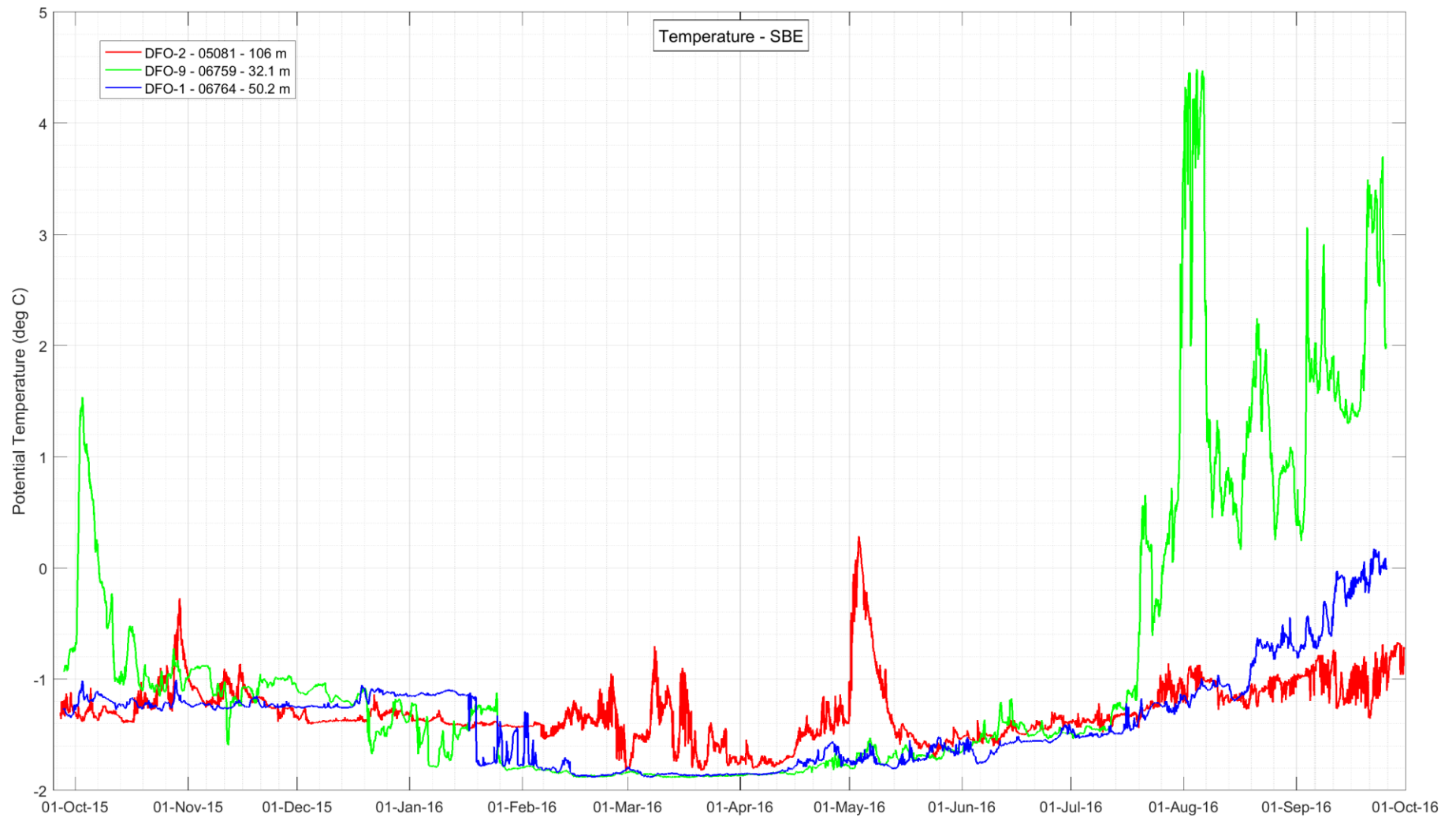


Figure 50: Temperature time-series recorded at DFO-2-15, DFO-1-15, and DFO-9-15 from 2015 to 2016. The legend shows the serial number and depth of each CT logger.

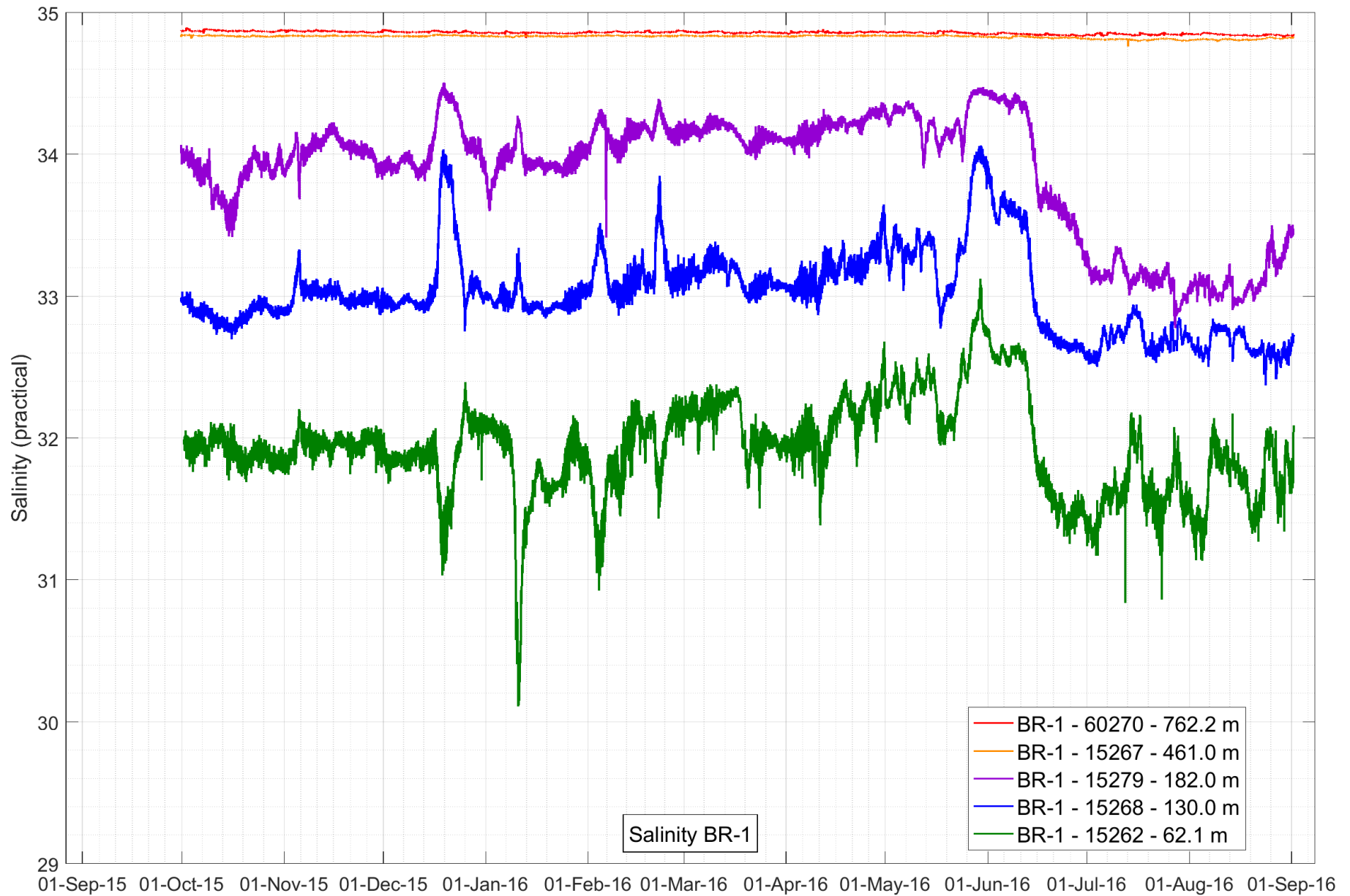


Figure 51: Salinity time-series recorded at BR-1-15 from 2015 to 2016. The legend shows the serial number and depth of each CT logger.

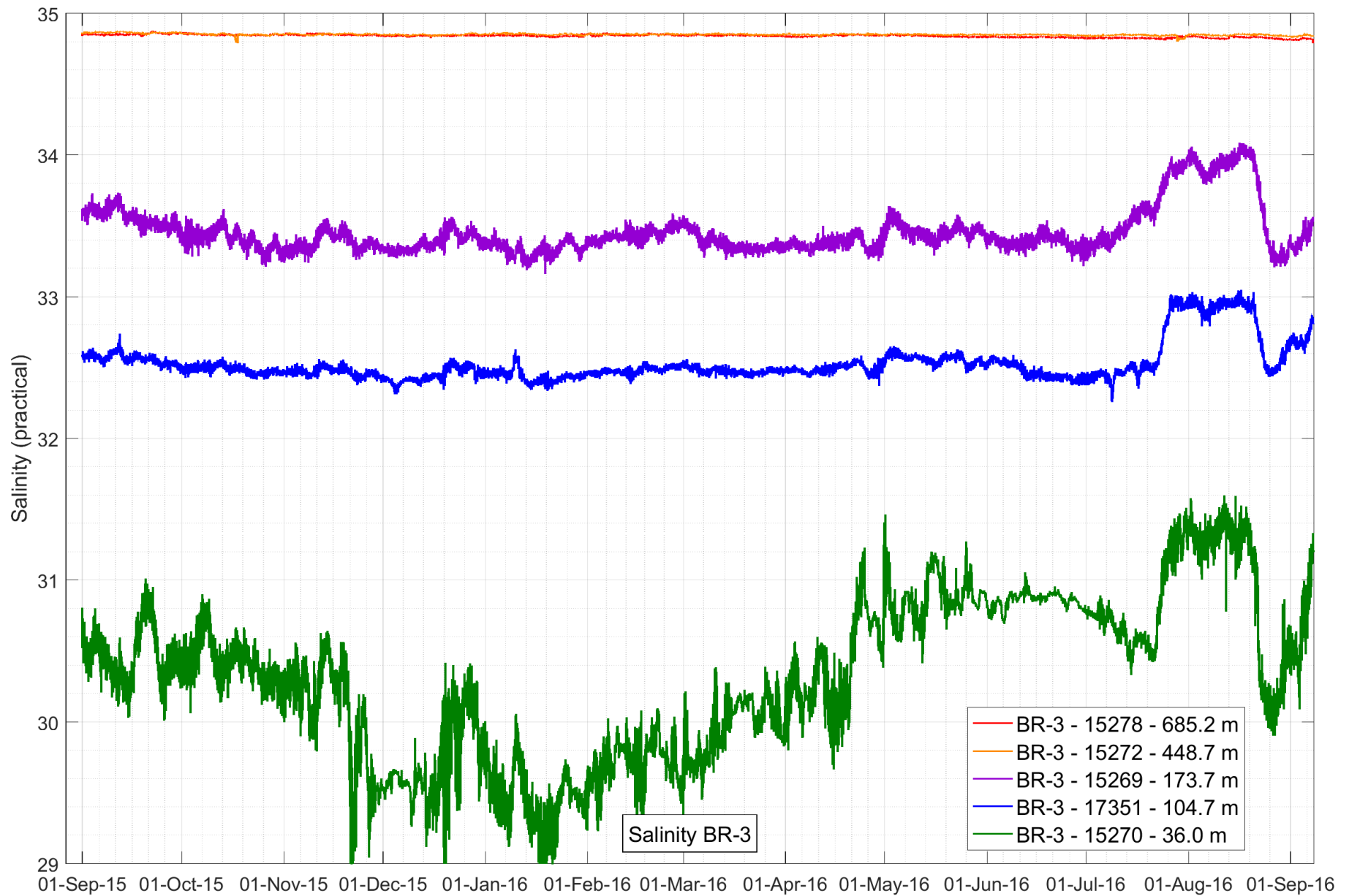


Figure 52: Salinity time-series recorded at BR-3-15 from 2015 to 2016. The legend shows the serial number and depth of each CT logger.

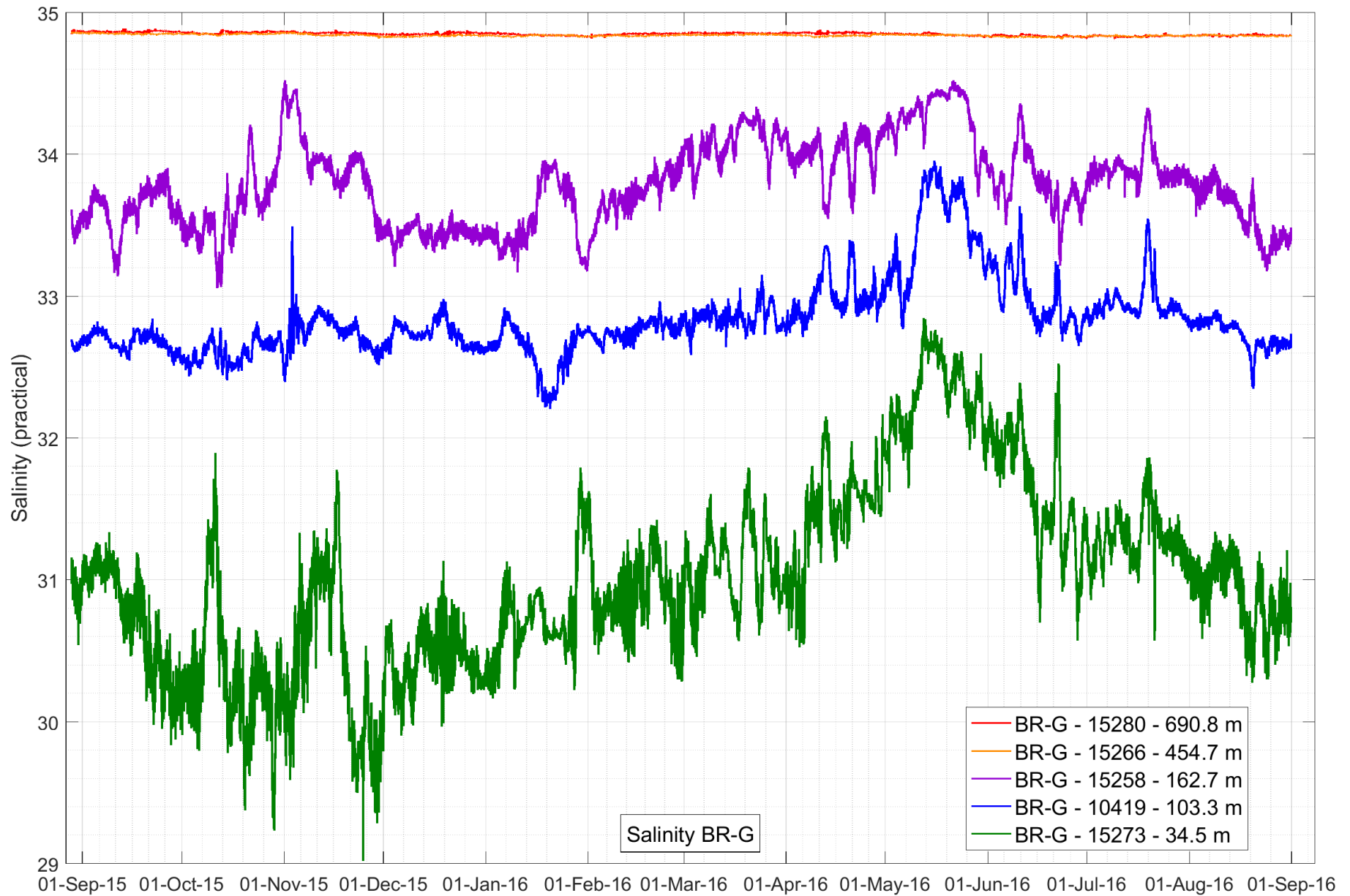


Figure 53: Salinity time-series recorded at BR-G-15 from 2015 to 2016. The legend shows the serial number and depth of each CT logger.

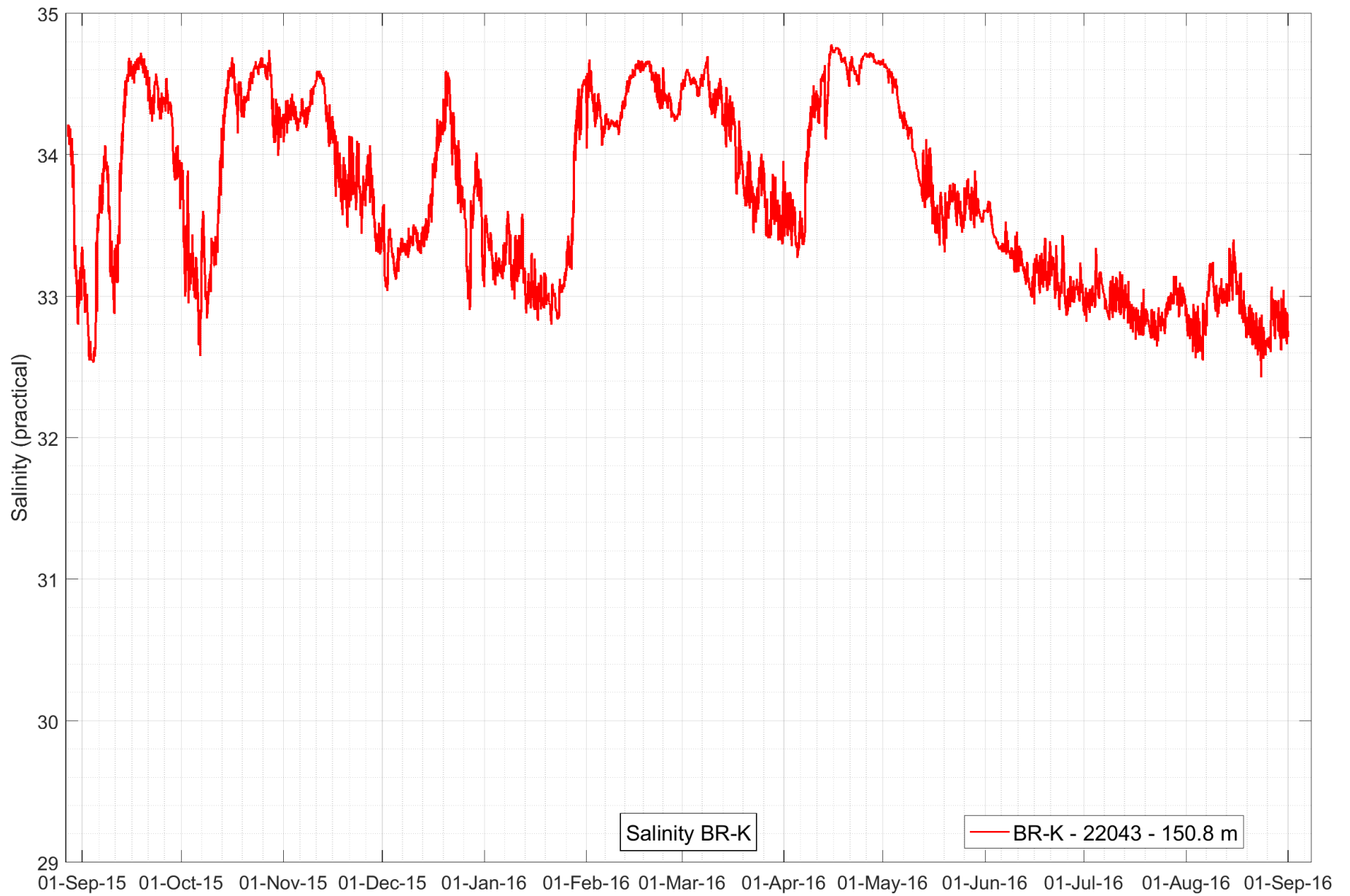


Figure 54: Salinity time-series recorded at BR-K-15 from 2015 to 2016. The legend shows the serial number and depth of each CT logger.

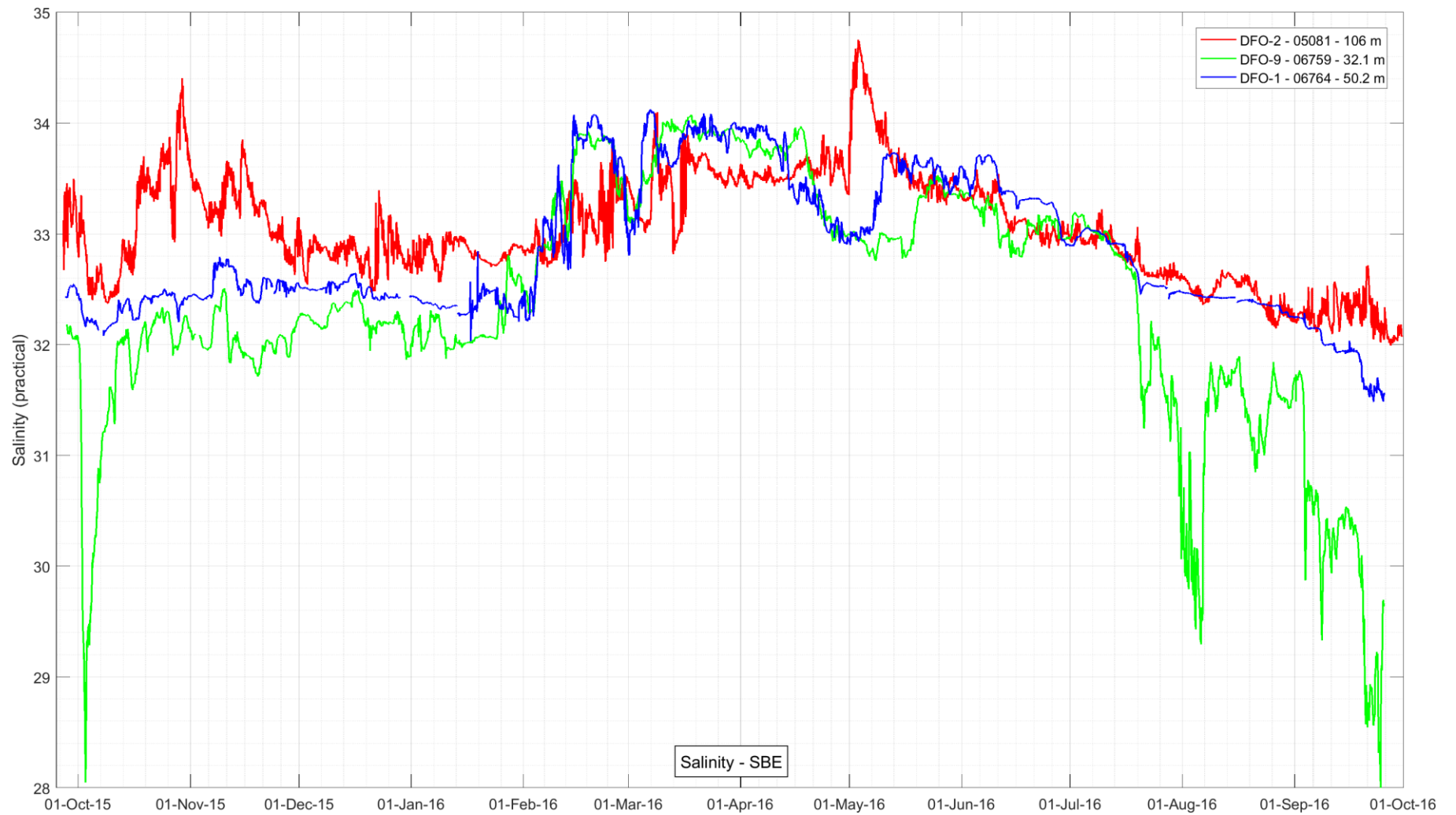


Figure 55: Salinity time-series recorded at DFO-2-15, DFO-1-15, and DFO-9-15 from 2015 to 2016. The legend shows the serial number and depth of each CT logger.

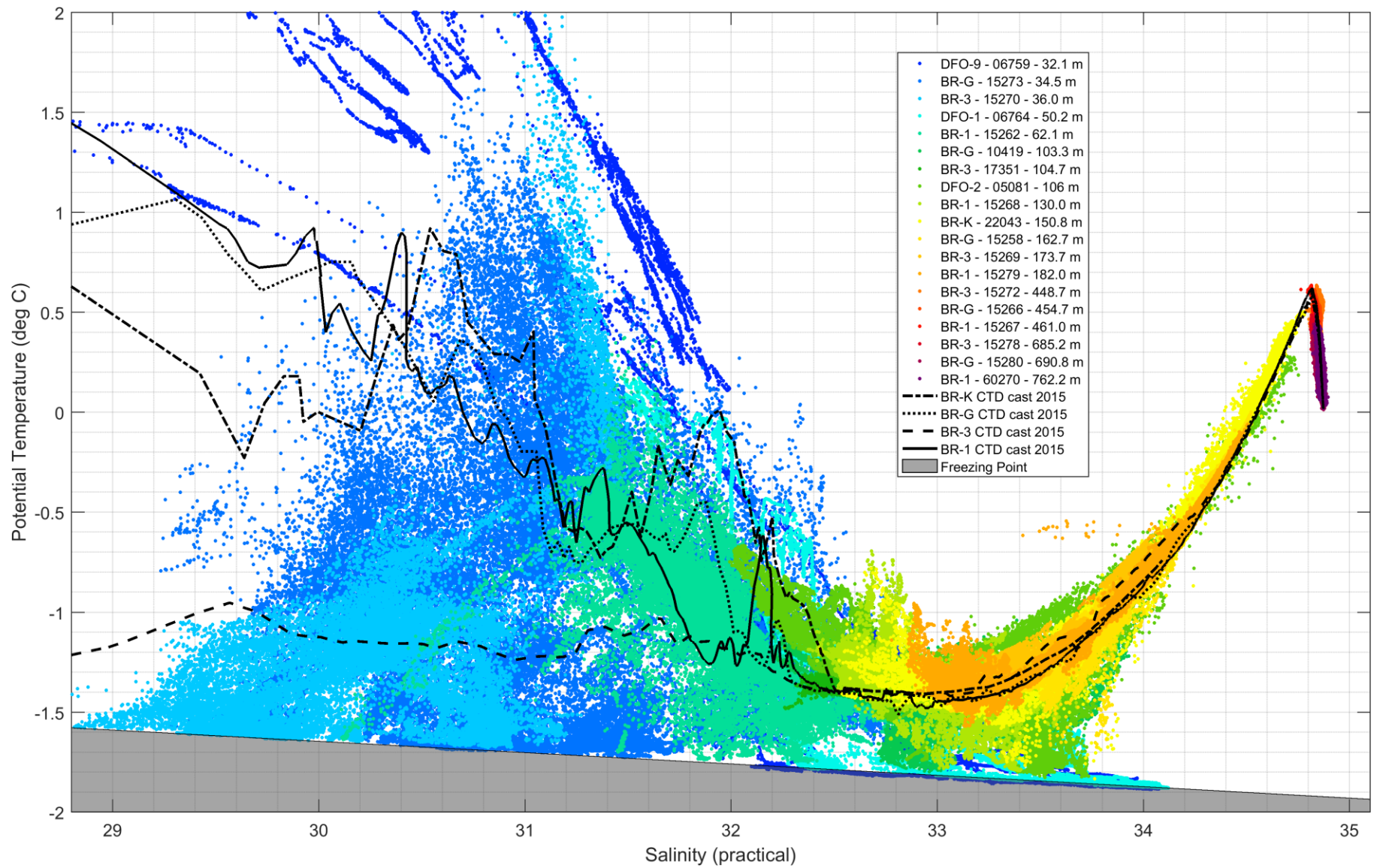


Figure 56: Temperature-salinity diagram constructed upon all data acquired with the CT loggers attached to the moorings BR-1, BR-3, BR-G, BR-K, DFO-2, DFO-1, and DFO-9 from 2015 to 2016. CTD profile data taken at mooring locations during the CCGS Amundsen and Laurier cruises in 2015 are depicted by the 4 black lines.

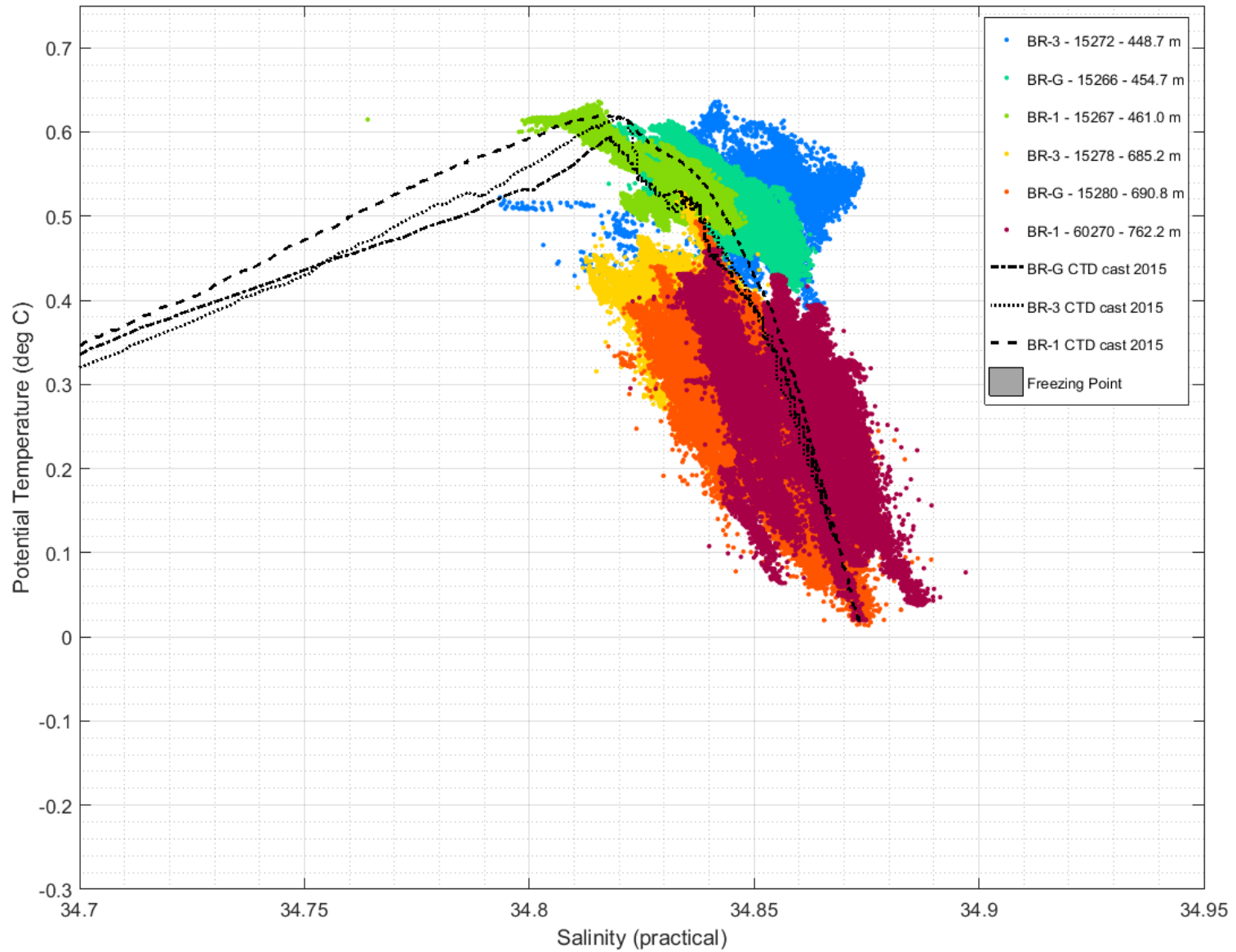


Figure 57: Zoom on the temperature-salinity diagram constructed upon data acquired with the deep CT loggers (>400 m) attached to the slope moorings BR-1, BR-3 and BR-G from 2015 to 2016. CTD profile data taken at mooring locations during the CCGS Amundsen and Laurier cruises in 2015 are depicted by the 3 black lines.

3.4 Biogeochemical Fluxes

This section of the report provides a preliminary assessment of biogeochemical implications of the physical oceanography setting presented in the sections above. Within iBO, automated sediment traps are deployed at 2 depths on the longer slope moorings (see section 2.1.1) to provide insights on the biological regime and cycle of marine productivity in the offshore domain of the southeastern Beaufort Sea. This includes the export of organic carbon as well as information on the planktonic food web, the community of small organisms that supports upper trophic levels, such as fish and marine mammals.

The analyses conducted on trap samples at Université Laval include measurements of total particulate matter, particulate organic carbon, phytoplankton cells and zooplankton. The goal of these analyses is to investigate inter-annual variations in primary and secondary production in relation to changes in ice cover and water temperature in the Beaufort Sea. Preliminary results for phytoplankton cells export obtained at the 3 mooring sites show that diatom export peaked at the end of May and beginning of July at the two mooring sites located on the continental slope of the southern Beaufort Sea, from which ice cleared very early in 2016, in late April (Figure 58). Increased diatom fluxes occurred later in July and August at the mooring site off Banks Island and were very low in contrast to southern sites (Figure 58).

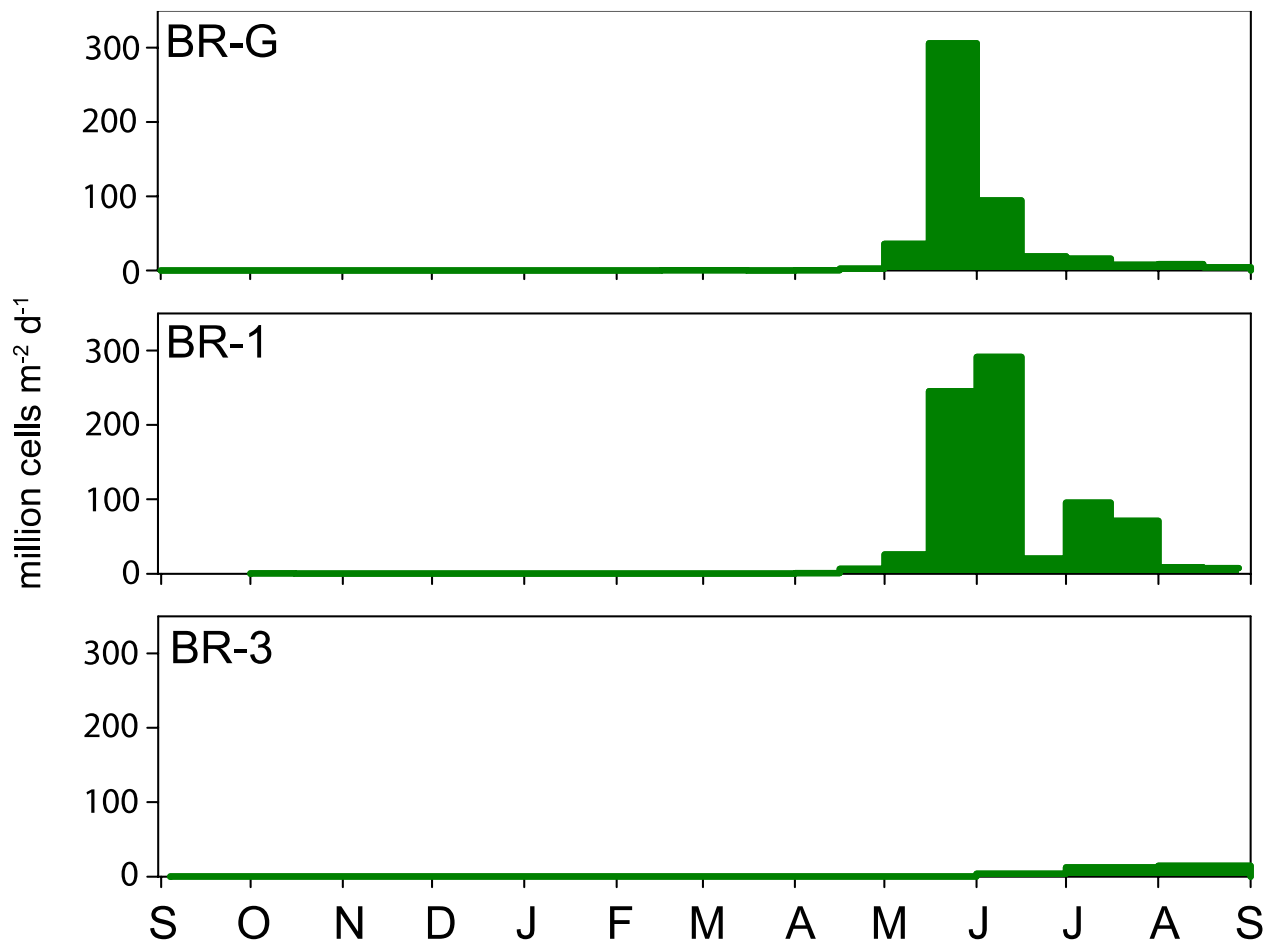


Figure 58: Time-series of diatom fluxes in 2015-2016 in the Beaufort Sea

The ice algae *Nitzschia frigida* is used as an indicator of opening of leads, break-up and open water and is always one of the first diatom species observed at the onset of the biologically productive season in the Arctic Ocean. Fluxes of *N. frigida* were recorded at the end of April on the Mackenzie shelf, consistent with a very early ice break-up, while they occurred later in June west of Banks Island (Figure 59).

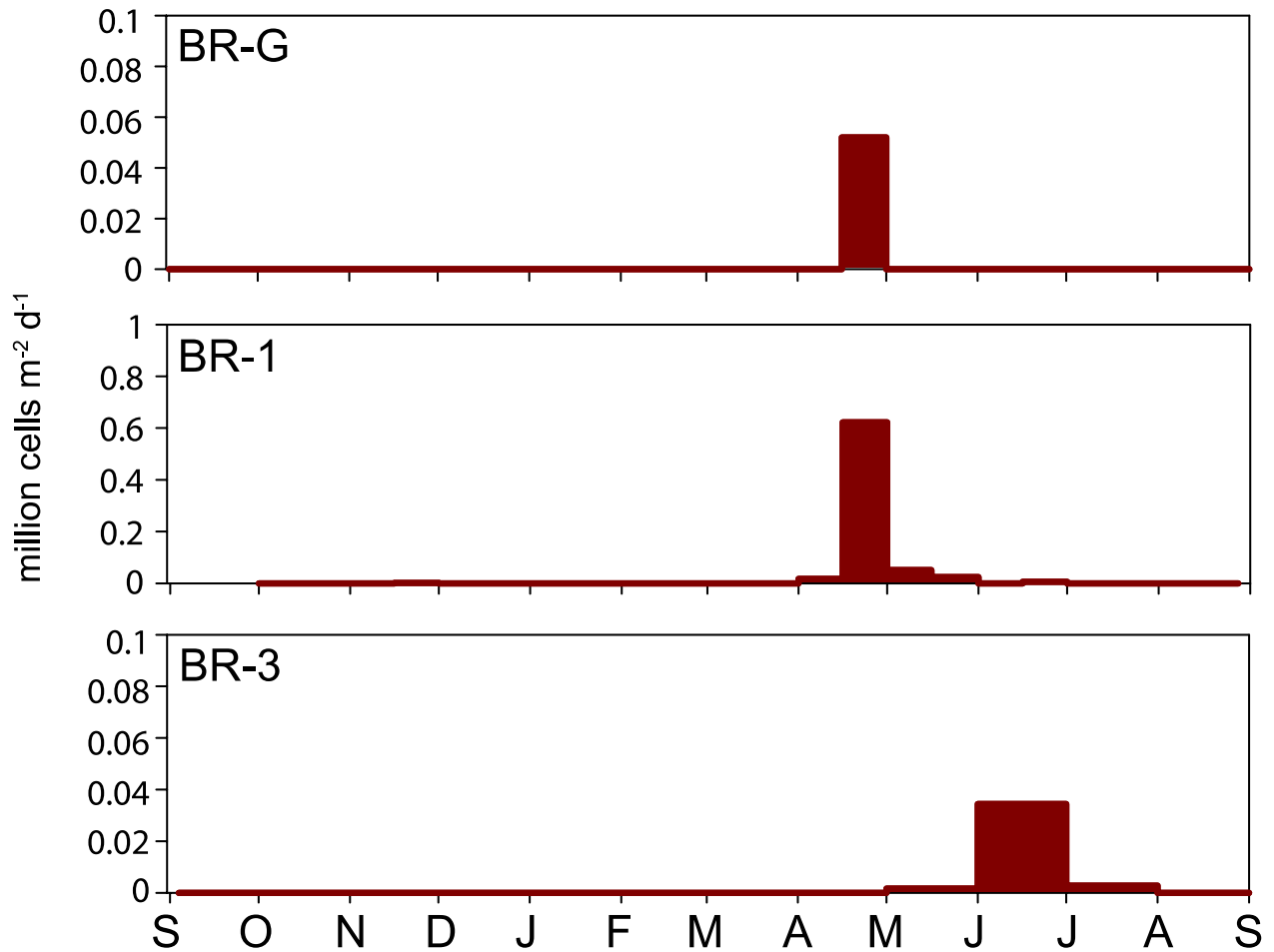


Figure 59: Time-series of the ice algae *Nitzschia frigida* fluxes in 2015-2016 in the Beaufort Sea

4.0 CONCLUSIONS

This section of the report provides additional discussion on the 2015-2016 QA/QC dataset available thus far. Concluding remarks on features of interest are provided in section 4.1. Lessons learned from the 2016 field operations are summarized in section 4.2. At this stage of the project, the lessons learned and recommendations are currently being addressed to provide for more robust and secure future mooring deployments in 2017; and to increase the overall quality of the dataset. Objectives and priorities for 2017-2018 are also presented in section 4.3, including an outlook of the foreseeable milestones for the third year of the iBO scientific program.

4.1 Concluding Remarks on the 2015-2016 Dataset

This report is aimed at providing an initial review of the available QA/QC data from the 7 iBO moorings recovered in 2016. Valid data have been presented for current meters, current profilers, and CT loggers deployed at all moorings. The percentage of valid data for current meters and profilers average 88.1% (see Appendix D for further details), while it is 99.95% for CT sensors. The QA/QC dataset for these instruments is readily available as Matlab© and formatted Text files (ASCII) provided as a data deliverable (see Appendix C). In addition, an initial outlook on biological activity over the slope was presented using a portion of the sediment trap data. The primary features of interest observed in the 2015-2016 dataset include the following:

- Sea ice break up was observed in 2016, approximately 6 weeks ahead of normal. The minimum regional sea ice concentration by the end of summer ranked as second lowest on record, just above the 2012 minimum by less than 3%. Further analyses linking regional sea ice coverage and mooring data recorded over the last few years, especially those from the IPS, should be conducted to assess if any pre-conditioning state or early warning sign of this rapid sea ice decline in 2016 is discernable.
- Wind conditions over the Beaufort Sea in summer 2016 were substantially different than in 2015 as a result of distinct atmospheric patterns. Sea level pressures were higher than average over the central Arctic Ocean in 2015, which generated weak to moderate easterly winds over the entire Beaufort. By contrast, conditions were generally stormy in 2016 and sea level pressures were much lower than average, fostering a dipole pattern with relatively westerlies in the northern Beaufort and weak easterlies over the continental shelf. These distinct wind regimes influenced surface currents (upper 50 m) along the slope of the Mackenzie Shelf (BR-G, -K, -01, and DFO-2), with most frequent directions following the wind patterns. However, surface currents near Banks Island (BR-03) were steadily to the south while surface currents on the inner-to-mid shelf (DFO-1, -9) were directed to the east-southeast in both years. This suggests that wind might not be the primary forcing factor of surface currents at BR-03, DFO-1 and -9 and further investigation is warranted to assess the role of buoyancy and inertial motions.
- Surface currents over the central slope were also generally stronger and less directionally variable in 2016 than in 2015. As a general rule, current speeds greater than 40 cm/s near the surface were approximately 5 times more frequent in 2016 than in 2015 at BR-G and BR-K. Ongoing analyses on the IPS data should provide an indication of how wave conditions were influenced by the stronger wind regime in 2016.
- Near-bottom current patterns were relatively similar in both 2014-2015 and 2015-2016. Currents along the slope generally follow the bathymetric contours, with a mean direction towards the eastern quadrant. Reversals in the current direction are more frequent at BR-K than at any other slope moorings, suggesting that this site reacts promptly to external forcings, in accordance with the dynamics of a shelfbreak jet (see next point). At the deeper sites BR-G and -03, currents near the bottom at 700 m were approximately 20-25% stronger than in the mid-water column, suggesting an effective transfer of energy to the deep water

layers at these sites. However, this trend was not observed at BR-01 and further analyses are required to understand the mechanisms underlying spatial variability in bottom currents. On the inner to mid shelf, bottom currents are variable and generally follow the same patterns as the surface currents.

- Maximum instantaneous current speeds in 2015-2016 were recorded at BR-K (up to 75-85 cm/s throughout the water column), suggesting that the upper slope is likely the region where the strongest sub-surface currents occur each year (see also last's year report; ArcticNet et al., 2016). Hence, the BR-K site allows tracking the core of the narrow shelf break jet (10-15 km) in terms of both magnitude and direction. It provides key information to complement the neighboring DFO-2 and BR-G moorings providing a more comprehensive view of ocean circulation in the vicinity of the exploration leases. In particular, temperature-salinity properties near the bottom at BR-K and DFO-2 showed relatively large fluctuations that appear to be the result of upwelling/downwelling cycles along the slope, the latter warrant further investigation to assess any trend in their frequency and magnitude based on multi-year data.
- As in 2014-2015, eddy-like features were identified visually in the current speed/direction and temperature-salinity time-series (ArcticNet et al., 2016). In 2015-2016, numerous eddies were detected at BR-01 throughout the winter. Further analyses should focus on the inter-annual and spatial variability of eddy activity in order to understand their propagation route and potential to carry over long distances specific physio-chemical properties such as heat, freshwater and nutrients (based on temperature-salinity signature).
- An unusual warming of surface waters was detected at BR-03 near Banks Island in late summer 2016 while sea ice coverage was still around 50% at this location. Interestingly, manifestations of this sudden temperature increase were seen at 36 and 174 m, but not at 105 m near the core of the Pacific Winter water mass.
- Export of particulate organic matter was particularly early and pronounced in 2016 when compared to 2015. Biological activity in the vicinity of Banks Island also appears to have been much stronger in 2016 than in the preceding year. Further analyses on biogeochemical fluxes could be made to understand trends and patterns in primary productivity in the Beaufort Sea in the context of receding sea ice and warming waters.

4.2 2016 Fieldwork Lessons Learned and Recommendations

This section of the report identifies lessons learned and recommendations from work on the Amundsen and Laurier during the 2016 iBO Program that are currently being addressed to improve future mooring deployments and recoveries. The list of recommendations has been finalized following the iBO TAC Meeting that was hosted as part of the ArcticNet Annual Scientific Meeting, Winnipeg, in December 2016 (see Appendix B).

- The compasses of ADCPs recovered in 2016 that could not be verified in Kugluktuk in the wake of Leg 3a due to logistical constraints should be checked prior to any further re-deployment. Similarly, the compasses of all ADCPs and current-meters deployed in 2016 need to be verified after their recovery in 2017 since no general calibration/verification activity was conducted prior to the campaign.
- The bulkhead connector (dummy plug) of all Nortek Aquadopp instruments should be carefully inspected to detect early onset of pin corrosion and rubber fatigue. The replacement of older cables and connectors as part of routine maintenance is advised.
- Special care should be taken when closing the end cap of the TRDI external battery housing to avoid the possibility of O-rings slipping away from their proper position. The size and model of the O-ring should also be verified given that many TRDI O-rings are similar, although they serve different purposes.

- Communication problem with TRDI WHS ADCP #3778 should be further investigated since the cause for the intermittent communication failure could not be identified aboard the *Amundsen*. The instrument should also be tested for proper functionality. A service repair at the manufactory is advised if communication remains problematic.
- A custom-made plastic bushing should be developed for the large stainless eyes of the swiveling Aquadopp in-line frames in order to replace the tygon tube approach that does not meet the expected standards for iBO moorings. The slightly-corroded Aquadopp frames with fin should be replaced by new ones prior to the next campaign;
- In addition to testing whether a given Technicap trap motor functions properly, the direction of the rotation should be checked prior to deployment;
- Long Ranger ADCPs deployed in the Beaufort Sea should be programmed using the High Power Mode since a combination of Low Power Mode, elevated ambient noise due to ice, wind or waves, and low scatterer concentrations due to the influence of impoverished waters of the Canada Basin could result in partial data loss.
- Bathymetry of the deployment site should be carefully evaluated for risks associated with mooring drift and longer-than-usual ship re-positioning. Bathymetry variability should be examined by an expert multibeam personnel from the bridge during the deployment operation in order to avoid mishap in the deployment location.
- Robust 316 Wichard stainless steel shackles should be purchased for 2017 in order to replace the galvanized shackles typically used above the Nortek and TRDI ADCP cages.

4.3 Objectives and Milestones for 2017-2018

Objectives of iBO for 2017-2018 are centered on the recovery and redeployment of the 7 iBO moorings from the CGGS Sir Wilfrid Laurier during its annual Arctic expedition to the Beaufort Sea (September 19 to October 6, 2017). Foreseeable milestones for 2017-2018 are listed in Table 17. This includes the finalization of the QA/QC for 2015-2016 data (primarily IPS data) and the upcoming processing of 2016-2017 datasets recovered from the Laurier. Other activities such as TAC operational meetings, equipment mob/demob, and verification of ADCP compasses to address field logistic, instrumentation performance, and data processing are planned to ensure a timely development of the project in 2017-2018. Communication activities will be primarily focused on stakeholder consultations and participation to the Arctic Change conference, Quebec City, December 2017.

Table 17: 2017-2018 iBO Milestones

Milestone	Date
Presentation of the iBO program at the IGC meeting, Aklavik	March 16, 2017
Pre-field 2017 Operational Conference Call Meeting	May 1, 2017
Instrumentation maintenance completed at DFO and ArcticNet	May 15, 2017
Technical Advisory Committee Conference Call - Summer Meeting	August 1, 2017
Recovery and redeployment of iBO moorings onboard the Laurier	October 6, 2017
Annual Technical Advisory Committee Meeting, Arctic Change Conference, Quebec	December 11, 2017

Finalization of data processing of IPS 2016-2017 and related reporting	December 31, 2017
QA/QC of ADCP and CT logger 2016-2017 data	March 31, 2017
iBO Technical Report 2017 Submitted	March 31, 2018

With iBO entering its third year, the iBO TAC also plans to develop a State of the Beaufort Sea (SBS) Report that would merge historical mooring data from DFO and ArcticNet with newly-acquired datasets from iBO. This report would represent a major outcome or deliverable of iBO, assuming that additional manpower and financial resources would support the development of this product over 2017-2019, i.e. beyond the current data collection scope. The roadmap and structure of the SBS Report are currently being outlined with a first developmental phase consisting of stakeholder consultations, including with the Inuvialuit communities, oil and gas industry, governmental departments, and academic partners of iBO. Through these consultations, our objective is to align the content of the SBS Report with the needs and requirements pertaining to the present status of oil and gas development in the Canadian Beaufort Sea. A first consultation effort was undertaken on March 16, 2017 at the Inuvialuit Game Council (IGC) meeting in Aklavik, NWT to seek feedback for the proposed development of the SBS Report. Chapter leads and sub-teams will be confirmed in the wake of stakeholder consultations, although it is expected that the iBO TAC and close colleagues will form the core of the writing team.

At this stage we envision that the major goal of the SBS report would be to review and update our understanding of the marine physical environment of the Canadian Beaufort Sea as based on IPS, ADCP and CT time-series data from DFO and ArcticNet. Connecting the shelf and slope mooring datasets within an integrated approach has not been conducted prior to iBO, whereas the need for a true regional perspective spanning more than a decade is needed to provide baseline knowledge on the extremely variable Beaufort marine environment. The central chapters of the SBS Report would thus deal with sea ice and water column dynamics, which would likely be supplemented by an introductory chapter on atmospheric forcings and by a side chapter on ecosystem variability inferred from sediment trap data. Including elements of predictive modelling and forecasting would also be possible, but contingent to available funding and commitment of external collaborators to iBO. This preliminary SBS Report structure and the related table of content is expected to be refined following stakeholder consultations and discussion with Indigenous and Northern Affairs Canada (INAC) who is currently developing a Strategic Regional Environmental Assessment (SREA) for the Beaufort Sea as a follow-up to BREA. The community consultation conducted on March 16, 2017 validated the notion that a thorough understanding of the physical environment provided by the SBS Report would represent a key building block of the SREA.

A general roadmap for the development of the SBS Report is provided in Figure 60. The roadmap is organised around three main phases. The first phase starts in March 2017 and should comprise stakeholder consultations, team and budget build-up, and preliminary data analysis and drafting of the report structure by chapter leads. The second phase is expected to start with a kick-off meeting at the Arctic Change 2017 conference and should focus on data analyses, figure development and writing of the report. A project update to stakeholders will also be part of phase 2 to further align the proposed report content to actual needs and requirements. A first complete draft of the report is expected to be generated at the end of phase 2. The final phase will consist of revision and adjustment following review of the draft report by stakeholders. Enhanced interactions with INAC are expected during phase 3 in order to generate a product that would become a key element of the broader SREA. The final SBS report is expected to be delivered by December 2019, assuming that all phases could be conducted without any delay.

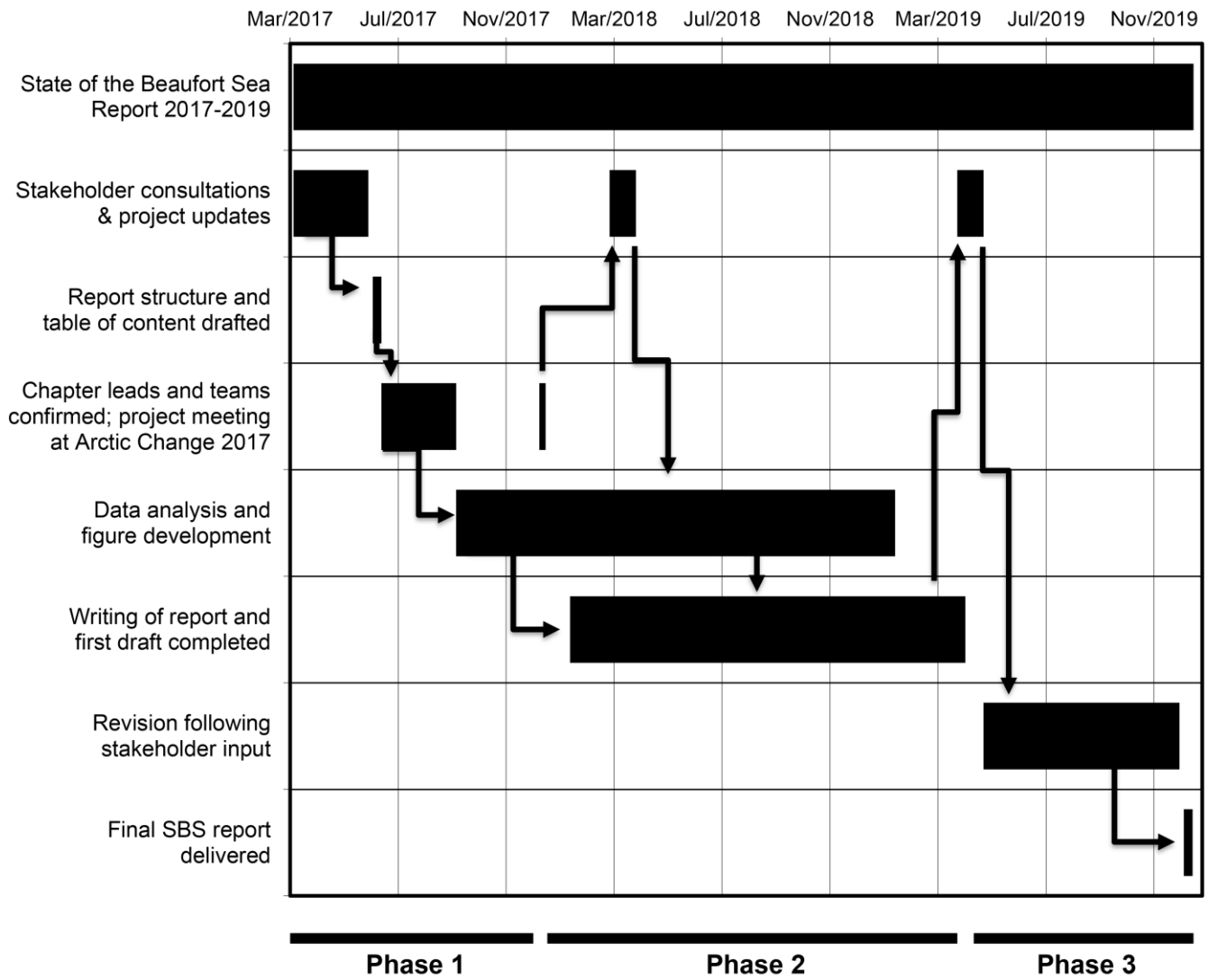


Figure 60: General roadmap for the potential development of the State of the Beaufort Sea Report over 2017-2019, pending the availability of additional manpower and financial resources to support the development of this product over 2017-2019

5.0 REFERENCES

- ArcticNet Inc., Fisheries and Oceans, Golder Associates Ltd. (2016). Integrated Beaufort Observatory (iBO) 2015 Technical Project Report. 4 August 2016.
- Aagaard, K., 1984. The Beaufort Undercurrent. In: Barnes, P.W., Schell, D.M., Reimnitz, E. (Eds.), *The Alaskan Beaufort Sea: Ecosystems and Environments*. Academic Press, New York, pp. 47–74.
- ASL Environmental Sciences Inc. 2015. IPS Processing Toolbox User's Guide. Report by ASL Environmental Sciences Inc., Victoria BC, Canada, 136 pp.
- Barber, D.G., Hanesiak, J.M., 2004. Meteorological forcing of sea ice concentrations in the southern Beaufort Sea over the period 1979 to 2000. *J. Geophys. Res. (C Oceans)* 109, C06014.
- Blasco, S., Bennett, R., Brent, T., Burton, M., Campbell, P., Carr, E., Covill, R., Dallimore, S., Davies, E., Hughes-Clarke, J., Issler, D., Leonard, L., MacKillop, K., Mazzotti, S., Patton, E., Rogers, G., Shearer, J. and White, M., 2013. 2010 State of Knowledge: Beaufort Sea Seabed Geohazards Associated with Offshore Hydrocarbon Development; Geological Survey of Canada, Open File 6989, 340 p. doi:10.4095/292616
- Canadian Ice Service (CIS). 2016. Seasonal summary. North American Arctic Waters. Summer 2016. 28 pp.
- Carmack, E.C., MacDonald, R.W., 2002. Oceanography of the Canadian Shelf of the Beaufort Sea: a Setting for Marine Life. *Arctic* 55, suppl. 1, 29-45.
- Dmitrenko, I. A., Kirillov, S. A., Forest, A., Gratton, Y., Volkov, D. L., Williams, W. J., Lukovich, J. V., Belanger, C. and Barber, D. G. 2016, Shelfbreak current over the Canadian Beaufort Sea continental slope: Wind-driven events in January 2005. *J. Geophys. Res. Oceans*. Accepted Author Manuscript. doi:10.1002/2015JC011514
- Fissel, D. B., Marko, J. R., Melling, H. 2008, (July). Advances in marine ice profiling for oil and gas applications. In *Proceedings of the Ictech 2008 Conference*.
- Forest, A., Osborne, P. D., Fortier, L., Sampei, M., and Lowings, M. G. 2015. Physical forcings and intense shelf–slope fluxes of particulate matter in the halocline waters of the Canadian Beaufort Sea during winter. *Continental Shelf Research*, 101, 1-21.
- Galley, R. J., Else, B. G. T., Prinsenber, S. J., Babb, D., Barber, D. G. 2013. Summer Sea Ice Concentration, Motion, and Thickness Near Areas of Proposed Offshore Oil and Gas Development in the Canadian Beaufort Sea—2009. *Arctic*, 105-116.
- Giovando, L.F., Herlinveaux, R.H., 1981. A discussion of factors influencing dispersion of pollutants in the Beaufort Sea. *Pacific Marine Science Report* 81-4, p. 198.
- Golder Associates Inc (Golder). 2013. *2013 Instrument Compass Calibration Technical Memorandum*. 13-1334-0031. June 2013.
- _____. 2014. *2014 BREA Current Meter Instrument Compass Calibration Summary*. Technical Memorandum.
- _____. 2015. ArcticNet 2015 Leg 3a Safety Incident Report: Benthos Locator Overpressure. Memorandum
- _____. 2016a. Integrated Beaufort Observatory (iBO) Mooring Field Report 2015. Technical Memorandum. April 5, 2016.

- _____. 2016b. Integrated Beaufort Observatory (iBO) Mooring Field Report 2016. Technical Memorandum. Report Number: 1406102-R-Rev0-3000-3002.
- Institute of Ocean Sciences – Fisheries and Oceans Canada (IOS-DFO). Integrated Beaufort Observatory 2016 Field Expedition Report. September 20 – October 14, 2016. Ed. By H. Melling. IOS Cruise 2016-13 (2016006PGC)
- Integrated Ocean Observing System (IOOS). 2015. Manual for Real-Time Quality Control of In-Situ Current Observations: A Guide to Quality Control and Quality Assurance of Acoustic Doppler Current Profiler Observations. Version 2.0 October 2015.
- Kulikov, E.A., Carmack, E.C., Macdonald, R.W., 1998. Flow variability at the continental shelf break of the Mackenzie Shelf in the Beaufort Sea. *Journal of Geophysical Research. C. Oceans* 103, 12,725-712,741.
- Lansard, B., Mucci, A., Miller, L. A., Macdonald, R. W., Gratton, Y. 2012. Seasonal variability of water mass distribution in the southeastern Beaufort Sea determined by total alkalinity and $\delta^{18}O$. *J. Geophys. Res. (C Oceans* 117(C3).
- Macdonald, R.W., Paton, D.W., Carmack, E.C., Omstedt, A., 1995. The freshwater budget and under-ice spreading of Mackenzie River water in the Canadian Beaufort Sea based on salinity and $d^{18}O/d^{16}O$ measurements in water and ice. *J. Geophys. Res. (C Oceans)* 100, 895-919.
- Macdonald, R.W., Solomon, S.M., Cranston, R.E., Welch, H.E., Yunker, M.B., Gobeil, C., 1998. A sediment and organic carbon budget for the Canadian Beaufort Shelf. *Marine Geology* 144, 255-273.
- Melling, H., 1993. The formation of a haline shelf front in wintertime in an ice-covered arctic sea. *Continental Shelf Research* 13, 1123–1147.
- Melling, H., Riedel, D.A. 2004. Draft and Movement of Pack Ice in the Beaufort Sea: A Time-Series Presentation April 1990 - August 1999. Canadian Technical Report of Hydrography and Ocean Sciences 238, v + 24 pp.
- Melling, H., Johnston, P. H., Riedel, D.A. 1995. Measurements of the underside topography of sea ice by moored subsea sonar. *Journal of Atmospheric and Oceanic Technology*, 12(3), 589-602.
- Melling, H., Gratton, Y., Ingram, G. 2001. Ocean circulation within the North Water polynya of Baffin Bay. *Atmosphere-Ocean*, 39(3), 301-325.
- Nortek AS (Nortek). 2013. Comprehensive Manual. December 2013.
- O'Brien, M.C., Macdonald, R.W., Melling, H., Iseki, K., 2006. Particle fluxes and geochemistry on the Canadian Beaufort Shelf: Implications for sediment transport and deposition. *Continental Shelf Research* 26, 41-81.
- Pickart, R.S., 2004. Shelfbreak circulation in the Alaskan Beaufort Sea: Mean structure and variability. *J. Geophys. Res. (C Oceans)* 109, C04024.
- Pickart, R.S., Schulze, L.M., Moore, G.W.K., Charette, M.A., Arrigo, K.R., van Dijken, G., Danielson, S.L., 2013. Long-term trends of upwelling and impacts on primary productivity in the Alaskan Beaufort Sea. *Deep Sea Research Part I: Oceanographic Research Papers* 79, 106-121.
- RBR-Global (RBR). 2016. Ruskin User Guide. Latest version available at: <https://rbr-global.com/support/software>.
- Beardsley, R. C., and L. K. Rosenfeld 1983, Introduction to the CODE-1 moored array and large-scale data report, in CODE-1: Moored Array and Large-Scale Data Report, edited by L. K. Rosenfeld, Tech. Rep. WHOI-83-23, CODE Tech. Rep. 21, pp. 1216, Woods Hole Oceanogr. Inst., Woods Hole, Mass.

- Sequoia Scientific. 2008. Processing LISST-100 and LISST-100X Data in MATLAB. Online Article (last update: 11 July 2012). <http://www.sequoiasci.com/article/processing-lisst-100-and-lisst-100x-data-in-matlab/>.
- Teledyne RDI (TRDI). 2014. Monitor, Sentinel, Mariner, Long Ranger, and Quartermaster Commands and Output Data Format. P/N 957-6156-00. Revised March 2014.
- Teledyne RDI (TRDI). 2006. Acoustic Doppler Current Profiler Principles of Operation: A Practical Primer. P/N 951-6069-00. December 2006.
- von Appen, W. J., Pickart, R. S. 2012. Two configurations of the western Arctic shelfbreak current in summer. *Journal of Physical Oceanography*, 42(3), 329-351.
- Williams, W. J., Melling, H., Carmack, E. C., & Ingram, R. G. 2008. Kugmallit Valley as a conduit for cross-shelf exchange on the Mackenzie Shelf in the Beaufort Sea. *Journal of Geophysical Research: Oceans*, 113(C2).
- Woodgate, R. A. and Holroyd, A.E. 2011. Correction of Teledyne Acoustic Doppler Current Profiler (ADCP) Bottom-Track Range Measurements for Instrument Pitch and Roll. University of Washington Technical Report: available at <http://psc.apl.washington.edu/BeringStrait.html>

Appendix A. 2015-2016 Final Mooring Diagrams

The final mooring diagrams 2015-2016 are provided below. Instrument depths correspond to the measured depth (for instruments equipped with a pressure sensor) or estimated for each instrument throughout the deployment period.

DEPTH (m)

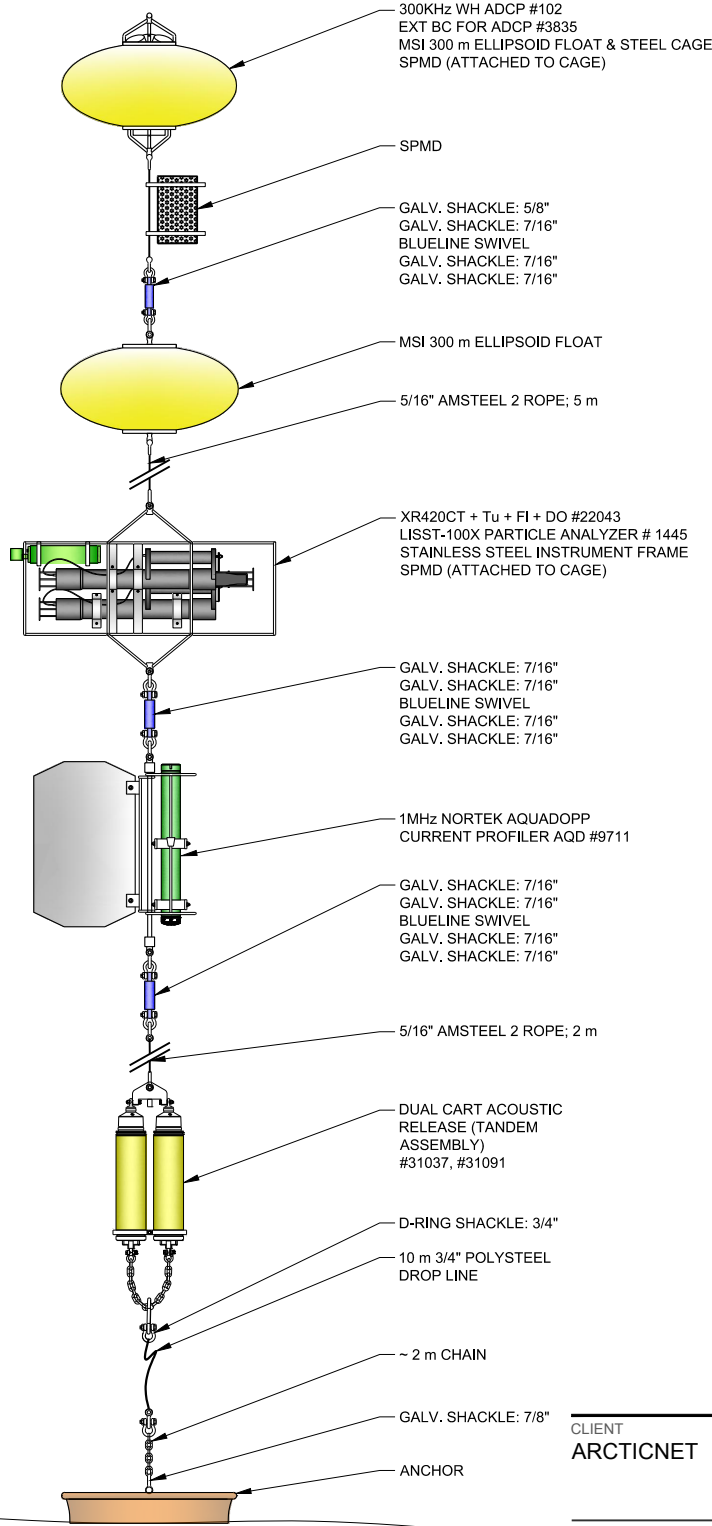
COMPONENT

145.0

150.8

152.2

168.9



NOT TO SCALE

CLIENT
ARCTICNET

PROJECT
IBO

TITLE
2015-2016 MOORING DIAGRAM BR-K

CONSULTANT

YYYY-MM-DD 2017-03-02

PREPARED REDMOND

DESIGN GC

REVIEW GC

APPROVED EB



PROJECT No.
1406102

PHASE
4000

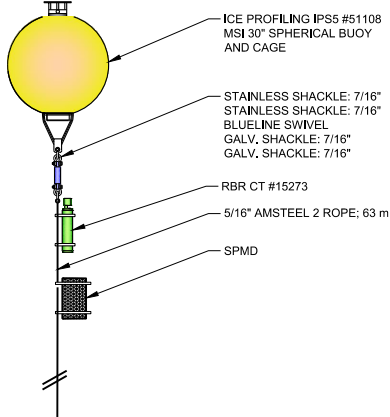
Rev.
A

FIGURE
1

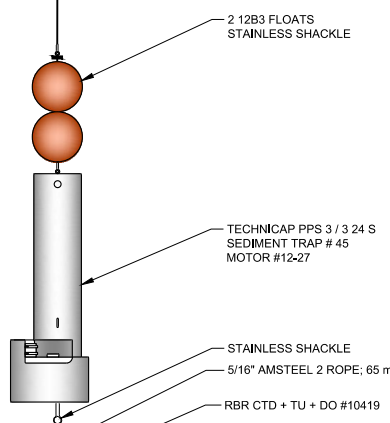
DEPTH (m)

COMPONENT

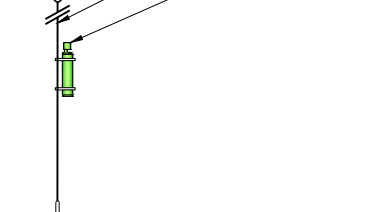
34.5



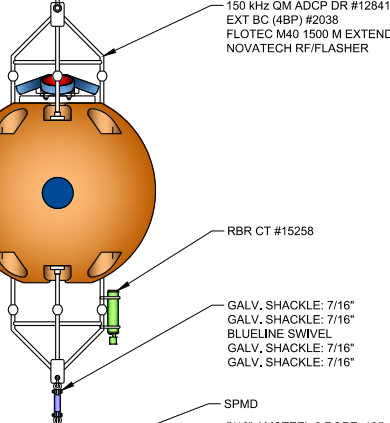
105



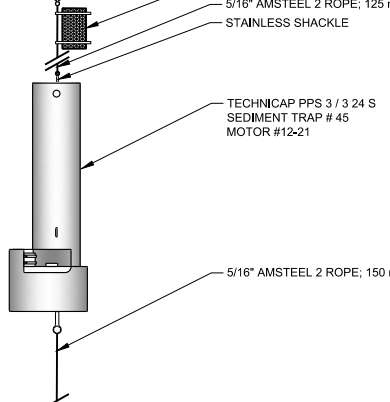
106.4



160.7



162.7

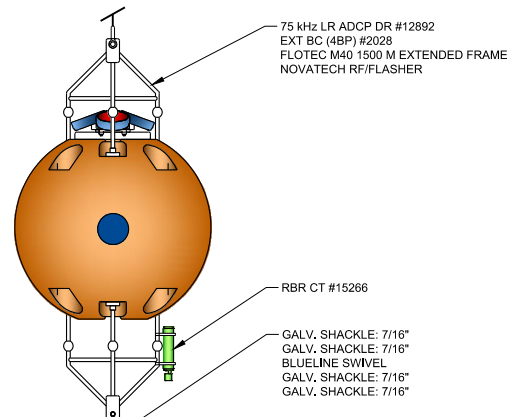


310

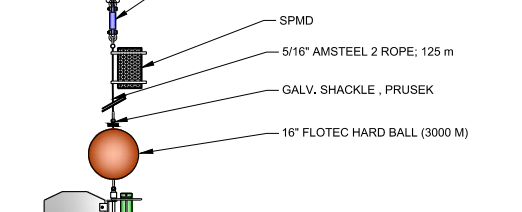
DEPTH (m)

COMPONENT

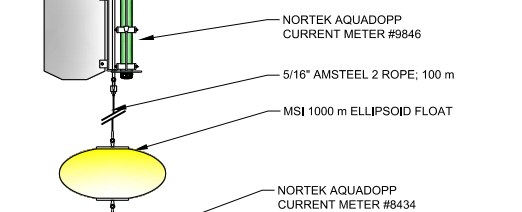
452.7



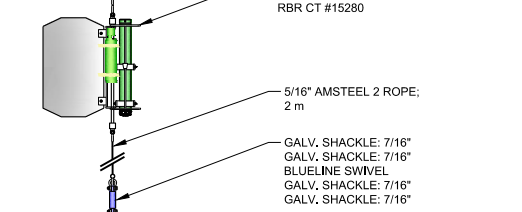
454.7



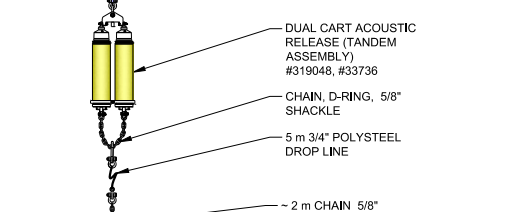
580.9



690.8



700.3



NOT TO SCALE

CLIENT
ARCTICNET

PROJECT
IBO

TITLE
2015-2016 MOORING DIAGRAM BR-G

CONSULTANT



YYYY-MM-DD 2017-03-02

PREPARED REDMOND

DESIGN GC

REVIEW GC

APPROVED EB

PROJECT No.
1406102

PHASE
4000

Rev.
A

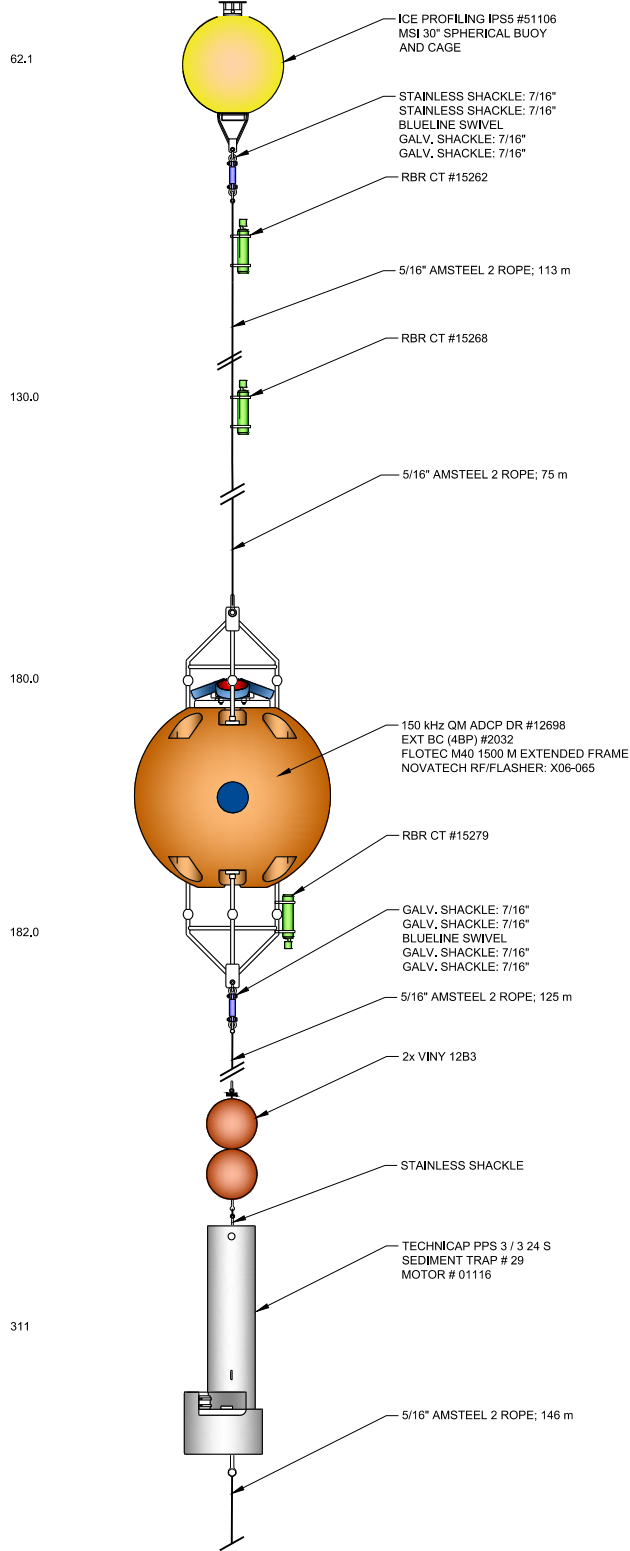
FIGURE
2

Path: \\redmond\geomat\geomat\GOLDER\COSTAL_GRP\REDMOND\99_PROJECTS\1406102_Arc\Sheet_Beaufort4000_Output\IBO2_PRODUCTION\DWG\1_File Name: 1406102_4000_002.dwg

IF THIS MEASUREMENT DOES NOT MATCH WHAT IS SHOWN, THE SHEET SIZE HAS BEEN MODIFIED FROM ANSIA

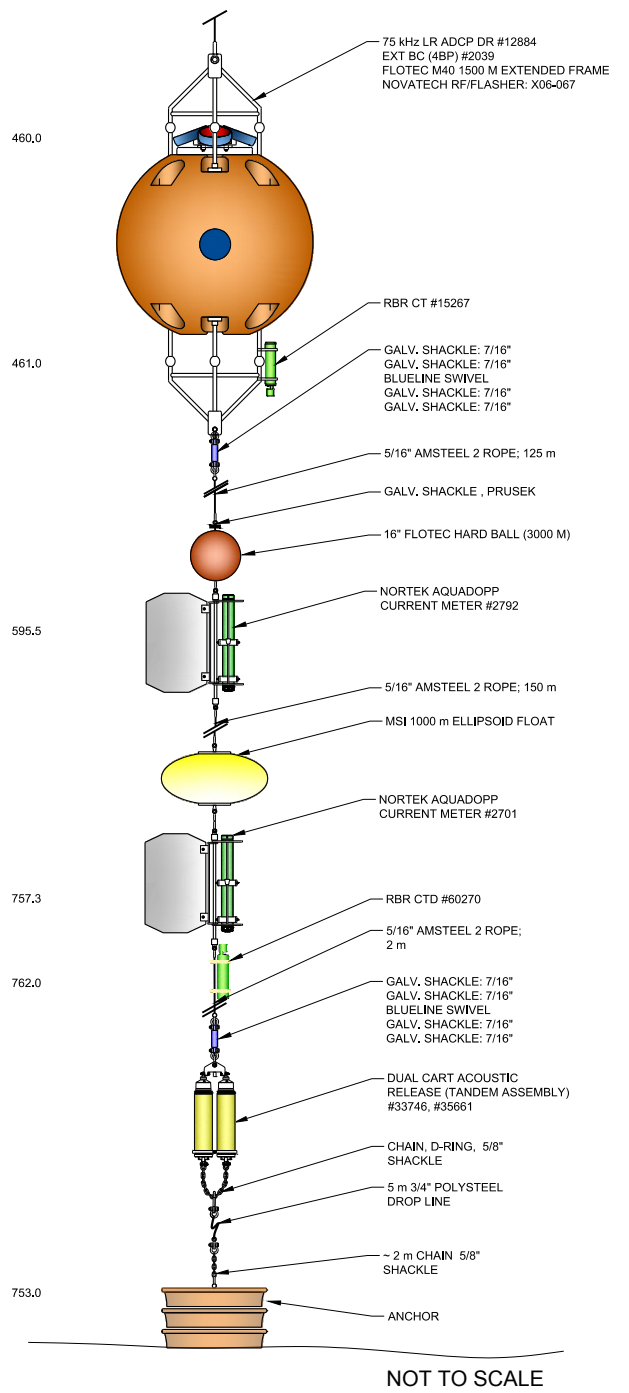
DEPTH (m)

COMPONENT



DEPTH (m)

COMPONENT



CLIENT
ARCTICNET

PROJECT
IBO

TITLE
2015-2016 MOORING DIAGRAM BR-1

CONSULTANT

YYYY-MM-DD 2017-03-02

PREPARED REDMOND

DESIGN GC

REVIEW GC

APPROVED EB



PROJECT No.
1406102

PHASE
4000

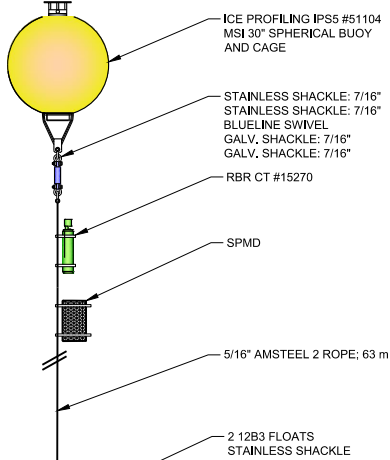
Rev.
A

FIGURE
3

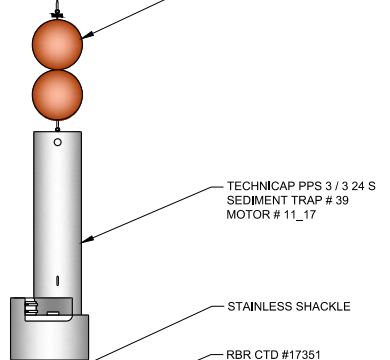
DEPTH (m)

COMPONENT

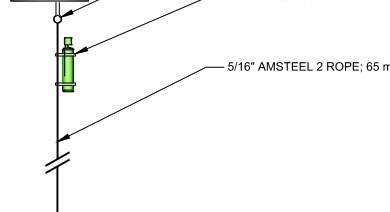
36.0



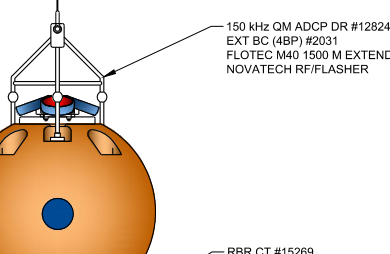
103



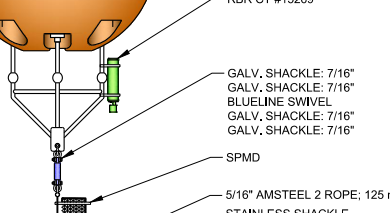
104.6



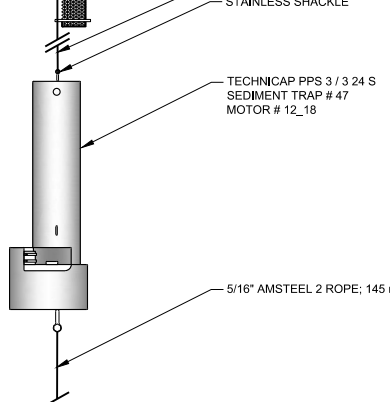
171.7



173.7



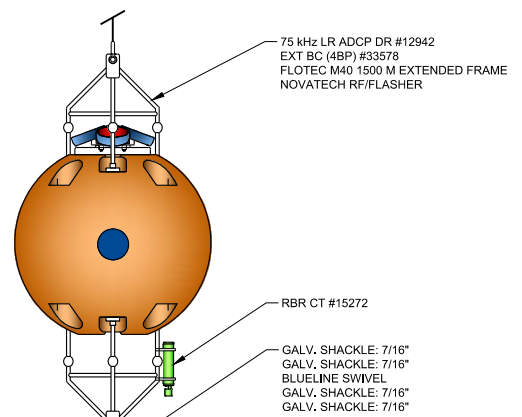
310



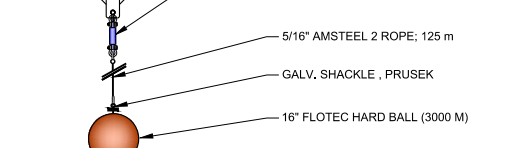
DEPTH (m)

COMPONENT

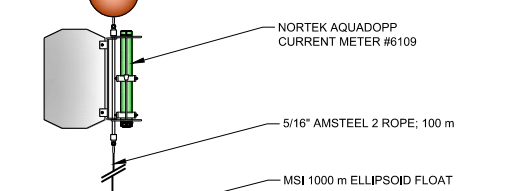
446.7



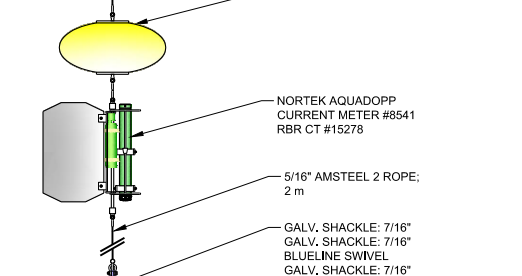
448.7



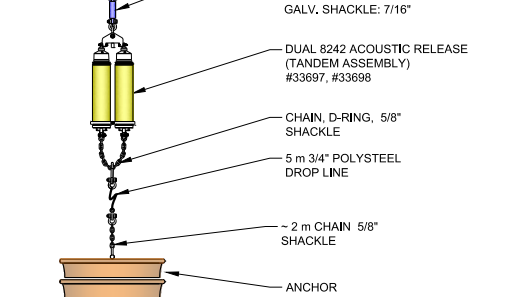
574.7



685.2



689.4



NOT TO SCALE

CLIENT
ARCTICNET

PROJECT
IBO

TITLE
2015-2016 MOORING DIAGRAM BR-3

CONSULTANT



YYYY-MM-DD 2017-03-02

PREPARED REDMOND

DESIGN GC

REVIEW GC

APPROVED EB

PROJECT No.
1406102

PHASE
4000

Rev.
A

FIGURE
4

Use a kevlar loop tied to the hook so that the cut end pulls through the lugs on deployment

Lift point

40 m

Grappling loop (poly or kevlar rope)

IPS4 Ice-profiling Sonar (short fat)

Stainless steel frame
5 Vinyl floats w/ hockey-puck stops
Pieps beacon w/ bracket
SBE37 vertical on frame

SBE37-SM

Isolation bushing kit

7/16" shackle
7/16" shackle
1/4" plastic eye

Mooring used at IBO16-2

Inclination: 83.1° H = 6940 nT

65 m: 1/4" kevlar

Use a kevlar loop tied to frame. The cut end should pull through the opening

Lift point

(non-magnetic link)

1/4" plastic eye
7/16" shackle (stainless)
7/16" shackle (stainless)

107 m

RDI Narrowband ADCP 300 kHz

Stainless frame
4 Vinyl floats w/ hockey-puck stops
Stabilizing vane (14" x 30")

SBE37-SM

Isolation bushing kit

7/16" shackle
1/2" shackle
3T bronze swivel
5/8" + 1/2" shackles

CART tandem release transponder

Galvanized drop ring

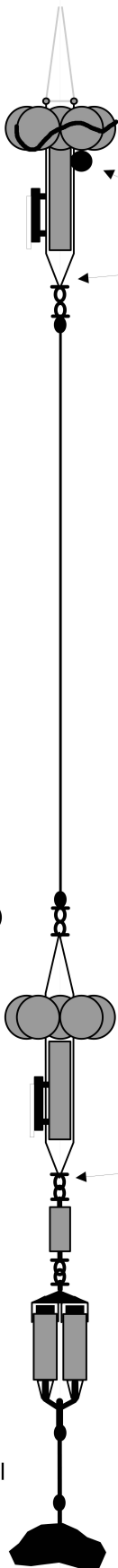
5/8" plastic eye

1 m: 5/8" polysteel

5/8" plastic eye
3/4" shackle

112 m

800-lb anchor (railway wheel)

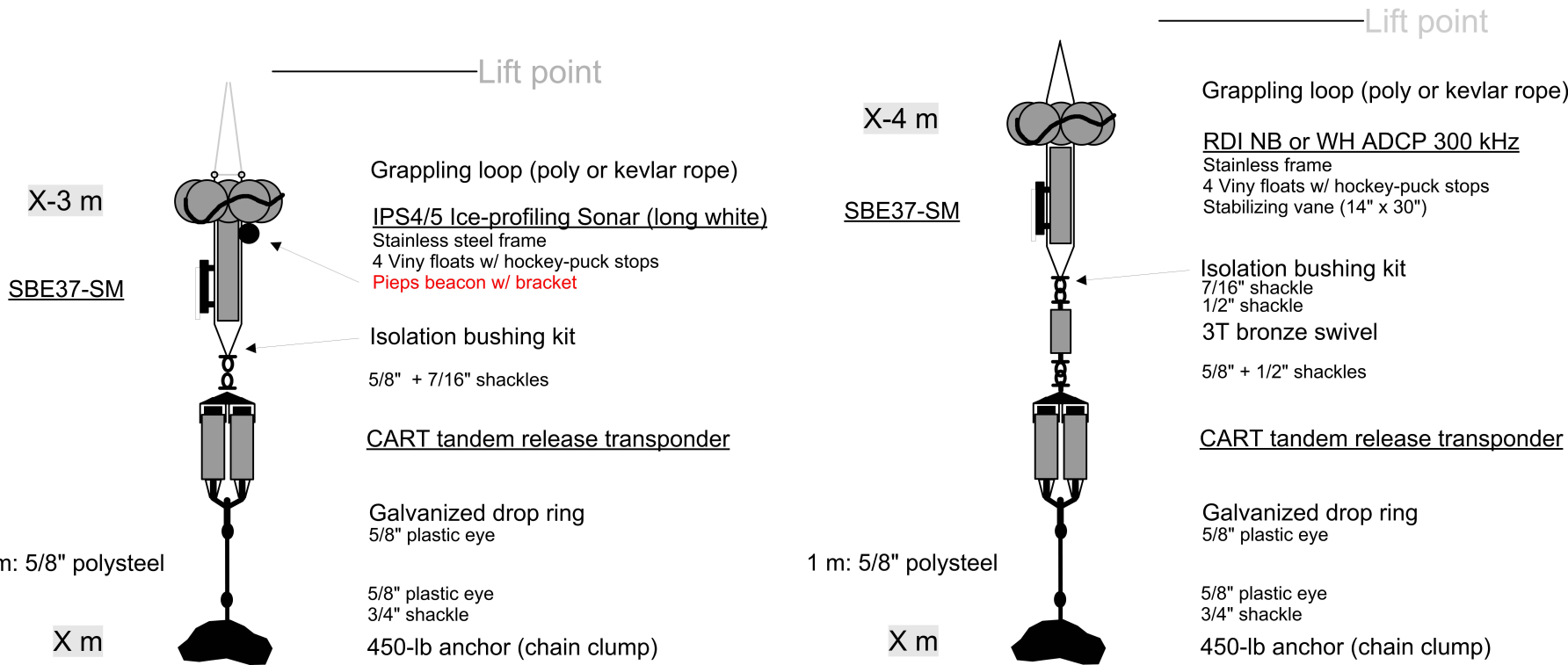


Moorings used at IBO16-1, IBO16-9

Beaufort Sea. Depths: 35-55 m

Inclination ~ 82.7° H ~ 7321 nT

Use a kevlar loop tied to the hook
The cut end should pull through the
lugs on deployment



integrated Beaufort Observatory (iBO) 2016 Annual Meeting

Minutes

Technical Advisory Committee Meeting

ArcticNet Annual Scientific Meeting 2016

RBC Convention Center, Winnipeg, Room 15S

6 December 2016, 8:30 AM – 12:00 PM

Present: Alexandre Forest, Golder; Anissa Merzouk, ArcticNet; Catherine Lalande, U. Laval; Humfrey Melling, IOS-DFO; Luc Michaud, ArcticNet; Mike Smith, IOL; Shawn Meredyk, ArcticNet

Regrets: Keith Lévesque, ArcticNet; Phil Osborne, Golder

Meeting started at 8:30 AM (CST)

1. Welcome and introduction

2. Approval of agenda

The meeting's agenda was presented and approved unanimously.

3. Meeting objectives

The last TAC meeting was held on August 10, 2016 and aimed at planning the upcoming expeditions on the *Amundsen* and *Laurier*, reviewing the 2014-2015 data processing schedule, and discussing the iBO collaboration framework.

This annual meeting at the ArcticNet ASM is an important opportunity for TAC members to meet in person, review last year's activities and plan for the future. The meeting aimed to review the following items:

- 2016 field activities and lessons learned
- 2015-16 mooring data recovery success
- Review of the 2015 technical data report
- Coordination of the 2016 technical data report
- Status of collaborations and data availability
- Early planning of 2017 field campaign(s)

4. 2016 field activities

A total of 7 iBO moorings were recovered and deployed in the Beaufort Sea using the CCGS *Amundsen*, from August 25 to September 17, and the CCGS *Sir Wilfrid Laurier*, from September 20 to October 17. Four moorings (BR-K, BR-G, BR-1 and BR-3) were recovered, serviced and re-deployed successfully from the *Amundsen* while three moorings (DFO-1, DFO-2 and DFO-9) were turned over from the *Laurier*. Good teamwork and well-established Health and Safety procedures resulted in no incidents being reported during field operations.

a. CCGS *Sir Wilfrid Laurier*

Operations on the *Laurier* were carried out between August 26 and September 28. Clear weather and light ice conditions prevailed during operations in the Beaufort Sea. The map of the Beaufort Sea with the *Laurier* cruise track and the ice edge, showed an interesting ice tongue feature west of Banks Island.

The *Laurier* carried out a total of 15 mooring deployments as part of different programs, including iBO and MARES. In addition to the mooring work, the *Laurier* conducted operations for the Marine Geohazard program near DFO-2 and at a sentinel site on the Chukchi Plateau in collaboration with NOAA. A glider equipped with multiple sensors was also deployed near the Mackenzie Trough, carrying out profiles right up to the surface and providing complementary information to sub-surface moorings.

The MARES mooring array stretches perpendicular to the Yukon Shelf from 40 to 760 m, hooking up to iBO mooring BR-1. The array targets upwelling events and moorings are equipped with IPS, current meters and ADCPs, and in some cases, nitrate and CO₂ sensors. The MARES program is expected to be renewed for another year until 2018.

No major malfunctions occurred with mooring instruments although one CART release failed and one WH ADCP (from the WHOI program) could not be calibrated. DFO provided substitutes for both instruments. Reduced sensitivity for one beam from a DFO NB-ADCP was observed and the minor implications for data quality will be investigated during data processing. Also, one ASL IPS in the Chukchi Sea from the Shell/ASL program did not record any echoes.

Seabed mapping operations focused on hazards posed by unstable terrain. Chimney structures surveyed in 2013 were re-surveyed and substantial changes over 3 years were observed at mud expulsion features. A gully feature generated by a landslide was characterized by a methane-based ecosystem with tube worm colonies. Two AUVs equipped with novel sensors were deployed in Ajurak Block to carry out sub-bottom seafloor mapping with the MBARI expert team. The AUV dives aimed to complement past *Amundsen* multibeam surveys and generate detailed seafloor maps. The resulting bathymetry data could be accessible, and the annotated video would be of special interest.

The year 2016 was a light ice year, but was very different from 2012, when the record low ice extent was observed. Higher SST were recorded in 2012 in southern Beaufort Sea due to atmospheric patterns and the flushing of ice through Fram Strait. The underway TSG data collected by the *Laurier* in 2012 and 2016 were compared.

b. CCGS *Amundsen*

Recoveries

Mooring recovery operations were all successfully conducted although BR-1-15 was found to be deeper than expected. Data recovery rates of instruments on the 2015 moorings were good: IPS 100%, ADCPs 86% (one did not work), AQD and CNL 99.6% (although one ADQ is still under investigation), CT loggers 100%, sediment traps 100%, and LISST 100%.

One IPS partially slipped out of its cage during recovery, but the rope that was implemented as a mitigation procedure to prevent loss of equipment worked as expected. Additional mitigation measures will be assessed in 2017. One ADCP battery housing was recovered with a squashed O-Ring, which leaked and caused a failure in the instrument recording. Although these seals are thoroughly checked when closing the cap of the external housing, this event stresses the importance of double-checking the placement of the seals.

One Long-Ranger was set to low-power mode instead of high-power to potentially improve battery life following recommendations based on the analysis of BREA Long-Ranger ADCPs. These settings resulted in unexpected loss of data quality in the upper water column over the year due to a combination of low scatter concentration and low power. The applicability of the low-power to Arctic waters should be discussed with the manufacturer.

ACTION: HM to keep TAC informed of its exchange with TRDI about the appropriateness of low-power mode for Arctic waters.

One Nortek AQD deployed at intermediate depths on BR-3 was recovered with a corroded connector pin. Data availability from this instrument is under investigation. Instruments on BR-3 successfully recorded ocean currents from surface to bottom, so the potential loss of data is not expected to have a major impact on the 2015-16 dataset. All AQD connectors will be thoroughly inspected and changed if needed prior to future deployments.

One sediment trap motor turned in the wrong direction so both the turning direction and proper motor functioning will be checked in the future. Low power on a sediment trap motor (BR-G B) also led to 4 cups not turning properly and thus collecting more particles (2 months in the same cup). It was suggested that a firmware update be implemented to check the motor's rotation and to increase the likelihood of the cups turning in such cases.

ACTION: SM to mention this solution to Technicap for a firmware update to the sediment traps motors to ensure cups are turning properly.

In 2015, a benthos pinger over-pressurized and exploded in the lab, causing a minor injury to a staff member, and new Health and Safety procedures for these instruments were put in place in 2016. Revised instructions were provided to the crew before recovery, all instruments were inspected and vented on deck, and 4 new instruments equipped with metal caps rather than plastic were bought. No leaked benthos pinger was reported in 2016, but all of the old pingers were discarded according to the new procedures.

Signs of minor galvanic corrosion were observed on Aquadopp in-line frames although the shackles on these frames were intact. In 2016, redeployed cages used only heavy duty Tygon tubes not susceptible to brittling. It was suggested that custom-made bushings should be made for the Aquadopp frames to address this issue.

BR-3-15 was recovered with a highly corroded galvanized shackle found in the Aquadopp in-line frame near the bottom. The eyes of the frame were intact and only the galvanized shackle had corroded substantially, likely the sign of impurities in the metal. H&S and operational procedures are already in place to prevent losing instruments during recovery due to failing shackles, but these procedures will be further improved following this event. Additional protection will also be put in place to avoid galvanic contact creating corrosion on the eyes of the frames.

BR-1-15 was recovered with an imploded Viny float because it was deployed too deep (at ~300 m) while the maximum deployment depth is 200 m. BR-1-15 was also deployed deeper (~770 m) than the target depth of 750 m. This apparently did not affect the IPS depth (62 m) due to longer rope lengths on this mooring. The discrepancy may have resulted from rope stretch over time (dating from BREA moorings of early 2010s), so all ropes on moorings deployed in 2016 were changed. Further review and processing of data from the long moorings (BR-1, BR-3 and BR-G) is needed to evaluate the impact of these discrepancies for data quality.

Deployments

Deployment operations followed improved procedures established at the 2015 Annual TAC Meeting (e.g. lithium batteries and high power mode on ADCPs, new Amsteel ropes, etc.) and all were successfully and safely conducted. All instruments were programmed for one year except BR-3, for two years. Steep bathymetric gradients and difficulty in positioning the ship during deployment of BR-3 led to the mooring free-falling about 30 m deeper than planned. This resulted in the IPS being at its detection limit depth, so a second mooring line was deployed 1-km south of BR-3 along the route of ice drift with an IPS at the correct depth.

ACTION: Operational and Health and Safety procedures for mooring operations to be reviewed based on the lessons learned in 2016.

5. Reporting and data availability

a. 2014-2015 technical report

A first draft of the 2014-2015 technical report was produced in April 2016 with a revised version in August. The focus of the report was on ocean currents collected from ADCPs and current-meters and temperature and salinity variability from the CT sensors. A second version of these datasets is now available, as well as data on particle fluxes from the sediment traps. Highlights of these updated datasets were presented, including an in-depth analysis of an upwelling event and associated circulation patterns at the shelf break during Fall 2014.

An addendum to the 2014-2015 technical report will be produced to present the IPS data. Data processing was queued at ASL to complete three deep locations in December with the next 3 expected in January. Deeper analysis of the IPS datasets will impact the delivery time and cost of processing. It was decided a quick processing should be done with higher level of detail for case studies, features of interest and extreme events. Forecasting ability should be kept in mind in selecting these features, such as detecting patterns in drift of multi-year ice floes before they reach the southern Beaufort Sea.

ACTION: HM to produce a 2014-15 IPS data report, based on the processing reports produced by ASL, by 01 March 2017.

b. 2015-2016 technical report

The technical report for 2015-16 will use last year's report as a template but could possibly include more data products (i.e. progressive vector diagrams and inter-annual comparisons). The report is due 31 March 2017.

c. Toward a State of the Beaufort Sea Report

It is important to think strategically about the outputs and outcomes of the iBO project with a goal of maintaining the Beaufort Sea Observatory in the long term. The production of a State of the Beaufort Sea Report would serve as the main iBO product for this funding cycle (2015-2019). The Report would be published in 2019 with a draft prepared by mid-2018.

The State of the Beaufort Sea Report would build on the iBO technical reports produced from 2015 to 2018 and would focus on the ocean and sea ice regimes in the region. The Report would also include datasets generated during the different Beaufort Sea Mooring Programs over the years to generate long time series: ArcticNet-Industry and BREA (2009-2014) and further back (DFO datasets). A tentative Table of Content with suggested Chapter Leads and key collaborators was presented. Although biogeochemical fluxes would be presented, the Report will present no biological data. The biology aspects could be integrated later into the larger DFO State of the ocean report, developed independently.

Concerns were raised that the writing of a State of the Beaufort Sea report will represent a lot of work to uniformize formats and scales, and to manage deadlines and the people involved. Examples of recent publications were presented to highlight the work already being done on these datasets or ancillary data (e.g. Sigmond et al. 2016, Forest et al. in prep., King et al in prep., Melling and Asplin work on ArcticNet-Industry datasets (2009-2011)). The Beaufort Sea Ice and Ocean Regime chaired by iBO and hosted at the ASM would be a good opportunity to network with potential contributors to the report.

d. Data availability

ESRF and IOL are being provided with the QA/QC'd data as the datasets are processed and an addendum to the 2014-15 technical report will be produced. Interested users can contact the iBO TAC to request access to the data but the iBO datasets will also be made publicly available on the Polar Data Catalogue in January 2017 using a login-restricted access. Concerns were raised that although ESRF agreed with making the data public in an email to iBO directors, this may not reflect the terms of the contract.

ACTION: AM to clarify with ESRF if the contract allows making the data available, and take appropriate steps to amend the contract if necessary.

e. Financial and project progress reports

The upcoming project progress reports and financial reports due to ESRF and IOL were presented.

6. Planning of the Beaufort Sea campaign(s) 2017

The draft expedition schedule for the *Amundsen* in 2017 was presented. Three large programs will participate in the expedition: BaySys, ArcticNet and the Nunavik Inuit Health Survey. The ArcticNet campaign in the Beaufort Sea/Mackenzie Shelf area, including the iBO mooring program, cannot be carried out on the *Amundsen* due to time constraints. Other research vessels were considered to complete ArcticNet's western Arctic work, including the CCGS *Laurier* if it can accommodate the mooring program.

The *Laurier* could carry out the ArcticNet-iBO mooring program although turning over all the moorings with only two weeks of ship time will be challenging. Three berths could be made available for ArcticNet-iBO personnel, who can collaborate with the DFO (and possibly MARES) team to carry out mooring operations. Space on deck and in the hold of the *Laurier* can also be made available for the *Amundsen* equipment. The *Laurier* could also potentially welcome MWOs as part of the IOL collaboration on the iBO program.

The *Laurier* will be mobilized in early July and all the *Amundsen* equipment must be in Victoria by 28 June.

Note that if *Amundsen* personnel board or disembark the ship through the US, they will need passports and appropriate medical coverage.

ACTION: AM to check clearance requirements to access the *Laurier* and take appropriate steps if *Amundsen* personnel need to re-apply.

ACTION: HM to update the *Amundsen* team on the *Laurier* expedition, double-check if the collaboration agreement between ArcticNet and DFO Science requires amendments, and send an estimate of ship time costs.

Meeting adjourned at 12:00 PM (CST).

Appendix C. Data deliverable

In addition to this report, we issue the available oceanographic data that was processed and quality checked following the methods described in section 2.4. The data is provided electronically. This data is provided as a draft and could be subject to further revisions. The data are provided as Matlab and ASCII files for the following instruments:

Mooring	Mooring depth (m)	Instrument	Serial Number	Instrument depth (m)
BR-1-15	753.0	RBR XR-420 CT	15262	62.1
		RBR XR420 CT	15268	130.0
		TRDI QM ADCP 150 kHz	12698	180.0
		RBR XR420 CT	15279	182.0
		TRDI LR ADCP 75 kHz	12884	460.0
		RBR XR-420 CT	15267	461.0
		Aquadopp DW 2 MHz	2792	595.5
		Aquadopp DW 2 MHz	2701	757.3
		RBR Concerto CTD	60270	762.0
BR-3-15	689.4	RBR XR-420 CT	15270	36.0
		RBR XR-420 CTD	17351	104.6
		TRDI QM ADCP 150 kHz	12824	171.7
		RBR XR-420 CT	15269	173.7
		TRDI LR ADCP 75 kHz	12942	446.7
		RBR XR-420 CT	15272	448.7
		Aquadopp DW 2 MHz	6109	574.7
		Aquadopp DW 2 MHz	8541	685.2
		RBR XR-420 CT	15278	685.2
BR-G-15	700.3	RBR XR420 CT	15273	34.5
		RBR XR-420 CT-Tu-DO	10419	106.4
		TRDI QM ADCP 150 kHz	12841	160.7
		RBR XR-420 CT	15258	162.7
		TRDI LR ADCP 75 kHz	12892	452.7
		RBR XR-420 CT	15266	454.7
		Aquadopp DW 2 MHz	9846	580.9
		Aquadopp DW 2 MHz	8434	690.8
BR-K-15	168.9	TRDI WHS ADCP 300 kHz	102	145.0
		RBR XR-420 CT-Tu-FI-DO	22043	150.8
		Aquadopp Profiler 1 MHz	9711	152.2
DFO-2-15	110.8	TRDI NB ADCP 300kHz	464	107.0
DFO-1-15	54.8	TRDI NB ADCP 300kHz	506	51.0
DFO-9-15	35.5	TRDI WHS ADCP 300kHz	12414	32.0

Appendix D. Summary Statistics of Ocean Currents

Table 18: Summary statistics of current speed, vector-averaged direction and number of valid records by bin depth at BR-1-15 based on the data acquired with the QM ADCP #12698 from 2015 to 2016. Bin depths flagged manually as part of the QA/QC are highlighted in red.

Bin Depth (m)	Min Speed (m/s)	1%ile Speed (m/s)	5%ile Speed (m/s)	25%ile Speed (m/s)	Median Speed (m/s)	Mean Speed (m/s)	75%ile Speed (m/s)	95%ile Speed (m/s)	99%ile Speed (m/s)	Max Speed (m/s)	Standard Deviation Speed (m/s)	Vector-Averaged Direction (deg TN)	Number of Valid Records	% of Valid Data (%)
14.8	0.00	0.01	0.02	0.04	0.07	0.09	0.12	0.26	0.35	0.53	0.08	266.1	27,012	83.6
19.8	0.00	0.01	0.03	0.08	0.13	0.15	0.21	0.36	0.46	0.61	0.10	266.8	29,526	91.3
23.8	0.00	0.01	0.03	0.08	0.13	0.16	0.22	0.37	0.47	0.62	0.11	261.3	31,889	98.7
27.8	0.00	0.01	0.03	0.08	0.13	0.15	0.21	0.37	0.46	0.59	0.11	258.9	31,940	98.8
31.8	0.00	0.01	0.03	0.07	0.12	0.15	0.21	0.36	0.45	0.58	0.10	257.0	32,015	99.0
35.8	0.00	0.01	0.03	0.07	0.12	0.15	0.21	0.36	0.44	0.58	0.10	255.6	32,051	99.2
39.8	0.00	0.01	0.03	0.07	0.13	0.15	0.21	0.35	0.43	0.58	0.10	255.3	32,069	99.2
43.8	0.00	0.01	0.03	0.07	0.12	0.15	0.20	0.34	0.42	0.58	0.10	254.9	32,072	99.2
47.8	0.00	0.01	0.03	0.07	0.12	0.14	0.20	0.33	0.41	0.59	0.10	254.8	32,047	99.1
51.8	0.00	0.01	0.03	0.07	0.12	0.14	0.20	0.33	0.41	0.56	0.09	254.8	32,055	99.2
55.8	0.00	0.01	0.03	0.07	0.12	0.14	0.19	0.33	0.41	0.55	0.09	254.6	32,047	99.1
59.8	0.00	0.01	0.03	0.07	0.12	0.14	0.19	0.32	0.41	0.56	0.09	254.7	32,029	99.1
63.8	0.00	0.01	0.03	0.07	0.12	0.14	0.19	0.32	0.40	0.54	0.09	255.1	32,044	99.1
67.8	0.00	0.01	0.02	0.06	0.09	0.11	0.14	0.29	0.39	0.55	0.08	253.1	32,102	99.3
71.8	0.00	0.01	0.02	0.06	0.09	0.10	0.13	0.26	0.39	0.56	0.07	252.0	32,146	99.4
75.8	0.00	0.01	0.03	0.07	0.11	0.13	0.18	0.29	0.37	0.56	0.08	255.4	32,090	99.3
79.8	0.00	0.01	0.03	0.07	0.11	0.14	0.19	0.32	0.40	0.58	0.09	256.3	32,116	99.4
83.8	0.00	0.01	0.03	0.07	0.11	0.14	0.18	0.33	0.42	0.57	0.09	256.9	32,154	99.5
87.8	0.00	0.01	0.03	0.07	0.11	0.14	0.18	0.33	0.42	0.57	0.09	257.1	32,174	99.5
91.8	0.00	0.01	0.03	0.07	0.11	0.14	0.18	0.33	0.43	0.56	0.10	257.5	32,205	99.6
95.8	0.00	0.01	0.03	0.07	0.11	0.14	0.19	0.33	0.43	0.54	0.10	258.1	32,220	99.7
99.8	0.00	0.01	0.03	0.07	0.11	0.14	0.18	0.34	0.43	0.55	0.10	258.5	32,239	99.7

103.8	0.00	0.01	0.03	0.07	0.11	0.14	0.19	0.34	0.44	0.56	0.10	259.1	32,249	99.8
107.8	0.00	0.01	0.03	0.07	0.11	0.14	0.18	0.34	0.44	0.60	0.10	259.8	32,267	99.8
111.8	0.00	0.01	0.03	0.06	0.11	0.14	0.18	0.35	0.44	0.57	0.10	260.0	32,279	99.9
115.8	0.00	0.01	0.03	0.06	0.11	0.14	0.18	0.35	0.45	0.58	0.10	260.2	32,291	99.9
119.8	0.00	0.01	0.02	0.06	0.10	0.13	0.18	0.35	0.45	0.57	0.10	260.9	32,302	99.9
123.8	0.00	0.01	0.02	0.06	0.10	0.13	0.18	0.35	0.46	0.58	0.10	261.3	32,307	99.9
127.8	0.00	0.01	0.02	0.06	0.10	0.13	0.17	0.35	0.46	0.59	0.10	261.5	32,311	100.0
131.8	0.00	0.01	0.02	0.04	0.08	0.11	0.15	0.34	0.45	0.59	0.10	262.2	32,321	100.0
135.8	0.00	0.01	0.02	0.06	0.09	0.13	0.16	0.35	0.46	0.59	0.10	261.8	32,317	100.0
139.8	0.00	0.01	0.02	0.05	0.09	0.12	0.16	0.35	0.46	0.60	0.10	262.1	32,320	100.0
143.8	0.00	0.01	0.02	0.05	0.09	0.12	0.15	0.36	0.45	0.63	0.10	261.9	32,322	100.0
147.8	0.00	0.01	0.02	0.05	0.08	0.12	0.15	0.36	0.46	0.63	0.10	262.2	32,323	100.0
151.8	0.00	0.01	0.02	0.05	0.08	0.12	0.14	0.36	0.45	0.62	0.10	262.8	32,324	100.0
155.8	0.00	0.01	0.02	0.05	0.08	0.11	0.14	0.36	0.45	0.61	0.10	263.2	32,324	100.0
159.8	0.00	0.01	0.02	0.04	0.07	0.11	0.13	0.35	0.45	0.63	0.10	263.4	32,324	100.0
163.8	0.00	0.01	0.02	0.04	0.07	0.11	0.12	0.35	0.44	0.61	0.10	263.6	32,324	100.0
167.8	0.00	0.01	0.02	0.04	0.07	0.10	0.12	0.34	0.44	0.61	0.10	263.8	32,324	100.0
171.8	0.00	0.01	0.02	0.04	0.06	0.10	0.11	0.34	0.44	0.58	0.10	264.8	32,324	100.0

Table 19: Summary statistics of current speed, vector-averaged direction and number of valid records by bin depth at BR-1-15 based on the data acquired with the LR ADCP #12884 from 2015 to 2016.

Bin Depth (m)	Min Speed (m/s)	1%ile Speed (m/s)	5%ile Speed (m/s)	25%ile Speed (m/s)	Median Speed (m/s)	Mean Speed (m/s)	75%ile Speed (m/s)	95%ile Speed (m/s)	99%ile Speed (m/s)	Max Speed (m/s)	Standard Deviation Speed (m/s)	Vector-Averaged Direction (deg TN)	Number of Valid Records	% of Valid Data (%)
52.6	0.00	0.01	0.02	0.06	0.09	0.11	0.14	0.30	0.38	0.49	0.08	229.0	10,963	67.8
68.6	0.00	0.01	0.02	0.05	0.08	0.10	0.13	0.27	0.37	0.52	0.08	222.6	8,858	54.8
84.6	0.00	0.01	0.02	0.05	0.09	0.10	0.13	0.27	0.38	0.52	0.08	214.9	8,347	51.6
100.6	0.00	0.01	0.02	0.05	0.08	0.11	0.14	0.28	0.37	0.53	0.08	214.2	8,830	54.6
116.6	0.00	0.01	0.02	0.05	0.08	0.11	0.14	0.29	0.39	0.52	0.08	222.5	9,804	60.7

132.6	0.00	0.01	0.02	0.05	0.07	0.10	0.13	0.33	0.43	0.58	0.09	228.5	11,449	70.8
148.6	0.00	0.01	0.02	0.04	0.07	0.10	0.11	0.34	0.44	0.59	0.10	230.0	12,517	77.4
164.6	0.00	0.01	0.01	0.03	0.06	0.09	0.10	0.33	0.44	0.61	0.10	228.9	13,452	83.2
180.6	0.00	0.01	0.01	0.03	0.05	0.08	0.09	0.31	0.42	0.53	0.09	228.4	14,066	87.0
196.6	0.00	0.01	0.01	0.03	0.04	0.07	0.08	0.27	0.38	0.48	0.08	227.4	14,665	90.7
212.6	0.00	0.00	0.01	0.02	0.04	0.07	0.07	0.25	0.34	0.41	0.07	224.7	15,162	93.8
228.6	0.00	0.00	0.01	0.02	0.04	0.06	0.06	0.20	0.29	0.37	0.06	220.8	15,523	96.0
244.6	0.00	0.00	0.01	0.02	0.03	0.05	0.06	0.15	0.23	0.32	0.05	216.2	15,731	97.3
260.6	0.00	0.00	0.01	0.02	0.03	0.04	0.05	0.12	0.17	0.28	0.03	207.9	15,872	98.2
276.6	0.00	0.00	0.01	0.02	0.03	0.04	0.05	0.10	0.14	0.20	0.03	194.9	15,965	98.8
292.6	0.00	0.00	0.01	0.02	0.03	0.03	0.04	0.08	0.12	0.24	0.02	182.4	16,032	99.2
308.6	0.00	0.00	0.01	0.02	0.03	0.03	0.04	0.07	0.10	0.15	0.02	168.9	16,066	99.4
324.6	0.00	0.00	0.01	0.02	0.02	0.03	0.04	0.06	0.08	0.12	0.02	154.4	16,073	99.4
340.6	0.00	0.00	0.01	0.02	0.03	0.03	0.04	0.06	0.08	0.14	0.02	146.1	16,071	99.4
356.6	0.00	0.00	0.01	0.02	0.03	0.03	0.04	0.06	0.08	0.14	0.02	140.9	16,111	99.7
372.6	0.00	0.00	0.01	0.02	0.02	0.03	0.04	0.06	0.08	0.15	0.02	135.3	16,136	99.8
388.6	0.00	0.00	0.01	0.02	0.02	0.03	0.04	0.06	0.08	0.14	0.02	131.3	16,144	99.9
404.6	0.00	0.00	0.01	0.02	0.02	0.03	0.04	0.06	0.08	0.13	0.02	129.1	16,147	99.9
420.6	0.00	0.00	0.01	0.02	0.02	0.03	0.04	0.06	0.08	0.13	0.02	126.4	16,158	100.0
436.6	0.00	0.00	0.01	0.02	0.02	0.03	0.04	0.06	0.08	0.13	0.02	115.0	16,162	100.0

Table 20: Summary statistics of current speed, vector-averaged direction and number of valid records at 595.6 and 757.3 m depth at BR-1-15 as based on the data acquired with the Aquadopp DW #2792 and #2701 from 2015 to 2016.

Bin Depth (m)	Min Speed (m/s)	1%ile Speed (m/s)	5%ile Speed (m/s)	25%ile Speed (m/s)	Median Speed (m/s)	Mean Speed (m/s)	75%ile Speed (m/s)	95%ile Speed (m/s)	99%ile Speed (m/s)	Max Speed (m/s)	Standard Deviation Speed (m/s)	Vector-Averaged Direction (deg TN)	Number of Valid Records	% of Valid Data (%)
595.6	0.00	0.00	0.01	0.02	0.03	0.03	0.04	0.06	0.08	0.11	0.02	75.7	16,162	100.0
757.3	0.00	0.00	0.01	0.01	0.03	0.03	0.04	0.08	0.11	0.16	0.02	106.5	15,811	100.0

Table 21: Summary statistics of current speed, vector-averaged direction and number of valid records by bin depth at BR-3-15 based on the data acquired with the LR ADCP #12942 from 2015 to 2016. Bin depths flagged manually as part of the QA/QC are highlighted in red.

Bin Depth (m)	Min Speed (m/s)	1%ile Speed (m/s)	5%ile Speed (m/s)	25%ile Speed (m/s)	Median Speed (m/s)	Mean Speed (m/s)	75%ile Speed (m/s)	95%ile Speed (m/s)	99%ile Speed (m/s)	Max Speed (m/s)	Standard Deviation Speed (m/s)	Vector-Averaged Direction (deg TN)	Number of Valid Records	% of Valid Data (%)
54.4	0.00	0.01	0.02	0.04	0.07	0.07	0.10	0.15	0.19	0.29	0.04	175.0	8,835	98.7
70.4	0.00	0.01	0.02	0.04	0.06	0.07	0.09	0.14	0.17	0.28	0.04	171.2	8,785	98.1
86.4	0.00	0.01	0.01	0.03	0.05	0.06	0.08	0.12	0.16	0.30	0.03	166.5	8,730	97.5
102.4	0.00	0.01	0.01	0.03	0.05	0.06	0.07	0.12	0.15	0.32	0.03	166.8	8,754	97.8
118.4	0.00	0.01	0.01	0.03	0.05	0.05	0.07	0.11	0.15	0.28	0.03	165.1	8,800	98.3
134.4	0.00	0.01	0.01	0.03	0.05	0.06	0.07	0.11	0.15	0.30	0.03	164.2	8,825	98.6
150.4	0.00	0.01	0.02	0.03	0.05	0.06	0.08	0.12	0.17	0.30	0.03	162.0	8,844	98.8
166.4	0.00	0.01	0.01	0.03	0.05	0.06	0.07	0.12	0.18	0.31	0.03	155.3	8,866	99.0
182.4	0.00	0.01	0.01	0.03	0.05	0.05	0.07	0.11	0.18	0.29	0.03	141.5	8,893	99.3
198.4	0.00	0.01	0.01	0.03	0.05	0.05	0.07	0.11	0.16	0.27	0.03	101.8	8,908	99.5
214.4	0.00	0.01	0.01	0.03	0.05	0.05	0.07	0.11	0.15	0.28	0.03	40.9	8,923	99.7
230.4	0.00	0.01	0.01	0.03	0.05	0.05	0.07	0.11	0.14	0.23	0.03	16.1	8,925	99.7
246.4	0.00	0.01	0.01	0.03	0.05	0.05	0.07	0.11	0.14	0.34	0.03	2.5	8,943	99.9
262.4	0.00	0.01	0.01	0.03	0.05	0.05	0.07	0.11	0.14	0.21	0.03	356.6	8,947	99.9
278.4	0.00	0.01	0.01	0.03	0.05	0.05	0.07	0.11	0.14	0.25	0.03	357.0	8,952	100.0
294.4	0.00	0.01	0.01	0.03	0.04	0.05	0.07	0.10	0.13	0.20	0.03	355.3	8,952	100.0
310.4	0.00	0.00	0.01	0.03	0.04	0.05	0.06	0.10	0.12	0.20	0.03	355.1	8,952	100.0
326.4	0.00	0.01	0.01	0.03	0.05	0.05	0.07	0.11	0.14	0.20	0.03	354.5	8,952	100.0
342.4	0.00	0.01	0.01	0.03	0.05	0.05	0.07	0.11	0.14	0.20	0.03	352.7	8,952	100.0
358.4	0.00	0.01	0.01	0.03	0.05	0.05	0.07	0.11	0.14	0.21	0.03	355.0	8,952	100.0
374.4	0.00	0.01	0.01	0.03	0.05	0.05	0.07	0.11	0.14	0.21	0.03	355.2	8,952	100.0
390.4	0.00	0.01	0.01	0.03	0.05	0.05	0.07	0.11	0.15	0.21	0.03	355.6	8,952	100.0
406.4	0.00	0.01	0.01	0.03	0.05	0.05	0.07	0.11	0.14	0.20	0.03	356.6	8,952	100.0
422.4	0.00	0.01	0.01	0.03	0.05	0.05	0.07	0.11	0.15	0.23	0.03	354.9	8,952	100.0

Table 22: Summary statistics of current speed, vector-averaged direction and number of valid records at 574.7 and 685.2 m depth at BR-3-15 as based on the data acquired with the Aquadopp DW #6109 and #8541 from 2015 to 2016.

Bin Depth (m)	Min Speed (m/s)	1%ile Speed (m/s)	5%ile Speed (m/s)	25%ile Speed (m/s)	Median Speed (m/s)	Mean Speed (m/s)	75%ile Speed (m/s)	95%ile Speed (m/s)	99%ile Speed (m/s)	Max Speed (m/s)	Standard Deviation Speed (m/s)	Vector-Averaged Direction (deg TN)	Number of Valid Records	% of Valid Data (%)
574.7	0.00	0.01	0.01	0.03	0.05	0.06	0.09	0.13	0.16	0.20	0.04	325.5	3,643	40.7
685.2	0.00	0.01	0.01	0.04	0.07	0.08	0.11	0.17	0.21	0.31	0.05	331.5	8,952	100.0

Table 23: Summary statistics of current speed, vector-averaged direction and number of valid records by bin depth at BR-G-15 based on the data acquired with the QM ADCP #12841 from 2015 to 2016. Bin depths flagged manually as part of the QA/QC are highlighted in red.

Bin Depth (m)	Min Speed (m/s)	1%ile Speed (m/s)	5%ile Speed (m/s)	25%ile Speed (m/s)	Median Speed (m/s)	Mean Speed (m/s)	75%ile Speed (m/s)	95%ile Speed (m/s)	99%ile Speed (m/s)	Max Speed (m/s)	Standard Deviation Speed (m/s)	Vector-Averaged Direction (deg TN)	Number of Valid Records	% of Valid Data (%)
16.5	0.00	0.02	0.04	0.09	0.15	0.16	0.21	0.31	0.38	0.56	0.08	265.2	31,462	88.8
20.5	0.00	0.02	0.04	0.10	0.17	0.19	0.26	0.40	0.47	0.60	0.11	272.8	35,220	99.4
24.5	0.00	0.02	0.04	0.10	0.17	0.19	0.26	0.41	0.50	0.62	0.11	271.1	35,327	99.7
28.5	0.00	0.02	0.04	0.10	0.17	0.18	0.25	0.40	0.48	0.65	0.11	267.7	35,330	99.7
32.5	0.00	0.02	0.04	0.10	0.17	0.18	0.25	0.38	0.47	0.64	0.11	264.8	35,309	99.6
36.5	0.00	0.02	0.04	0.10	0.17	0.18	0.25	0.37	0.46	0.66	0.10	262.7	35,323	99.7
40.5	0.00	0.02	0.04	0.09	0.16	0.17	0.24	0.36	0.45	0.65	0.10	262.1	35,297	99.6
44.5	0.00	0.01	0.03	0.09	0.15	0.17	0.23	0.35	0.44	0.67	0.10	261.8	35,305	99.6
48.5	0.00	0.02	0.04	0.09	0.16	0.17	0.23	0.35	0.43	0.67	0.10	259.9	35,305	99.6
52.5	0.00	0.02	0.04	0.09	0.16	0.17	0.23	0.34	0.43	0.69	0.10	258.4	35,341	99.7
56.5	0.00	0.01	0.03	0.09	0.15	0.16	0.22	0.34	0.43	0.72	0.10	257.8	35,332	99.7
60.5	0.00	0.01	0.03	0.09	0.15	0.16	0.22	0.34	0.42	0.77	0.10	257.9	35,330	99.7
64.5	0.00	0.02	0.03	0.09	0.15	0.16	0.22	0.33	0.43	0.82	0.10	257.7	35,326	99.7
68.5	0.00	0.01	0.03	0.09	0.15	0.16	0.22	0.33	0.43	0.80	0.10	258.4	35,325	99.7
72.5	0.00	0.01	0.03	0.09	0.15	0.16	0.22	0.33	0.43	0.83	0.10	258.5	35,333	99.7
76.5	0.00	0.01	0.03	0.09	0.15	0.16	0.21	0.33	0.43	0.80	0.10	258.8	35,334	99.7

80.5	0.00	0.01	0.03	0.09	0.15	0.16	0.21	0.33	0.43	0.80	0.10	259.0	35,354	99.7
84.5	0.00	0.01	0.03	0.09	0.15	0.16	0.21	0.33	0.43	0.81	0.10	260.0	35,374	99.8
88.5	0.00	0.01	0.03	0.09	0.14	0.16	0.21	0.33	0.44	0.80	0.09	260.1	35,388	99.8
92.5	0.00	0.01	0.03	0.09	0.14	0.16	0.21	0.32	0.44	0.79	0.09	259.8	35,405	99.9
96.5	0.00	0.01	0.03	0.09	0.14	0.16	0.21	0.32	0.45	0.77	0.09	259.6	35,417	99.9
100.5	0.00	0.01	0.03	0.09	0.14	0.15	0.20	0.32	0.44	0.79	0.09	261.1	35,425	99.9
104.5	0.00	0.01	0.02	0.05	0.07	0.10	0.11	0.28	0.39	0.84	0.09	273.3	35,442	100.0
108.5	0.00	0.01	0.03	0.05	0.08	0.10	0.13	0.24	0.30	0.74	0.07	271.5	35,442	100.0
112.5	0.00	0.02	0.04	0.09	0.14	0.15	0.20	0.29	0.34	0.49	0.08	261.0	35,402	99.9
116.5	0.00	0.02	0.04	0.09	0.14	0.15	0.20	0.31	0.41	0.62	0.08	260.8	35,414	99.9
120.5	0.00	0.02	0.03	0.09	0.14	0.15	0.19	0.30	0.41	0.72	0.09	261.7	35,444	100.0
124.5	0.00	0.02	0.03	0.09	0.14	0.15	0.19	0.29	0.40	0.74	0.08	262.9	35,444	100.0
128.5	0.00	0.01	0.03	0.08	0.13	0.14	0.19	0.28	0.39	0.73	0.08	263.8	35,445	100.0
132.5	0.00	0.01	0.03	0.08	0.13	0.14	0.19	0.28	0.38	0.69	0.08	263.3	35,445	100.0
136.5	0.00	0.01	0.03	0.08	0.13	0.14	0.18	0.27	0.36	0.67	0.08	262.7	35,445	100.0
140.5	0.00	0.01	0.03	0.08	0.12	0.13	0.18	0.26	0.35	0.66	0.07	262.7	35,445	100.0
144.5	0.00	0.01	0.03	0.07	0.12	0.13	0.17	0.25	0.33	0.64	0.07	263.9	35,445	100.0
148.5	0.00	0.01	0.03	0.07	0.11	0.12	0.17	0.24	0.32	0.61	0.07	264.6	35,445	100.0
152.5	0.00	0.01	0.03	0.07	0.11	0.12	0.16	0.24	0.31	0.61	0.07	266.2	35,445	100.0

Table 24: Summary statistics of current speed, vector-averaged direction and number of valid records by bin depth at BR-G-15 based on the data acquired with the LR ADCP #12892 from 2015 to 2016.

Bin Depth (m)	Min Speed (m/s)	1%ile Speed (m/s)	5%ile Speed (m/s)	25%ile Speed (m/s)	Median Speed (m/s)	Mean Speed (m/s)	75%ile Speed (m/s)	95%ile Speed (m/s)	99%ile Speed (m/s)	Max Speed (m/s)	Standard Deviation Speed (m/s)	Vector-Averaged Direction (deg TN)	Number of Valid Records	% of Valid Data (%)
44.7	0.00	0.01	0.03	0.07	0.11	0.12	0.16	0.27	0.36	1.10	0.08	269.8	15,660	88.4
60.7	0.00	0.01	0.03	0.08	0.15	0.16	0.21	0.33	0.41	0.63	0.09	273.6	17,407	98.2
76.7	0.00	0.01	0.03	0.08	0.14	0.16	0.21	0.32	0.42	0.61	0.09	274.1	17,262	97.4

92.7	0.00	0.01	0.03	0.08	0.14	0.15	0.21	0.33	0.43	0.76	0.09	274.4	17,267	97.4
108.7	0.00	0.01	0.03	0.09	0.14	0.15	0.20	0.31	0.41	0.76	0.09	274.0	17,399	98.2
124.7	0.00	0.01	0.03	0.08	0.13	0.14	0.19	0.30	0.39	0.79	0.08	274.4	17,490	98.7
140.7	0.00	0.01	0.03	0.07	0.12	0.13	0.17	0.25	0.32	0.72	0.07	273.6	17,562	99.1
156.7	0.00	0.01	0.03	0.06	0.10	0.11	0.16	0.24	0.31	0.65	0.07	275.0	17,610	99.4
172.7	0.00	0.01	0.02	0.05	0.09	0.10	0.13	0.21	0.27	0.56	0.06	276.2	17,644	99.6
188.7	0.00	0.01	0.02	0.04	0.07	0.08	0.11	0.19	0.24	0.53	0.05	277.0	17,674	99.7
204.7	0.00	0.01	0.02	0.04	0.06	0.07	0.09	0.16	0.22	0.37	0.05	278.1	17,699	99.9
220.7	0.00	0.01	0.01	0.03	0.06	0.06	0.08	0.14	0.19	0.30	0.04	279.8	17,710	99.9
236.7	0.00	0.01	0.01	0.03	0.05	0.06	0.07	0.12	0.17	0.24	0.03	282.3	17,719	100.0
252.7	0.00	0.01	0.01	0.03	0.05	0.05	0.07	0.11	0.15	0.26	0.03	285.1	17,722	100.0
268.7	0.00	0.01	0.01	0.03	0.04	0.05	0.06	0.10	0.14	0.20	0.03	291.6	17,720	100.0
284.7	0.00	0.01	0.01	0.03	0.04	0.05	0.06	0.10	0.13	0.19	0.03	296.2	17,721	100.0
300.7	0.00	0.01	0.01	0.03	0.04	0.04	0.06	0.09	0.12	0.21	0.03	302.1	17,722	100.0
316.7	0.00	0.01	0.01	0.03	0.04	0.04	0.06	0.09	0.12	0.21	0.02	307.1	17,722	100.0
332.7	0.00	0.01	0.01	0.03	0.04	0.04	0.06	0.09	0.12	0.19	0.02	311.6	17,722	100.0
348.7	0.00	0.01	0.01	0.03	0.04	0.04	0.06	0.09	0.12	0.18	0.02	316.4	17,722	100.0
364.7	0.00	0.00	0.01	0.03	0.04	0.04	0.06	0.09	0.12	0.20	0.02	322.4	17,722	100.0
380.7	0.00	0.00	0.01	0.02	0.04	0.04	0.06	0.09	0.12	0.19	0.02	326.1	17,722	100.0
396.7	0.00	0.00	0.01	0.02	0.04	0.04	0.06	0.09	0.12	0.19	0.02	329.6	17,722	100.0
412.7	0.00	0.00	0.01	0.02	0.04	0.04	0.06	0.09	0.12	0.23	0.02	334.2	17,722	100.0
428.7	0.00	0.00	0.01	0.03	0.04	0.04	0.06	0.09	0.12	0.18	0.02	336.2	17,722	100.0

Table 25: Summary statistics of current speed, vector-averaged direction and number of valid records at 580.9 and 690.8 m depth at BR-G-15 as based on the data acquired with the Aquadopp DW #9846 and #8434 from 2015 to 2016.

Bin Depth (m)	Min Speed (m/s)	1%ile Speed (m/s)	5%ile Speed (m/s)	25%ile Speed (m/s)	Median Speed (m/s)	Mean Speed (m/s)	75%ile Speed (m/s)	95%ile Speed (m/s)	99%ile Speed (m/s)	Max Speed (m/s)	Standard Deviation Speed (m/s)	Vector-Averaged Direction (deg TN)	Number of Valid Records	% of Valid Data (%)
580.9	0.00	0.00	0.01	0.02	0.04	0.04	0.05	0.09	0.11	0.16	0.02	33.7	17,723	100.0

690.8	0.00	0.00	0.01	0.02	0.04	0.05	0.07	0.12	0.16	0.24	0.04	52.2	17,723	100.0
-------	------	------	------	------	------	------	------	------	------	------	------	------	--------	-------

Table 26: Summary statistics of current speed, vector-averaged direction and number of valid records by bin depth at BR-K-15 based on the data acquired with the WHS ADCP #102 from 2015 to 2016.

Bin Depth (m)	Min Speed (m/s)	1%ile Speed (m/s)	5%ile Speed (m/s)	25%ile Speed (m/s)	Median Speed (m/s)	Mean Speed (m/s)	75%ile Speed (m/s)	95%ile Speed (m/s)	99%ile Speed (m/s)	Max Speed (m/s)	Standard Deviation Speed (m/s)	Vector-Averaged Direction (deg TN)	Number of Valid Records	% of Valid Data (%)
22.9	0.00	0.01	0.03	0.08	0.14	0.16	0.22	0.35	0.54	0.85	0.11	253.4	13,207	74.3
30.9	0.00	0.02	0.03	0.08	0.14	0.16	0.21	0.33	0.52	0.75	0.10	342.4	15,478	87.0
38.9	0.00	0.01	0.03	0.08	0.13	0.15	0.21	0.32	0.51	0.70	0.10	50.7	16,794	94.4
46.9	0.00	0.01	0.03	0.08	0.14	0.16	0.21	0.32	0.51	0.73	0.10	59.5	17,463	98.2
54.9	0.00	0.02	0.03	0.09	0.15	0.16	0.22	0.34	0.51	0.76	0.10	64.3	17,651	99.3
62.9	0.00	0.02	0.03	0.09	0.16	0.17	0.23	0.37	0.53	0.79	0.11	64.8	17,746	99.8
70.9	0.00	0.02	0.03	0.09	0.16	0.18	0.24	0.41	0.57	0.89	0.12	64.6	17,779	100.0
78.9	0.00	0.02	0.03	0.10	0.17	0.19	0.26	0.43	0.60	0.95	0.13	64.4	17,783	100.0
86.9	0.00	0.02	0.04	0.10	0.18	0.20	0.28	0.46	0.60	0.92	0.14	63.9	17,784	100.0
94.9	0.00	0.02	0.04	0.10	0.18	0.21	0.30	0.47	0.60	0.85	0.14	62.8	17,784	100.0
102.9	0.00	0.02	0.04	0.10	0.19	0.21	0.31	0.48	0.59	0.82	0.14	61.2	17,784	100.0
110.9	0.00	0.02	0.04	0.11	0.19	0.21	0.30	0.47	0.58	0.78	0.14	60.0	17,784	100.0
118.9	0.00	0.02	0.04	0.10	0.18	0.21	0.29	0.46	0.57	0.78	0.13	59.2	17,784	100.0
126.9	0.00	0.01	0.03	0.10	0.18	0.20	0.28	0.44	0.56	0.75	0.13	58.6	17,784	100.0
134.9	0.00	0.01	0.03	0.09	0.16	0.18	0.26	0.41	0.53	0.73	0.12	59.8	17,784	100.0

Table 27: Summary statistics of current speed, vector-averaged direction and number of valid records by bin depth at DFO-2-15 based on the data acquired with the NB ADCP #464 from 2015 to 2016.

Bin Depth (m)	Min Speed (m/s)	1%ile Speed (m/s)	5%ile Speed (m/s)	25%ile Speed (m/s)	Median Speed (m/s)	Mean Speed (m/s)	75%ile Speed (m/s)	95%ile Speed (m/s)	99%ile Speed (m/s)	Max Speed (m/s)	Standard Deviation Speed (m/s)	Vector-Averaged Direction (deg TN)	Number of Valid Records	% of Valid Data (%)
11.1	0.00	0.01	0.02	0.05	0.09	0.10	0.14	0.22	0.28	0.51	0.06	160.1	14,248	81.5
15.0	0.00	0.01	0.02	0.05	0.09	0.10	0.14	0.21	0.27	0.48	0.06	171.8	17,325	99.1

18.9	0.00	0.01	0.02	0.05	0.09	0.10	0.13	0.21	0.28	0.40	0.06	171.1	17,456	99.9
22.7	0.00	0.01	0.02	0.05	0.09	0.10	0.13	0.22	0.29	0.40	0.06	170.2	17,477	100.0
26.6	0.00	0.01	0.02	0.05	0.09	0.10	0.13	0.22	0.29	0.40	0.06	168.3	17,477	100.0
30.5	0.00	0.01	0.02	0.05	0.09	0.10	0.13	0.23	0.29	0.40	0.06	166.0	17,477	100.0
34.4	0.00	0.01	0.02	0.05	0.09	0.10	0.13	0.23	0.29	0.41	0.06	164.4	17,469	99.9
38.3	0.00	0.01	0.02	0.06	0.09	0.10	0.13	0.23	0.30	0.42	0.06	162.4	17,466	99.9
42.2	0.00	0.01	0.02	0.05	0.09	0.10	0.13	0.23	0.30	0.41	0.06	160.2	17,465	99.9
46.1	0.00	0.01	0.02	0.06	0.09	0.10	0.13	0.23	0.29	0.40	0.06	156.5	17,479	100.0

Table 28: Summary statistics of current speed, vector-averaged direction and number of valid records by bin depth at DFO-1-15 based on the data acquired with the NB ADCP #506 from 2015 to 2016.

Bin Depth (m)	Min Speed (m/s)	1%ile Speed (m/s)	5%ile Speed (m/s)	25%ile Speed (m/s)	Median Speed (m/s)	Mean Speed (m/s)	75%ile Speed (m/s)	95%ile Speed (m/s)	99%ile Speed (m/s)	Max Speed (m/s)	Standard Deviation Speed (m/s)	Vector-Averaged Direction (deg TN)	Number of Valid Records	% of Valid Data (%)
19.3	0.00	0.01	0.02	0.05	0.09	0.10	0.14	0.23	0.36	0.60	0.07	244.0	5,883	33.2
23.2	0.00	0.01	0.03	0.07	0.11	0.13	0.17	0.29	0.38	0.64	0.08	237.1	12,478	70.3
27.1	0.00	0.01	0.03	0.08	0.12	0.14	0.18	0.30	0.38	0.61	0.08	237.0	12,209	68.8
31.0	0.00	0.01	0.03	0.07	0.12	0.13	0.18	0.29	0.37	0.54	0.08	235.6	13,895	78.3
34.9	0.00	0.01	0.03	0.07	0.12	0.13	0.17	0.27	0.36	0.49	0.08	231.9	15,093	85.1
38.8	0.00	0.01	0.03	0.07	0.11	0.13	0.17	0.27	0.34	0.48	0.07	231.3	16,101	90.8
42.7	0.00	0.01	0.03	0.07	0.11	0.13	0.17	0.26	0.33	0.51	0.07	232.5	16,725	94.3
46.6	0.00	0.01	0.03	0.07	0.11	0.12	0.17	0.26	0.33	0.49	0.07	229.1	17,065	96.2
50.5	0.00	0.01	0.03	0.07	0.11	0.12	0.16	0.25	0.33	0.44	0.07	227.6	17,144	96.6
58.3	0.00	0.01	0.03	0.07	0.11	0.12	0.16	0.25	0.32	0.42	0.07	211.5	17,612	99.3
62.2	0.00	0.01	0.03	0.07	0.11	0.12	0.16	0.25	0.32	0.45	0.07	195.7	17,622	99.3
66.1	0.00	0.01	0.03	0.07	0.11	0.12	0.16	0.25	0.31	0.42	0.07	160.1	17,611	99.3
70.0	0.00	0.01	0.03	0.06	0.10	0.12	0.15	0.25	0.31	0.40	0.07	113.3	17,635	99.4
73.9	0.00	0.01	0.03	0.06	0.10	0.11	0.15	0.24	0.31	0.37	0.07	86.7	17,582	99.1
77.8	0.00	0.01	0.03	0.06	0.10	0.11	0.15	0.24	0.31	0.39	0.07	74.9	17,635	99.4

81.7	0.00	0.01	0.02	0.06	0.10	0.11	0.15	0.24	0.30	0.39	0.07	68.2	17,643	99.4
85.6	0.00	0.01	0.02	0.06	0.09	0.11	0.15	0.24	0.30	0.42	0.07	61.8	17,671	99.6
89.5	0.00	0.01	0.02	0.05	0.09	0.10	0.14	0.23	0.29	0.42	0.07	56.8	17,687	99.7
93.4	0.00	0.01	0.02	0.05	0.08	0.10	0.13	0.22	0.28	0.40	0.06	54.3	17,674	99.6
97.3	0.00	0.01	0.02	0.05	0.08	0.10	0.13	0.22	0.28	0.39	0.06	52.7	17,693	99.7
101.2	0.00	0.01	0.02	0.04	0.08	0.09	0.13	0.21	0.27	0.38	0.06	55.8	17,740	100.0

Table 29: Summary statistics of current speed, vector-averaged direction and number of valid records by bin depth at DFO-9-15 based on the data acquired with the WHS ADCP #12414 from 2015 to 2016.

Bin Depth (m)	Min Speed (m/s)	1%ile Speed (m/s)	5%ile Speed (m/s)	25%ile Speed (m/s)	Median Speed (m/s)	Mean Speed (m/s)	75%ile Speed (m/s)	95%ile Speed (m/s)	99%ile Speed (m/s)	Max Speed (m/s)	Standard Deviation Speed (m/s)	Vector-Averaged Direction (deg TN)	Number of Valid Records	% of Valid Data (%)
2.8	0.00	0.01	0.03	0.08	0.15	0.18	0.25	0.45	0.61	1.00	0.13	238.6	10,603	60.7
3.8	0.00	0.01	0.02	0.06	0.13	0.16	0.22	0.39	0.56	0.91	0.12	269.2	14,975	85.8
4.8	0.00	0.01	0.02	0.06	0.12	0.15	0.21	0.36	0.52	0.89	0.11	268.0	15,660	89.7
5.8	0.00	0.01	0.02	0.05	0.11	0.14	0.19	0.34	0.50	0.84	0.11	263.2	16,195	92.8
6.8	0.00	0.01	0.02	0.05	0.10	0.13	0.18	0.33	0.48	0.79	0.10	256.1	16,794	96.2
7.8	0.00	0.01	0.02	0.05	0.10	0.12	0.17	0.31	0.47	0.78	0.10	250.1	17,022	97.5
8.8	0.00	0.01	0.02	0.05	0.10	0.12	0.17	0.30	0.45	0.71	0.09	244.2	17,119	98.0
9.8	0.00	0.01	0.02	0.05	0.09	0.12	0.16	0.29	0.42	0.64	0.09	237.9	17,299	99.1
10.8	0.00	0.01	0.02	0.05	0.09	0.11	0.16	0.28	0.41	0.58	0.09	235.1	17,364	99.4
11.8	0.00	0.01	0.02	0.05	0.09	0.11	0.15	0.27	0.39	0.56	0.08	228.8	17,390	99.6
12.8	0.00	0.01	0.02	0.05	0.09	0.11	0.15	0.26	0.37	0.56	0.08	222.1	17,408	99.7
13.8	0.00	0.01	0.02	0.05	0.09	0.11	0.15	0.26	0.36	0.59	0.08	215.2	17,394	99.6
14.8	0.00	0.01	0.02	0.05	0.09	0.11	0.14	0.25	0.36	0.59	0.07	209.8	17,403	99.7
15.8	0.00	0.01	0.02	0.06	0.09	0.11	0.14	0.25	0.35	0.63	0.07	207.9	17,400	99.7
16.8	0.00	0.01	0.02	0.06	0.09	0.11	0.14	0.24	0.34	0.60	0.07	207.4	17,392	99.6
17.8	0.00	0.01	0.02	0.06	0.09	0.10	0.14	0.24	0.32	0.56	0.07	206.7	17,398	99.6
18.8	0.00	0.01	0.02	0.06	0.09	0.10	0.14	0.23	0.32	0.57	0.07	203.7	17,392	99.6

19.8	0.00	0.01	0.02	0.05	0.09	0.10	0.13	0.22	0.31	0.58	0.07	201.9	17,383	99.6
20.8	0.00	0.01	0.02	0.05	0.09	0.10	0.13	0.22	0.31	0.55	0.06	202.5	17,390	99.6
21.8	0.00	0.01	0.02	0.05	0.08	0.10	0.13	0.22	0.30	0.48	0.06	203.3	17,394	99.6
22.8	0.00	0.01	0.02	0.05	0.08	0.09	0.13	0.21	0.30	0.44	0.06	204.1	17,393	99.6
23.8	0.00	0.01	0.02	0.05	0.08	0.09	0.12	0.21	0.30	0.39	0.06	203.7	17,403	99.7
24.8	0.00	0.01	0.02	0.04	0.07	0.09	0.12	0.21	0.29	0.39	0.06	202.8	17,403	99.7
25.8	0.00	0.01	0.02	0.04	0.07	0.09	0.12	0.21	0.29	0.38	0.06	201.3	17,410	99.7
26.8	0.00	0.01	0.02	0.04	0.07	0.08	0.11	0.20	0.29	0.38	0.06	200.5	17,416	99.7
27.8	0.00	0.01	0.01	0.04	0.07	0.08	0.11	0.20	0.29	0.39	0.06	200.1	17,459	100.0

integrated Beaufort Observatory

2017 Technical Project Report



Edited by:

ArcticNet Inc.
Fisheries and Oceans Canada
Golder Associates Ltd.

Table of Contents

1.0	INTRODUCTION.....	1
1.1	Report Organization.....	3
1.2	Physical Setting of the Study Area.....	3
2.0	MATERIAL AND METHODS	5
2.1	Taut-line Mooring Design.....	5
2.1.1	Slope Moorings	5
2.1.2	Shelf Moorings	6
2.2	Compass Calibration and Verification.....	7
2.3	Mooring Recovery and Deployment.....	8
2.3.1	Shipboard Mooring Operations.....	9
2.4	Data Processing and QA/QC.....	10
2.4.1	Current Meters and Current Profilers.....	10
2.4.2	Temperature-Salinity Loggers	13
2.4.3	Ice Profiling Sonars and Ice velocity.....	14
2.4.4	Sediment Traps	14
3.0	RESULTS AND DISCUSSION	15
3.1	Sea Ice Conditions.....	15
3.2	Ocean Currents	17
3.2.1	Mooring BR-1	18
3.2.2	Mooring BR-3	31
3.2.3	Mooring BR-G	43
3.2.4	Mooring BR-K.....	55
3.2.5	Mooring DFO-2.....	62
3.2.6	Mooring DFO-1.....	67
3.2.7	Mooring DFO-9.....	71
3.2.8	Spatial Variability of Surface and Bottom Currents in Open Water.....	75
3.3	Temperature and Salinity.....	78
3.4	Biogeochemical Fluxes.....	94
4.0	CONCLUSIONS.....	95
4.1	Concluding Remarks on the 2016-2017 Dataset	95
4.2	2017 Fieldwork Lessons Learned and Recommendations	96

4.3	Objectives and Milestones for 2018-2019.....	97
-----	--	----

5.0 REFERENCES..... 99

TABLES

Table 1: Mean Error of TRDI Compasses (10 Degree Increment).....	8
Table 2: 2016-2017 Mooring Recovery Summary.....	8
Table 3: 2017-2018 Mooring Deployment Summary.....	9
Table 4: Magnetic declination values for 2016-2017 iBO Moorings	11
Table 5: Angles chosen to describe the along-slope/shelf current component for each iBO mooring.....	17
Table 6: Selected bin depths to characterize circulation patterns throughout the water column.....	17
Table 7: Summary of current profilers and current meters clock drift, first and last good record, and percentage of raw data return on iBO moorings from 2016 to 2017.....	18
Table 8: Annual statistics of current speed and direction at BR-1-16 from selected bin depths representative of water mass variability in the Beaufort Sea (see Table 6 for water mass description).....	24
Table 9: Annual statistics of current speed and direction at BR-3-16 from selected bin depths representative of water mass variability in the Beaufort Sea (see Table 6 for water mass description).....	36
Table 10: Annual statistics of current speed and direction at BR-G-16 from selected bin depths representative of water mass variability in the Beaufort Sea (see Table 6 for water mass description).....	48
Table 11: Annual statistics of current speed and direction at BR-K-16 from selected bin depths representative of water mass variability in the Beaufort Sea (see Table 6 for water mass description).....	58
Table 12: Annual statistics of current speed and direction at DFO-2-16 from selected bin depths representative of water mass variability in the Beaufort Sea (see Table 6 for water mass description).....	64
Table 13: Annual statistics of current speed and direction at DFO-1-16 from a selected bin depth representative of the Polar-mixed layer (see Table 6 for water mass description).....	69
Table 14: Annual statistics of current speed and direction at DFO-9-16 from a selected bin depth representative of the Polar-mixed layer (see Table 6 for water mass description).....	73
Table 15: Summary of CT data logger clock drift and percentage of raw data return on iBO moorings from 2016 to 2017.....	80
Table 16: Summary of valid and flagged data from CT loggers deployed on the BR slope moorings from 2016 to 2017. See Table 15 for the instrument model associated with each serial number.....	81
Table 17: 2018-2019 iBO Milestones.....	98
Table 18: Summary statistics of current speed, vector-averaged direction and number of valid records by bin depth at BR-1-16 based on the data acquired with the QM ADCP #12823 from 2016 to 2017. Bin depths flagged manually as part of the QA/QC are highlighted in red.....	104
Table 19: Summary statistics of current speed, vector-averaged direction and number of valid records by bin depth at BR-1-16 based on the data acquired with the LR ADCP #12943 from 2016 to 2017.....	106
Table 20: Summary statistics of current speed, vector-averaged direction and number of valid records at 590.5 and 745.2 m depth at BR-1-16 as based on the data acquired with the Aquadopp DW #8543 and #8448 from 2016 to 2017.....	107
Table 21: Summary statistics of current speed, vector-averaged direction and number of valid records by bin depth at BR-3-16 based on the data acquired with the QM ADCP #8784 from 2016 to 2017. Bin depths flagged manually as part of the QA/QC are highlighted in red.....	107
Table 22: Summary statistics of current speed, vector-averaged direction and number of valid records by bin depth at BR-3-16 based on the data acquired with the LR ADCP #18785 from 2016 to 2017.....	109

Table 23: Summary statistics of current speed, vector-averaged direction and number of valid records at 601.5 and 712.8 m depth at BR-3-16 as based on the data acquired with the Aquadopp DW #8447 and #9473 from 2016 to 2017. 110

Table 24: Summary statistics of current speed, vector-averaged direction and number of valid records by bin depth at BR-G-16 based on the data acquired with the QM ADCP #12699 from 2016 to 2017. Bin depths flagged manually as part of the QA/QC are highlighted in red. 110

Table 25: Summary statistics of current speed, vector-averaged direction and number of valid records by bin depth at BR-G-16 based on the data acquired with the LR ADCP #13079 from 2016 to 2017. 112

Table 26: Summary statistics of current speed, vector-averaged direction and number of valid records at 564.8 and 674.3 m depth at BR-G-16 as based on the data acquired with the Aquadopp DW #8419 and #8442 from 2016 to 2017. 113

Table 27: Summary statistics of current speed, vector-averaged direction and number of valid records by bin depth at BR-K-16 based on the data acquired with the WHS ADCP #7844 from 2016 to 2017. 113

Table 28: Summary statistics of current speed, vector-averaged direction and number of valid records by bin depth at BR-K-16 based on the data acquired with the Nortek Aquadopp Profiler #1147 from 2016 to 2017. Bin depths flagged manually as part of the QA/QC are highlighted in red. 114

Table 29: Summary statistics of current speed, vector-averaged direction and number of valid records by bin depth at DFO-2-16 based on the data acquired with the NB ADCP #586 from 2016 to 2017. 115

Table 30: Summary statistics of current speed, vector-averaged direction and number of valid records by bin depth at DFO-1-16 based on the data acquired with the WHS ADCP #12463 from 2016 to 2017. 116

Table 31: Summary statistics of current speed, vector-averaged direction and number of valid records by bin depth at DFO-9-16 based on the data acquired with the WHS ADCP #2412 from 2016 to 2017. 117

FIGURES

Figure 1: Bathymetric map of the Canadian Beaufort Sea showing the location of iBO moorings (in red). Moorings from partner projects (ArcticNet, DFO, MARES/BOEM) are also shown on the map but are not detailed in the present report).2

Figure 2: Weekly ice coverage by stage of development for the season 2016 (March – September 2016) as based on daily ice charts from Canadian Ice services. Brown: old ice. Green: first-year ice. Pink/purple: New/Young ice. Red line: average sea ice concentration 1992-2010. Data source: Ice graph 2.5, <http://iceweb1.cis.ec.gc.ca/IceGraph/>. 15

Figure 3: Sea ice concentration (% coverage) for a 12.5 X 12.5 km pixel area over each iBO mooring during 2016-2017 as derived from SSM/I satellite imagery. The black line shows the mean ice concentration over 1992-2016 within each pixel. ... 16

Figure 4: Time-series of current speed, current direction and along-slope current component at mooring BR-1-16 measured by the QM ADCP #12823. The black line depicts the instrument depth.20

Figure 5: Time-series of current speed, current direction and along-slope current component at mooring BR-1-16 measured by the LR ADCP #12943. The black line depicts the instrument depth.21

Figure 6: Time-series of current speed, current direction and along-slope current component at 591 m at mooring BR-1-16 measured by the Aquadopp #8543.22

Figure 7: Time-series of current speed, current direction and along-slope current component at 745 m at mooring BR-1-16 measured by the Aquadopp #8448.23

Figure 8: Seasonal current roses at 29 m depth (bin cell #35) at BR-1-16 measured by the QM ADCP #12823. Data are low-pass filtered. Roses indicate the direction toward which currents flow. Seasons are defined following the meteorological convention (Fall: October-December; Winter: January-March; Spring: April-June; Summer: July-September).25

Figure 9: Seasonal current roses at 129 m depth (bin cell #10) at BR-1-16 measured by the QM ADCP #12823. Data are low-pass filtered. Roses indicate the direction toward which currents flow. Seasons are defined following the meteorological convention (Fall: October-December; Winter: January-March; Spring: April-June; Summer: July-September).26

Figure 10: Seasonal current roses at 226 m depth (bin cell #14) at BR-1-16 measured by the LR ADCP #12943. Data are low-pass filtered. Roses indicate the direction toward which currents flow. Seasons are defined following the meteorological convention (Fall: October-December; Winter: January-March; Spring: April-June; Summer: July-September).27

Figure 11: Seasonal current roses at 354 m depth (bin cell #6) at BR-1-16 measured by the LR ADCP #12943. Data are low-pass filtered. Roses indicate the direction toward which currents flow. Seasons are defined following the meteorological convention (Fall: October-December; Winter: January-March; Spring: April-June; Summer: July-September).28

Figure 12: Seasonal current roses at 591 m depth at BR-1-16 measured by the Aquadopp #8543. Data are low-pass filtered. Roses indicate the direction toward which currents flow. Seasons are defined following the meteorological convention (Fall: October-December; Winter: January-March; Spring: April-June; Summer: July-September).....29

Figure 13: Seasonal current roses at 745 m depth at BR-1-16 measured by the Aquadopp #8448. Data are low-pass filtered. Roses indicate the direction toward which currents flow. Seasons are defined following the meteorological convention (Fall: October-December; Winter: January-March; Spring: April-June; Summer: July-September).....30

Figure 14: Time-series of current speed, current direction and along-slope current component at mooring BR-3-16 measured by the QM ADCP #8784. The black line depicts the instrument depth.32

Figure 15: Time-series of current speed, current direction and along-slope current component at mooring BR-3-16 measured by the LR ADCP #18785. The black line depicts the instrument depth.33

Figure 16: Time-series of current speed, current direction and along-slope current component at 602 m at mooring BR-3-16 as obtained with the Aquadopp #8447.34

Figure 17: Time-series of current speed, current direction and along-slope current component at 713 m at mooring BR-3-16 as obtained with the Aquadopp #9473.35

Figure 18: Seasonal current roses at 19 m depth (bin cell #46) at BR-3-16 measured by the QM ADCP #8784. Data are low-pass filtered. Roses point toward where the currents are going. Seasons are defined following the meteorological convention (Fall: October-December; Winter: January-March; Spring: April-June; Summer: July-September).....37

Figure 19: Seasonal current roses at 131 m depth (bin cell #18) at BR-3-16 measured by the QM ADCP #8784. Data are low-pass filtered. Roses indicate the direction toward which currents flow. Seasons are defined following the meteorological convention (Fall: October-December; Winter: January-March; Spring: April-June; Summer: July-September).38

Figure 20: Seasonal current roses at 216 m depth (bin cell #17) at BR-3-16 measured by the LR ADCP #18785. Data are low-pass filtered. Roses indicate the direction toward which currents flow. Seasons are defined following the meteorological convention (Fall: October-December; Winter: January-March; Spring: April-June; Summer: July-September).39

Figure 21: Seasonal current roses at 344 m depth (bin cell #9) at BR-3-16 measured by the LR ADCP #18785. Data are low-pass filtered. Roses indicate the direction toward which currents flow. Seasons are defined following the meteorological convention (Fall: October-December; Winter: January-March; Spring: April-June; Summer: July-September).40

Figure 22: Seasonal current roses at 602 m depth at BR-3-16 measured by the Aquadopp #8447. Data are low-pass filtered. Roses indicate the direction toward which currents flow. Seasons are defined following the meteorological convention (Fall: October-December; Winter: January-March; Spring: April-June; Summer: July-September).....41

Figure 23: Seasonal current roses at 713 m depth at BR-3-16 measured by the Aquadopp #9473. Data are low-pass filtered. Roses indicate the direction toward which currents flow. Seasons are defined following the meteorological convention (Fall: October-December; Winter: January-March; Spring: April-June; Summer: July-September).....42

Figure 24: Time-series of current speed, current direction and along-slope current component at mooring BR-G-16 measured by the QM ADCP #12699. The black line depicts the instrument depth.44

Figure 25: Time-series of current speed, current direction and along-slope current component at mooring BR-G-16 measured by the LR ADCP #13079. The black line depicts the instrument depth.45

Figure 26: Time-series of current speed, current direction and along-slope current component at 565 m at mooring BR-G-16 measured by the Aquadopp #8419.46

Figure 27: Time-series of current speed, current direction and along-slope current component at 674 m at mooring BR-G-16 measured by the Aquadopp #8442.47

Figure 28: Seasonal current roses at 29 m depth (bin cell #35) at BR-G-16 measured by the QM ADCP #12699. Data are low-pass filtered. Roses indicate the direction toward which currents flow. Seasons are defined following the meteorological convention (Fall: October-December; Winter: January-March; Spring: April-June; Summer: July-September). 49

Figure 29: Seasonal current roses at 133 m depth (bin cell #9) at BR-G-16 measured by the QM ADCP #12699. Data are low-pass filtered. Roses indicate the direction toward which currents flow. Seasons are defined following the meteorological convention (Fall: October-December; Winter: January-March; Spring: April-June; Summer: July-September). 50

Figure 30: Seasonal current roses at 220 m depth (bin cell #14) at BR-G-16 measured by the LR ADCP #13079. Data are low-pass filtered. Roses indicate the direction toward which currents flow. Seasons are defined following the meteorological convention (Fall: October-December; Winter: January-March; Spring: April-June; Summer: July-September). 51

Figure 31: Seasonal current roses at 348 m depth (bin cell #6) at BR-G-16 measured by the LR ADCP #13079. Data are low-pass filtered. Roses indicate the direction toward which currents flow. Seasons are defined following the meteorological convention (Fall: October-December; Winter: January-March; Spring: April-June; Summer: July-September). 52

Figure 32: Seasonal current roses at 565 m depth at BR-G-16 measured by the Aquadopp #8419. Data are low-pass filtered. Roses indicate the direction toward which currents flow. Seasons are defined following the meteorological convention (Fall: October-December; Winter: January-March; Spring: April-June; Summer: July-September)..... 53

Figure 33: Seasonal current roses at 674 m depth at BR-G-16 measured by the Aquadopp #8442. Data are low-pass filtered. Roses indicate the direction toward which currents flow. Seasons are defined following the meteorological convention (Fall: October-December; Winter: January-March; Spring: April-June; Summer: July-September)..... 54

Figure 34: Time-series of current speed, current direction and along-slope current component at mooring BR-K-16 measured by the WHS ADCP #7844. The black line depicts the instrument depth. 56

Figure 35: Time-series of current speed, current direction and along-slope current component at mooring BR-K-16 measured by the Aquadopp Profiler #11147. The black line depicts the instrument depth. 57

Figure 36: Seasonal current roses at 21 m depth (bin cell #14) at BR-K-16 measured by the WHS ADCP #7844. Data are low-pass filtered. Roses indicate the direction toward which currents flow. Seasons are defined following the meteorological convention (Fall: October-December; Winter: January-March; Spring: April-June; Summer: July-September). 59

Figure 37: Seasonal current roses at 125 m depth (bin cell #1) at BR-K-16 measured by the WHS ADCP #7844. Data are low-pass filtered. Roses indicate the direction toward which currents flow. Seasons are defined following the meteorological convention (Fall: October-December; Winter: January-March; Spring: April-June; Summer: July-September). 60

Figure 38: Seasonal current roses at 163 m depth (bin cell #14) at BR-K-16 measured by the Aquadopp Profiler #11147. Data are low-pass filtered. Roses indicate the direction toward which currents flow. Seasons are defined following the meteorological convention (Fall: October-December; Winter: January-March; Spring: April-June; Summer: July-September). 61

Figure 39: Time-series of current speed, current direction and along-slope current component at mooring DFO-2-16 measured by the NB ADCP #586. The black line depicts the instrument depth. 63

Figure 40: Seasonal current roses at 20 m depth at DFO-2-16 as based on low-pass filtered data from bin cell #22 measured by the NB ADCP #586. Roses indicate the direction toward which currents flow. Seasons are defined following the meteorological convention (Fall: October-December; Winter: January-March; Spring: April-June; Summer: July-September). 65

Figure 41: Seasonal current roses at 102 m depth at DFO-2-16 as based on low-pass filtered data from bin cell #1 measured by the NB ADCP #586. Roses indicate the direction toward which currents flow. Seasons are defined following the meteorological convention (Fall: October-December; Winter: January-March; Spring: April-June; Summer: July-September). 66

Figure 42: Time-series of current speed, current direction and along-slope current component at mooring DFO-1-16 measured by the NB ADCP #12463. The black line depicts the instrument depth..... 68

Figure 43: Seasonal current roses at 19 m depth at DFO-1-16 as based on low-pass filtered data from bin cell #15 measured by the WHS ADCP #12463. Roses indicate the direction toward which currents flow. Seasons are defined following the meteorological convention (Fall: October-December; Winter: January-March; Spring: April-June; Summer: July-September). 70

Figure 44: Time-series of current speed, current direction and along-slope current component at mooring DFO-9-16 measured by the WHS ADCP #2412. The black line depicts the instrument depth. 72

Figure 45: Seasonal current roses at 20 m depth at DFO-9-16 as based on low-pass filtered data from bin cell #8 measured by the WHS ADCP #2412. Roses indicate the direction toward which currents flow. Seasons are defined following the meteorological convention (Fall: October-December; Winter: January-March; Spring: April-June; Summer: July-September). 74

Figure 46: Near-surface currents for the open water season for low-pass filtered current velocity data from the bin depth nearest bin depth to 50 m at all moorings except DFO-1 and DFO-9 which are closest to a bin depth of 20 m. Data when sea ice was present (winter-spring) were filtered out. Roses indicate toward where the current is flowing. 76

Figure 47: Near-bottom currents for the open water season for low-pass filtered current velocity data from the bin depth nearest to bottom at each location. Data when sea ice was present (winter-spring) were filtered out. Roses indicate toward where the current is flowing. 77

Figure 48: Temperature time-series measured at BR-1-16 from 2016 to 2017. The legend shows the serial number and depth of each CT logger. 82

Figure 49: Temperature time-series recorded at BR-3-16 from 2016 to 2017. The legend shows the serial number and depth of each CT logger. 83

Figure 50: Temperature time-series recorded at BR-G-16 from 2016 to 2017. The legend shows the serial number and depth of each CT logger. 84

Figure 51: Temperature time-series recorded at BR-K-16 from 2016 to 2017. The legend shows the serial number and depth of each CT logger. 85

Figure 52: Temperature time-series recorded at DFO-2-16, DFO-1-16, and DFO-9-16 from 2016 to 2017. The legend shows the serial number and depth of each CT logger. 86

Figure 53: Salinity time-series recorded at BR-1-16 from 2016 to 2017. The legend shows the serial number and depth of each CT logger. 87

Figure 54: Salinity time-series recorded at BR-3-16 from 2016 to 2017. The legend shows the serial number and depth of each CT logger. 88

Figure 55: Salinity time-series recorded at BR-G-16 from 2016 to 2017. The legend shows the serial number and depth of each CT logger. 89

Figure 56: Salinity time-series recorded at BR-K-16 from 2016 to 2017. The legend shows the serial number and depth of each CT logger. 90

Figure 57: Salinity time-series recorded at DFO-2-16, DFO-1-16, and DFO-9-16 from 2016 to 2017. The legend shows the serial number and depth of each CT logger. 91

Figure 58: Temperature-salinity diagram constructed with all data acquired by the CT loggers attached to the moorings BR-1, BR-3, BR-G, BR-K, DFO-2, DFO-1, and DFO-9 from 2016 to 2017. CTD profile data taken at mooring locations during the CCGS Laurier cruises in 2017 are depicted by the 4 black lines. 92

Figure 59: Zoom on the temperature-salinity diagram constructed with data acquired by the deep CT loggers (>400 m) attached to the slope moorings BR-1, BR-3 and BR-G from 2016 to 2017. CTD profile data taken at mooring locations during the CCGS Laurier cruises in 2017 are depicted by the 3 black lines. 93

Figure 60: Diatom fluxes from September 2016 to September 2017 in the Beaufort Sea 94

APPENDICES

- Appendix A. 2016-2017 Final Mooring Diagrams
- Appendix B. Data deliverable
- Appendix C. Summary Statistics of Ocean Currents

1.0 INTRODUCTION

The beginning of ice and ocean monitoring in the Canadian Beaufort Sea can be traced back to the 1980's when oceanographic moorings were deployed by Fisheries and Oceans Canada (DFO) in partnership with the oil and gas industry to document ice, wave and surge hazards and ocean current variability. During the next two decades, programs that involved government, industry and indigenous peoples injected funding to maintain year-round observations through DFO moorings that focused primarily on the continental shelf and the deep Canada Basin. In the mid-2000's, ArcticNet Inc. established the Long-Term Oceanic Observatories (LTOO) project to maintain moorings in the southeastern Beaufort Sea that were first deployed as part of the Canadian Arctic Shelf Exchange Study (CASES: 2002-2004); these brought a focus on the intervening continental slope which had received little prior attention. The LTOO project has been sustained since then through collaborations with different programs, such as partnerships with the oil and gas industry (2009-2011) and through the Beaufort Regional Environmental Assessment (BREA: 2011-2015).

The integrated Beaufort Observatory (iBO) was conceived as a means of fostering synergy among the primary long term mooring programs in the Beaufort Sea, enabling: 1) continuation of the time series at key locations; 2) synthesis of observations collected over the past three decades. This technical report describes the activities undertaken as part of the third year of iBO from April 1, 2017 to March 31, 2018. iBO is a four-year program (2015-2018) managed by ArcticNet in partnership with DFO and Golder Associates Ltd. (Golder). The program is supported by the Environmental Study Research Funds (ESRF) and Imperial Oil Resources Ventures Limited (IORVL). iBO aims to contribute key oceanographic information and understanding required for decisions on environmental stewardship and on industrial development and its regulation in the Canadian Beaufort Sea.

The iBO program contributes to the development of regional syntheses of ocean circulation, sea ice observations and biogeochemical fluxes that will include:

- Information on the magnitude, extent and return period of extreme ice features and of hazardous sea conditions – waves, surge and strong current;
- Ice and ocean datasets to document and interpret inter-annual variability of ice circulation, ocean circulation and particulate matter fluxes in relation to various environmental forcing factors;
- Data to support the development and evaluation of accurate numerical prediction models for operational ocean forecasting and the validation/verification of regional research models for simulating ice, seawater and oil spill trajectories.

The activities conducted under the umbrella of the iBO program during 2017-2018 include the turnaround of 7 moorings deployed in 2016, either from CCGS Amundsen or from CCGS Sir Wilfrid Laurier (Laurier). Together, these 7 moorings (Figure 1) constitute the backbone of iBO, providing an ice and ocean dataset of regional scope. In a larger context, iBO activities in 2017-2018 also included the organization of a Technical Advisory Committee (TAC) meeting at the ArcticNet Annual Scientific Meeting to review field operations and data recovery. In March and April, the iBO team began Phase 1 of the Variability of the Beaufort Ice-Ocean Environment Synthesis Report to be developed over 2018-2021. Phase 1 consists of 3 subtasks: develop a Table of Contents and methods for the Synthesis Report, commence dialog with relevant Inuvialuit stakeholders, and provide a review of ongoing research in the Beaufort Sea. The Synthesis Report will be a building block of the Indigenous and Northern Affairs Canada (INAC) Beaufort Regional Strategic Environmental Assessment (BRSEA).

The goal of the present technical report is to provide a summary of the data acquired from the 7 iBO installations in 2016 to 2017 which represent an extension of key time-series initiated through ArcticNet/BREA and DFO over

the preceding years. Only the 2016-2017 data that have been processed thus far are presented in this report and includes all current meter, current profiler, and temperature-salinity data and part of the biogeochemical flux data. Data sets from the ice profiling sonars (IPS) currently being processed will be added to the final 2016-2017 data record, since the availability of processed IPS data is delayed by about a year relative to processed ADCP and CT sensor data. In conclusion, we identify lessons learned stemming from the 2017 operations and define objectives and priorities for 2018-2019.

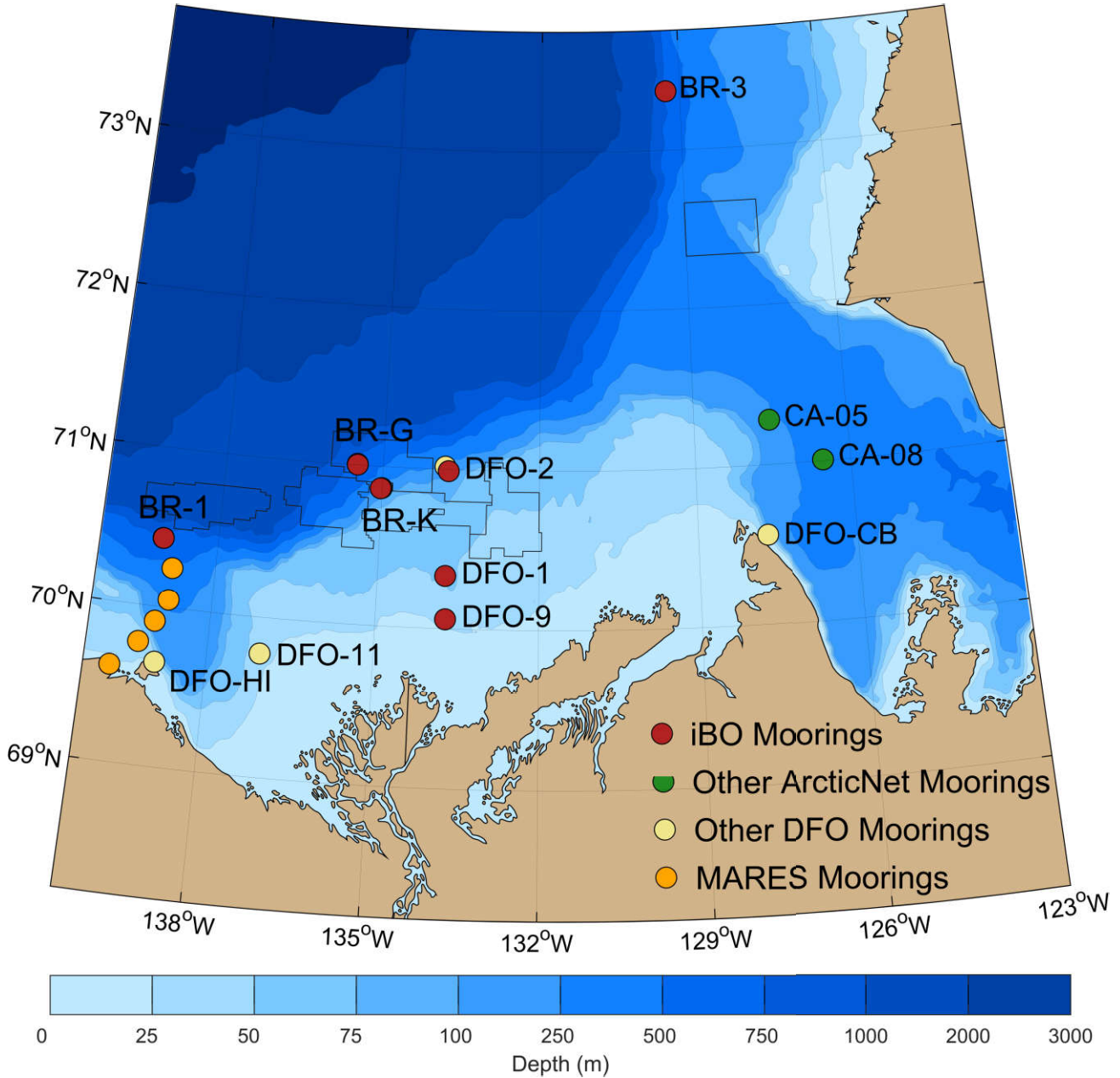


Figure 1: Bathymetric map of the Canadian Beaufort Sea showing the location of iBO moorings (in red). Moorings from partner projects (ArcticNet, DFO, MARES/BOEM) are also shown on the map but are not detailed in the present report).

1.1 Report Organization

This report provides an overview of the physical setting of the study area in section 1.2. A summary of iBO mooring design, field calibration activities, and shipboard mooring operations conducted onboard the CCGS Laurier in 2017 are provided in sections 2.1 through 2.3. Description of the post-processing and QA/QC procedures applied to the recovered data and samples is presented in section 2.4. Section 3.0 provides a review of the processed datasets for the 7 iBO moorings shown in Figure 1 (red dots), with the exception of the data from the IPS during 2016-17 for which there is presently no budget and the particle-size analyzer which is not currently being completed. Data are grouped by parameter: section 0 provides a detailed overview of the ocean current speed and direction recorded throughout the water column at all 7 moorings; section 3.2.8 provides a review of water mass variability based on temperature and salinity records; and section 3.4 presents preliminary data from sediment traps. Appendix A provides the final mooring diagrams for 2016-2017. Appendix B lists the electronic files provided as a data deliverable with this report. Appendix C provides a tabular summary of descriptive statistics pertaining to ocean currents measured at the 7 iBO moorings in 2016-2017.

1.2 Physical Setting of the Study Area

The Canadian Beaufort Shelf (Figure 1) is a narrow Arctic shelf (120 km width × 530 km length) comprised of a series of plateaus separated by shallow channels (Blasco et al., 2013). The shelf break is located at 80-100 m depth where the slope angle increases to 2-6° toward the deep Canada Basin. The region is greatly influenced by the Mackenzie River, which is the largest Arctic river in terms of sediment load ($\sim 127 \times 10^6 \text{ t y}^{-1}$) and the fourth largest in terms of freshwater discharge ($330 \text{ km}^3 \text{ y}^{-1}$) (Macdonald et al. 1998).

Ice cover in the region undergoes a seasonal cycle with considerable inter-annual variability. Galley et al. (2013) recently documented that no significant trend in summer sea ice concentration on the mid-to upper slope of the central shelf has been measured from 1996 to 2010, although off the shelf to the northwest, a decrease in old sea ice concentration compensated by an increase in first-year sea ice is apparent. Typically, seasonal sea ice begins to form in October in the coastal sector and by early to mid-November the ice cover is consolidated over the entire region (<http://iceweb1.cis.ec.gc.ca/30Atlas/page1.xhtml?region=WA&lang=en>; Carmack and Macdonald, 2002). In winter, land-fast ice forms in the nearshore out to about the 20 m isobath and an ice rubble field (i.e. the *stamukhi*; Giovando and Herlinveaux 1981), which includes grounded ice, develops at the outer edge of the land-fast ice. Beyond the *stamukhi*, a recurrent flaw lead separates the land-fast ice from the moving pack ice that typically drifts westward driven by prevailing wind (Macdonald et al. 1995). The Cape Bathurst Polynya centered at the mouth of the Amundsen Gulf is part of the flaw lead system that borders the Beaufort Sea (Barber and Hanesiak 2004). The summer retreat of the ice to the north-west driven by the seasonal increase in east wind (<http://iceweb1.cis.ec.gc.ca/30Atlas/page1.xhtml?region=WA&lang=en>) causes widening of the flaw lead typically in June, but sometimes as much as 6 weeks earlier.

On the inner to mid-shelf, ice drift, ocean circulation, and the trajectory of the Mackenzie River plume, are highly variable and linked to wind dynamics (Melling, 1993; Melling and Riedel 1994; O'Brien et al. 2006). Over the outer shelf and on the slope, large-scale surface circulation (upper 50 m) is dominated by westward-flowing current of the Beaufort Gyre (Ingram et al. 2008). The water mass that occupies the upper 50 m is the Arctic Surface Water with salinity of $\sim 30\text{-}31$ (practical scale) on average in winter, but this value changes markedly with river input and the growth and melt of ice. From 50 to 200 m depth near the shelf break, a submerged stream of north-eastward flow delineates the Beaufort under-current (Forest et al. 2015; Dmitrenko et al. 2016), the eastward continuation of a feature first described in the Alaskan Beaufort Sea (Aagaard 1984; Pickart 2004; von Appen and Pickart

2012). This current is 10-15 km in width and topographically steered along the upper slope; it predominately transports Arctic water of Pacific origin (salinity ~33), but some water of Atlantic origin (salinity 34.0-34.9) which typically dominates the 200-1000 m layer of the water column is entrained at times. This under-current is subject to frequent wind-forced reversals to the west which are commonly associated with upwelling (Aagaard 1984; Pickart et al. 2013). The under-current is the strongest circulation feature in the area and intrinsic to shelf-slope exchange of water in the Beaufort (e.g. Kulikov et al. 1998; Williams et al. 2008). At 20-30 km from the shelf edge, the eastward shelfbreak jet is no longer present and the mean current in the upper 200 m is westward within the anti-cyclonic motion of the Beaufort Gyre (Forest et al. 2015). Mesoscale eddies frequent the region beyond the shelf edge.

2.0 MATERIAL AND METHODS

This section of the report provides detailed information on the tautline mooring design and instrumentation of iBO moorings (section 2.1), compass calibration activities for current meters and current profilers (section 2.2), and mooring recovery and deployment operations aboard the CCGS Laurier (section 2.3). A description of the QA/QC processing steps for each moored instrument is provided in section 2.4.

2.1 Taut-line Mooring Design

2.1.1 Slope Moorings

The slope moorings array consists of 3 similarly designed long moorings (BR-1, BR-G and BR-3) located on the middle continental slope (~700-750 m depth) and one short mooring (BR-K) located on the upper slope near the shelf edge (~170 m depth; Figure 1). Mooring diagrams (as deployed) for 2016-2017 are included in Appendix A.

The longer moorings on the lower slope consist of the following key components:

- ASL Ice Profiling Sonar (IPS) was used at approximately 60 m depth to measure ice draft and non-directional waves during intervals of open water. IPS were mounted in 30-inch spherical syntactic foam floats (Mooring Systems Inc. - MSI).
- 150 kHz Teledyne RD Instruments (TRDI) Quarter Master Acoustic Doppler Current Profiler (QM ADCP) were used at approximately 180 m water depth to profile upper water column currents at 4 m vertical resolution and measure ice velocity using a Bottom-Track feature. The QM ADCPs were mounted up-looking in 40-inch syntactic foam floats (Flotation Technologies - DeepWater Buoyancy).
- 75 kHz TRDI Long Ranger ADCP (LR ADCP) were used at approximately 450 m water depth to measure water velocity profiles at 16 m vertical resolution. The LR ADCPs were mounted up-looking in 40-inch syntactic foam floats (Flotation Technologies).
- Two high frequency short-range (<1 m) Nortek Aquadopp DW (AQD) single point current meters were used to measure water velocity at approximately 10 m and 110 m above the bottom. Each Nortek AQD was equipped with a vane to hold the heading nearly constant for the duration of each ensemble interval.
- Two Technicap PPS 3/3-24S 24 cup sequential sediment traps were deployed between the IPS, QM ADCP and LR ADCP to record the annual cycle in vertical particle flux.
- RBR or Seabird SBE37SM Conductivity and Temperature (CT) loggers were installed at approximately 60 m, 130 m, 180 m, and 450 m water depth, as well as 10 m above the bottom. These instruments measure water temperature and salinity and are used to compute sound speed to improve IPS and ADCP processing.
- Various smaller syntactic foam floats were distributed along the mooring as required.
- Tandem Edgetech CART or Oceano acoustic transponder releases were used as the primary locating and recovery devices.

The shallow (upper slope) mooring consisted of the following key components:

- A 300 kHz TRDI Workhorse Sentinel ADCP (WHS ADCP) was used at approximately 140 m water depth to profile currents with a vertical resolution of 8 m, as well as to measure ice velocity using the Bottom-Track feature. The WHS ADCPs were mounted upward looking in 33-inch syntactic foam ellipsoid floats manufactured by MSI.
- A RBR CT logger with auxiliary sensors to measure turbidity, dissolved oxygen, and chlorophyll fluorescence was installed at approximately 18 m above the bed.
- A Sequoia LISST 100X laser diffraction system was located 18 m above the seafloor to provide measurements of particle size distributions and associated volume concentrations in the lower water column. The LISST measurements help to better quantify the seasonal and annual variability of vertical and horizontal fluxes of inorganic solids.
- A 1 MHz Nortek Aquadopp profiling current meter (AQP) was mounted down-looking below the LISST to provide details of the flow and acoustic backscatter structure near the seafloor on the upper slope. The AQP's measure three-dimensional current velocities and provide a measure of acoustic backscatter intensity in 2 m range bins from the bottom to about 16 m above seabed. Combined with the velocity profile information from upward looking ADCP's the profilers provide a detailed and nearly complete view of the water column vertical structure.
- An additional syntactic foam ellipsoid float was located above the LISST cage to provide floatation for the lower portion of the mooring.
- Edgetech (Model CART) acoustic transponder releases in tandem were used as the primary recovery device.

Improvements and changes made in 2017 to the iBO moorings with respect to the 2016 moorings included the following:

- Removal of the Sequoia LISST 100X laser diffraction system from the shallow mooring BR-K.
- Replacement, on mooring BR-1, of the tandem ORE 8242 releases with Oceano releases to facilitate the turnaround of the mooring since no spare 8242s were available in the instrument pool.
- Removal of the lower hardball float from above the Nortek Aquadopp on the offshore slope moorings because the added buoyancy was deemed unnecessary, and their attachment to the mooring posed a safety issue for mooring deployment and recovery.

2.1.2 Shelf Moorings

The moorings at all three shelf locations (DFO-9, DFO-1, and DFO-2; Figure 1) have similar design (Appendix A). They are located at approximately the 28 m, 55 m and 110 m isobaths, respectively; DFO-2 is on the upper continental slope and DFO-2 and DFO-9 lie within the Kugmallit sea valley. Recording instruments at the two shallower sites (DFO-9 and DFO-1) are placed on two separate nearby (50-150 m separation) moorings so as to keep the equipment near the seabed safe from drifting ice and to avoid interference between the two sonars used for observations. The depth at the third site is sufficient that the instruments are located one above the other on a single mooring.

The moorings at all three sites support the following instruments:

- ASL IPS are located at 30-50 m depth to measure ice draft and non-directional waves during intervals of open water. IPS of three types are in use: original IPS4 units operating at 200-kHz acoustic frequency; updated W-IPS4 units operating at 420 or 895 kHz and measuring wave height as well as ice draft; IPS5 units operating at 420 kHz with increased data storage capacity. IPS are mounted in light-weight stainless steel frames each supported by a collar of four 14-inch spherical plastic floats (Viny Inc. Model 12B3).
- 300-kHz TRDI ADCPs are located about 4 m above the seabed to measure ocean current at 4 m vertical resolution between about 6-m elevation above the seabed to about 15-m depth below the surface, plus ice velocity. ADCPs of two types are in use: original narrow-band ADCPs (NB-ADCP) and newer broad-band WHS-ADCPs. The NB ADCPs operating with higher signal-noise ratio and better magnetic compasses are favoured for Arctic use. ADCPs are mounted in light-weight stainless steel frames each supported by a collar of four 14-inch spherical plastic floats (Viny Inc. Model 12B3) and equipped with vane so that the ADCP heading remains stable throughout a measurement interval. The frame is coupled into the mooring through a swivel.
- CT loggers (Seacat SBE37: Sea Bird Electronics Inc.) are installed on the frame with each ADCP, about 3 m above the seabed. They record the temperature and salinity of water within the bottom boundary layer and provide sensitive indication of water mass shifts associated with up-welling and down-welling motions.
- Acoustic transponder releases (Model CART: ORE Edgetech) were mounted in tandem 1 m above the mooring's deadweight anchor. The CART is the device used to locate each mooring and to enable its recovery by unhooking the buoyant part of the mooring from its heavy anchor. Two transponding releases are used in parallel for redundancy in this essential function.

2.2 Compass Calibration and Verification

Compass calibration is an important consideration for current meters deployed in the Canadian Beaufort Sea due to the reduced magnitude of the horizontal component of the Earth's magnetic field in the Canadian Arctic, less than one third of its value in southern Canada. Calibration and verification of the current meter compasses near the approximate geomagnetic latitude where they will be deployed is advisable prior to deployment. Moreover, care must be taken to eliminate all sources of magnetic interference from the instrument-supporting cages on the mooring and similarly also in the immediate vicinity of the calibration activities. For this reason, calibration activities cannot take place onboard the Laurier.

The compass calibration procedure for TRDI current meters corrects for both soft iron effect (i.e. distortion of the Earth's magnetic field by local ferrous metal) and hard iron effects (i.e. magnetic influence from magnetic material in the vicinity of the instrument, such as mooring hardware and batteries). Nortek's compass calibration for Aquadopp and Continental instruments only corrects for hard iron effects and not for soft iron effects.

Summaries of compass calibration and verification activity are provided in the iBO 2017 field reports from the Laurier expedition (Golder 2018; IOS-DFO 2017). In 2017 compass calibration and verification was completed for two TRDI WHS 300 kHz ADCPs (#7844 and #8682) on September 18, 2017 prior to the crew change for the Leg 3a expedition at the Kugluktuk airfield. The TRDI WHS 300 kHz ADCPs were re-calibrated during the cruise on September 28, 2017 at Herschel Island to obtain an improved result. Calibrations of DFO instruments deployed from the Laurier were conducted on September 18, 2017 at the Kugluktuk airfield and at Herschel Island on September 28, 2017.

Table 1 provides a summary of the post-verification compass errors (calculated from readings made in 10 degree increments) for the verification activities conducted in September 2017. In the last column of Table 1, the mean calculated error is the accuracy of the compass; this value has been used in processing to correct the compass reading. For the instruments deployed on the BR moorings, where stabilizing vanes were not used with the current meters, the value of standard deviation in the same column represents the precision of that correction; the largest value of 1.3° indicates that uncorrected errors ranged over $\pm 1.8^\circ$ (for a sine wave) as the heading of the instrument varied. For instruments deployed which were equipped with stabilizing vanes (DFO moorings), the residual non-linearity – summarized as a standard deviation Table 1 – was used in calibration so that the precision in all cases is approximately 1°.

Table 1: Mean Error of TRDI Compasses (10 Degree Increment).

Instrument	Serial Number	Mooring	Mean Calculated Error \pm Standard Deviation around the Compass (degrees)
TRDI WHS ADCP	7844	BR-K-17	0.9 \pm 0.6
TRDI WHS ADCP	8682	Not used	2.3 \pm 1.3
TRDI NB-ADCP	0586	DFO-2	± 1.5
TRDI WHS-ADCP	12463	DFO-1	± 1.5
TRDI WHS ADCP	02412	DFO-9	± 1.5

2.3 Mooring Recovery and Deployment

This section of the report provides details on iBO mooring recovery and deployment operations conducted aboard the CCGS Sir Wilfrid-Laurier (section 2.3.1) during the 2017 fieldwork. Coordinates and depths of the mooring at their recovery and re-deployment are provided in Table 2 and Table 3.

Table 2: 2016-2017 Mooring Recovery Summary

Mooring	Latitude (WGS84)	Longitude (WGS84)	Water Depth (m)	2016 Deployment Date and Time (UTC)	2017 Recovery Date and Time (UTC)
BR-K-16	70° 51.7920' N	135° 1.47146' W	166	Sep-05-2016 00:18	Sep-26-2017 21:57
BR-G-16	71° 00.1148' N	135° 29.4372' W	699	Sep-04-2016 17:58	Oct-01-2017 14:56
BR-1-16	70° 26.0135' N	139° 01.6081' W	754	Sep-03-2016 02:49	Sep-27-2017 15:55
BR-3-16	73° 24.5273' N	129° 21.7590' W	718	Sep-09-2016 00:39	Sep-23-2017 17:20
BR-3B-16	73° 24.0661' N	129° 21.2336' W	690	Sep-13-2016 21:40	Sep-23-2017 14:56
DFO-2-16	70° 59.3590' N	133° 44.6363' W	111	Sep-30-2016 15:42	Sep-26-2017 15:27
DFO-1a-16	70° 20.0310' N	133° 44.3690' W	55	Sep-25-2016 21:53	Sep-30-2017 19:08
DFO-1b-16	70° 20.0350' N	133° 44.4520' W	55	Sep-25-2016 21:55	Sep-30-2017 19:21
DFO-9a-16	70° 03.5339' N	133° 42.9176' W	31	Sep-25-2016 18:17	Sep-30-2017 14:56
DFO-9b-16	70° 03.5013' N	133° 42.9369' W	31	Sep-25-2016 18:13	Sep-30-2017 14:41

Table 3: 2017-2018 Mooring Deployment Summary

Mooring	Latitude (WGS84)	Longitude (WGS84)	Water Depth (m)	2017 Deployment Date and Time (UTC)
BR-K-17	70° 51.7923' N	135° 01.4506' W	165	Oct-01-2017 01:07
BR-G-17	71° 00.0918' N	135° 29.5331' W	699	Oct-01-2017 19:54
BR-1-17	70° 25.9911' N	139° 01.5892' W	759	Oct-02-2017 15:38
BR-3-17	73° 24.0855' N	129° 21.0377' W	690	Sep-24-2017 00:02
DFO-2-17	70° 59.3540' N	133° 44.6670' W	109	Sep-26-2017 15:55
DFO-1a-17	70° 20.0250' N	133° 44.3538' W	55	Sep-30-2017 19:39
DFO-1b-17	70° 20.0300' N	133° 44.4380' W	55	Sep-30-2017 19:36
DFO-9a-17	70° 03.5024' N	133° 42.9247' W	35	Sep-30-2017 16:16
DFO-9b-17	70° 03.5309' N	133° 42.8695' W	35	Sep-30-2017 16:02

2.3.1 Shipboard Mooring Operations

Steps for mooring recovery aboard the CCGS Laurier generally included:

- pre-operations Job Safety Assessment (JSA) meeting, an operational planning meeting, and a toolbox meeting (on deck);
- interrogate the mooring to determine range;
- maneuver ship into position depending on prevailing drift, wind and sea state;
- conduct a conductivity, temperature and depth (CTD) cast to provide overlapping water column data for data processing; relative timing of CTD cast varies with logistic constraints on the Sir Wilfrid Laurier
- enable the acoustic release and send a command to release the mooring;
- mooring positioned relative to the bow of the ship for recovery;
- lift mooring elements onto the foredeck and take instruments off the mooring as they are brought on deck, then take the mooring apart (i.e., a complete disassembly of the mooring);
- inspect and rinse instruments with freshwater and stow in plastic bins;
- transfer to equipment lab spaces for inspection and data recovery;
- immediately download data from the instruments if re-using, otherwise as schedule permits;
- perform preliminary review and graphical inspection of the data if re-using the instrument, otherwise as schedule permits;
- store and secure the instruments onboard the ship, and
- service and maintain the instruments, including any required trouble-shooting or field repair.

All mooring recovery operations were conducted safely and successfully on the foredeck and from the FRC, when involved. Servicing of the mooring instruments involved the following steps:

- opening the housing (if required) and inspecting interior for corrosion, and other damage;

- changing the batteries (if required), and replacing desiccant (if applicable);
- cleaning the o-ring surfaces and re-greasing and replacing or cleaning all o-rings;
- running a trial delayed-start deployment using instrument's internal power with computer disconnected, followed by upload and inspection of data record;
- programming the instrument for deployment;
- completing a record of programming (screenshots and paper record sheets).

Before programming and deployment of instruments on the moorings, standard manufacturer procedures and pre-deployment tests were followed to provide verification of instrument operation. Instruments were generally programmed for a 1-year deployment. However, those at BR-3 were programmed for two years' operations because at this northerly location west of Banks Island ice can in some years preclude mooring recovery operations. This mooring was also equipped with Oceano acoustic releases that have an extended battery life of at least 2 years. A contingency phase was implemented for all Ice Profilers in order to continue measurements in the event that the mooring might not be recovered in the fall of 2018.

Steps in the mooring deployment were as follows:

- confirm the design of the mooring particulars to meet the site's constraints;
- review the lifting plan and JSA;
- assemble the mooring on deck (using the original configuration or a modified configuration, as appropriate);
- conduct a toolbox meeting on-deck;
- deploy the mooring;
- enable and interrogate the acoustic release;
- perform triangulation to determine the actual location of the mooring, as distinct from the drop point;
- disable the acoustic release; and
- perform CTD cast.

2.4 Data Processing and QA/QC

2.4.1 Current Meters and Current Profilers

This section of the report provides a summary of QA/QC procedure applied to current meters and current profilers deployed on both BR and DFO moorings. The QA/QC procedure of current profilers on BR mooring differs slightly from that applied to DFO instruments (see details below). For all moorings, pressure sensors on the TRDI ADCPs were zeroed at the time of setup in order to account for atmospheric pressure in the depth calculation performed by the instrument. Processing routines were used to convert pressure measured by the Nortek AQDs, to water depth; pressure measurements in air before and after the instrument deployment were averaged to represent mean atmospheric pressure. For BR moorings, processing of the ASCII files from Nortek AQDs or MATLAB® binary files from TRDI ADCPs was completed using MATLAB® software. For DFO moorings, data were processed

using the in-house software and routines (the IOS SHELL suite) from DFO, which produce ASCII multi-line header files and multiple ASCII data files. These DFO ASCII files were converted into the BR mooring file format (MATLAB® binary and Text files) for plotting, analyses and to be provided as a data deliverable.

Processing and quality-checking of the current time-series data consisted of the following steps:

- 1) Measurements made by the instrument while it was out of the water, as determined from pressure readings, were removed.

East and North horizontal components of velocities were corrected to true north based on local magnetic declination. An annual average magnetic declination was used for the deployment period based on the Natural Resources Canada numerical model for the International Geomagnetic Reference Field 2012 (IGRF-12; <http://www.geomag.nrcan.gc.ca/calc/mdcal-eng.php>). The summary of magnetic declination values each for each mooring is listed in Table 4.

Table 4: Magnetic declination values for 2016-2017 iBO Moorings

Mooring	Magnetic Declination [degrees East]
BR-G-16	22.2
BR-K-16	22.3
BR-3-16	22.7
BR-1-16	21.4
DFO-2-16	22.4
DFO-1-16	22.3
DFO-9-16	22.3

- 2) Compass readings from the ADCPs at the DFO moorings were further corrected for compass non-linearity using a polynomial approximation to compass response as a function of instrument geomagnetic heading (section 2.2). This can span a range that exceeds 10° peak to peak, depending on the instrument and its battery. The geomagnetic field near the Beaufort coast is considered close enough to that at the locations at moorings offshore that the measured polynomial correction is applicable offshore¹. No polynomial correction was applied to the indicated directions of TRDI ADCPs at the BR sites because the ±4-degree root-mean-square non-linearity was considered acceptable (TRDI 2014).
- 3) Acoustic amplitude was plotted for each beam to check the quality of the instrument signal return and filtered for amplitudes below the noise floor for the respective instrument (Nortek 2013; TRDI 2014).
- 4) Nominal depths of echo intensity and velocity data from TRDI ADCPs deployed at the DFO sites were calculated using a spline interpolation along each beam that corrects for the effects of changing pitch and roll. Nominal depths from the TRDI ADCPs deployed at the BR moorings were calculated using the default bin mapping method (nearest vertical bin) for TRDI ADCPs (TRDI 2014) that uses the 20° beam slant angle. The latter approach provides similar results to the spline interpolation method in the cases that the tilt is lower than 10° (>99.5% of time for each time series).

¹ The strengths of the horizontal component and the declination angles of geomagnetic field at Kuglugtuk and Herschel Island at the time of writing were respectively: 6468 and 8405 nT and 81.5° & 82.9°.

- 5) For ADCPs deployed at the BR moorings, the following steps were applied to filter data and to identify and flag data that were considered as suspicious:
 - a) Data were filtered for side-lobe interference using the beam slant angle of the instrument. For the Nortek Aquadopp profiler at BR-K, this value was 25° (Nortek 2013) and for the TRDI ADCPs this value was 20° (for all LR, QM and WHS ADCPs) or 30° (for NB ADCP on DFO-2). At BR moorings the filter correction was calculated as the product of the instrument depth and the cosine of the slant angle plus one range bin. The filtered range approximately corresponds to the top 10% of the range to surface or bottom depending on whether the instrument was up-looking or down-looking (only the Aquadopp profiler at BR-K).
 - b) For TRDI instruments, datasets were filtered using the Percent Good (PG) values. Data points with a combined PG4 and PG1 value of less than 25% (TRDI 2014; IOS 2015) were removed from the dataset. The PG value is a data-quality indicator that reports the percentage (0 to 100) of valid data collected for each depth cell of the velocity profile using the four beams (PG4) and three beams (PG3). It is an indicator of the following criteria: low correlation, large error velocity and fish detection (false target threshold) (TRDI 2006).
 - c) Time series data from ancillary sensors on the current profilers were inspected for QA/QC purposes. Nortek recommends that the instrument tilt not exceed a maximum of 10° for measurement of currents (Nortek 2013) and TRDI recommends a maximum tilt limit of 15° (TRDI 2014). Data when tilt was exceeding the respective thresholds were flagged as part of the QA/QC.
 - d) Data were further filtered using the error velocity (TRDI instruments only) and maximum vertical velocity thresholds. The error velocity is a measure of the homogeneity of water movement across the span of the 4 inclined sonar beams. The data from TRDI ADCPs on BR slope moorings were filtered for vertical velocities greater than 0.1 m/s and error velocities greater than 0.15 m/s (i.e. arbitrary values based on error velocity thresholds developed as part of the BREA program).
 - e) Additional visual inspection guided the flagging of (subjectively) suspicious bin values.
 - f) Bottom track ranges (WHS and QM) are corrected for pitch and roll following the methodology of Woodgate and Holroyd (2011). Note that bottom track velocities are uncorrected for an up-looking ADCP (the bottom track function defaults to being used down-looking from a vessel). Velocity polarity should be inverted before use as ice velocities.
- 6) For ADCPs deployed at the DFO sites, a multi-stage decision tree was applied to identify and flag data judged to be of little value by a variety of criteria. These criteria include:
 - a) Surface interference: Eliminating surface interference at the DFO sites used the same methodology as at BR sites, except that the ADCP-measured range to the surface (water-ice or water-air) was used in place of the ADCP's depth.
 - b) Beam-to-beam differences: Ensemble values masked if more than three differences between beams exceed 8 counts.
 - c) Extreme strong echo: Ensemble values masked because at least one beam differs from the others by more than 25 counts.
 - d) Extr+Diffs: ensemble values masked due to combined conditions of 2 & 3.
 - e) PercentGood < 25: Ensemble values masked because fewer than 25% of the ping data yielded 3 or 4 beam solutions.

- f) Low Amplitude: Ensemble values masked because 1 or more beams have amplitude of less than 1 counts.
- g) Error Velocity: Ensemble values masked because the so-called error velocity (actually the difference between independent values of vertical velocity) exceeded 2.8 times the standard deviation of the time series (approximately the 99th percentile). The editing threshold here and in the next step were not fixed but set adaptively.
- h) VertVel: Ensemble values masked because the vertical velocity exceeded 2.8 times the standard deviations of the time series (approximately the 99th percentile).

Final QA/QC time-series data from ADCPs are usually gappy and can be difficult to use in some applications. To generate continuous time series of data at sub-tidal frequencies, the final processing step for DFO was the complex demodulation of the time-series within over-lapping 12-hour windows (e.g. Melling et al. 2001). This additional step was not applied to the current data delivered as part of Appendix B. Instead a low-pass filter (PL66TN, Beardsley and Rosenfeld 1983) was applied to selected bin depth time-series for each instrument data (interpolated linearly to 1-hour intervals for consistency) in order to construct seasonal current roses (16 directions, 22.5° bins) of the sub-tidal current component as presented in section 0.

2.4.2 Temperature-Salinity Loggers

Data were extracted from the RBR sensors using Ruskin® software (RBR 2016) and from Sea Bird sensors using Sea Bird Electronics software. Time-series from BR moorings were processed and plotted using MATLAB® scripts, whereas the same task was accomplished by DFO using in-house IOS SHELL routines.

For CT sensors on the BR moorings time series were clipped for out-of-water values and evaluated visually for data quality. In addition, an automated filter is applied to the conductivity and temperature data to flag potential spikes from the data time-series using a seven-sample moving window. All values outside of ± 1.5 standard deviations about the moving window mean that could be considered spikes are flagged; spikes in conductivity are far more common than spikes in temperature. Any spikes identified in the temperature or conductivity time-series cause the corresponding salinity values also to be flagged because salinity is temperature and conductivity dependent.

In addition, the temperature and salinity data from all moorings were verified and corrected for accuracy against nearby CTD casts acquired at the time of deployment in 2017. Since appreciable drift in sensor calibration rarely occurs for temperature, the assessment of calibration drift is normally carried out for conductivity; it is done on the basis of potential temperature versus salinity plots. For Sea Bird sensors, drift in conductivity calibration is usually associated with silting or bio-fouling, For the RBR sensors a calibration shift from laboratory values can occur via intrusion of mooring components (conducting or non-conducting lines, support structure, etc.) into the (20-cm diameter) sensing volume for conductivity.

2.4.3 Ice Profiling Sonars and Ice velocity

Processing and QA/QC data from IPS 2014-2017 is currently underway and results are expected to be presented as part of upcoming complementary reports provided by DFO and ASL Environmental Sciences Ltd (ASL). It should be noted, however, that all the IPS at the 7 iBO moorings and all CT loggers at the DFO moorings functioned properly and provided complete datasets from 2016 to 2017 with a total of 100% of raw data return. The derivation of ice draft from IPS signal data employs well-established methods that have been developed during the processing of many dozens of IPS datasets over the past three decades (Melling et al. 1995; Melling and Riedel, 2004; Fissel et al. 2008).

There are many steps in the processing of IPS signal data to ice draft. The procedures for detection of erroneous target data and for calibration of zero ice draft in particular are meticulous and require considerable experience. It is not useful to document the process here in detail. The interested reader is referred to Melling et al. (1995) and Melling and Riedel (2004).

Ice velocity is derived from data provided by TRDI's patented bottom-track firmware in the WHS and QM ADCPs (see section 2.1). It can also be derived from binned water-column data recorded by LR ADCPs if certain conditions are met. The ASL procedures for deriving reliable estimates of ice velocity from ADCP data are numerous. Moreover, a certain level of subjectivity must be tolerated in the analysis because greatly varying conditions at the target (rough or smooth ice; continuous or broken ice cover; rough seas or calm seas; other targets yielding plausible echoes; etc.) generate ambiguity. The interested reader is referred to more thorough discussions provided by Melling and Riedel (2004) and ASL (2015).

2.4.4 Sediment Traps

Each of the BR moorings on the middle continental slope was equipped with two automated sediment traps (at approximately 125 and 310 m depth) to record the annual cycle in vertical particle flux (inorganic sediments, organic carbon and particulate nitrogen) and plankton community composition in the upper water column. Four of the six traps provided complete particle flux time-series as expected. Two sediment traps did not provide any samples due to rotation problems: BR-G-16 (upper trap) and BR-3-16 (upper). In the case of BR-G, the motor rotated in the wrong direction and at BR-3 there was a problem with the fit of the teeth on the motor and carousel which caused the carousel to stop rotating after 2 cups. The motor from BR-G has been taken out of service.

Analyses on the sediment trap samples are underway at Université Laval. As a first step, sediment trap samples were split to prepare a subsample for the measurements of total particulate matter (TPM), particulate organic carbon (POC), and particulate nitrogen (PN). The subsamples will be filtered, weighed and processed on the CHN elemental analyzer for TPM, POC and PN values. In addition, zooplankton actively entering the sediment traps (named "swimmers") and that are present in the subsample were removed. Zooplankton organisms will be identified to the lowest species possible to monitor the seasonal and inter-annual fluctuation in the zooplankton community structure. Aliquots are also used for the enumeration and identification of phytoplankton cells to indirectly assess the magnitude, timing, and composition of the phytoplankton spring bloom.

3.0 RESULTS AND DISCUSSION

This section of the report summarizes measurements of currents, salinity, temperature, and sediment trap data collected in the 2016-2017 deployment interval. A description of sea ice conditions is provided for context.

3.1 Sea Ice Conditions

The southern Beaufort was characterised by early sea ice breakup in 2017 (similar to 2016 but not as severe), approximately 6 weeks ahead of normal according to Canadian Ice Services (CIS 2017). Weekly ice coverage by stage of development for the season 2017 is provided in Figure 2. Open water was already present in the region by the end of May and throughout the summer ice coverage remained near record lows in the Beaufort Sea. Sea ice concentration over each mooring location as obtained from SSM/I satellite imagery (12.5 x 12.5 km pixel resolution) is provided in Figure 3. Sea ice growth in the fall was delayed by approximately 2 weeks. In the spring, sea ice concentration declined to near zero at most of the mooring sites at the end of May except for DFO-1 on the shelf where breakup occurred almost a month earlier. At BR-3 sea ice persisted near the average through summer. The regional seasonal ice coverage minimum in September 2017 was near 18.7%, the eighth lowest coverage on record.

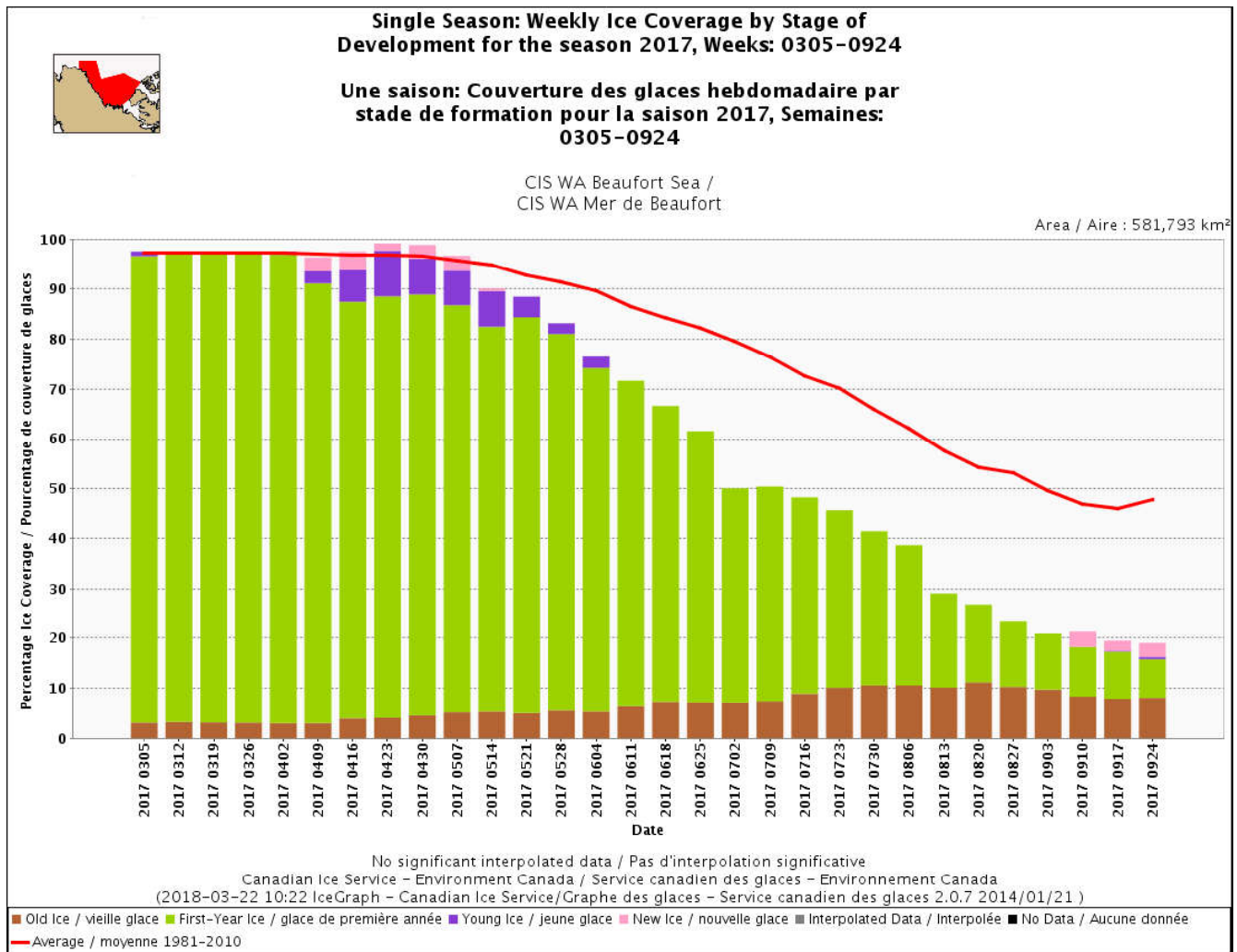


Figure 2: Weekly ice coverage by stage of development for the season 2016 (March – September 2016) as based on daily ice charts from Canadian Ice services. Brown: old ice. Green: first-year ice. Pink/purple: New/Young ice. Red line: average sea ice concentration 1992-2010. Data source: Ice graph 2.5, <http://iceweb1.cis.ec.gc.ca/IceGraph/>.

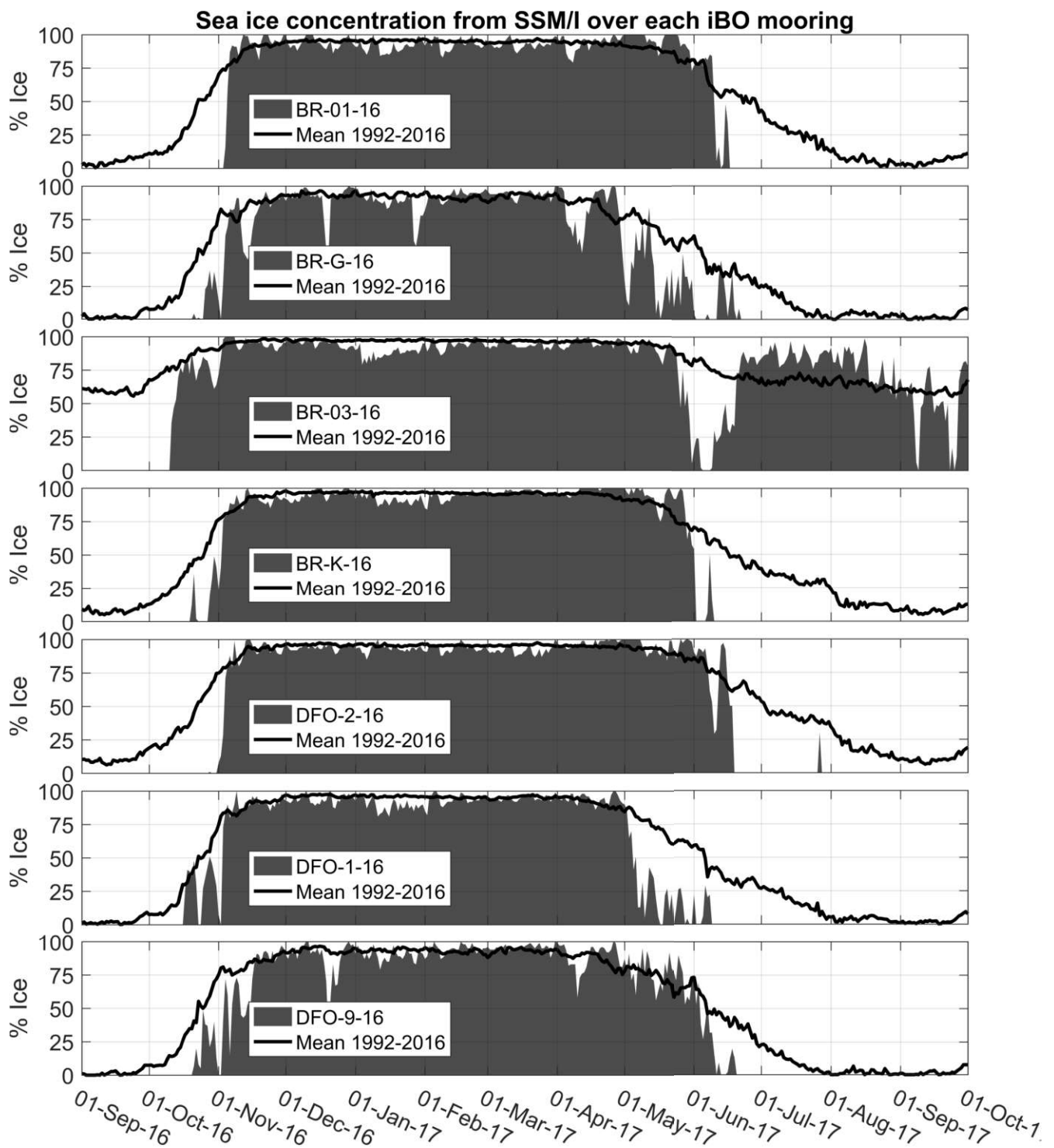


Figure 3: Sea ice concentration (% coverage) for a 12.5 X 12.5 km pixel area over each iBO mooring during 2016-2017 as derived from SSM/I satellite imagery. The black line shows the mean ice concentration over 1992-2016 within each pixel.

3.2 Ocean Currents

Processed data for all current profilers and current meters from the 7 iBO moorings for 2016 to 2017 are presented in this section of the report. For each instrument, time-series plots of current speed, current direction and along-isobath current speed are presented. The along-isobath component of current typically dominates current variability over the continental slope (Williams et al. 2008; Forest et al. 2015; Dmitrenko et al. 2016). The along-isobath direction was estimated as the heading of the bathymetric contour at each mooring location (Table 5) with respect to true North; this is consistent with previous mooring studies that described the along-isobath flow. The along-isobath direction is indicated by a bold line in current rose plots. Annual statistics of current speed and direction for selected bin depths (nearest available bins to those listed in Table 6) are also provided to characterize the net behaviour of ocean currents with depth.

Seasonal current roses based on the sub-tidal component of current velocity were constructed for the same selected bin depths (Table 6) to contrast the temporal variability of ocean circulation patterns in relation to the distinct water masses and water mass boundaries. The sub-tidal component was obtained by applying a low-pass filter with a half-amplitude period of 33 hours to each selected time-series linearly interpolated over 1-hour intervals (PL66TN, Beardsley and Rosenfeld 1983). In addition, a complete tabular summary of current speed descriptive statistics, vector-averaged direction and number of valid records is provided for every bin depth of each instrument in Appendix C. Meta-data for each instrument (i.e. serial number, mean instrument depth, date and time of first and last good record, and percentage of raw data return) are provided in Table 7.

Table 5: Angles chosen to describe the along-slope/shelf current component for each iBO mooring.

Mooring	Angle, degrees True North (TN)
BR-1	78
BR-3	0
BR-G, BR-K, DFO-2	52
DFO-9 ¹	90
DFO-1 ¹	10

¹Note: DFO-1 and DFO-9 are located in the Kugmallit sea valley where the isobaths are sharply bent. The angles at these two sites were adjusted for the expected flow conditions across the valley.

Table 6: Selected bin depths to characterize circulation patterns throughout the water column.

Approximate Bin Depth (m)	Rationale (based on Lansard et al. 2012)
20	Near-surface circulation within the Polar-Mixed Layer (salinity \approx 31-32)
130	Core of the Pacific Halocline water mass (salinity \approx 33)
220	Boundary between the Pacific Halocline and Atlantic water
350	Mid-depth of the water column over the slope, core of the Atlantic Water mass (salinity \approx 34.8)
550	Deep circulation over the slope, lower portion of the Atlantic water mass
700	Near-bottom circulation at the boundary between the Fram Strait and Barents Sea branches of Atlantic water (salinity \approx 34.9)

Table 7: Summary of current profilers and current meters clock drift, first and last good record, and percentage of raw data return on iBO moorings from 2016 to 2017.

Mooring	Instrument	Serial number	Depth (m)	Clock Drift (mm:ss)	First Good Record (UTC)	Last Good Record (UTC)	Raw Data Return ¹
BR-01-16	TRDI QM ADCP 150 kHz	12823	173.7	00:23	Sep-03-2016 3:00:00	Sep-27-2017 15:00:00	100.0%
BR-01-16	Nortek Aquadopp DW	8448	745.2	00:43	03-Sep-2016 03:00:00	Sep-27-2017 15:30:00	100.0%
BR-01-16	Nortek Aquadopp DW	8543	590.5	01:26	03-Sep-2016 03:00:00	May-20-2017 0:53:00	66.5%
BR-01-16	TRDI LR ADCP 75 kHz	12943	458.7	02:12	Sep-03-2016 3:00:00	Sep-27-2017 15:30:00	100.0%
BR-03-16	Nortek Aquadopp DW	8447	601.5	00:50	Sep-09-2016 1:00:00	Sep-23-2017 16:00:00	100.0%
BR-03-16	Nortek Aquadopp DW	9473	712.8	00:43	Sep-09-2016 0:00:00	Sep-23-2017 17:00:00	100.0%
BR-03-16	TRDI QM ADCP 150 kHz	8784	143.4	09:27	Sep-09-2016 1:00:00	Sep-23-2017 16:30:00	100.0%
BR-03-16	TRDI LR ADCP 75 kHz	18785	496.9	08:03	Sep-09-2016 1:00:00	Sep-23-2017 17:00:00	100.0%
BR-G-16	Nortek Aquadopp DW	8419	564.8	00:22	Sep-04-2016 18:30:00	Oct-01-2017 14:30:00	100.0%
BR-G-16	Nortek Aquadopp DW	8442	674.3	00:23	Sep-04-2016 18:30:00	Oct-01-2017 14:30:00	100.0%
BR-G-16	TRDI LR ADCP 75 kHz	13079	452.7	00:15	Sep-04-2016 18:30:00	Oct-01-2017 14:30:00	100.0%
BR-G-16	TRDI QM ADCP 150 kHz	12699	173.6	00:19	Sep-04-2016 18:00:00	Oct-01-2017 14:30:00	100.0%
BR-K-16	Nortek Aquadopp Profiler	11147	148.6	00:41	Sep-05-2016 1:00:00	Sep-26-2017 23:00:00	100.0%
BR-K-16	TRDI WHS ADCP 300 kHz	7844	135.6	09:30	Sep-05-2016 0:30:00	Aug-11-2017 4:30:00	87.9%
DFO-2-16	TRDI NB ADCP 300 kHz	586	108.0	08:43	Sep-30-2016 16:00:00	Sep-26-2017 17:00:00	100.0%
DFO-1-16	TRDI NB ADCP 300 kHz	12463	51.0	02:32	Sep-25-2016 22:00:00	Sep-30-2017 19:30:00	100.0%
DFO-9-16	TRDI WHS ADCP 300 kHz	2412	31.5	01:48	Sep-25-2016 18:30:00	Sep-30-2017 16:30:00	100.0%

¹Note: The raw data return is based on the number of records (including bad data) during the period from the mooring deployment to the mooring recovery.

3.2.1 Mooring BR-1

Time-series plots of current speed, direction, and along-slope current from the QM ADCP, LR ADCP and the two Aquadopp DW deployed at BR-1 from 2016 to 2017 are provided in Figure 4 through Figure 7. The data in the QM and LR ADCP plots are filtered for bins with PG4+PG1 values less than 25%, bins affected by sidelobe interference and for error velocity thresholds as described in section 2.4.1. The first valid bin depth for QM ADCP #12823 at BR-1-16 after removing sidelobe interference was 29.4 m (bin cell 35) and contains 95% valid data (Appendix C). Bin depths between 57 and 61 m (bin cells 27 and 28) of the QM ADCP appear to be affected by the presence of the IPS float and cage, which resulted in reflection observed in the echo intensity (not shown) and a general decrease in current speed at these depths. A reflection was also observed at bin depths between 121 and 129 m (bin cells 10-12) due to the sediment trap and CT sensor frame located at this depth. Bin cells

10,11,12,27, and 28 of QM ADCP #12823 were manually flagged as part of the QA/QC and data from these bin depths should be treated carefully before being used in further analyses. The pressure time series from the QM ADCP #12823 recorded fluctuations on the order of 2 to 4 m during the latter half of the deployment which do not correspond to changes in depth during mooring layover, indicating a potential malfunction of the pressure sensor. The pressure time series from this instrument should be used with caution.

The LR ADCP #12943 measured currents at BR-1-16 did not appear to have been impacted by interference with other parts of the mooring (Figure 5). The first valid bin depth for this instrument was 50.5 m (bin cell 25) with 98% valid data (Appendix C). The overall data return was high, with only a few intervals of data loss in summer 2016 in the upper water column at bin depths 146 m and shallower (bin cells 19 to 25). The percentage valid data is 98% or greater in all depth bins. The data quality is improved versus the 2015 deployment, likely due to changing the instrument setting on the LR ADCP from Low Power mode to High Power mode in 2016 and upgrading batteries from standard alkaline to high-capacity Lithium packs. The deep Aquadopps current meters #8543 (590.5 m) and #8448 (745.2 m) provided time-series with a percentage of valid data return of 66.5% and 100% for each instrument, respectively (Figure 6, Figure 7 and Appendix C). Current meter #8543 is suspected to have stopped prematurely on May 20, 2017 due to a bad battery.

Mean current speeds at BR-1-16 ranged from 10 to 18 cm/s in the upper 200 m of the water column; and from 4 to 8 cm/s below 200 m (Table 8, Appendix C). Vector-averaged directions were typically to the west-northwest (270-360°TN) for all bin depths down to 200 m. Below 200 m the direction transitions to the north-northeast, directions below 275 m are consistently to the east (90-100°TN). Aquadopps at 591 m and 745 m measured an average direction to the east of 70°TN and 95°TN, respectively. The maximum current speed measured for unflagged bins was 69 cm/s on September 26, 2017 at 29 m depth during westward currents. Intermittent intervals of stronger currents (>50 cm/s, with stronger values centered around 50 to 100 m) to the north-northeast and northwest were generally measured from June through August 2017 when the region was ice free. These events are presumably driven by strong winds, however the depth-intensified patterns (Figure 4) suggest that the wind forcing is not local. Strong north and eastward-directed currents (>50 cm/s) were also measured in the winter from December 2016 through February 2017. These events have a strong along-slope component.

Seasonal current roses (low-pass filtered) for selected bin depths at mooring BR-1-16 are provided in Figure 8 through Figure 13. The strong westward current event (>50 cm/s) detected in the upper water column from June through August (spring and summer) is particularly visible in the summer current roses at the near surface (29 m, Figure 8). Lower in the water column, at the depths of Atlantic water mass, low-pass filtered currents were generally weak (<10 cm/s) and variable around the compass (Figure 11 and Figure 12). Near the bottom at 591 and 745 m, most frequent currents were directed to the east or south (across the slope toward the shelf; Figure 132 and 13).

BR-1; QM Broadband 153.6 kHz; 70.43310 N, 139.02700 W; 2016-2017; Instr. #12823

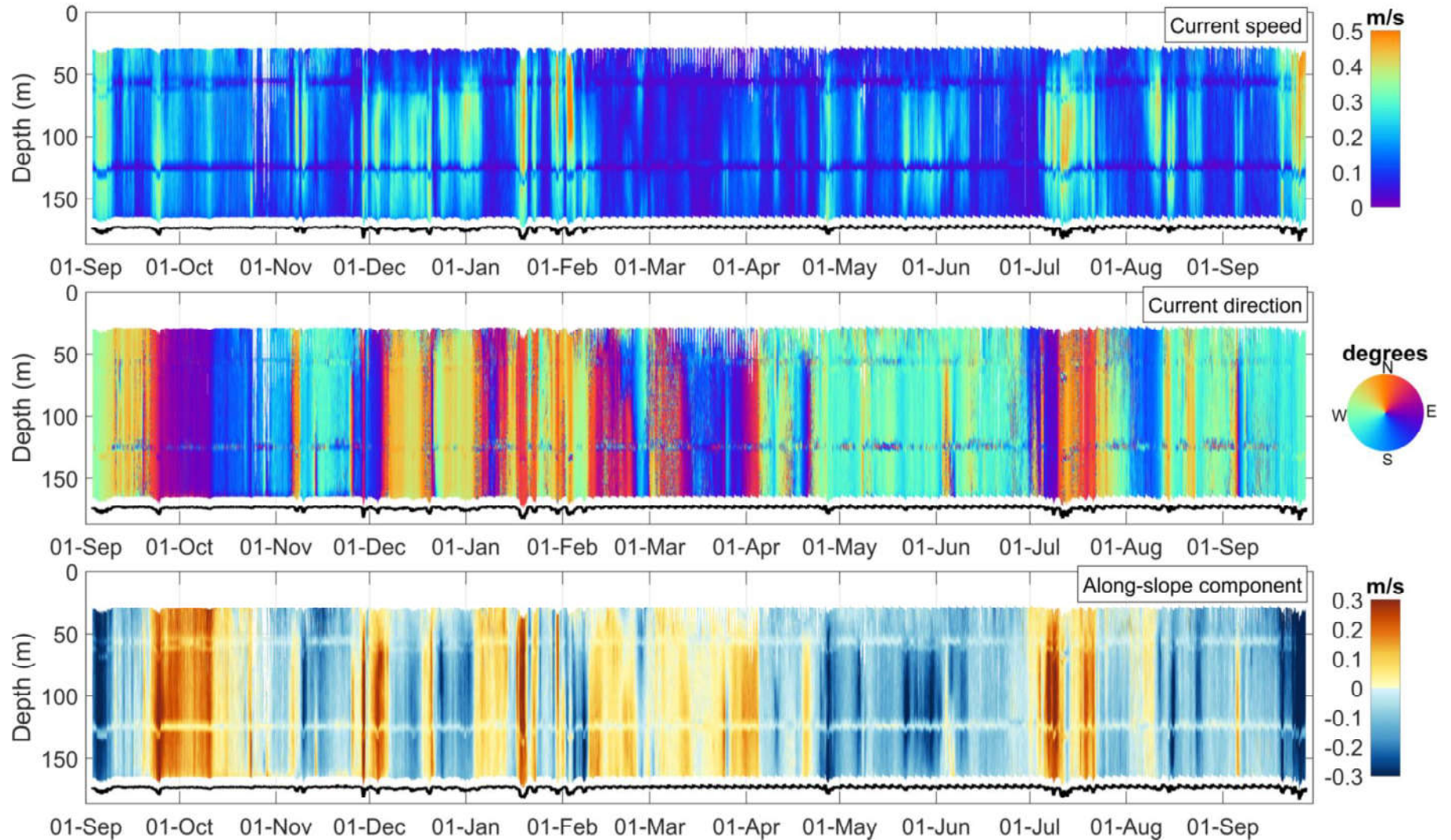


Figure 4: Time-series of current speed, current direction and along-slope current component at mooring BR-1-16 measured by the QM ADCP #12823. The black line depicts the instrument depth.

BR-1; LR Broadband 76.8 kHz; 70.43310 N, 139.02700 W; 2016-2017; Instr. #12943

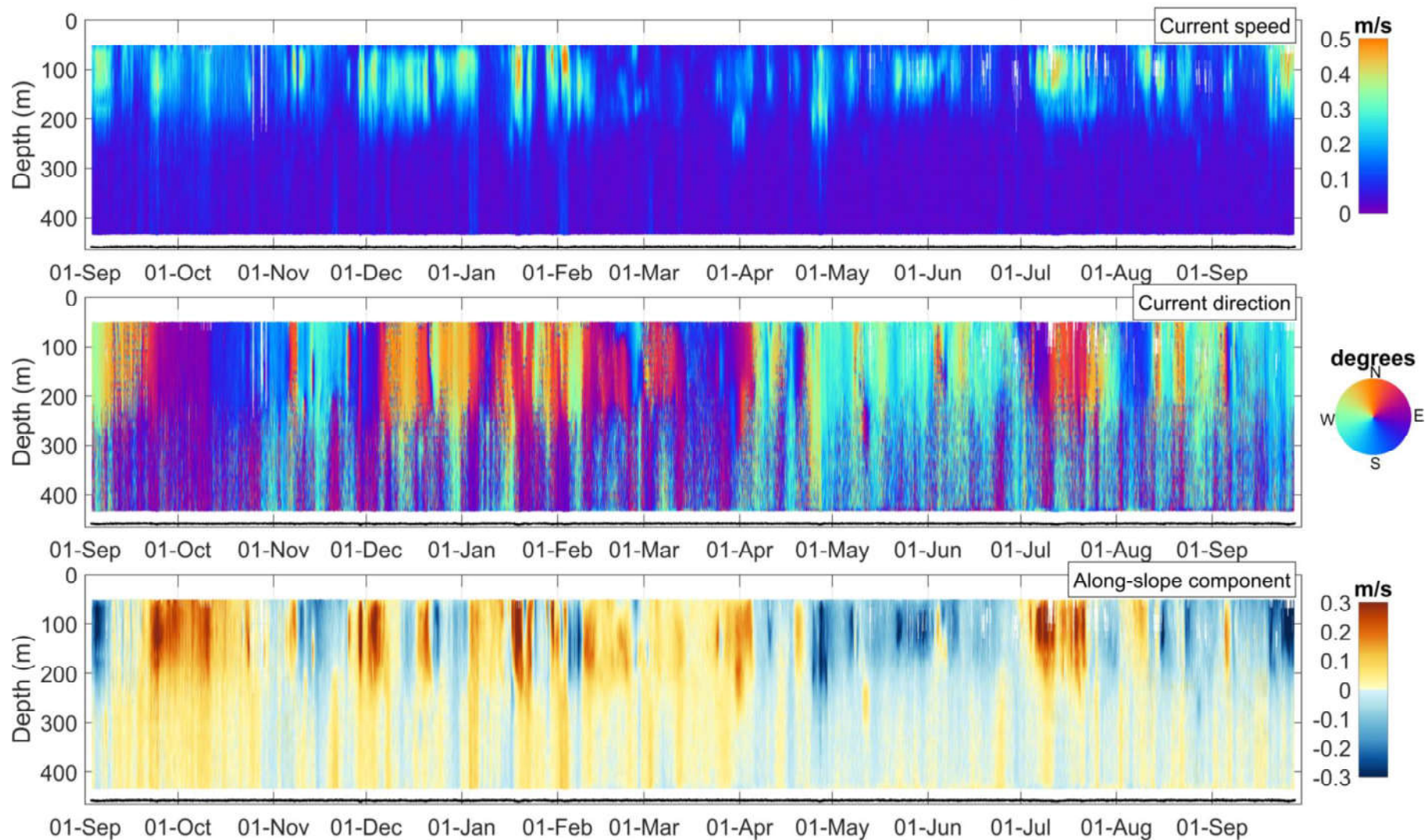


Figure 5: Time-series of current speed, current direction and along-slope current component at mooring BR-1-16 measured by the LR ADCP #12943. The black line depicts the instrument depth.

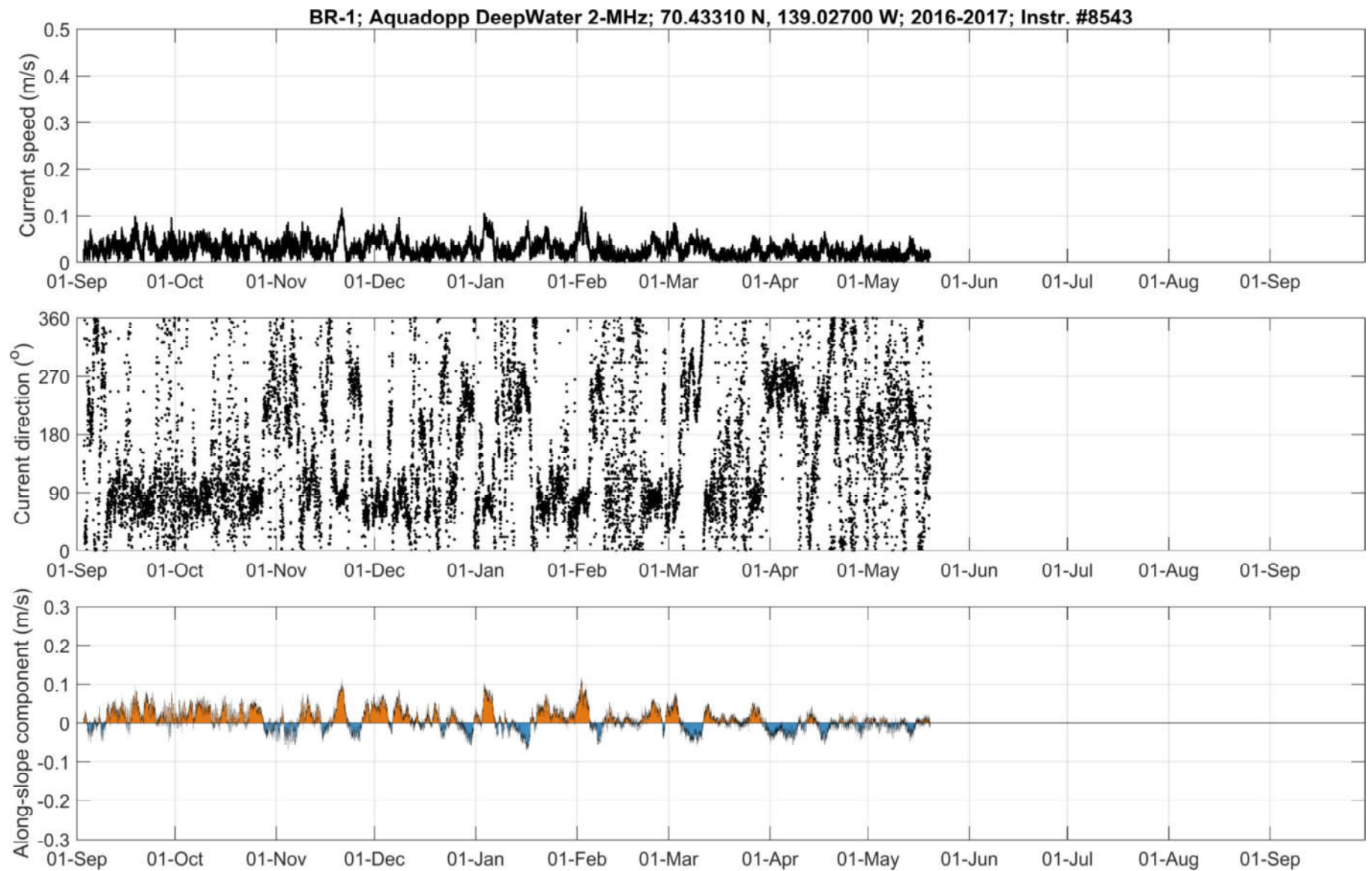


Figure 6: Time-series of current speed, current direction and along-slope current component at 591 m at mooring BR-1-16 measured by the Aquadopp #8543.

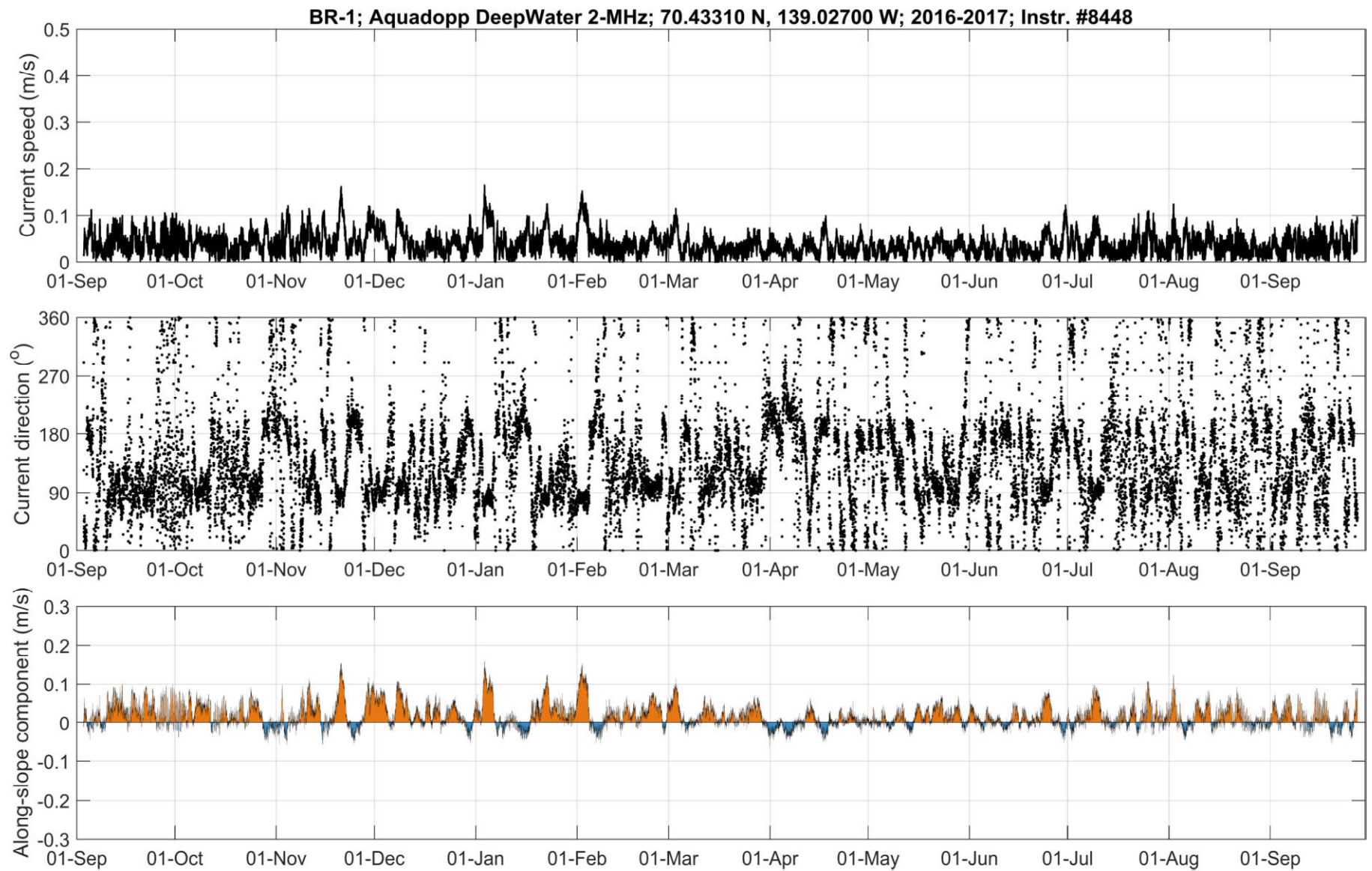


Figure 7: Time-series of current speed, current direction and along-slope current component at 745 m at mooring BR-1-16 measured by the Aquadopp #8448.

Table 8: Annual statistics of current speed and direction at BR-1-16 from selected bin depths representative of water mass variability in the Beaufort Sea (see Table 6 for water mass description).

Bin Depth (m)	Median Speed (m/s)	Mean Speed (m/s)	75%ile Speed (m/s)	95%ile Speed (m/s)	99%ile Speed (m/s)	Max Speed (m/s)	Standard Deviation Speed (m/s)	Vector-Averaged Direction (deg TN)
29.4	0.11	0.13	0.18	0.31	0.43	0.69	0.09	276.9
129.3	0.14	0.15	0.20	0.29	0.33	0.39	0.08	302.7
226.5	0.06	0.07	0.09	0.14	0.19	0.39	0.04	41.5
354.5	0.04	0.04	0.05	0.08	0.11	0.17	0.02	97.9
590.5	0.03	0.03	0.04	0.06	0.08	0.12	0.02	69.8
745.2	0.03	0.04	0.05	0.09	0.11	0.17	0.02	94.7

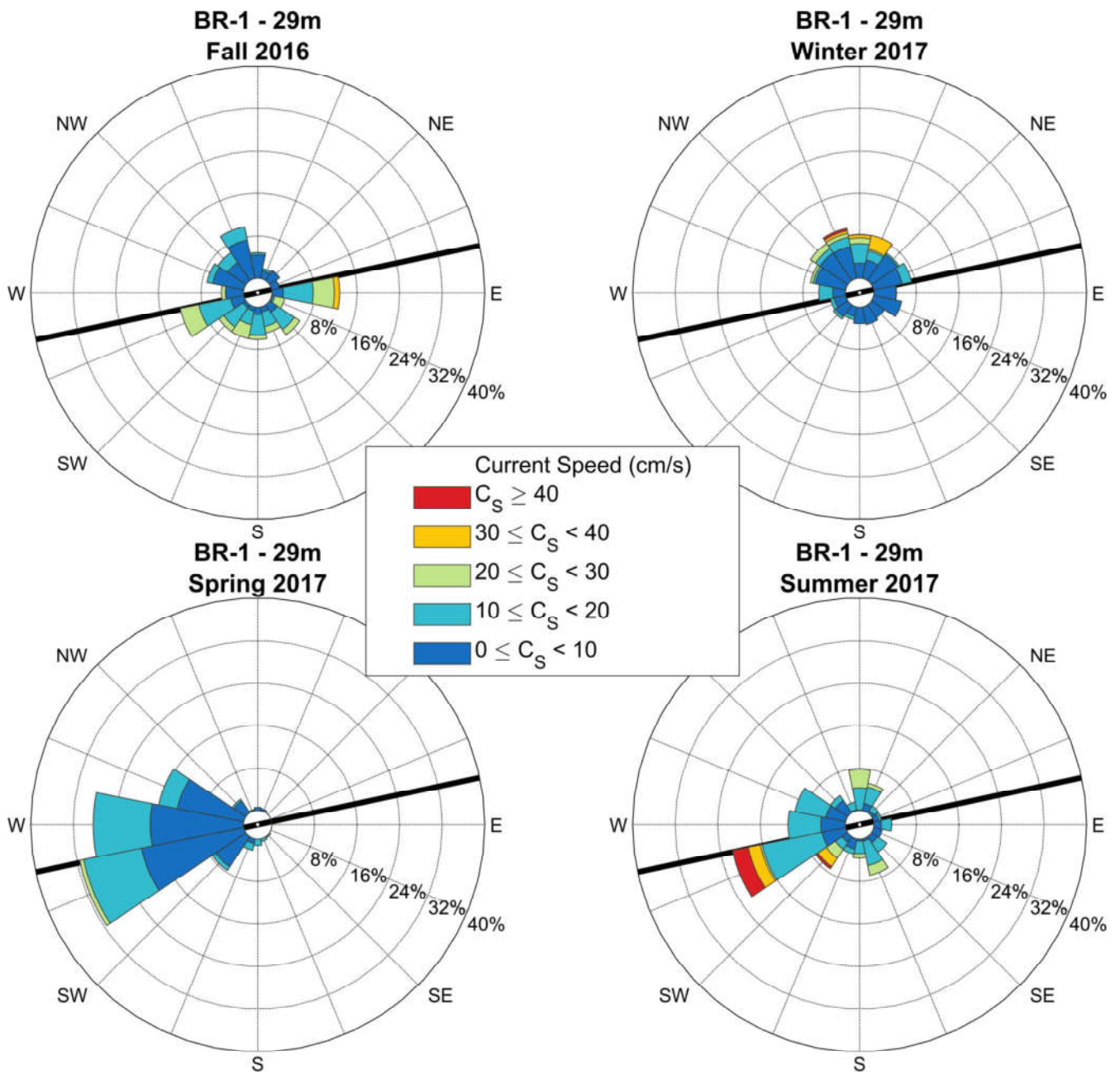


Figure 8: Seasonal current roses at 29 m depth (bin cell #35) at BR-1-16 measured by the QM ADCP #12823. Data are low-pass filtered. Roses indicate the direction toward which currents flow. Seasons are defined following the meteorological convention (Fall: October-December; Winter: January-March; Spring: April-June; Summer: July-September).

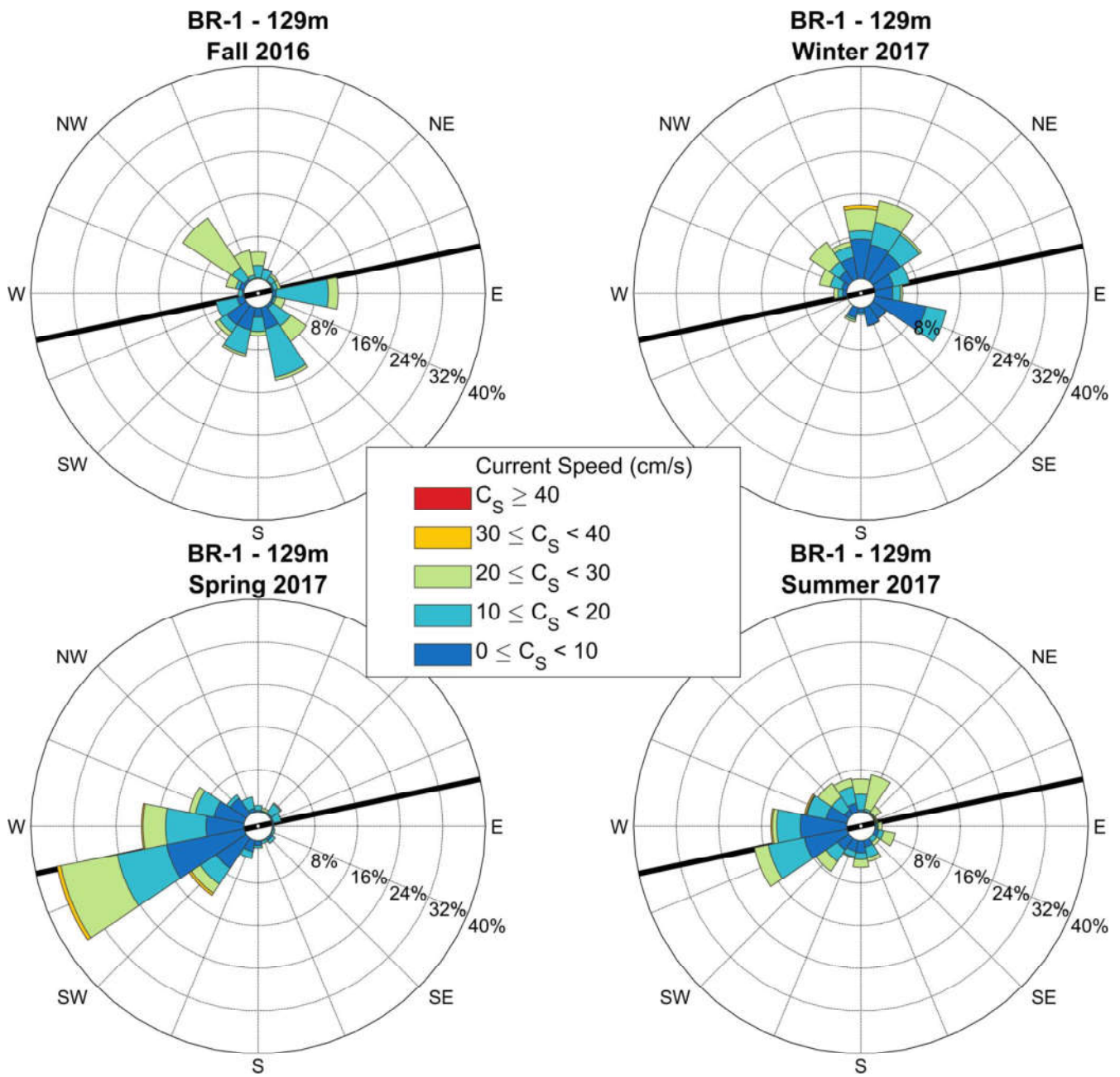


Figure 9: Seasonal current roses at 129 m depth (bin cell #10) at BR-1-16 measured by the QM ADCP #12823. Data are low-pass filtered. Roses indicate the direction toward which currents flow. Seasons are defined following the meteorological convention (Fall: October-December; Winter: January-March; Spring: April-June; Summer: July-September).

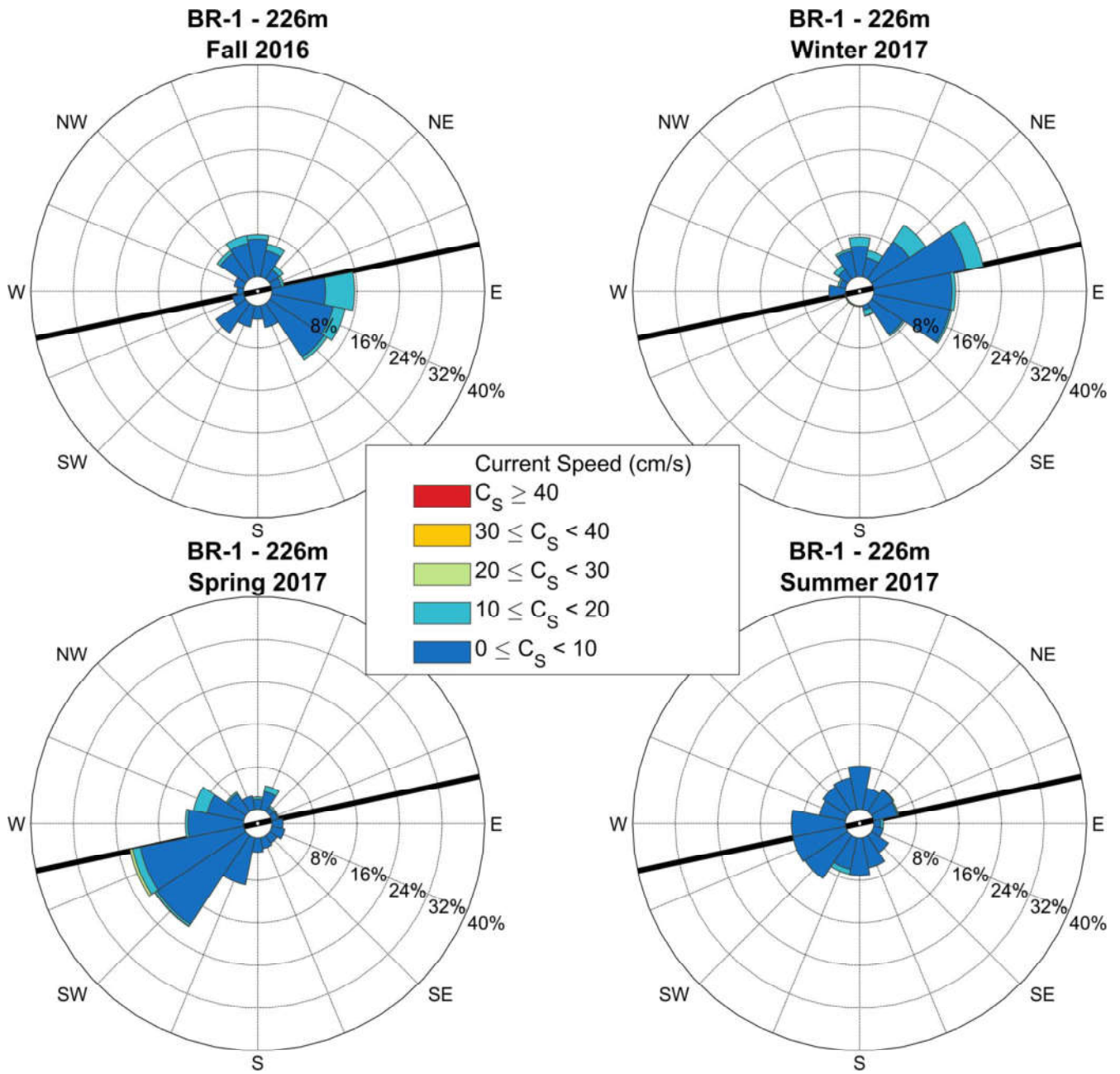


Figure 10: Seasonal current roses at 226 m depth (bin cell #14) at BR-1-16 measured by the LR ADCP #12943. Data are low-pass filtered. Roses indicate the direction toward which currents flow. Seasons are defined following the meteorological convention (Fall: October-December; Winter: January-March; Spring: April-June; Summer: July-September).

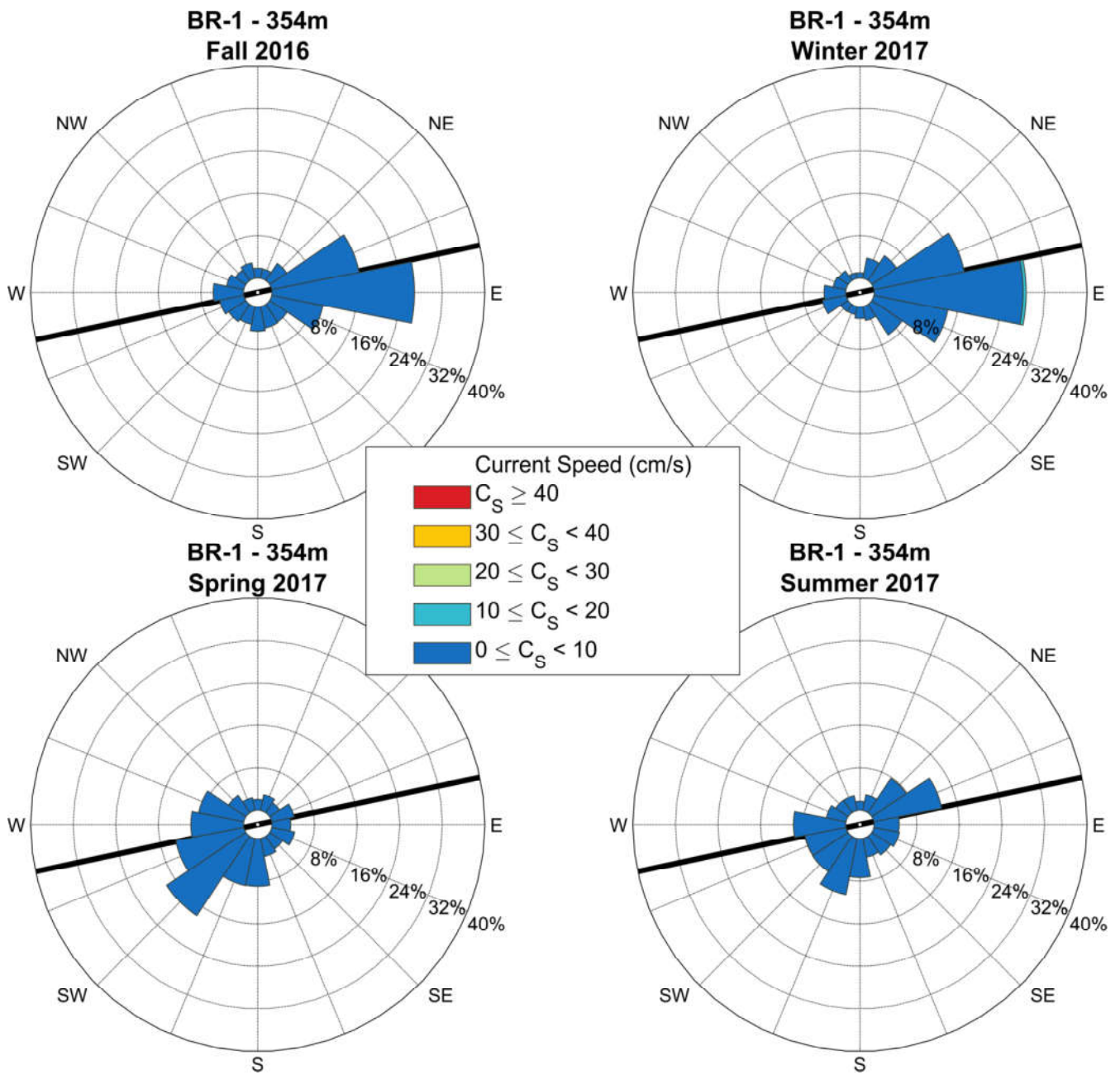


Figure 11: Seasonal current roses at 354 m depth (bin cell #6) at BR-1-16 measured by the LR ADCP #12943. Data are low-pass filtered. Roses indicate the direction toward which currents flow. Seasons are defined following the meteorological convention (Fall: October-December; Winter: January-March; Spring: April-June; Summer: July-September).

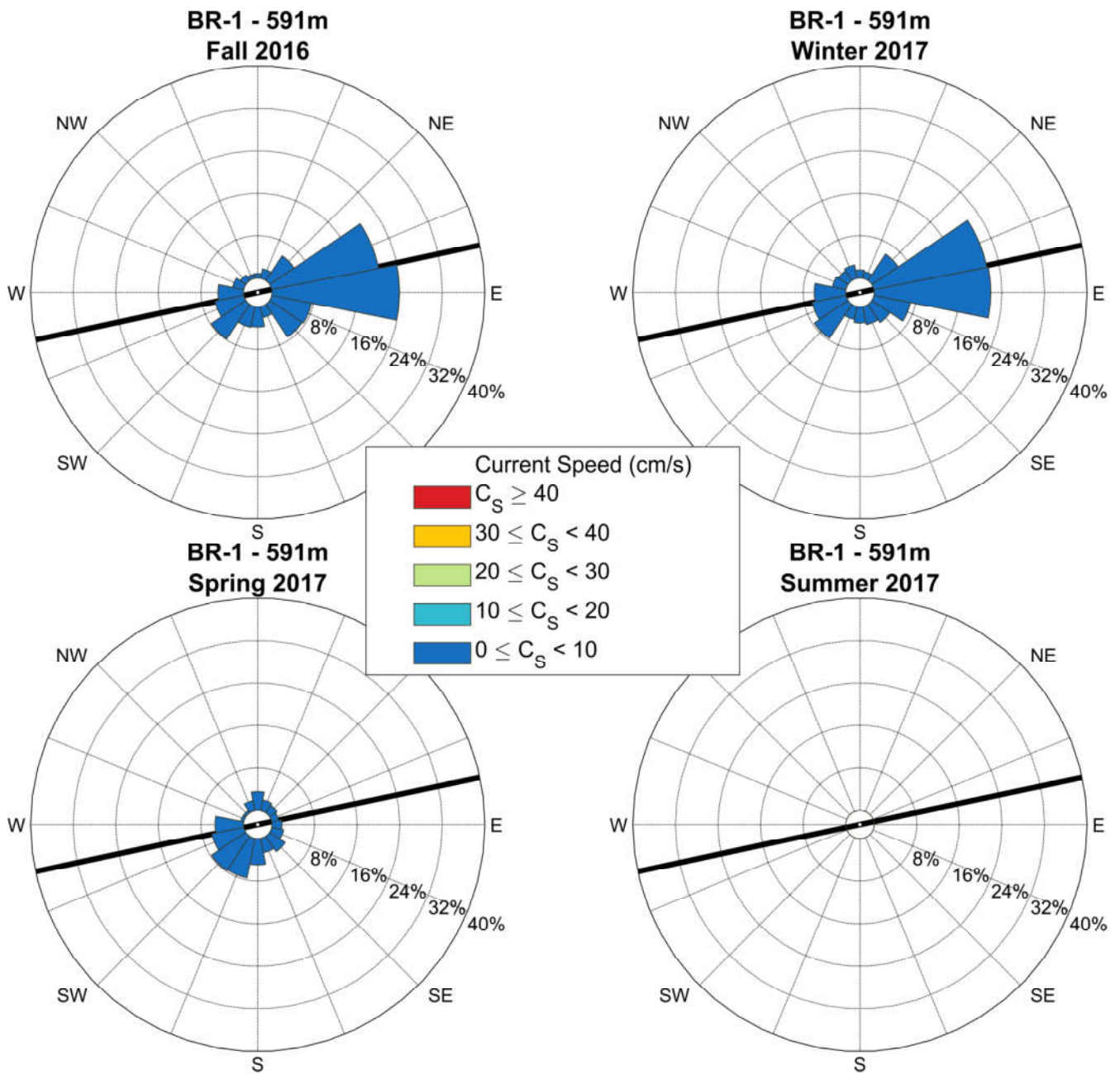


Figure 12: Seasonal current roses at 591 m depth at BR-1-16 measured by the Aquadopp #8543. Data are low-pass filtered. Roses indicate the direction toward which currents flow. Seasons are defined following the meteorological convention (Fall: October-December; Winter: January-March; Spring: April-June; Summer: July-September).

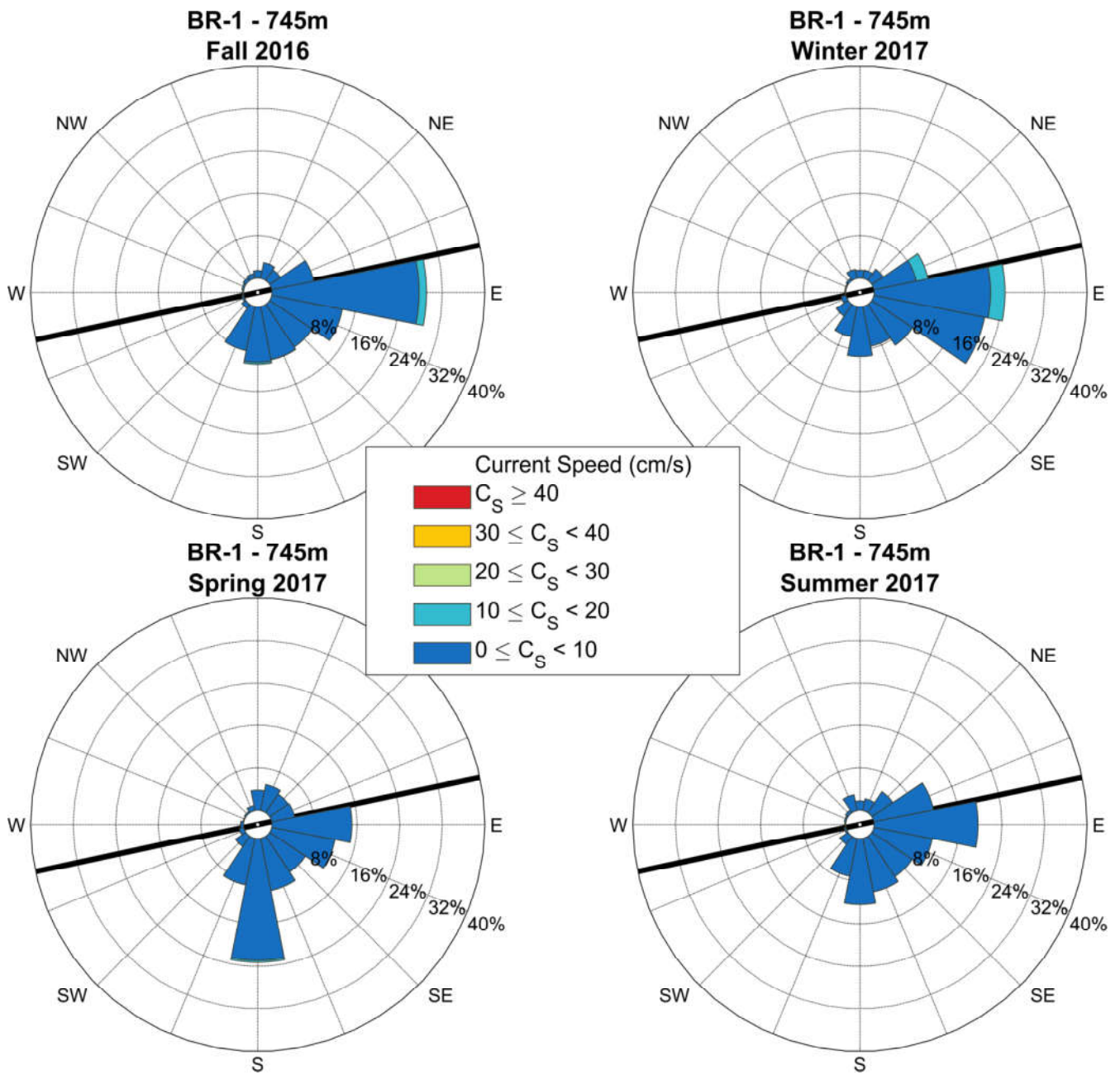


Figure 13: Seasonal current roses at 745 m depth at BR-1-16 measured by the Aquadopp #8448. Data are low-pass filtered. Roses indicate the direction toward which currents flow. Seasons are defined following the meteorological convention (Fall: October-December; Winter: January-March; Spring: April-June; Summer: July-September).

3.2.2 Mooring BR-3

Time-series plots of current speed, direction, and along-slope current component from the QM ADCP, LR ADCP and the two Aquadopp DW deployed at BR-3 from 2016 to 2017 are provided in Figure 15 through Figure 17. The first valid bin depth for QM ADCP #8784 at BR-3-16 after removing sidelobe interference was 18.9 m (bin cell 46), although this bin depth contains only 89% valid data (Appendix C). Bin depths 95 to 99 m (bin cells 26 and 27) of the QM ADCP appear to be affected by the presence of the IPS float and cage, which resulted in reflection observed in the echo intensity (not shown) and a general decrease in current speed at these depths. A reflection was also observed at bin depths 159 to 163 m (bin cells 10 and 11) due to the sediment trap and CT sensor frame located at this depth. Bin cells 10, 11, 26, and 27 of QM ADCP #12698 were manually flagged as part of the QA/QC and data from these bin depths should be treated carefully before being used in further analyses. A partial data loss of the upper water column (>100 m) in April, May, and July 2017 is likely related to the QM ADCP being deployed near the upper limit of its operating range in this environment. The pressure time series from the QM ADCP #8784 appears to have malfunctioned as it recorded depth fluctuations on the order of 3 to 6 m during most of the deployment which do not correspond to changes in depth from mooring layover and also measured a mean water depth approximately 50 m shallower than expected. Due to the suspected malfunction of the sensor, the depth time-series was replaced with a nominal depth of 207.2 m calculated using the mean depth of SBE CT logger #10851 and the 50 m length of line separating the instruments.

The LR ADCP #18785 at BR-3-16 provided a complete annual dataset. The first valid bin depth for the LR ADCP #18785 at BR-3-16 was 56.4 m (bin cell 27) with 97% valid data (Appendix C). The percentage of valid records was greater than 94% at all bin depths for this instrument. Partial data loss possibly linked to high intensity of ambient sound generated by sea ice or wind/waves at the surface was observed only at brief intervals in May and June 2017 again in late-August and September 2017 at this location (Figure 15). The deep Aquadopp current meters #8447 (601.5 m) and #9473 (712.8 m) provided complete time-series with 100% valid data (Figure 16, 17, and Appendix C).

Mean current speeds at BR-3-16 ranged from 6 to 9 cm/s in the upper 200 m of the water column; and from 5 to 7 cm/s below 200 m (Table 8, Appendix C). Vector-averaged directions were typically to the south (175-195°TN) for all bin depths down to 200 m. Below 200 m the vector averaged directions are consistently to the north-northwest (335-360°TN). The maximum current speed measured for un-flagged bins at BR-3-16 was 48 cm/s towards the south on September 9, 2017 at the near surface bin at 19 m depth (Appendix C). Another event of with current speeds of 15 to 20 cm/s magnitude was measured throughout the water column above approximately 200 m depth from February 1 to 7, 2017 towards the north. Overall current speeds in the lower water column are quiescent with only 5% of the entire LR ADCP current speed dataset at BR-3-16 exceeding 10 cm/s (Appendix C).

Seasonal current roses (low-pass filtered) for selected bin depths at mooring BR-3-16 are provided in Figure 18 through Figure 23. The current roses illustrate that the dominant flow direction in the upper water column (19 m to 131 m) is southward, particularly during the spring and summer intervals. In the lower portion of the water column (216 m to 713 m) northward currents are dominant however there is some bi-directionality in the currents at 216, 344, and 602 m water depth. Currents at the lower most Aquadopp (713 m) are unidirectionally to the north.

BR-3; QM Broadband 153.6 kHz; 73.41017 N, 129.36267 W; 2016-2017; Instr. #8784

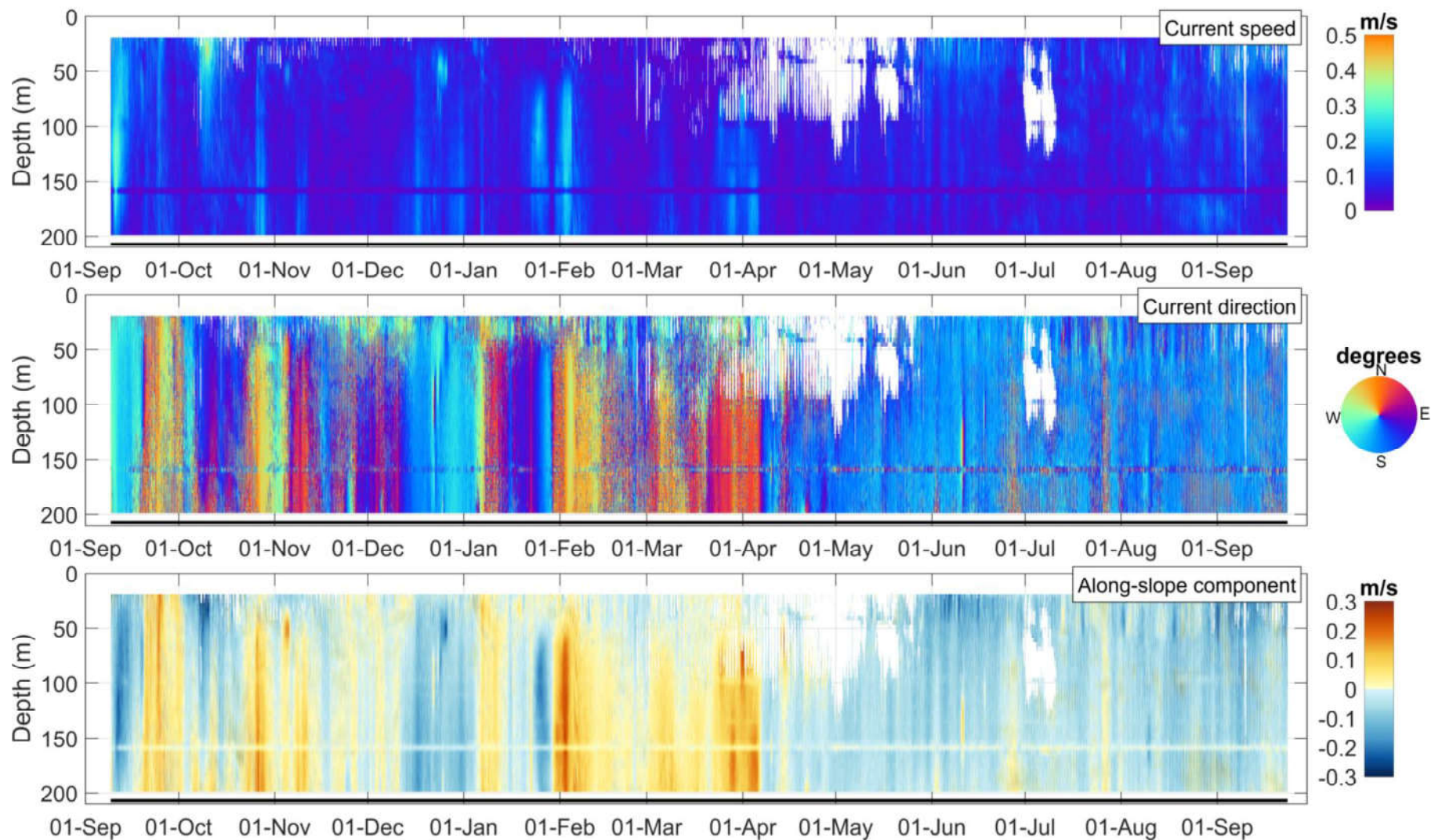


Figure 14: Time-series of current speed, current direction and along-slope current component at mooring BR-3-16 measured by the QM ADCP #8784. The black line depicts the instrument depth.

BR-3; LR Broadband 76.8 kHz; 73.41017 N, 129.36267 W; 2016-2017; Instr. #18785

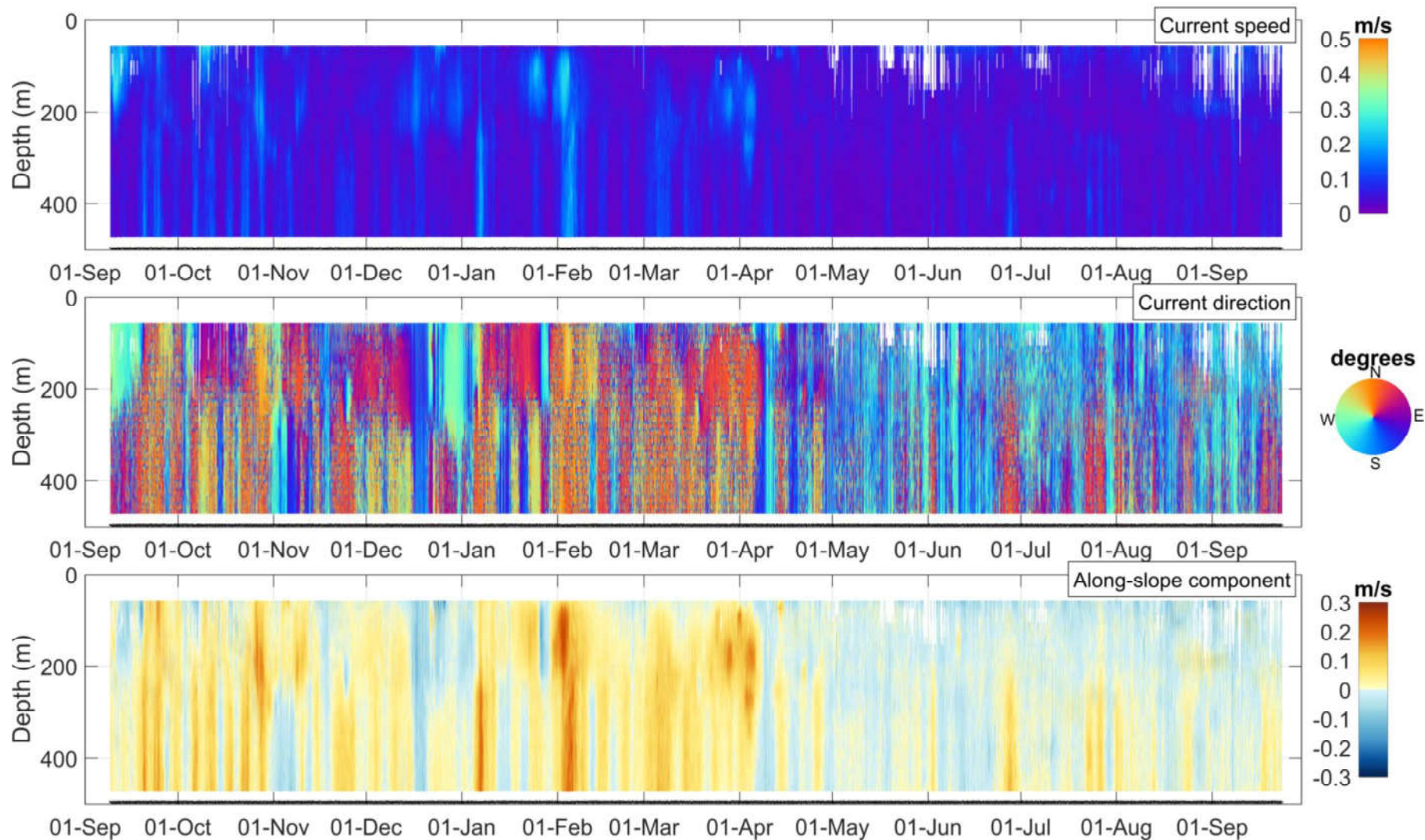


Figure 15: Time-series of current speed, current direction and along-slope current component at mooring BR-3-16 measured by the LR ADCP #18785. The black line depicts the instrument depth.

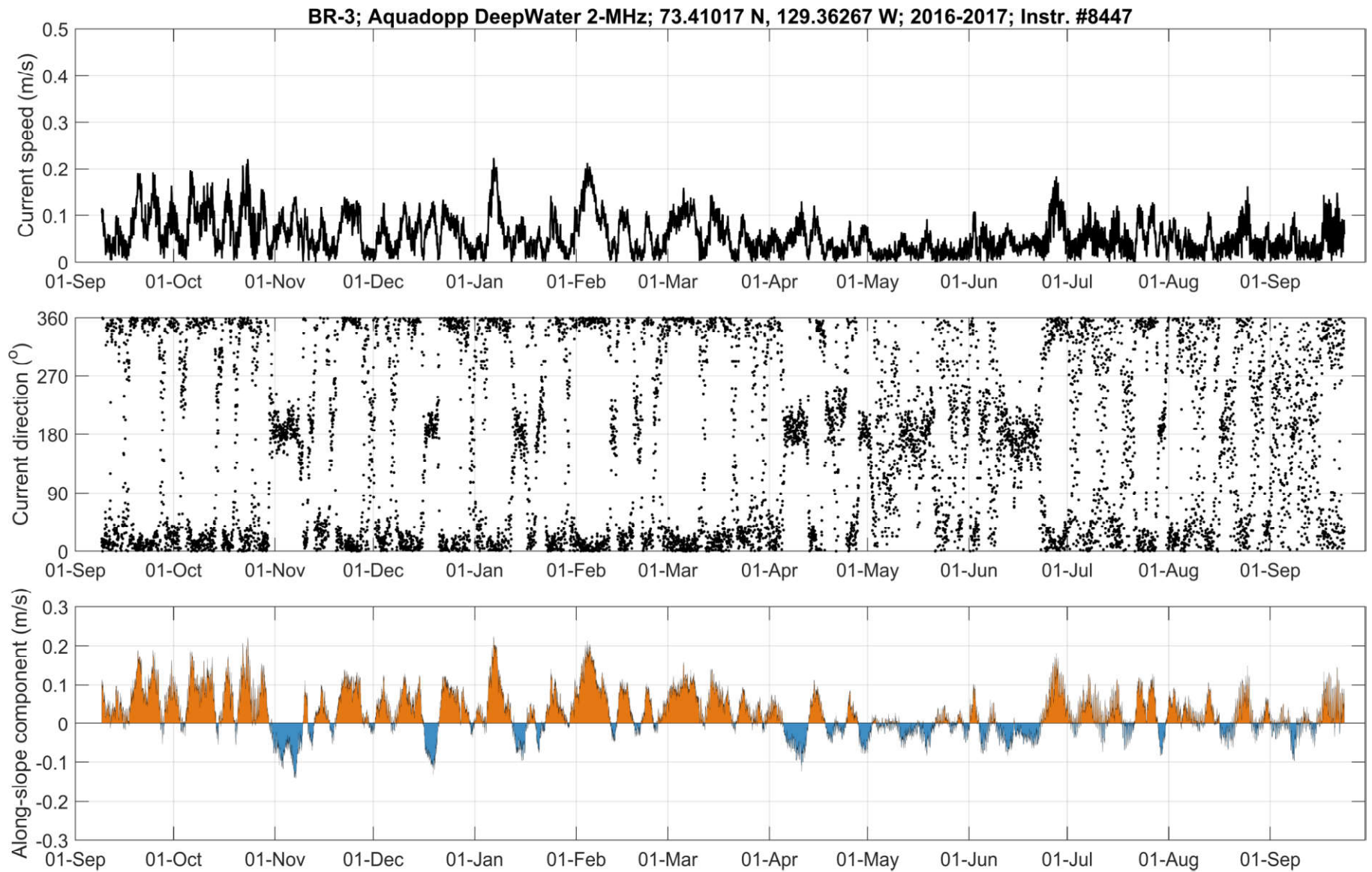


Figure 16: Time-series of current speed, current direction and along-slope current component at 602 m at mooring BR-3-16 as obtained with the Aquadopp #8447.

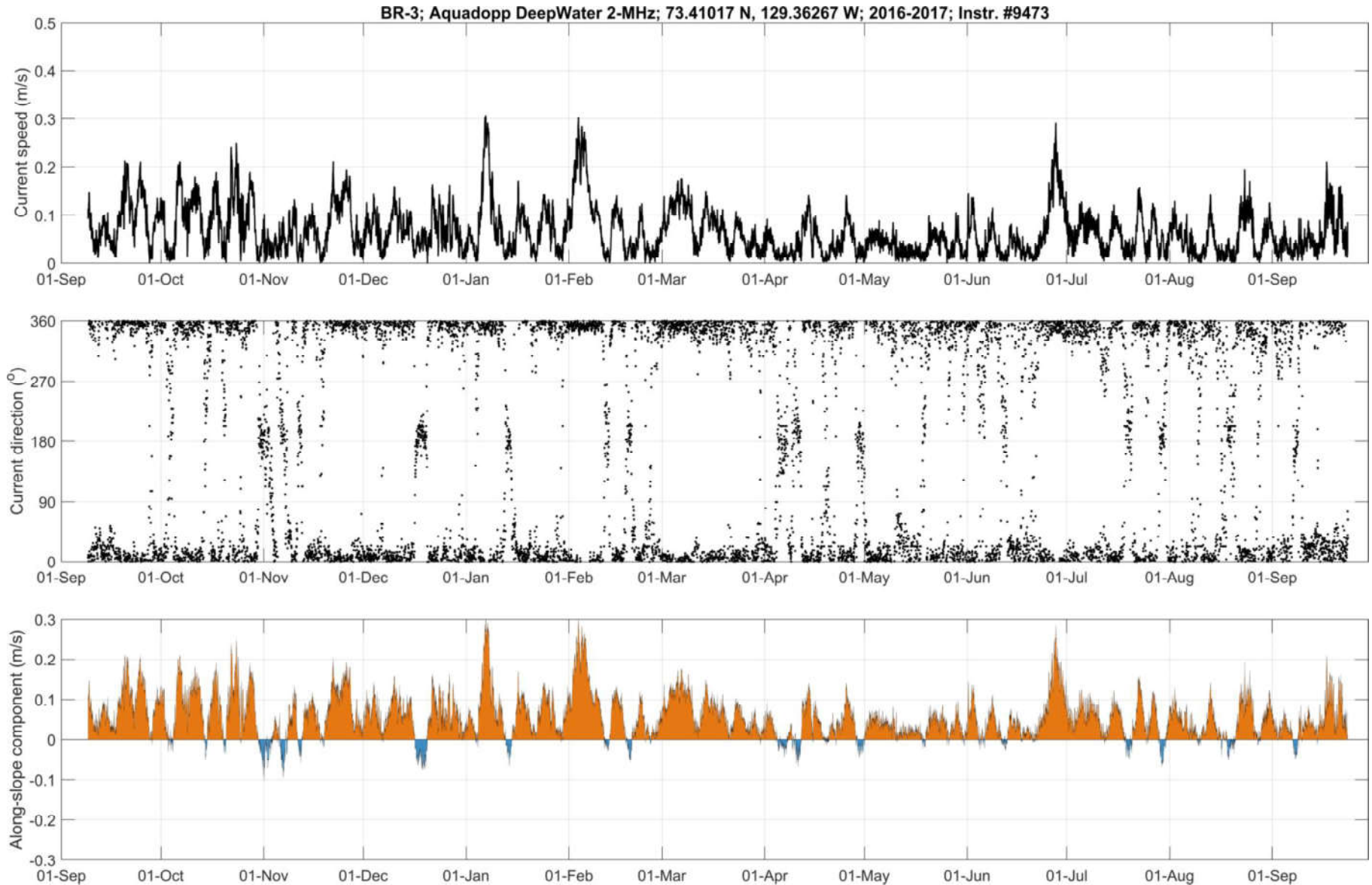


Figure 17: Time-series of current speed, current direction and along-slope current component at 713 m at mooring BR-3-16 as obtained with the Aquadopp #9473.

Table 9: Annual statistics of current speed and direction at BR-3-16 from selected bin depths representative of water mass variability in the Beaufort Sea (see Table 6 for water mass description).

Bin Depth (m)	Median Speed (m/s)	Mean Speed (m/s)	75%ile Speed (m/s)	95%ile Speed (m/s)	99%ile Speed (m/s)	Max Speed (m/s)	Standard Deviation Speed (m/s)	Vector-Averaged Direction (deg TN)
18.9	0.06	0.08	0.10	0.21	0.30	0.48	0.06	191.5
130.9	0.06	0.07	0.09	0.15	0.23	0.34	0.04	179.1
216.4	0.05	0.06	0.08	0.13	0.17	0.24	0.04	359.6
344.4	0.04	0.05	0.06	0.11	0.16	0.22	0.03	353.9
601.5	0.05	0.06	0.08	0.13	0.18	0.22	0.04	343.0
712.8	0.05	0.07	0.09	0.16	0.24	0.31	0.05	336.1

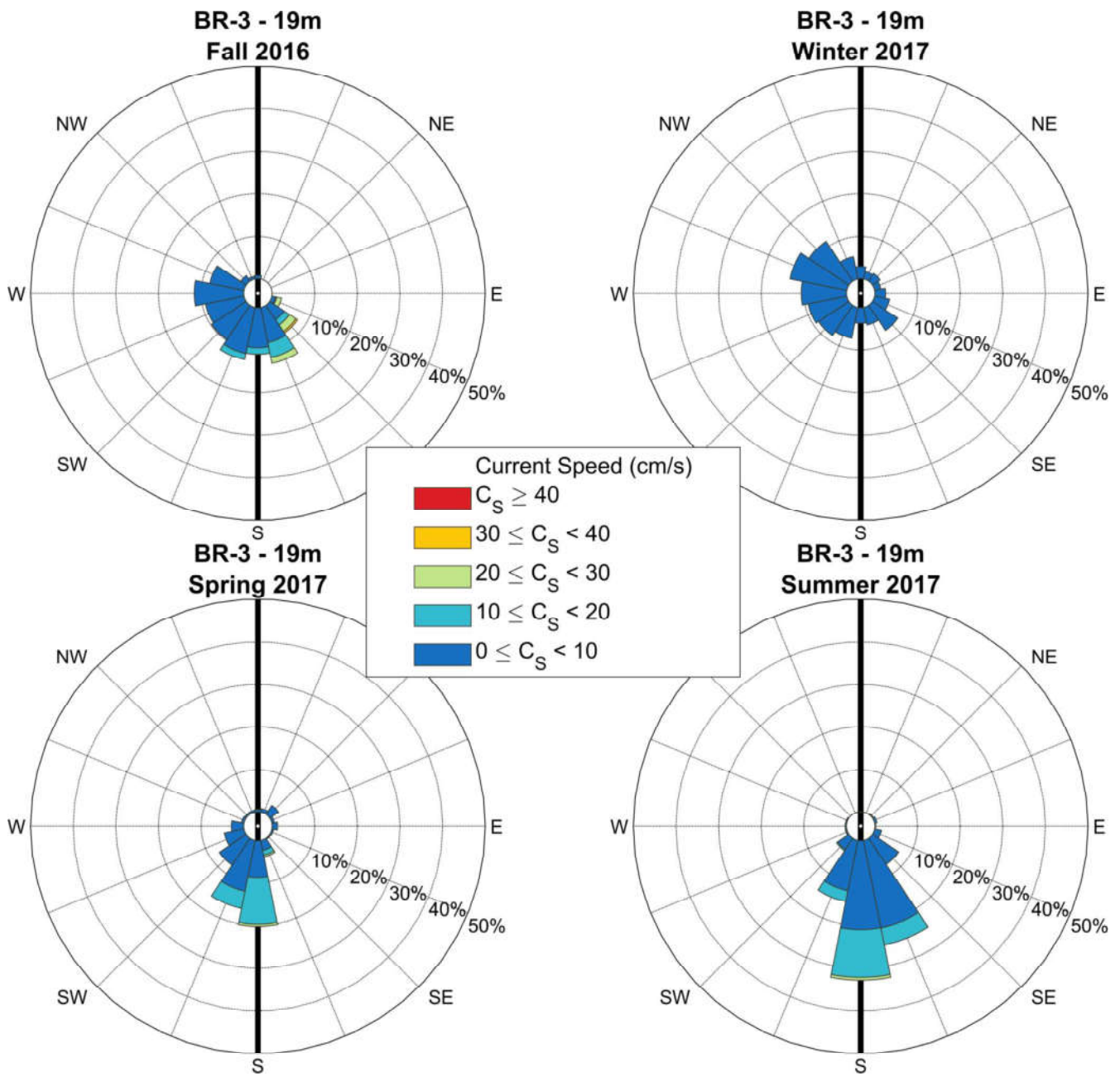


Figure 18: Seasonal current roses at 19 m depth (bin cell #46) at BR-3-16 measured by the QM ADCP #8784. Data are low-pass filtered. Roses point toward where the currents are going. Seasons are defined following the meteorological convention (Fall: October-December; Winter: January-March; Spring: April-June; Summer: July-September).

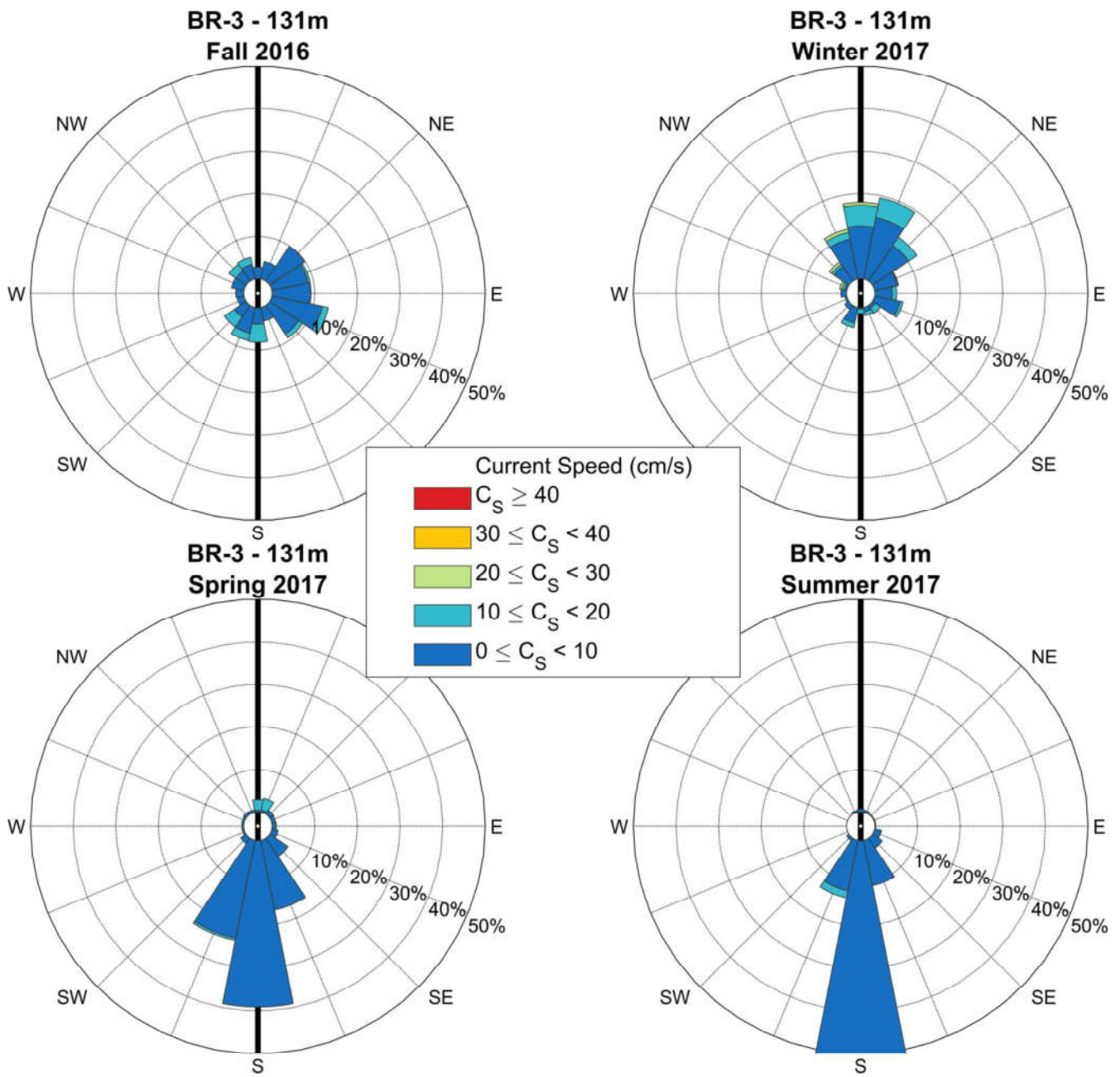


Figure 19: Seasonal current roses at 131 m depth (bin cell #18) at BR-3-16 measured by the QM ADCP #8784. Data are low-pass filtered. Roses indicate the direction toward which currents flow. Seasons are defined following the meteorological convention (Fall: October-December; Winter: January-March; Spring: April-June; Summer: July-September).

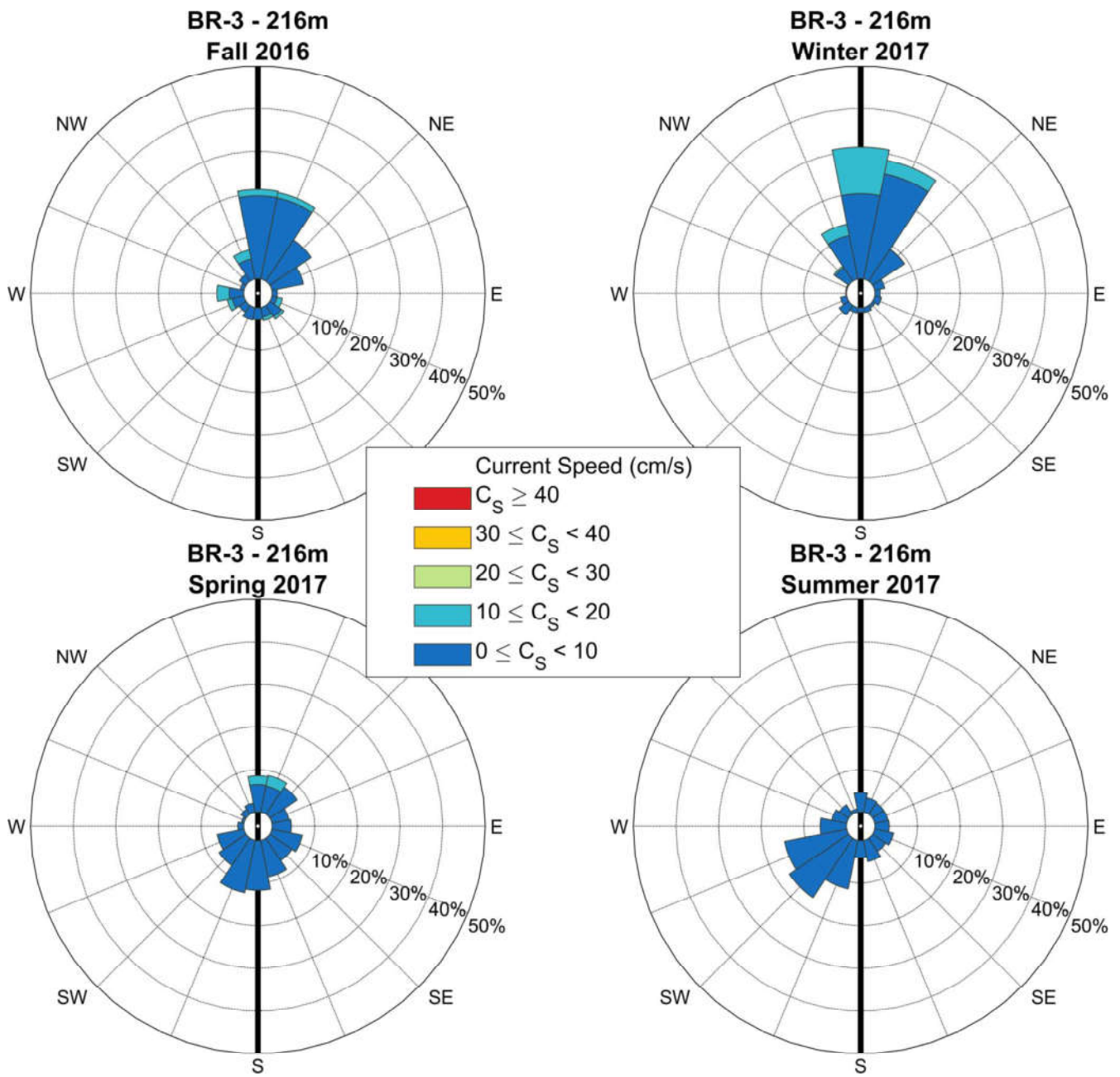


Figure 20: Seasonal current roses at 216 m depth (bin cell #17) at BR-3-16 measured by the LR ADCP #18785. Data are low-pass filtered. Roses indicate the direction toward which currents flow. Seasons are defined following the meteorological convention (Fall: October-December; Winter: January-March; Spring: April-June; Summer: July-September).

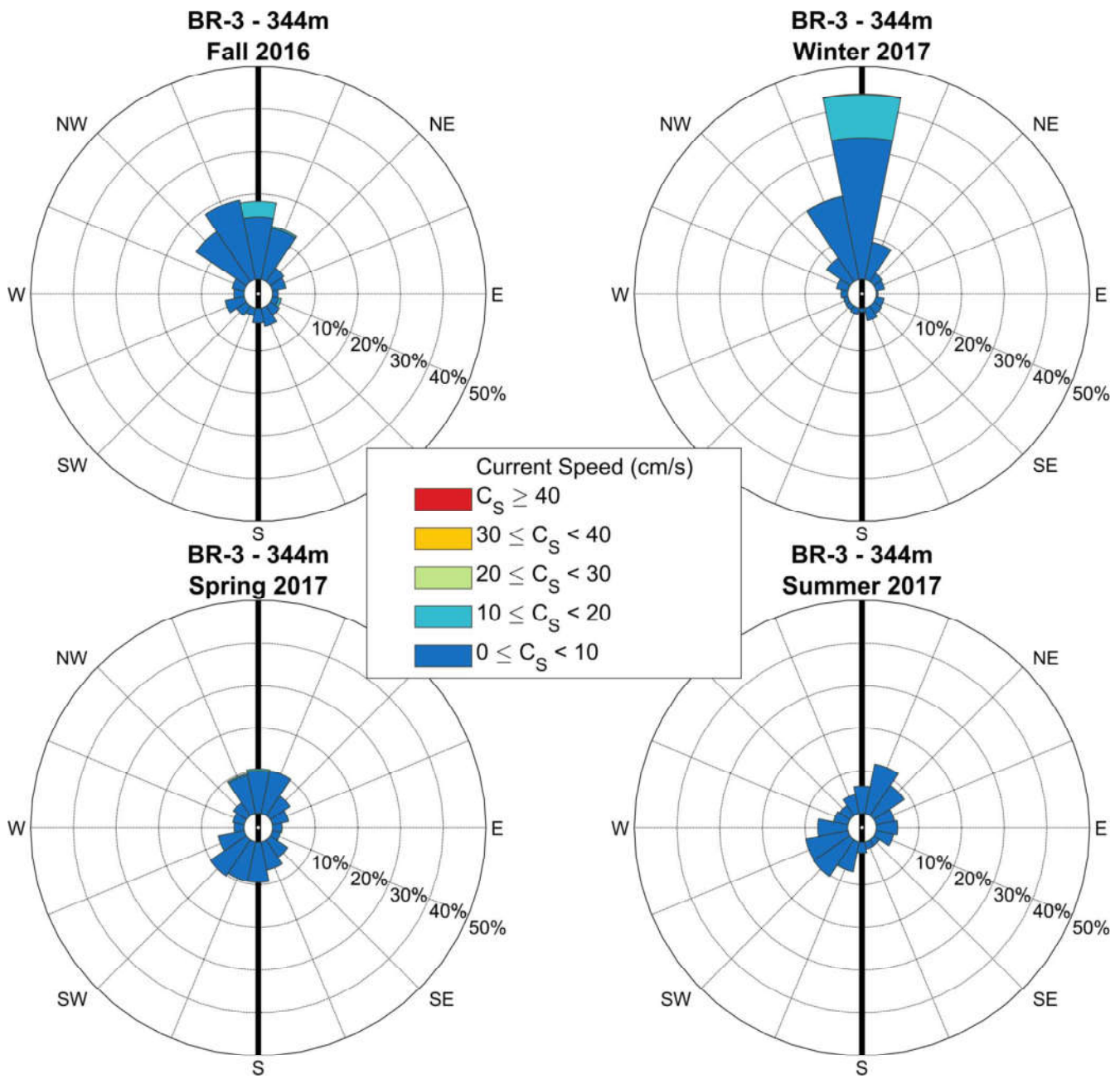


Figure 21: Seasonal current roses at 344 m depth (bin cell #9) at BR-3-16 measured by the LR ADCP #18785. Data are low-pass filtered. Roses indicate the direction toward which currents flow. Seasons are defined following the meteorological convention (Fall: October-December; Winter: January-March; Spring: April-June; Summer: July-September).

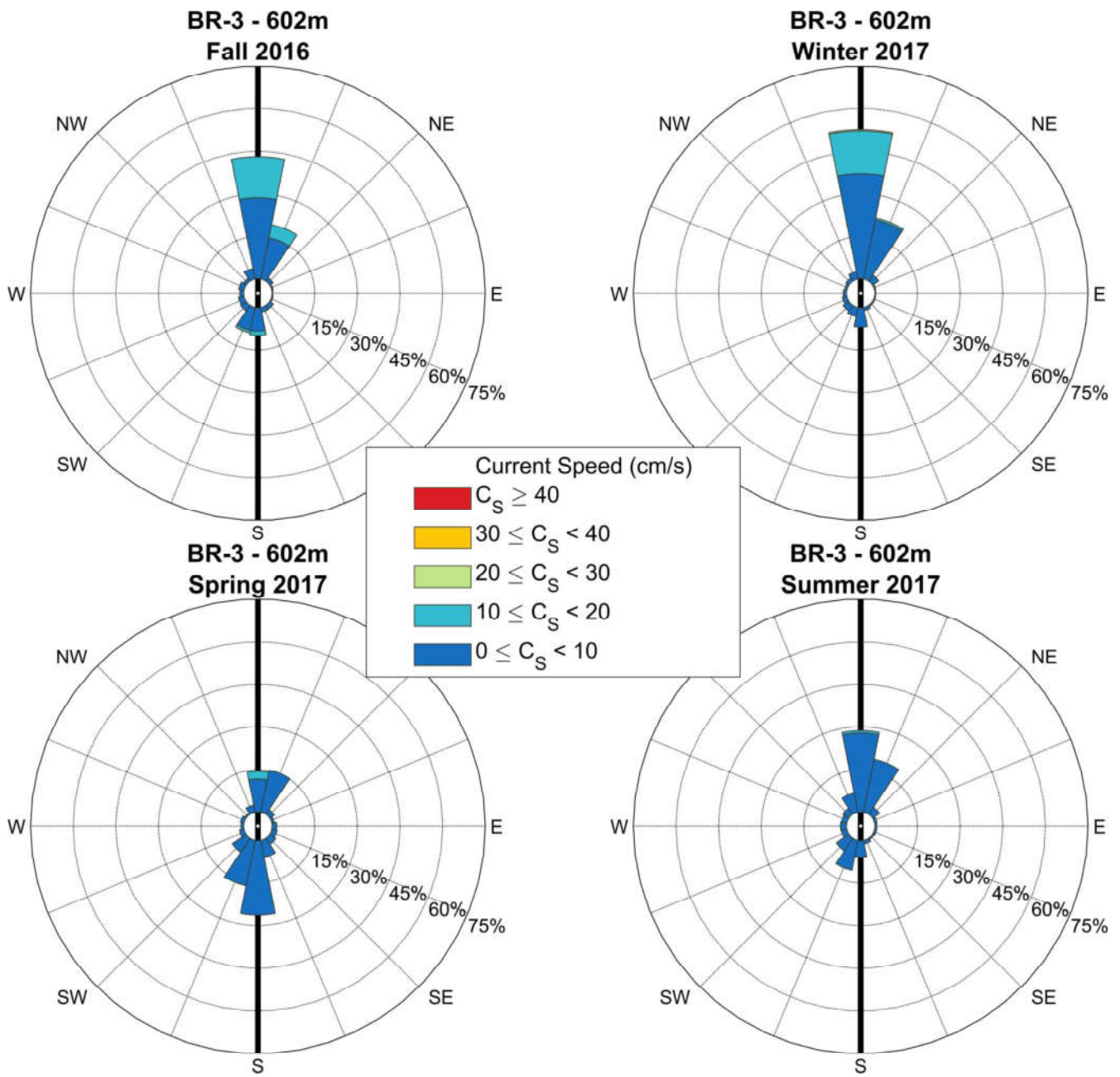


Figure 22: Seasonal current roses at 602 m depth at BR-3-16 measured by the Aquadopp #8447. Data are low-pass filtered. Roses indicate the direction toward which currents flow. Seasons are defined following the meteorological convention (Fall: October-December; Winter: January-March; Spring: April-June; Summer: July-September).

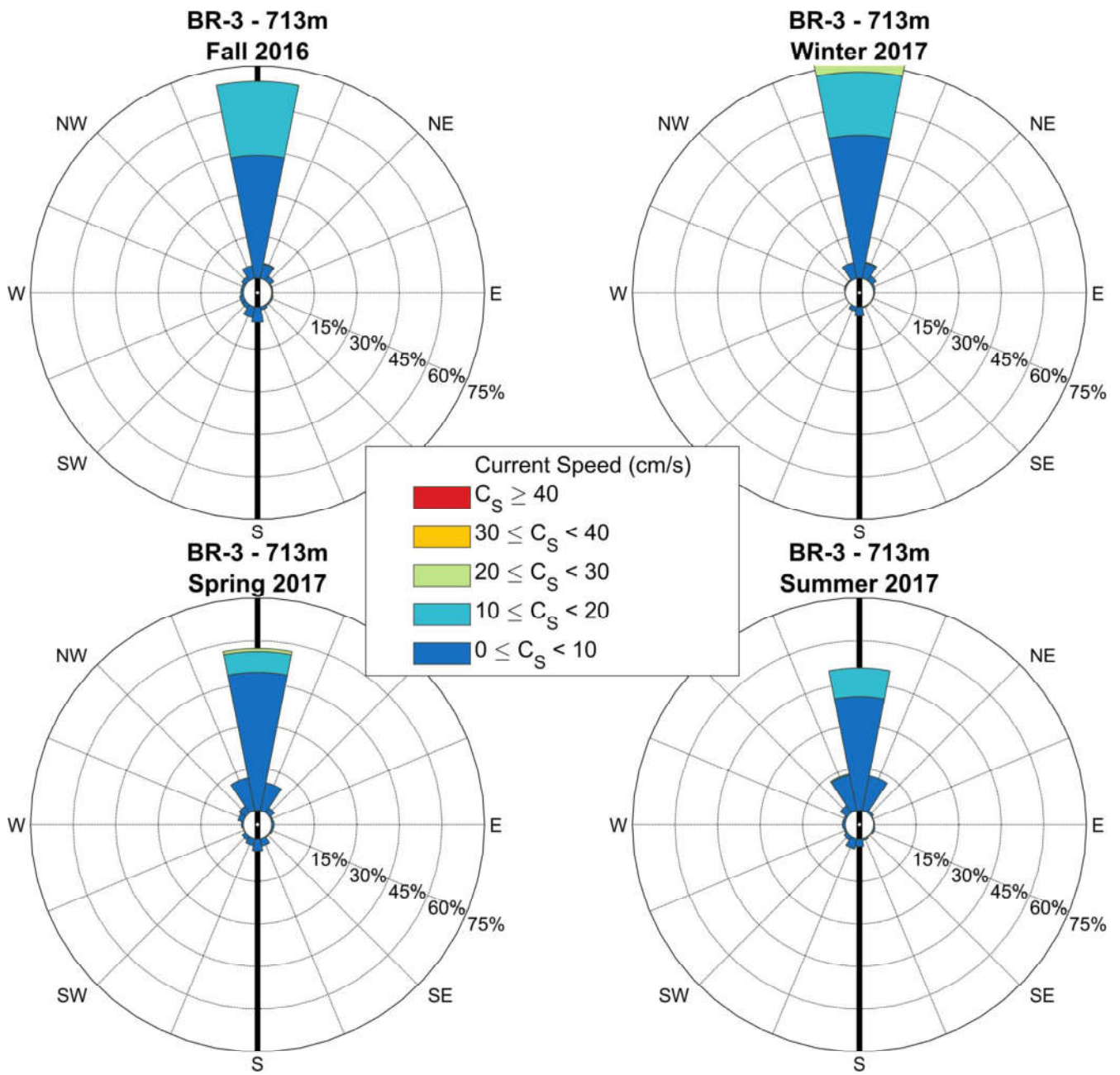


Figure 23: Seasonal current roses at 713 m depth at BR-3-16 measured by the Aquadopp #9473. Data are low-pass filtered. Roses indicate the direction toward which currents flow. Seasons are defined following the meteorological convention (Fall: October-December; Winter: January-March; Spring: April-June; Summer: July-September).

3.2.3 Mooring BR-G

Time-series plots of current speed, direction, and along-slope current component from the QM ADCP, LR ADCP and the two Aquadopp DW deployed at BR-G from 2016 to 2017 are provided in Figure 24 through Figure 27. The first valid bin depth for the QM ADCP #12699 at BR-G-16 after removing sidelobe interference was 29.2 m (bin cell 35) with 97% valid data (Appendix C). Bin depths 121 to 129 m (bin cells 10, 11 and 12) were affected by the presence of the upper sediment trap (as at BR-1 and BR-3), which resulted in reflection observed in the echo intensity (not shown) and a general decrease in current speed at these depths. A reflection was also observed at bin depths between 61 and 65 m (bin cells 26 and 27) due to the IPS float and cage. Accordingly, bin cells 10 to 12 and 26 to 27 for QM ADCP #12699 were manually flagged as part of the QA/QC and data from these bin depths should be treated carefully before being used in further analyses. The pressure time series from the QM ADCP #12699 recorded fluctuations on the order of 2 to 4 m (similar to the QM ADCP at BR-1) during most of the deployment which do not correspond to changes in depth due to mooring layover, indicating a potential malfunction of the pressure sensor. The pressure time series from this instrument should be used with caution.

The LR ADCP #13079 did not show any sign of suspicious bins due to interference with other parts of the mooring (Figure 25). The first valid bin depth for this instrument was 44.4 m (bin cell 25) with 84% valid data (Appendix C). Partial data loss possibly linked to high intensity of ambient sound generated by sea ice or wind/waves at the surface was observed briefly in October 2016 and spring-summer 2017 (Figure 25). The deep Aquadopp current meters #8419 (564.8 m) and #8442 (674.3 m) provided complete time-series with 100% valid data for each instrument (Figure 26, Figure 27, and Appendix C).

Mean current speeds at BR-G-16 ranged from 8 to 14 cm/s in the upper 200 m of the water column; and from 4 to 7 cm/s below 200 m (Table 10, Appendix C). Vector-averaged directions were typically to the southwest (225-240°TN) for all bins down to 200 m depth. Below 200 m currents veer progressively to the south and east in the LR ADCP dataset. In the lower water column, vector-averaged direction from the deep Aquadopps at 565 and 674 m was to the northeast along the slope (25-50°TN). The maximum current speed at BR-G-16 was 110 cm/s towards the west on September 20, 2016 at 101 m depth, measured by the QM ADCP. The maximum was measured during a strong event recorded by both the QM and LR ADCP in the upper water column above 125 m and which lasted several days. The instrument tilt was near, but did not exceed, the 15-degree threshold for reliable measurements during this event. A few other strong events (current speeds >50 cm/s) were measured in both of the time-series from January through March towards the northeast and east.

Seasonal current roses (low-pass filtered) for selected bin depths at mooring BR-G-16 are provided in Figure 28 through Figure 33. The strongest near surface currents (29 m, Figure 28) occur in the spring and summer. Stronger subsurface currents (133 m, Figure 29) occur in the winter, spring and summer. Directions in the upper water column are primarily bi-directional and along-slope, varying between the northeast and southwest. Below 200 m, currents are relatively weak and are typically less than 10 cm/s, with directions oriented along-slope to the northeast, with the exception of a reversal to the southwest in the spring at and above 220 m in the water column. Current speed and direction in the lowermost section of the water column (565 and 674 m, Figure 32 and Figure 33) were generally similar and uniformly to the east-northeast along the slope.

BR-G; QM Broadband 153.6 kHz; 71.00213 N, 135.49078 W; 2016-2017; Instr. #12699

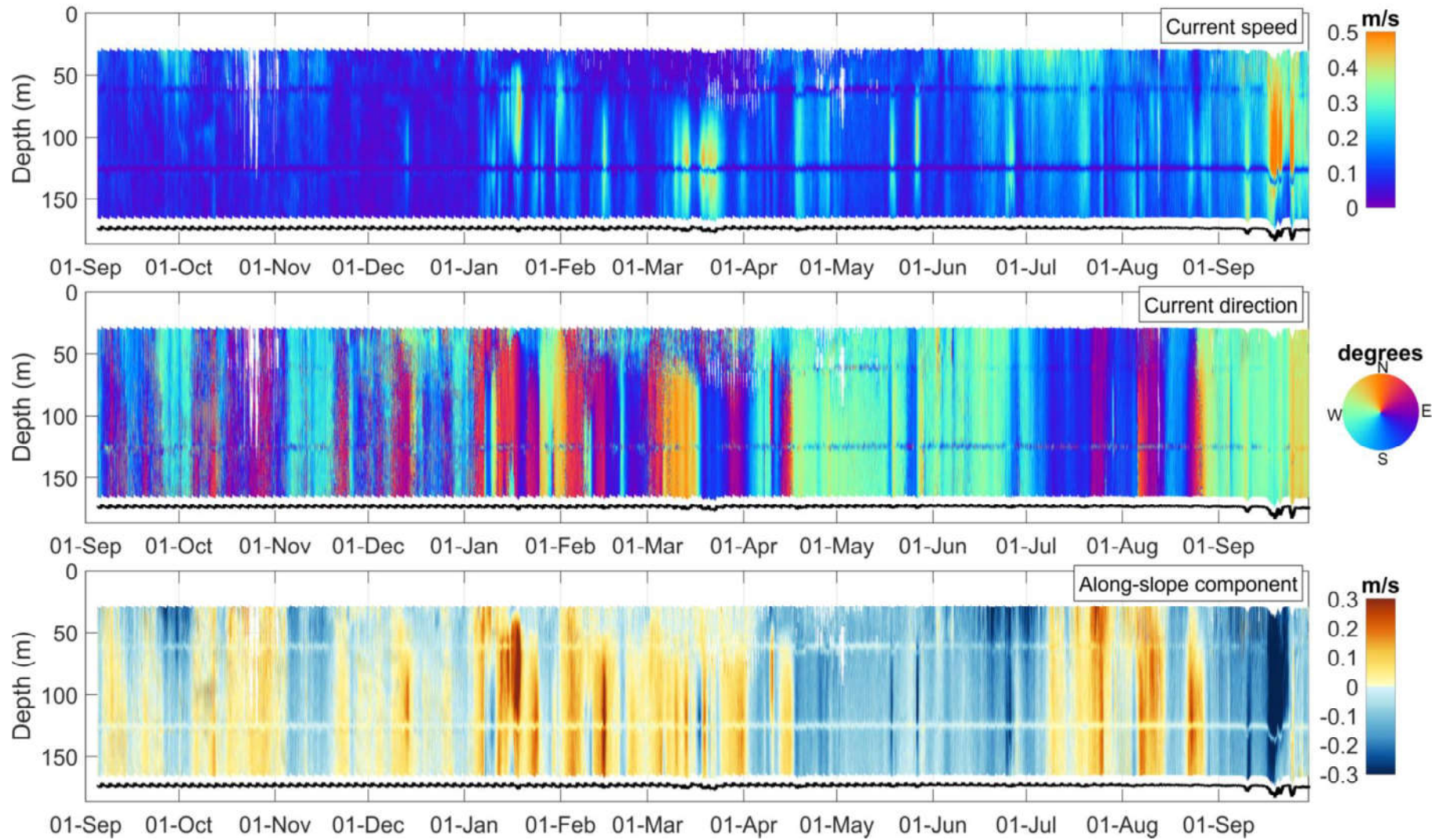


Figure 24: Time-series of current speed, current direction and along-slope current component at mooring BR-G-16 measured by the QM ADCP #12699. The black line depicts the instrument depth.

BR-G; LR Broadband 76.8 kHz; 71.00213 N, 135.49078 W; 2016-2017; Instr. #13079

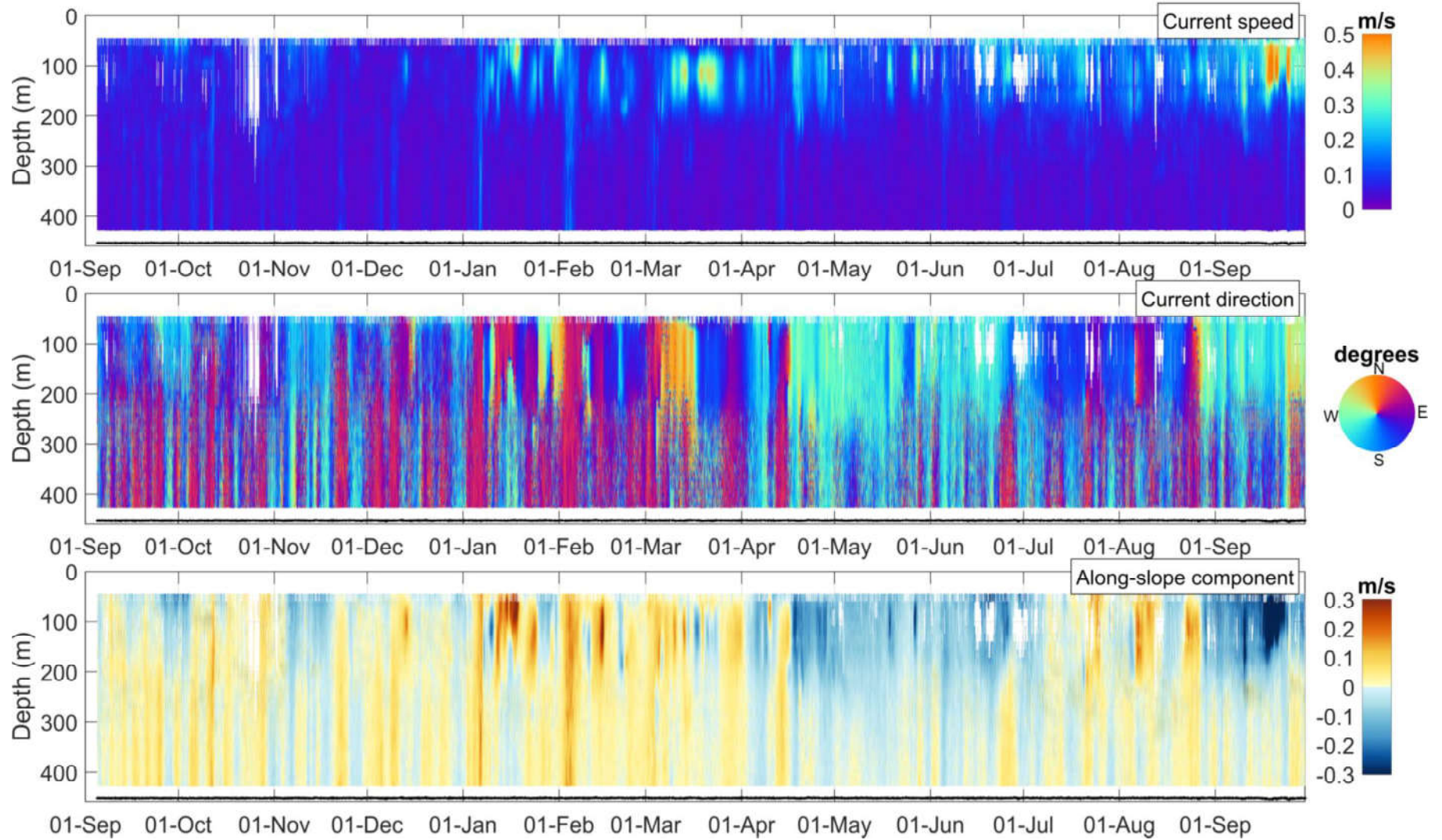


Figure 25: Time-series of current speed, current direction and along-slope current component at mooring BR-G-16 measured by the LR ADCP #13079. The black line depicts the instrument depth.

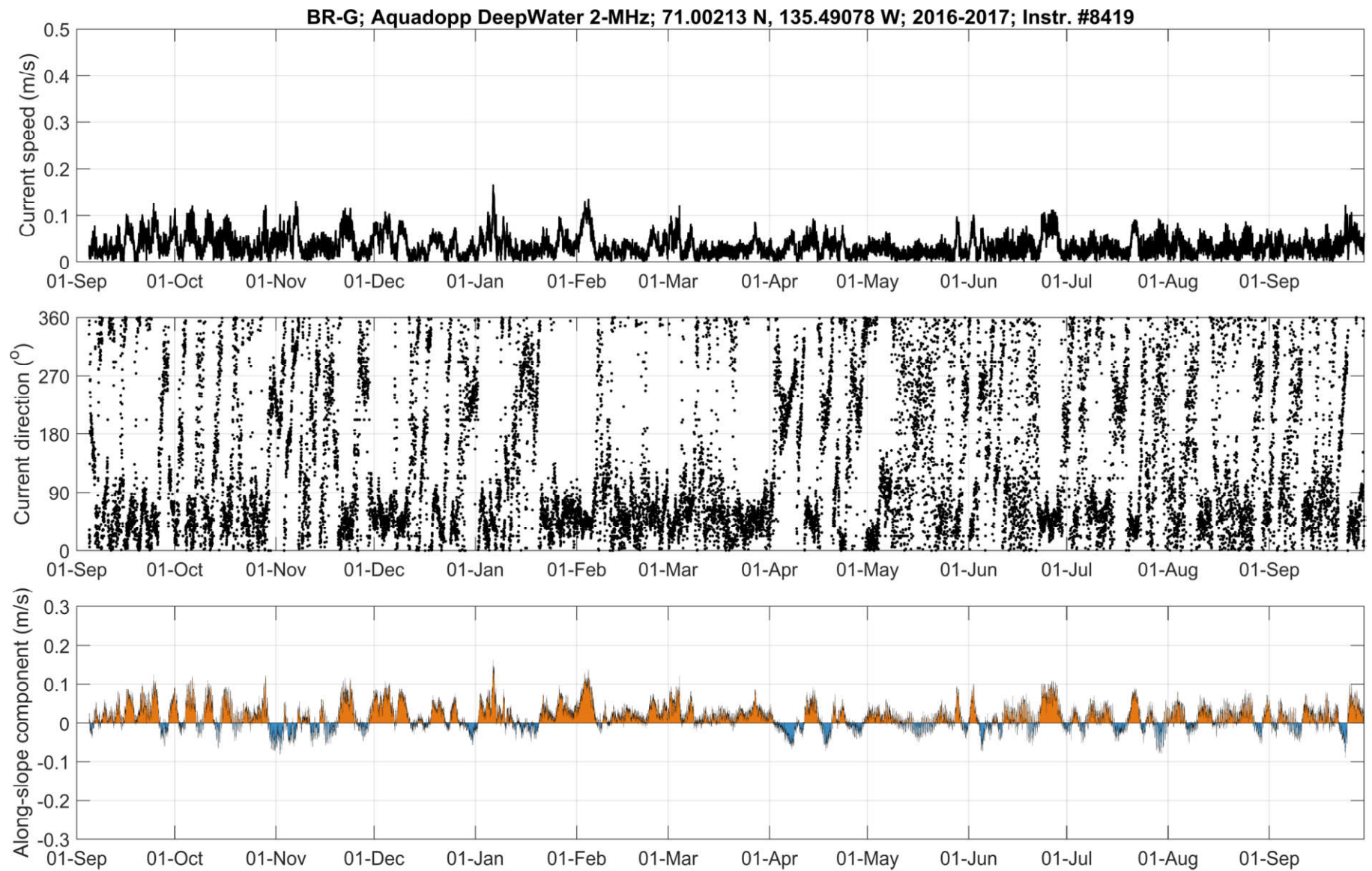


Figure 26: Time-series of current speed, current direction and along-slope current component at 565 m at mooring BR-G-16 measured by the Aquadopp #8419.

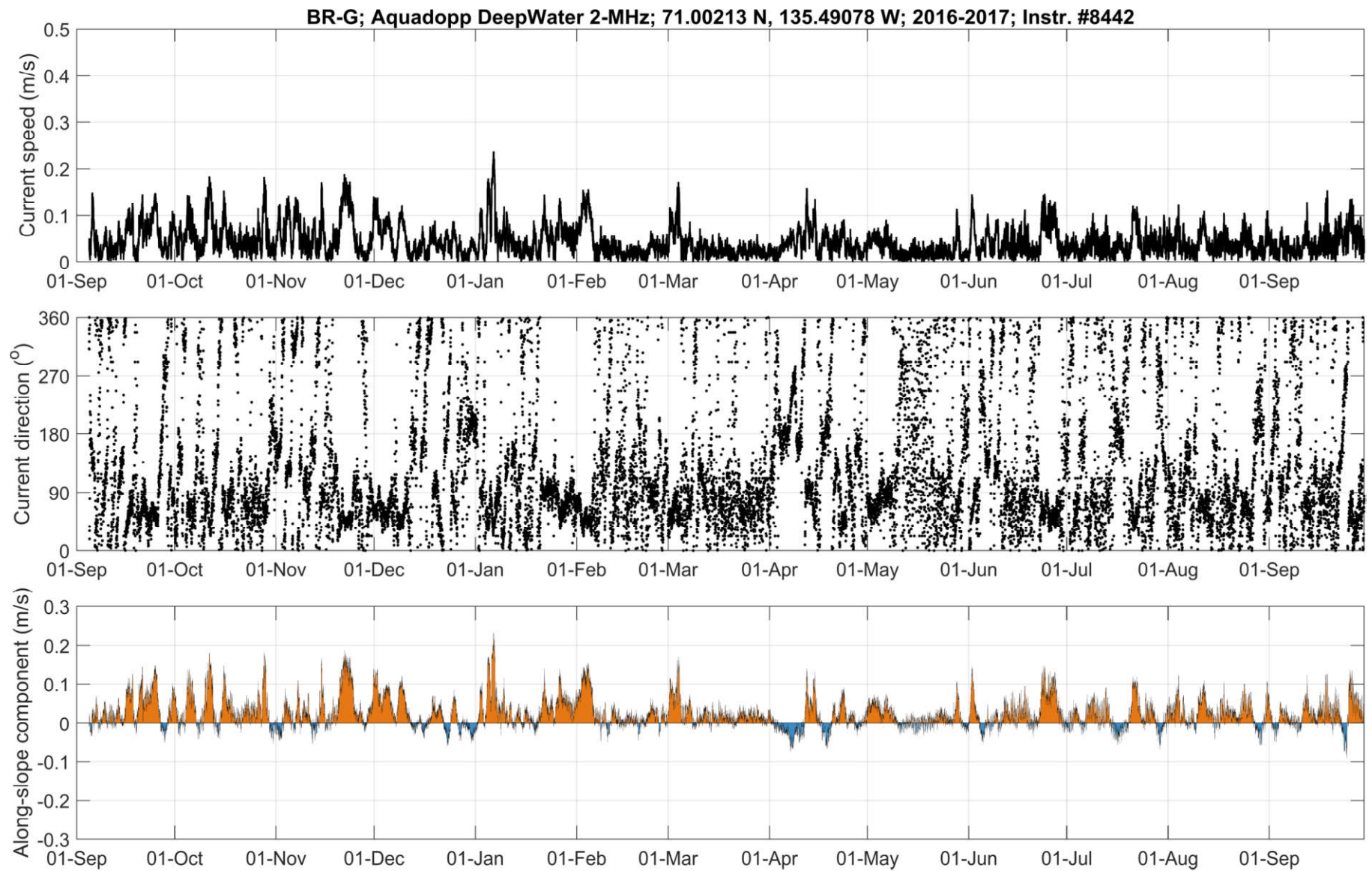


Figure 27: Time-series of current speed, current direction and along-slope current component at 674 m at mooring BR-G-16 measured by the Aquadopp #8442.

Table 10: Annual statistics of current speed and direction at BR-G-16 from selected bin depths representative of water mass variability in the Beaufort Sea (see Table 6 for water mass description).

Bin Depth (m)	Median Speed (m/s)	Mean Speed (m/s)	75%ile Speed (m/s)	95%ile Speed (m/s)	99%ile Speed (m/s)	Max Speed (m/s)	Standard Deviation Speed (m/s)	Vector-Averaged Direction (deg TN)
29.2	0.11	0.14	0.20	0.33	0.40	0.52	0.10	225.5
133.2	0.11	0.13	0.17	0.30	0.40	0.51	0.08	234.7
220.2	0.06	0.06	0.08	0.12	0.16	0.44	0.06	133.9
348.2	0.04	0.04	0.05	0.08	0.11	0.30	0.02	59.2
564.8	0.03	0.04	0.05	0.08	0.10	0.17	0.02	24.1
674.3	0.04	0.04	0.06	0.11	0.15	0.24	0.03	50.4

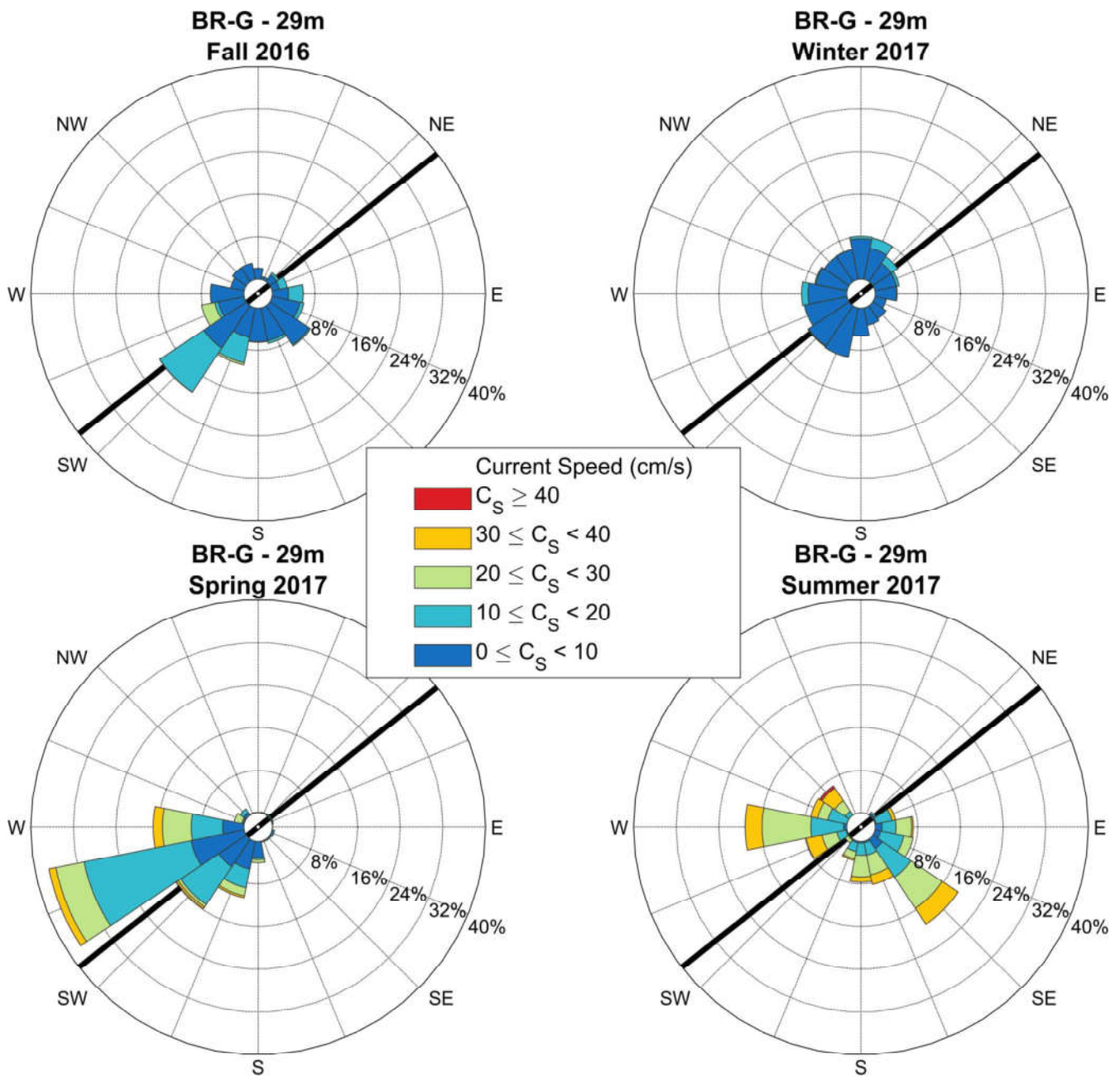


Figure 28: Seasonal current roses at 29 m depth (bin cell #35) at BR-G-16 measured by the QM ADCP #12699. Data are low-pass filtered. Roses indicate the direction toward which currents flow. Seasons are defined following the meteorological convention (Fall: October-December; Winter: January-March; Spring: April-June; Summer: July-September).

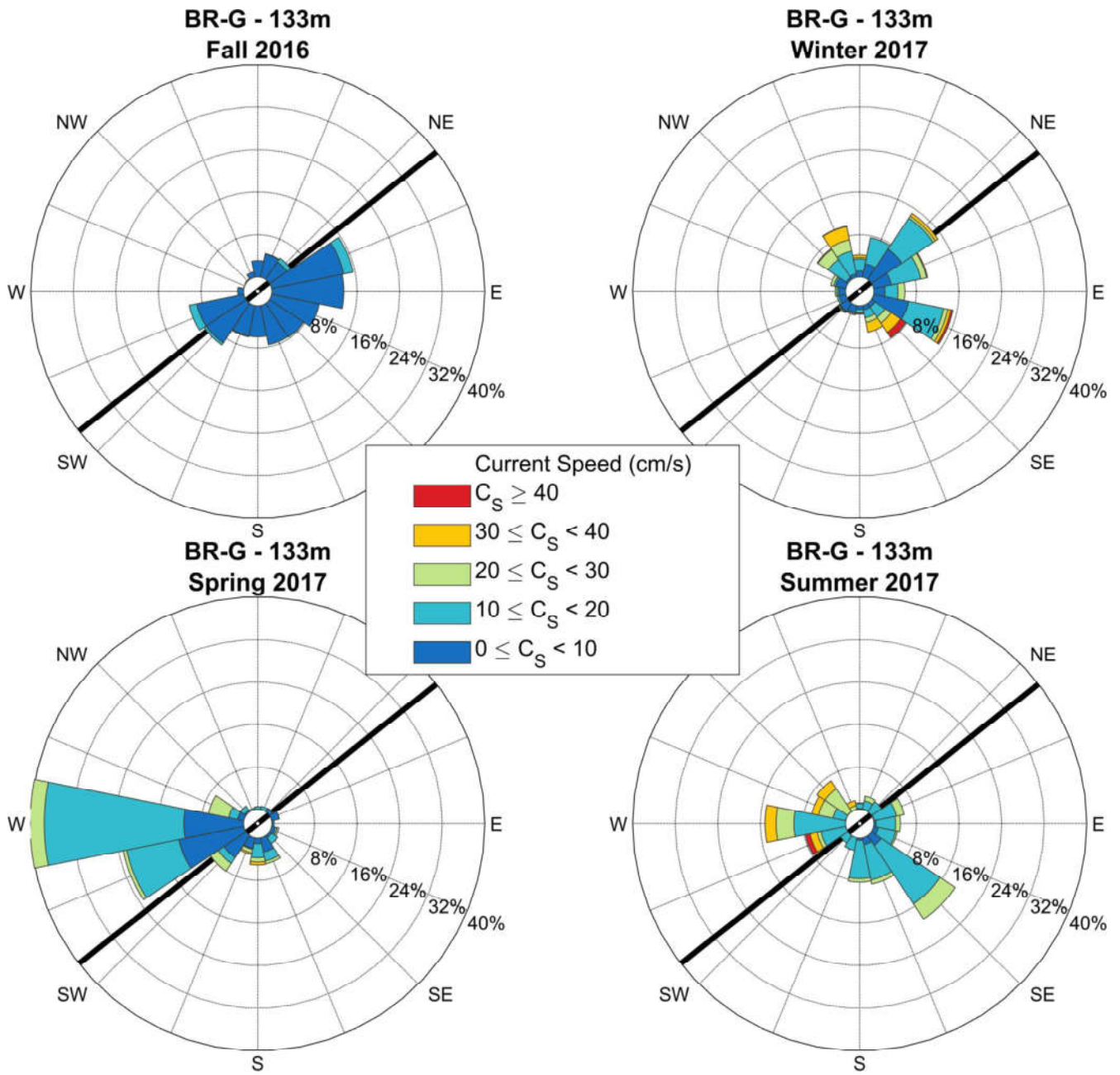


Figure 29: Seasonal current roses at 133 m depth (bin cell #9) at BR-G-16 measured by the QM ADCP #12699. Data are low-pass filtered. Roses indicate the direction toward which currents flow. Seasons are defined following the meteorological convention (Fall: October-December; Winter: January-March; Spring: April-June; Summer: July-September).

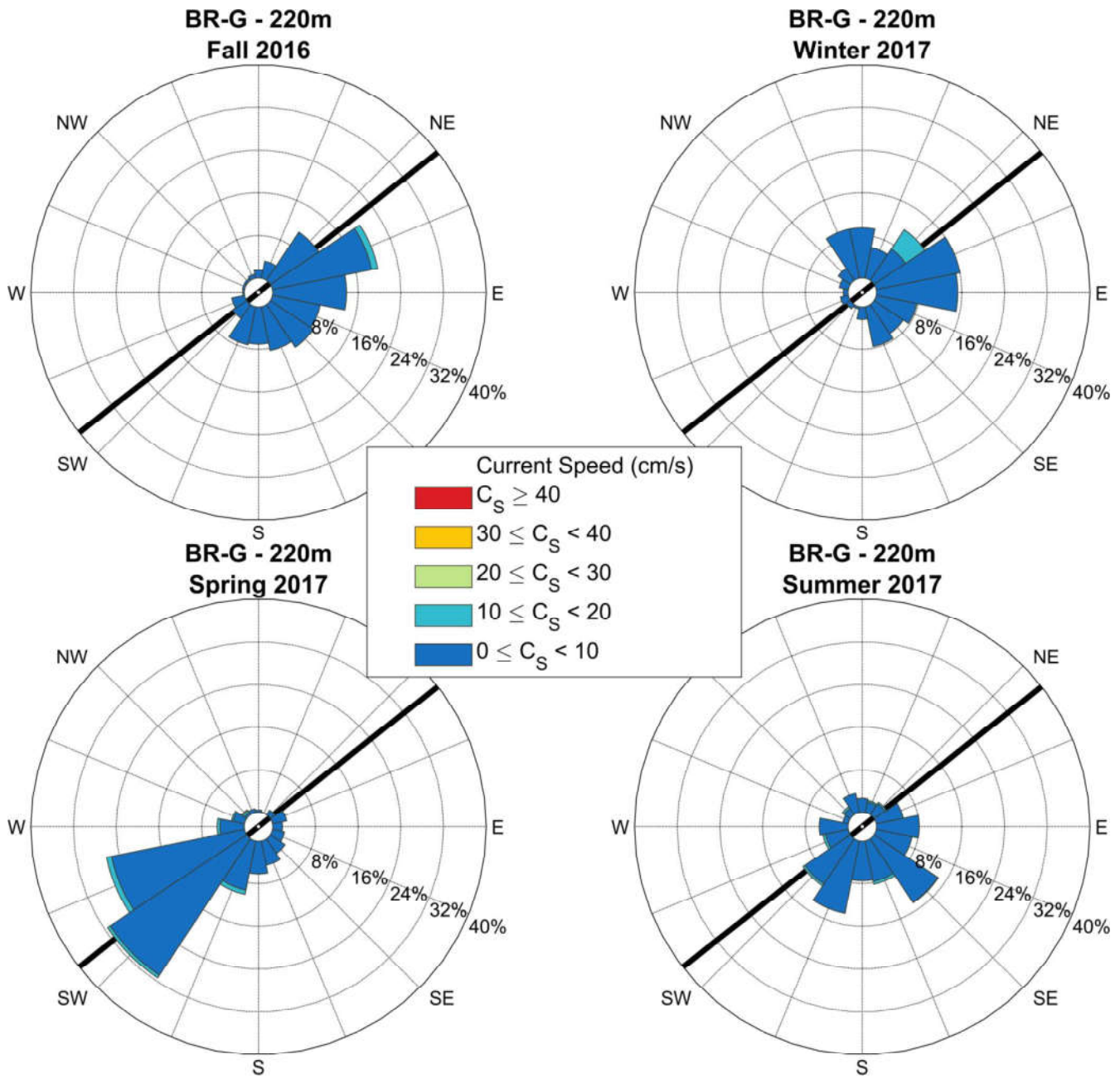


Figure 30: Seasonal current roses at 220 m depth (bin cell #14) at BR-G-16 measured by the LR ADCP #13079. Data are low-pass filtered. Roses indicate the direction toward which currents flow. Seasons are defined following the meteorological convention (Fall: October-December; Winter: January-March; Spring: April-June; Summer: July-September).

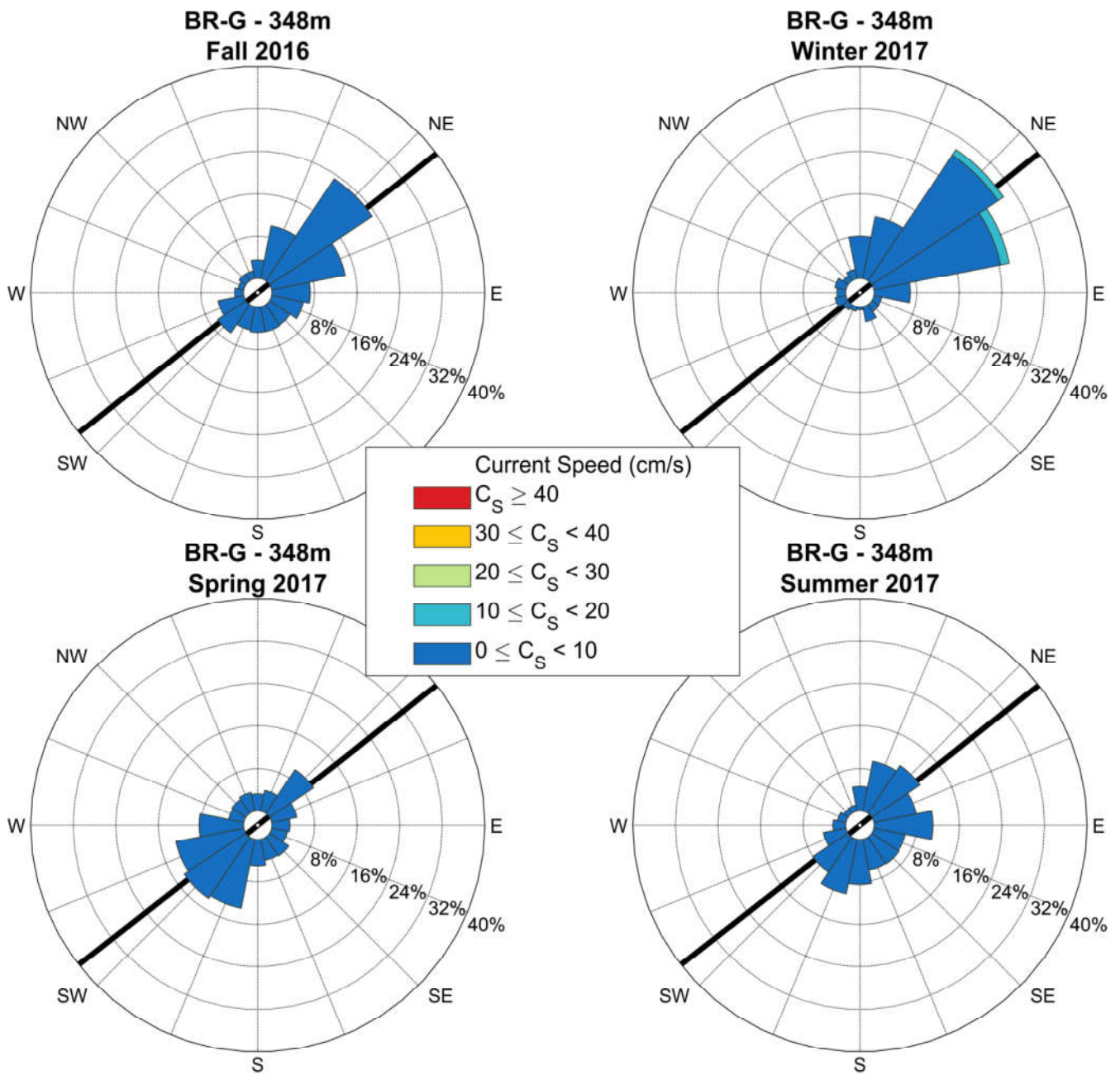


Figure 31: Seasonal current roses at 348 m depth (bin cell #6) at BR-G-16 measured by the LR ADCP #13079. Data are low-pass filtered. Roses indicate the direction toward which currents flow. Seasons are defined following the meteorological convention (Fall: October-December; Winter: January-March; Spring: April-June; Summer: July-September).

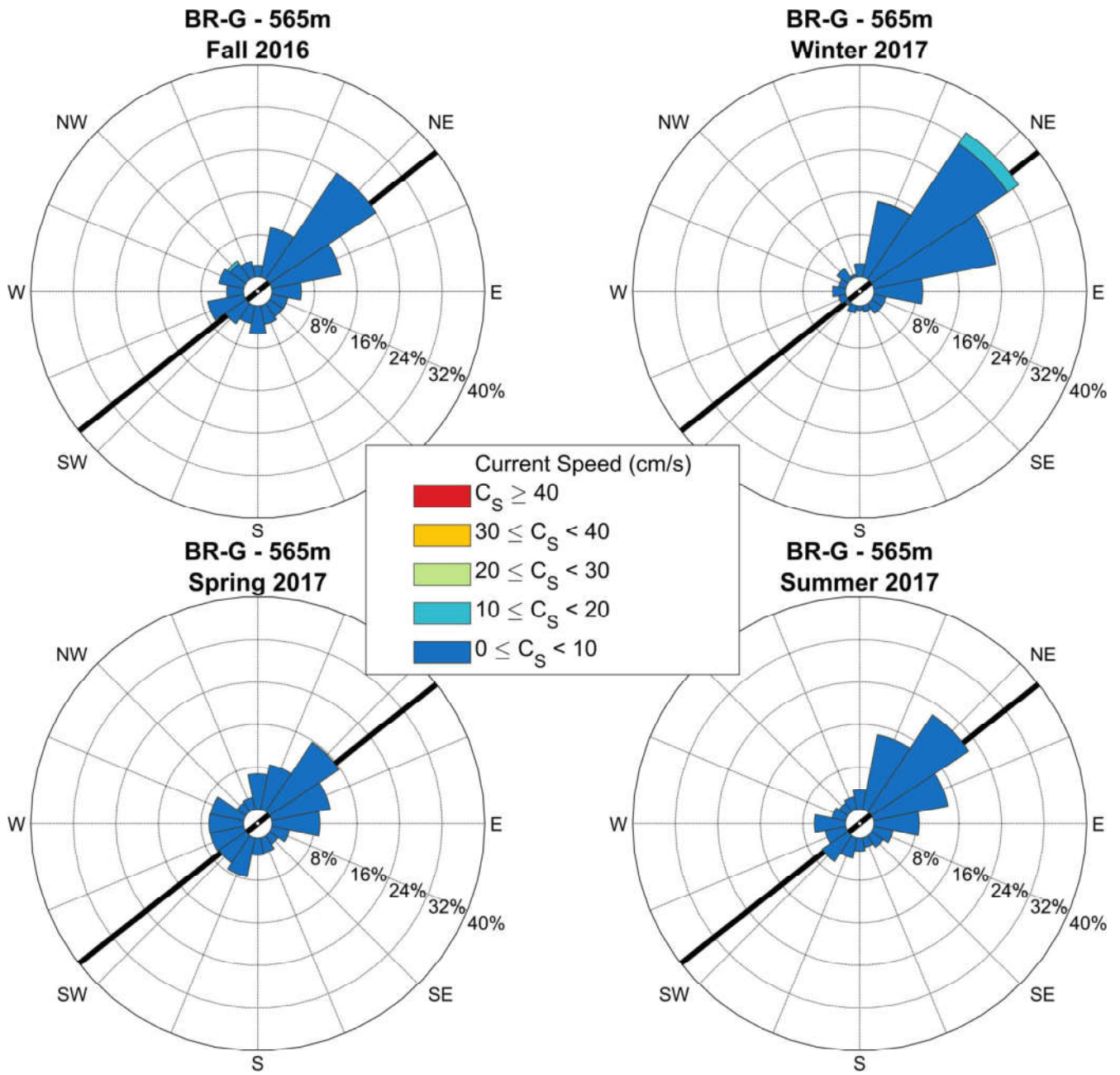


Figure 32: Seasonal current roses at 565 m depth at BR-G-16 measured by the Aquadopp #8419. Data are low-pass filtered. Roses indicate the direction toward which currents flow. Seasons are defined following the meteorological convention (Fall: October-December; Winter: January-March; Spring: April-June; Summer: July-September).

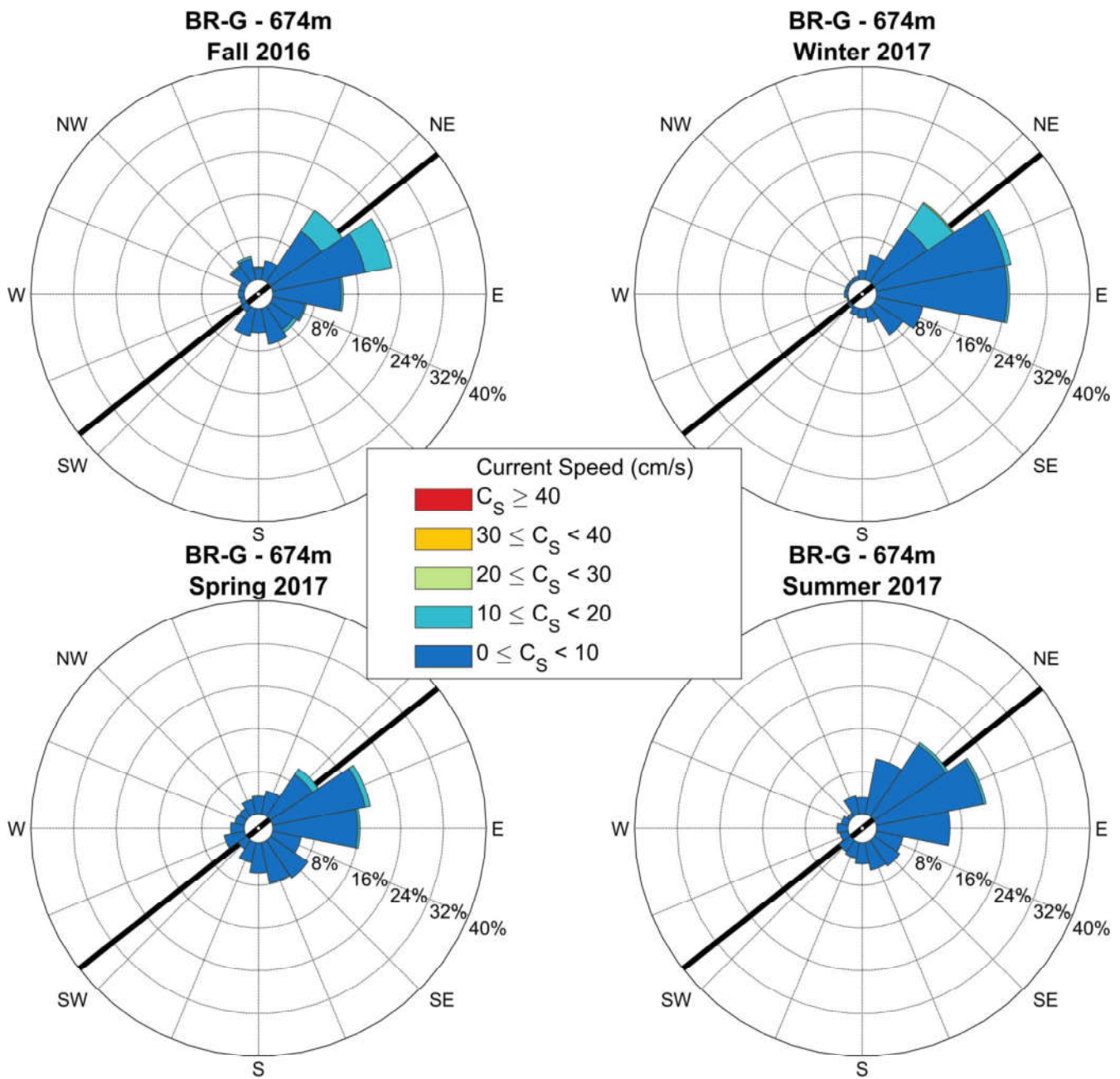


Figure 33: Seasonal current roses at 674 m depth at BR-G-16 measured by the Aquadopp #8442. Data are low-pass filtered. Roses indicate the direction toward which currents flow. Seasons are defined following the meteorological convention (Fall: October-December; Winter: January-March; Spring: April-June; Summer: July-September).

3.2.4 Mooring BR-K

Time-series plots of current speed, direction, and along-slope current component from the WHS ADCP and Nortek Aquadopp Profiler deployed at the upper slope mooring BR-K from 2016 to 2017 are provided in Figure 34 and Figure 35. The WHS ADCP stopped recording prematurely on August 11, 2017 due to a suspected issue with the data card. The first valid bin depth for the WHS ADCP #7844 at BR-K-16 after removing sidelobe interference was 21.4 m (bin cell 14) with only 23% of the recorded data valid (Appendix C). The WHS ADCP experienced significant data loss in the upper column with valid data ranging from 23% to 95% at 85 m water depth and above. The data loss appears to be a result of poor signal return in the upper water column as a result of being deployed inadvertently using the broadband setting (WB0) which reduced the profiling range in comparison to narrow band (WB1). No bin depth was manually flagged due to possible interference with other parts of the mooring for this instrument as part of the QA/QC procedure.

The down-looking Aquadopp Profiler #1147 at BR-K-16 provided a complete annual dataset of bottom currents on the upper slope (Figure 35). One suspicious bin cell at 150.0 m depth (bin cell 1) was manually flagged as part of the QA/QC process (Appendix C). This bin depth was likely affected by the presence of the acoustic release tandem kit located approximately 2 m below the Aquadopp, which resulted in reflection observed in the echo intensity and suspicious current direction at this depth (Figure 35). The data from other bin depths were of high quality with 100% valid data for all bin cells.

Mean current speeds at BR-K-16 measured by the WHS ADCP ranged from 12 to 18 cm/s throughout the water column (Appendix C, Table 11). Vector-averaged directions were uniformly to the east (75-100°TN) at all bin depths. Mean current speeds measured by the Nortek Aquadopp Profiler ranged from 7 to 11 cm/s throughout the water column (Appendix C, Table 11). Vector-averaged directions were uniformly to the east-northeast in the near-bottom depth bins (50-75°TN) at all bin depths.

Maximum current speed measured at BR-K-16 was 108 cm/s on January 7, 2017 at 53 m depth during a strong current event measured across all water depths at the mooring. Current direction during the event was uniformly to the northeast (50-65°TN) in the upper water column measured by the WHS ADCP, consistent with an intensification of the Beaufort shelfbreak jet flowing within 10-15 km of the shelf edge on the upper slope (see section 1.2). Several other relatively strong current speed events (>50 cm/s) were recorded at BR-K throughout the data record characterized by both a strong positive (northeast) and negative along-slope current component (southwest).

Seasonal current roses (low-pass filtered) for selected bin depths at mooring BR-K-16 are provided in Figure 36 to Figure 37. The currents in the at 21 m and 125 m show a strong bi-direction signal, particularly at 125 m which reflects the presence of the shelfbreak jet alternating with wind-forced reversals to the southwest. Near-bottom currents are primarily uni-directional towards the northeast, reflecting the persistence of the shelfbreak undercurrent at this depth.

BR-K; WH Broadband 307.2 kHz; 70.86325 N, 135.02415 W; 2016-2017; Instr. #7844

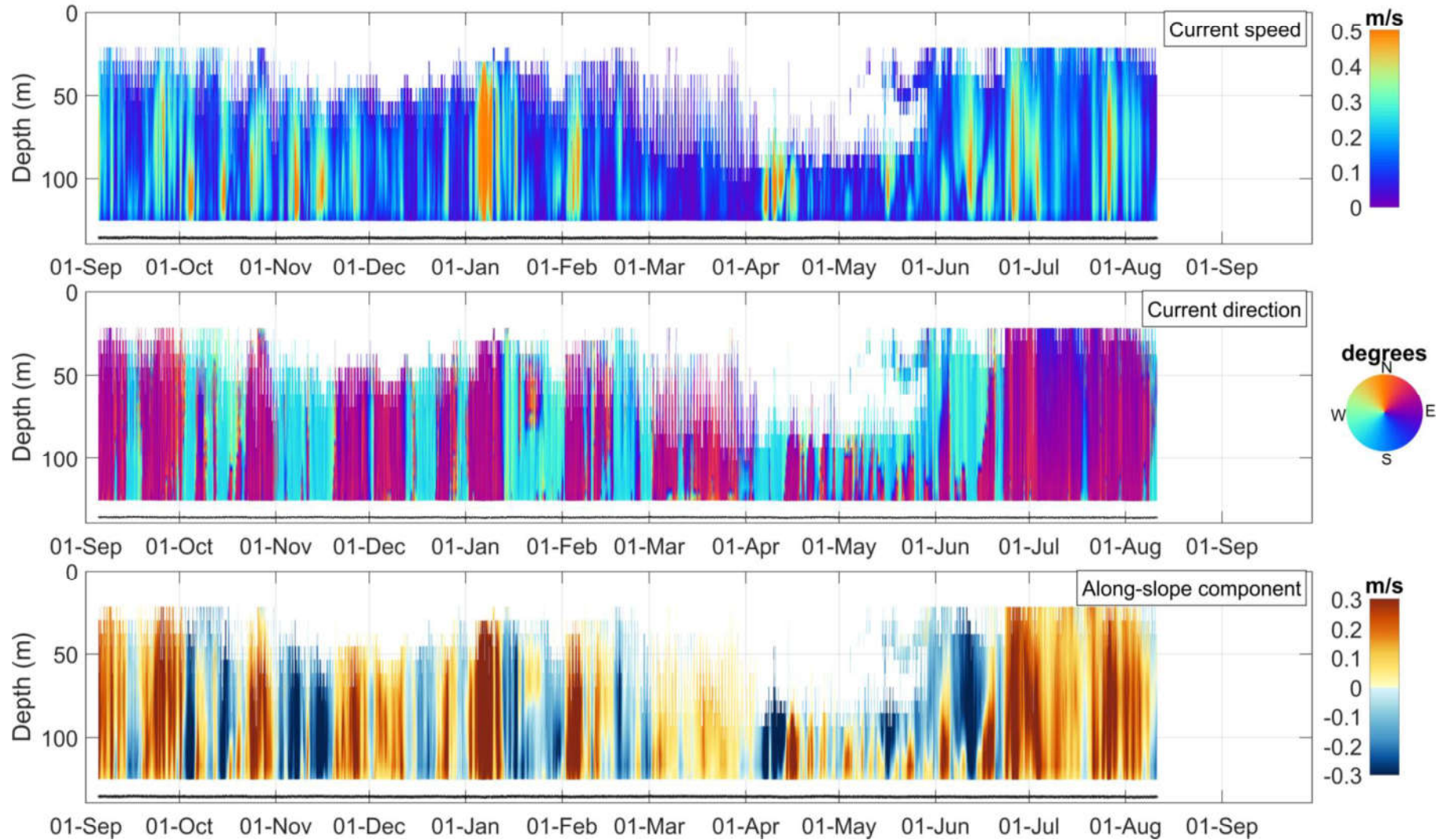


Figure 34: Time-series of current speed, current direction and along-slope current component at mooring BR-K-16 measured by the WHS ADCP #7844. The black line depicts the instrument depth.

BR-K; Aquadopp Profiler 1-MHz; 70.86325 N, 135.02415 W; 2016-2017; Instr. #11147

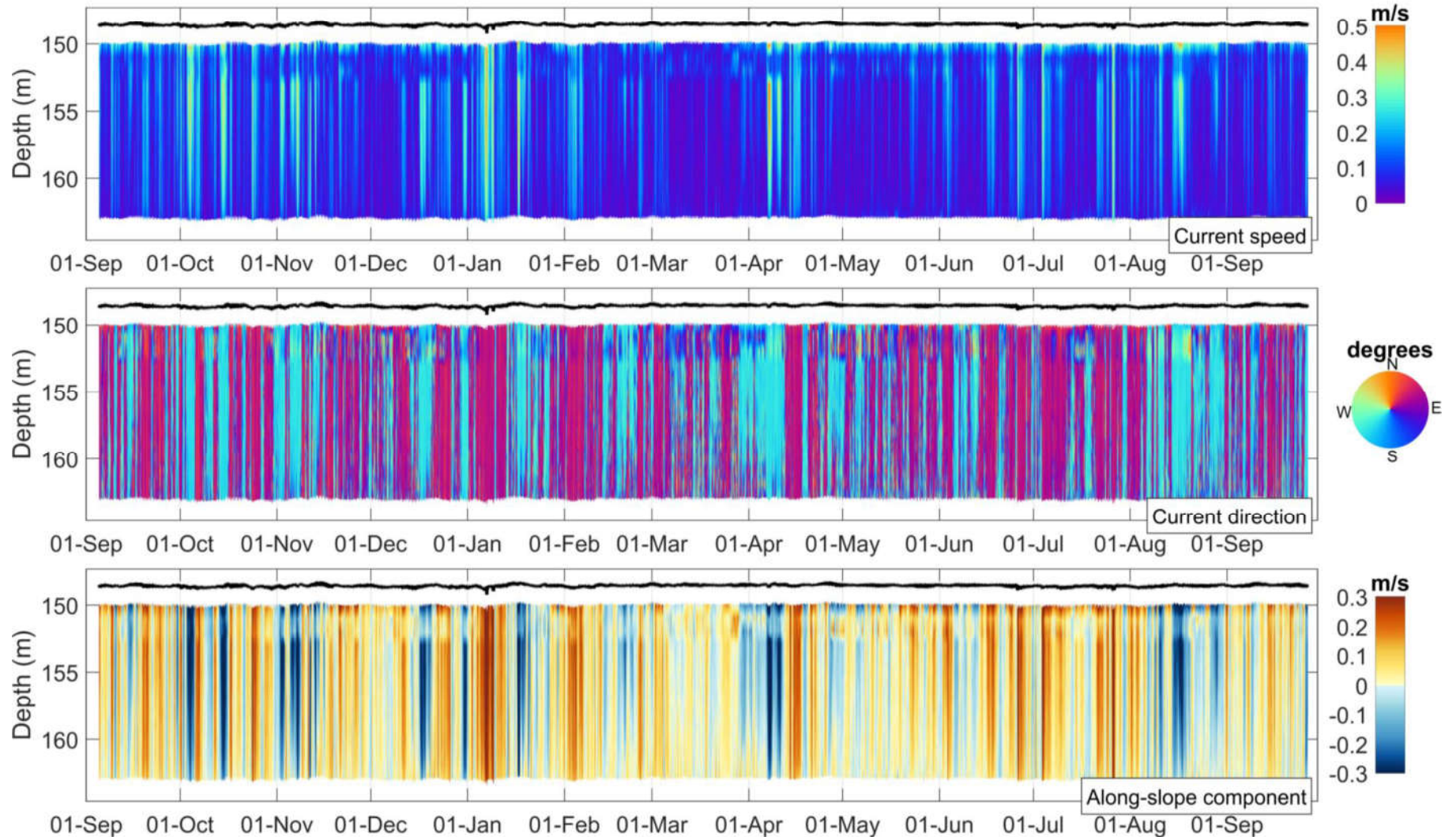


Figure 35: Time-series of current speed, current direction and along-slope current component at mooring BR-K-16 measured by the Aquadopp Profiler #11147. The black line depicts the instrument depth.

Table 11: Annual statistics of current speed and direction at BR-K-16 from selected bin depths representative of water mass variability in the Beaufort Sea (see Table 6 for water mass description).

Bin Depth (m)	Median Speed (m/s)	Mean Speed (m/s)	75%ile Speed (m/s)	95%ile Speed (m/s)	99%ile Speed (m/s)	Max Speed (m/s)	Standard Deviation Speed (m/s)	Vector-Averaged Direction (deg TN)
21.4	0.14	0.15	0.20	0.29	0.37	0.49	0.08	99.8
125.4	0.09	0.12	0.16	0.29	0.42	0.72	0.09	74.5
163.0 (near bottom)	0.06	0.07	0.09	0.17	0.23	0.38	0.05	53.2

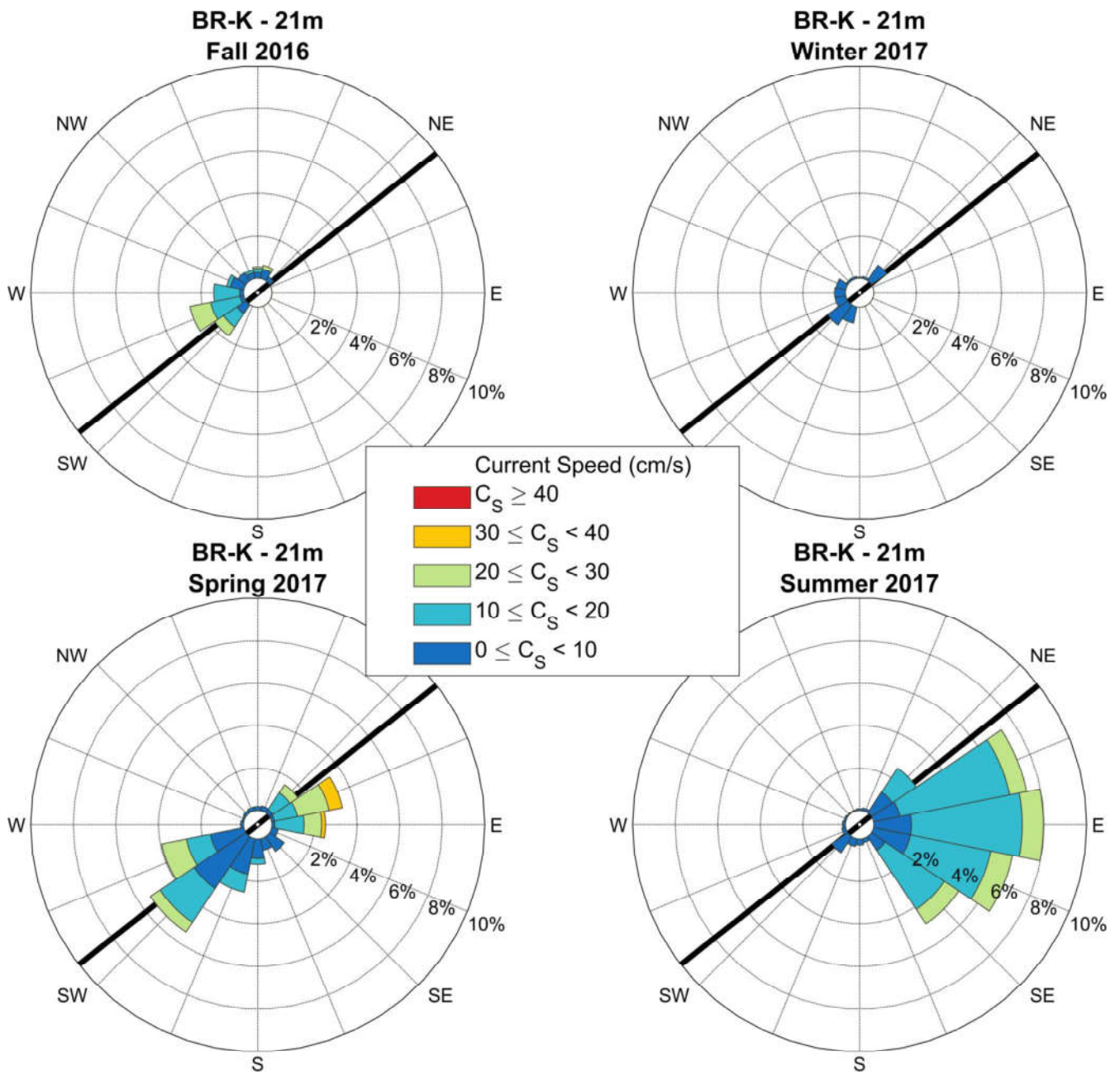


Figure 36: Seasonal current roses at 21 m depth (bin cell #14) at BR-K-16 measured by the WHS ADCP #7844. Data are low-pass filtered. Roses indicate the direction toward which currents flow. Seasons are defined following the meteorological convention (Fall: October-December; Winter: January-March; Spring: April-June; Summer: July-September).

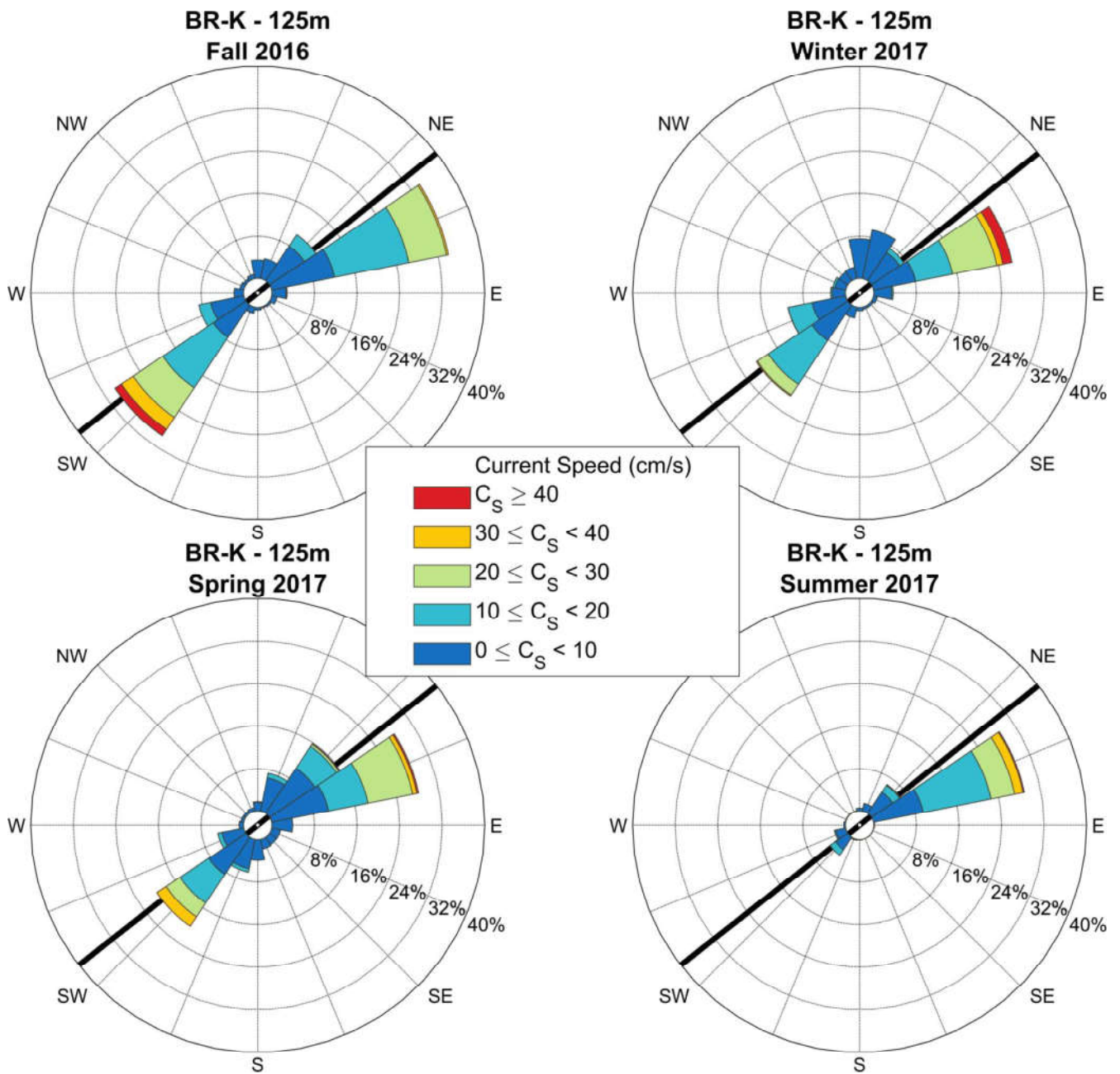


Figure 37: Seasonal current roses at 125 m depth (bin cell #1) at BR-K-16 measured by the WHS ADCP #7844. Data are low-pass filtered. Roses indicate the direction toward which currents flow. Seasons are defined following the meteorological convention (Fall: October-December; Winter: January-March; Spring: April-June; Summer: July-September).

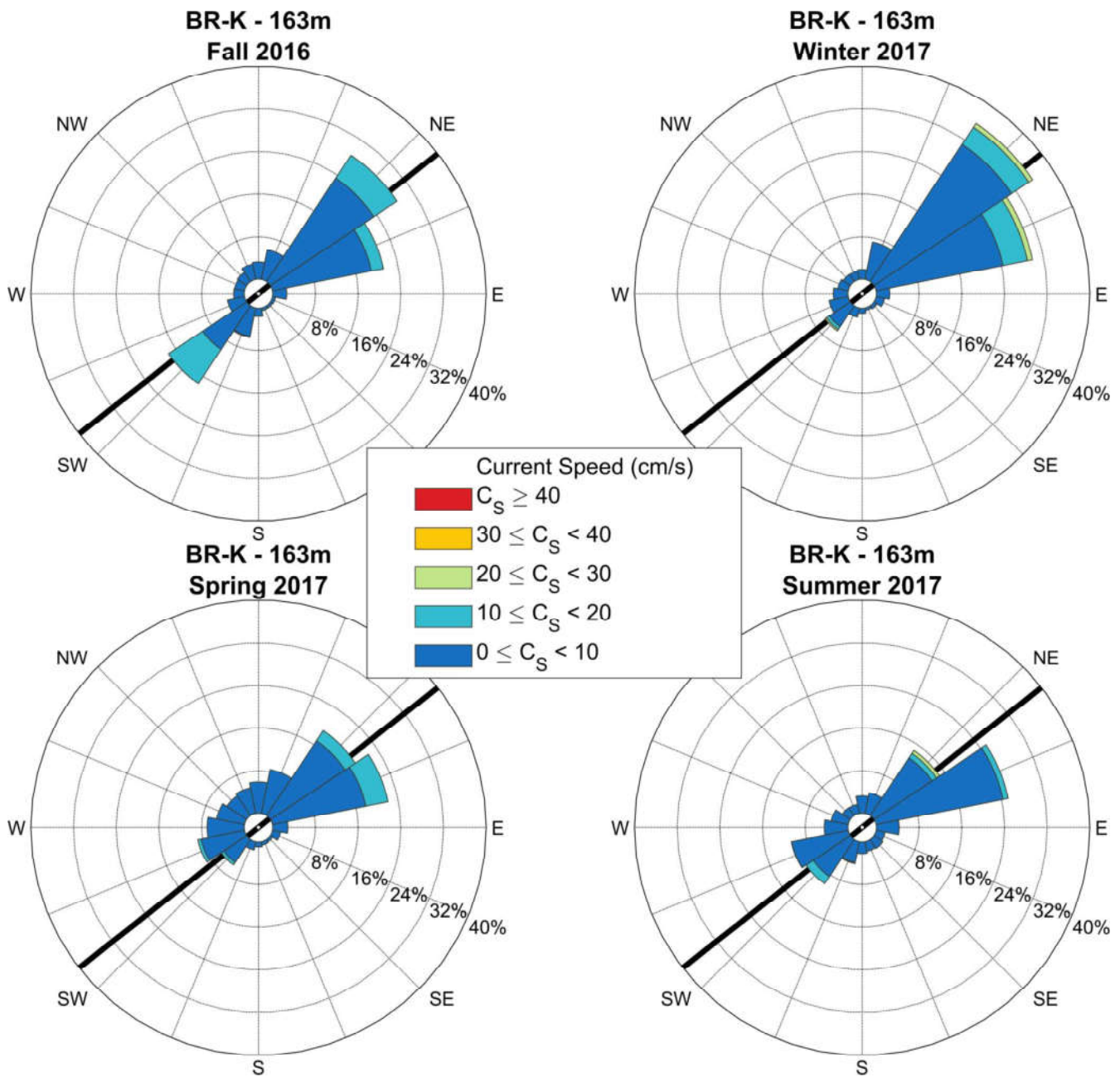


Figure 38: Seasonal current roses at 163 m depth (bin cell #14) at BR-K-16 measured by the Aquadopp Profiler #11147. Data are low-pass filtered. Roses indicate the direction toward which currents flow. Seasons are defined following the meteorological convention (Fall: October-December; Winter: January-March; Spring: April-June; Summer: July-September).

3.2.5 Mooring DFO-2

A time-series plot of current speed, direction, and along-slope current component from the NB ADCP deployed at the outer shelf mooring DFO-2 from 2016 to 2017 is provided in Figure 39. The data in the NB ADCP plot are filtered for bins with PG4 values less than 25%, bins affected by sidelobe interference and for error velocity thresholds and other masks as described in section 2.4.1. The first valid bin depth for the NB ADCP #586 at DFO-2-15 after removing sidelobe interference was 16.1 m (bin cell 23) with a percentage of valid data of 41% (Appendix C). The percentage of valid data below the uppermost valid bin depth ranged from 88% to 100%. Bins at 47 and 51 m (bin cells 14 and 15) were flagged for this instrument as part of the QA/QC procedure for suspected interference with the IPS on the mooring and should be treated carefully before being used in further analyses.

Mean current speeds at DFO-2-16 ranged from 7 to 12 cm/s throughout the water column, with the stronger mean currents typically near the surface (Appendix C, Table 12). Maximum current speed at DFO-2-16 was 60 cm/s on September 7, 2017 at the 20 m depth bin (Appendix C) during a strong event towards the southwest. Seasonal current roses (low-pass filtered) for selected bin depths at mooring DFO-2-16 are provided in Figure 40 and Figure 41. Current roses show currents are primarily bi-directional, orientated along the slope at this site. The strongest currents at 20 m were measured during the fall and summer seasons when the site is ice free.

DFO-2; NB ADCP 300kHz; 70.9893 N, 133.7439 W; 2016-2017; Instr. #586; 108 m depth

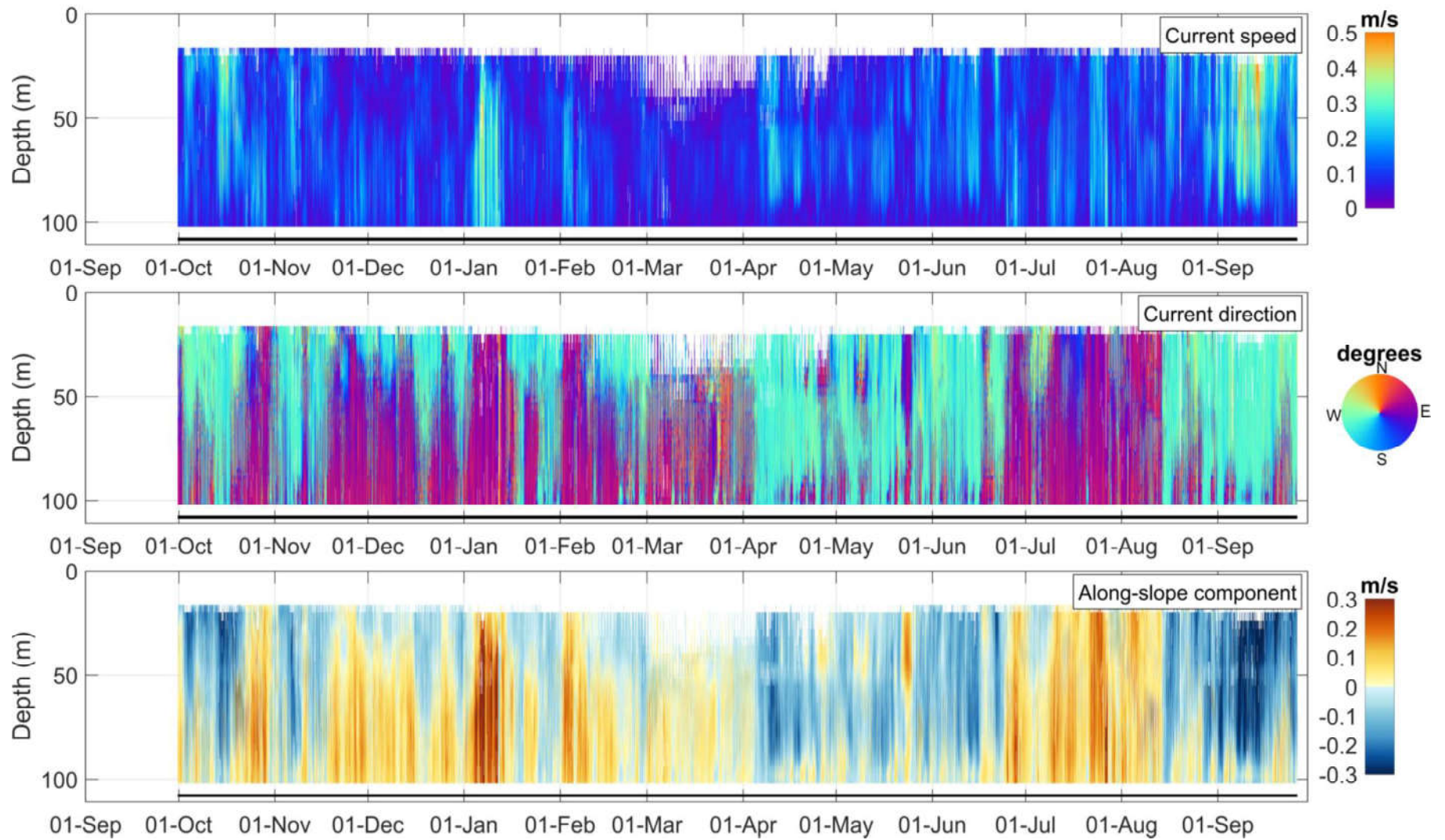


Figure 39: Time-series of current speed, current direction and along-slope current component at mooring DFO-2-16 measured the NB ADCP #586. The black line depicts the instrument depth.

Table 12: Annual statistics of current speed and direction at DFO-2-16 from selected bin depths representative of water mass variability in the Beaufort Sea (see Table 6 for water mass description).

Bin Depth (m)	Median Speed (m/s)	Mean Speed (m/s)	75%ile Speed (m/s)	95%ile Speed (m/s)	99%ile Speed (m/s)	Max Speed (m/s)	Standard Deviation Speed (m/s)	Vector-Averaged Direction (deg TN)
20.0	0.09	0.11	0.15	0.26	0.36	0.49	0.08	244.5
102.1	0.06	0.07	0.10	0.17	0.25	0.47	0.05	53.1

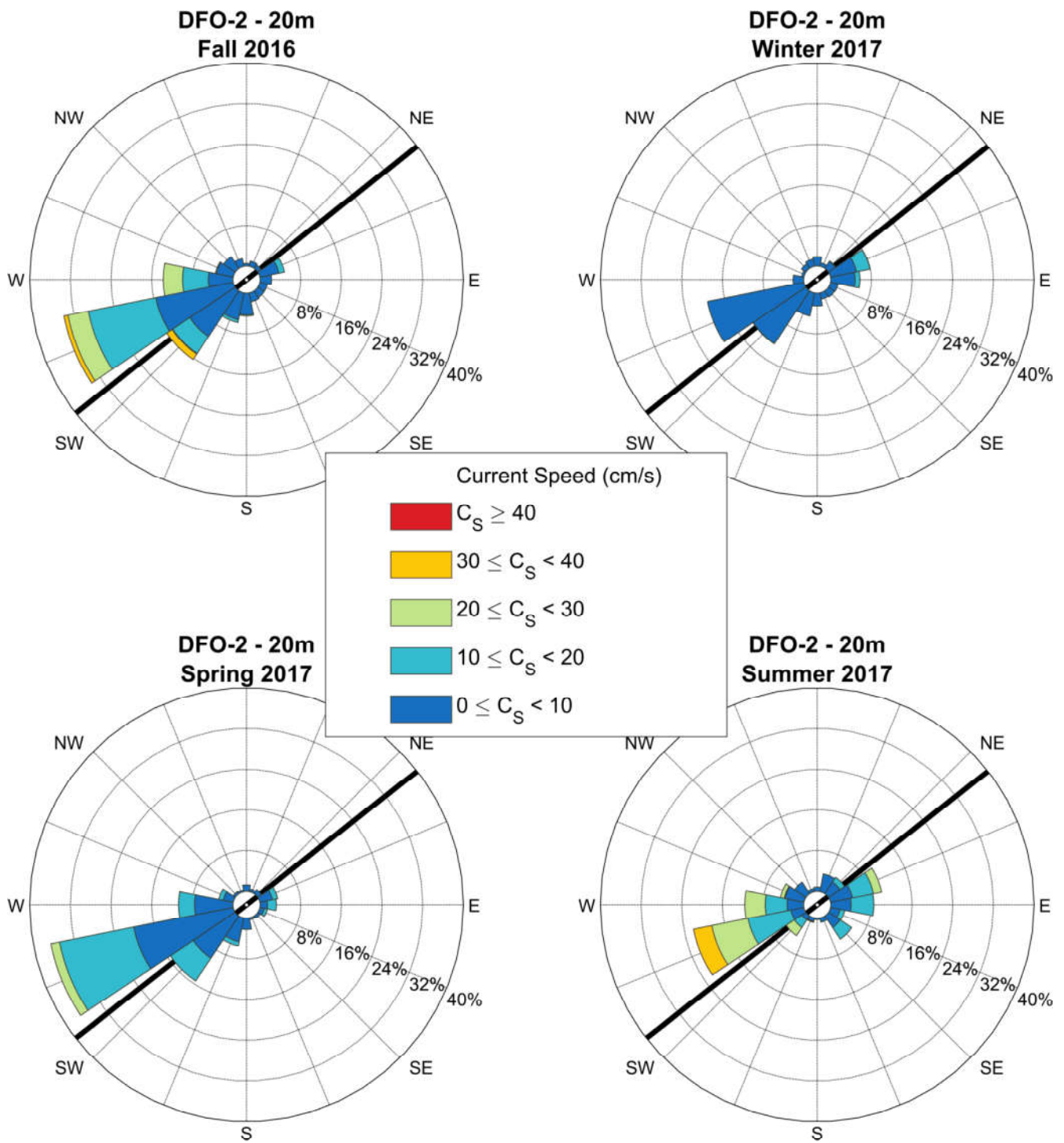


Figure 40: Seasonal current roses at 20 m depth at DFO-2-16 as based on low-pass filtered data from bin cell #22 measured by the NB ADCP #586. Roses indicate the direction toward which currents flow. Seasons are defined following the meteorological convention (Fall: October-December; Winter: January-March; Spring: April-June; Summer: July-September).

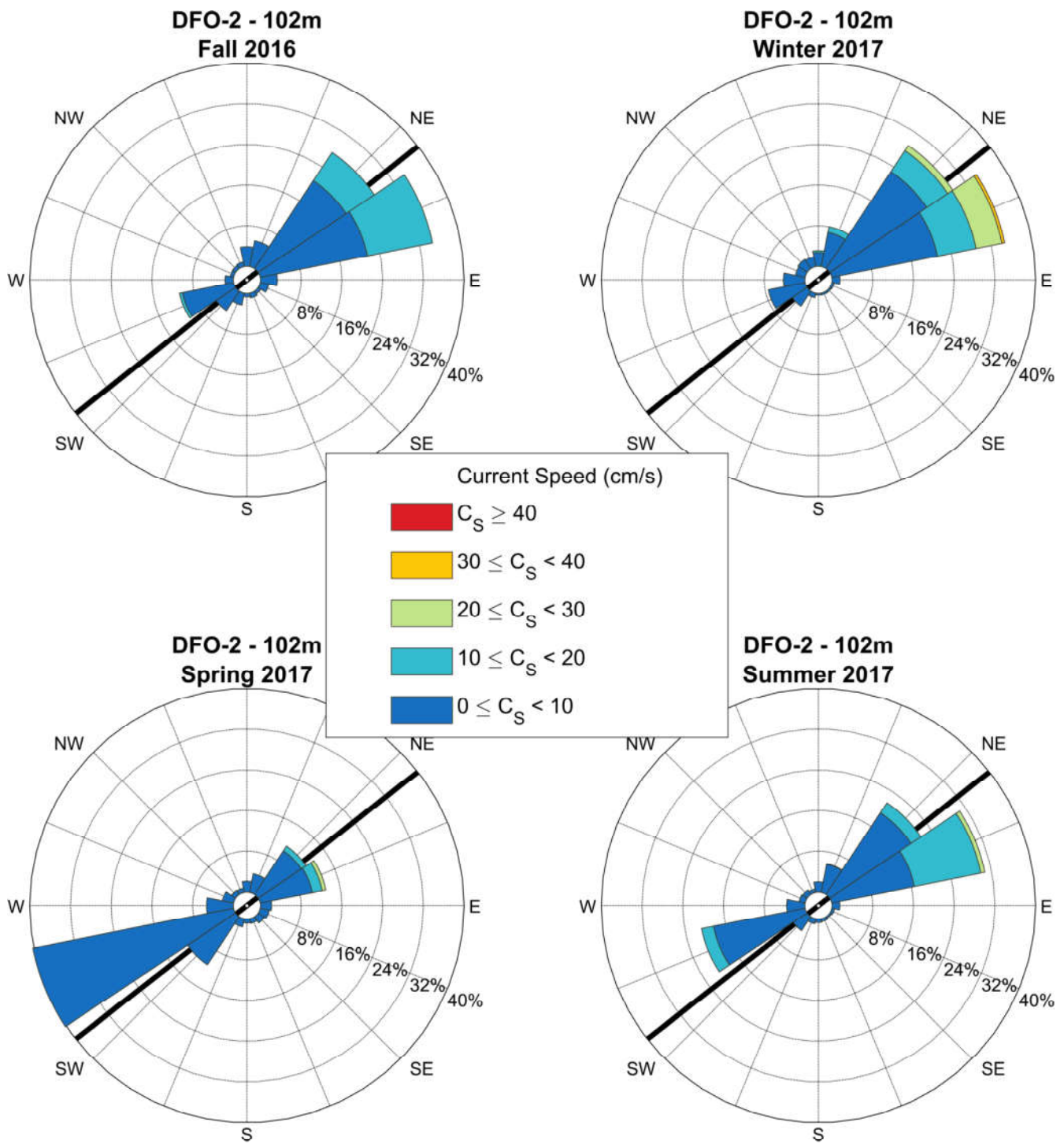


Figure 41: Seasonal current roses at 102 m depth at DFO-2-16 as based on low-pass filtered data from bin cell #1 measured by the NB ADCP #586. Roses indicate the direction toward which currents flow. Seasons are defined following the meteorological convention (Fall: October-December; Winter: January-March; Spring: April-June; Summer: July-September).

3.2.6 Mooring DFO-1

A time-series plot of current speed, direction, and along-slope current component from the WHS ADCP deployed at the mid-shelf mooring DFO-1 from 2016 to 2017 is provided in Figure 42. The data in the WHS ADCP plot are filtered for bins with PG4 values less than 25%, bins affected by sidelobe interference and for error velocity thresholds and other masks as described in section 2.4.1. The first valid bin depth for the WHS ADCP #12463 at DFO-1-16 after removing sidelobe interference was 6.8 m (bin cell 21) with 74% valid data (Appendix C). Percentage of valid data below the uppermost valid bin depth ranged from 89% to 100%. No bin depth was manually flagged for this instrument as part of the QA/QC procedure.

Mean current speeds at the mid-shelf site DFO-1-16 is 9 to 11 cm/s throughout the water column, with no discernable vertical pattern in current speed intensity (Appendix C, Table 13). Vector-averaged directions are consistently oriented towards the south. Maximum current speed at this site was 68 cm/s on July 25, 2017 measured in the upper portion of the water column at 6.8 m depth (Appendix C). Seasonal current roses (low-pass filtered) for one bin depth (18.9 m) in the middle of the water column at mooring DFO-1-16 are provided in Figure 43. Current directions are highly variable at this site, but are typically orientated towards the southern quadrants.

DFO-1; WHS 300 307.2kHz; 70.3338 N, 133.7395 W; 2016-2017; Instr. #12463; 51 m depth

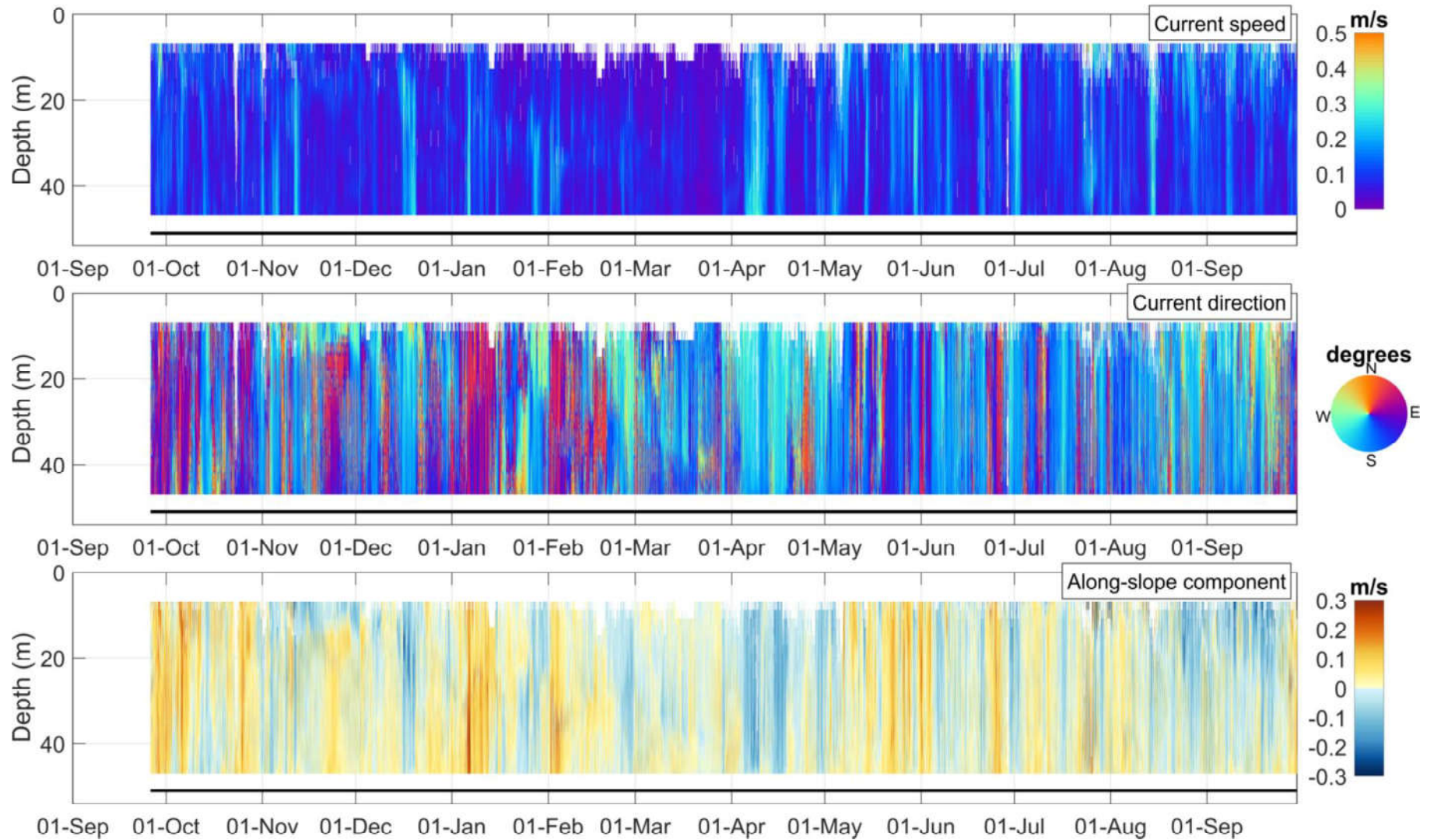


Figure 42: Time-series of current speed, current direction and along-slope current component at mooring DFO-1-16 measured by the NB ADCP #12463. The black line depicts the instrument depth.

Table 13: Annual statistics of current speed and direction at DFO-1-16 from a selected bin depth representative of the Polar-mixed layer (see Table 6 for water mass description).

Bin Depth (m)	Median Speed (m/s)	Mean Speed (m/s)	75%ile Speed (m/s)	95%ile Speed (m/s)	99%ile Speed (m/s)	Max Speed (m/s)	Standard Deviation Speed (m/s)	Vector-Averaged Direction (deg TN)
18.9	0.08	0.09	0.13	0.20	0.26	0.38	0.06	184.4

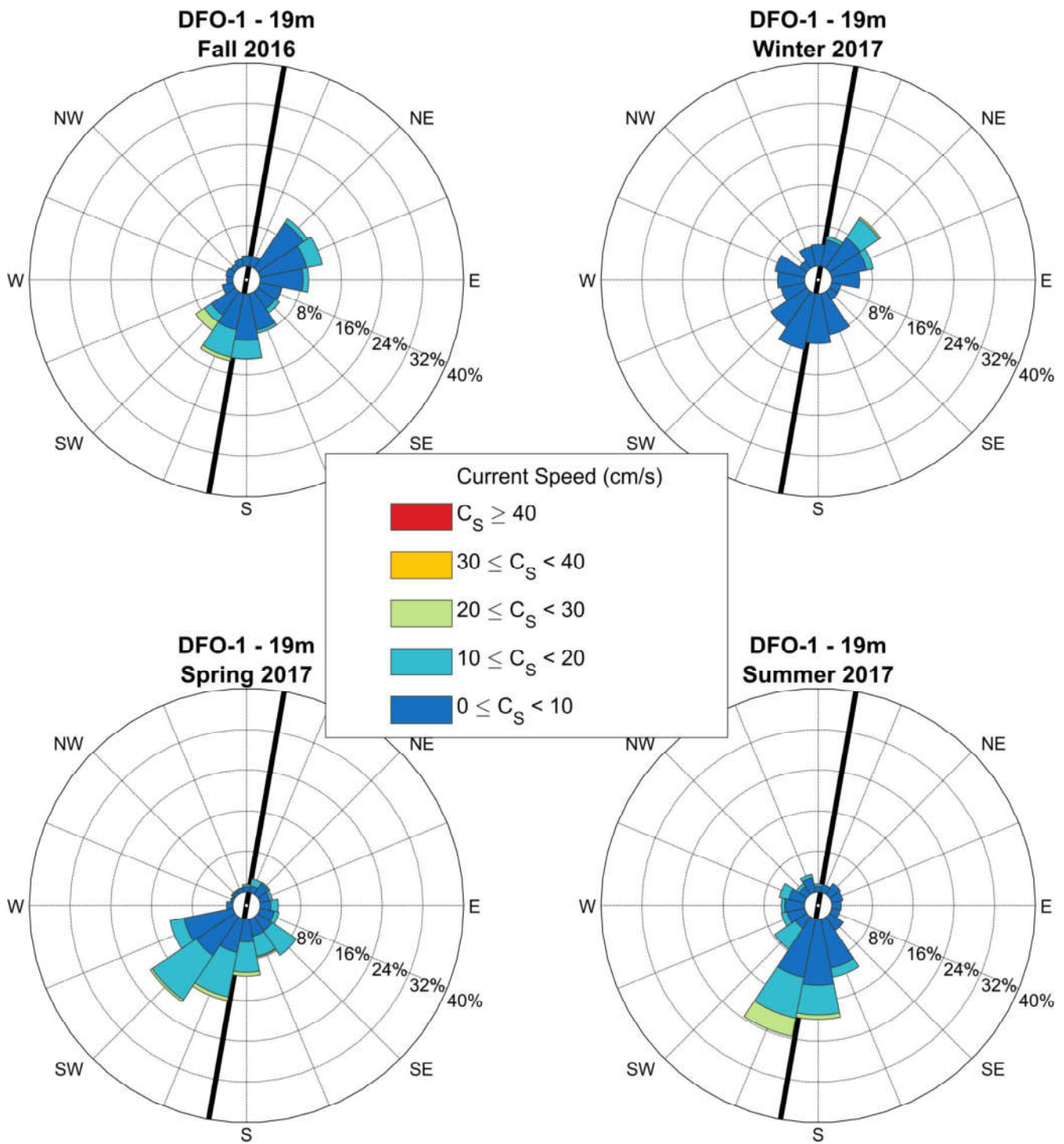


Figure 43: Seasonal current roses at 19 m depth at DFO-1-16 as based on low-pass filtered data from bin cell #15 measured by the WHS ADCP #12463. Roses indicate the direction toward which currents flow. Seasons are defined following the meteorological convention (Fall: October-December; Winter: January-March; Spring: April-June; Summer: July-September).

3.2.7 Mooring DFO-9

A time-series plot of current speed, direction, and along-slope current component from the WHS ADCP deployed at the inner shelf mooring DFO-9 from 2016 to 2017 is provided in Figure 44. The data in the WHS ADCP plot are filtered for bins with PG4 values less than 25%, bins affected by sidelobe interference and for error velocity thresholds and other masks as described in section 2.4.1. The first valid bin depth for the WHS ADCP #2412 at DFO-9-16 after removing sidelobe interference was 3.3 m (bin cell 26) with a percentage of valid data of 40% (Appendix C). Percentage of valid data below the uppermost valid bin depth ranged from 61 to 100%. The dataset at mooring DFO-9 was affected by echoes returned from sloping sidewalls of the dredge pit the mooring was located in. The mooring was located too close to the edge of the pit and the echoes caused unrealistic results (anomalies on the order of 10 cm/s). These anomalies were filtered using modified data masks.

Based on the valid data collected at DFO-9-16, mean current speeds at this site range from 6 to 16 cm/s throughout the water column, with the stronger mean currents typically near the surface (Table 14, Appendix C). Vector-averaged directions were all towards west and southwest with the exception of the lowermost bins which were oriented towards the south. Maximum current speed at DFO-9-16 was 86 cm/s on August 14, 2017 at the 5.3 m depth bin. Seasonal current roses (low-pass filtered) for one bin depth (20.8 m) at mooring DFO-9-16 are provided in Figure 45. Current directions are primarily bi-directional at this location, aligned along the slope.

DFO-9; WHS 300 307.2kHz; 70.0589 N, 133.7153 W; 2016-2017; Instr. #2412; 31.5 m depth

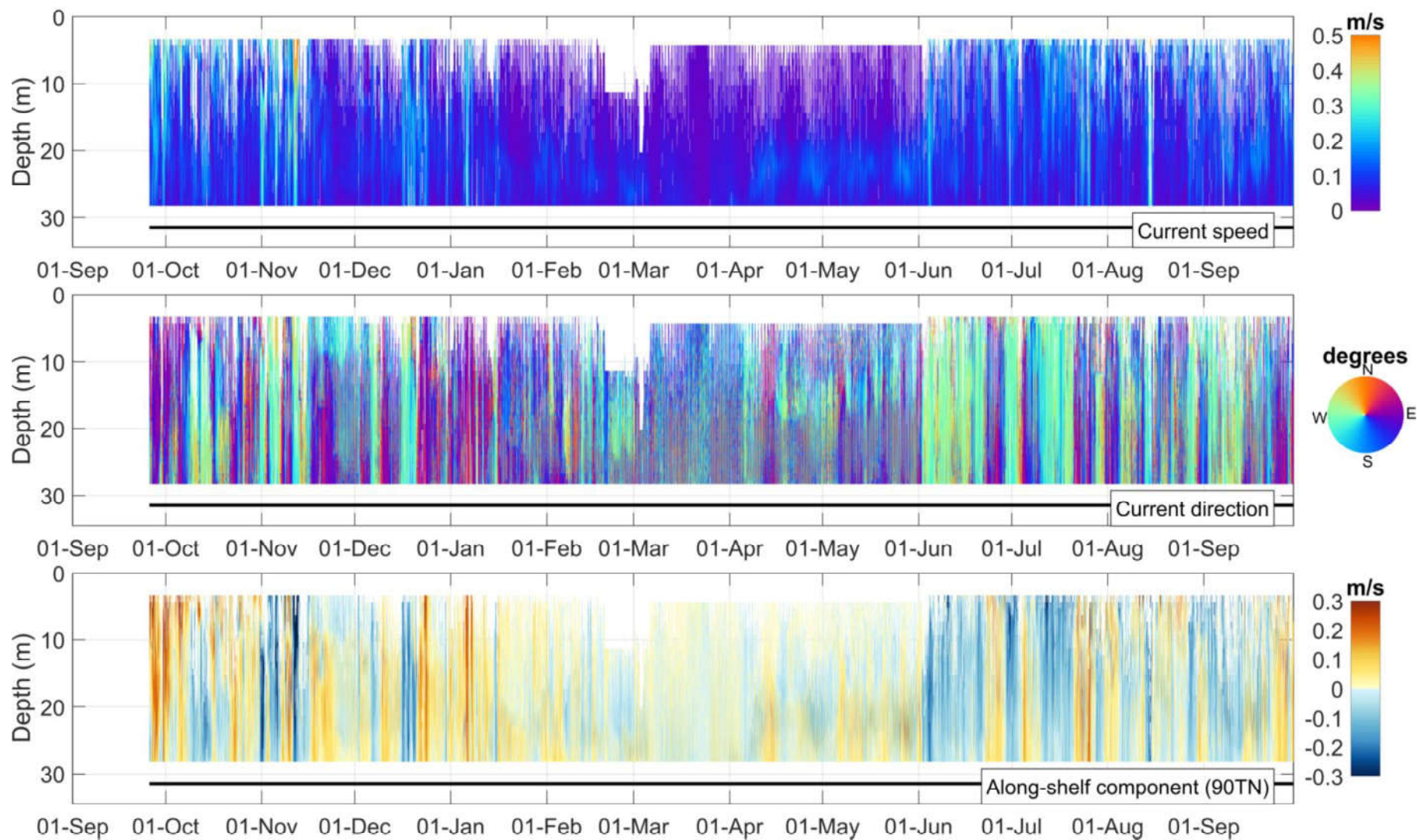


Figure 44: Time-series of current speed, current direction and along-slope current component at mooring DFO-9-16 measured by the WHS ADCP #2412. The black line depicts the instrument depth.

Table 14: Annual statistics of current speed and direction at DFO-9-16 from a selected bin depth representative of the Polar-mixed layer (see Table 6 for water mass description).

Bin Depth (m)	Median Speed (m/s)	Mean Speed (m/s)	75%ile Speed (m/s)	95%ile Speed (m/s)	99%ile Speed (m/s)	Max Speed (m/s)	Standard Deviation Speed (m/s)	Vector-Averaged Direction (deg TN)
20.3	0.08	0.09	0.11	0.19	0.27	0.48	0.06	272.6

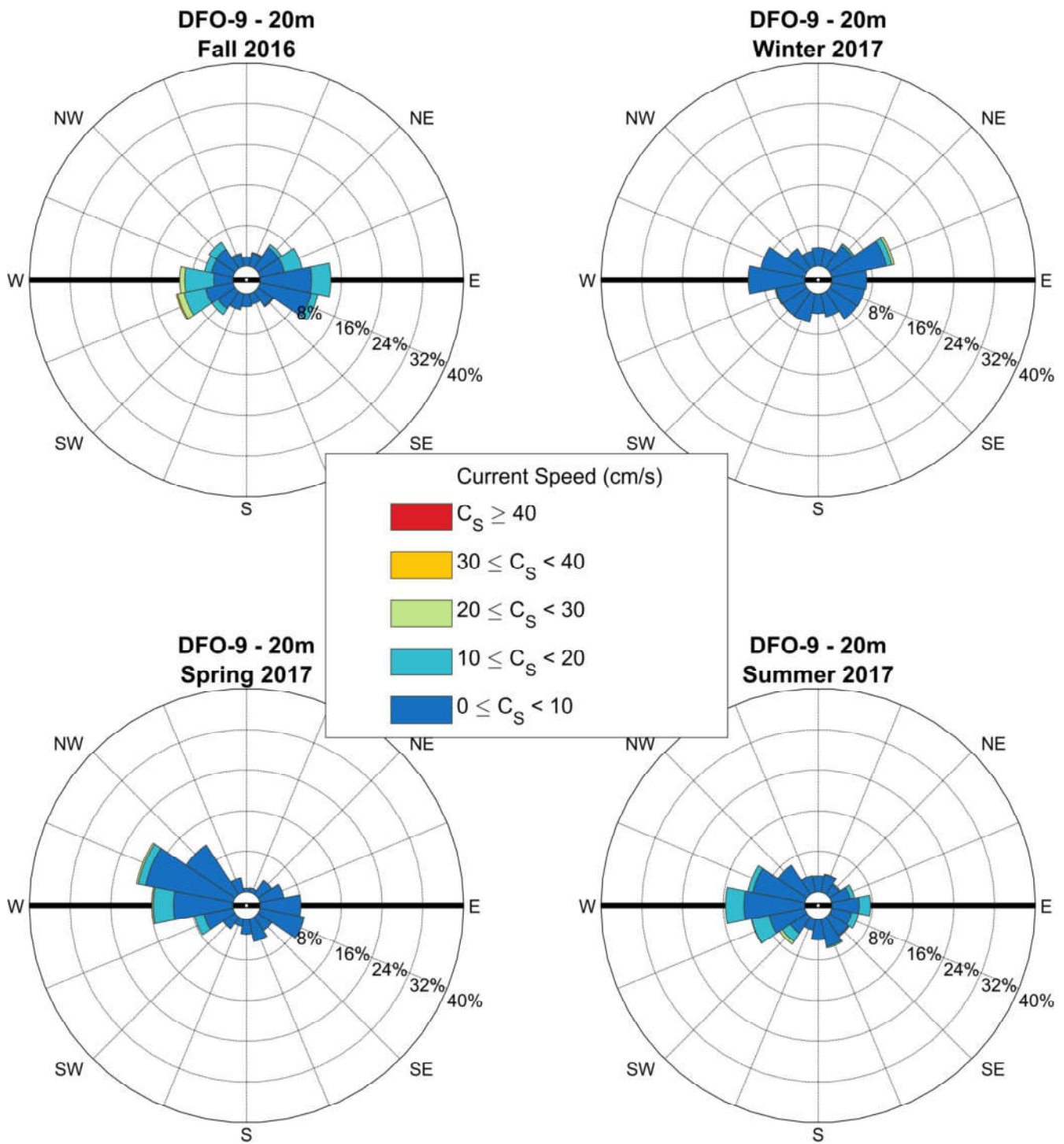


Figure 45: Seasonal current roses at 20 m depth at DFO-9-16 as based on low-pass filtered data from bin cell #8 measured by the WHS ADCP #2412. Roses indicate the direction toward which currents flow. Seasons are defined following the meteorological convention (Fall: October-December; Winter: January-March; Spring: April-June; Summer: July-September).

3.2.8 Spatial Variability of Surface and Bottom Currents in Open Water

Near-surface and near-bottom currents (low-pass filtered) during the open water season (June to October) were mapped as current roses in Figure 46 and Figure 47 to provide an overview of ocean circulation variability during the operational season in the southeastern Beaufort Sea. Each map represents current variability during a composite open water season, which is based on the initial (fall) and final (summer) sampling period of a given deployment year. Merging of multi-annual datasets and generation of actual current patterns per year is planned at a later stage of the iBO program as part of the planned Synthesis Report (see section 4.3).

The currents roses illustrate that the dominant surface circulation pattern in open water during 2016-2017 at BR-G, BR-1, and BR-3 (Figure 46) was in accord with the anti-cyclonic (clockwise) motion of the Beaufort Gyre with directions generally to the south-southwest along the slope and shelf break. The surface currents at BR-G and BR-3 show some directional variability, but the strongest currents are towards the southwest. By contrast, surface currents at BR-K during open water conditions showed a different pattern, with a dominance of northeastward currents.

Near-bottom currents during summer and fall (Figure 47) in 2016-2017 were predominantly toward the northeast at BR-1, BR-K, and BR-G and to the north at BR-3. Occasional reversals to the southwest were observed at BR-K. Near-bottom currents were strongest at BR-3 on average. Near-bottom currents at BR-G, BR-3, and BR-K generally follow the bathymetric contours at their respective location; at BR-1 more directional variability is observed in the bottom currents than at the other sites.

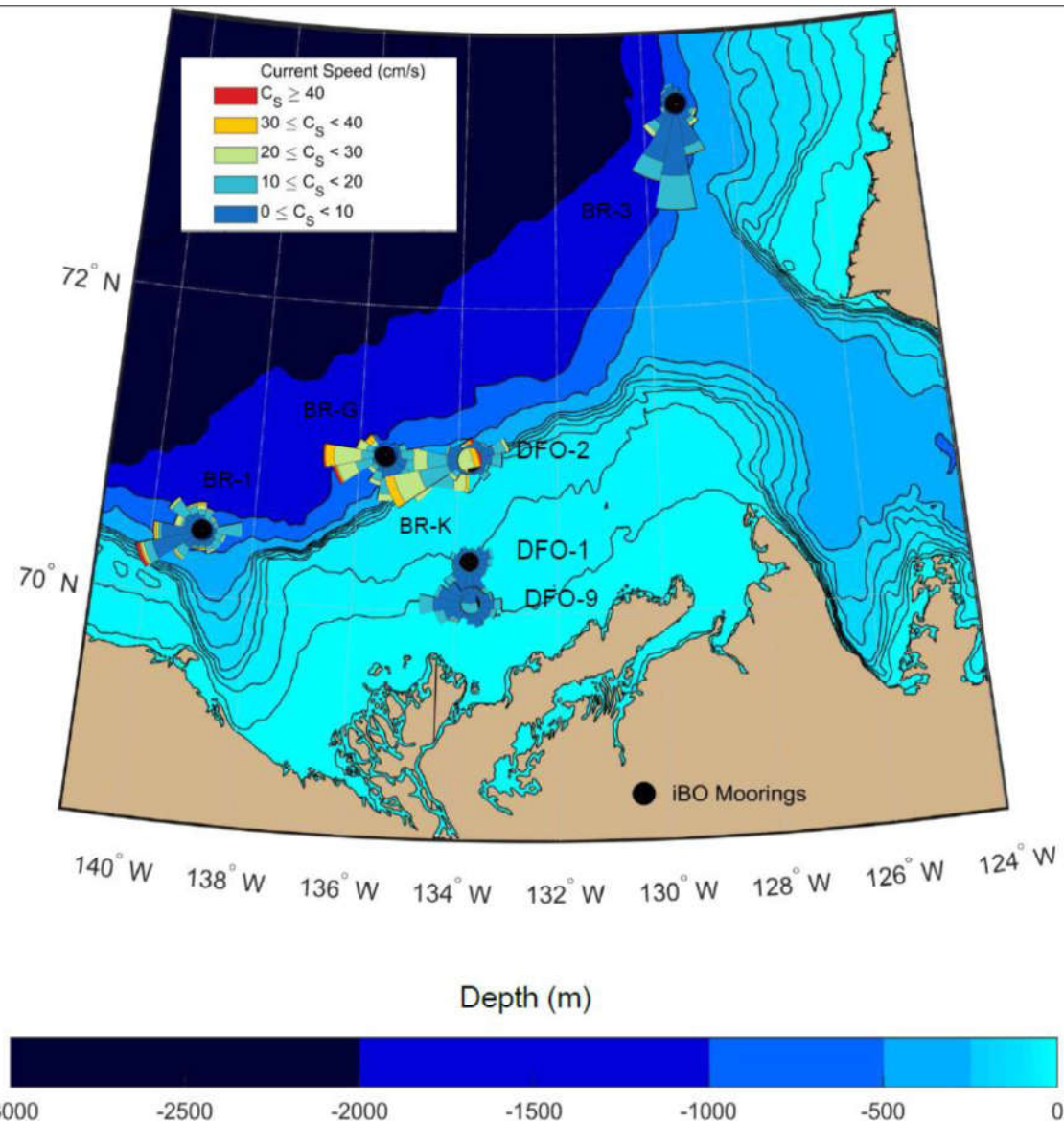


Figure 46: Near-surface currents for the open water season for low-pass filtered current velocity data from the bin depth nearest bin depth to 50 m at all moorings except DFO-1 and DFO-9 which are closest to a bin depth of 20 m. Data when sea ice was present (winter-spring) were filtered out. Roses indicate toward where the current is flowing.

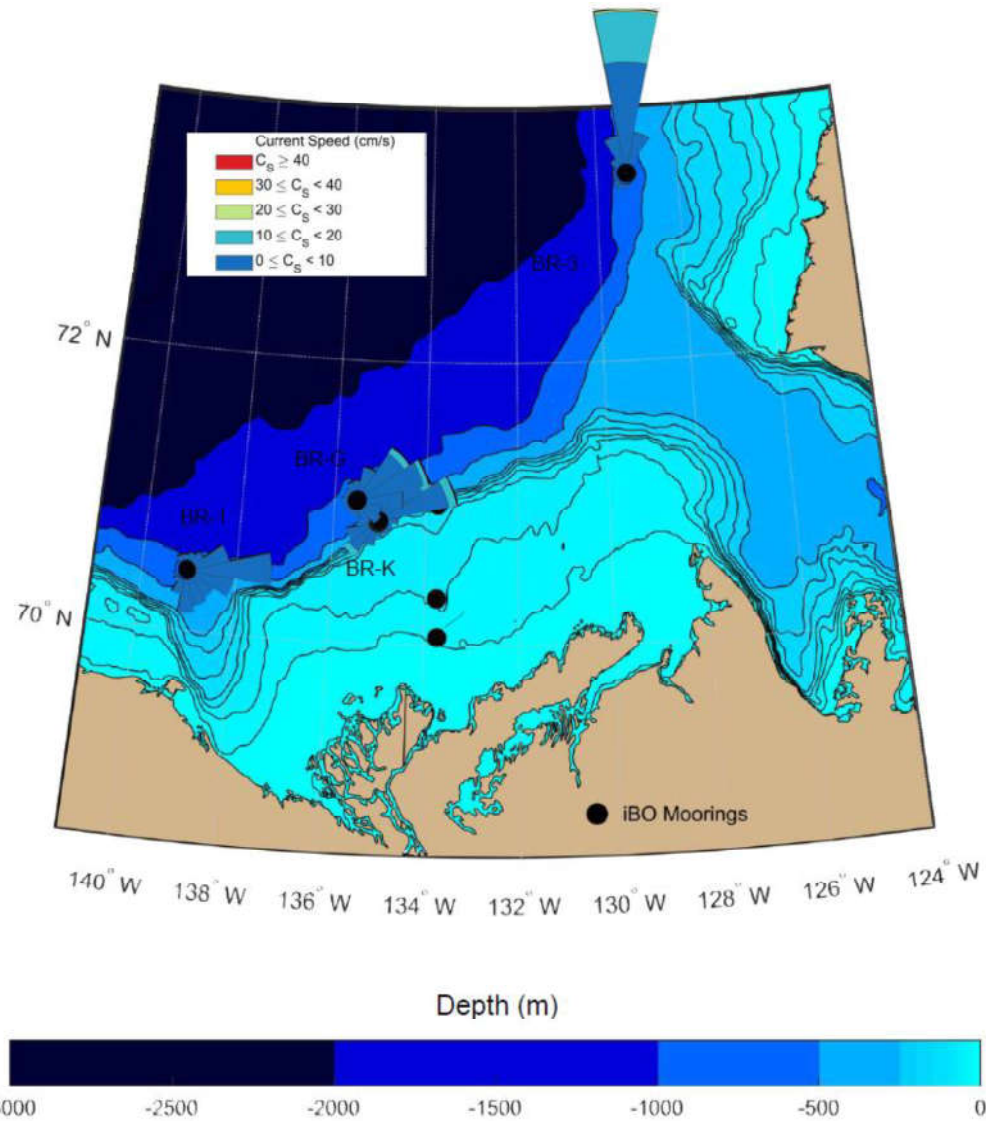


Figure 47: Near-bottom currents for the open water season for low-pass filtered current velocity data from the bin depth nearest to bottom at each location. Data when sea ice was present (winter-spring) were filtered out. Roses indicate toward where the current is flowing.

3.3 Temperature and Salinity

The summary of CT logger data recovery success on iBO moorings from 2016 to 2017 is provided in Table 15. A summary of valid and flagged data (suspicious spikes) for each processed CT sensor is provided in Table 16 for the BR moorings. Statistics are not presented for the DFO moorings due to differences in the QA/QC processing methodology.

Processed temperature and salinity data from all CT loggers deployed on BR moorings from 2016 to 2017 are presented using time-series plots of temperature and salinity at each mooring. Temperature time-series recorded at moorings BR-1, BR-3, BR-G and BR-K are presented in Figure 48 through Figure 51. Salinity time-series for the same moorings are provided in Figure 53 through Figure 56. Temperature and salinity time-series for DFO moorings are combined into two plots in Figure 52 and Figure 57. Data from temperature-salinity time-series presented below were filtered for spike-like values that were detected using the method described in section 2.4.2. Missing data were replaced by linearly-interpolated values in the time-series plots. A temperature-salinity diagram is also provided in Figure 58, which combines all QA/QC data from the moored CT loggers (also filtered for spikes, but not interpolated for missing values) as well as water column profile data from CTD casts conducted at mooring deployment in 2017 aboard the *Laurier*.

The temperature time-series recorded at discrete depths varying from 32 to 742 m on the slope illustrate the typical vertical layering in temperature in the Beaufort Sea (e.g. Lansard et al. 2012 and references therein), although marked temporal variability was observed, particularly at BR-G (Figure 50) and BR-1 (Figure 48). Temperature was most variable in the upper 200 m of the water column, with temperature varying from around 1.5°C down to around -1.5°C with the exception of the shelf moorings DFO-2 (upper CT logger) and DFO-9 which varied to as warm as 2.6°C. Rapid transitions from relatively cold to relatively warm (and vice-versa) temperature were often detected in the upper 200 m. For example, the most extreme was an increase from -0.3 to 1.5°C recorded at 50 m at BR-G in mid August 2017 (Figure 50) and simultaneous increases in salinity and temperature were also recorded at 120 and 175 m water depth, suggesting an intrusion of deep water. No simultaneous increase in salinity was recorded at 50 m water depth..

At 148 m water depth at BR-K on the upper slope, approximately six notable increases in temperature (from -1.4 to 0.4°C) were recorded throughout the time-series from September 2016 to October 2016 (Figure 51). Each fluctuation varied from -1.4°C up to -1.0 to 0.2°C occurring over 1 to 3 week intervals. Corresponding increases in salinity from 33 up to 34.5 (Figure 56) concurrent with a negative along-slope current component is likely a sign of upwelling of deep waters at the shelf break.

Likewise temperature, salinity time-series showed that most of the variability in terms of water-mass physical properties occurs in the upper 200 m (Figure 53 through Figure 56). Contrary to temperature, salinity is monotonically increasing with depth in the Beaufort Sea. Over the slope in 2015 to 2016, salinity from 450 to 740 m depth occupied a very narrow range from 34.7 to 34.9, while salinity in the upper 200 m ranged from 27.7 (DFO-9, 32 m in January 2017) up to 34.8 (at DFO-2, BR-K, BR-G, and BR-3 51).

The temperature-salinity diagram combining all data from the CT loggers provides a way to further characterize the different water masses occupying the water column at mooring locations from 2016 to 2017 (Figure 58). This diagram provides evidence that most of the variability in the water column is taking place in the upper 200 m. It also illustrates the lack of Beaufort Sea Winter Water (BSWW), described in Jackson et al. (2015) as cold salty (33) water capable of halocline ventilation. The T-S diagram shows no seawater near the freezing point in the salinity range of 31 to 34.

The visual comparison between CTD cast data from 2017 and the moored CT sensor data provides a preliminary assessment of the accuracy of the CT sensor data. Instruments in the upper 200 m did not appear to be affected by any visible bias given their consistency with respect to the freezing line and the expected variability in the shape of the halocline (i.e. between ~32.0 and 34.7 salinity) that changes over time due to upwelling/downwelling and other mixing processes.

The deeper CT logger instruments (>400 m) did show some offset with respect to the CTD cast data collected in 2016. A zoom on the narrow domain of the temperature-salinity variability in the lower portion of the Atlantic water mass is shown in Figure 59. These instruments were visually corrected to the CTD cast data to address individual instrument-specific offsets or miscalculation in the relationship linking pressure to conductivity and potential temperature. It should be noted that the RBR CT loggers do not include an integrated pressure sensor. Depth of RBR CT sensors needs to be estimated on the basis of other nearby instruments which is a likely a source of the observed biases.

Table 15: Summary of CT data logger clock drift and percentage of raw data return on iBO moorings from 2016 to 2017.

Mooring	Instrument	Serial number	Depth (m)	Clock Drift (mm:ss)	First Good Record (UTC)	Last Good Record (UTC)	Raw Data Return (%)
BR-01-16	RBR XR420 CT	15263	50	01:13	Sep-03-2016 3:00:00	Sep-27-2017 15:40:00	100.0%
BR-01-16	SBE37 Microcat	12235	118.8	00:14	Sep-04-2016 3:00:00	Sep-28-2017 15:50:00	100.0%
BR-01-16	RBR XR420 CT	15274	174.7	00:36	Sep-03-2016 3:10:00	Sep-27-2017 15:30:00	100.0%
BR-01-16	RBR XR420 CT	17352	459.7	00:57	Sep-03-2016 3:20:00	Sep-27-2017 15:40:00	100.0%
BR-01-16	SBE37 Microcat	10850	741.1	00:03	Sep-04-2016 3:00:00	Sep-28-2017 15:50:00	100.0%
BR-03-16	RBR XR420 CT	61550	89	00:45	Sep-09-2016 0:50:00	Sep-23-2017 17:20:00	100.0%
BR-03-16	SBE37 Microcat	10851	157.2	00:00	Sep-10-2016 1:00:00	Sep-24-2017 17:20:00	100.0%
BR-03-16	RBR XR420 CT	61551	208.2	00:39	Sep-09-2016 1:00:00	Sep-23-2017 17:20:00	100.0%
BR-03-16	RBR XR420 CT	15281	497.9	01:01	Sep-09-2016 1:00:00	Sep-23-2017 16:30:00	100.0%
BR-03-16	SBE37 Microcat	10849	713.3	00:07	Sep-10-2016 0:50:00	Sep-24-2017 17:20:00	100.0%
BR-03B-16	SBE37 Microcat	10196	50.1	00:05	Sep-14-2016 21:50:00	Sep-24-2017 15:00:00	98.7%
BR-G-16	RBR XR420 CT	15271	50	00:34	Sep-04-2016 18:40:00	Oct-01-2017 14:40:00	100.0%
BR-G-16	SBE37 Microcat	12236	119.5	00:04	Sep-05-2016 18:10:01	Oct-02-2017 14:50:00	100.0%
BR-G-16	RBR XR420 CT	15264	174.6	00:50	Sep-04-2016 18:10:00	Oct-01-2017 14:40:00	100.0%
BR-G-16	RBR XR420 CT	15275	453.7	00:46	Sep-04-2016 18:30:00	Oct-01-2017 14:30:00	100.0%
BR-G-16	SBE37 Microcat	10852	685.6	00:10	Sep-05-2016 18:10:00	Oct-02-2017 14:50:00	100.0%
BR-K-16	RBR XR420 CT-Tu-DO-FI	17112	147.6	00:55	Sep-05-2016 2:00:00	Sep-26-2017 20:00:00	100.0%
DFO-9-16	SBE37 Microcat	6762	32.0	01:12	Sep-25-2016 18:30:00	Sep-30-2017 17:00:00	100.0%
DFO-1-16	SBE37 Microcat	5886	52.0	00:59	Sep-25-2016 22:00:00	Sep-30-2017 20:00:00	100.0%
DFO-2-16	SBE37 Microcat	4992	41.5	00:22	Sep-30-2016 15:45:00	Sep-26-2017 16:45:00	100.0%
DFO-2-16	SBE37 Microcat	5889	109.0	05:24	Sep-30-2016 15:45:00	Sep-26-2017 16:00:00	100.0%

Table 16: Summary of valid and flagged data from CT loggers deployed on the BR slope moorings from 2016 to 2017. See Table 15 for the instrument model associated with each serial number.

Mooring	Serial number	Depth (m)	Number of Valid Conductivity Records	Number of Flagged Conductivity Records	% of Valid and Un-flagged Conductivity Records (%)	Number of Valid Temperature Records	Number of Flagged Temperature Records	% of Valid and Un-flagged Temperature Records (%)
BR-01-16	15263	50	56,093	24	100.0%	56,093	44	100.0%
BR-01-16	12235	118.8	56,094	128	99.8%	56,094	64	99.8%
BR-01-16	15274	174.7	56,091	9	100.0%	56,091	7	100.0%
BR-01-16	17352	459.7	56,091	11	100.0%	56,091	7	100.0%
BR-01-16	10850	741.1	56,094	15	100.0%	56,094	9	100.0%
BR-03-16	61550	89	54,676	7	100.0%	54,676	14	100.0%
BR-03-16	10851	157.2	54,675	7	100.0%	54,675	7	100.0%
BR-03-16	61551	208.2	54,675	7	100.0%	54,675	7	100.0%
BR-03-16	15281	497.9	18,224	49	99.7%	18,224	9	99.7%
BR-03-16	10849	713.3	54,676	15	100.0%	54,676	1	100.0%
BR-03B-16	10196	50.1	53,960	7	100.0%	53,960	53	100.0%
BR-G-16	15271	50	56,425	19	100.0%	56,425	59	100.0%
BR-G-16	12236	119.5	56,429	8	100.0%	56,429	125	100.0%
BR-G-16	15264	174.6	56,428	8	100.0%	56,428	0	100.0%
BR-G-16	15275	453.7	56,425	85	99.8%	56,425	50	99.8%
BR-G-16	10852	685.6	56,429	10	100.0%	56,429	6	100.0%
BR-K-16	17112	147.6	9,284	7	99.9%	9,284	8	99.9%

Note: The percentage of valid data is based on the total number of records returned by the instrument from deployment to recovery. Data from DFO moorings are not presented here due to the difference in methodology for data processing.

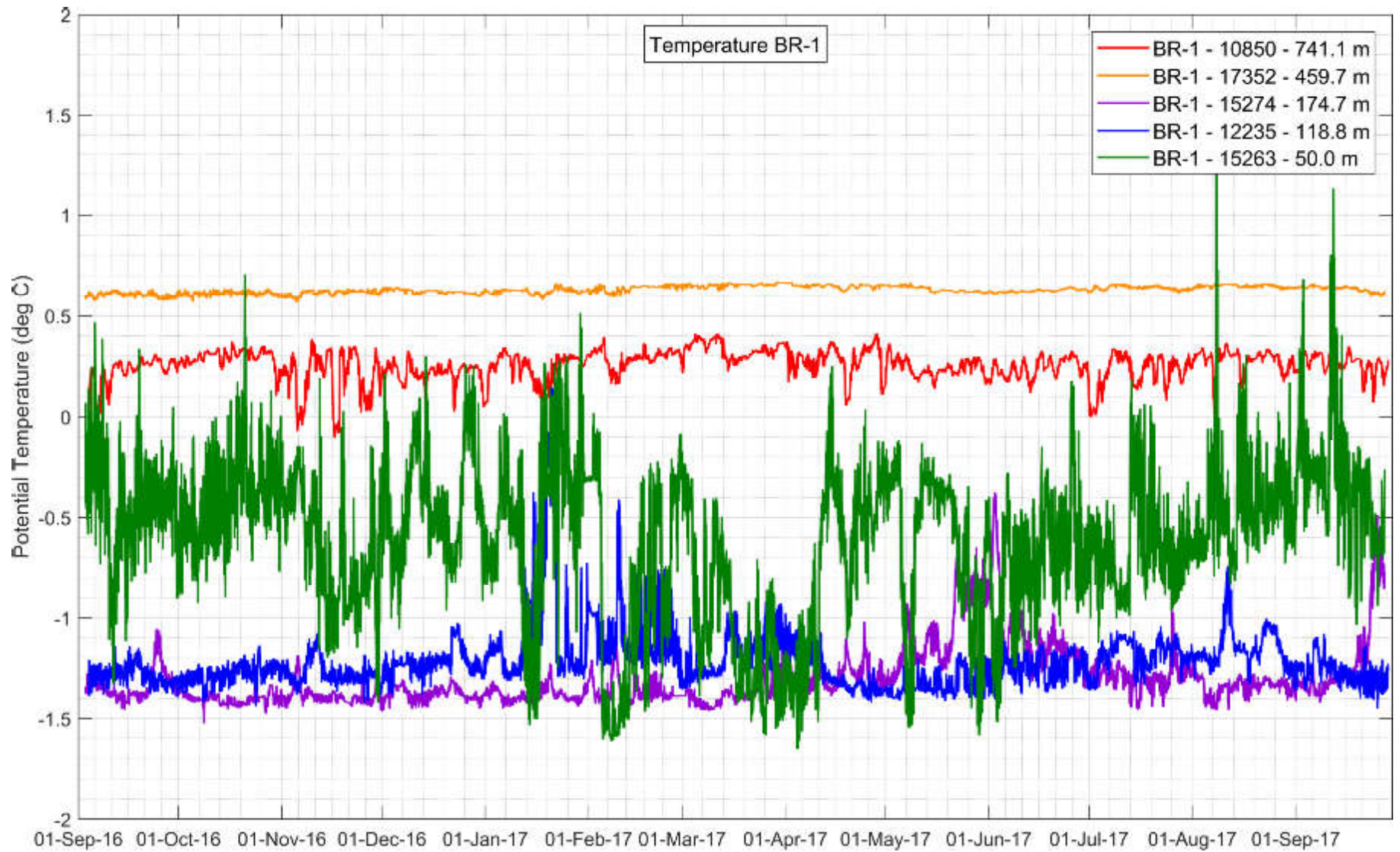
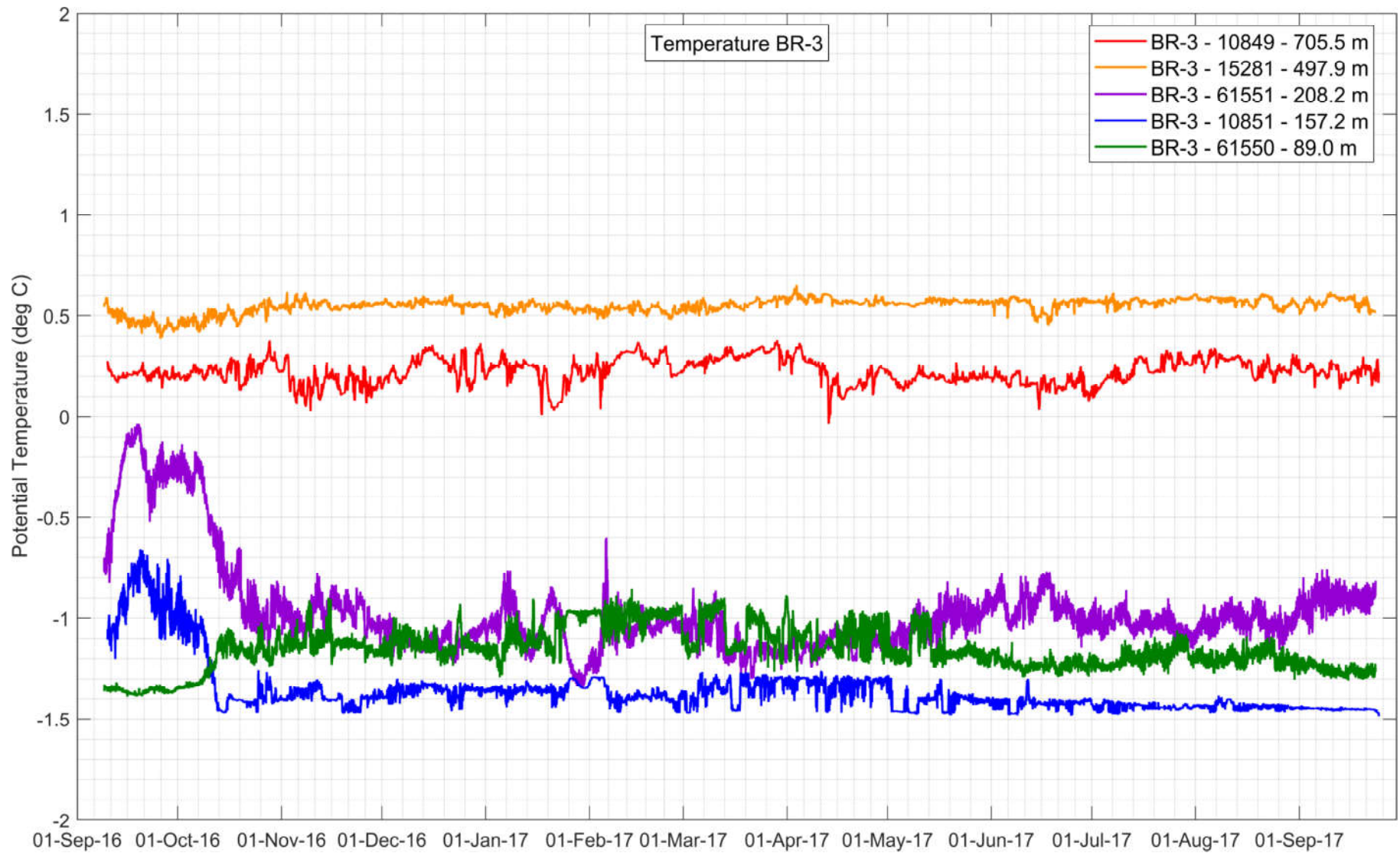
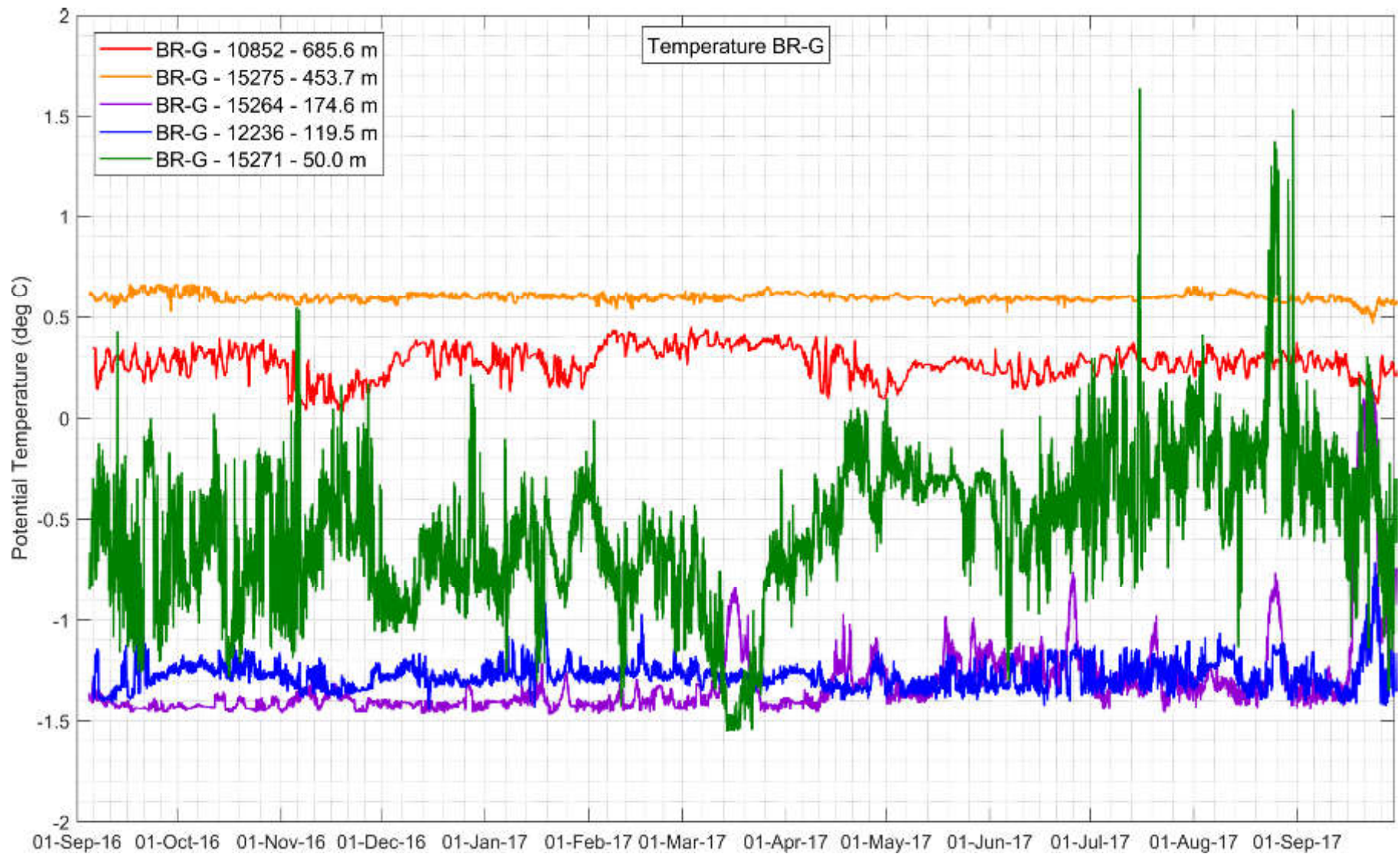
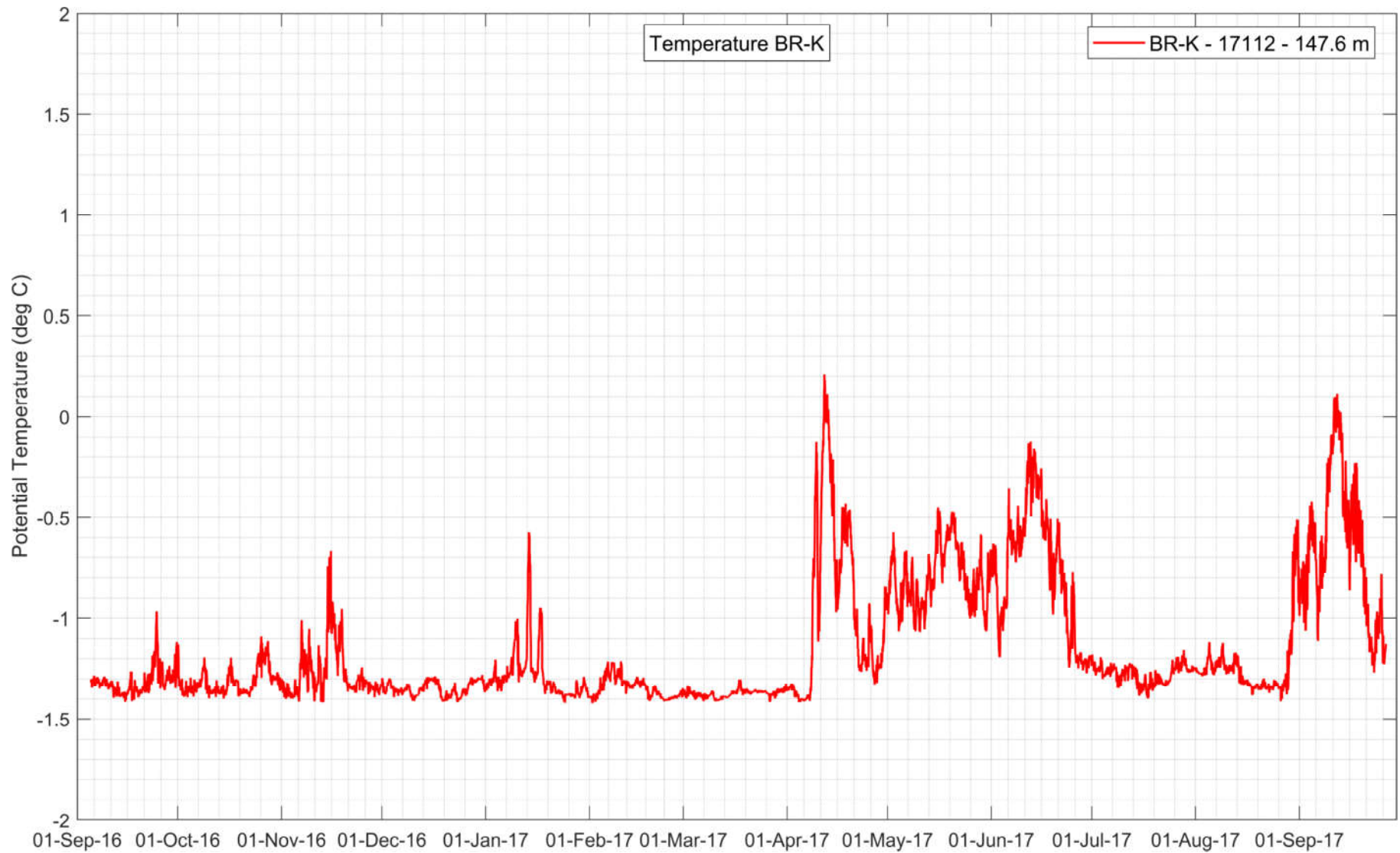


Figure 48: Temperature time-series measured at BR-1-16 from 2016 to 2017. The legend shows the serial number and depth of each CT logger.







01-Sep-16 01-Oct-16 01-Nov-16 01-Dec-16 01-Jan-17 01-Feb-17 01-Mar-17 01-Apr-17 01-May-17 01-Jun-17 01-Jul-17 01-Aug-17 01-Sep-17
 Figure 51: Temperature time-series recorded at BR-K-16 from 2016 to 2017. The legend shows the serial number and depth of each CT logger.

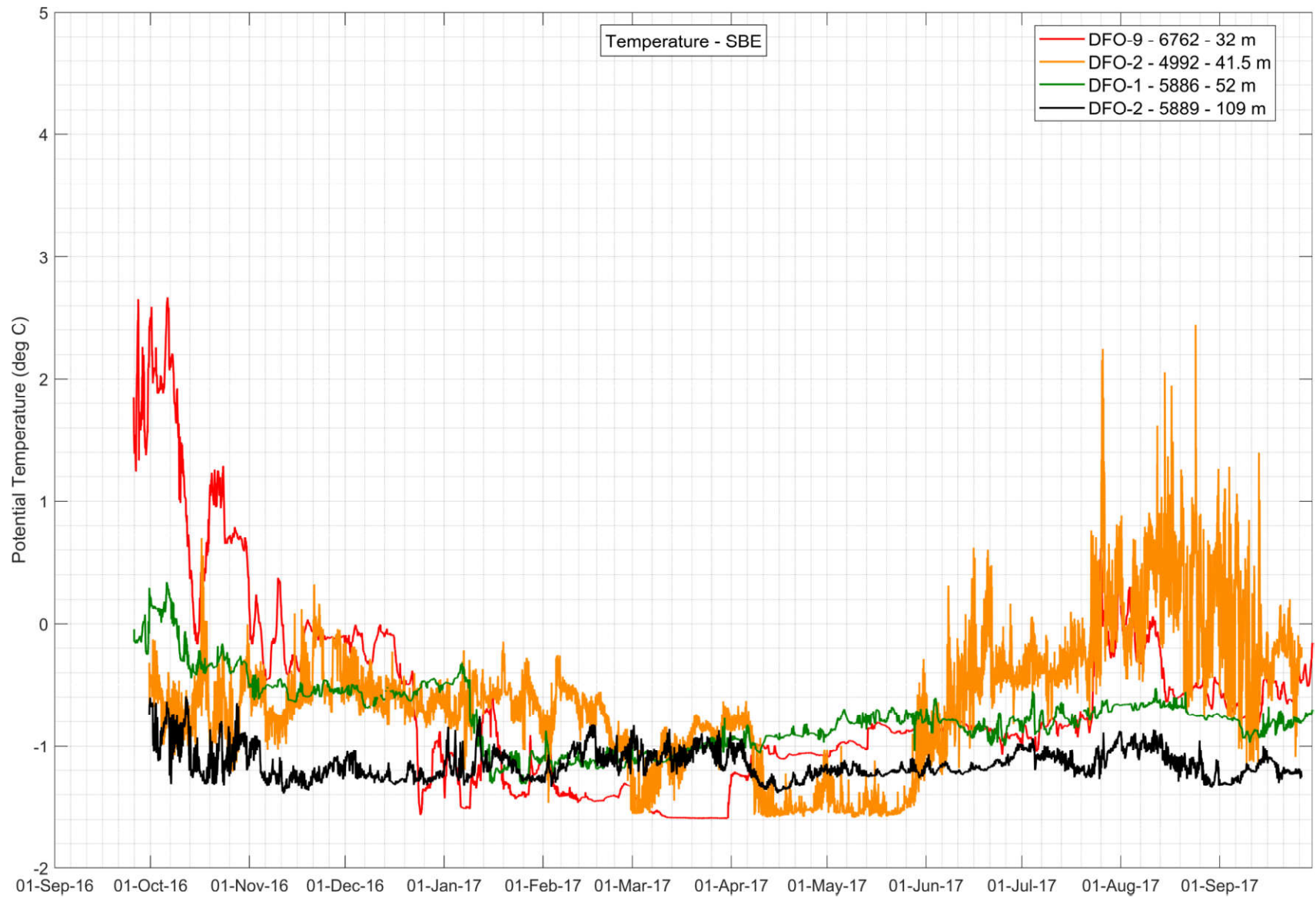


Figure 52: Temperature time-series recorded at DFO-2-16, DFO-1-16, and DFO-9-16 from 2016 to 2017. The legend shows the serial number and depth of each CT logger.

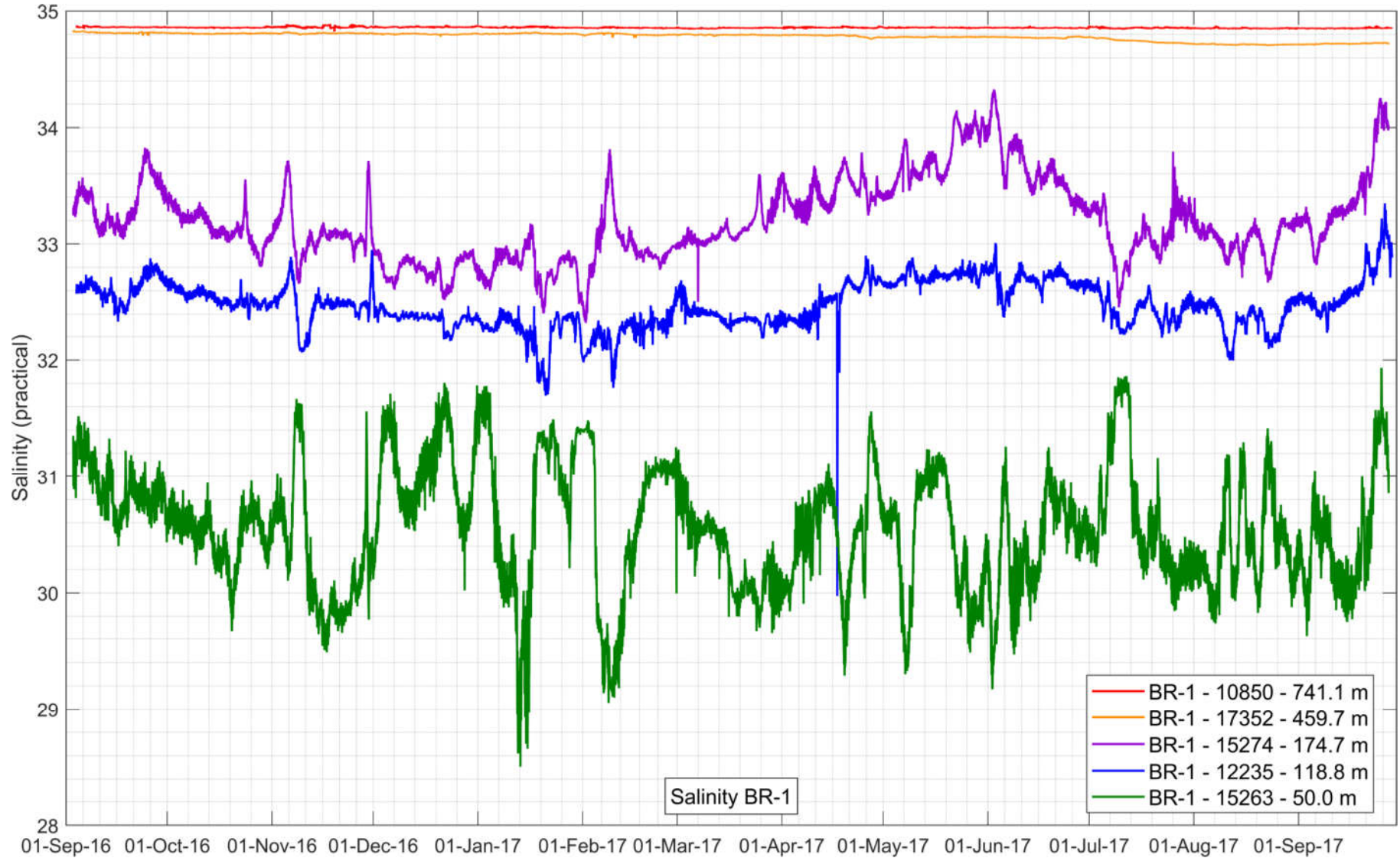


Figure 53: Salinity time-series recorded at BR-1-16 from 2016 to 2017. The legend shows the serial number and depth of each CT logger.

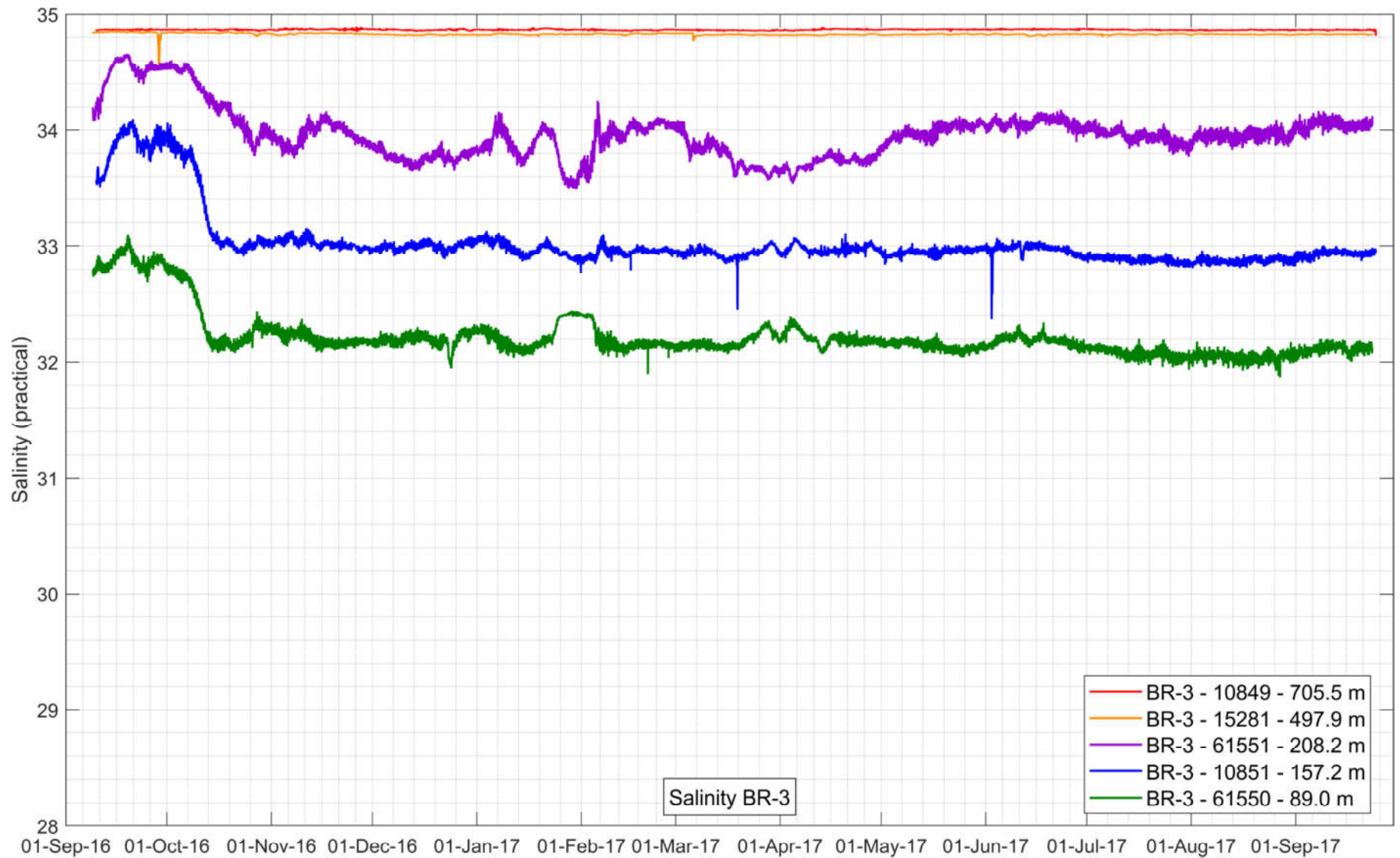


Figure 54: Salinity time-series recorded at BR-3-16 from 2016 to 2017. The legend shows the serial number and depth of each CT logger.

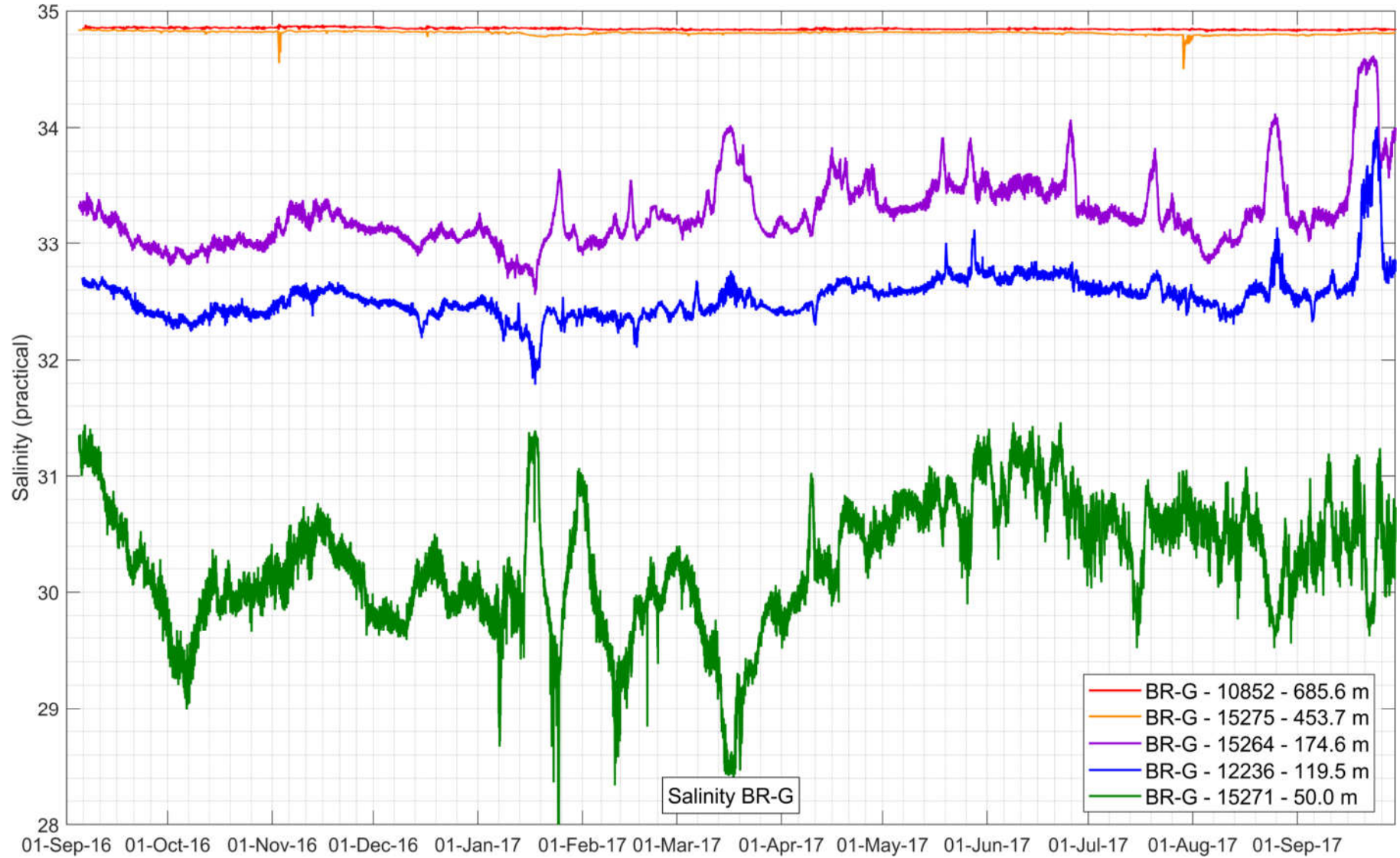


Figure 55: Salinity time-series recorded at BR-G-16 from 2016 to 2017. The legend shows the serial number and depth of each CT logger.



Figure 56: Salinity time-series recorded at BR-K-16 from 2016 to 2017. The legend shows the serial number and depth of each CT logger.

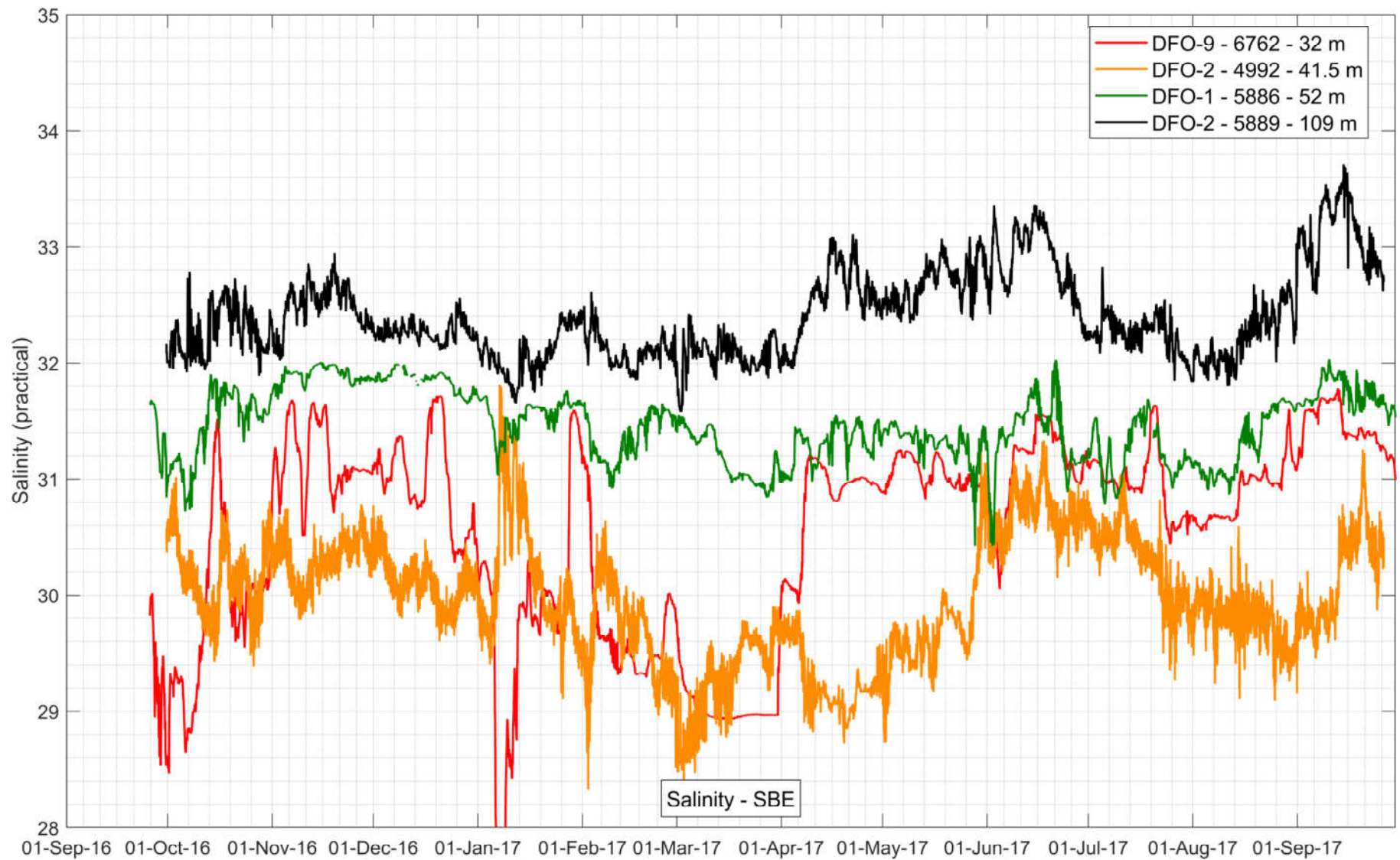


Figure 57: Salinity time-series recorded at DFO-2-16, DFO-1-16, and DFO-9-16 from 2016 to 2017. The legend shows the serial number and depth of each CT logger.

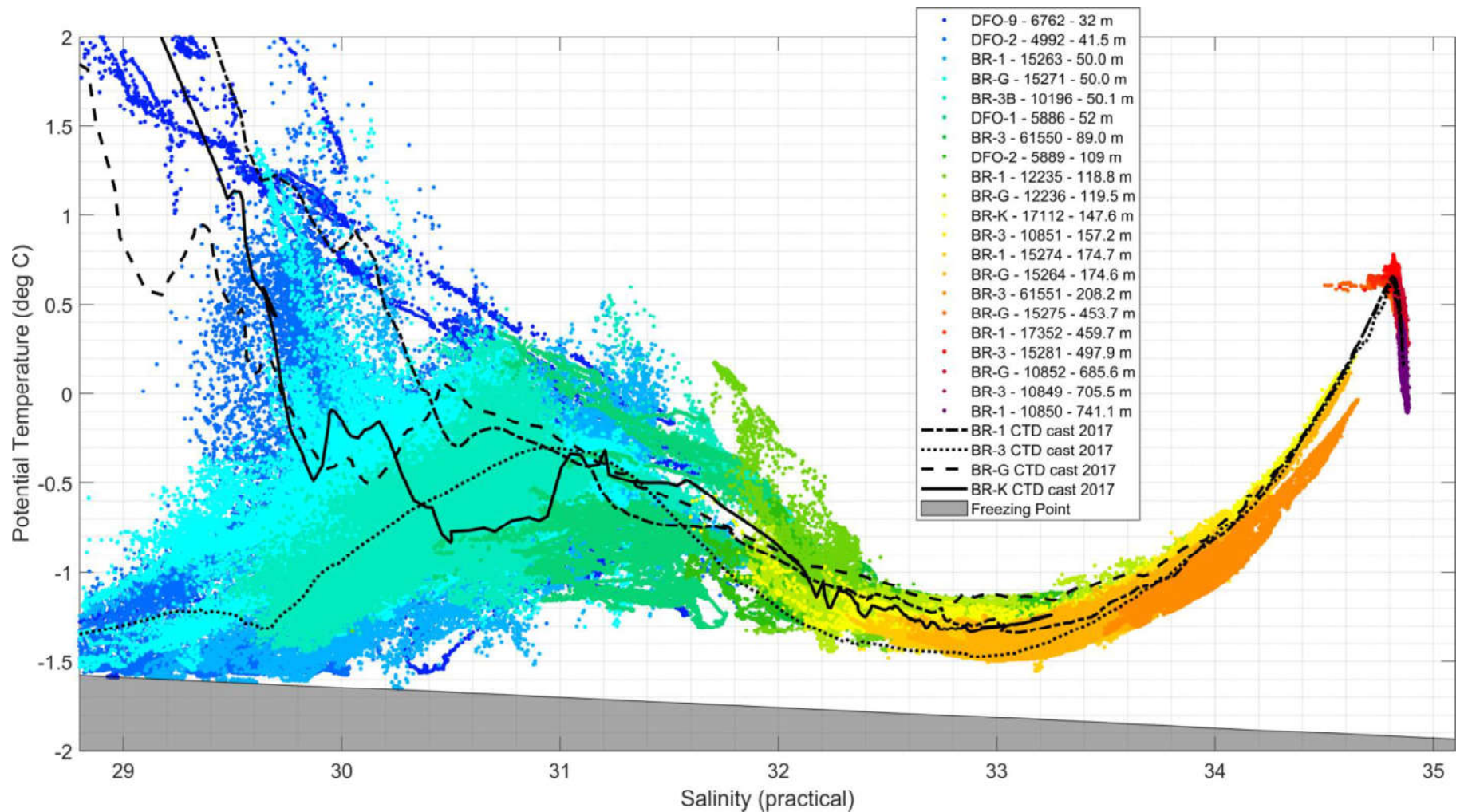


Figure 58: Temperature-salinity diagram constructed with all data acquired by the CT loggers attached to the moorings BR-1, BR-3, BR-G, BR-K, DFO-2, DFO-1, and DFO-9 from 2016 to 2017. CTD profile data taken at mooring locations during the CCGS Laurier cruises in 2017 are depicted by the 4 black lines.

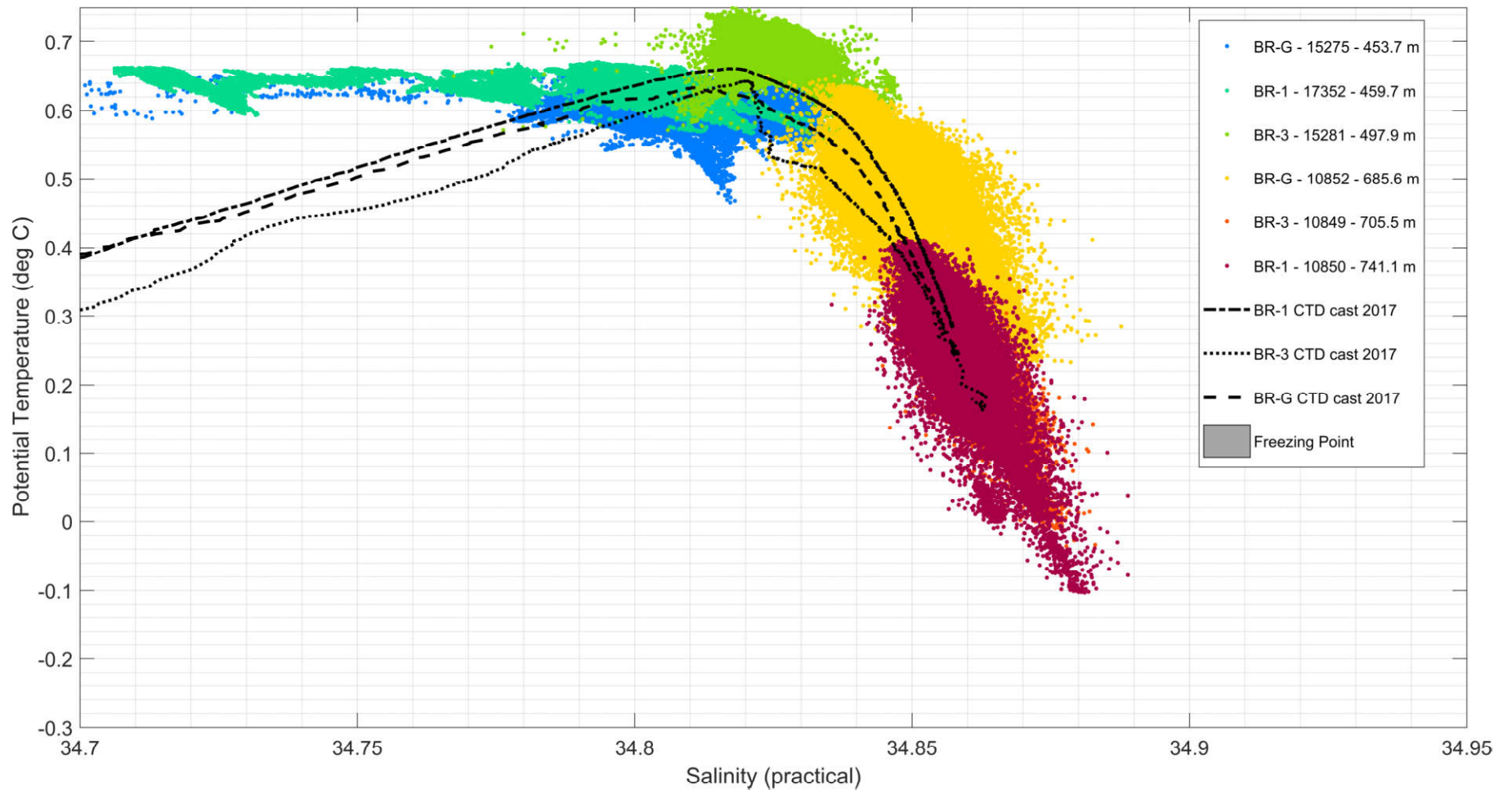


Figure 59: Zoom on the temperature-salinity diagram constructed with data acquired by the deep CT loggers (>400 m) attached to the slope moorings BR-1, BR-3 and BR-G from 2016 to 2017. CTD profile data taken at mooring locations during the CCGS Laurier cruises in 2017 are depicted by the 3 black lines.

3.4 Biogeochemical Fluxes

Analyses of the sediment trap samples, including measurements of total particulate matter, particulate organic carbon, and microscopic identification of phytoplankton cells, are partially completed. Preliminary results for phytoplankton cells export indicate sustained diatom fluxes at the shallow BR-1 position from the end of June to the end of August, with an increasing proportion of cells without chloroplasts reflecting the progression of the phytoplankton bloom (Figure 60). Diatom fluxes were lower at the deeper BR-G sediment trap but still indicated an increase in export at the end of June on the shelf. Although diatom fluxes were relatively high during autumn at BR-3 off Banks Island, only very low diatom fluxes (not visible) were recorded during spring and summer in 2017.

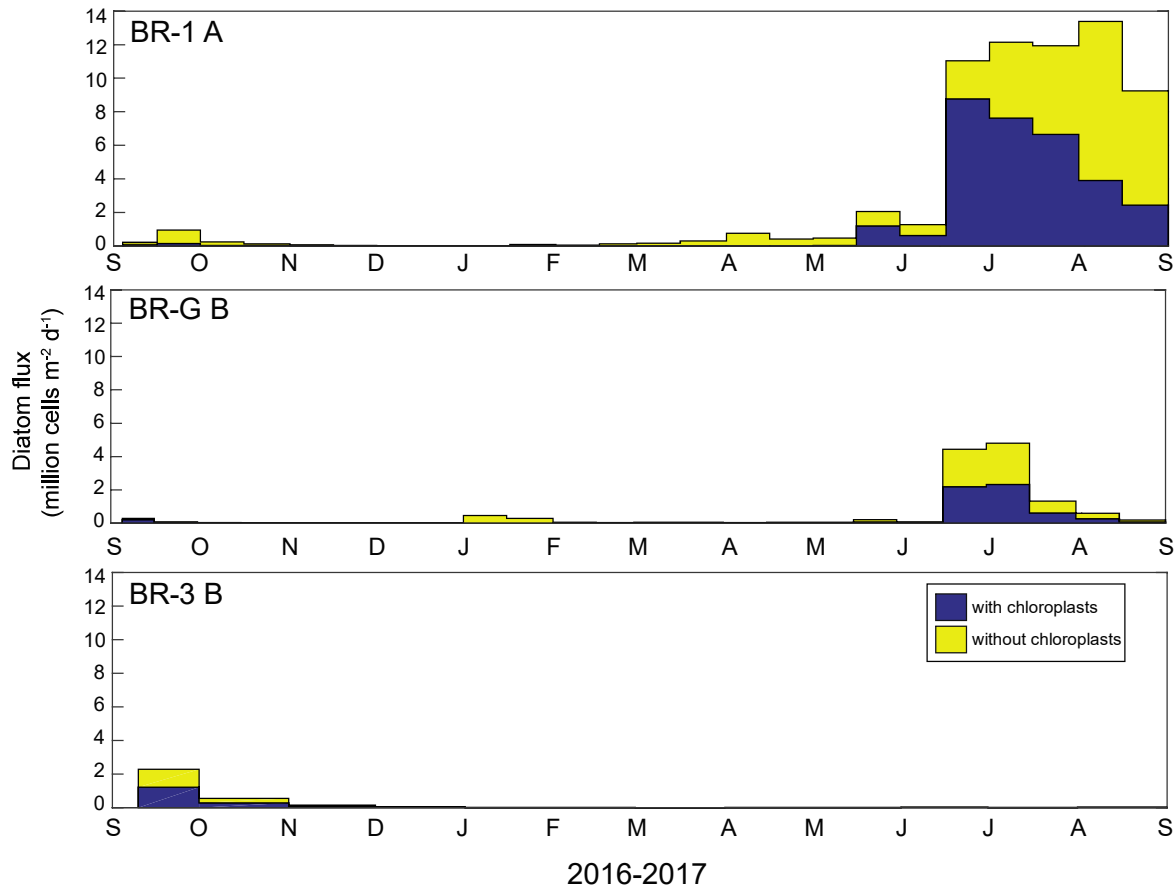


Figure 60: Diatom fluxes from September 2016 to September 2017 in the Beaufort Sea

4.0 CONCLUSIONS

This section of the report provides additional discussion on the 2016-2017 QA/QC dataset available thus far. Concluding remarks on features of interest are provided in section 4.1. Lessons learned from the 2017 field operations are summarized in section 4.2. At this stage of the project, the lessons learned and recommendations are currently being addressed to provide for more robust and secure future mooring deployments; and to increase the overall quality of the dataset. Objectives and priorities for 2018-2019 are also presented in section 4.3, including an outlook of the milestones for the fourth year of the iBO scientific program.

4.1 Concluding Remarks on the 2016-2017 Dataset

This report is aimed at providing an initial review of the available QA/QC data from the 7 iBO moorings recovered in 2017. Valid data have been presented for current meters, current profilers, and CT loggers deployed at all moorings. The percentage of valid data for current meters and profilers average 93.1% (see Appendix C for further details), while it is 99.94% for CT sensors. The QA/QC dataset for these instruments is readily available as Matlab© and formatted Text files (ASCII) provided as a data deliverable (see Appendix B). In addition, an initial outlook on biological activity over the slope was presented using a portion of the sediment trap data. The primary features of interest observed in the 2016-2017 dataset include the following:

- Sea ice break up was observed in 2017 approximately 6 weeks ahead of normal. The minimum regional sea ice concentration by the end of summer ranked as the eighth lowest on record, at 18.7%. Forthcoming processing analysis of the ice data from the IPS will help link the regional sea ice coverage and mooring data recorded over the last few years.
- Surface currents during open water at BR-1, BR-G, and BR-3 were generally towards the south-southwest in accord with the anti-cyclonic (clockwise) motion of the Beaufort Gyre. By contrast, surface currents at BR-K during open water conditions showed a different pattern, with a dominance of northeastward currents.
- Near-bottom current patterns were relatively similar to measurements from both 2014-2015 and 2015-2016. Currents along the slope generally follow the bathymetric contours, with a mean direction towards the northeast (BR-1, BR-G, BR-K) and north (BR-3). Reversals in the bottom current direction are most frequent at BR-K than at any other slope mooring, which suggests that this site reacts promptly to external forcings, in accordance with the dynamics of a shelf-break jet (see next point). Of the deep moorings, bottom currents were strongest at BR-3.
- Maximum instantaneous current speeds in 2016-2017 were recorded at BR-K and BR-G (up to 110 cm/s throughout the water column), consistent with magnitudes measured in previous years. Mean current speeds through the water column at BR-1, BR-G, BR-K, and BR-3 were between 6-18 cm/s, also consistent with mean speeds measured in the previous year(2015-2016).
- The temperature and salinity time-series showed that most of the variability in terms of water mass physical properties occurs in the upper 200 m. Several temperature and salinity events were recorded concurrent with a negative along-slope current component, These events are a likely sign of upwelling of deep waters at the shelf break. The time-series are indicate a lack of BSWW in comparison to 2015-2016.
- Preliminary analysis of the sediment trap data indicates that biological activity appears to have been much weaker at all of the mooring sites when compared to 2016 or 2015. Diatom fluxes at BR-3 were particularly low, a result of ice cover which persisted most of the summer. Further analyses on biogeochemical fluxes should be made to understand trends and patterns in primary productivity in the Beaufort Sea.

4.2 2017 Fieldwork Lessons Learned and Recommendations

This section of the report identifies lessons learned and recommendations from work on the Laurier during the 2017 iBO Program that are currently being addressed to improve future mooring deployments and recoveries. The list of recommendations has been finalized following the iBO TAC Meeting that was hosted as part of the ArcticNet Annual Scientific Meeting, Quebec City, in December 2017. The recommendations are provided below for three categories (instrument maintenance, mooring design and equipment, field work and logistics):

Instrument maintenance:

- The bulkhead connector (including interior) of all Nortek Aquadopp instruments should be carefully inspected to detect early onset of pin corrosion due to rubber fatigue or brittleness. The replacement of older cables and connectors as part of routine maintenance is advised.
- Bottom tracking firmware (used for measuring ice keel velocities) should be installed on all 300 kHz WHS ADCPs. The 300 kHz WHS ADCP #8682 did not have the correct firmware version installed and could not be used as planned on mooring BR-K.
- Oceano releases: The connection to the top ring on the tandem Oceano releases needs improvement to ensure it is properly isolated from shackles and the releases. A more robust solution should be investigated prior to their next usage.
- Benthos releases: All units should be set-up with Tilt enabled at start up if we were to use them again. This would allow a better understanding of the mooring orientation and would aid in the understanding of the situation. The new stainless steel tandem kits should not be used on moorings until further discussion with Benthos.

Mooring design and equipment:

- Additional high-strength plastic mounting clamps for RBR CT loggers should be purchased for attaching the instruments to the line or mooring frames. Mounting clamps are more robust and easier to install than stainless steel hose clamps, which were used for mounting several of the instruments in 2017 due to a lack of plastic clamps.
- In the future it is preferable to use RBR sensors with depth sensor in order to enhance the data set, to aid in the QA/QC process and mooring line analysis. Several depth capable units are now available.
- High-quality cable ties suitable for cold temperatures should be obtained for mousing mooring shackles. Cable ties that were sent for use on the Laurier in 2017 were of poor quality and broke frequently during tightening. Arctic brand cable ties with an 80-pound breaking strength have been used successfully in the past.
- In general, connections between frames, mooring lines, and acoustic releases need more planning to avoid the usage of varying metal types in close proximity and the use of variable quality hardware components. If metal to metal contact between dissimilar components cannot be avoided, then appropriate plastic bushings should be made or acquired in advance to properly isolate dissimilar metals. Bushings should be installed on spare instrument cages in advance to avoid difficulty in locating properly fitted bushing while onboard the cruise. Instrument cages and hardware which require special attention: Nortek stainless steel cages, acoustic releases (all types), and sediment traps.

- It is best practice to maintain consistency in mooring hardware and instrumentation and use materials from reputable suppliers and vendors with a history of success in past long-term Arctic Ocean deployments. The mooring team should avoid testing or substituting new hardware that is not provided or endorsed by the manufacturer or reviewed by the mooring design lead or ocean engineer whether for financial or logistical reasons. Mooring designs and changes to moorings should be kept simple so that mooring components can be easily tracked and for diagnosis of issues.

Fieldwork and logistics:

- The batteries of instruments that failed should be set aside for analysis and not discarded. This may help determining the cause of the failure.
- More detailed notes and photos should be collected when recovering sediment traps to assist in the diagnosis of problems.
- The original schedule for Leg 3a on the Laurier was ambitious and optimistic for three mooring programs at the end of September in the Arctic Ocean. Early utilization of much of our poor weather caused the schedule to slip by several days. Poor weather also precluded disembarkation via helicopter to Inuvik, resulting in expensive changes to airplane tickets. While it is difficult to plan for the many factors involved in the ship-to-shore transfer, it is important to keep in mind possible delays when purchasing airplane tickets. Alternatively, disembarkation could be restricted to locations where ship-to-shore transfers can be reliably accomplished.
- One solution for dealing with the limited available ship time in the Arctic is for the program to reduce the number of moorings to be serviced in any given year by increasing the deployment duration of selected moorings from 1 to 2 years. This could save money and reduce the time pressure on the mooring program. However, it increases the risk of equipment and data loss due to corrosion.
- Work space in the between decks hold was very tight because of the multiple moorings program on Leg 3a. Future work on the Laurier should carefully consider packing and organization of equipment to efficiently use space and sufficient time should be allowed for movement and re-organization of equipment in the hold. Laboratories in other parts of the ship can also be utilized to free up space in the between decks hold.
- Several of the M40 floats escaped their lashings and rolled around on the truck bed during the transit from Quebec City to IOS in Sidney in June. The ship has given notice that they will not load M40 floats on board the Laurier in the future unless they are packaged so that they can be reliably secured against movement. ArcticNet will look into building effective and stackable packaging for these floats.

4.3 Objectives and Milestones for 2018-2019

Objectives of iBO for 2018-2019 are centered on the recovery of the 7 iBO moorings from the CGGS Sir Wilfrid Laurier during its annual Arctic expedition to the Beaufort Sea (tentatively scheduled for September 25 to October 14, 2018). Milestones for 2018-2019 are provided in Table 17. This includes the finalization of the QA/QC for 2016-2017 data (primarily IPS data) and the upcoming processing of 2016-2017 datasets recovered from the Laurier. Other activities such as operational meetings, equipment mob/demob, and verification of ADCP compasses to address field logistics, instrumentation performance, and data processing are planned to ensure a timely development of the project in 2018-2019.

Table 17: 2018-2019 iBO Milestones

Milestone	Date
Completion of Phase 1 of BRSEA Synthesis Report	April 30, 2018
Technical Advisory Committee Conference Call - Spring Meeting	May 15, 2018
Pre-field 2017 Operational Conference Call Meeting	July 2018
Recovery of iBO moorings onboard the Laurier	September 25, 2018 to October 14, 2018
ArcticNet Annual Science Meeting, Ottawa	December 10 to 14, 2018
Finalization of data processing of IPS 2017-2018 and related reporting	December 31, 2018
Presentation of the iBO program at the Inuvialuit Game Council (IGC) meeting, Tuktoyaktuk or Winnipeg	Spring 2019
QA/QC of ADCP and CT logger 2017-2018 data	March 31, 2019
iBO Technical Report 2018 Submitted	March 31, 2019

With iBO entering its fourth and final year, the iBO TAC is proposing to develop a Synthesis Report which will be a basic building block for the Indigenous and Northern Affairs Canada (INAC) Beaufort Sea Regional Strategic Environmental Assessment (BRSEA). The Synthesis Report will link up-to-date scientific knowledge on the ice-ocean environment of the Beaufort Sea to issues important to environmental assessment and decision-making in relation to Beaufort offshore exploration and development, particularly for oil & gas. This will be completed primarily by synthesizing the 8 years (2009-2017) of enhanced observations of the marine physical environment by Industry, ArcticNet, and Fisheries and Oceans Canada (DFO) along with existing data and Inuvialuit Traditional Knowledge.

Phase 1 of the Synthesis Report consists of 3 subtasks: develop a Table of Contents and methods for the Synthesis Report, commence dialog with relevant Inuvialuit stakeholders, and provide a review of ongoing research in the Beaufort Sea. Phase 1 is planned to be completed at the end of April 2018 with Phase 2 (development of the Synthesis Report) beginning thereafter. Completion of the Synthesis Report would represent a major outcome and deliverable of iBO. The broad objectives of the Synthesis Report include:

- Synthesis of ice-ocean data from 2009-2017
- Contribute to validation of modelling tools
 - Use ocean data during selected events to evaluate simulations of a high-resolution operational ocean forecast model (Environment and Climate Change Canada (ECCC) and DFO's Regional Ice-Ocean Prediction System (RIOPS), <http://navigator.oceansdata.ca>) and to provide insight into the present value of this predictive tool in ocean management and crisis response.
- Link ice-ocean processes to broader applications
 - Identify notable occurrences and follow in detail their development, climax and decay as case studies of circumstances that require industry and government planning.
 - Engage stakeholders in applying the science so that our output is relevant, comprehensible and useful in considerations of offshore development.

5.0 REFERENCES

- ArcticNet Inc., Fisheries and Oceans, Golder Associates Ltd. (2016). Integrated Beaufort Observatory (iBO) 2015 Technical Project Report. 4 August 2016.
- Aagaard, K., 1984. The Beaufort Undercurrent. In: Barnes, P.W., Schell, D.M., Reimnitz, E. (Eds.), *The Alaskan Beaufort Sea: Ecosystems and Environments*. Academic Press, New York, pp. 47–74.
- ASL Environmental Sciences Inc. 2015. IPS Processing Toolbox User's Guide. Report by ASL Environmental Sciences Inc., Victoria BC, Canada, 136 pp.
- Barber, D.G., Hanesiak, J.M., 2004. Meteorological forcing of sea ice concentrations in the southern Beaufort Sea over the period 1979 to 2000. *J. Geophys. Res. (C Oceans)* 109, C06014.
- Blasco, S., Bennett, R., Brent, T., Burton, M., Campbell, P., Carr, E., Covill, R., Dallimore, S., Davies, E., Hughes-Clarke, J., Issler, D., Leonard, L., MacKillop, K., Mazzotti, S., Patton, E., Rogers, G., Shearer, J. and White, M., 2013. 2010 State of Knowledge: Beaufort Sea Seabed Geohazards Associated with Offshore Hydrocarbon Development; Geological Survey of Canada, Open File 6989, 340 p. doi:10.4095/292616
- Canadian Ice Service (CIS). 2017. Seasonal summary. North American Arctic Waters. Summer 2017. 31 pp.
- Carmack, E.C., MacDonald, R.W., 2002. Oceanography of the Canadian Shelf of the Beaufort Sea: a Setting for Marine Life. *Arctic* 55, suppl. 1, 29-45.
- Dmitrenko, I. A., Kirillov, S. A., Forest, A., Gratton, Y., Volkov, D. L., Williams, W. J., Lukovich, J. V., Belanger, C. and Barber, D. G. 2016, Shelfbreak current over the Canadian Beaufort Sea continental slope: Wind-driven events in January 2005. *J. Geophys. Res. Oceans*. Accepted Author Manuscript. doi:10.1002/2015JC011514
- Fissel, D. B., Marko, J. R., Melling, H. 2008, (July). Advances in marine ice profiling for oil and gas applications. In *Proceedings of the Icetech 2008 Conference*.
- Forest, A., Osborne, P. D., Fortier, L., Sampei, M., and Lowings, M. G. 2015. Physical forcings and intense shelf–slope fluxes of particulate matter in the halocline waters of the Canadian Beaufort Sea during winter. *Continental Shelf Research*, 101, 1-21.
- Galley, R. J., Else, B. G. T., Prinsenber, S. J., Babb, D., Barber, D. G. 2013. Summer Sea Ice Concentration, Motion, and Thickness Near Areas of Proposed Offshore Oil and Gas Development in the Canadian Beaufort Sea—2009. *Arctic*, 105-116.
- Giovando, L.F., Herlinveaux, R.H., 1981. A discussion of factors influencing dispersion of pollutants in the Beaufort Sea. *Pacific Marine Science Report* 81-4, p. 198.
- Golder Associates Ltd. (Golder). 2018. Integrated Beaufort Observatory (iBO) Mooring Field Report 2017. Technical Report. Report Number 1775762-R-Rev0-2017.
- Institute of Ocean Sciences – Fisheries and Oceans Canada (IOS-DFO). Integrated Beaufort Observatory 2017 Field Expedition Report. September 15 – October 9, 2017. Ed. By H. Melling. IOS Cruise 2017-97
- Integrated Ocean Observing System (IOOS). 2015. Manual for Real-Time Quality Control of In-Situ Current Observations: A Guide to Quality Control and Quality Assurance of Acoustic Doppler Current Profiler Observations. Version 2.0 October 2015.

- Jackson, J. M., H. Melling, J. V. Lukovich, D. Fissel, and D. G. Barber (2015), Formation of winter water on the Canadian Beaufort shelf: New insight from observations during 2009–2011, *J. Geophys. Res. Oceans*, 120, doi:10.1002/2015JC010812.
- Kulikov, E.A., Carmack, E.C., Macdonald, R.W., 1998. Flow variability at the continental shelf break of the Mackenzie Shelf in the Beaufort Sea. *Journal of Geophysical Research. C. Oceans* 103, 12,725-712,741.
- Lansard, B., Mucci, A., Miller, L. A., Macdonald, R. W., Gratton, Y. 2012. Seasonal variability of water mass distribution in the southeastern Beaufort Sea determined by total alkalinity and $\delta^{18}\text{O}$. *J. Geophys. Res. (C Oceans* 117(C3).
- Macdonald, R.W., Paton, D.W., Carmack, E.C., Omstedt, A., 1995. The freshwater budget and under-ice spreading of Mackenzie River water in the Canadian Beaufort Sea based on salinity and $d^{18}\text{O}/d^{16}\text{O}$ measurements in water and ice. *J. Geophys. Res. (C Oceans)* 100, 895-919.
- Macdonald, R.W., Solomon, S.M., Cranston, R.E., Welch, H.E., Yunker, M.B., Gobeil, C., 1998. A sediment and organic carbon budget for the Canadian Beaufort Shelf. *Marine Geology* 144, 255-273.
- Melling, H., 1993. The formation of a haline shelf front in wintertime in an ice-covered arctic sea. *Continental Shelf Research* 13, 1123–1147.
- Melling, H., Riedel, D.A. 2004. Draft and Movement of Pack Ice in the Beaufort Sea: A Time-Series Presentation April 1990 - August 1999. *Canadian Technical Report of Hydrography and Ocean Sciences* 238, v + 24 pp.
- Melling, H., Johnston, P. H., Riedel, D.A. 1995. Measurements of the underside topography of sea ice by moored subsea sonar. *Journal of Atmospheric and Oceanic Technology*, 12(3), 589-602.
- Melling, H., Gratton, Y., Ingram, G. 2001. Ocean circulation within the North Water polynya of Baffin Bay. *Atmosphere-Ocean*, 39(3), 301-325.
- Nortek AS (Nortek). 2013. Comprehensive Manual. December 2013.
- O'Brien, M.C., Macdonald, R.W., Melling, H., Iseki, K., 2006. Particle fluxes and geochemistry on the Canadian Beaufort Shelf: Implications for sediment transport and deposition. *Continental Shelf Research* 26, 41-81.
- Pickart, R.S., 2004. Shelfbreak circulation in the Alaskan Beaufort Sea: Mean structure and variability. *J. Geophys. Res. (C Oceans)* 109, C04024.
- Pickart, R.S., Schulze, L.M., Moore, G.W.K., Charette, M.A., Arrigo, K.R., van Dijken, G., Danielson, S.L., 2013. Long-term trends of upwelling and impacts on primary productivity in the Alaskan Beaufort Sea. *Deep Sea Research Part I: Oceanographic Research Papers* 79, 106-121.
- RBR-Global (RBR). 2016. Ruskin User Guide. Latest version available at: <https://rbr-global.com/support/software>.
- Beardsley, R. C., and L. K. Rosenfeld 1983, Introduction to the CODE-1 moored array and large-scale data report, in *CODE-1: Moored Array and Large-Scale Data Report*, edited by L. K. Rosenfeld, Tech. Rep. WHOI-83-23, CODE Tech. Rep. 21, pp. 1216, Woods Hole Oceanogr. Inst., Woods Hole, Mass.
- Sequoia Scientific. 2008. Processing LISST-100 and LISST-100X Data in MATLAB. Online Article (last update: 11 July 2012). <http://www.sequoiasci.com/article/processing-lisst-100-and-lisst-100x-data-in-matlab/>.
- Teledyne RDI (TRDI). 2014. Monitor, Sentinel, Mariner, Long Ranger, and Quartermaster Commands and Output Data Format. P/N 957-6156-00. Revised March 2014.
- Teledyne RDI (TRDI). 2006. Acoustic Doppler Current Profiler Principles of Operation: A Practical Primer. P/N 951-6069-00. December 2006.

- von Appen, W. J., Pickart, R. S. 2012. Two configurations of the western Arctic shelfbreak current in summer. *Journal of Physical Oceanography*, 42(3), 329-351.
- Williams, W. J., Melling, H., Carmack, E. C., & Ingram, R. G. 2008. Kugmallit Valley as a conduit for cross-shelf exchange on the Mackenzie Shelf in the Beaufort Sea. *Journal of Geophysical Research: Oceans*, 113(C2).
- Woodgate, R. A. and Holroyd, A.E. 2011. Correction of Teledyne Acoustic Doppler Current Profiler (ADCP) Bottom-Track Range Measurements for Instrument Pitch and Roll. University of Washington Technical Report: available at <http://psc.apl.washington.edu/BeringStrait.html>

Appendix A. 2016-2017 Final Mooring Diagrams

The final mooring diagrams 2016-2017 are provided below. Instrument depths correspond to the planned depth for each instrument throughout the deployment period.

BR3-16

Lat: 70° 24.5273' N (Triangulated Position)
 Long: 129° 21.7590' W (Triangulated Position)

Site Depth : 690m
 Slope near Banks Island



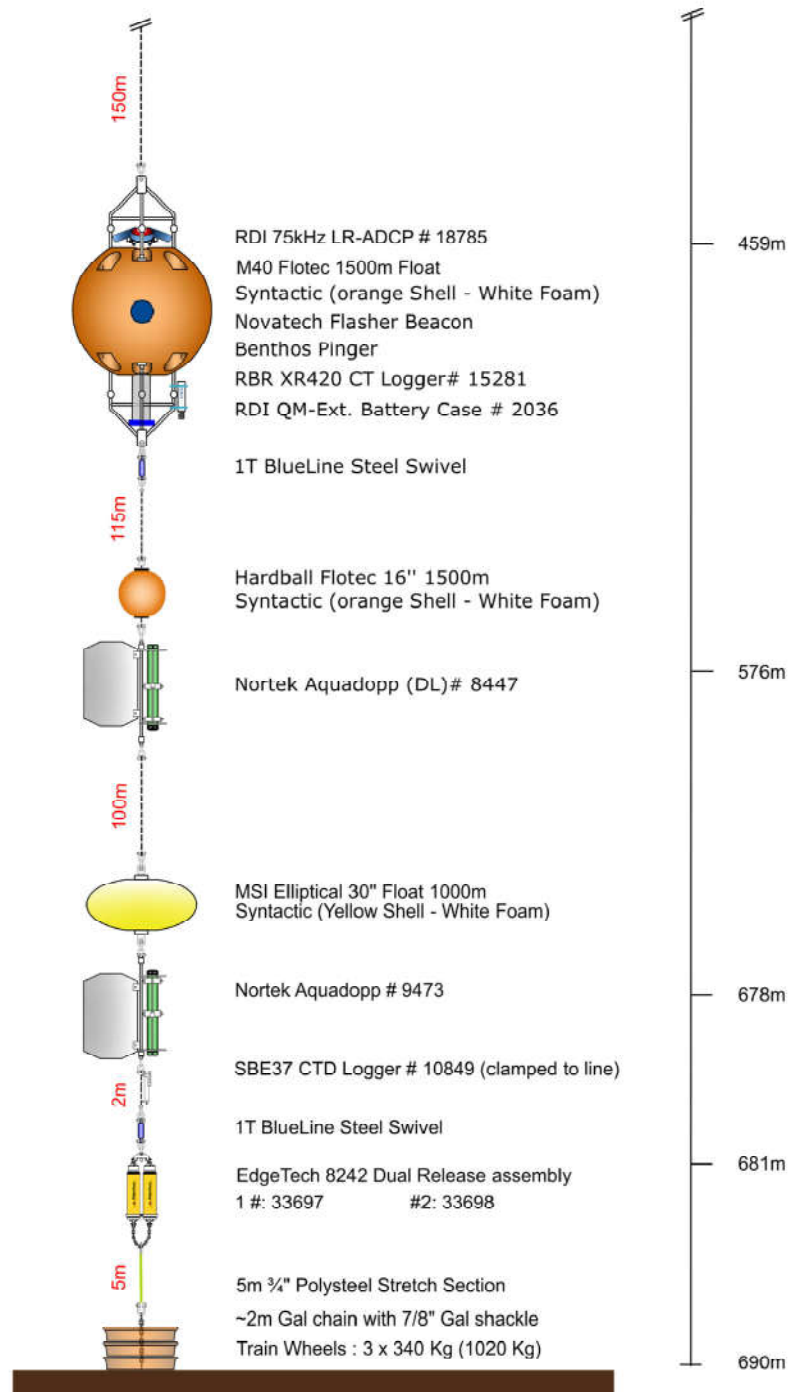
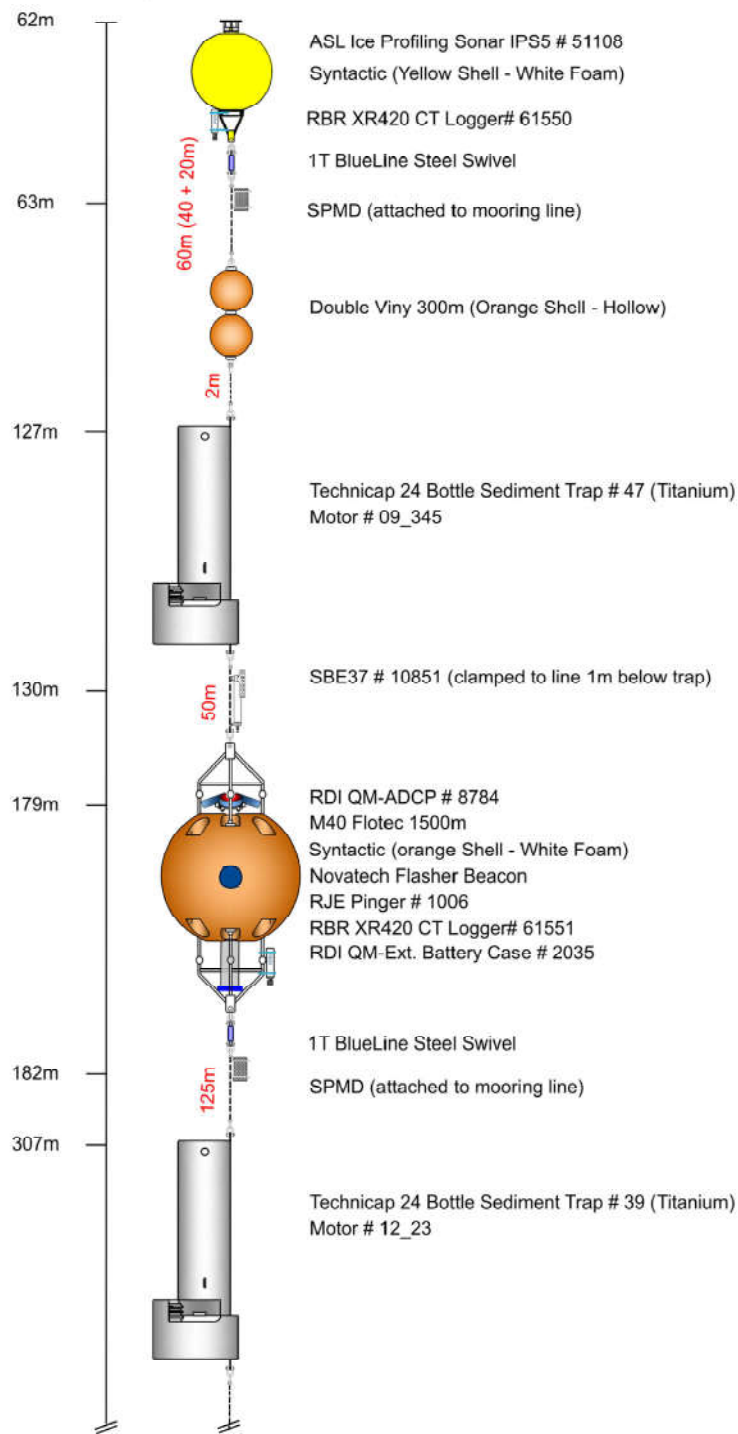
Instrument Target Depth

Component Details

* Mooring Line : Amsteel II 5/16"

Component Details

Instrument Target Depth



Appendix B. Data deliverable

In addition to this report, we issue the available oceanographic data that was processed and quality checked following the methods described in section 2.4. The data is provided electronically. This data is provided as a draft and could be subject to further revisions. The data are provided as Matlab and ASCII files for the following instruments:

Mooring	Mooring depth (m)	Instrument	Serial Number	Instrument depth (m)
BR-1-16	754	RBR XR420 CT	15263	50.0
		SBE37 Microcat	12235	118.8
		TRDI QM ADCP 150 kHz	12823	173.7
		RBR XR420 CT	15274	174.7
		TRDI LR ADCP 75 kHz	12943	458.7
		RBR XR420 CT	17352	459.7
		Nortek Aquadopp DW	8543	590.5
		SBE37 Microcat	10850	741.1
		Nortek Aquadopp DW	8448	745.2
BR-3-16	718	RBR XR420 CT	61550	89.0
		TRDI QM ADCP 150 kHz	8784	144.4
		RBR XR420 CT	61551	207.2
		SBE37 Microcat	10851	208.2
		TRDI LR ADCP 75 kHz	18785	496.9
		RBR XR420 CT	15281	497.9
		Nortek Aquadopp DW	8447	601.5
		Nortek Aquadopp DW	9473	712.8
		SBE37 Microcat	10849	713.3
BR-3B-16	690	SBE37 Microcat	10196	50.1
BR-G-16	699	RBR XR420 CT	15271	50.0
		SBE37 Microcat	12236	119.5
		TRDI QM ADCP 150 kHz	12699	173.6
		RBR XR420 CT	15264	174.6
		TRDI LR ADCP 75 kHz	13079	452.7
		RBR XR420 CT	15275	453.7
		Nortek Aquadopp DW	8419	564.8
		Nortek Aquadopp DW	8442	674.3
		SBE37 Microcat	10852	685.6
BR-K-16	166	TRDI WHS ADCP 300 kHz	7844	135.6
		RBR XR420 CT-Tu-DO-FI	17112	134.6
		Nortek Aquadopp Profiler	11147	148.6
DFO-2-16		TRDI NB ADCP 300kHz	0586	109
DFO-1-16		TRDI WHS ADCP 300kHz	12463	51
DFO-9-16		TRDI WHS ADCP 300kHz	02412	31

Appendix C. Summary Statistics of Ocean Currents

Table 18: Summary statistics of current speed, vector-averaged direction and number of valid records by bin depth at BR-1-16 based on the data acquired with the QM ADCP #12823 from 2016 to 2017. Bin depths flagged manually as part of the QA/QC are highlighted in red.

Bin Depth (m)	Min Speed (m/s)	1%ile Speed (m/s)	5%ile Speed (m/s)	25%ile Speed (m/s)	Median Speed (m/s)	Mean Speed (m/s)	75%ile Speed (m/s)	95%ile Speed (m/s)	99%ile Speed (m/s)	Max Speed (m/s)	Standard Deviation Speed (m/s)	Vector-Averaged Direction (deg TN)	Number of Valid Records	% of Valid Data (%)
29.4	0.0	0.01	0.03	0.07	0.11	0.13	0.18	0.31	0.43	0.69	0.09	276.9	35,548	95.1
33.4	0.0	0.01	0.03	0.07	0.12	0.14	0.18	0.30	0.44	0.65	0.09	278.0	35,604	95.2
37.4	0.0	0.01	0.03	0.08	0.12	0.14	0.18	0.30	0.45	0.61	0.09	280.0	35,852	95.9
41.4	0.0	0.02	0.03	0.08	0.12	0.14	0.18	0.30	0.45	0.61	0.09	281.3	36,181	96.8
45.4	0.0	0.02	0.04	0.08	0.13	0.14	0.19	0.31	0.45	0.63	0.09	282.9	36,464	97.5
49.4	0.0	0.02	0.04	0.08	0.13	0.14	0.18	0.31	0.45	0.63	0.09	283.8	36,678	98.1
53.3	0.0	0.01	0.03	0.06	0.09	0.11	0.14	0.28	0.43	0.61	0.08	289.8	37,252	99.6
57.3	0.0	0.00	0.01	0.03	0.06	0.10	0.15	0.33	0.46	0.64	0.11	308.0	37,364	99.9
61.3	0.0	0.02	0.04	0.08	0.12	0.14	0.17	0.31	0.45	0.63	0.09	286.7	36,945	98.8
65.3	0.0	0.02	0.04	0.09	0.15	0.16	0.22	0.34	0.45	0.64	0.09	288.4	36,984	98.9
69.3	0.0	0.02	0.04	0.09	0.15	0.17	0.23	0.37	0.46	0.63	0.10	291.0	37,053	99.1
73.3	0.0	0.02	0.04	0.09	0.15	0.17	0.23	0.37	0.46	0.64	0.10	292.7	37,100	99.2
77.3	0.0	0.02	0.04	0.09	0.15	0.17	0.23	0.37	0.46	0.65	0.10	293.2	37,128	99.3
81.3	0.0	0.02	0.04	0.09	0.15	0.17	0.23	0.38	0.46	0.63	0.10	294.0	37,153	99.4
85.3	0.0	0.02	0.04	0.09	0.15	0.17	0.23	0.38	0.46	0.62	0.10	294.8	37,168	99.4
89.3	0.0	0.02	0.04	0.09	0.15	0.17	0.24	0.37	0.46	0.60	0.10	295.4	37,173	99.4
93.3	0.0	0.02	0.04	0.09	0.15	0.17	0.24	0.37	0.45	0.59	0.10	296.1	37,176	99.4
97.3	0.0	0.02	0.04	0.09	0.15	0.17	0.24	0.37	0.45	0.55	0.10	297.0	37,182	99.4
101.4	0.0	0.02	0.04	0.09	0.15	0.17	0.24	0.37	0.44	0.54	0.10	297.9	37,185	99.4
105.4	0.0	0.02	0.04	0.09	0.15	0.17	0.24	0.37	0.44	0.57	0.10	299.1	37,197	99.5
109.3	0.0	0.02	0.04	0.09	0.15	0.17	0.24	0.36	0.43	0.59	0.10	299.5	37,213	99.5
113.3	0.0	0.02	0.04	0.09	0.15	0.17	0.24	0.36	0.43	0.60	0.10	300.0	37,233	99.6

Bin Depth (m)	Min Speed (m/s)	1%ile Speed (m/s)	5%ile Speed (m/s)	25%ile Speed (m/s)	Median Speed (m/s)	Mean Speed (m/s)	75%ile Speed (m/s)	95%ile Speed (m/s)	99%ile Speed (m/s)	Max Speed (m/s)	Standard Deviation Speed (m/s)	Vector-Averaged Direction (deg TN)	Number of Valid Records	% of Valid Data (%)
117.3	0.0	0.02	0.04	0.09	0.15	0.17	0.23	0.36	0.42	0.55	0.10	301.0	37,252	99.6
121.3	0.0	0.01	0.02	0.06	0.10	0.12	0.15	0.32	0.39	0.57	0.09	310.4	37,343	99.9
125.3	0.0	0.00	0.01	0.02	0.04	0.05	0.06	0.16	0.21	0.39	0.05	337.1	37,393	100.0
129.3	0.0	0.01	0.03	0.08	0.14	0.15	0.20	0.29	0.33	0.39	0.08	302.7	37,327	99.8
133.3	0.0	0.02	0.04	0.09	0.15	0.16	0.23	0.33	0.39	0.50	0.09	302.1	37,315	99.8
137.3	0.0	0.02	0.04	0.09	0.14	0.16	0.22	0.33	0.39	0.53	0.09	302.8	37,329	99.8
141.3	0.0	0.02	0.04	0.09	0.14	0.16	0.22	0.32	0.38	0.49	0.09	302.9	37,344	99.9
145.3	0.0	0.02	0.04	0.09	0.14	0.15	0.21	0.31	0.37	0.49	0.08	303.5	37,365	99.9
149.3	0.0	0.02	0.04	0.08	0.14	0.15	0.20	0.30	0.36	0.48	0.08	304.2	37,381	100.0
153.3	0.0	0.02	0.04	0.08	0.13	0.14	0.20	0.29	0.35	0.47	0.08	304.6	37,391	100.0
157.3	0.0	0.02	0.03	0.08	0.13	0.14	0.19	0.28	0.34	0.45	0.08	305.4	37,392	100.0
161.3	0.0	0.02	0.03	0.08	0.12	0.13	0.18	0.27	0.33	0.45	0.07	305.3	37,393	100.0
165.3	0.0	0.01	0.03	0.07	0.11	0.12	0.16	0.25	0.31	0.42	0.07	305.7	37,393	100.0

Table 19: Summary statistics of current speed, vector-averaged direction and number of valid records by bin depth at BR-1-16 based on the data acquired with the LR ADCP #12943 from 2016 to 2017.

Bin Depth (m)	Min Speed (m/s)	1%ile Speed (m/s)	5%ile Speed (m/s)	25%ile Speed (m/s)	Median Speed (m/s)	Mean Speed (m/s)	75%ile Speed (m/s)	95%ile Speed (m/s)	99%ile Speed (m/s)	Max Speed (m/s)	Standard Deviation Speed (m/s)	Vector-Averaged Direction (deg TN)	Number of Valid Records	% of Valid Data (%)
50.5	0.0	0.02	0.04	0.08	0.12	0.13	0.17	0.27	0.38	0.65	0.08	301.4	18,381	98.3
66.5	0.0	0.02	0.04	0.09	0.14	0.16	0.22	0.36	0.45	0.65	0.10	331.3	18,458	98.7
82.5	0.0	0.02	0.04	0.09	0.16	0.17	0.24	0.37	0.47	0.64	0.10	343.2	18,321	98.0
98.5	0.0	0.02	0.04	0.10	0.16	0.18	0.24	0.37	0.45	0.56	0.10	351.6	18,286	97.8
114.5	0.0	0.02	0.04	0.09	0.16	0.17	0.24	0.36	0.43	0.55	0.10	353.9	18,408	98.4
130.5	0.0	0.02	0.04	0.09	0.15	0.17	0.23	0.34	0.40	0.51	0.09	356.7	18,517	99.0
146.5	0.0	0.02	0.04	0.09	0.14	0.15	0.21	0.29	0.35	0.44	0.08	358.6	18,602	99.5
162.5	0.0	0.02	0.04	0.08	0.13	0.13	0.18	0.26	0.31	0.44	0.07	2.2	18,632	99.6
178.5	0.0	0.01	0.03	0.07	0.11	0.12	0.16	0.24	0.30	0.42	0.07	10.0	18,648	99.7
194.5	0.0	0.01	0.02	0.06	0.09	0.10	0.13	0.21	0.27	0.36	0.06	19.3	18,663	99.8
210.5	0.0	0.01	0.02	0.05	0.07	0.08	0.11	0.17	0.22	0.40	0.05	28.4	18,679	99.9
226.5	0.0	0.01	0.02	0.04	0.06	0.07	0.09	0.14	0.19	0.39	0.04	41.5	18,695	100.0
242.5	0.0	0.01	0.01	0.03	0.05	0.06	0.07	0.12	0.16	0.25	0.03	61.5	18,697	100.0
258.5	0.0	0.01	0.01	0.03	0.05	0.05	0.07	0.11	0.14	0.21	0.03	76.4	18,697	100.0
274.5	0.0	0.01	0.01	0.03	0.04	0.05	0.06	0.10	0.13	0.18	0.03	89.2	18,697	100.0
290.5	0.0	0.00	0.01	0.03	0.04	0.04	0.06	0.09	0.12	0.19	0.02	92.5	18,697	100.0
306.5	0.0	0.00	0.01	0.02	0.04	0.04	0.05	0.08	0.10	0.16	0.02	100.6	18,697	100.0
322.5	0.0	0.00	0.01	0.02	0.04	0.04	0.05	0.08	0.11	0.17	0.02	98.6	18,697	100.0
338.5	0.0	0.00	0.01	0.02	0.04	0.04	0.05	0.08	0.11	0.18	0.02	96.8	18,697	100.0
354.5	0.0	0.00	0.01	0.02	0.04	0.04	0.05	0.08	0.11	0.17	0.02	97.9	18,697	100.0
370.5	0.0	0.00	0.01	0.02	0.04	0.04	0.05	0.08	0.11	0.18	0.02	97.7	18,697	100.0
386.5	0.0	0.00	0.01	0.02	0.03	0.04	0.05	0.08	0.10	0.16	0.02	95.4	18,697	100.0
402.5	0.0	0.00	0.01	0.02	0.03	0.04	0.05	0.08	0.11	0.16	0.02	93.2	18,697	100.0
418.5	0.0	0.00	0.01	0.02	0.03	0.04	0.05	0.08	0.10	0.18	0.02	92.2	18,697	100.0
434.5	0.0	0.00	0.01	0.02	0.04	0.04	0.05	0.08	0.10	0.20	0.02	91.4	18,697	100.0

Table 20: Summary statistics of current speed, vector-averaged direction and number of valid records at 590.5 and 745.2 m depth at BR-1-16 as based on the data acquired with the Aquadopp DW #8543 and #8448 from 2016 to 2017.

Bin Depth (m)	Min Speed (m/s)	1%ile Speed (m/s)	5%ile Speed (m/s)	25%ile Speed (m/s)	Median Speed (m/s)	Mean Speed (m/s)	75%ile Speed (m/s)	95%ile Speed (m/s)	99%ile Speed (m/s)	Max Speed (m/s)	Standard Deviation Speed (m/s)	Vector-Averaged Direction (deg TN)	Number of Valid Records	% of Valid Data (%)
590.5	0.0	0.00	0.01	0.02	0.03	0.03	0.04	0.06	0.08	0.12	0.02	69.8	12,431	66.5
745.2	0.0	0.00	0.01	0.02	0.03	0.04	0.05	0.09	0.11	0.17	0.02	94.7	18,698	100.0

Table 21: Summary statistics of current speed, vector-averaged direction and number of valid records by bin depth at BR-3-16 based on the data acquired with the QM ADCP #8784 from 2016 to 2017. Bin depths flagged manually as part of the QA/QC are highlighted in red.

Bin Depth (m)	Min Speed (m/s)	1%ile Speed (m/s)	5%ile Speed (m/s)	25%ile Speed (m/s)	Median Speed (m/s)	Mean Speed (m/s)	75%ile Speed (m/s)	95%ile Speed (m/s)	99%ile Speed (m/s)	Max Speed (m/s)	Standard Deviation Speed (m/s)	Vector-Averaged Direction (deg TN)	Number of Valid Records	% of Valid Data (%)
18.9	0.00	0.01	0.01	0.04	0.06	0.08	0.10	0.21	0.30	0.48	0.06	191.5	16,383	89.9
22.9	0.00	0.01	0.02	0.04	0.07	0.09	0.12	0.21	0.29	0.44	0.06	192.7	16,164	88.7
26.9	0.00	0.01	0.02	0.04	0.08	0.09	0.12	0.21	0.29	0.45	0.06	191.9	16,232	89.1
30.9	0.00	0.01	0.02	0.04	0.08	0.09	0.12	0.20	0.29	0.47	0.06	191.1	16,099	88.3
34.9	0.00	0.01	0.02	0.04	0.08	0.09	0.12	0.20	0.29	0.46	0.06	192.0	16,310	89.5
38.9	0.00	0.01	0.02	0.04	0.07	0.09	0.12	0.20	0.28	0.44	0.06	191.7	16,846	92.4
42.9	0.00	0.01	0.02	0.04	0.07	0.09	0.12	0.20	0.27	0.37	0.06	190.9	16,850	92.5
46.9	0.00	0.01	0.02	0.04	0.07	0.08	0.12	0.20	0.26	0.35	0.06	190.4	16,366	89.8
50.9	0.00	0.01	0.02	0.04	0.07	0.08	0.11	0.19	0.25	0.36	0.05	190.3	16,200	88.9
54.9	0.00	0.01	0.02	0.04	0.07	0.08	0.11	0.19	0.24	0.36	0.05	189.4	16,144	88.6
58.9	0.00	0.01	0.02	0.04	0.07	0.08	0.11	0.18	0.23	0.35	0.05	188.1	16,118	88.4
62.9	0.00	0.01	0.02	0.04	0.07	0.08	0.10	0.17	0.23	0.30	0.05	186.9	16,126	88.5
66.9	0.00	0.01	0.02	0.04	0.07	0.08	0.10	0.17	0.22	0.34	0.05	185.9	16,093	88.3
70.9	0.00	0.01	0.02	0.04	0.07	0.08	0.10	0.18	0.23	0.34	0.05	185.2	16,113	88.4
74.9	0.00	0.01	0.02	0.04	0.07	0.08	0.10	0.18	0.23	0.30	0.05	182.9	16,172	88.7
78.9	0.00	0.01	0.02	0.04	0.07	0.08	0.10	0.18	0.23	0.30	0.05	182.8	16,282	89.3
82.9	0.00	0.01	0.02	0.04	0.07	0.08	0.10	0.18	0.24	0.33	0.05	181.7	16,406	90.0
86.9	0.00	0.01	0.02	0.04	0.07	0.08	0.10	0.18	0.24	0.32	0.05	181.3	16,638	91.3
90.9	0.00	0.01	0.02	0.04	0.07	0.08	0.10	0.18	0.24	0.31	0.05	179.3	16,904	92.8
94.9	0.00	0.01	0.02	0.04	0.06	0.07	0.09	0.16	0.23	0.30	0.05	178.2	17,697	97.1

Bin Depth (m)	Min Speed (m/s)	1%ile Speed (m/s)	5%ile Speed (m/s)	25%ile Speed (m/s)	Median Speed (m/s)	Mean Speed (m/s)	75%ile Speed (m/s)	95%ile Speed (m/s)	99%ile Speed (m/s)	Max Speed (m/s)	Standard Deviation Speed (m/s)	Vector-Averaged Direction (deg TN)	Number of Valid Records	% of Valid Data (%)
98.9	0.00	0.01	0.02	0.04	0.06	0.07	0.09	0.16	0.23	0.33	0.05	177.6	17,699	97.1
102.9	0.00	0.01	0.02	0.04	0.07	0.08	0.10	0.17	0.24	0.33	0.05	175.9	17,575	96.4
106.9	0.00	0.01	0.02	0.04	0.07	0.08	0.10	0.17	0.24	0.33	0.05	175.9	17,722	97.2
110.9	0.00	0.01	0.02	0.04	0.07	0.07	0.10	0.16	0.24	0.34	0.05	175.3	17,874	98.1
114.9	0.00	0.01	0.02	0.04	0.07	0.07	0.10	0.16	0.24	0.34	0.05	175.8	17,966	98.6
118.9	0.00	0.01	0.02	0.04	0.07	0.07	0.10	0.16	0.24	0.35	0.05	176.6	18,055	99.1
122.9	0.00	0.01	0.02	0.04	0.06	0.07	0.09	0.16	0.24	0.35	0.05	176.8	18,133	99.5
126.9	0.00	0.01	0.02	0.04	0.06	0.07	0.09	0.15	0.24	0.33	0.04	177.8	18,183	99.8
130.9	0.00	0.01	0.02	0.04	0.06	0.07	0.09	0.15	0.23	0.34	0.04	179.1	18,206	99.9
134.9	0.00	0.01	0.02	0.04	0.06	0.07	0.09	0.15	0.23	0.34	0.04	181.3	18,216	100.0
138.9	0.00	0.01	0.02	0.04	0.06	0.07	0.09	0.15	0.23	0.34	0.04	180.8	18,216	100.0
142.9	0.00	0.01	0.02	0.04	0.06	0.07	0.10	0.16	0.22	0.34	0.04	181.3	18,218	100.0
146.9	0.00	0.01	0.02	0.04	0.06	0.07	0.09	0.16	0.21	0.33	0.04	183.6	18,219	100.0
150.9	0.00	0.01	0.02	0.04	0.06	0.07	0.09	0.16	0.21	0.34	0.04	183.4	18,222	100.0
154.9	0.00	0.01	0.01	0.03	0.05	0.06	0.08	0.14	0.19	0.35	0.04	184.2	18,221	100.0
158.9	0.00	0.00	0.00	0.01	0.02	0.02	0.02	0.04	0.06	0.28	0.02	35.7	18,224	100.0
162.9	0.00	0.01	0.02	0.04	0.07	0.07	0.10	0.16	0.21	0.33	0.04	182.7	18,223	100.0
166.9	0.00	0.01	0.02	0.04	0.06	0.07	0.10	0.16	0.21	0.31	0.04	182.9	18,224	100.0
170.9	0.00	0.01	0.02	0.04	0.06	0.07	0.10	0.16	0.21	0.30	0.04	183.6	18,223	100.0
174.9	0.00	0.01	0.02	0.04	0.06	0.07	0.10	0.16	0.21	0.31	0.04	184.2	18,224	100.0
178.9	0.00	0.01	0.02	0.04	0.06	0.07	0.09	0.16	0.21	0.30	0.04	186.4	18,224	100.0
182.9	0.00	0.01	0.02	0.04	0.06	0.07	0.09	0.16	0.21	0.29	0.04	188.8	18,224	100.0
186.9	0.00	0.01	0.02	0.04	0.06	0.07	0.09	0.16	0.20	0.28	0.04	197.4	18,224	100.0
190.9	0.00	0.01	0.02	0.04	0.06	0.07	0.09	0.15	0.20	0.28	0.04	215.7	18,224	100.0
194.9	0.00	0.01	0.02	0.04	0.06	0.07	0.09	0.15	0.20	0.26	0.04	257.5	18,224	100.0
198.9	0.00	0.01	0.02	0.04	0.06	0.06	0.09	0.14	0.19	0.26	0.04	309.6	18,224	100.0

Table 22: Summary statistics of current speed, vector-averaged direction and number of valid records by bin depth at BR-3-16 based on the data acquired with the LR ADCP #18785 from 2016 to 2017.

Bin Depth (m)	Min Speed (m/s)	1%ile Speed (m/s)	5%ile Speed (m/s)	25%ile Speed (m/s)	Median Speed (m/s)	Mean Speed (m/s)	75%ile Speed (m/s)	95%ile Speed (m/s)	99%ile Speed (m/s)	Max Speed (m/s)	Standard Deviation Speed (m/s)	Vector-Averaged Direction (deg TN)	Number of Valid Records	% of Valid Data (%)
56.4	0.0	0.01	0.01	0.04	0.06	0.07	0.10	0.17	0.23	0.34	0.05	206.7	8,827	96.9
72.4	0.0	0.01	0.01	0.04	0.06	0.07	0.09	0.16	0.22	0.28	0.04	222.8	8,625	94.7
88.4	0.0	0.01	0.01	0.03	0.06	0.07	0.09	0.16	0.22	0.37	0.04	322.0	8,523	93.5
104.4	0.0	0.01	0.01	0.03	0.05	0.06	0.08	0.15	0.23	0.30	0.04	1.5	8,619	94.6
120.4	0.0	0.01	0.01	0.03	0.05	0.06	0.08	0.15	0.23	0.32	0.04	7.5	8,740	95.9
136.4	0.0	0.01	0.01	0.03	0.05	0.06	0.08	0.14	0.22	0.34	0.04	3.8	8,858	97.2
152.4	0.0	0.01	0.01	0.03	0.05	0.06	0.08	0.15	0.21	0.30	0.04	1.1	8,985	98.6
168.4	0.0	0.01	0.01	0.03	0.05	0.06	0.08	0.15	0.20	0.29	0.04	2.1	9,045	99.3
184.4	0.0	0.01	0.01	0.03	0.05	0.06	0.08	0.15	0.19	0.24	0.04	3.1	9,073	99.6
200.4	0.0	0.01	0.01	0.03	0.05	0.06	0.08	0.14	0.19	0.26	0.04	2.6	9,085	99.7
216.4	0.0	0.01	0.01	0.03	0.05	0.06	0.08	0.13	0.17	0.24	0.04	359.6	9,100	99.9
232.4	0.0	0.01	0.01	0.03	0.05	0.05	0.07	0.12	0.16	0.23	0.03	357.1	9,102	99.9
248.4	0.0	0.01	0.01	0.03	0.05	0.05	0.07	0.12	0.17	0.23	0.03	355.3	9,104	99.9
264.4	0.0	0.01	0.01	0.03	0.05	0.05	0.07	0.12	0.17	0.24	0.03	353.0	9,104	99.9
280.4	0.0	0.01	0.01	0.03	0.04	0.05	0.07	0.12	0.17	0.24	0.03	351.3	9,108	100.0
296.4	0.0	0.01	0.01	0.03	0.04	0.05	0.06	0.11	0.15	0.23	0.03	352.0	9,110	100.0
312.4	0.0	0.00	0.01	0.03	0.04	0.05	0.06	0.11	0.15	0.24	0.03	353.2	9,112	100.0
328.4	0.0	0.00	0.01	0.03	0.04	0.05	0.06	0.11	0.16	0.23	0.03	355.0	9,112	100.0
344.4	0.0	0.00	0.01	0.03	0.04	0.05	0.06	0.11	0.16	0.22	0.03	353.9	9,112	100.0
360.4	0.0	0.00	0.01	0.02	0.04	0.05	0.06	0.10	0.16	0.24	0.03	355.2	9,112	100.0
376.4	0.0	0.01	0.01	0.03	0.04	0.05	0.07	0.11	0.17	0.25	0.03	355.3	9,112	100.0
392.4	0.0	0.00	0.01	0.03	0.04	0.05	0.07	0.11	0.16	0.24	0.03	356.1	9,112	100.0
408.4	0.0	0.00	0.01	0.03	0.04	0.05	0.07	0.11	0.17	0.25	0.03	356.6	9,112	100.0
424.4	0.0	0.00	0.01	0.03	0.04	0.05	0.07	0.12	0.17	0.23	0.03	357.7	9,112	100.0
440.4	0.0	0.00	0.01	0.03	0.04	0.05	0.07	0.12	0.17	0.22	0.03	358.1	9,112	100.0
456.4	0.0	0.00	0.01	0.03	0.04	0.05	0.07	0.12	0.17	0.24	0.03	357.7	9,112	100.0
472.4	0.0	0.00	0.01	0.03	0.05	0.05	0.07	0.12	0.17	0.25	0.04	1.3	9,112	100.0

Table 23: Summary statistics of current speed, vector-averaged direction and number of valid records at 601.5 and 712.8 m depth at BR-3-16 as based on the data acquired with the Aquadopp DW #8447 and #9473 from 2016 to 2017.

Bin Depth (m)	Min Speed (m/s)	1%ile Speed (m/s)	5%ile Speed (m/s)	25%ile Speed (m/s)	Median Speed (m/s)	Mean Speed (m/s)	75%ile Speed (m/s)	95%ile Speed (m/s)	99%ile Speed (m/s)	Max Speed (m/s)	Standard Deviation Speed (m/s)	Vector-Averaged Direction (deg TN)	Number of Valid Records	% of Valid Data (%)
601.5	0.0	0.00	0.01	0.03	0.05	0.06	0.08	0.13	0.18	0.22	0.04	343.0	9,112	100.0
712.8	0.0	0.00	0.01	0.03	0.05	0.07	0.09	0.16	0.24	0.31	0.05	336.1	9,113	100.0

Table 24: Summary statistics of current speed, vector-averaged direction and number of valid records by bin depth at BR-G-16 based on the data acquired with the QM ADCP #12699 from 2016 to 2017. Bin depths flagged manually as part of the QA/QC are highlighted in red.

Bin Depth (m)	Min Speed (m/s)	1%ile Speed (m/s)	5%ile Speed (m/s)	25%ile Speed (m/s)	Median Speed (m/s)	Mean Speed (m/s)	75%ile Speed (m/s)	95%ile Speed (m/s)	99%ile Speed (m/s)	Max Speed (m/s)	Standard Deviation Speed (m/s)	Vector-Averaged Direction (deg TN)	Number of Valid Records	% of Valid Data (%)
29.2	0.0	0.01	0.02	0.06	0.11	0.14	0.20	0.33	0.40	0.52	0.10	225.5	36,404	96.8
33.2	0.0	0.01	0.02	0.06	0.11	0.14	0.19	0.32	0.39	0.55	0.09	226.4	36,781	97.8
37.2	0.0	0.01	0.02	0.06	0.11	0.13	0.19	0.32	0.39	0.52	0.09	227.2	36,965	98.3
41.2	0.0	0.01	0.02	0.06	0.12	0.13	0.19	0.31	0.40	0.51	0.09	227.6	36,997	98.3
45.2	0.0	0.01	0.02	0.06	0.12	0.13	0.19	0.31	0.40	0.51	0.09	228.7	37,022	98.4
49.2	0.0	0.01	0.02	0.07	0.12	0.13	0.18	0.30	0.41	0.50	0.09	228.9	36,937	98.2
53.2	0.0	0.01	0.03	0.07	0.12	0.13	0.18	0.29	0.41	0.51	0.09	229.2	36,837	97.9
57.2	0.0	0.01	0.03	0.07	0.12	0.13	0.18	0.28	0.42	0.55	0.08	230.5	36,605	97.3
61.2	0.0	0.01	0.01	0.03	0.06	0.09	0.12	0.26	0.42	0.57	0.08	230.4	37,370	99.3
65.2	0.0	0.01	0.03	0.06	0.11	0.12	0.16	0.27	0.43	0.59	0.08	230.3	37,125	98.7
69.2	0.0	0.01	0.03	0.07	0.12	0.13	0.18	0.29	0.43	0.59	0.08	233.4	37,083	98.6
73.2	0.0	0.01	0.03	0.08	0.12	0.14	0.18	0.29	0.45	0.63	0.09	233.2	37,192	98.9
77.2	0.0	0.01	0.03	0.07	0.12	0.14	0.18	0.29	0.45	0.68	0.09	233.4	37,306	99.2
81.2	0.0	0.01	0.03	0.08	0.12	0.14	0.18	0.29	0.46	0.75	0.09	234.3	37,347	99.3
85.2	0.0	0.01	0.03	0.07	0.12	0.14	0.18	0.30	0.47	0.71	0.09	234.7	37,357	99.3
89.2	0.0	0.01	0.03	0.08	0.12	0.14	0.18	0.31	0.49	0.73	0.09	236.6	37,376	99.4
93.2	0.0	0.01	0.03	0.08	0.12	0.14	0.18	0.31	0.50	0.76	0.09	237.3	37,399	99.4

Bin Depth (m)	Min Speed (m/s)	1%ile Speed (m/s)	5%ile Speed (m/s)	25%ile Speed (m/s)	Median Speed (m/s)	Mean Speed (m/s)	75%ile Speed (m/s)	95%ile Speed (m/s)	99%ile Speed (m/s)	Max Speed (m/s)	Standard Deviation Speed (m/s)	Vector-Averaged Direction (deg TN)	Number of Valid Records	% of Valid Data (%)
97.2	0.0	0.01	0.03	0.08	0.12	0.14	0.18	0.32	0.50	0.81	0.10	238.4	37,411	99.5
101.2	0.0	0.01	0.03	0.07	0.12	0.14	0.18	0.33	0.51	0.82	0.10	239.2	37,430	99.5
105.2	0.0	0.01	0.03	0.07	0.12	0.14	0.18	0.34	0.51	0.79	0.10	239.7	37,442	99.5
109.2	0.0	0.01	0.03	0.07	0.12	0.14	0.18	0.34	0.51	0.78	0.10	240.1	37,479	99.6
113.2	0.0	0.01	0.03	0.07	0.12	0.14	0.18	0.33	0.50	0.74	0.10	239.8	37,508	99.7
117.2	0.0	0.01	0.03	0.07	0.12	0.14	0.18	0.33	0.50	0.72	0.10	240.0	37,536	99.8
121.2	0.0	0.02	0.03	0.07	0.11	0.13	0.15	0.29	0.47	0.69	0.08	233.9	37,525	99.8
125.2	0.0	0.00	0.00	0.01	0.02	0.03	0.03	0.08	0.26	0.58	0.04	270.0	37,616	100.0
129.2	0.0	0.01	0.03	0.07	0.11	0.12	0.16	0.27	0.36	0.48	0.07	224.7	37,587	99.9
133.2	0.0	0.01	0.03	0.07	0.11	0.13	0.17	0.30	0.40	0.51	0.08	234.7	37,607	100.0
137.2	0.0	0.01	0.03	0.07	0.11	0.13	0.17	0.29	0.40	0.50	0.08	233.3	37,614	100.0
141.2	0.0	0.01	0.03	0.07	0.11	0.13	0.17	0.28	0.38	0.52	0.08	232.0	37,615	100.0
145.2	0.0	0.01	0.03	0.07	0.11	0.12	0.16	0.27	0.36	0.48	0.08	231.3	37,617	100.0
149.2	0.0	0.01	0.03	0.06	0.11	0.12	0.16	0.26	0.35	0.48	0.07	231.9	37,618	100.0
153.2	0.0	0.01	0.02	0.06	0.10	0.12	0.15	0.25	0.33	0.46	0.07	231.2	37,618	100.0
157.2	0.0	0.01	0.02	0.06	0.10	0.11	0.15	0.24	0.32	0.46	0.07	230.4	37,618	100.0
161.2	0.0	0.01	0.02	0.06	0.10	0.11	0.15	0.23	0.30	0.46	0.07	230.7	37,618	100.0
165.2	0.0	0.01	0.02	0.06	0.10	0.11	0.14	0.22	0.28	0.45	0.06	230.7	37,618	100.0

Table 25: Summary statistics of current speed, vector-averaged direction and number of valid records by bin depth at BR-G-16 based on the data acquired with the LR ADCP #13079 from 2016 to 2017.

Bin Depth (m)	Min Speed (m/s)	1%ile Speed (m/s)	5%ile Speed (m/s)	25%ile Speed (m/s)	Median Speed (m/s)	Mean Speed (m/s)	75%ile Speed (m/s)	95%ile Speed (m/s)	99%ile Speed (m/s)	Max Speed (m/s)	Standard Deviation Speed (m/s)	Vector-Averaged Direction (deg TN)	Number of Valid Records	% of Valid Data (%)
44.4	0.0	0.01	0.02	0.06	0.11	0.12	0.17	0.27	0.33	0.48	0.08	200.8	15,767	83.8
60.2	0.0	0.01	0.03	0.07	0.12	0.13	0.17	0.29	0.43	0.57	0.08	199.3	18,502	98.4
76.2	0.0	0.01	0.03	0.07	0.12	0.13	0.18	0.29	0.44	0.64	0.09	192.7	18,129	96.4
92.2	0.0	0.01	0.03	0.07	0.12	0.14	0.18	0.32	0.47	0.73	0.09	189.0	17,678	94.0
108.2	0.0	0.01	0.03	0.07	0.12	0.14	0.18	0.33	0.48	0.72	0.10	188.3	17,595	93.5
124.2	0.0	0.01	0.03	0.07	0.11	0.13	0.17	0.30	0.45	0.59	0.09	185.8	17,777	94.5
140.2	0.0	0.01	0.03	0.06	0.10	0.11	0.15	0.25	0.35	0.46	0.07	183.5	18,267	97.1
156.2	0.0	0.01	0.03	0.06	0.10	0.11	0.15	0.23	0.28	0.44	0.06	177.4	18,405	97.9
172.2	0.0	0.01	0.02	0.06	0.09	0.10	0.13	0.19	0.24	0.44	0.05	172.7	18,576	98.8
188.2	0.0	0.01	0.02	0.05	0.07	0.08	0.11	0.16	0.21	0.40	0.04	163.7	18,636	99.1
204.2	0.0	0.01	0.02	0.04	0.06	0.07	0.09	0.14	0.18	0.40	0.04	151.5	18,703	99.4
220.2	0.0	0.01	0.02	0.04	0.06	0.06	0.08	0.12	0.16	0.44	0.03	133.9	18,744	99.7
236.2	0.0	0.01	0.01	0.03	0.05	0.05	0.07	0.11	0.15	0.41	0.03	108.7	18,780	99.8
252.2	0.0	0.01	0.01	0.03	0.05	0.05	0.07	0.10	0.14	0.35	0.03	87.1	18,792	99.9
268.2	0.0	0.01	0.01	0.03	0.04	0.05	0.06	0.10	0.13	0.39	0.03	75.3	18,795	99.9
284.2	0.0	0.01	0.01	0.03	0.04	0.05	0.06	0.09	0.13	0.34	0.03	69.1	18,803	100.0
300.2	0.0	0.00	0.01	0.03	0.04	0.04	0.06	0.09	0.12	0.34	0.02	65.3	18,806	100.0
316.2	0.0	0.00	0.01	0.02	0.04	0.04	0.05	0.08	0.11	0.33	0.02	62.5	18,807	100.0
332.2	0.0	0.00	0.01	0.02	0.04	0.04	0.05	0.09	0.11	0.34	0.02	61.4	18,808	100.0
348.2	0.0	0.00	0.01	0.02	0.04	0.04	0.05	0.08	0.11	0.30	0.02	59.2	18,809	100.0
364.2	0.0	0.00	0.01	0.02	0.04	0.04	0.05	0.08	0.11	0.32	0.02	56.1	18,809	100.0
380.2	0.0	0.00	0.01	0.02	0.04	0.04	0.05	0.08	0.11	0.38	0.02	53.3	18,809	100.0
396.2	0.0	0.00	0.01	0.02	0.04	0.04	0.05	0.08	0.11	0.40	0.02	52.2	18,809	100.0
412.2	0.0	0.00	0.01	0.02	0.04	0.04	0.05	0.08	0.12	0.38	0.02	48.6	18,809	100.0
428.2	0.0	0.00	0.01	0.02	0.04	0.04	0.05	0.08	0.12	0.38	0.02	45.5	18,809	100.0

Table 26: Summary statistics of current speed, vector-averaged direction and number of valid records at 564.8 and 674.3 m depth at BR-G-16 as based on the data acquired with the Aquadopp DW #8419 and #8442 from 2016 to 2017.

Bin Depth (m)	Min Speed (m/s)	1%ile Speed (m/s)	5%ile Speed (m/s)	25%ile Speed (m/s)	Median Speed (m/s)	Mean Speed (m/s)	75%ile Speed (m/s)	95%ile Speed (m/s)	99%ile Speed (m/s)	Max Speed (m/s)	Standard Deviation Speed (m/s)	Vector-Averaged Direction (deg TN)	Number of Valid Records	% of Valid Data (%)
564.8	0.0	0.00	0.01	0.02	0.03	0.04	0.05	0.08	0.10	0.17	0.02	24.1	18,809	100.0
674.3	0.0	0.00	0.01	0.02	0.04	0.04	0.06	0.11	0.15	0.24	0.03	50.4	18,809	100.0

Table 27: Summary statistics of current speed, vector-averaged direction and number of valid records by bin depth at BR-K-16 based on the data acquired with the WHS ADCP #7844 from 2016 to 2017.

Bin Depth (m)	Min Speed (m/s)	1%ile Speed (m/s)	5%ile Speed (m/s)	25%ile Speed (m/s)	Median Speed (m/s)	Mean Speed (m/s)	75%ile Speed (m/s)	95%ile Speed (m/s)	99%ile Speed (m/s)	Max Speed (m/s)	Standard Deviation Speed (m/s)	Vector-Averaged Direction (deg TN)	Number of Valid Records	% of Valid Data (%)
21.4	0.0	0.01	0.03	0.08	0.14	0.15	0.20	0.29	0.37	0.49	0.08	99.8	3,718	22.8
29.4	0.0	0.01	0.03	0.08	0.13	0.14	0.19	0.30	0.38	0.54	0.08	95.2	6,090	37.3
37.4	0.0	0.01	0.03	0.07	0.13	0.14	0.19	0.31	0.44	0.69	0.09	97.1	8,460	51.8
45.4	0.0	0.01	0.03	0.07	0.12	0.14	0.19	0.33	0.47	0.98	0.10	94.7	10,584	64.8
53.4	0.0	0.01	0.03	0.07	0.12	0.15	0.20	0.35	0.52	1.08	0.11	88.6	11,739	71.9
61.4	0.0	0.01	0.03	0.08	0.13	0.16	0.22	0.37	0.54	1.04	0.12	86.4	12,616	77.3
69.4	0.0	0.01	0.03	0.08	0.14	0.17	0.24	0.38	0.55	1.03	0.12	85.5	13,310	81.5
77.4	0.0	0.01	0.03	0.08	0.15	0.18	0.25	0.39	0.56	0.97	0.12	88.7	14,200	87.0
85.4	0.0	0.01	0.03	0.08	0.15	0.18	0.25	0.41	0.56	0.94	0.13	95.4	15,566	95.3
93.4	0.0	0.01	0.03	0.08	0.15	0.18	0.25	0.43	0.57	0.92	0.13	96.9	16,276	99.7
101.4	0.0	0.01	0.03	0.08	0.15	0.18	0.25	0.46	0.59	0.87	0.13	92.9	16,329	100.0
109.4	0.0	0.01	0.03	0.08	0.15	0.18	0.25	0.45	0.58	0.84	0.13	85.9	16,329	100.0
117.4	0.0	0.01	0.03	0.08	0.15	0.17	0.24	0.41	0.55	0.79	0.12	80.1	16,329	100.0
125.4	0.0	0.01	0.02	0.05	0.09	0.12	0.16	0.29	0.42	0.72	0.09	74.5	16,329	100.0

Table 28: Summary statistics of current speed, vector-averaged direction and number of valid records by bin depth at BR-K-16 based on the data acquired with the Nortek Aquadopp Profiler #1147 from 2016 to 2017. Bin depths flagged manually as part of the QA/QC are highlighted in red.

Bin Depth (m)	Min Speed (m/s)	1%ile Speed (m/s)	5%ile Speed (m/s)	25%ile Speed (m/s)	Median Speed (m/s)	Mean Speed (m/s)	75%ile Speed (m/s)	95%ile Speed (m/s)	99%ile Speed (m/s)	Max Speed (m/s)	Standard Deviation Speed (m/s)	Vector-Averaged Direction (deg TN)	Number of Valid Records	% of Valid Data (%)
150.0	0.0	0.02	0.05	0.12	0.19	0.20	0.26	0.37	0.46	0.63	0.10	51.7	9,277	99.9
151.0	0.0	0.01	0.02	0.06	0.09	0.10	0.13	0.22	0.31	0.56	0.06	75.2	9,285	100.0
152.0	0.0	0.01	0.02	0.06	0.09	0.11	0.15	0.25	0.33	0.55	0.07	69	9,285	100.0
153.0	0.0	0.01	0.02	0.05	0.09	0.11	0.15	0.29	0.40	0.56	0.09	74.6	9,285	100.0
154.0	0.0	0.01	0.02	0.05	0.08	0.11	0.15	0.29	0.39	0.53	0.09	75.9	9,285	100.0
155.0	0.0	0.01	0.02	0.04	0.08	0.11	0.14	0.28	0.38	0.55	0.08	75.6	9,285	100.0
156.0	0.0	0.01	0.02	0.04	0.08	0.10	0.14	0.27	0.38	0.53	0.08	74	9,285	100.0
157.0	0.0	0.01	0.01	0.04	0.07	0.10	0.13	0.26	0.37	0.53	0.08	72.8	9,285	100.0
158.0	0.0	0.01	0.01	0.04	0.07	0.09	0.13	0.25	0.36	0.51	0.08	71.5	9,285	100.0
159.0	0.0	0.01	0.01	0.04	0.07	0.09	0.12	0.24	0.34	0.51	0.07	69.9	9,285	100.0
160.0	0.0	0.01	0.01	0.03	0.06	0.08	0.11	0.23	0.33	0.47	0.07	68.5	9,285	100.0
161.0	0.0	0.01	0.01	0.03	0.06	0.08	0.11	0.21	0.31	0.46	0.06	65.8	9,285	100.0
162.0	0.0	0.01	0.01	0.03	0.06	0.07	0.10	0.19	0.29	0.45	0.06	62.8	9,285	100.0
163.0	0.0	0.01	0.01	0.03	0.06	0.07	0.09	0.17	0.23	0.38	0.05	53.2	9,285	100.0

Table 29: Summary statistics of current speed, vector-averaged direction and number of valid records by bin depth at DFO-2-16 based on the data acquired with the NB ADCP #586 from 2016 to 2017.

Bin Depth (m)	Min Speed (m/s)	1%ile Speed (m/s)	5%ile Speed (m/s)	25%ile Speed (m/s)	Median Speed (m/s)	Mean Speed (m/s)	75%ile Speed (m/s)	95%ile Speed (m/s)	99%ile Speed (m/s)	Max Speed (m/s)	Standard Deviation Speed (m/s)	Vector-Averaged Direction (deg TN)	Number of Valid Records	% of Valid Data (%)
16.1	0.0	0.01	0.02	0.04	0.07	0.08	0.11	0.19	0.26	0.41	0.06	251.6	7,040	41
20.0	0.0	0.01	0.02	0.05	0.09	0.11	0.15	0.26	0.36	0.49	0.08	244.5	15,187	88
23.9	0.0	0.01	0.02	0.05	0.09	0.11	0.15	0.28	0.39	0.58	0.08	243.9	15,509	90
27.8	0.0	0.01	0.02	0.05	0.09	0.11	0.15	0.28	0.40	0.60	0.08	243.5	15,884	92
31.8	0.0	0.01	0.02	0.05	0.09	0.11	0.15	0.27	0.39	0.57	0.08	242.8	16,374	95
35.7	0.0	0.01	0.02	0.05	0.09	0.11	0.15	0.27	0.38	0.55	0.08	242.2	16,794	97
39.6	0.0	0.01	0.02	0.05	0.09	0.11	0.15	0.26	0.38	0.55	0.08	241.6	17,182	99
43.5	0.0	0.01	0.02	0.05	0.09	0.11	0.15	0.26	0.37	0.54	0.08	241.2	17,182	99
47.4	0.0	0.01	0.02	0.05	0.09	0.11	0.14	0.24	0.36	0.53	0.07	239.9	17,109	99
51.3	0.0	0.01	0.02	0.06	0.09	0.11	0.14	0.24	0.36	0.50	0.07	239.8	17,203	99
55.2	0.0	0.01	0.03	0.06	0.10	0.12	0.15	0.27	0.36	0.50	0.08	240.3	17,277	100
59.1	0.0	0.01	0.03	0.06	0.10	0.12	0.16	0.27	0.36	0.49	0.07	240.3	17,280	100
63.0	0.0	0.01	0.03	0.07	0.11	0.12	0.16	0.27	0.36	0.50	0.07	239.4	17,290	100
66.9	0.0	0.01	0.03	0.07	0.11	0.12	0.16	0.27	0.35	0.47	0.07	239.3	17,287	100
70.9	0.0	0.01	0.03	0.07	0.11	0.12	0.16	0.27	0.35	0.49	0.07	243.0	17,290	100
74.8	0.0	0.01	0.03	0.07	0.11	0.12	0.16	0.26	0.34	0.49	0.07	258.3	17,288	100
78.7	0.0	0.01	0.03	0.07	0.11	0.12	0.16	0.25	0.34	0.50	0.07	18.3	17,291	100
82.6	0.0	0.01	0.03	0.06	0.10	0.11	0.15	0.25	0.33	0.50	0.07	42.9	17,284	100
86.5	0.0	0.01	0.02	0.06	0.09	0.11	0.14	0.23	0.31	0.52	0.07	47.8	17,286	100
90.4	0.0	0.01	0.02	0.05	0.08	0.10	0.13	0.21	0.28	0.53	0.06	50.3	17,278	100
94.3	0.0	0.01	0.02	0.05	0.08	0.09	0.12	0.20	0.27	0.50	0.06	52.9	17,285	100
98.2	0.0	0.01	0.02	0.04	0.06	0.08	0.10	0.19	0.26	0.48	0.05	55.2	17,284	100
102.1	0.0	0.01	0.01	0.04	0.06	0.07	0.10	0.17	0.25	0.47	0.05	53.1	17,324	100

Table 30: Summary statistics of current speed, vector-averaged direction and number of valid records by bin depth at DFO-1-16 based on the data acquired with the WHS ADCP #12463 from 2016 to 2017.

Bin Depth (m)	Min Speed (m/s)	1%ile Speed (m/s)	5%ile Speed (m/s)	25%ile Speed (m/s)	Median Speed (m/s)	Mean Speed (m/s)	75%ile Speed (m/s)	95%ile Speed (m/s)	99%ile Speed (m/s)	Max Speed (m/s)	Standard Deviation Speed (m/s)	Vector-Averaged Direction (deg TN)	Number of Valid Records	% of Valid Data (%)
6.8	0.0	0.01	0.02	0.05	0.09	0.11	0.15	0.26	0.37	0.68	0.08	203.6	13,208	74
8.8	0.0	0.01	0.02	0.05	0.09	0.10	0.14	0.24	0.34	0.64	0.07	201.4	15,827	89
10.8	0.0	0.01	0.02	0.05	0.08	0.10	0.13	0.22	0.30	0.56	0.07	197.5	16,816	95
12.8	0.0	0.01	0.02	0.05	0.08	0.10	0.13	0.22	0.28	0.42	0.06	193.4	17,212	97
14.8	0.0	0.01	0.02	0.05	0.08	0.09	0.13	0.21	0.27	0.42	0.06	189.5	17,470	98
16.9	0.0	0.01	0.02	0.05	0.08	0.09	0.13	0.21	0.27	0.40	0.06	186.8	17,557	99
18.9	0.0	0.01	0.02	0.05	0.08	0.09	0.13	0.20	0.26	0.38	0.06	184.4	17,610	99
20.9	0.0	0.01	0.02	0.05	0.08	0.09	0.12	0.20	0.26	0.36	0.06	183.4	17,629	99
22.9	0.0	0.01	0.02	0.05	0.08	0.09	0.12	0.20	0.26	0.35	0.06	181.8	17,659	99
24.9	0.0	0.01	0.02	0.05	0.08	0.09	0.12	0.20	0.26	0.36	0.06	179.4	17,682	100
26.9	0.0	0.01	0.02	0.05	0.08	0.09	0.12	0.20	0.26	0.37	0.06	177.4	17,691	100
28.9	0.0	0.01	0.02	0.05	0.08	0.09	0.12	0.20	0.26	0.40	0.06	176.4	17,708	100
30.9	0.0	0.01	0.02	0.05	0.08	0.09	0.12	0.20	0.26	0.40	0.06	174.5	17,697	100
32.9	0.0	0.01	0.02	0.05	0.08	0.09	0.12	0.20	0.26	0.40	0.06	172.8	17,696	100
34.9	0.0	0.01	0.02	0.05	0.08	0.09	0.12	0.20	0.27	0.40	0.06	170.7	17,707	100
36.9	0.0	0.01	0.02	0.05	0.08	0.09	0.12	0.20	0.28	0.40	0.06	168.5	17,725	100
38.9	0.0	0.01	0.02	0.05	0.08	0.09	0.12	0.21	0.27	0.40	0.06	167.0	17,728	100
40.9	0.0	0.01	0.02	0.05	0.08	0.09	0.12	0.21	0.27	0.39	0.06	164.7	17,725	100
42.9	0.0	0.01	0.02	0.05	0.08	0.09	0.12	0.20	0.27	0.40	0.06	162.3	17,732	100
44.9	0.0	0.01	0.02	0.05	0.08	0.09	0.12	0.21	0.27	0.39	0.06	160.0	17,739	100
46.9	0.0	0.01	0.02	0.04	0.07	0.09	0.11	0.20	0.27	0.36	0.06	157.2	17,751	100

Table 31: Summary statistics of current speed, vector-averaged direction and number of valid records by bin depth at DFO-9-16 based on the data acquired with the WHS ADCP #2412 from 2016 to 2017.

Bin Depth (m)	Min Speed (m/s)	1%ile Speed (m/s)	5%ile Speed (m/s)	25%ile Speed (m/s)	Median Speed (m/s)	Mean Speed (m/s)	75%ile Speed (m/s)	95%ile Speed (m/s)	99%ile Speed (m/s)	Max Speed (m/s)	Standard Deviation Speed (m/s)	Vector-Averaged Direction (deg TN)	Number of Valid Records	% of Valid Data (%)
3.3	0.0	0.01	0.03	0.07	0.14	0.16	0.23	0.37	0.54	0.84	0.11	296.8	7,042	40
4.3	0.0	0.01	0.01	0.04	0.09	0.12	0.17	0.30	0.47	0.82	0.10	279.7	10,906	61
5.3	0.0	0.00	0.01	0.03	0.08	0.10	0.15	0.27	0.41	0.86	0.09	254.6	11,828	67
6.3	0.0	0.01	0.01	0.03	0.07	0.10	0.14	0.26	0.39	0.73	0.09	238.7	12,459	70
7.3	0.0	0.01	0.01	0.03	0.07	0.09	0.13	0.24	0.38	0.70	0.08	235.1	13,112	74
8.3	0.0	0.00	0.01	0.03	0.06	0.09	0.12	0.23	0.35	0.69	0.07	230.9	13,795	78
9.3	0.0	0.00	0.01	0.03	0.06	0.08	0.12	0.22	0.32	0.68	0.07	230.3	14,394	81
10.3	0.0	0.00	0.01	0.03	0.06	0.08	0.12	0.21	0.30	0.60	0.07	229.5	14,871	84
11.3	0.0	0.00	0.01	0.03	0.06	0.08	0.12	0.21	0.28	0.57	0.07	230.1	15,615	88
12.3	0.0	0.00	0.01	0.03	0.06	0.08	0.11	0.20	0.28	0.56	0.06	232.1	15,960	90
13.3	0.0	0.01	0.01	0.03	0.06	0.08	0.11	0.20	0.28	0.52	0.06	235.7	16,337	92
14.3	0.0	0.01	0.01	0.03	0.06	0.08	0.11	0.20	0.28	0.51	0.06	239.2	16,642	94
15.3	0.0	0.01	0.01	0.03	0.06	0.08	0.11	0.20	0.28	0.56	0.06	243.2	16,938	95
16.3	0.0	0.01	0.01	0.04	0.06	0.08	0.11	0.20	0.28	0.57	0.06	249.8	17,155	97
17.3	0.0	0.01	0.02	0.04	0.07	0.08	0.11	0.20	0.28	0.57	0.06	256.4	17,313	98
18.3	0.0	0.01	0.02	0.04	0.07	0.08	0.11	0.19	0.27	0.53	0.06	261.5	17,448	98
19.3	0.0	0.01	0.02	0.05	0.07	0.09	0.11	0.19	0.27	0.51	0.06	267.4	17,535	99
20.3	0.0	0.01	0.02	0.05	0.08	0.09	0.11	0.19	0.27	0.48	0.06	272.6	17,636	99
21.3	0.0	0.01	0.02	0.05	0.08	0.09	0.12	0.19	0.26	0.48	0.05	274.4	17,669	100
22.3	0.0	0.01	0.02	0.05	0.08	0.09	0.12	0.18	0.26	0.43	0.05	275.0	17,675	100
23.3	0.0	0.01	0.02	0.05	0.08	0.09	0.11	0.18	0.25	0.40	0.05	275.7	17,661	99
24.3	0.0	0.01	0.02	0.05	0.07	0.08	0.11	0.17	0.25	0.37	0.05	276.0	17,664	100
25.3	0.0	0.01	0.02	0.04	0.07	0.08	0.10	0.16	0.24	0.38	0.05	270.5	17,663	99
26.3	0.0	0.01	0.02	0.04	0.06	0.07	0.09	0.15	0.23	0.38	0.05	202.5	17,666	100
27.3	0.0	0.01	0.02	0.04	0.06	0.07	0.09	0.14	0.22	0.35	0.04	150.6	17,649	99
28.3	0.0	0.01	0.01	0.03	0.06	0.06	0.08	0.14	0.22	0.38	0.04	174.3	17,747	100

Executive Summary

This report describes the 2018-2019 activities of the integrated Beaufort Observatory (iBO), a four-year program (2015-2018) managed by ArcticNet in partnership with Fisheries and Oceans Canada and Golder Associates Ltd. iBO is supported by the Environmental Studies Research Fund and Imperial Oil Resources Ventures Limited. iBO aims to contribute key oceanographic information required for decisions on development and regulations in the offshore Canadian Beaufort Sea by extending existing time-series measurements and integrating regional understanding of the shelf and slope environment through year-round measurements acquired by autonomous measuring systems on subsurface moorings.

The activities described in this report focus on the turnaround of 2 of 7 moorings which constitute the backbone of the iBO observational program, initially deployed in 2014. Five of the 7 moorings could not be recovered in 2018 due to greater than normal ice concentration in the southern Beaufort Sea. These provide the means to obtain a regionally-integrated ice and ocean dataset. The main goal of this report is to provide an initial review of the dataset acquired during 2017-2018 through the operation of these 2 moorings. Only the data components processed thus far are presented; these include all current meter and current profiler data, and temperature-salinity data. Budget is not available under the current Environmental Studies Research Fund (ESRF) funding to process the complete ice-profiling sonar dataset due to the intensive nature of data processing requirements. The data is therefore being processed under a separate budget with support from DFO. Analyses on the sediment trap samples are currently pending additional funding from the LTOO project. Data acquired using ice-profiling sonar and sediment traps will be presented as an addendum to the present report at a later date as funding becomes available for processing of the data.

For each presented dataset, the spatial and temporal variability is discussed and events of interest that warrant further investigation are identified. A statistical analysis of the mean current patterns near the surface and near the bottom is provided. The concluding remarks provide a summary of oceanographic phenomena that could be targeted for further study. Lessons learned stemming from the 2018 operations as well as objectives and milestones for iBO in 2019-2020 are also summarized. Finally, a summary of the full iBO 2014-2018 dataset is provided which includes an overview of the data recovery success and inter-annual trends within the program measurement interval.

Table of Contents

1.0	INTRODUCTION.....	1
1.1	Report Organization.....	3
1.2	Physical Setting of the Study Area.....	3
2.0	MATERIAL AND METHODS.....	5
2.1	Taut-line Mooring Design.....	5
2.1.1	Slope Moorings	5
2.1.2	Shelf Moorings	6
2.2	Compass Calibration and Verification.....	7
2.3	Mooring Recovery and Deployment.....	8
2.3.1	Shipboard Mooring Operations.....	8
2.4	Data Processing and QA/QC	10
2.4.1	Current Meters and Current Profilers	10
2.4.2	Temperature-Salinity Loggers	12
2.4.3	Ice Profiling Sonars and Ice velocity.....	13
2.4.4	Sediment Traps	13
3.0	RESULTS AND DISCUSSION	14
3.1	Sea Ice Conditions.....	14
3.2	Ocean Currents	17
3.2.1	Mooring BR-1	19
3.2.2	Mooring DFO-9.....	26
3.2.3	Spatial Variability of Surface and Bottom Currents in Open Water.....	30
3.3	Temperature and Salinity.....	33
3.4	Summary of 2014-2018 iBO dataset.....	40
4.0	CONCLUSIONS.....	43
4.1	Concluding Remarks on the 2017-2018 Dataset	43
4.2	2018 Fieldwork Lessons Learned and Recommendations	43
4.3	Objectives and Milestones for 2019-2020.....	44
4.4	Concluding Remarks on the 2014-2018 iBO Program.....	46
5.0	REFERENCES.....	47

TABLES

Table 1: Mean Error of Current Meter Compasses (10 Degree Increment).	7
Table 2: 2017-2018 Mooring Recovery Summary	8
Table 3: 2018-2019 Mooring Deployment Summary	8
Table 4: Magnetic declination values for 2017-2018 iBO Moorings	10
Table 5: Status of IPS dataset processing for 2014 to 2018.	13
Table 6: Angles chosen to describe the along-slope/shelf current component for each iBO mooring.	17
Table 7: Selected bin depths to characterize circulation patterns throughout the water column.	17
Table 8: Summary of current profilers and current meters clock drift, first and last good record, and percentage of raw data return on iBO moorings from 2017 to 2018.	18
Table 9: Annual statistics of current speed and direction at BR-1-17 from selected bin depths representative of water mass variability in the Beaufort Sea (see Table 6 for water mass description).	22
Table 10: Annual statistics of current speed and direction at DFO-9-17 from a selected bin depth representative of the Polar-mixed layer (see Table 6 for water mass description).	28
Table 11: Summary of CT data logger clock drift and percentage of raw data return on iBO moorings from 2017 to 2018.	34
Table 12: Summary of valid and flagged data from CT loggers deployed on the BR slope moorings from 2017 to 2018. See Table 10 for the instrument model associated with each serial number.	34
Table 13: 2018-2019 iBO Milestones	45
Table 14: Summary statistics of current speed, vector-averaged direction and number of valid records by bin depth at BR-1-17 based on the data acquired with the QM ADCP #12824 from 2017 to 2018. Bin depths flagged manually as part of the QA/QC are highlighted in red.	57
Table 15: Summary statistics of current speed, vector-averaged direction and number of valid records at 586.2 m depth at BR-1-17 as based on the data acquired with the Aquadopp DW #2792 from 2017 to 2018.	58
Table 16: Summary statistics of current speed, vector-averaged direction and number of valid records by bin depth at DFO-9-16 based on the data acquired with the WHS ADCP #12414 from 2017 to 2018.	59

FIGURES

Figure 1: Bathymetric map of the Canadian Beaufort Sea showing the location of iBO moorings (in red). Moorings from partner projects (ArcticNet, DFO, MARES/BOEM) are also shown on the map but are not detailed in the present report).	2
Figure 2: Weekly southern Beaufort ice coverage by stage of development for the season 2018 (February – October 2018) as based on daily ice charts from Canadian Ice services. Brown: old ice. Green: first-year ice. Pink/purple: New/Young ice. Red line: average sea ice concentration 1981-2010. Data source: Ice graph 2.5, http://iceweb1.cis.ec.gc.ca/IceGraph/	14
Figure 3: Sea ice concentration (% coverage) for a 12.5 X 12.5 km pixel area over each iBO mooring during 2017-2018 as derived from SSM/I satellite imagery. The black line shows the mean ice concentration over 2009-2018 within each pixel and the red-dashed line corresponds to the date of the satellite image shown in Figure 4.	15
Figure 4: Satellite image from June 4, 2018 (image from NASA Earthview / MODIS https://worldview.earthdata.nasa.gov/).	16
Figure 5: Time-series of current speed, current direction and along-slope current component at mooring BR-1-17 measured by the QM ADCP #12824. The black line depicts the instrument depth.	20
Figure 6: Time-series of current speed, current direction and along-slope current component at 586 m at mooring BR-1-17 measured by the Aquadopp #2792.	21
Figure 7: Seasonal current roses at 32 m depth (bin cell #35) at BR-1-17 measured by the QM ADCP #12824. Data are low-pass filtered. Roses indicate the direction toward which currents flow. Seasons are defined following the meteorological	

convention (Fall: October-December; Winter: January-March; Spring: April-June; Summer: July-September). Black line indicates the angle chosen to describe the along-slope/shelf current.23

Figure 8: Seasonal current roses at 128 m depth (bin cell #11) at BR-1-17 measured by the QM ADCP #12824. Data are low-pass filtered. Roses indicate the direction toward which currents flow. Seasons are defined following the meteorological convention (Fall: October-December; Winter: January-March; Spring: April-June; Summer: July-September). Black line indicates the angle chosen to describe the along-slope/shelf current.24

Figure 9: Seasonal current roses at 586 m depth at BR-1-17 measured by the Aquadopp #8448. Data are low-pass filtered. Roses indicate the direction toward which currents flow. Seasons are defined following the meteorological convention (Fall: October-December; Winter: January-March; Spring: April-June; Summer: July-September). Black line indicates the angle chosen to describe the along-slope/shelf current.25

Figure 10: Time-series of current speed, current direction and along-slope current component at mooring DFO-9-17 measured by the WHS ADCP #12414. The black line depicts the instrument depth.27

Figure 11: Seasonal current roses at 20 m depth at DFO-9-17 as based on low-pass filtered data from bin cell #9 measured by the WHS ADCP #12414. Roses indicate the direction toward which currents flow. Seasons are defined following the meteorological convention (Fall: October-December; Winter: January-March; Spring: April-June; Summer: July-September). Black line indicates the angle chosen to describe the along-slope/shelf current.29

Figure 12: Near-surface currents for the open water season for low-pass filtered current velocity data from the bin depth nearest bin depth to 20 m at BR-1 and 5 m at DFO-9. Data when sea ice was present (winter-spring) were filtered out. Roses indicate toward where the current is flowing.31

Figure 13: Near-bottom currents for the open water season for low-pass filtered current velocity data from the bin depth nearest to bottom at each location. Data when sea ice was present (winter-spring) were filtered out. Roses indicate toward where the current is flowing.32

Figure 14: Temperature time-series measured at BR-1-17 from 2017 to 2018. The legend shows the serial number and depth of each CT logger.35

Figure 15: Temperature time-series recorded at DFO-9-17 from 2017 to 2018. The legend shows the serial number and depth of each CT logger.36

Figure 16: Salinity time-series recorded at BR-1-17 from 2017 to 2018. The legend shows the serial number and depth of each CT logger.37

Figure 17: Salinity time-series recorded at DFO-9-17 from 2017 to 2018. The legend shows the serial number and depth of each CT logger.38

Figure 18: Temperature-salinity diagram constructed with all data acquired by the CT loggers attached to the moorings BR-1 and DFO-9 from 2017 to 2018. CTD profile data taken at BR-1 during the CCGS Laurier cruises in 2018 are depicted by the black line.39

APPENDICES

Appendix A. 2017-2018 Final Mooring Diagrams

Appendix B. Technical Advisory Committee Meeting 2018 Minutes

Appendix C. Data deliverable

Appendix D. Summary Statistics of Ocean Currents

1.0 INTRODUCTION

The beginning of ice and ocean monitoring in the Canadian Beaufort Sea can be traced back to the 1980's when oceanographic moorings were deployed by Fisheries and Oceans Canada (DFO) in partnership with the oil and gas industry to document ice, wave and surge hazards and ocean current variability. During the next two decades, programs that involved government, industry and indigenous peoples injected funding to maintain year-round observations through DFO moorings that focused primarily on the continental shelf and the deep Canada Basin. In the mid-2000's, ArcticNet Inc. established the Long-Term Oceanic Observatories (LTOO) project to maintain moorings in the southeastern Beaufort Sea that were first deployed as part of the Canadian Arctic Shelf Exchange Study (CASES: 2002-2004); these brought a focus on the intervening continental slope which had received little prior attention. The LTOO project has been sustained since then through collaborations with different programs, such as partnerships with the oil and gas industry (2009-2011) and through the Beaufort Regional Environmental Assessment (BREA: 2011-2015).

The integrated Beaufort Observatory (iBO) was conceived as a means of fostering synergy among the primary long term mooring programs in the Beaufort Sea, enabling: 1) continuation of the time series at key locations; 2) synthesis of observations collected over the past three decades. This technical report describes the activities undertaken as part of the fourth year of iBO from April 1, 2018 to March 31, 2019 and also provides a summary of the four-year iBO dataset. iBO is a four-year program (2015-2018) managed by ArcticNet in partnership with DFO and Golder Associates Ltd. (Golder). The program is supported by the Environmental Studies Research Fund (ESRF) and Imperial Oil Resources Ventures Limited (IORVL). iBO aims to contribute key oceanographic information and understanding required for decisions on environmental stewardship and on industrial development and its regulation in the Canadian Beaufort Sea.

The iBO program contributes to the development of regional syntheses of ocean circulation, sea ice observations and biogeochemical fluxes that will include:

- Information on the magnitude, extent and return period of extreme ice features and of hazardous sea conditions – waves, surge and strong current;
- Ice and ocean datasets to document and interpret inter-annual variability of ice circulation, ocean circulation and particulate matter fluxes in relation to various environmental forcing factors;
- Data to support the development and evaluation of accurate numerical prediction models for operational ocean forecasting and the validation/verification of regional research models for simulating ice, seawater and oil spill trajectories.

The activities conducted under the umbrella of the iBO program during 2018-2019 included the recovery of 2 of 7 moorings deployed in 2017 from CCGS Sir Wilfrid Laurier (Laurier); the remaining 5 mooring could not be recovered in 2018 due to greater than normal ice coverage in the southern Beaufort. Together, these 7 moorings (Figure 1) constitute the backbone of iBO, providing an ice and ocean dataset of regional scope. In a larger context, iBO activities in 2018-2019 also included the organization of a Technical Advisory Committee (TAC) meeting at the ArcticNet Annual Scientific Meeting to review field operations and data recovery.

In December 2018 through April 2019, the iBO team began Phase 2 of the Variability of the Beaufort Ice-Ocean Environment Synthesis Report to be developed over 2018-2021. The Synthesis Report will be a building block of the Indigenous and Northern Affairs Canada (INAC) Beaufort Regional Strategic Environmental Assessment (BRSEA). The goal of Phase 2 is to develop an informative document summarizing the physical marine environment by incorporating analysis and review of existing data and new data obtained from the mooring observatories, and state-of-the-art modelling products. Phase 2 also seeks to continue liaison and coordination with relevant Inuvialuit and Industry stakeholder in the Beaufort Sea for communication and delivery of research and data products.

The goal of the present technical report is to provide a summary of the data acquired from the 2 iBO installations in 2017 to 2018 which represent an extension of key time-series initiated through ArcticNet/BREA and DFO over the preceding years. Only the 2017-2018 data that have been processed thus far are presented in this report and includes all current meter, current profiler, and temperature-salinity data. The data set from the ice profiling sonar (IPS) at DFO-9 is currently queued for processing and there is presently no funding to process IPS data from BR-1. In conclusion, we identify lessons learned stemming from the 2018 operations and define objectives and priorities for 2019-2020. Additionally, a brief summary and conclusions from the full dataset acquired during the iBO program from 2014 to 2018 is provided following the presentation of the 2017-2018 dataset.

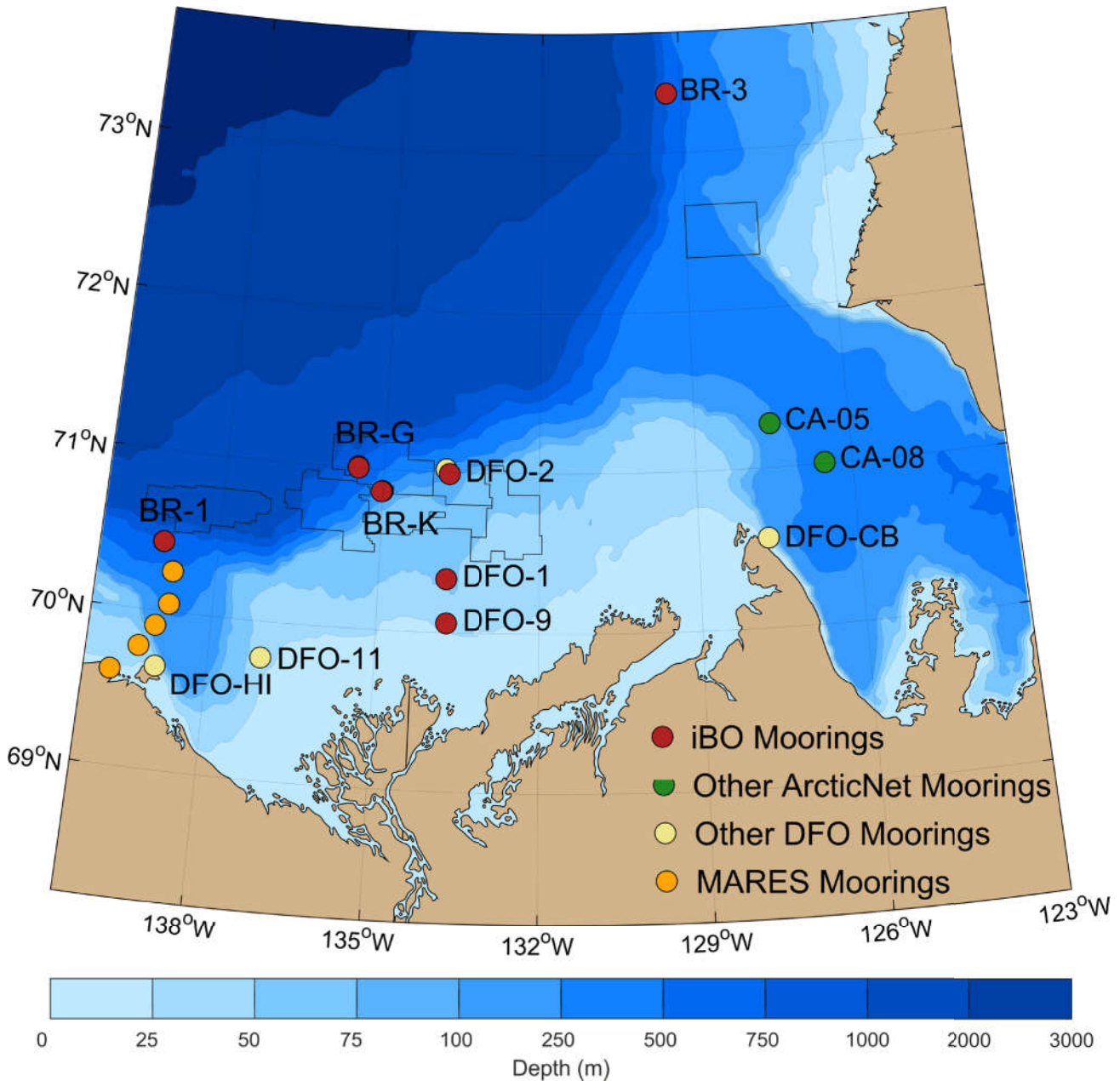


Figure 1: Bathymetric map of the Canadian Beaufort Sea showing the location of iBO moorings (in red). Moorings from partner projects (ArcticNet, DFO, MARES/BOEM) are also shown on the map but are not detailed in the present report).

1.1 Report Organization

This report provides an overview of the physical setting of the study area in section 1.2. A summary of iBO mooring design, field calibration activities, and shipboard mooring operations conducted onboard the CCGS Laurier in 2018 are provided in sections 2.1 through 2.3. Description of the post-processing and QA/QC procedures applied to the recovered data and samples is presented in section 2.4. Section 3.0 provides a review of the processed datasets for the 2 iBO moorings (BR-1 and DFO-9) shown in Figure 1 (red dots), with the exception of the data from the IPS and sediment traps for which the QA/QC. Budget is not available under ESRF to process the IPS data due to the intensive nature of the data and are being processed under a separate budget with support from DFO. Data are grouped by parameter: section 3.1 provide a summary of the sea ice conditions, section 3.2 provides a detailed overview of the ocean current speed and direction recorded throughout the water column at both moorings; and section 3.2.3 provides a review of water mass variability based on temperature and salinity records. Section 3.4 provides a summary of the full 2014-2018 dataset. Section 4 summarizes initial observations on the 2017-2018 dataset, lessons learned from the fieldwork, objectives for 2019-2020, and concluding remarks on the 2014-2018 dataset. The appendices provide the final mooring diagrams for 2017-2018 (Appendix A) and summaries of the TAC and Beaufort Sea Collaboration meetings (Appendix B) hosted as part of the ArcticNet Annual Scientific Meeting, Ottawa, in December 2018. Appendix C lists the electronic files provided as a data deliverable with this report. Appendix D provides a tabular summary of descriptive statistics pertaining to ocean currents measured at the 2 iBO moorings in 2017-2018.

1.2 Physical Setting of the Study Area

The Canadian Beaufort Shelf (Figure 1) is a narrow Arctic shelf (120 km width × 530 km length) comprised of a series of plateaus separated by shallow channels (Blasco et al., 2013). The shelfbreak is located at 80-100 m depth where the slope angle increases to 2-6° toward the deep Canada Basin. The region is greatly influenced by the Mackenzie River, which is the largest Arctic river in terms of sediment load ($\sim 127 \times 10^6$ t per year) and the fourth largest in terms of freshwater discharge ($330 \text{ km}^3 \text{ yr}^{-1}$) (Macdonald et al. 1998).

Ice cover in the region undergoes a seasonal cycle with considerable inter-annual variability. Galley et al. (2013) recently documented that no significant trend in summer sea ice concentration on the mid-to upper slope of the central shelf has been measured from 1996 to 2010, although off the shelf to the northwest, a decrease in old sea ice concentration compensated by an increase in first-year sea ice is apparent. Typically, seasonal sea ice begins to form in October in the coastal sector and by early to mid-November the ice cover is consolidated over the entire region (<http://iceweb1.cis.ec.gc.ca/30Atlas/page1.xhtml?region=WA&lang=en>; Carmack and Macdonald, 2002). In winter, landfast ice forms in the nearshore out to about the 20 m isobath and an ice rubble field (i.e. the stamukhi; Giovando and Herlinveaux 1981), which includes grounded ice, develops at the outer edge of the landfast ice. Beyond the stamukhi, a recurrent flaw lead separates the landfast ice from the moving pack ice that typically drifts westward driven by [prevailing wind (Macdonald et al. 1995). The Cape Bathurst Polynya centered at the mouth of the Amundsen Gulf is part of the flaw lead system that borders the Beaufort Sea (Barber and Hanesiak 2004). The summer retreat of the ice to the north-west driven by the seasonal increase in east wind (<http://iceweb1.cis.ec.gc.ca/30Atlas/page1.xhtml?region=WA&lang=en>) causes widening of the flaw lead typically in June, but sometimes as much as 6 weeks earlier.

On the inner to mid-shelf, ice drift, ocean circulation, and the trajectory of the Mackenzie River plume, are highly variable and linked to wind dynamics (Melling, 1993; Melling and Riedel 1994; O'Brien et al. 2006). Over the outer shelf and on the slope, large-scale surface circulation (upper 50 m) is dominated by westward-flowing current of

the Beaufort Gyre (Ingram et al. 2008). The water mass that occupies the upper 50 m (polar mixed-layer) is the Arctic Surface Water with salinity of ~30-31 (practical scale) on average in winter, but this value changes markedly with river input and the growth and melt of ice. From 50 to 200 m depth near the shelfbreak, a submerged stream of north-eastward flow delineates the Beaufort under-current (Forest et al. 2015; Dmitrenko et al. 2016), the eastward continuation of a feature first described in the Alaskan Beaufort Sea (Aagaard 1984; Pickart 2004; von Appen and Pickart 2012). This current is 10-15 km in width and topographically steered along the upper slope; it predominately transports Arctic water of Pacific origin (salinity ~33), but some water of Atlantic origin (salinity 34.0-34.9) which typically dominates the 200-1000 m layer of the water column is entrained at times. This under-current is subject to frequent wind-forced reversals to the west which are commonly associated with upwelling (Aagaard 1984; Pickart et al. 2013). The under-current is the strongest circulation feature in the area and intrinsic to shelf-slope exchange of water in the Beaufort (e.g. Kulikov et al. 1998; Williams et al. 2008). At 20-30 km from the shelf edge, the eastward shelfbreak jet is no longer present and the mean current in the upper 200 m is westward within the anti-cyclonic motion of the Beaufort Gyre (Forest et al. 2015). Mesoscale eddies frequent the region beyond the shelf edge.

2.0 MATERIAL AND METHODS

This section of the report provides detailed information on the tautline mooring design and instrumentation of iBO moorings (section 2.1), compass calibration activities for current meters and current profilers (section 2.2), and mooring recovery and deployment operations aboard the CCGS Laurier (section 2.3). A description of the QA/QC processing steps for each moored instrument is provided in section 2.4.

2.1 Taut-line Mooring Design

2.1.1 Slope Moorings

The slope moorings array consists of 3 similarly designed long moorings (BR-1, BR-G and BR-3) located on the middle continental slope (~700-750 m depth) and one short mooring (BR-K) located on the upper slope near the shelf edge (~170 m depth; Figure 1). Mooring diagrams (as deployed) for 2017-2018 are included in Appendix A.

The longer moorings on the lower slope consist of the following key components:

- ASL Ice Profiling Sonar (IPS) was used at approximately 60 m depth to measure ice draft and non-directional waves during intervals of open water. IPS were mounted in 30-inch spherical syntactic foam floats (Mooring Systems Inc. - MSI).
- 150 kHz Teledyne RD Instruments (TRDI) Quarter Master Acoustic Doppler Current Profiler (QM ADCP) were used at approximately 180 m water depth to profile upper water column currents at 4 m vertical resolution and measure ice velocity using a Bottom-Track feature. The QM ADCPs were mounted up-looking in 40-inch syntactic foam floats (Flotation Technologies - DeepWater Buoyancy).
- 75 kHz TRDI Long Ranger ADCP (LR ADCP) were used at approximately 450 m water depth to measure water velocity profiles at 16 m vertical resolution. The LR ADCPs were mounted up-looking in 40-inch syntactic foam floats (Flotation Technologies).
- Two high frequency short-range (<1 m) Nortek Aquadopp DW (AQD) single point current meters were used to measure water velocity at approximately 10 m and 110 m above the bottom. Each Nortek AQD was equipped with a vane to hold the heading nearly constant for the duration of each ensemble interval.
- Two Technicap PPS 3/3-24S 24 cup sequential sediment traps were deployed between the IPS, QM ADCP and LR ADCP to record the annual cycle in vertical particle flux.
- RBR or Seabird SBE37SM Conductivity and Temperature (CT) loggers were installed at approximately 60 m, 130 m, 180 m, and 450 m water depth, as well as 10 m above the bottom. These instruments measure water temperature and salinity and are used to compute sound speed to improve IPS and ADCP processing.
- Various smaller syntactic foam floats were distributed along the mooring as required.
- Tandem Edgetech CART or Oceano acoustic transponder releases were used as the primary locating and recovery devices.

The shallow (upper slope) mooring consisted of the following key components:

- A 300 kHz TRDI Workhorse Sentinel ADCP (WHS ADCP) was used at approximately 140 m water depth to profile currents with a vertical resolution of 8 m, as well as to measure ice velocity using the Bottom-Track feature. The WHS ADCPs were mounted upward looking in 33-inch syntactic foam ellipsoid floats manufactured by MSI.
- A RBR CT logger with auxiliary sensors to measure turbidity, dissolved oxygen, and chlorophyll fluorescence was installed at approximately 18 m above the bed.
- A Sequoia LISST 100X laser diffraction system was located 18 m above the seafloor to provide measurements of particle size distributions and associated volume concentrations in the lower water column. The LISST measurements help to better quantify the seasonal and annual variability of vertical and horizontal fluxes of inorganic solids.
- A 1 MHz Nortek Aquadopp profiling current meter (AQP) was mounted down-looking below the LISST to provide details of the flow and acoustic backscatter structure near the seafloor on the upper slope. The AQP's measure three-dimensional current velocities and provide a measure of acoustic backscatter intensity in 2 m range bins from the bottom to about 16 m above seabed. Combined with the velocity profile information from upward looking ADCP's the profilers provide a detailed and near complete view of the water column vertical structure.
- An additional syntactic foam ellipsoid float was located above the LISST cage to provide floatation for the lower portion of the mooring.
- Edgetech (Model CART) acoustic transponder releases in tandem were used as the primary recovery device.

2.1.2 Shelf Moorings

The moorings at all three shelf locations (DFO-9, DFO-1, and DFO-2; Figure 1) have similar design (Appendix A). They are located at approximately the 28 m, 55 m and 110 m isobaths, respectively; DFO-2 is on the upper continental slope and DFO-2 and DFO-9 lie within the Kugmallit sea valley. Recording instruments at the two shallower sites (DFO-9 and DFO-1) are placed on two separate nearby (50-150 m separation) moorings so as to keep the equipment near the seabed safe from drifting ice and to avoid interference between the two sonars used for observations. The depth at the third site is sufficient that the instruments are located one above the other on a single mooring.

The moorings at all three sites support the following instruments:

- ASL IPS are located at 30-50 m depth to measure ice draft and non-directional waves during intervals of open water. IPS of three types are in use: original IPS4 units operating at 200-kHz acoustic frequency; updated W-IPS4 units operating at 420 or 895 kHz and measuring wave height as well as ice draft; IPS5 units operating at 420 kHz with increased data storage capacity. IPS are mounted in light-weight stainless steel frames each supported by a collar of four 14-inch spherical plastic floats (Viny Inc. Model 12B3).
- 300-kHz TRDI ADCPs are located about 4 m above the seabed to measure ocean current at 4 m vertical resolution between about 6-m elevation above the seabed to about 15-m depth below the surface, plus ice velocity. ADCPs of two types are in use: original narrow-band ADCPs (NB-ADCP) and newer broad-band WHS-ADCPs. The NB ADCPs operating with higher signal-noise ratio and better magnetic compasses are favoured for Arctic use. ADCPs are mounted in light-weight stainless steel frames each supported by a collar

of four 14-inch spherical plastic floats (Viny Inc. Model 12B3) and equipped with vane so that the ADCP heading remains stable throughout a measurement interval. The frame is coupled into the mooring through a swivel.

- CT loggers (Seacat SBE37: Sea Bird Electronics Inc.) are installed on the frame with each ADCP, about 3 m above the seabed. They record the temperature and salinity of water within the bottom boundary layer and provide sensitive indication of water mass shifts associated with up-welling and down-welling motions.
- Acoustic transponder releases (Model CART: ORE Edgetech) were mounted in tandem 1 m above the mooring's deadweight anchor. The CART is the device used to locate each mooring and to enable its recovery by unhooking the buoyant part of the mooring from its heavy anchor. Two transponding releases are used in parallel for redundancy in this essential function.

2.2 Compass Calibration and Verification

Compass calibration is an important consideration for current meters deployed in the Canadian Beaufort Sea due to the reduced magnitude of the horizontal component of the Earth's magnetic field in the Canadian Arctic, less than one third of its value in southern Canada. Calibration and verification of the current meter compasses near the approximate geomagnetic latitude where they will be deployed is advisable prior to deployment. Moreover, care must be taken to eliminate all sources of magnetic interference from the instrument-supporting cages on the mooring and similarly also in the immediate vicinity of the calibration activities. For this reason, calibration activities cannot take place onboard the Laurier.

The compass calibration procedure for TRDI current meters corrects for both soft iron effect (i.e. distortion of the Earth's magnetic field by local ferrous metal) and hard iron effects (i.e. magnetic influence from magnetic material in the vicinity of the instrument, such as mooring hardware and batteries). Nortek's compass calibration for Aquadopp and Continental instruments only corrects for hard iron effects and not for soft iron effects.

A summary of compass calibration and verification activity are provided in the iBO 2018 field report from the Laurier expedition (IOS-DFO 2018). In 2018 compass calibration and verification was completed for four TRDI WHS 300 kHz ADCPs on September 26, 2018 prior to the crew change for the Leg 3a expedition at the Kugluktuk airfield. A second calibration of two Nortek Aquadopp current meters was completed on the shore of Thesinger Bay, Banks Island on October 6, 2018.

Table 1 provides a summary of the post-verification compass errors (calculated from readings made in 10 degree increments) for the verification activities conducted in October 2018 and the calibration results for the ADCP recovered from DFO-9-17 (previous calibration results for BR moorings were reported previously). In the last column of Table 1, the mean calculated error is the accuracy of the compass; this value has been used in processing to correct the compass reading (DFO moorings only).

Table 1: Mean Error of Current Meter Compasses (10 Degree Increment).

Instrument	Serial Number	Mooring	Mean Calculated Error \pm Standard Deviation around the Compass (degrees)
Nortek Aquadopp	2754	Not used	0.26 \pm 1.58
Nortek Aquadopp	2758	Not used	0.16 \pm 5.06
TRDI WHS ADCP ¹	12414	DFO-9-17	1.0 \pm 0.9, based on calibration at Kugluktuk airport

Notes: ¹Calibration prior to deployment in September 2017.

2.3 Mooring Recovery and Deployment

This section of the report provides details on iBO mooring recovery and deployment operations conducted aboard the CCGS Sir Wilfrid-Laurier (section 2.3.1) during the 2018 fieldwork. Coordinates and depths of the mooring at their recovery and re-deployment are provided in Table 2 and Table 3.

Table 2: 2017-2018 Mooring Recovery Summary

Mooring	Latitude (WGS84)	Longitude (WGS84)	Water Depth (m)	2017 Deployment Date and Time (UTC)	2018 Recovery Date and Time (UTC)
BR-1-17	70° 25.9911' N	139° 01.5892' W	759	Oct-02-2017 15:38	Oct-10-2018 16:00
DFO-9a-17	70° 20.0300' N	133° 44.4380' W	35	Sep-30-2017 19:36	Oct-09-2018 20:00
DFO-9b-17	70° 03.5024' N	133° 42.9247' W	35	Sep-30-2017 16:16	Oct-09-2018 20:00
DFO-9c-17	70° 03.5309' N	133° 42.8695' W	35	Sep-30-2017 16:02	Oct-09-2018 20:00

Table 3: 2018-2019 Mooring Deployment Summary

Mooring	Latitude (WGS84)	Longitude (WGS84)	Water Depth (m)	2017 Deployment Date and Time (UTC)
DFO-9a-18	70° 03.5372' N	133° 42.9754' W	36	Oct-09-2018 22:25
DFO-9b-18	70° 03.5309' N	133° 42.9353' W	36	Oct-09-2018 22:23
DFO-1a-18	70° 14.6475' N	133° 31.6191' W	52	Oct-09-2018 02:37
DFO-1b-18	70° 14.7711' N	133° 32.0233' W	53	Oct-10-2018 01:05

2.3.1 Shipboard Mooring Operations

Steps for mooring recovery aboard the CCGS Laurier generally included:

- pre-operations Job Safety Assessment (JSA) meeting, an operational planning meeting, and a toolbox meeting (on deck);
- interrogate the mooring to determine range;
- maneuver ship into position depending on prevailing drift, wind and sea state;
- conduct a conductivity, temperature and depth (CTD) cast to provide overlapping water column data for data processing; relative timing of CTD cast varies with logistic constraints on the Sir Wilfrid Laurier
- enable the acoustic release and send a command to release the mooring;
- mooring positioned relative to the bow of the ship for recovery;
- lift mooring elements onto the foredeck and take instruments off the mooring as they are brought on deck, then take the mooring apart (i.e., a complete disassembly of the mooring);
- inspect and rinse instruments with freshwater and stow in plastic bins;
- transfer of equipment lab spaces for inspection and data recovery;
- immediately download data from the instruments if re-using, otherwise as schedule permits;

- perform preliminary review and graphical inspection of the data if re-using the instrument, otherwise as schedule permits;
- store and secure the instruments onboard the ship, and
- service and maintain the instruments, including any required trouble-shooting or field repair.

All mooring recovery operations were conducted safely and successfully on the foredeck and from the FRC, when involved. Servicing of the mooring instruments involved the following steps:

- opening the housing (if required) and inspecting interior for corrosion, and other damage;
- changing the batteries (if required), and replacing desiccant (if applicable);
- cleaning the o-ring surfaces and re-greasing and replacing or cleaning all o-rings;
- running a trial delayed-start deployment using instrument's internal power with computer disconnected, followed by upload and inspection of data record;
- programming the instrument for deployment;
- completing a record of programming (screenshots and paper record sheets).

Before programming and deployment of instruments on the moorings, standard manufacturer procedures and pre-deployment tests were followed to provide verification of instrument operation. Instruments were generally programmed for a 1-year deployment. However, those at BR-3 were programmed in 2017 for two years' operations because at this northerly location west of Banks Island ice can in some years preclude mooring recovery operations. This mooring was also equipped with Oceano acoustic releases that have an extended battery life of at least 2 years. A contingency phase was implemented for all Ice Profilers in order to continue measurements in the event that the mooring might not be recovered in the fall of 2018.

Steps in the mooring deployment typically consist of the following:

- confirm the design of the mooring particulars to meet the site's constraints;
- review the lifting plan and JSA;
- assemble the mooring on deck (using the original configuration or a modified configuration, as appropriate);
- conduct a toolbox meeting on-deck;
- deploy the mooring;
- enable and interrogate the acoustic release;
- perform triangulation to determine the actual location of the mooring, as distinct from the drop point;
- disable the acoustic release; and
- perform CTD cast.

2.4 Data Processing and QA/QC

2.4.1 Current Meters and Current Profilers

This section of the report provides a summary of QA/QC procedure applied to current meters and current profilers deployed on both BR and DFO moorings. The QA/QC procedure of current profilers on BR mooring differs slightly from that applied to DFO instruments (see details below). For all moorings, pressure sensors on the TRDI ADCPs were zeroed at the time of setup in order to account for atmospheric pressure in the depth calculation performed by the instrument. Processing routines were used to convert pressure measured by the Nortek AQDs, to water depth; pressure measurements in air before and after the instrument deployment were averaged to represent mean atmospheric pressure. For BR moorings, processing of the ASCII files from Nortek AQDs or MATLAB® binary files from TRDI ADCPs was completed using MATLAB® software. For DFO moorings, data was processed using the in-house software and routines (the IOS SHELL suite) from DFO, which produce ASCII multi-line header files and multiple ASCII data files. These DFO ASCII files were converted into the BR mooring file format (MATLAB® binary and Text files) for plotting, analyses and to be provided as a data deliverable.

Processing and quality-checking of the current time-series data consisted of the following steps:

- 1) Measurements made by the instrument while it was out of the water, as determined from pressure readings, were removed.
- 2) East and North horizontal components of velocities were corrected to true north based on local magnetic declination. An annual average magnetic declination was used for the deployment period based on the Natural Resources Canada numerical model for the International Geomagnetic Reference Field 2012 (IGRF-12; <http://www.geomag.nrcan.gc.ca/calc/mdcal-eng.php>). The summary of magnetic declination values each for each mooring is listed in Table 4.

Table 4: Magnetic declination values for 2017-2018 iBO Moorings

Mooring	Magnetic Declination [degrees East]
BR-1-17	21.5
DFO-9-17	21.7

- 3) Compass readings from the ADCPs at the DFO moorings were further corrected for compass non-linearity using a polynomial approximation to compass response as a function of instrument geomagnetic heading (section 2.2). This can span a range that exceeds 10° peak to peak, depending on the instrument and its battery. The geomagnetic field near the Beaufort coast is considered close enough to the locations of moorings so that the measured polynomial correction is applicable offshore¹. No polynomial correction was applied to the indicated directions of TRDI ADCPs at the BR sites because the ±4 degree root-mean-square non-linearity was considered acceptable (TRDI 2014).
- 4) Acoustic amplitude was plotted for each beam to check the quality of the instrument signal return and filtered for amplitudes below the noise floor for the respective instrument (Nortek 2013; TRDI 2014).
- 5) Nominal depths of echo intensity and velocity data from TRDI ADCPs deployed at the DFO sites were calculated using a spline interpolation along each beam that corrects for the effects of changing pitch and roll. Nominal depths from the TRDI ADCPs deployed at the BR moorings were calculated using the default bin mapping method (nearest vertical bin) for TRDI ADCPs (TRDI 2014) that uses the 20° beam slant angle.

¹ The strengths of the horizontal component and the declination angles of geomagnetic field at Kuglugtuk at the time of writing were 6468 and 81.5°.

The latter approach provides similar results to the spline interpolation method in the cases that the tilt is lower than 10° (>99.5% of time for each time series).

- 6) For ADCPs deployed at the BR moorings, the following steps were applied to filter data and to identify and flag data that were considered as suspicious:
 - a) Data were filtered for sidelobe interference using the beam slant angle of the instrument. For the TRDI ADCPs this value was 20° (for all LR, QM and WHS ADCPs) or 30° (for NB ADCPs on DFO-2 and DFO-1). At BR moorings the filter correction was calculated as the product of the instrument depth and the cosine of the slant angle plus one range bin. The filtered range approximately corresponds to the top 10% of the range to surface or bottom depending on whether the instrument was up-looking or down-looking (only the Aquadopp profiler at BR-K).
 - b) For TRDI instruments, datasets were filtered using the Percent Good (PG) values. Data points with a combined PG4 and PG1 value of less than 25% (TRDI 2014; IOS 2015) were removed from the dataset. The PG value is a data-quality indicator that reports the percentage (0 to 100) of valid data collected for each depth cell of the velocity profile using the four beams (PG4) and three beams (PG3). It is an indicator of the following criteria: low correlation, large error velocity and fish detection (false target threshold) (TRDI 2006).
 - c) Time series data from ancillary sensors on the current profilers were inspected for QA/QC purposes. Nortek recommends that the instrument tilt not exceed a maximum of 10° for measurement of currents (Nortek 2013) and TRDI recommends a maximum tilt limit of 15° (TRDI 2014). Data when tilt was exceeding the respective thresholds were flagged as part of the QA/QC.
 - d) Data were further filtered using the error velocity (TRDI instruments only) and maximum vertical velocity thresholds. The error velocity is a measure of the homogeneity of water movement across the span of the 4 inclined sonar beams. The data from TRDI ADCPs on BR slope moorings were filtered for vertical velocities greater than 0.1 m/s and error velocities greater than 0.15 m/s (i.e. arbitrary values based on error velocity thresholds developed as part of the BREA program).
 - e) Additional visual inspection guided the flagging of (subjectively) suspicious bin values.
 - f) Bottom track ranges (WHS and QM) are corrected for pitch and roll following the methodology of Woodgate and Holroyd (2011). Note that bottom track velocities are uncorrected for an up-looking ADCP (the bottom track function defaults to being used down-looking from a vessel). Velocity polarity should be inverted before use as ice velocities.
- 7) For ADCPs deployed at the DFO sites, a multi-stage decision tree was applied to identify and flag data judged to be of little value by a variety of criteria. These criteria include:
 - a) Surface interference: Eliminating surface interference at the DFO sites used the same methodology as at BR sites, except that the ADCP-measured range to the surface (water-ice or water-air) was used in place of the ADCP's depth.
 - b) Beam-to-beam differences: Ensemble values masked if more than three differences between beams exceed 8 counts.
 - c) Extreme strong echo: Ensemble values masked because at least one beam differs from the others by more than 25 counts.
 - d) Extr+Diffs: ensemble values masked due to combined conditions of 2 & 3.

- e) PercentGood < 25: Ensemble values masked because fewer than 25% of the ping data yielded 3 or 4 beam solutions.
- f) Low Amplitude: Ensemble values masked because 1 or more beams have amplitude of less than 1 counts.
- g) Error Velocity: Ensemble values masked because the so-called error velocity (actually the difference between independent values of vertical velocity) exceeded 2.8 times the standard deviation of the time series (approximately the 99th percentile). The editing threshold here and in the next step were not fixed but set adaptively.
- h) VertVel: Ensemble values masked because the vertical velocity exceeded 2.8 times the standard deviations of the time series (approximately the 99th percentile).

Final QA/QC time-series data from ADCPs are usually gappy and can be difficult to use in some applications. To generate continuous time series of data at sub-tidal frequencies, the final processing step for DFO was the complex demodulation of the time-series within over-lapping 12-hour windows (e.g. Melling et al. 2001). This additional step was not applied to the current data delivered as part of Appendix C. Instead a low-pass filter (PL66TN, Beardsley and Rosenfeld 1983) was applied to selected bin depth time-series for each instrument data (interpolated linearly to 1-hour intervals for consistency) in order to construct seasonal current roses (16 directions, 22.5° bins) of the sub-tidal current component as presented in section 3.2.

2.4.2 Temperature-Salinity Loggers

Data were extracted from the RBR sensors using Ruskin® software (RBR 2016) and from Sea Bird sensors using Sea Bird Electronics software. Time-series from BR moorings were processed and plotted using MATLAB® scripts, whereas the same task was accomplished by DFO using in-house IOS SHELL routines.

For CT sensors on the BR moorings time series were clipped for out-of-water values and evaluated visually for data quality. In addition, an automated filter is applied to the conductivity and temperature data to flag potential spikes from the data time-series using a seven-sample moving window. All values outside of ± 1.5 standard deviations about the moving window mean that could be considered spikes are flagged; spikes in conductivity are far more common than spikes in temperature. Any spikes identified in the temperature or conductivity time-series cause the corresponding salinity values also to be flagged because salinity is temperature and conductivity dependent.

In addition, the temperature and salinity data from all moorings were verified and corrected for accuracy against nearby CTD casts acquired at the time of recovery in 2018. Since appreciable drift in sensor calibration rarely occurs for temperature, the assessment of calibration drift is normally carried out for conductivity; it is done on the basis of potential temperature versus salinity plots. For Sea Bird sensors, drift in conductivity calibration is usually associated with silting or bio-fouling. For the RBR sensors a calibration shift from laboratory values can occur via intrusion of mooring components (conducting or non-conducting lines, support structure, etc.) into the (20-cm diameter) sensing volume for conductivity. No correction was required for the CT sensors at BR-1 for 2017 to 2018. The conductivity at DFO-9 drifted to a lower value during 2017-18. The salinity from the SBE37 just prior to recovery was about 0.18 lower than the CTD. An adjustment was made in processing to increase conductivity linearly from zero to 0.18 during the deployment.

2.4.3 Ice Profiling Sonars and Ice velocity

Processing and QA/QC data from a partial IPS dataset for 2014-2018 is currently underway and results are expected to be presented as part of upcoming complementary reports provided by DFO and ASL Environmental Sciences Ltd (ASL). No funding currently exists for processing of the IPS datasets at the BR moorings beginning in 2016. Table 5 provides a summary of the processing status for the IPS dataset from each mooring for 2014 to 2018. It should be noted, however, that the IPS and all CT loggers at the BR-1 and DFO-9 moorings functioned properly and provided complete datasets from 2017 to 2018 with a total of 100% of raw data return. The derivation of ice draft from IPS signal data employs well-established methods that have been developed during the processing of many dozens of IPS datasets over the past three decades (Melling et al. 1995; Melling and Riedel, 2004; Fissel et al. 2008). Data and available QA/QC reports for IPS are available on request.

Table 5: Status of IPS dataset processing for 2014 to 2018.

Bin Depth (m)	2014-2015	2015-2016	2016-2017	2017-2018
BR-3	Complete	At early stage (ice velocity)	Processing not funded	Processing not funded (no data available)
BR-G	Complete	Processing not funded	Processing not funded	Processing not funded (no data available)
BR-1	Complete	At early stage (ice velocity)	Processing not funded	Processing not funded
BR-K	Processing not funded	Processing not funded	Processing not funded	Processing not funded (no data available)
DFO-2	Complete	At mid-stage (draft calibration)	Queued for processing	No data available
DFO-1	Complete	Complete	Queued for processing	No data available
DFO-9	Complete	Complete	Queued for processing	Queued for processing

There are many steps in the processing of IPS signal data to ice draft. The procedures for detection of erroneous target data and for calibration of zero ice draft in particular are meticulous and require considerable experience. It is not useful to document the process here in detail. The interested reader is referred to Melling et al. (1995) and Melling and Riedel (2004).

Ice velocity is derived from data provided by TRDI's patented bottom-track firmware in the WHS and QM ADCPs (see section 2.1). It can also be derived from binned water-column data recorded by LR ADCPs if certain conditions are met. The ASL procedures for deriving reliable estimates of ice velocity from ADCP data are numerous. Moreover, a certain level of subjectivity must be tolerated in the analysis because greatly varying conditions at the target (rough or smooth ice; continuous or broken ice cover; rough seas or calm seas; other targets yielding plausible echoes; etc.) generate ambiguity. The interested reader is referred to more thorough discussions provided by Melling and Riedel (2004) and ASL (2015).

2.4.4 Sediment Traps

Each of the BR moorings on the middle continental slope was equipped with two automated sediment traps (at approximately 125 and 310 m depth) to record the annual cycle in vertical particle flux (inorganic sediments, organic carbon and particulate nitrogen) and plankton community composition in the upper water column. One of the two traps recovered from BR-1 provided complete particle flux time-series as expected. One sediment trap did not provide any samples due to installation problems. Analyses on the sediment trap samples are currently pending additional funding from the LTOO project.

3.0 RESULTS AND DISCUSSION

This section of the report summarizes measurements of currents, salinity, and temperature data collected in the 2017-2018 deployment interval. A description of sea ice conditions is provided for context.

3.1 Sea Ice Conditions

The southern Beaufort was characterised by earlier than normal breakup at the beginning of June 2018 followed by greater than normal ice concentration through September according to Canadian Ice Services (CIS 2018). Weekly ice coverage by stage of development for the season 2018 is provided in Figure 2. Sea ice concentration over each mooring location as obtained from SSM/I satellite imagery (12.5 x 12.5 km pixel resolution) is provided in Figure 3. The red line indicates the date (June 4) of the satellite photo of the southern Beaufort Sea following ice breakup. The photo in Figure 4 shows open water at all the mooring sites except BR-3. Sea ice at BR-3 persisted near the average through summer. At the beginning of September, persistent northwesterly winds pushed pack ice from the west and northwest of Banks Island into the western entrance of Amundsen Gulf and onto Cape Bathurst and the Tuktoyaktuk Peninsula by early October (CIS 2018). The regional seasonal ice coverage minimum in September 2018 was at 33.1%, near the median for 1968 to 2018.

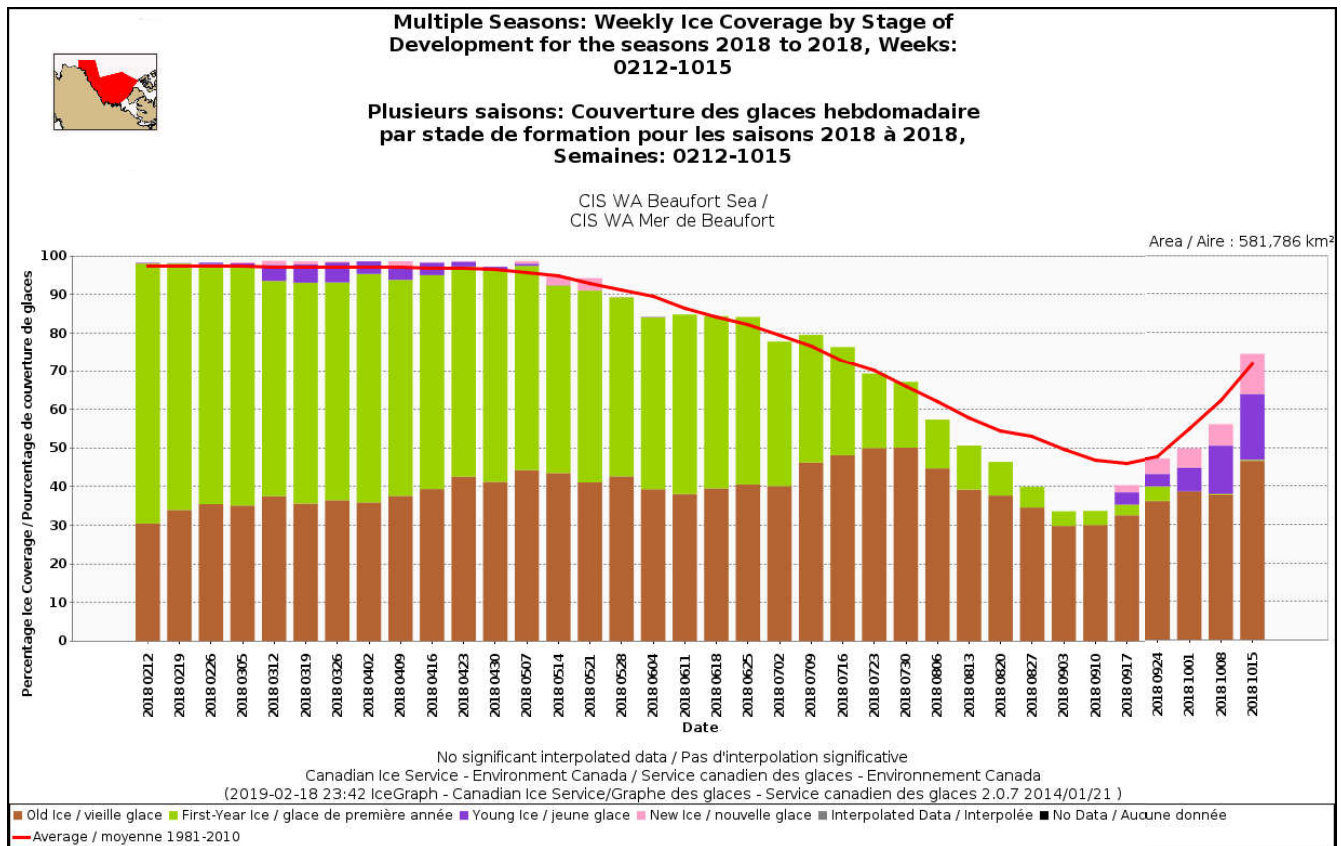


Figure 2: Weekly southern Beaufort ice coverage by stage of development for the season 2018 (February – October 2018) as based on daily ice charts from Canadian Ice services. Brown: old ice. Green: first-year ice. Pink/purple: New/Young ice. Red line: average sea ice concentration 1981-2010. Data source: Ice graph 2.5, <http://iceweb1.cis.ec.gc.ca/IceGraph/>.

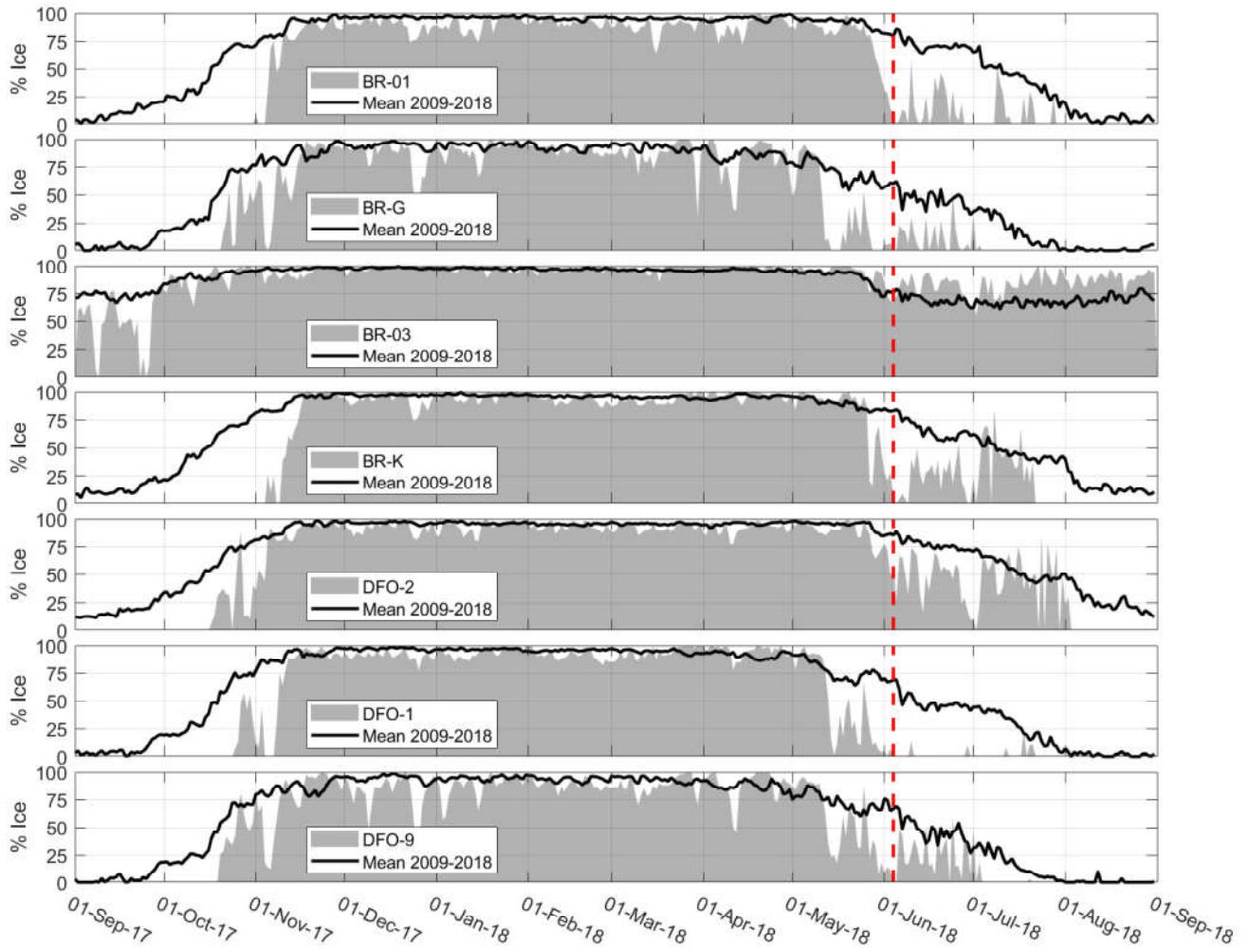


Figure 3: Sea ice concentration (% coverage) for a 12.5 X 12.5 km pixel area over each iBO mooring during 2017-2018 as derived from SSM/I satellite imagery. The black line shows the mean ice concentration over 2009-2018 within each pixel and the red-dashed line corresponds to the date of the satellite image shown in Figure 4.

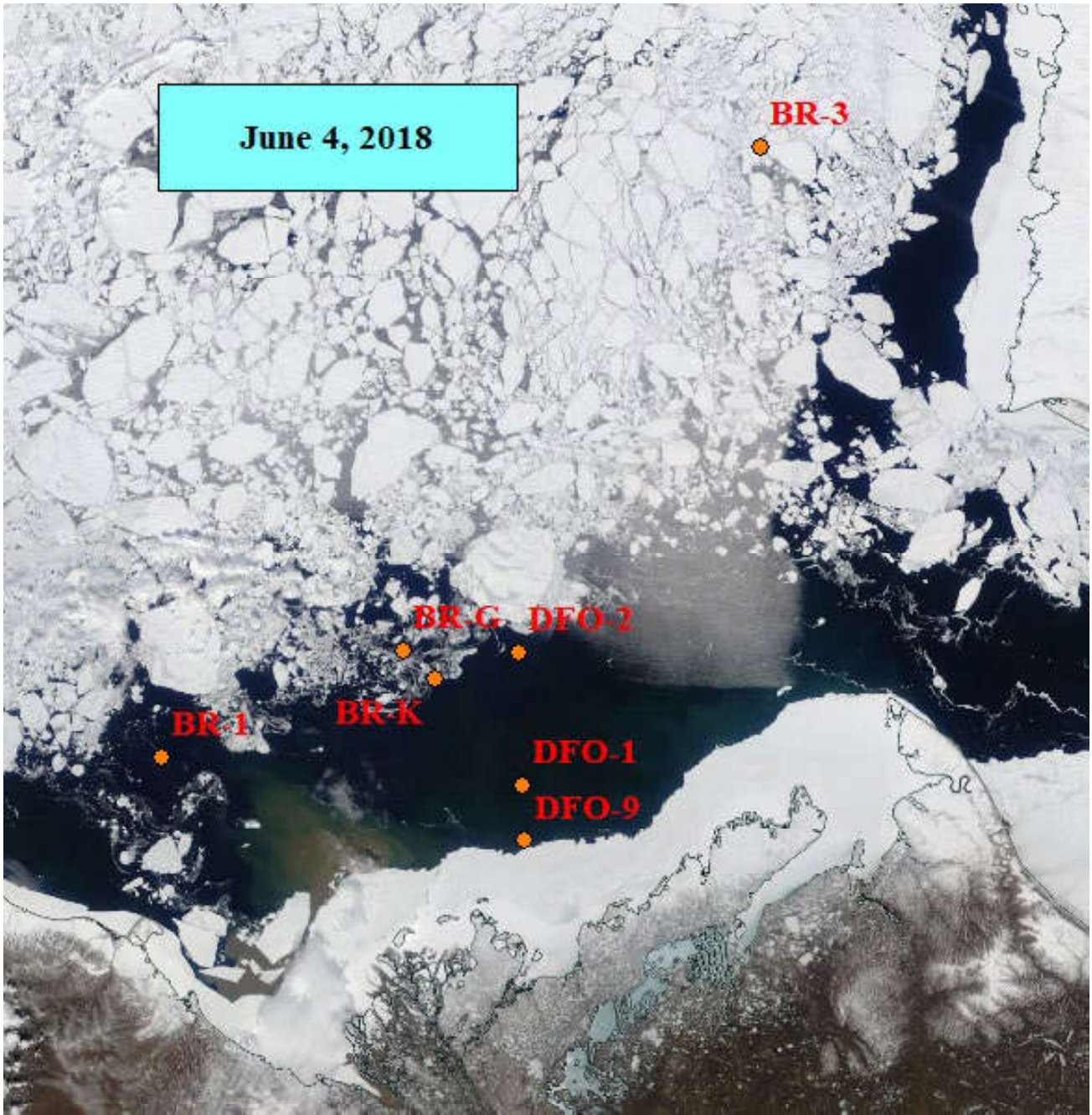


Figure 4: Satellite image from June 4, 2018 (image from NASA Earthview / MODIS <https://worldview.earthdata.nasa.gov/>).

3.2 Ocean Currents

Processed data for all current profilers and current meters from the 2 iBO moorings for 2017 to 2018 are presented in this section of the report. For each instrument, a time-series plot of current speed, current direction and along-isobath current speed is presented. The along-isobath component of current typically dominates current variability over the continental slope (Williams et al. 2008; Forest et al. 2015; Dmitrenko et al. 2016). The along-isobath direction was estimated as the heading of the bathymetric contour at each mooring location (Table 6) with respect to true North; this is consistent with previous mooring studies that described the along-isobath flow. The along-isobath direction is indicated by a bold line in current rose plots. Annual statistics of current speed and direction for selected bin depths (nearest available bins to those listed in Table 7) are also provided to characterize the net behaviour of ocean currents with depth.

Seasonal current roses based on the sub-tidal component of current velocity were constructed for the same selected bin depths (Table 7) to contrast the temporal variability of ocean circulation patterns in relation to the distinct water masses and water mass boundaries. The sub-tidal component was obtained by applying a low-pass filter with a half-amplitude period of 33 hours to each selected time-series linearly interpolated over 1-hour intervals (PL66TN, Beardsley and Rosenfeld 1983). In addition, a complete tabular summary of current speed descriptive statistics, vector-averaged direction and number of valid records is provided for every bin depth of each instrument in Appendix D. Meta-data for each instrument (i.e. serial number, mean instrument depth, date and time of first and last good record, and percentage of raw data return) is provided in Table 8.

Table 6: Angles chosen to describe the along-slope/shelf current component for each iBO mooring.

Mooring	Angle, degrees True North (TN)
BR-1	78
BR-3	0
BR-G, BR-K, DFO-2	52
DFO-9 ¹	90
DFO-1 ¹	10

¹Note: DFO-1 and DFO-9 are located in the Kugmallit sea valley where the isobaths are sharply bent. The angles at these two sites were adjusted for the expected flow conditions across the valley.

Table 7: Selected bin depths to characterize circulation patterns throughout the water column.

Approximate Bin Depth (m)	Rationale (based on Lansard et al. 2012)
20	Near-surface circulation within the Polar-Mixed Layer (salinity \approx 31-32)
130	Core of the Pacific Halocline water mass (salinity \approx 33)
220	Boundary between the Pacific Halocline and Atlantic water
350	Mid-depth of the water column over the slope, core of the Atlantic Water mass (salinity \approx 34.8)
550	Deep circulation over the slope, lower portion of the Atlantic water mass
700	Near-bottom circulation at the boundary between the Fram Strait and Barents Sea branches of Atlantic water (salinity \approx 34.9)

Table 8: Summary of current profilers and current meters clock drift, first and last good record, and percentage of raw data return on iBO moorings from 2017 to 2018.

Mooring	Instrument	Serial number	Depth (m)	Clock Drift (mm:ss)	First Good Record (UTC)	Last Good Record (UTC)	Raw Data Return ¹
BR-01-17	TRDI QM ADCP 150 kHz	12824	176	04:43	Oct-02-2017 15:45:00	Oct-10-2018 16:29:00	100%
BR-01-17	TRDI LR ADCP 75 kHz	12884	462	N/A	N/A	N/A	0.0%
BR-01-17	Nortek Aquadopp DW	2792	586	01:17	Oct-02-2017 16:00:00	Oct-10-2018 16:30:00	100%
BR-01-17	Nortek Aquadopp DW	9839	742	N/A	N/A	N/A	0.0%
DFO-9-17	TRDI WHS ADCP 300 kHz	12414	31	08:45	Sep-30-2017 16:30:00	Oct-09-2018 20:08:44	100%

¹Note: The raw data return is based on the number of records (including bad data) during the period from the mooring deployment to the mooring recovery.

3.2.1 Mooring BR-1

Time-series plots of current speed, direction, and along-slope current from the QM ADCP and one Aquadopps DW deployed at BR-1 from 2017 to 2018 are provided in Figure 5 and Figure 6. No data were available from the LR ADCP or second Aquadopps DW at BR-1 due to instrument failures. The data in the QM ADCP plots are filtered for bins with PG4+PG1 values less than 25%, bins affected by sidelobe interference and for error velocity thresholds as described in section 2.4.1. The first valid bin depth for QM ADCP #12824 at BR-1-17 after removing sidelobe interference was 15.9 m (bin cell 39) and contains 85% valid data (Appendix D). The bin depth at 59.8 m (bin cell 28) of the QM ADCP appears to be affected by the presence of the IPS float and cage, which resulted in a reflection observed in the echo intensity (not shown) and a general decrease in current speed at these depths. A reflection was also observed at bin depths between 123.8 and 131.3 m (bin cells 10-12) due to the sediment trap and CT sensor frame located at this depth. Bin cells 10,11,12, and 28 of QM ADCP #12824 were manually flagged as part of the QA/QC and data from these bin depths should be treated carefully before being used in further analyses. The pressure time series from the QM ADCP #12824 recorded fluctuations on the order of 2 to 4 m during the deployment which do not correspond to changes in depth during mooring layover, indicating a potential malfunction of the pressure sensor. The pressure time series from this instrument should be used with caution. The Aquadopps DW current meter #2792 at 586 m provided a time-series with 100% valid data return (Figure 6, Appendix D).

Mean current speeds at BR-1-17 ranged from 10 to 19 cm/s in the upper 170 m of the water column; and 3 cm/s at a depth of 586 m (Table 9, Appendix D). Vector-averaged directions were typically to the west-southwest (200-260°TN) for all bin depths down to 130 m. Between 130 m and 170 m the vector-averaged direction transitions to the south (150-200°TN). The Aquadopps at 586 m measured an average direction to the east at 75°TN. The maximum current speed measured for un-flagged bins was 67 cm/s on June 27, 2018 at 116 m depth during a strong but short-lived (1-2 days) pulse with current direction along-slope to the northeast. Several other intermittent intervals of stronger currents (>50 cm/s, with strongest values centered around 50 to 150 m) to the north-northeast were measured in late March, late April/early May, and early August 2018. These events, which all have a strong along-slope component, are presumably driven by strong winds, however the depth-intensified patterns (Figure 5) suggest that the wind forcing is not local. Several shorter-lived and lower intensity pulses of current directed along-slope to the northeast were measured between October 2017 and December 2017.

Seasonal current roses (low-pass filtered) for selected bin depths at mooring BR-1-17 are provided in Figure 7 through Figure 9. Predominant current directions in the upper water column (32 m) are to the west in the fall, winter, and spring and are more variable in the summer when stronger northeast directed currents were measured. Lower in the water column at 128 m the currents were variable and generally less than 20 cm/s; in winter and spring the most frequent currents were directed north or south (across the slope). Near the bottom at 586 m, low-pass filtered currents were generally weak (<10 cm/s) with increased variability (Figure 9) but with a dominant direction to the northeast along-slope.

BR-1; QM Broadband 153.6 kHz; 70.43318 N, 139.02649 W; 2017-2018; Instr. #12824

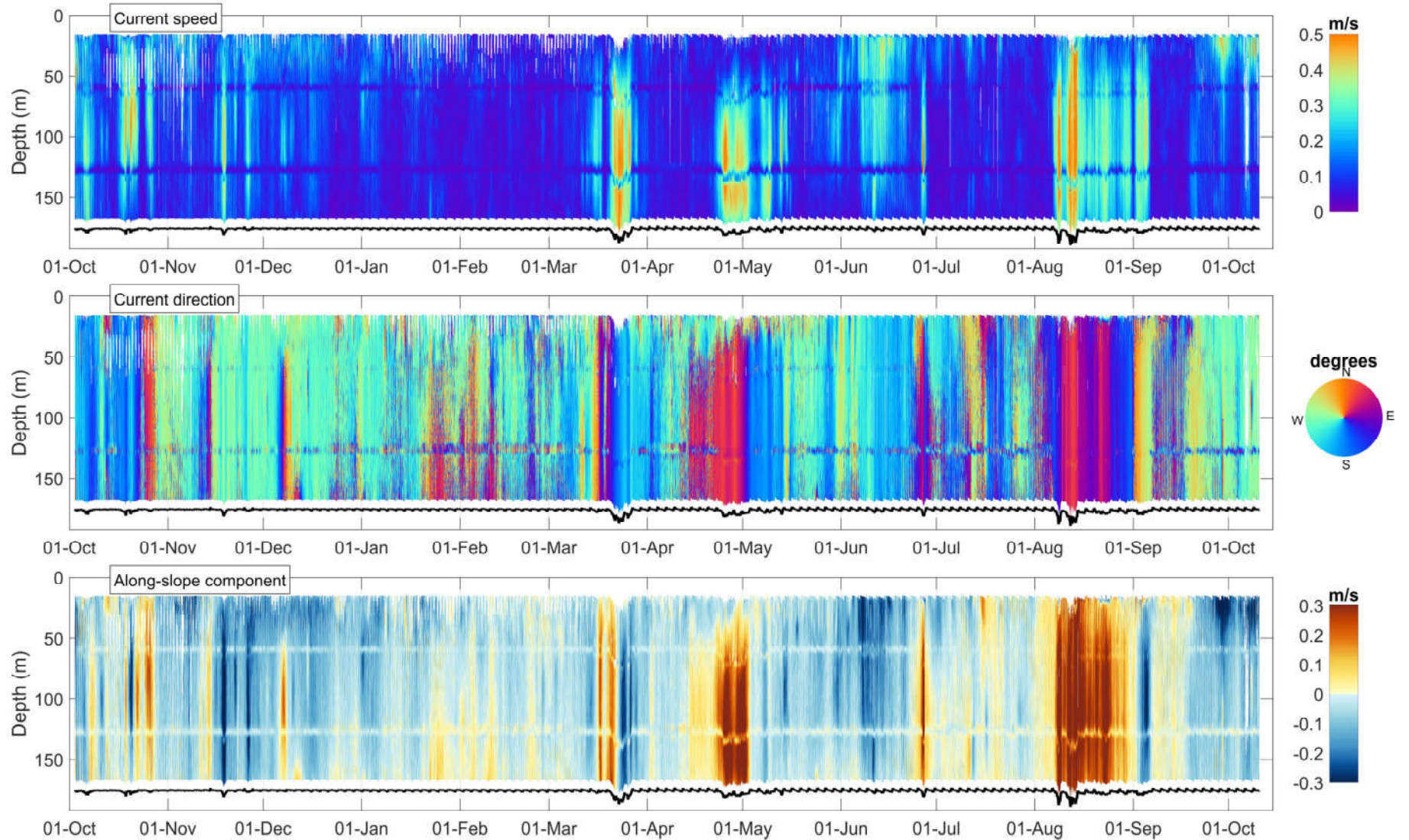


Figure 5: Time-series of current speed, current direction and along-slope current component at mooring BR-1-17 measured by the QM ADCP #12824. The black line depicts the instrument depth.

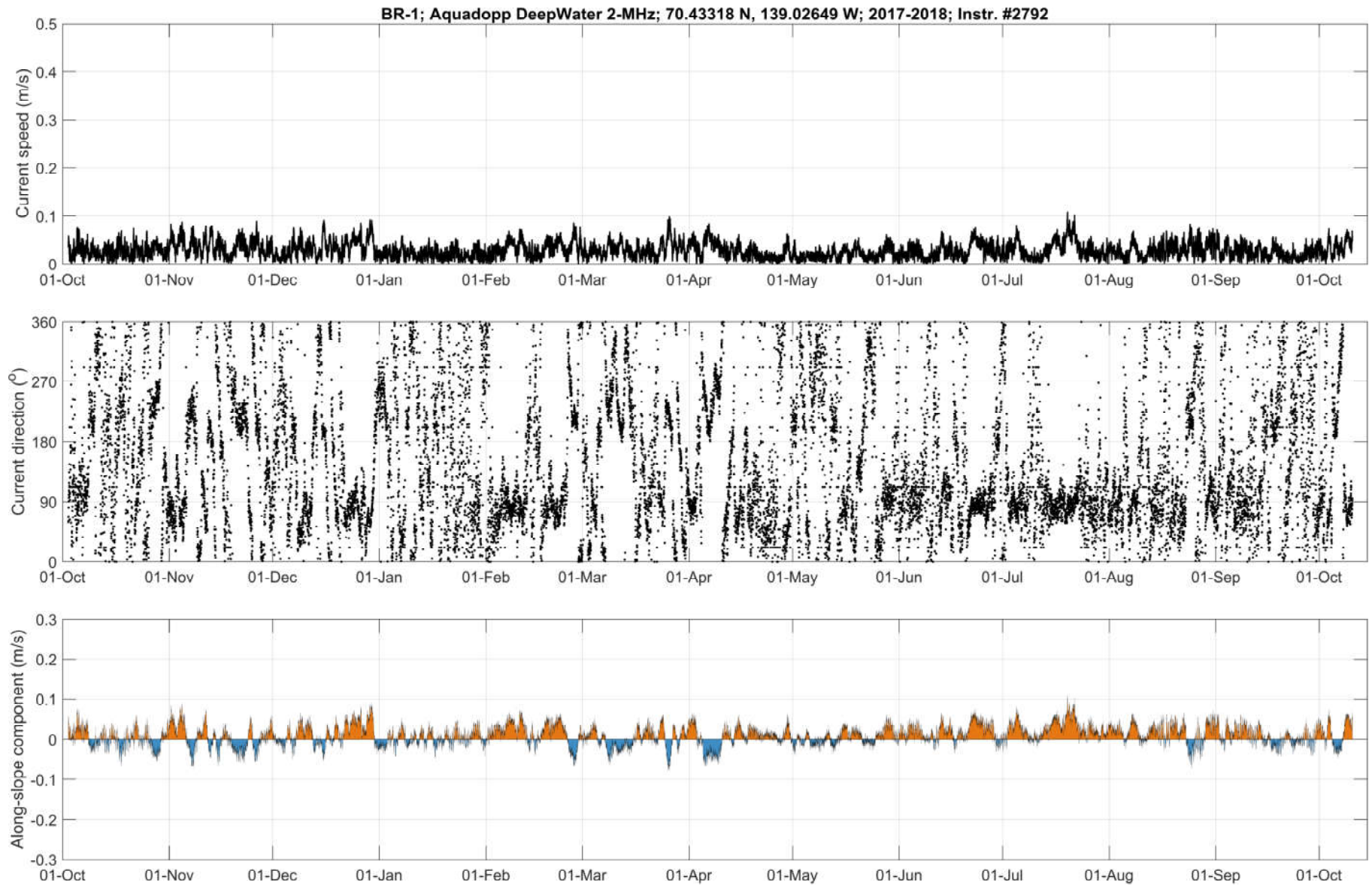


Figure 6: Time-series of current speed, current direction and along-slope current component at 586 m at mooring BR-1-17 measured by the Aquadopp #2792.

Table 9: Annual statistics of current speed and direction at BR-1-17 from selected bin depths representative of water mass variability in the Beaufort Sea (see Table 7 for water mass description).

Bin Depth (m)	Median Speed (m/s)	Mean Speed (m/s)	75%ile Speed (m/s)	95%ile Speed (m/s)	99%ile Speed (m/s)	Max Speed (m/s)	Standard Deviation Speed (m/s)	Vector-Averaged Direction (deg TN)
32	0.12	0.13	0.18	0.30	0.41	0.60	0.09	249.2
136	0.09	0.13	0.16	0.37	0.47	0.56	0.11	198.0
586	0.03	0.03	0.04	0.06	0.08	0.11	0.02	75.8

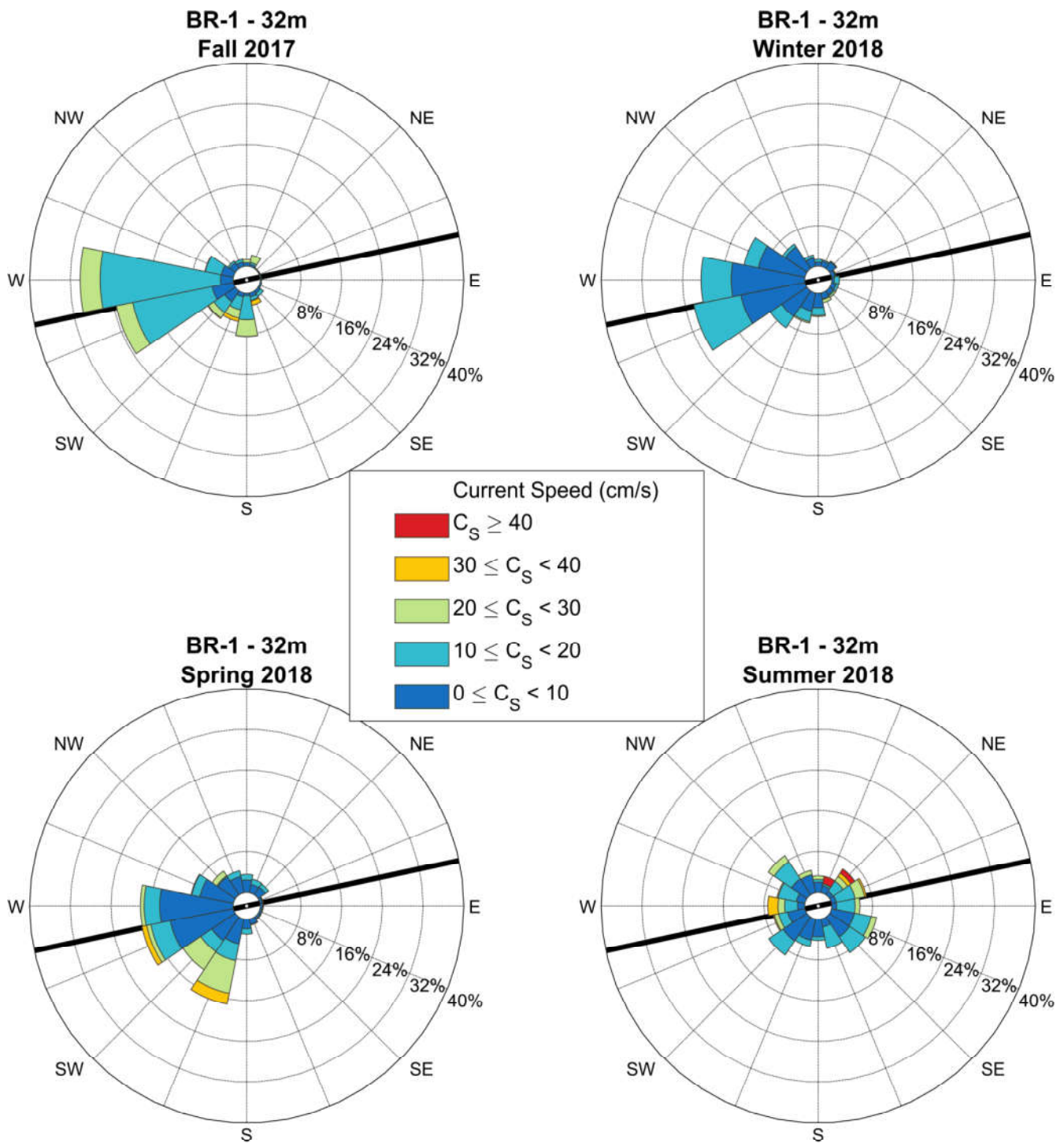


Figure 7: Seasonal current roses at 32 m depth (bin cell #35) at BR-1-17 measured by the QM ADCP #12824. Data are low-pass filtered. Roses indicate the direction toward which currents flow. Seasons are defined following the meteorological convention (Fall: October-December; Winter: January-March; Spring: April-June; Summer: July-September). Black line indicates the angle chosen to describe the along-slope/shelf current.

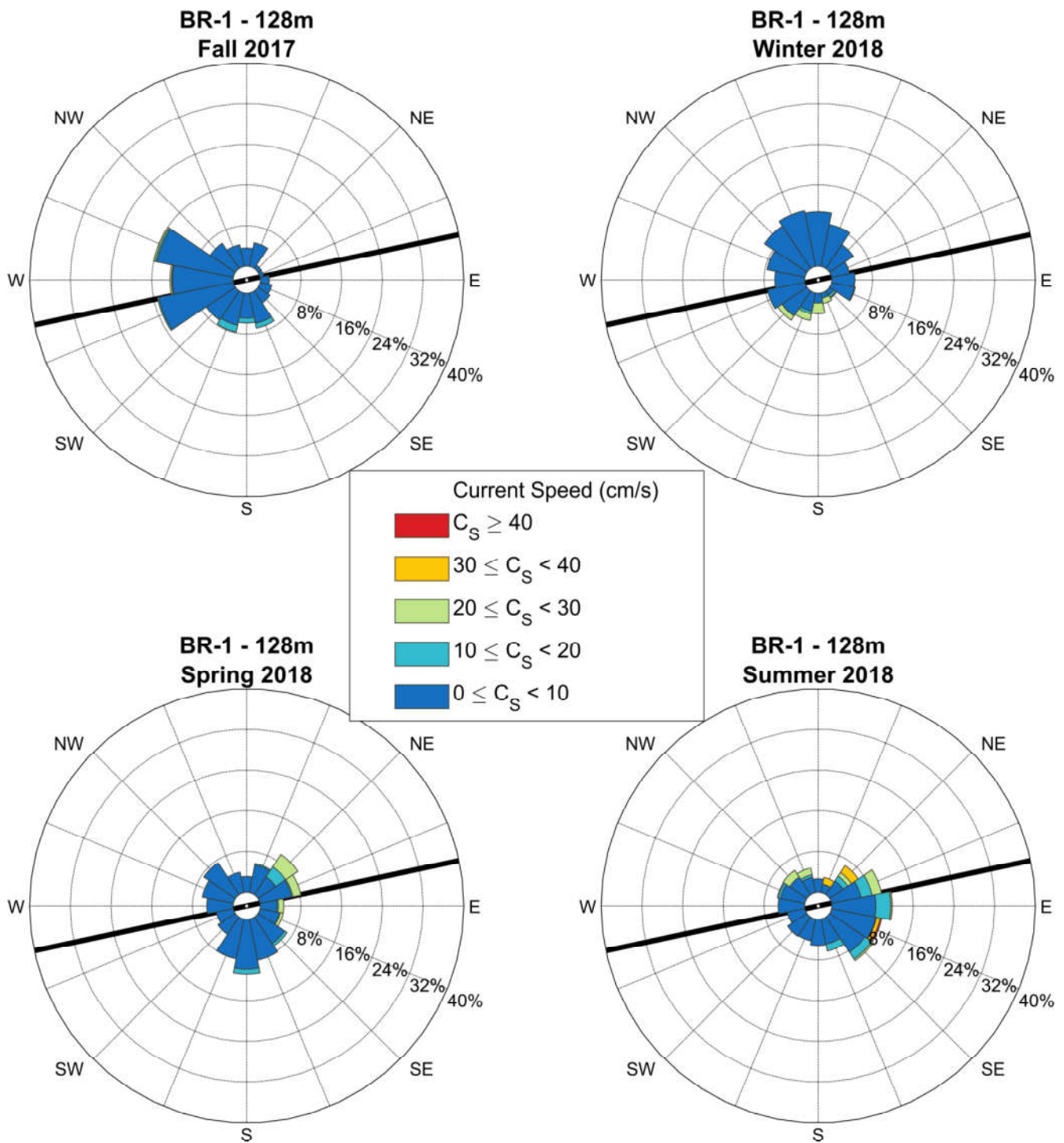


Figure 8: Seasonal current roses at 128 m depth (bin cell #11) at BR-1-17 measured by the QM ADCP #12824. Data are low-pass filtered. Roses indicate the direction toward which currents flow. Seasons are defined following the meteorological convention (Fall: October-December; Winter: January-March; Spring: April-June; Summer: July-September). Black line indicates the angle chosen to describe the along-slope/shelf current.

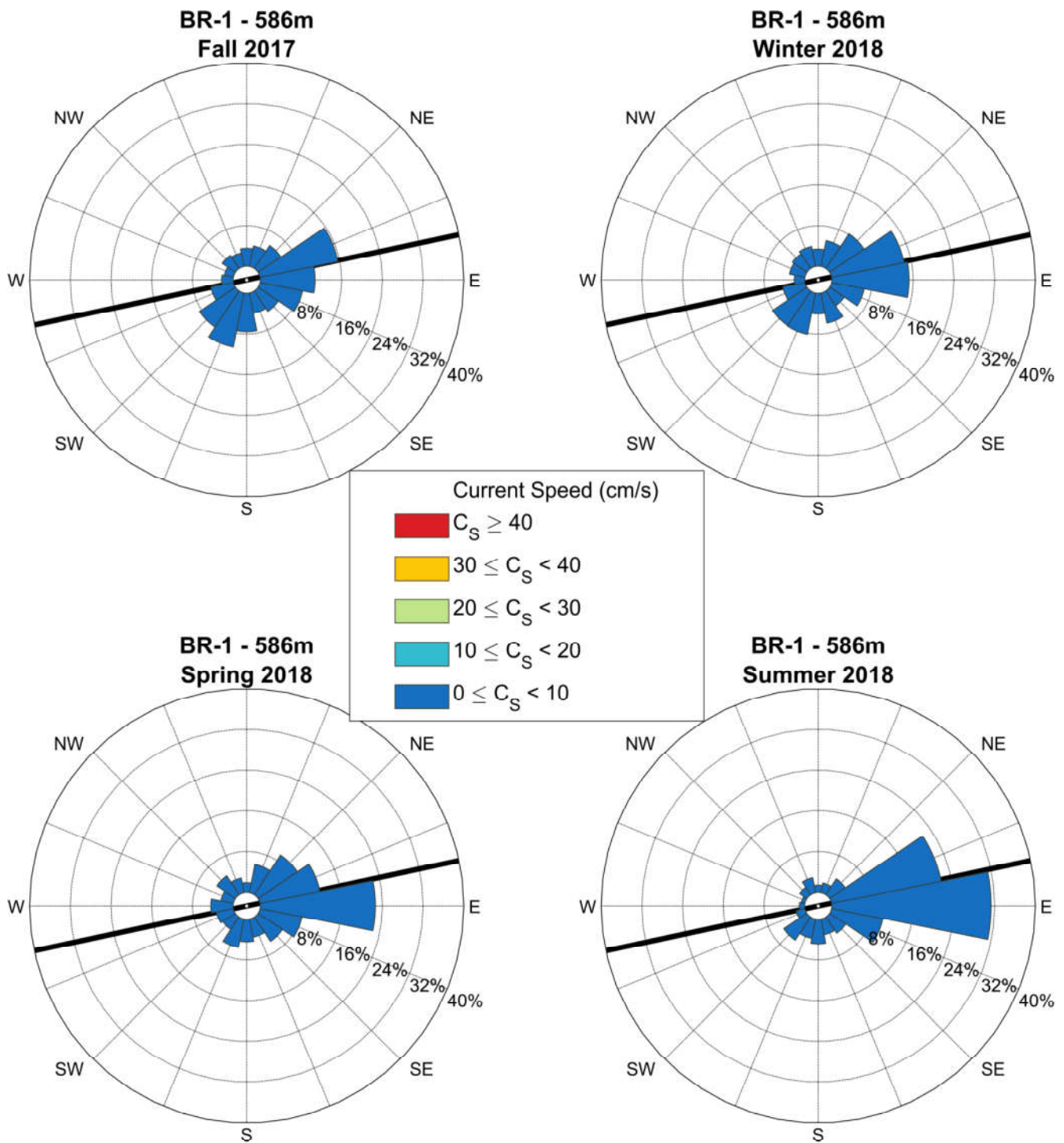


Figure 9: Seasonal current roses at 586 m depth at BR-1-17 measured by the Aquadopp #8448. Data are low-pass filtered. Roses indicate the direction toward which currents flow. Seasons are defined following the meteorological convention (Fall: October-December; Winter: January-March; Spring: April-June; Summer: July-September). Black line indicates the angle chosen to describe the along-slope/shelf current.

3.2.2 Mooring DFO-9

A time-series plot of current speed, direction, and along-slope current component from the WHS ADCP deployed at the inner shelf mooring DFO-9 from 2017 to 2018 is provided in Figure 10. The data in the WHS ADCP plot are filtered for bins with PG4 values less than 25%, bins affected by sidelobe interference and for error velocity thresholds and other masks as described in section 2.4.1. The first valid bin depth for the WHS ADCP #12414 at DFO-9-17 after removing sidelobe interference was 5.0 m (bin cell 24) with a percentage of valid data of 70% (Appendix D). Percentage of valid data below the uppermost valid bin depth ranged from 70 to 100%.

Based on the valid data collected at DFO-9-17, mean current speeds at this site range from 8 to 17 cm/s throughout the water column, with the stronger mean currents typically near the surface (Table 10, Appendix D). Vector-averaged directions were all towards the east-northeast (35-90°TN) in the upper 18 m of the water column and towards the west and southwest in the lowermost bins. Maximum current speed at DFO-9-17 was 108 cm/s on September 1, 2018 at the 5.0 m depth bin during a strong northeasterly flow event. Seasonal current roses (low-pass filtered) for one bin depth (20.0 m) at mooring DFO-9-16 are provided in Figure 11. The roses show current directions are strongly bi-directional at this location, frequently in alignment along the shelf. The strongest currents occur most frequently in the summer months.

DFO-9; WHS 300 307.2kHz; 70.0584 N, 133.7154 W; 2017-2018; Instr. #12414; 31 m depth

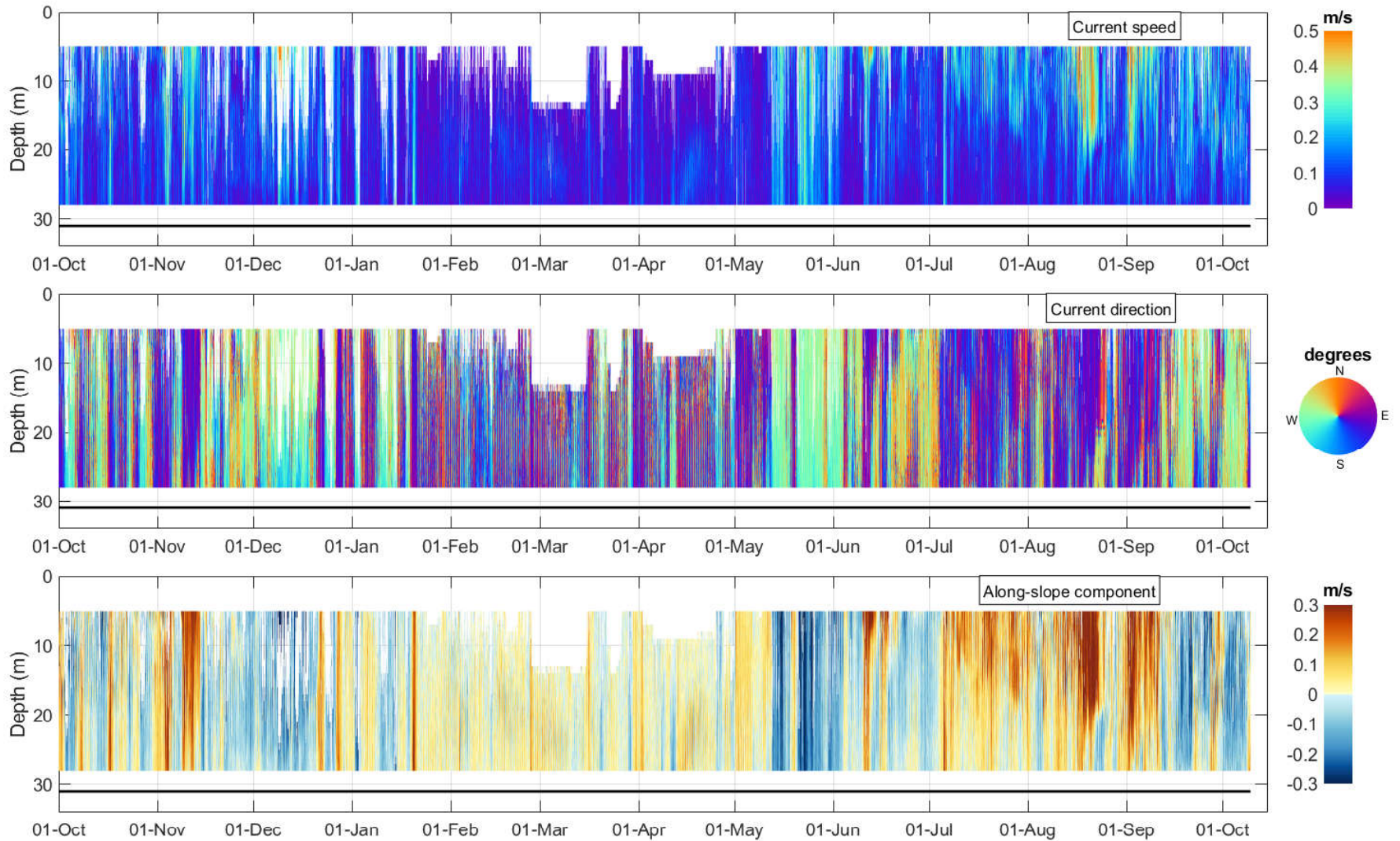


Figure 10: Time-series of current speed, current direction and along-slope current component at mooring DFO-9-17 measured by the WHS ADCP #12414. The black line depicts the instrument depth.

Table 10: Annual statistics of current speed and direction at DFO-9-17 from a selected bin depth representative of the Polar-mixed layer (see Table 7 for water mass description).

Bin Depth (m)	Median Speed (m/s)	Mean Speed (m/s)	75%ile Speed (m/s)	95%ile Speed (m/s)	99%ile Speed (m/s)	Max Speed (m/s)	Standard Deviation Speed (m/s)	Vector-Averaged Direction (deg TN)
20.0	0.09	0.10	0.14	0.23	0.31	0.49	0.07	241.0

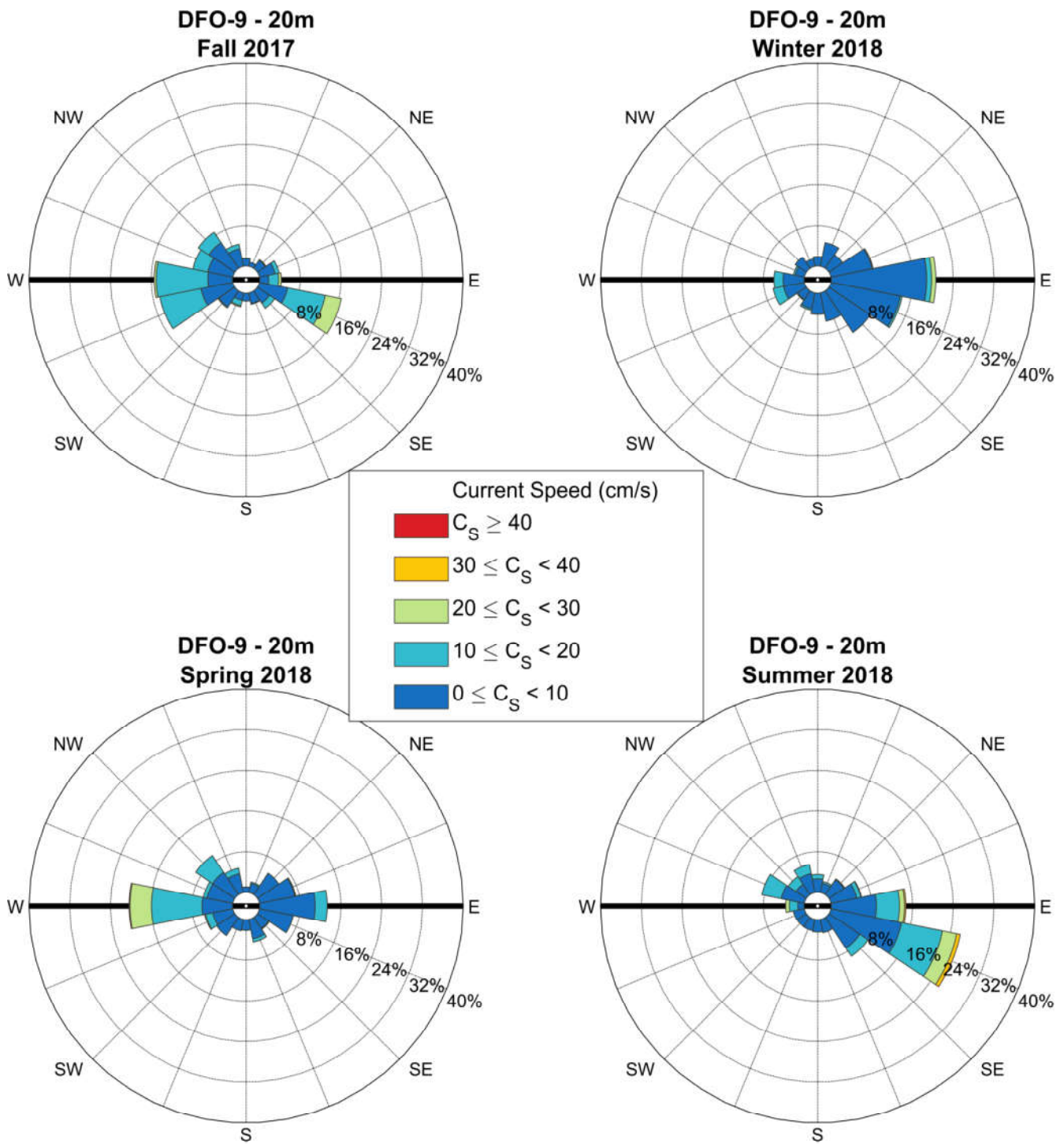


Figure 11: Seasonal current roses at 20 m depth at DFO-9-17 as based on low-pass filtered data from bin cell #9 measured by the WHS ADCP #12414. Roses indicate the direction toward which currents flow. Seasons are defined following the meteorological convention (Fall: October-December; Winter: January-March; Spring: April-June; Summer: July-September). Black line indicates the angle chosen to describe the along-slope/shelf current.

3.2.3 Spatial Variability of Surface and Bottom Currents in Open Water

Near-surface and near-bottom currents (low-pass filtered) during the open water season (June to October) were mapped as current roses in Figure 12 to Figure 13 provide an overview of current variability at the two mooring sites (BR-1 and DFO-9) during the operational season in the southeastern Beaufort Sea. Each map represents current variability during a composite open water season, which is based on the initial (fall) and final (summer) sampling period of a given deployment year.

The currents roses (Figure 12) illustrate the dominant surface currents in open water during 2017-2018 at BR-1 was in accord with the anti-cyclonic (clockwise) motion of the Beaufort Gyre with directions generally to the southwest along the slope. A few strong reversals in current direction to the northeast are observed in the surface current rose. At DFO-9 the surface currents in open water are bi-directional, dominantly to the southeast and northwest likely driven by wind forcing on the shelf.

Near-bottom currents during summer and fall (Figure 13) in 2017-2018 were predominantly toward the northeast at BR-1 generally following the bathymetric contours. Near-bottom currents at DFO-9, like the surface currents, are bi-directional, but with greater variability than at the surface.

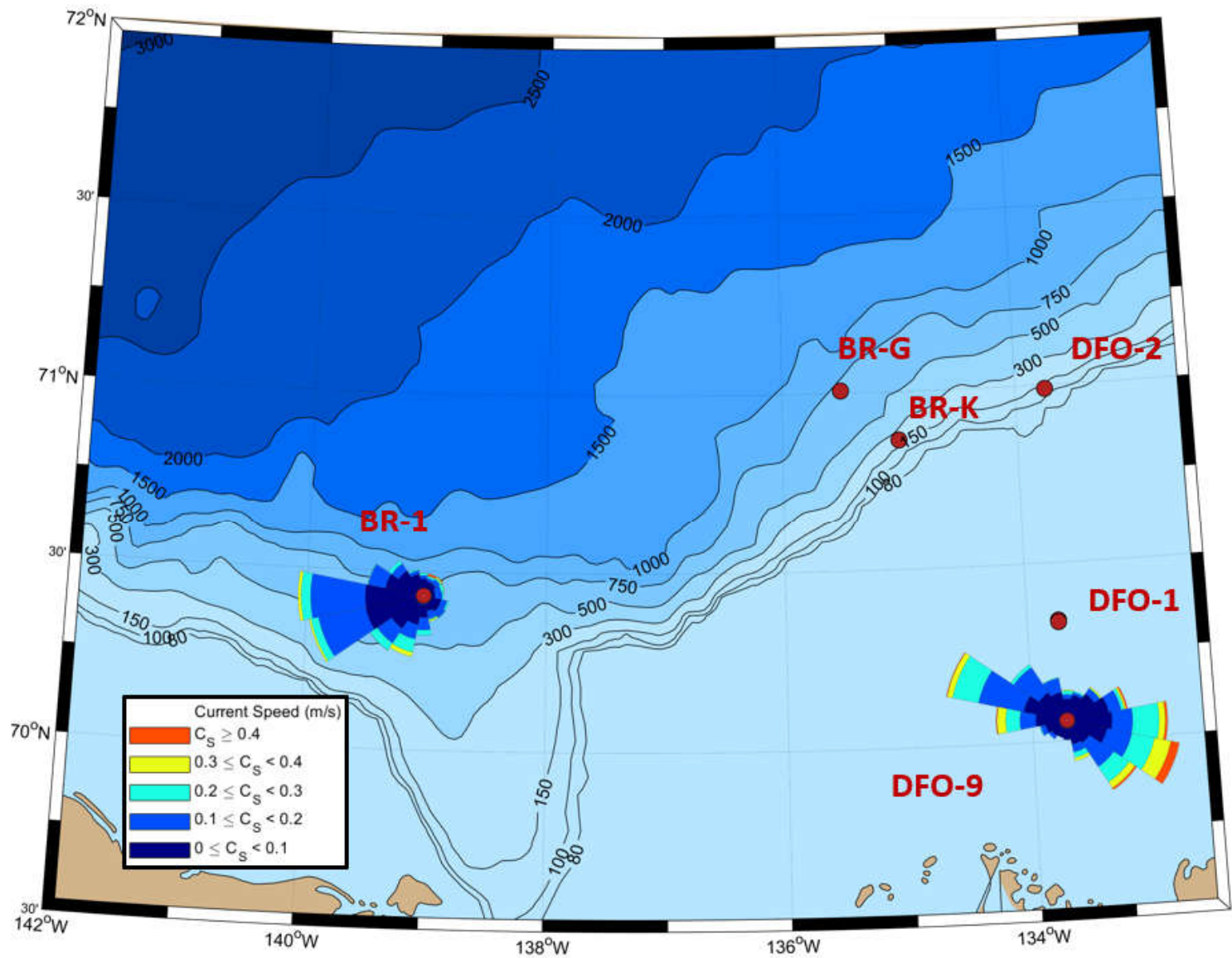


Figure 12: Near-surface currents for the open water season for low-pass filtered current velocity data from the bin depth nearest bin depth to 20 m at BR-1 and 5 m at DFO-9. Data when sea ice was present (winter-spring) were filtered out. Roses indicate toward where the current is flowing.

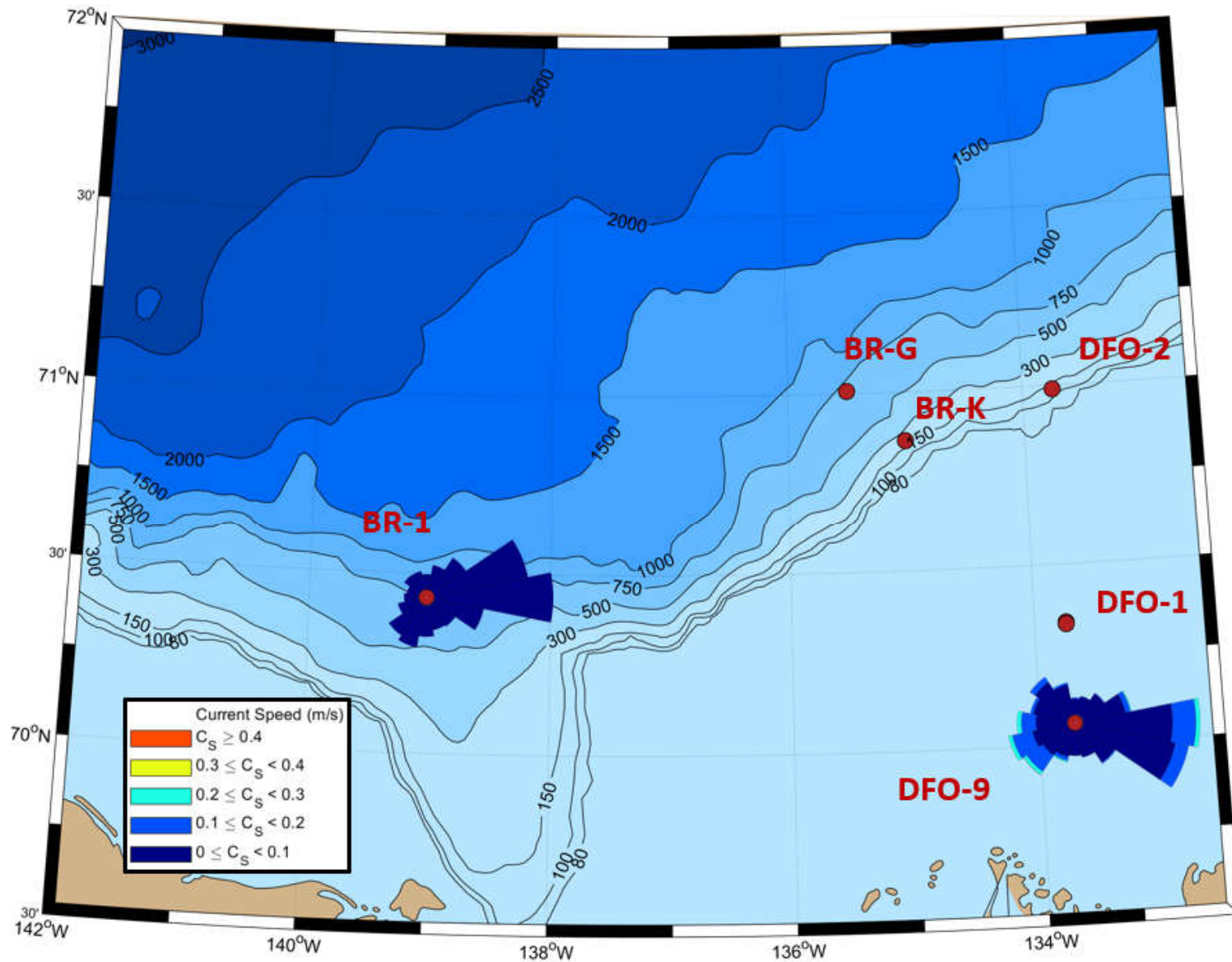


Figure 13: Near-bottom currents for the open water season for low-pass filtered current velocity data from the bin depth nearest to bottom at each location. Data when sea ice was present (winter-spring) were filtered out. Roses indicate toward where the current is flowing.

3.3 Temperature and Salinity

The summary of CT logger data recovery success on iBO moorings from 2017 to 2018 is provided in Table 11. A summary of valid and flagged data (suspicious spikes) for each processed CT sensor is provided in Table 12 for the BR-1 mooring. Statistics are not presented for the DFO mooring due to differences in the QA/QC processing methodology.

Processed temperature and salinity data from all CT loggers deployed on BR moorings from 2017 to 2018 are presented using time-series plots of temperature and salinity at each mooring. Temperature time-series recorded at mooring BR-1 are presented in Figure 14. Salinity time-series for the same moorings are provided in Figure 16. Temperature and salinity time-series for DFO-9 are provided in Figure 15 and Figure 17. Data from temperature-salinity time-series presented below were filtered for spike-like values that were detected using the method described in section 2.4.2. Missing data were replaced by linearly-interpolated values in the time-series plots. A temperature-salinity diagram is also provided in Figure 18, which combines all QA/QC data from the moored CT loggers (also filtered for spikes, but not interpolated for missing values) as well as water column profile data from CTD casts conducted at mooring deployment in 2018 aboard the Laurier.

The temperature time-series recorded at discrete depths varying from 32 to 742 m on the slope at BR-1 illustrate the typical vertical layering in temperature in the Beaufort Sea (e.g. Lansard et al. 2012 and references therein). Temperature at BR-1 was most variable in the upper 200 m of the water column, with temperature varying from around 0.1°C down to -1.7°C. Variability was even greater at the CT logger on DFO-9 on the shelf which varied in temperature from 0.6°C to -1.8°C. Variability at DFO-9 was greatest during the summer ice-free months. Rapid transitions from relatively cold to relatively warm (and vice-versa) temperature were often detected in the upper 200 m at both moorings. For example, the most extreme was an increase from -1.0 to 0.6°C recorded at 32 m at DFO-9 in late August 2017 (Figure 15).

Likewise temperature, the salinity time-series showed that most of the variability in terms of water mass physical properties occurs in the upper 200 m (Figure 16 through Figure 17). Contrary to temperature, salinity is monotonically increasing with depth in the Beaufort Sea. On the slope in 2017 to 2018, salinity from 450 to 740 m depth occupied a very narrow range from 34.7 to 34.9, while salinity in the upper 200 m ranged from 27.9 (DFO-9, 32 m on November 12, 2017) up to 34.5 (BR-1 at 177 m in late October 2017). Several rapid transitions from in salinity (increases up to 1.5) were measured in the upper 200 m at BR-1, notably in late October 2017, mid-March 2018, late May 2018, and in August 2018 which were concurrent with a strong negative along-slope current, indicating a possible upwelling condition.

The temperature-salinity diagram combining all data from the CT loggers provides a way to further characterize the different water masses occupying the water column at mooring locations from 2017 to 2018 (Figure 18). This diagram provides evidence that most of the variability in the water column is taking place in the upper 200 m. It also illustrates the presence of Beaufort Sea Winter Water (BSWW), described in Jackson et al. (2015) as cold salty (33) water near the freezing point capable of halocline ventilation. BSWW was not observed at the mooring sites in 2016 to 2017 but was observed in 2015 to 2016.

The visual comparison between CTD cast data from 2018 and the moored CT sensor data provides a preliminary assessment of the accuracy of the CT sensor data. Instruments in the upper 200 m did not appear to be affected by any visible bias given their consistency with respect to the freezing line and the expected variability in the shape of the halocline (i.e. between ~32.0 and 34.7 salinity) that changes over time due to upwelling/downwelling and other mixing processes. The deeper CT logger instruments (>400 m) also did not show any offset with respect to the CTD cast data collected in 2018 and were therefore not corrected.

Table 11: Summary of CT data logger clock drift and percentage of raw data return on iBO moorings from 2017 to 2018.

Mooring	Instrument	Serial number	Depth (m)	Clock Drift (mm:ss)	First Good Record (UTC)	Last Good Record (UTC)	Raw Data Return (%)
BR-01-17	RBR XR420 CT	15266	62	01:27	Oct-02-2017 16:00:00	Oct-10-2018 17:00:00	100%
BR-01-17	SBE37 Microcat	12235	122	00:00	Oct-02-2017 16:00:00	Oct-10-2018 17:00:00	100%
BR-01-17	RBR XR420 CT	15263	177	01:15	Oct-02-2017 16:00:00	Oct-10-2018 17:00:00	100%
BR-01-17	RBR XR420 CT	15274	462	00:26	Oct-02-2017 16:00:00	Oct-10-2018 17:00:00	100%
BR-01-17	SBE37 Microcat	10850	742	00:00	Oct-02-2017 16:00:00	Oct-10-2018 17:00:00	100%
DFO-9-17	SBE37 Microcat	6728	32.5	00:03	Sep-30-2017 16:15:00	Oct-09-2018 15:55:	100%

Table 12: Summary of valid and flagged data from CT loggers deployed on the BR slope moorings from 2017 to 2018. See Table 11 for the instrument model associated with each serial number.

Mooring	Serial number	Depth (m)	Number of Valid Conductivity Records	Number of Flagged Conductivity Records	% of Valid and Un-flagged Conductivity Records (%)	Number of Valid Temperature Records	Number of Flagged Temperature Records	% of Valid and Un-flagged Temperature Records (%)
BR-01-17	15266	62	53,719	24	100.0%	53,719	11	100.0%
BR-01-17	12235	122	53,719	75	99.9%	53,719	42	99.9%
BR-01-17	15263	177	53,719	7	100.0%	53,719	7	100.0%
BR-01-17	15274	462	53,719	16	100.0%	53,719	9	100.0%
BR-01-17	10850	742	53,719	9	100.0%	53,719	5	100.0%

Note: The percentage of valid data is based on the total number of records returned by the instrument from deployment to recovery. Data from DFO moorings are not presented here due to the difference in methodology for data processing.

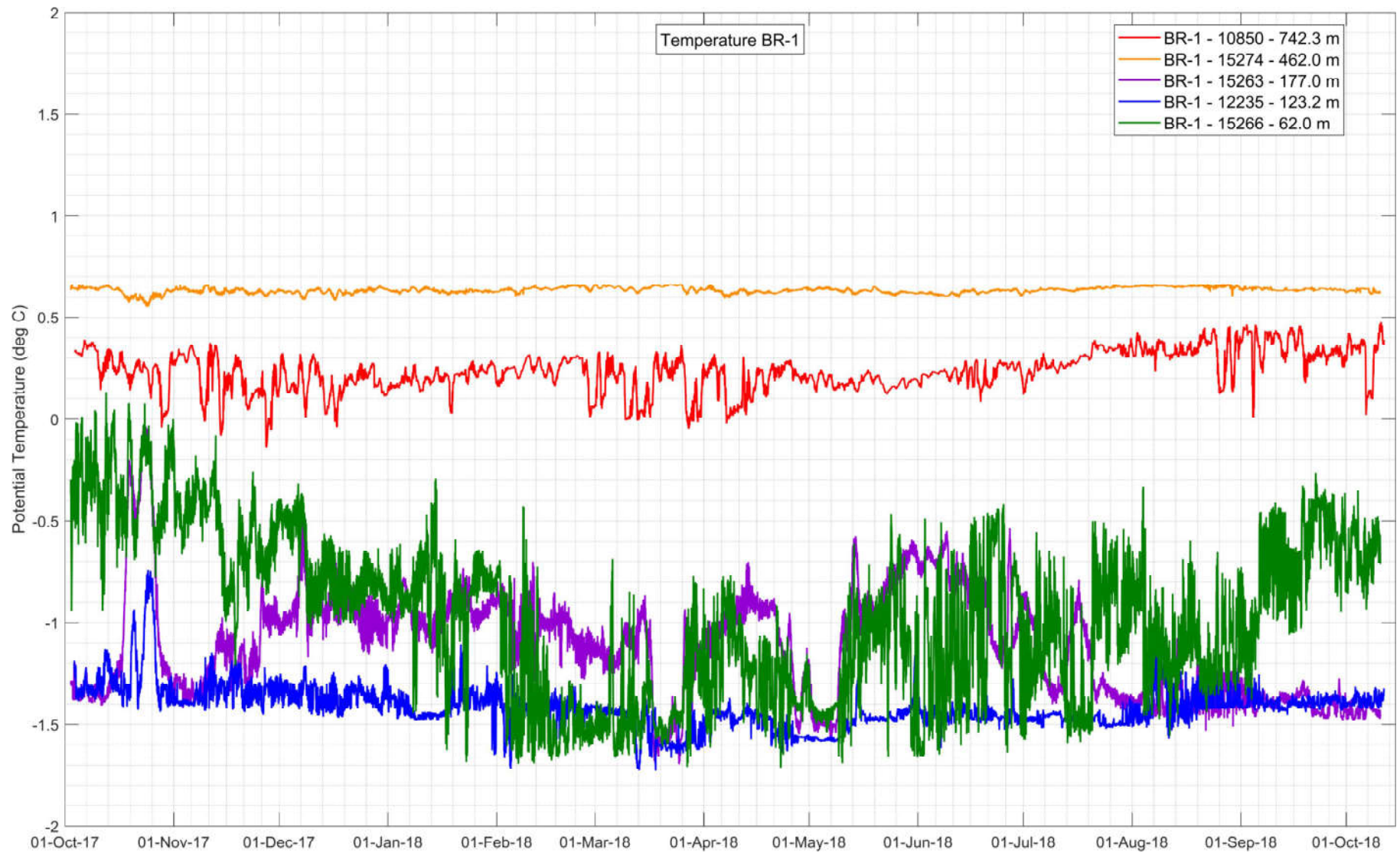


Figure 14: Temperature time-series measured at BR-1-17 from 2017 to 2018. The legend shows the serial number and depth of each CT logger.

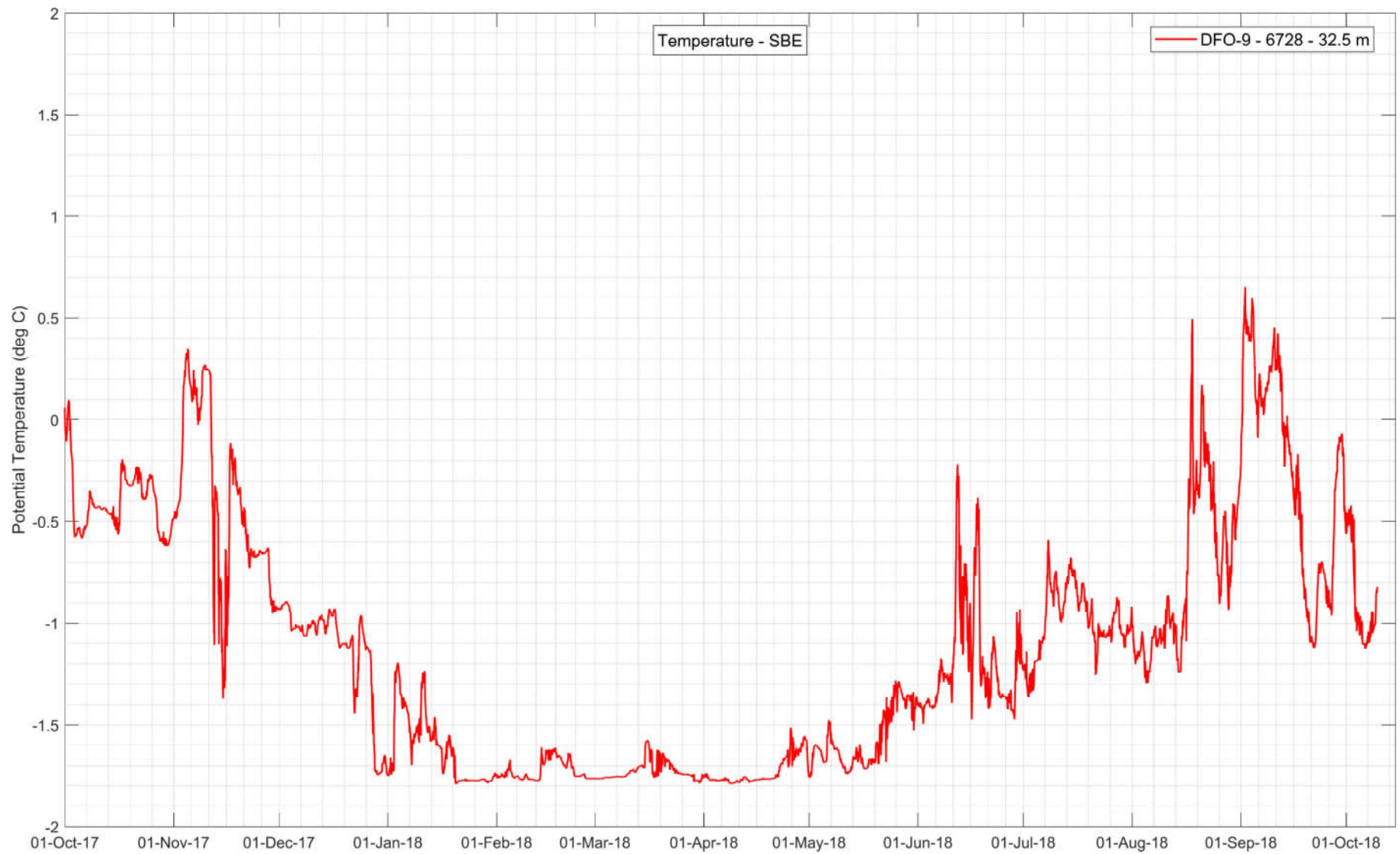


Figure 15: Temperature time-series recorded at DFO-9-17 from 2017 to 2018. The legend shows the serial number and depth of each CT logger.

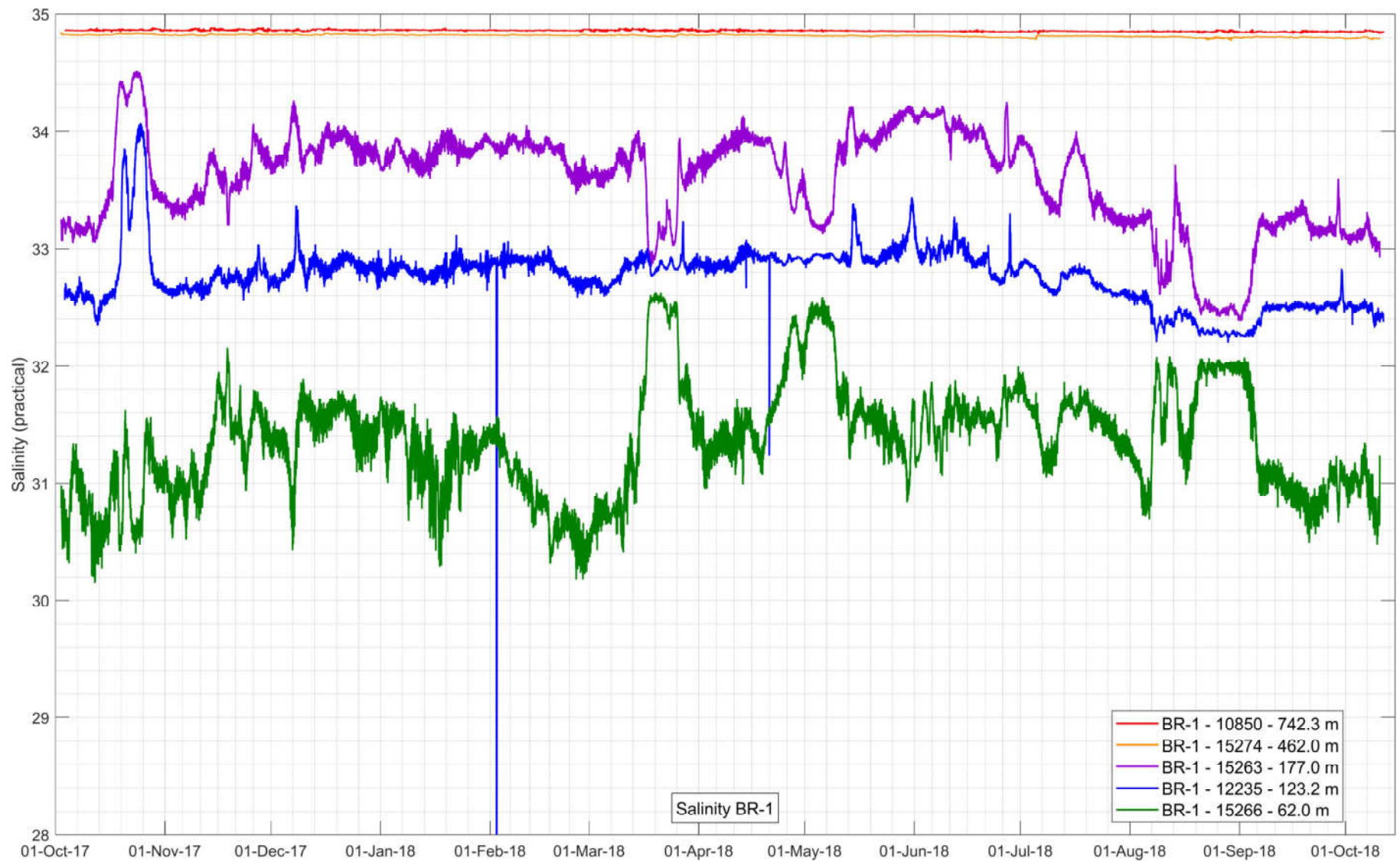


Figure 16: Salinity time-series recorded at BR-1-17 from 2017 to 2018. The legend shows the serial number and depth of each CT logger.



Figure 17: Salinity time-series recorded at DFO-9-17 from 2017 to 2018. The legend shows the serial number and depth of each CT logger.

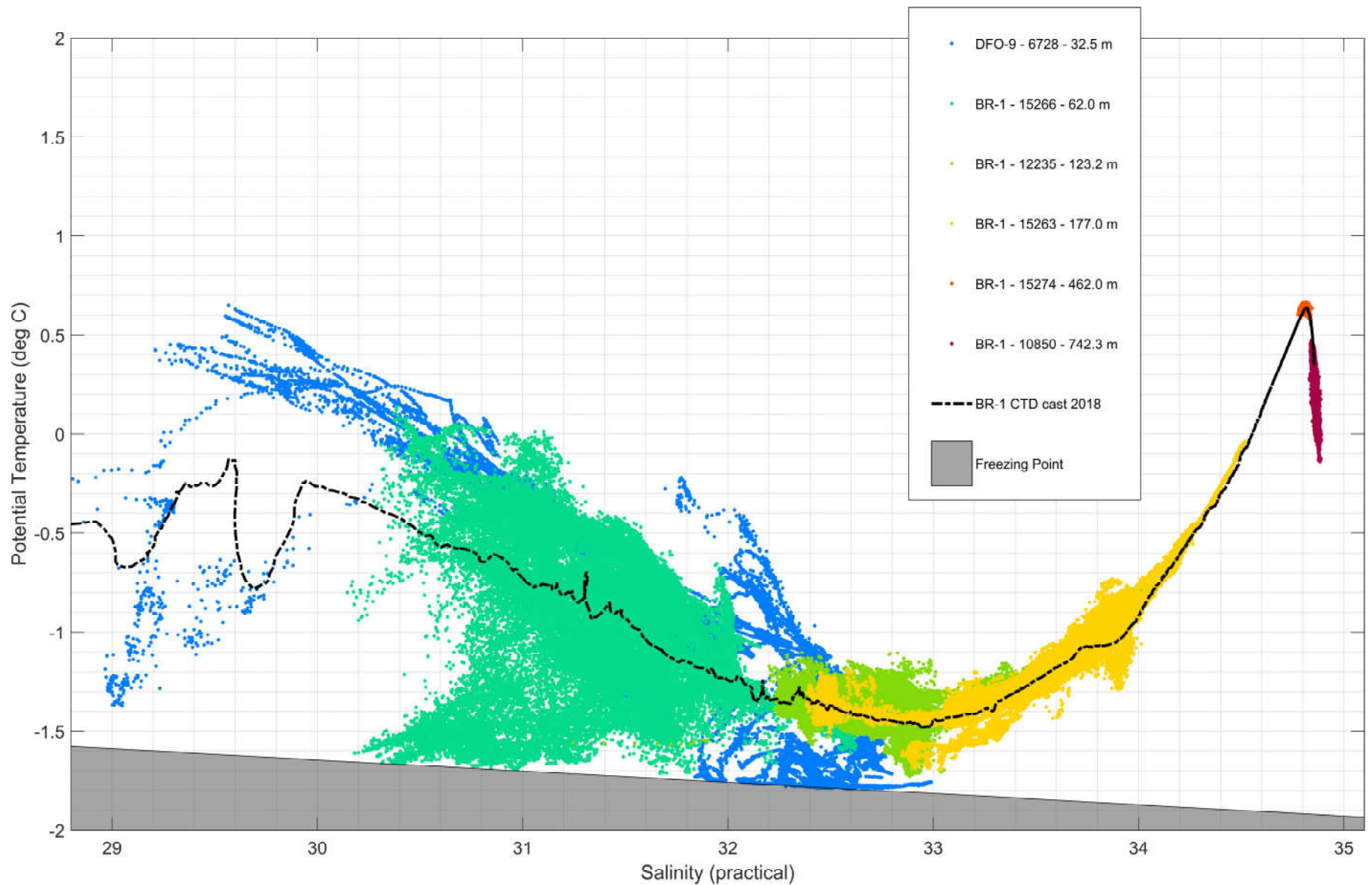


Figure 18: Temperature-salinity diagram constructed with all data acquired by the CT loggers attached to the moorings BR-1 and DFO-9 from 2017 to 2018. CTD profile data taken at BR-1 during the CCGS Laurier cruises in 2018 are depicted by the black line.

3.4 Summary of 2014-2018 iBO dataset

This section of the report summarizes measurements of sea ice conditions, currents, salinity, and temperature data collected during the four-year iBO program and presented in the 2015, 2016, 2017, and 2018 Technical Project Reports (ArcticNet et al. 2016, 2017, and 2018). Table 13 provides a summary of the valid data by percentage (data remaining after filtering and processing) by instrument type at each mooring from 2014 to 2018. Data recovery was consistently at or near 100% for CT loggers and IPS instruments, while the data recovery for ADCPs was 90%. The high data recovery rates reflect the success of the iBO field program and attention to quality control and resulted in a near-continuous dataset at 7 mooring sites from 2014-2018 with few gaps. Data from 5 moorings are pending as they remain unrecovered due to unfavorable ice conditions in 2018 (a recovery attempt will be made in summer 2019 for these moorings).

Table 13: Valid data (%) by mooring and instrument type for the four-year iBO program.

Years	BR-K			BR-G			BR-1			BR-3		
	ADCP	CT	IPS	ADCP	CT	IPS	ADCP	CT	IPS	ADCP	CT	IPS
2014-2015	98.5	68.0	100	98.8	99.9	100	99.2	99.9	100	99.8	99.9	100
2015-2016	98.4	99.9	100	99.6	99.9	100	96.0	99.9	100	60.0	99.9	100
2016-2017	73.2	100	100	99.3	99.9	100	91.2	99.9	100	98.5	99.9	100
2017-2018	Not recovered			Not recovered			49.6	100	100	Not recovered		

Years	DFO-1			DFO-2			DFO-9		
	ADCP	CT	IPS	ADCP	CT	IPS	ADCP	CT	IPS
2014-2015	83.4	100	100	99.3	100	100	77.8	100	100
2015-2016	98.0	100	100	90.8	100	100	96.7	100	100
2016-2017	97.5	100	100	95.4	100	100	88.5	100	100
2017-2018	Not recovered			Not recovered			91.1	100	100

Note: IPS data are reported as % of recovered data

Sea ice conditions

A summary of sea ice conditions in the southern Beaufort Sea from 2015 to 2018 is provided in Table 14. Sea ice in 2015, 2016, 2017, and 2018 were characterized by earlier than normal break up in the spring. Regional (Beaufort Sea) seasonal ice coverage minima were in the top ten lowest on record for 2015 to 2017 while 2018 was near the median due to persistent northwesterly winds in late summer which pushed pack ice from the west and northwest of Banks Island into the southern Beaufort Sea. Processing and QA/QC data of the IPS dataset for 2014-2018 is in various stages of progress pending available funds (described in more detail in section 2.4.3). Currently available results from the iBO IPS dataset show that ice is changing more slowly over the Mackenzie shelf than further north in the Canada Basin. On the Mackenzie shelf, decadal trends show that the ice-free season is now longer and the ice slightly thinner by about 6 cm.

Table 14: Summary of sea ice conditions in the southern Beaufort Sea from 2014 to 2018.

Year	Ice break-Up ¹	Regional seasonal ice coverage minimum
2015	June (4 weeks ahead of normal)	14.8% (fifth lowest on record)
2016	May (6 weeks ahead of normal)	4.9% (second lowest on record)
2017	May (6 weeks ahead of normal)	18.7% (eighth lowest on record)
2018	June (4 weeks ahead of normal)	33.1% (near the median on record)

Note: ¹As described by the Canadian Ice Service season summary for North American Arctic Waters. The interval from 1981 to 2010 is used to define average conditions. See Sea Ice Climatic Atlas for the Northern Canadian Waters 1981-2010 for more detail.

Ocean Currents

Current profilers and current meters at the 7 mooring sites provided measurements of ocean current through the water column from 2014 to 2018. The measurements allow currents across the shelf, shelf-break, and slope to be described and characterized in terms of multi-year mean conditions and variability and provide evidence and insight into large-scale circulation patterns (coastal current on the shelf, shelf-break jet, slope current, and Beaufort Gyre current on the lower slope) and smaller-scale patterns (eddy-like features and up-welling and down-welling events). Each dataset from 2014 to 2018 was illustrated with color contour plots of current speed, direction, and along-slope component of current. Seasonal current roses for selected bin depths were provided to contrast the temporal variability of ocean circulation patterns in relation to the distinct water masses and water mass boundaries. Finally, annual statistics of current speed and direction provide a characterization of the behaviour of ocean currents with depth.

Table 15 provides a summary of the annual mean and max speeds from 2014 to 2018 at the bin depths selected to characterize the circulation patterns throughout the water column (see Table 7 for further description). The maximum current speeds are typically observed in the near-surface bins where wind-driven currents are strongest. On the lower slope moorings (BR-1, BR-3, and BR-G) current speeds are consistently weak (mean speed <8 cm/s) with low variability below 220 m depth. Current speeds are weakest at BR-3, except near-bottom (700 m) currents which are stronger than in the mid-water column suggesting an effective transfer of energy to deep water at this site (more investigation is required to understand the mechanism for this). On the upper slope (BR-K and DFO-2) more variability is observed in the current speeds, a result of the dynamics of the shelf-break jet at these sites. Current speeds across the shelf (DFO-1 and DFO-9) are relatively uniform and weak; possibly due to being driven by a buoyant coastal current rather than wind forcing.

Table 15: Summary of the annual mean and max speeds at the bin depths selected to characterize the circulation patterns throughout the water column for 2014-2017.

Approximate Water Depth (m)	BR-1 ¹	BR-3	BR-G	BR-K	DFO-2	DFO-1	DFO-9 ¹
	Range in annual mean speeds 2014-2018 (max speed 2014-2018), cm/s						
20	11-15 (87)	7-8 (48)	13-19 (92)	12-16 (85)	11-13 (64)	8-10 (42)	8-10 (61)
130	10-15 (59)	6-7 (34)	13-14 (69)	12-20 (75)	7-9 (47)		
220	3-7 (41)	5-6 (33)	6-8 (44)				
350	3-5 (43)	5-6 (26)	4-5 (30)				
550	3 (13)	5-6 (22)	4 (21)				
700	3-4 (20)	7-8 (34)	4-5 (30)				

Note: ¹Includes 2017-2018 deployment.

Temperature and Salinity

CT loggers at the 7 mooring sites provided measurements of temperature and salinity at discrete depths from approximately 30 to 740 m and provide evidence of layering of water masses and indication of water mass shifts associated with events such as up-welling and down-welling motions. The CT logger data are illustrated with time-series of loggers on each mooring and using a temperature-salinity diagram combining all data from the CT loggers to further characterize the different water masses occupying the water column at the moorings. The majority of variability in terms of water mass physical variability occurs in the upper 200 m of the water column. Water mass shifts resulting in the upper 200 m from up-welling or down-welling were identified primarily on the slope moorings (BR-1, BR-3, BR-G, and BR-K) throughout the year but most frequently during the summer months when wind-driven currents are most important. Deep Atlantic Water (450 to 740 m) consistently occurs between a very narrow range of salinity from 34.7 to 34.9 and temperatures from -0.3°C to 0.7°C .

Biogeochemical fluxes

Sediment traps deployed at 2 depths on longer slope moorings provide insights on the biological regime and cycle marine productivity in the offshore domain of the southern Beaufort Sea. Sediment trap data from BR-1, BR-G, and BR-3 were analyzed for 2014 to 2017 while analyses on the sediment trap samples from 2017 to 2018 are currently pending additional funding from the LTOO project. The results of the analyses show peak diatom fluxes are typically sustained from June through July or August and are ice-dependent. Diatom fluxes at BR-3 are low in contrast to the southern sites (BR-1 and BR-G).

4.0 CONCLUSIONS

This section of the report provides concluding remarks on features of interest from the 2017-2018 QA/QC dataset available thus far in Section 4.1 and lessons learned from the 2018 field operations are summarized in section 4.2. At this stage of the project, the lessons learned and recommendations are currently being addressed to provide for more robust and secure future mooring deployments; and to increase the overall quality of the dataset. Objectives and priorities for 2018-2019 are also presented in section 4.3, including an outlook of the milestones for the fourth year of the iBO scientific program.

4.1 Concluding Remarks on the 2017-2018 Dataset

This report is aimed at providing an initial review of the available QA/QC data from the 2 iBO moorings recovered in 2018. Valid data have been presented for current meters, current profilers, and CT loggers deployed at all moorings. The percentage of valid data for current meters and profilers averaged 49.6 % (see Appendix D for further details), while it is 100% for CT sensors. The QA/QC dataset for these instruments is readily available as Matlab© and formatted Text files (ASCII) provided as a data deliverable (see Appendix C). The primary features of interest observed in the 2017-2018 dataset include the following:

- Sea ice in 2018 was characterized by an earlier than normal break up in June followed by greater than normal ice concentration through September. The minimum regional sea ice concentration by the end of September was near the median for seasons on record at 33.1%.
- Surface currents during open water at BR-1 were generally towards the south-southwest in accord with the anti-cyclonic (clockwise) motion of the Beaufort Gyre. Several strong (>50 cm/s) reversals in current direction towards the northeast (along-slope) were observed throughout the year. Surface currents at DFO-9 in open water are bi-directional, dominantly to the southeast and northwest likely driven by wind forcing on the shelf.
- Near-bottom current patterns were relatively similar to measurements from previous years. Currents along the slope are weak (<10 cm/s) and generally follow the bathymetric contours, with a mean direction towards the northeast at BR-1. Currents on the shelf (DFO-9) are bi-directional, similar to those on the surface but with greater variability.
- Maximum current speed in 2017-2018 measured at BR-1 was 67 cm/s and the maximum current speed measured at DFO-9 was 108 cm/s, consistent with magnitudes measured in previous years. Mean current speeds through the water column at BR-1 were between 3-19 cm/s and 8-17 cm/s at DFO-9, also consistent with mean speeds measured in the previous years (2014-2017).
- The temperature and salinity time-series showed that most of the variability in terms of water mass physical properties occurs in the upper 200 m. Several temperature and salinity events were recorded concurrent with a positive along-slope current component which are a likely sign of upwelling of deep waters at the shelf break. The time-series are also noted for a presence of BSWW which is in contrast to 2016-2017.

4.2 2018 Fieldwork Lessons Learned and Recommendations

This section of the report identifies lessons learned and recommendations from work on the Laurier during the 2018 iBO Program that are currently being addressed to improve future mooring deployments and recoveries. The list of recommendations has been finalized following the iBO TAC Meeting that was hosted as part of the ArcticNet

Annual Scientific Meeting, Ottawa, in December 2018 (see Appendix B). The recommendations are provided below for three categories (instrument maintenance, mooring design and equipment, field work and logistics):

Instrument maintenance:

- The TRDI LR battery casing bulkhead connector was bent and thus broken which flooded the housing. It is suspected to have been caused by pulling on the battery cable to remove it when the connector was cold-hardened (in the forward hold). The connectors are brittle when cold; using a heat gun to warm up the connector before removing the cable may help prevent this in the future or replacing the connectors with new, less brittle rubber connectors from TRDI.
- The Nortek Aquadopp bulkhead connector leaked through the connector as it appeared to be loose, allowing water to enter via the connector. The bulkhead connectors on all Nortek instruments should be checked for replacement.
- The lower sediment trap on BR-1-17 rotating disc was not properly installed and was not in contact with the motor drive.

Mooring design and equipment:

- The drop chain galvanized shackles of BR-1-17 Tandem EdgeTech CART releases showed significant corrosion on the chain and attachment shackles, where the joint was under tension. The corrosion was possibly related to poor quality shackles or chain, though this is the first time this has been observed. This poses a recovery risk for moorings BR-G-17 and BR-K-17 in 2019, after two years being underwater.

Fieldwork and logistics:

- The schedule for Leg 3a on the Laurier was severely impacted by greater than normal ice concentration which prevented the recovery of 5 moorings. This reinforces the need to plan and design moorings for 2-year deployments intervals.
- Work space in the between decks hold was very tight because of the multiple moorings program on Leg 3a. Future work on the Laurier should carefully consider packing and organization of equipment to efficiently use space and sufficient time should be allowed for movement and re-organization of equipment in the hold. Laboratories in other parts of the ship can also be utilized to free up space in the between decks hold.

4.3 Objectives and Milestones for 2019-2020

Objectives of iBO for 2019-2020 are centered on the recovery of the 5 remaining iBO moorings from the CGGS Sir Wilfrid Laurier during its annual Arctic expedition to the Beaufort Sea (tentatively scheduled for September 25 to October 14, 2019). Milestones for 2019-2020 are provided in Table 16. This includes the finalization of the QA/QC for 2017-2018 data recovered from the Laurier in 2018. Other activities such as TAC operational meetings, equipment mob/demob, and verification of ADCP compasses to address field logistics, instrumentation performance, and data processing are planned to ensure a timely development of the project in 2019-2020.

Table 16: 2018-2019 iBO Milestones.

Milestone	Date
Presentation of the iBO program at the Inuvialuit Game Council (IGC) meeting, Inuvik	March 8, 2019
QA/QC of ADCP and CT logger 2017-2018 data	March 31, 2019
iBO Technical Report 2018 Submitted	March 31, 2019
Instrumentation maintenance completed at DFO and ArcticNet	Dec 2018-Mar 2019
Completion of BRSEA Synthesis Report (Phase 2 interim report)	May 31, 2019
Technical Advisory Committee Conference Call - Spring Meeting	May 15, 2019
Recovery of iBO moorings onboard the Laurier (tentative)	September 25, 2018 to October 14, 2018
Annual Technical Advisory Committee Meeting, ArcticNet Annual Science Meeting, Ottawa	December, 2019

With iBO completing its fourth and final year, the iBO TAC is developing a Synthesis Report which will be a basic building block for the Indigenous and Northern Affairs Canada (INAC) Beaufort Sea Regional Strategic Environmental Assessment (BRSEA). The Synthesis Report will link up-to-date scientific knowledge on the ice-ocean environment of the Beaufort Sea to issues important to environmental assessment and decision-making in relation to Beaufort offshore exploration and development, particularly for oil & gas. This will be completed primarily by synthesizing the 8 years (2009-2017) of enhanced observations of the marine physical environment by Industry, ArcticNet, and Fisheries and Oceans Canada (DFO) along with existing data and Inuvialuit Traditional Knowledge.

Phase 1, completed in 2018, of the Synthesis Report consisted of 3 subtasks: develop a Table of Contents and methods for the Synthesis Report, commence dialog with relevant Inuvialuit stakeholders, and provide a review of ongoing research in the Beaufort Sea. Phase 2 (development of the Synthesis Report) was commenced in December 2018. Completion of the Synthesis Report will represent a major outcome and deliverable of iBO. The broad objectives of the Synthesis Report include:

- Synthesis of ice-ocean data from 2009-2017
- Contribute to validation of modelling tools
 - Use ocean data during selected events to evaluate simulations of a high-resolution operational ocean forecast model (Environment and Climate Change Canada (ECCC) and DFO's Regional Ice-Ocean Prediction System (RIOPS), <http://navigator.oceansdata.ca>) and to provide insight into the present value of this predictive tool in ocean management and crisis response.
- Link ice-ocean processes to broader applications
 - Identify notable occurrences and follow in detail their development, climax and decay as case studies of circumstances that require industry and government planning.
 - Engage stakeholders in applying the science so that our output is relevant, comprehensible and useful in considerations of offshore development.

4.4 Concluding Remarks on the 2014-2018 iBO Program

This report provides a summary of the iBO program and 2014-2018 dataset following completion of the fourth and final year of the program. The following are key observations derived from the full dataset:

- The high data recovery rates (>90% on average) reflect the success of the iBO field program, attention to quality control detail, continuous application of lessons learned and have resulted in a near-continuous dataset at 7 mooring sites from 2014-2018 with few gaps.
- Sea ice conditions in the southern Beaufort Sea from 2015 to 2018 are characterized by earlier than normal break up in the spring and near record minimum seasonal ice coverage each September except for 2018. Available results from the iBO IPS dataset reflect a similar a trend towards longer ice-free seasons and slightly thinner ice.
- Current profilers and current meters at the 7 mooring sites provided measurements of ocean current through the water column from 2014 to 2018 and were used to characterize currents across the shelf, shelf-break, and slope and provide evidence and insight into large- and small-scale circulation patterns. Current speeds are consistent from year-to-year; similar large- and small-scale circulation patterns were observed from year-to-year with some temporal and spatial variation.
- The temperature and salinity time-series from 2014 to 2018 consistently show that most of the variability in terms of water mass physical properties occurs in the upper 200 m. Each year several water mass shifts resulting in the upper 200 m from up-welling or down-welling were identified primarily on the slope moorings. Below 200 m, temperature-salinity diagrams show little variability from year-to-year in water mass physical properties.

The near-continuous four-year dataset provides important insight into the marine physical environment of the southern Beaufort Sea. An initial review of the datasets has thus far been presented in yearly Technical Reports and has identified key features of the physical environment. The dataset provides the opportunity to further investigate and understand ice-ocean processes in the southern Beaufort Sea. An initial phase of this investigation is currently being completed as part of the BRSEA Synthesis Report, which aims to incorporate the dataset into the synthesis of 8 years of (2009-2017) of enhanced observations of the marine physical environment in the southern Beaufort Sea.

[https://golderassociates.sharepoint.com/sites/1896023/Deliverables/Issued to Client - Reserved for WP/1896023-005-R-Rev0/1896023-005-R-Rev0-iBO_2018_TechReport 06May_19.docx](https://golderassociates.sharepoint.com/sites/1896023/Deliverables/Issued%20to%20Client%20-%20Reserved%20for%20WP/1896023-005-R-Rev0/1896023-005-R-Rev0-iBO_2018_TechReport%2006May_19.docx)

5.0 REFERENCES

- ArcticNet Inc., Fisheries and Oceans, Golder Associates Ltd. (2016). Integrated Beaufort Observatory (iBO) 2015 Technical Project Report. 4 August 2016.
- ArcticNet Inc., Fisheries and Oceans, Golder Associates Ltd. (2017). Integrated Beaufort Observatory (iBO) 2016 Technical Project Report. 31 March 2017.
- ArcticNet Inc., Fisheries and Oceans, Golder Associates Ltd. (2018). Integrated Beaufort Observatory (iBO) 2017 Technical Project Report. June 2018.
- Aagaard, K., 1984. The Beaufort Undercurrent. In: Barnes, P.W., Schell, D.M., Reimnitz, E. (Eds.), *The Alaskan Beaufort Sea: Ecosystems and Environments*. Academic Press, New York, pp. 47–74.
- ASL Environmental Sciences Inc. 2015. IPS Processing Toolbox User's Guide. Report by ASL Environmental Sciences Inc., Victoria BC, Canada, 136 pp.
- Barber, D.G., Hanesiak, J.M., 2004. Meteorological forcing of sea ice concentrations in the southern Beaufort Sea over the period 1979 to 2000. *J. Geophys. Res. (C Oceans)* 109, C06014.
- Blasco, S., Bennett, R., Brent, T., Burton, M., Campbell, P., Carr, E., Covill, R., Dallimore, S., Davies, E., Hughes-Clarke, J., Issler, D., Leonard, L., MacKillop, K., Mazzotti, S., Patton, E., Rogers, G., Shearer, J. and White, M., 2013. 2010 State of Knowledge: Beaufort Sea Seabed Geohazards Associated with Offshore Hydrocarbon Development; Geological Survey of Canada, Open File 6989, 340 p. doi:10.4095/292616
- Canadian Ice Service (CIS). 2018. Seasonal summary. North American Arctic Waters. Summer 2018. 34 pp. https://www.canada.ca/content/dam/eccc/cisccg/seasonal_summaries/20181231_sumarsue_summer2018.pdf
- Carmack, E.C., MacDonald, R.W., 2002. Oceanography of the Canadian Shelf of the Beaufort Sea: a Setting for Marine Life. *Arctic* 55, suppl. 1, 29-45.
- Dmitrenko, I. A., Kirillov, S. A., Forest, A., Gratton, Y., Volkov, D. L., Williams, W. J., Lukovich, J. V., Belanger, C. and Barber, D. G. 2016, Shelfbreak current over the Canadian Beaufort Sea continental slope: Wind-driven events in January 2005. *J. Geophys. Res. Oceans*. Accepted Author Manuscript. doi:10.1002/2015JC011514
- Fissel, D. B., Marko, J. R., Melling, H. 2008, (July). Advances in marine ice profiling for oil and gas applications. In *Proceedings of the Ictech 2008 Conference*.
- Forest, A., Osborne, P. D., Fortier, L., Sampei, M., and Lowings, M. G. 2015. Physical forcings and intense shelf–slope fluxes of particulate matter in the halocline waters of the Canadian Beaufort Sea during winter. *Continental Shelf Research*, 101, 1-21.
- Galley, R. J., Else, B. G. T., Prinsenberg, S. J., Babb, D., Barber, D. G. 2013. Summer Sea Ice Concentration, Motion, and Thickness Near Areas of Proposed Offshore Oil and Gas Development in the Canadian Beaufort Sea—2009. *Arctic*, 105-116.
- Giovando, L.F., Herlinveaux, R.H., 1981. A discussion of factors influencing dispersion of pollutants in the Beaufort Sea. *Pacific Marine Science Report* 81-4, p. 198.
- Institute of Ocean Sciences – Fisheries and Oceans Canada (IOS-DFO). 2018. Arctic Marine Observatories 2018 Field Expedition Report. September 25 – October 18, 2018. Ed. By H. Melling. IOS Cruise 2018-06

- Integrated Ocean Observing System (IOOS). 2015. Manual for Real-Time Quality Control of In-Situ Current Observations: A Guide to Quality Control and Quality Assurance of Acoustic Doppler Current Profiler Observations. Version 2.0 October 2015.
- Jackson, J. M., H. Melling, J. V. Lukovich, D. Fissel, and D. G. Barber (2015), Formation of winter water on the Canadian Beaufort shelf: New insight from observations during 2009–2011, *J. Geophys. Res. Oceans*, 120, doi:10.1002/2015JC010812.
- Kulikov, E.A., Carmack, E.C., Macdonald, R.W., 1998. Flow variability at the continental shelf break of the Mackenzie Shelf in the Beaufort Sea. *Journal of Geophysical Research. C. Oceans* 103, 12,725-712,741.
- Lansard, B., Mucci, A., Miller, L. A., Macdonald, R. W., Gratton, Y. 2012. Seasonal variability of water mass distribution in the southeastern Beaufort Sea determined by total alkalinity and $\delta^{18}O$. *J. Geophys. Res. (C Oceans* 117(C3).
- Macdonald, R.W., Paton, D.W., Carmack, E.C., Omstedt, A., 1995. The freshwater budget and under-ice spreading of Mackenzie River water in the Canadian Beaufort Sea based on salinity and $d^{18}O/d^{16}O$ measurements in water and ice. *J. Geophys. Res. (C Oceans)* 100, 895-919.
- Macdonald, R.W., Solomon, S.M., Cranston, R.E., Welch, H.E., Yunker, M.B., Gobeil, C., 1998. A sediment and organic carbon budget for the Canadian Beaufort Shelf. *Marine Geology* 144, 255-273.
- Melling, H., 1993. The formation of a haline shelf front in wintertime in an ice-covered arctic sea. *Continental Shelf Research* 13, 1123–1147.
- Melling, H., Riedel, D.A. 2004. Draft and Movement of Pack Ice in the Beaufort Sea: A Time-Series Presentation April 1990 - August 1999. Canadian Technical Report of Hydrography and Ocean Sciences 238, v + 24 pp.
- Melling, H., Johnston, P. H., Riedel, D.A. 1995. Measurements of the underside topography of sea ice by moored subsea sonar. *Journal of Atmospheric and Oceanic Technology*, 12(3), 589-602.
- Melling, H., Gratton, Y., Ingram, G. 2001. Ocean circulation within the North Water polynya of Baffin Bay. *Atmosphere-Ocean*, 39(3), 301-325.
- Nortek AS (Nortek). 2013. Comprehensive Manual. December 2013.
- O'Brien, M.C., Macdonald, R.W., Melling, H., Iseki, K., 2006. Particle fluxes and geochemistry on the Canadian Beaufort Shelf: Implications for sediment transport and deposition. *Continental Shelf Research* 26, 41-81.
- Pickart, R.S., 2004. Shelfbreak circulation in the Alaskan Beaufort Sea: Mean structure and variability. *J. Geophys. Res. (C Oceans)* 109, C04024.
- Pickart, R.S., Schulze, L.M., Moore, G.W.K., Charette, M.A., Arrigo, K.R., van Dijken, G., Danielson, S.L., 2013. Long-term trends of upwelling and impacts on primary productivity in the Alaskan Beaufort Sea. *Deep Sea Research Part I: Oceanographic Research Papers* 79, 106-121.
- RBR-Global (RBR). 2016. Ruskin User Guide. Latest version available at: <https://rbr-global.com/support/software>.
- Beardsley, R. C., and L. K. Rosenfeld 1983, Introduction to the CODE-1 moored array and large-scale data report, in CODE-1: Moored Array and Large-Scale Data Report, edited by L. K. Rosenfeld, Tech. Rep. WHOI-83-23, CODE Tech. Rep. 21, pp. 1216, Woods Hole Oceanogr. Inst., Woods Hole, Mass.
- Sequoia Scientific. 2008. Processing LISST-100 and LISST-100X Data in MATLAB. Online Article (last update: 11 July 2012). <http://www.sequoiasci.com/article/processing-lisst-100-and-lisst-100x-data-in-matlab/>.

Teledyne RDI (TRDI). 2014. Monitor, Sentinel, Mariner, Long Ranger, and Quartermaster Commands and Output Data Format. P/N 957-6156-00. Revised March 2014.

Teledyne RDI (TRDI). 2006. Acoustic Doppler Current Profiler Principles of Operation: A Practical Primer. P/N 951-6069-00. December 2006.

von Appen, W. J., Pickart, R. S. 2012. Two configurations of the western Arctic shelfbreak current in summer. *Journal of Physical Oceanography*, 42(3), 329-351.

Williams, W. J., Melling, H., Carmack, E. C., & Ingram, R. G. 2008. Kugmallit Valley as a conduit for cross-shelf exchange on the Mackenzie Shelf in the Beaufort Sea. *Journal of Geophysical Research: Oceans*, 113(C2).

Woodgate, R. A. and Holroyd, A.E. 2011. Correction of Teledyne Acoustic Doppler Current Profiler (ADCP) Bottom-Track Range Measurements for Instrument Pitch and Roll. University of Washington Technical Report: available at <http://psc.apl.washington.edu/BeringStrait.html>

Appendix A. 2017-2018 Final Mooring Diagrams

The final mooring diagrams 2017-2018 are provided below. Instrument depths correspond to the planned depth for each instrument throughout the deployment period.

BR1-17

Lat: 70° 25.9911' N
 Long: 139° 01.5892' W

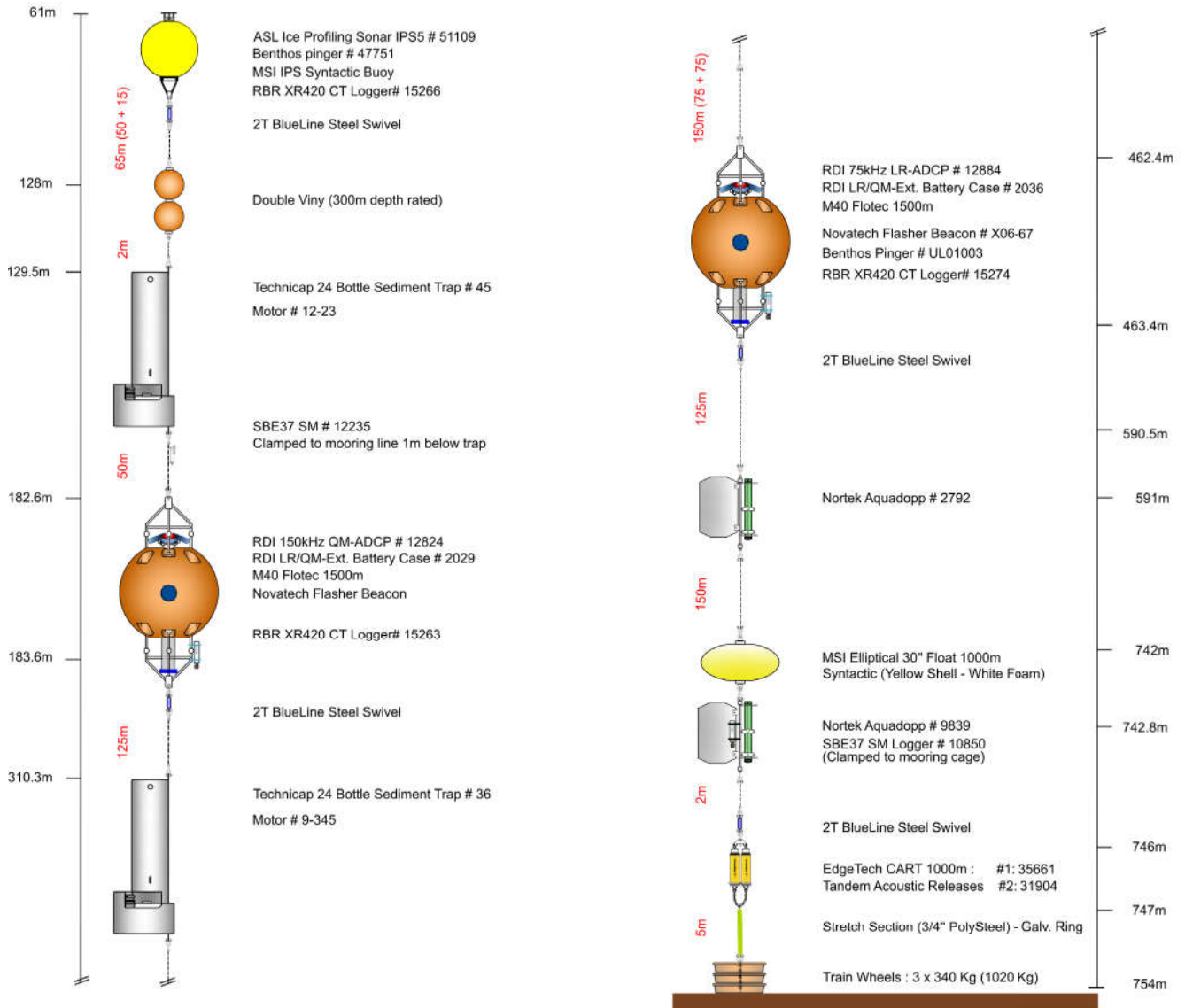
Site Depth : 759m
Slope in Mackenzie Trough (Beaufort Sea)



Instrument Target Depth

Component Details

* Amsteel II 5/16" - First deployed: 2016



BRG-17

Lat: 71° 0.0918' N
 Long: 135° 29.5331' W

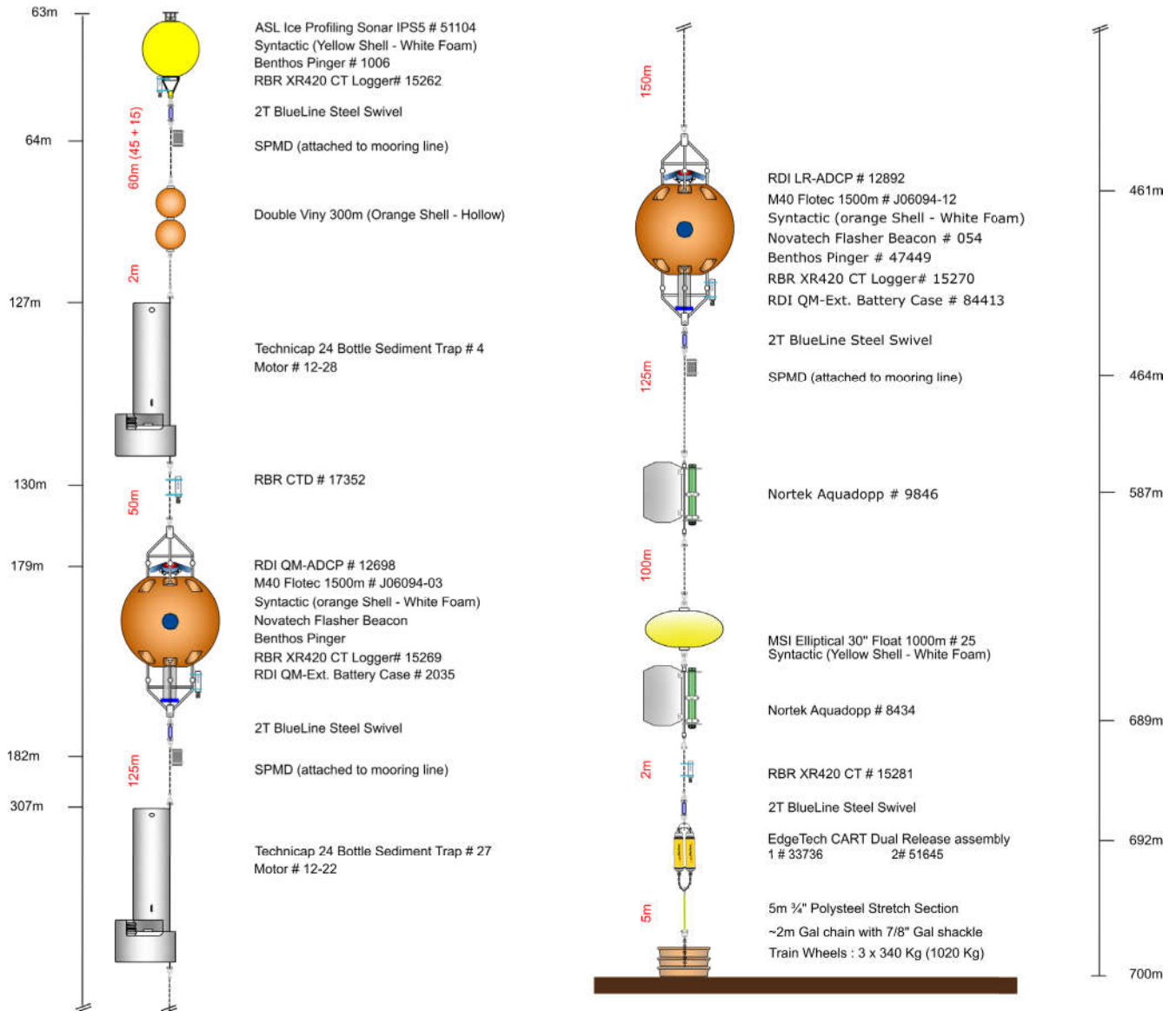
Site Depth : 699m Mooring Length : 637m
Slope in Pokak Area



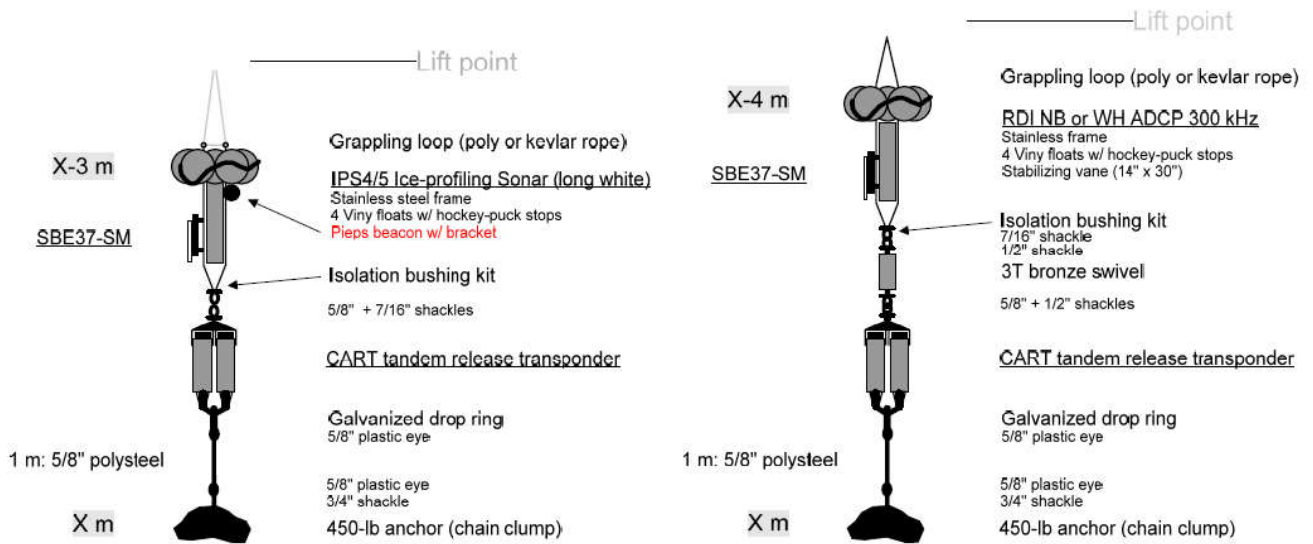
Instrument Target Depth

Component Details

* Mooring Line : Amsteel II 5/16" - First deployed: 2016



Short Taut-line Mooring Schematic for Installations at Cache Point Channel (ACW17-40), Cape Bathurst (CB17), IBO17-1, IBO17-9, IBO17-11 (Mackenzie Shelf), HI17 (Herschel Island)



Appendix B. Technical Advisory Committee Meeting 2018 Minutes

iBO Technical Advisory Committee meeting

ArcticNet ASM 2018

Ottawa - 11 December 2018 11:00

Attendees: Alex Forest, Anissa Merzouk, Shawn Meredyk, Catherine Lalonde, Kanae Komaki, Phil Osbourne, Greg Curtiss, Humfrey Melling

Minutes Summary: Anissa Merzouk, Shawn Meredyk

1 Summary of 2018 operations

A quick annual executive summary of the iBO Laurier moorings ops was presented. Which covered primarily things that went wrong and lessons learned. Shawn mentioned that working on the Laurier was positive and good team work. Difficult ice conditions and rough seas resulted in low data recovery rates from almost all mooring teams and for some instruments from mooring BR1-17. CA08-17 (ArcticNet / LTOO – DFO collaboration) had only one instrument (AURAL – hydrophone) that didn't work due to faulty hard drive, that stopped working after 2 months. BR1-17 had four problems;

1. TRDI battery casing bulkhead connector was bent and thus broken which flooded the housing. This may have happened due to cold temp in the hold and improper disconnecting technique (pulling to vertically on a cold-hardened connector).
2. Nortek Aquadopp bulkhead connector had leaked through the connector as it appeared to be loose, allowing water to enter via the connector.
3. Sediment Trap B had an improperly installed disc, which didn't make contact with the motor drive.
4. The drop chain galvanized shackles of BR1-17 Tandem EdgeTech CART releases showed significant corrosion on the chain and attachment shackles, where the joint was under tension. Possibly bad shackles and bad chain, though this is the first time this has been observed. This poses a recovery risk for moorings BRG-17 and BRK-17 in 2019, after two years being underwater.

It was noted that it was hard to see the broken rubber connector when covered in grease, which doesn't help prevent flooding through the bulkhead connector. The bulkhead connectors are brittle when cold and not compliant at 0°C or lower. These older impulse connectors are hard to gain access to and are not flexible when cold, which has resulted in TRDI changing their bulkhead rubber connectors to a softer rubber. Efforts should be made to buy new bulkhead connectors for TRDI battery casings. The cable connector leakage problem seen in the past was resolved with a new rubber type from TRDI, however, only one new cable was ordered and there are still old rubber types on almost all units. The problem is also with the bulkhead connectors on the ADCPs themselves.

On Mooring BR1-17, the Long Ranger worked well for 2 days. Trap B (main screw) wasn't installed correctly and the lower Aquadopp was destroyed by flooding through a loose connector, thus connectors will be replaced for 2019. The primary concern for the 2019 recoveries are galvanized steel shackle corrosion on the CART tandem release moorings (BRG-17 and BRK-17), as BR1-17 identified shackles showing galvanized corrosion on the CART release chain, where the shackle pins touched the chain (20% diameter of pin and chain was corroded). This is odd (never seen before) and difficult to

explain as nothing has changed in the equipment nor mooring design and the equipment was ordered from same places for the past 5 years.

There was a concern that these galvanized shackles could be fake Crosby shackles, therefore, one sample will be sent to Crosby to have it investigated. Entire batch of potential bad shackles put aside to be disposed of. New batch of shackles and chains will be ordered for 2019 from a different supplier (not Lamé), probably Wesco in Vancouver, BC. It was also requested to re-connect with Baly to inquire if he had any comments or suggestions as Shawn had seen that a different method was used to install the tie-wraps in shackles (crossing) in 2017, which may have provided an anoxic point of contact, though this is only speculation and is not likely.

Stainless Steel shackles continue to show corrosion where tension on points of contact with the trap were seen. The use of galvanized shackles and a spliced rope system in future should eliminate stainless shackles from the mooring design and decrease mooring loss due to corrosion.

1.1 Lessons Learned:

- a. TRDI external battery housing bulkhead connector on older models can become hard and susceptible to pin breakage and connector breakage underneath the pins, which is not visible if covered in grease. Use a heat gun where necessary and pull horizontally, also no grease around bulkhead connector, only the pins matting connection.
- b. Older used bulkhead connectors on Aquadopp units could be replaced or at the very least have the bolt tightened and new Loctite re-applied.
- c. The sediment trap disc installation should never need additional rubber inserts or anything of the sort, all traps and discs and motors have the same dimensions and thus if they don't fit well, then it isn't installed correctly.
- d. Hydrophones from the company Multiélectronique, namely the older model AURAL units are unreliable for long deployment durations and thus new hydrophones (i.e, JASCO G4, etc.) should be purchased for future deployments.
- e. New shackles and new chain will be purchased due to visible corrosion on the drop chain recovered from the CART releases from BR1-17. Verified true Crosby shackles and chain are required.

1.2 Action Items:

- a. Shawn to order new Crosby Shackles and chain.
- b. Shawn to order and replace necessary bulkhead connectors with new softer rubber type for TRDI external battery casings.
- c. Shawn to order new bulkhead connectors for Aquadopp units
- d. Shawn to splice 2/5m rope sections to sediment traps to eliminate stainless steel shackles from mooring. Also the safety line would be in-line spliced to the end points.

2 Laurier Mission in 2019

The goal in 2019 is to recover the remaining 2017 moorings BR-G, -K, -3 and CA05. This has already been confirmed that Amundsen will not go to Beaufort Sea in 2019 due to early return to Québec in September 2019. Thus the Laurier will conduct the iBO mooring operations in 2019 again.

Humfrey has mentioned that the leftover ship time from 2018 was not resolved yet. But that 13 days are too much to request and a lower expectation of 5 days would be more likely approved (end of December 2018 or early 2019). Humfrey had also mentioned that the Beaufort gyre cyclonic-anticyclonic weather patterns that indicate a possibility for heavy ice again in 2019 (see cruise report). Humfrey had also confirmed that the Laurier is returning to the west coast for dry-dock operations (vessel life extensions) in 2019 but that the program for the Laurier is again Sept-early Oct for Beaufort Sea mooring operations.

Alex had mentioned that he'll follow up with news of LTOO mooring program in the new year.

2.1 Actions Items:

- a. Humfrey to confirm the number of days of ship time that can be recovered from the 2018 mission, for use in 2019.
- b. Alex to follow-up with new of LTOO mooring program and which moorings from LTOO will be continued.

3 Update on LTOO Mooring Program

The Arcticnet program is in renewal for 5 years. Projects will be selected in march 2019 and there was some concern about linkages with northern communities being weak and that to continue the program, a service contract with Arcticnet via Amundsen science could be necessary. This service contract would remove the need to be heavily tied by indigenous engagement, like other Arcticnet projects would be. The network investigator would be Catherine Lalonde or Alex, and the deployment of possibly 2 moorings in the Beaufort Sea and possibly two other LTOO moorings in Baffin Bay are in preparation for big a project in 2021. We will know more in Feb-March 2019.

Catherine had mentioned that BRG was a priority along with one site in Amundsen Gulf (no preference but CA05 or CA08 were mentioned).

LTOO will become a collaborative project with Danny Dumont (UQAR) but led by Amundsen Science (AS) under a service contract by Arcticnet. Phil had mentioned that past experiences from industry collaborations concerning mammal observers, later involved in moorings program, worked well during BREA and could possibly fulfill the community engagement directive of future LTOO program requirements. Alex had mentioned that something could be worked out via possible training / internship incentives.

3.1 Action Items:

- a. See Section 2.1b (above)

4 Update on BRSEA

Funding from INAC to produce synthesis report with Kanae is a possibility, with emphasis on ice profiler data. Ed Ross had sent a report with a data table identifying which data has been and is in-progress. Humfrey mentioned that they do basic processing and that he himself does a five page statistics summary for his ice profiling data. Humfrey had mentioned that it is hard to get throughput from ASL at the moment because their analyst is on maternity leave, but she will be back in January 2019. Alex had mentioned the need to obtain these data and liaison with Humfrey to provide material or feedback with Kanae for the document for INAC.

Humfrey had mentioned that the 2014-15 data was delivered and that he had package snapshots from all moorings, however, 2015-16 didn't have much data available. BR1 has three years of data, BR3 has 2 years (email from 9 Oct) including BREA data, not just iBO. A spreadsheet detailing what has been processed will be produced from Humfrey.

If Kane chooses the assignment, she would visit Québec and/or go to Victoria to work with Humfrey and discuss and work on the IPS data.

Re-convening in January or February in 2019 to follow up on this would be needed since the INAC expects this data in the document. Humfrey mentioned that there are lots of IPS data, from MARES and others and identifying key data products and missing/gaps for the INAC report could be a way to focus the work for Kanae and Humfrey. Humfrey has already identified data of interest and has sent them via email. The time needed to process these data are of concern if the report is to be completed on-time, thus it was suggested to possibly sub-contract ice profiler data processing experts to accelerate the time-to-publish, though we must be careful not to undercut ASL. Phil had mentioned that the need to re-connect with ASL and inquire on status and if there is sufficient help available to proceed on schedule.

Greg is building a database and inventory for the INAC synthesis, providing access to data from 2009-2013 ADCPs from Humfrey. The goal is to show continuity of time series and Greg and Humfrey will work together in 2019 on this project.

Alex and Phil met with Martin Tremblay concerning the BRSEA Report which is due in April 2019.

The ESRF report is an expanded version of the cruise report and is a bonus report which is not required, but is nice to show them the extent the program. BR1-17 and IOS Site 9 (2017) QA/QC to be done by Greg and is to be included in this 2019 ESRF report.

4.1 Action Items:

- a. BRSEA report to be completed in 2019
- b. ESRF report to be completed in 2019

5 New opportunities

ESRF will not be renewed if Arctic oil and gas moratorium continues. This is a clear message from Evan Burchart at IOL. There is little funding for ship time if only LTOO mooring program is renewed. If ESRF is not renewed, our group needs to find new sources of funding and opportunities. Possibly the OPP or the DFO-Academic or MEOPAR options might be accessible to the group, though this is to be seen.

Humfrey mentioned that DFO would not provide many opportunities except from an academic discretionary fund.

There was some interest in possibly gaining access to MPA funding from DFO, but the only DFO MPA in the Arctic are in the NE Canada Basin next to the high Arctic islands. But the DFO Ocean sector (not sciences sector) controls these funds and the opportunity to gain access to these funds was not probable.

Alex had mentioned the NSERC CRD but that we would need academic and private sector partners. Dany Dumont or Louis Fortier could possibly be the academic partners. The CRD around collaborations with NRC to investigate pipeline off Melville Island could be an option but would only provide minimal funding (<300K). Phil had mentioned that an Innovation fund from Golder (100 k\$) as private partner could be possible, which could get us the Industry-academic collaboration needed for the NSERC CRD submission.

5.1 Action Items:

- a. Alex, Phil and Humfrey to find NSERC CRD collaborators for the funding submission

Appendix C. Data deliverable

In addition to this report, we issue the available oceanographic data that was processed and quality checked following the methods described in section 2.4. The data is provided electronically. This data is provided as a draft and could be subject to further revisions. The data are provided as Matlab and ASCII files for the following instruments:

Mooring	Mooring depth (m)	Instrument	Serial Number	Instrument depth (m)
BR-1-17	759	RBR XR420 CT	15263	50.0
		SBE37 Microcat	12235	118.8
		TRDI QM ADCP 150 kHz	12823	173.7
		RBR XR420 CT	15274	174.7
		TRDI LR ADCP 75 kHz	12943	458.7
		RBR XR420 CT	17352	459.7
		Nortek Aquadopp DW	8543	590.5
		SBE37 Microcat	10850	741.1
		Nortek Aquadopp DW	8448	745.2
DFO-9-17	35	TRDI WHS ADCP 300kHz	12414	31.0
		SBE37 Microcat	6728	32.5

Appendix D. Summary Statistics of Ocean Currents

Table 17: Summary statistics of current speed, vector-averaged direction and number of valid records by bin depth at BR-1-17 based on the data acquired with the QM ADCP #12824 from 2017 to 2018. Bin depths flagged manually as part of the QA/QC are highlighted in red.

Bin Depth (m)	Min Speed (m/s)	1%ile Speed (m/s)	5%ile Speed (m/s)	25%ile Speed (m/s)	Median Speed (m/s)	Mean Speed (m/s)	75%ile Speed (m/s)	95%ile Speed (m/s)	99%ile Speed (m/s)	Max Speed (m/s)	Standard Deviation Speed (m/s)	Vector-Averaged Direction (deg TN)	Number of Valid Records	% of Valid Data (%)
15.9	0.00	0.01	0.02	0.06	0.11	0.12	0.17	0.28	0.36	0.60	0.08	259.0	30,478	85.1
19.9	0.00	0.01	0.03	0.07	0.12	0.14	0.18	0.30	0.41	0.62	0.09	257.1	33,398	93.3
23.9	0.00	0.01	0.03	0.07	0.12	0.14	0.19	0.32	0.43	0.60	0.09	255.0	33,955	94.8
27.8	0.00	0.01	0.03	0.07	0.12	0.14	0.18	0.31	0.42	0.60	0.09	251.9	34,604	96.6
31.8	0.00	0.01	0.03	0.07	0.12	0.13	0.18	0.30	0.41	0.60	0.09	249.2	34,859	97.3
35.8	0.00	0.01	0.03	0.07	0.12	0.13	0.18	0.29	0.40	0.60	0.08	247.2	34,725	97.0
39.8	0.00	0.01	0.03	0.07	0.12	0.13	0.18	0.29	0.39	0.61	0.08	244.8	34,771	97.1
43.8	0.00	0.01	0.03	0.07	0.12	0.13	0.18	0.29	0.40	0.57	0.08	242.5	34,844	97.3
47.8	0.00	0.01	0.03	0.07	0.11	0.13	0.18	0.29	0.42	0.57	0.09	240.1	35,030	97.8
51.8	0.00	0.01	0.03	0.07	0.11	0.13	0.18	0.30	0.43	0.59	0.09	237.2	35,185	98.2
55.8	0.00	0.01	0.03	0.07	0.11	0.12	0.16	0.29	0.42	0.60	0.08	236.9	35,177	98.2
59.8	0.00	0.00	0.01	0.02	0.05	0.09	0.11	0.32	0.44	0.59	0.10	202.1	35,702	99.7
63.8	0.00	0.01	0.03	0.06	0.10	0.12	0.15	0.29	0.43	0.60	0.08	235.9	35,292	98.5
67.8	0.00	0.01	0.03	0.06	0.11	0.13	0.18	0.31	0.43	0.59	0.09	229.3	35,421	98.9
71.8	0.00	0.01	0.03	0.06	0.11	0.14	0.18	0.34	0.44	0.61	0.10	226.6	35,444	99.0
75.8	0.00	0.01	0.03	0.06	0.10	0.14	0.18	0.35	0.46	0.65	0.10	224.6	35,442	99.0
79.8	0.00	0.01	0.02	0.06	0.10	0.14	0.19	0.35	0.47	0.62	0.11	222.4	35,440	99.0
83.8	0.00	0.01	0.03	0.06	0.10	0.14	0.19	0.36	0.47	0.65	0.11	220.7	35,441	99.0
87.8	0.00	0.01	0.02	0.06	0.10	0.14	0.19	0.37	0.48	0.64	0.11	219.8	35,464	99.0
91.8	0.00	0.01	0.02	0.06	0.10	0.14	0.19	0.37	0.48	0.64	0.11	218.3	35,509	99.2
95.8	0.00	0.01	0.02	0.06	0.10	0.14	0.19	0.37	0.48	0.60	0.11	216.9	35,513	99.2

Bin Depth (m)	Min Speed (m/s)	1%ile Speed (m/s)	5%ile Speed (m/s)	25%ile Speed (m/s)	Median Speed (m/s)	Mean Speed (m/s)	75%ile Speed (m/s)	95%ile Speed (m/s)	99%ile Speed (m/s)	Max Speed (m/s)	Standard Deviation Speed (m/s)	Vector-Averaged Direction (deg TN)	Number of Valid Records	% of Valid Data (%)
99.8	0.00	0.01	0.02	0.06	0.10	0.14	0.19	0.38	0.49	0.61	0.11	215.9	35,545	99.3
103.8	0.00	0.01	0.02	0.06	0.10	0.14	0.19	0.38	0.49	0.61	0.11	214.4	35,562	99.3
107.8	0.00	0.01	0.02	0.06	0.10	0.14	0.18	0.38	0.49	0.61	0.11	212.7	35,590	99.4
111.8	0.00	0.01	0.02	0.06	0.10	0.14	0.18	0.38	0.49	0.66	0.11	211.0	35,609	99.4
115.8	0.00	0.01	0.02	0.06	0.10	0.14	0.18	0.38	0.49	0.67	0.11	209.6	35,630	99.5
119.8	0.00	0.01	0.02	0.06	0.10	0.13	0.18	0.38	0.49	0.64	0.11	207.7	35,656	99.6
123.8	0.00	0.01	0.02	0.05	0.08	0.11	0.12	0.35	0.47	0.61	0.10	184.9	35,759	99.9
127.8	0.00	0.00	0.01	0.02	0.03	0.05	0.05	0.22	0.32	0.51	0.06	87.1	35,811	100
131.8	0.00	0.01	0.02	0.05	0.09	0.12	0.16	0.30	0.35	0.49	0.08	211.8	35,754	99.8
135.8	0.00	0.01	0.02	0.05	0.09	0.13	0.16	0.37	0.47	0.56	0.11	198.0	35,768	99.9
139.8	0.00	0.01	0.02	0.05	0.09	0.13	0.16	0.37	0.47	0.57	0.11	194.3	35,787	99.9
143.8	0.00	0.01	0.02	0.05	0.09	0.12	0.16	0.37	0.46	0.57	0.11	190.3	35,804	100
147.8	0.00	0.01	0.02	0.05	0.08	0.12	0.15	0.37	0.46	0.56	0.10	186.6	35,810	100
151.8	0.00	0.01	0.02	0.05	0.08	0.12	0.15	0.36	0.44	0.60	0.10	181.5	35,812	100
155.8	0.00	0.01	0.02	0.05	0.08	0.11	0.14	0.35	0.43	0.58	0.10	176.9	35,812	100
159.8	0.00	0.01	0.02	0.05	0.08	0.11	0.14	0.34	0.42	0.57	0.10	172.0	35,812	100
163.8	0.00	0.01	0.02	0.04	0.07	0.10	0.13	0.32	0.40	0.57	0.09	165.5	35,812	100
167.8	0.00	0.01	0.02	0.04	0.07	0.10	0.12	0.30	0.39	0.54	0.09	154.7	35,812	100

Table 18: Summary statistics of current speed, vector-averaged direction and number of valid records at 586.2 m depth at BR-1-17 as based on the data acquired with the Aquadopp DW #2792 from 2017 to 2018.

Bin Depth (m)	Min Speed (m/s)	1%ile Speed (m/s)	5%ile Speed (m/s)	25%ile Speed (m/s)	Median Speed (m/s)	Mean Speed (m/s)	75%ile Speed (m/s)	95%ile Speed (m/s)	99%ile Speed (m/s)	Max Speed (m/s)	Standard Deviation Speed (m/s)	Vector-Averaged Direction (deg TN)	Number of Valid Records	% of Valid Data (%)
586.2	0.00	0.00	0.01	0.02	0.03	0.03	0.04	0.06	0.08	0.11	0.02	75.8	17,906	100

Table 19: Summary statistics of current speed, vector-averaged direction and number of valid records by bin depth at DFO-9-16 based on the data acquired with the WHS ADCP #12414 from 2017 to 2018.

Bin Depth (m)	Min Speed (m/s)	1%ile Speed (m/s)	5%ile Speed (m/s)	25%ile Speed (m/s)	Median Speed (m/s)	Mean Speed (m/s)	75%ile Speed (m/s)	95%ile Speed (m/s)	99%ile Speed (m/s)	Max Speed (m/s)	Standard Deviation Speed (m/s)	Vector-Averaged Direction (deg TN)	Number of Valid Records	% of Valid Data (%)
5.0	0.00	0.01	0.02	0.07	0.14	0.17	0.23	0.40	0.56	1.08	0.12	88.6	12,634	70.3
6.0	0.00	0.01	0.02	0.07	0.13	0.16	0.22	0.38	0.54	0.97	0.12	91.1	12,980	72.3
7.0	0.00	0.01	0.02	0.06	0.12	0.15	0.20	0.35	0.51	0.90	0.11	90.2	13,442	74.8
8.0	0.00	0.01	0.02	0.06	0.11	0.14	0.19	0.34	0.48	0.88	0.11	89.5	13,935	77.6
9.0	0.00	0.01	0.02	0.05	0.10	0.13	0.18	0.32	0.45	0.78	0.10	88.9	14,801	82.4
10.0	0.00	0.01	0.02	0.05	0.10	0.13	0.18	0.31	0.44	0.72	0.10	85.6	15,074	83.9
11.0	0.00	0.01	0.02	0.05	0.10	0.12	0.18	0.30	0.43	0.68	0.09	85.1	15,255	84.9
12.0	0.00	0.01	0.02	0.05	0.10	0.12	0.17	0.30	0.42	0.60	0.09	80.3	15,438	86.0
13.0	0.00	0.01	0.02	0.05	0.09	0.12	0.16	0.28	0.41	0.62	0.09	76.9	16,119	89.7
14.0	0.00	0.01	0.02	0.05	0.09	0.11	0.16	0.27	0.40	0.61	0.09	70.3	16,670	92.8
15.0	0.00	0.01	0.02	0.05	0.09	0.11	0.15	0.27	0.40	0.62	0.08	62.6	16,888	94.0
16.0	0.00	0.01	0.02	0.05	0.09	0.11	0.15	0.26	0.39	0.59	0.08	53.5	17,073	95.1
17.0	0.00	0.01	0.02	0.05	0.09	0.11	0.15	0.26	0.37	0.54	0.08	35.2	17,246	96.0
18.0	0.00	0.01	0.02	0.05	0.09	0.11	0.14	0.25	0.36	0.55	0.07	283.5	17,395	96.9
19.0	0.00	0.01	0.02	0.05	0.09	0.10	0.14	0.24	0.33	0.53	0.07	242.6	17,502	97.5
20.0	0.00	0.01	0.02	0.05	0.09	0.10	0.14	0.23	0.31	0.49	0.07	241.0	17,567	97.8
21.0	0.00	0.01	0.02	0.05	0.09	0.10	0.13	0.22	0.30	0.48	0.06	240.0	17,644	98.2
22.0	0.00	0.01	0.02	0.05	0.09	0.10	0.13	0.21	0.29	0.43	0.06	234.2	17,712	98.6
23.0	0.00	0.01	0.02	0.05	0.08	0.10	0.13	0.21	0.29	0.45	0.06	231.6	17,763	98.9
24.0	0.00	0.01	0.02	0.05	0.08	0.09	0.12	0.21	0.28	0.44	0.06	224.9	17,817	99.2
25.0	0.00	0.01	0.02	0.05	0.08	0.09	0.12	0.21	0.28	0.42	0.06	214.8	17,854	99.4
26.0	0.00	0.01	0.02	0.04	0.07	0.09	0.11	0.20	0.27	0.40	0.06	204.2	17,875	99.5
27.0	0.00	0.01	0.02	0.04	0.07	0.08	0.11	0.19	0.27	0.40	0.06	198.3	17,896	99.6
28.0	0.00	0.01	0.02	0.04	0.06	0.08	0.10	0.18	0.26	0.43	0.05	195.9	17,960	100.0